UNIVERSITÉ DE GRENOBLE

THÈSE

Pour obtenir le grade de

DOCTEUR DE L'UNIVERSITÉ DE GRENOBLE

Spécialité : **Physiologie Physiopathologies et Pharmacologie**

Arrêté ministériel : 7 août 2006

Présentée par

« Marcela Alejandra GONZÁLEZ GRANILLO »

Thèse dirigée par **« Professeur Valdur SAKS »** et
codirigée par **« Docteur Yves USSON »**

préparée au sein du **Laboratoire de Bioénergétique Fondamentale et Appliquée - INSERM U1055, UJF**
dans **l'École Doctorale Chimie et Science du Vivant**

La bioénergétique systémique moléculaire des cellules cardiaques : la relation structure-fonction dans la régulation du métabolisme énergétique compartmentalisé.

Thèse soutenue publiquement le **« 28 septembre 2012 »**,
devant le jury composé de :

M. Pierre DOS SANTOS
Professeur, Directeur du GIS CHU - UBxS, Rapporteur.
M. Yves TOURNEUR
CR1, Directeur d'INSERM U1060/UNI.LYON1/INRA135, Rapporteur.
M. François BOUCHER
Professeur, Directeur du TIMC-IMAG UM 5525, Président.
Mme. Anne CANTEREAU
Docteur, Ingénieur de recherche CNRS, Plateforme ImageUP, Membre.
M. Andrey KUZNETZOV
Docteur, D. Swaroski research laboratory IMU, Membre.
M. Uwe SCHLATTNER
Professeur, Directeur du LBFA-INSERM U1055, Membre.

UNIVERSITÉ DE GRENOBLE

DOCTORAL THESIS

To obtain the grade of

DOCTOR OF PHILOSOPHY AT THE UNIVESITY OF GRENOBLE

Specialty: **Physiology, Physiopathology and Pharmacology**

Arrêté ministériel : 7 août 2006

Presented by

« Marcela Alejandra GONZÁLEZ GRANILLO »

Supervised by **« Professor Valdur SAKS »** and
Co-supervised by **« Doctor Yves USSON »**

prepared at the **Laboratory of Fundamental and Applied Bioenergetics (LBFA) - INSERM U1055, UJF**
at **the doctoral school of chemistry and life sciences**.

Molecular system bioenergetics of cardiac muscle cells: structure-function relationship in regulation of compartmentalized energy metabolism.

Thesis defended in public on **« September 28th, 2012 »**, in front of the thesis jury. Composition of the jury:

Professor Pierre DOS SANTOS
Director of the GIS CHU - UBxS, Reviewer.
Professor Yves TOURNEUR
Director of the INSERM U1060/UNI.LYON1/ INRA135, Reviewer.
Professor François BOUCHER
Director du TIMC-IMAG UM 5525, President.
Anne CANTEREAU, PhD
Engineer of research at the CNRS, Platform ImageUP, Examiner.
Andrey KUZNETZOV, PhD
D. Swaroski research laboratory IMU, Examiner.
Professor Uwe SCHLATTNER
Director of the LBFA-INSERM U1055, Examiner.

TABLE OF CONTENTS

FIGURE INDEX

TABLE INDEX

ABBREVIATIONS

AK	Adenylate kinase
α-KG	α-ketoglutarate
KDH	α-ketoglutarate dehydrogenase
AMP	Adenosine monophosphate
ANC	Adenine nucleotide carrier
ANT	Adenine nucleotide translocase
β-FAO	β-fatty acids oxidation
BCK	Brain creatine kinase
Ca^{2+}	Calcium
CTT	Carboxyl-terminal tail
CoQ	Coenzyme-Q
Cr	Creatine
CK	Creatine kinase
Cyt *c*	Cytochrome *c*
Drp1	Dynamin-related protein 1
$\Delta\psi$	Electrochemical gradient
$\Delta\mu_{H+}$	Electrochemical potential of protons
ETF	Electron-transferring flavoprotein
ETC	Electron transport chain
G	Energy
S	Entropy
H	Enthalpy
DNA	Deoxyribonucleic acid
FAD	Flavin adenine dinucleotide
FMN	Flavinmononucleotide
FFA	Free fatty acids
G6P	Glucose-6-phosphate
GLUT-4	Glucose transporter-4
GTP	Guanosine triphosphate
GAPDH	Glycealdehyde-3-phosphate dehydrogenase
HK	Hexokinase
IMAC	Inner-membrane anion channel
P_i	Inorganic phosphate
IMS	Intermembrane space
ICEU	Intracellular energetic units
KHE	K^+/H^+ exchanger
MDH	Malate dehydrogenase
mitoK_{ATP}	Mitochondrial ATP-sensitiveK^+ channel
mtDNA	Mitochondrial deoxyribonucleic acid
mitoK_{ca}	Mitochondrial Ca^{2+}-activated K^+ channel
MCU	Mitochondrial Ca^{2+} uniporter
MtCK	Mitochondrial creatine kinase
$\Delta\psi_m$	Mitochondrial electrical potential energy
MIM	Mitochondrial inner membrane
MI	Mitochondrial interactosome
MOM	Mitochondrial outer membrane
MT	Microtubules
MAP	Microtubule associated protein
Mfn	Mitofusin
MB-CK	Muscle-brain creatine kinase

MCK	Muscle creatine kinase
M	Myosin
NHE	Na^+H^+exchanger
NAD^+	Niacin adenine dinucleotide
NADH	Nicotinamide adenine dinucleotide
NB HL-1	Non-beating HL-1
OPA1	Optic atrophy
PTP	Permeability transition pore
PiC	Phosphate Carrier
PFK	Phosphofructokinase
PCr	Phosphocreatine
PGK	3-phosphoglycerate kinase
PTM	Post-translational modifications
Δp	Proton motive force
PYR	Pyruvate
PDH	Pyruvate dehydrogenase
PK	Pyruvate kinase
ROS	Reactive oxidative species
RC	Respiratory chain
RNA	Ribonucleic acid
rRNA	Ribosomal ribonucleic acid
SR	Sarcoplasmic reticulum
STI	Soy trypsin inhibitor
SDH	Succinate dehydrogenase
T	Temperature
tRNA	Transfer ribonucleic acid
TCA	Tricarboxylic acids
Tn	Troponin
QH_2	Ubiquinol
VDAC	Voltage dependent anion channel

I. INTRODUCTION

1. PHILOSOPHICAL BACKGROUND

1.1. Systems Biology: general historical overview.

Systems Biology describes complex biological systems quantitatively at different levels. It involves the application of experimental, theoretical, and computational techniques to the study of biological organisms at the molecular, cellular, organ, organism, and population level. Its aim is to understand biological processes as integrated systems instead of isolated parts.

Systems biology's main principle is to consider the interactions between components of the system, resulting in new system-level properties, which do not exist when components are studied separately. An integrated system and specific biological function resulting from interactions between individual components and depends on these level properties. The main aim of each level is to maintain the whole organism's life. An empowering tool of Systems Biology is mathematical modeling based on firm experimental data, without it mathematical modeling is sometimes just like a computer game. The use of well-established mathematical models can help to merge concepts of dynamics, regulation and control of biological functions. Systems biology interprets biological phenomena as dynamic processes which inherent time resolution depends on the behavior studied [1].

On the other hand, the previous approach of reductionism studies each element of a living organism on its isolated state. It is useful in order to determine intrinsic characteristic properties of objects, which cannot be explored in their native fundamental state. Reductionism is based in the central dogma of molecular biology (Watson and Crick [2]) where information flows from DNA to RNA, from RNA to proteins, to then form protein networks, and so on up through the biological levels to that of the whole organism. This line of thought is well schematized by Denis Noble in his book "The Music of Life" that describes how the, reductionist casual chain begins with the central dogma that

information flows from DNA to proteins, strictly from bottom-up, and extends the same concept through all the higher levels [3].

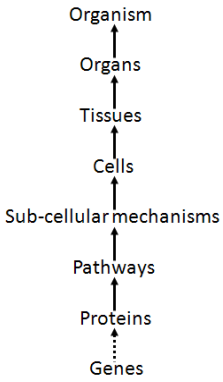

Figure 1. Reductionist causal chain: one-way system, from the genes to the organism. If it is known all about the lowest-level elements, genes and proteins, then everything about the organism would be clear. Taken from [3].

In addition, Denis Noble completed the previous diagram by adding the downward forms of causation, such as higher level triggering cell signaling and gene expression; these regulatory loops provide a fine control and a high degree of cellular organization.

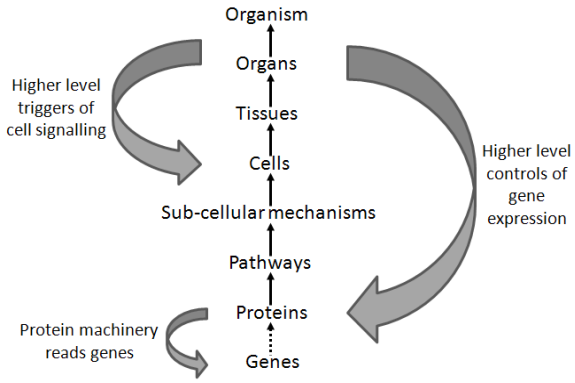

Figure 2. Downward causation: completed reductionist causal chain by the addition of downwards forms of causation. Higher levels trigger cell signaling and gene expression. Protein machinery reads and interprets gene coding. Loops of interacting downward and upward causation can be built between all levels of biological organization. Taken from [3].

By the addition of these loops, it can be seen that genes and proteins are involved and respond to an interaction of an organism with its environment, providing a physiological function and preserving life. Besides in "*The Music of Life*", Noble presents the ten principles of system biology [3].

Claude Bernard (1813-1878), a French physiologist and founder of experimental medicine and systems biology was according to Denis Noble. Through "*Introduction à l'étude de la Médicine*

Expérimentale" in 1865, Claude Bernard established the principles of system biology. In addition, he stated that 'the living organism does not really exist in the *milieu extérieur* but in the liquid *milieu intérieur*… a complex organism should be looked upon as an assemblage of simple organism… that live in the liquid *milieu intérieur*'; giving the first example of multilevel functionality through his concept of the constancy of the internal environment [4], called homeostasis nowadays.

From a philosophical point of view, systems biology follows the dialectic principles of the general historical developments described by a German philosopher, Georg Wilhelm Friedrich Hegel (1770-1831). Hegel considered the real knowledge as an understanding of not only part but the Whole, the Absolute Idea This Absolute Idea of a detailed knowledge of the integrated whole systems is what systems biology wants to understand (*i.e*. to know all about life in its complexity, an Absolute Idea of living systems) [5].

The dialectic consists of the thesis, antithesis and synthesis; this triadic movement is essential to understand the result. A thesis is first giving rise to its reaction, an antithesis contradicts or refutes the thesis, and a synthesis resolves the tension between a thesis and antithesis.

In addition, systems biology has been also favored by the works of Norbert Wiener (1894-1964), an American mathematician and founder of cybernetics. Cybernetics studies the structure and function of regulatory systems. Due to this, it plays a major role in systems biology, seeking to integrate different levels of information to understand how biological systems function. Wiener through cybernetics developed the theory of feedback regulation and its application to explain the mechanism of homeostasis [5].

Gathering the contributions of Bernard, Hegel and Wiener, it can be established that the development of biological science is a Hegelian dialect movement. In systems biology, these components are again studied in their interaction within the intact systems of interest. Finally, among these principles, transmission of information by feedback mechanisms is most important.

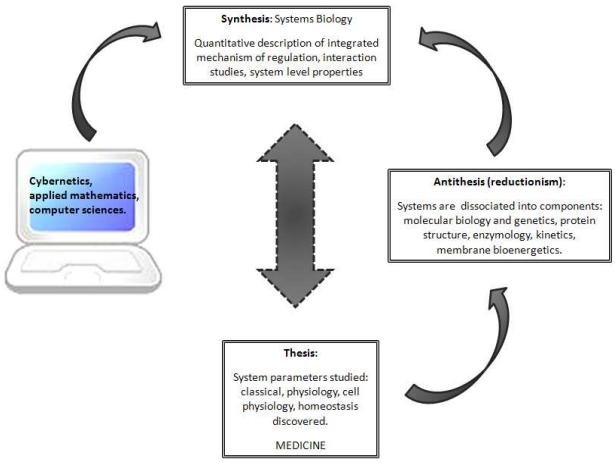

Figure 3. Hegelian logic of reflection and an approach of the biological sciences.

2. PRINCIPLES OF BIOENERGETICS

2.1. Molecular System Bioenergetics

Once the principles of system biology are applied to cellular bioenergetics, the field of Molecular System Bioenergetics arises, which includes the energy metabolism as integrated networks in spatial (organization) and temporal (dynamic) aspects [6].

Bioenergetics is the science that studies the energetic transformations within living cells, explaining how cells obtain energy to live and perform work : mechanically (via motility and contraction), osmotically (via ion transport), or chemically (via biosynthesis), and how a cell maintains its specific structure and metabolism [6].

The molecular system bioenergetics is the study of energy conversion in cells, which allows to explain many classical observations in the cellular physiology of respiration and to understand how a cell senses its energy status. By sensing its energy status the cell is able to adjust its functions under different living conditions. Moreover, it takes into account the spatial and temporal dynamics of intracellular interactions.

Therefore, living organisms are open systems that operate far from the thermodynamic equilibrium; they exchange both matter and energy with their surroundings. This is well described with the first law of thermodynamics that describes the principle of the conservation of energy *"in any physical or*

chemical change, the total amount of energy in the universe remains constant, although the form of the energy may exchange".

Moreover, the second law of thermodynamics establishes the tendency in nature toward ever-greater disorder in the universe "*the total entropy of the universe is continually increasing*". A process occurs as a result of increasing entropy in the universe. The theory of energy changes during chemical reaction at constant temperature (T), developed by J. Willard Gibbs, shows that the free energy (G) depends on entropy (S) and enthalpy (H):

$$\Delta G = \Delta H - T\Delta S$$

A spontaneously reacting system has always a negative ΔG. Therefore, cells carry out thermodynamically unfavorable energy-requiring (endergonic) reactions, cells couple these reactions to others in order to liberate free energy (exergonic reactions); then the overall process is the sum of the free energy changes, which is negative and never reaches equilibrium [7].

Living systems, take up nutrients - release waste products - and generate work and heat, and are characterized by being in a steady state; the total entropy change can be split into two contributing parts:

$$\Delta S = \Delta S_{\text{ext}} + \Delta S_{\text{int}}$$

where ΔS_{ext} is the entropy of catabolism and ΔS_{int} is the entropy of anabolism. In open systems the energy flows from chemical energy sources (carbohydrates, proteins and lipids) to cells where these substances are metabolized to maintain the living system.

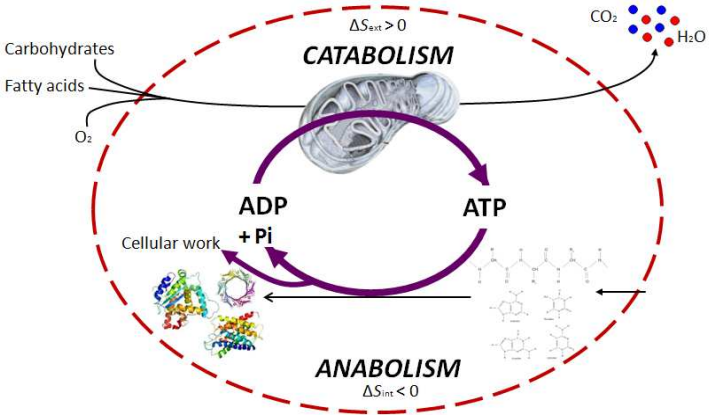

Figure 4. General scheme of cellular metabolism: exchange of matter and energy with the surrounding medium in the cell is called metabolism. The metabolism involves two general processes: catabolism (increases entropy within the surrounding medium) and anabolism (decreases the internal entropy). Both processes are coupled by reactions of cellular energetics, which are the center of cellular life.

Catabolism and anabolism coupling (metabolism) is the way through which free energy is extracted from the medium. Evolution has selected adenine nucleotides to fulfill this important task of coupling catabolism and anabolism (Fig. 4). Cellular energetics is based on synthesis and recycling reactions of ATP, ADP + P_i ↔ ATP + H_2O. Therefore, the mass action ratio of the reaction of ATP synthesis is usually expressed as:

$$\Gamma = \frac{[ATP]}{[ADP][P_i]}$$

A high mass action ratio for the reaction of ATP synthesis, supplies free energy for anabolic reactions in cellular work. The phosphorylation potential is the amount of free energy available in ATP system in cells, described as:

$$\Delta G_{ATP} = \Delta G^{\circ}_{ATP} + RT\, ln\, \frac{[ATP]}{[ADP][P_i]}$$

The energy obtained by this potential is used for several cellular processes, such as movement (contraction), ion transport and biosynthesis. We make use of molecular system bioenergetics to investigate the regulation of cardiac cells respiration and energy fluxes *in vivo*.

2.2. Energy metabolism in muscle cells.

The energy metabolism in living organisms is supported by the oxidation of substrates: carbohydrates and lipids; as well as amino acids which after deamination enter into carbohydrate oxidation pathway. The rate and efficiency of oxidative phosphorylation depend on the substrate source, carbohydrates and lipids, although both contribute to NAD^+ and FAD reduction; being the oxidative phosphorylation activity one element in the determination of the ratio of NADH to $FADH_2$ oxidation. In the heart fatty acids are the preferred fuel for mitochondrial respiration and account for 60-90% of energy production, with glucose oxidation making up 10-40% [8].

In 1948, Eugene Kennedy and Albert Lehninger discovered that mitochondria are the site of oxidative phosphorylation in eukaryotic cells. Moreover, mitochondria have an important role in thermogenesis, apoptosis, signaling, and regulation of ion homeostasis [7]. The word "Mitochondrion" comes from the Greek roots "mitos" - thread, and "chondrion" - grain or granule. It is involved in cellular ATP generation, apoptosis and necrosis processes [9].

Mitochondria have their circular own genome composed of 16-kilobase, its genome contains 37 genes essential for mitochondrial respiration function. Mammalian mitochondrial DNA (mtDNA) encodes 22 mitochondrial rRNAs, two mitochondrial tRNAs, and 13 proteins that make up parts of the oxidative phosphorylation complexes I, III, IV, and V [10].

Mitochondria are composed of compartments that carry out specialized functions:

- Mitochondrial outer membrane (MOM): encloses the entire organelle but it is freely permeable to molecules up to 5 KDa and ions due to the presence of the Voltage-Dependent Anion Channel (VDAC), being VDAC the most abundant protein and it has three isoforms in eukaryotic cells (VDAC1, VDAC2 and VDAC3)
- Intermembrane space (IMS)
- Mitochondrial inner membrane (MIM): forms internal compartments called cristae and inside of it we find the matrix. It is impermeable to most small molecules and ions, including

protons (H^+) due to the presence of cardiolipin, this establishes a proton-motive force across the MIM. The proton-motive force is generated by the complexes of the respiratory chain, also known as the electron transport chain (ETC). Moreover, it bears specific transporters which carry pyruvate, fatty acids, and amino acids or their α-keto derivatives into the matrix to follow the Krebs cycle. ADP and P_i are specifically transported into the matrix as newly synthesized ATP is transported out. It contains the respiratory electron carriers (complexes I-IV), ADP-ATP synthase (F_0F_1) or complex V, and other membrane transporters.

- Mitochondrial matrix: contains pyruvate dehydrogenase complex; citric acid cycle enzymes; fatty acid β-oxidation enzymes; amino acid oxidation enzymes; mitochondrial DNA (mtDNA), ribosomes; many other enzymes; ATP, ADP, P_i, Mg^{2+}, Ca^{2+}, K^+; and many soluble metabolic intermediates.

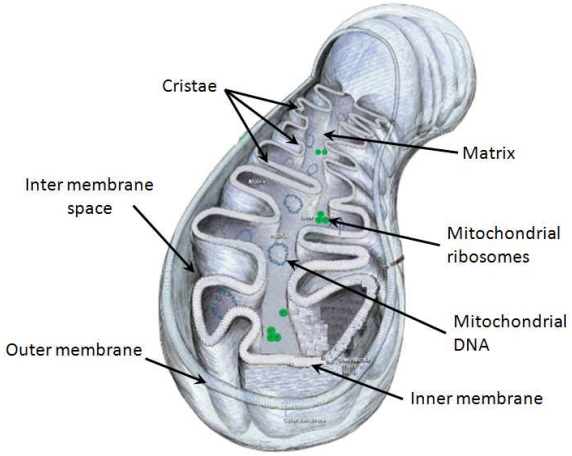

Figure 5. Mitochondrion: outer membrane, inter membrane space, inner membrane. The cristae are the internal compartments formed by the MIM. These regions expand the MIM, enhancing the ATP synthesis. The mitochondrial matrix is an aqueous solution of enzymes and intermediates of energy metabolism, mtDNA and ribosomes.

The content of mitochondria in skeletal muscles can vary from approximately 1% of cellular volume in the glycolytic muscles to up to 50% in the oxidative muscles. In adult cardiac cells, mitochondria occupy approximately 30-40% of the volume [11], whereas in neonatal cells mitochondrial volume occupies about 20% of the volume [12].

2.3. Electron transport chain (ETC)

In higher eukaryotes, the mitochondrial ETC has four major complexes. Each complex is a collection of proteins working together to produce the catalytic reducing power. The energy of electrons, liberated in a number of redox reactions, is translated into proton pumping by three large complexes (I, III and IV) [13]:

- Complex I: NADH-ubiquinone oxidoreductase, accepts electrons from NADH.
- Complex II: succinate oxidase-ubiquinone reductase, which oxidizes and accepts electrons from succinate, and reduces the ubiquinone pool.
    - Coenzyme-Q (CoQ): moves the electrons from complex I and II to complex III.
- Complex III: ubiquinol-cytochrome c oxidoreductase, which transfers electrons from ubiquinol to cytochrome *c*.
    - Cytochrome *c* (cyt *c*): moves the electrons from complex III to complex IV.
- Complex IV: cytochrome *c* oxydase, oxidizes cyt *c* and reduces molecular oxygen into water.

Thus, electron transport between complexes I to IV is coupled to extrusion of protons from the matrix though complexes I, III and IV into the IMS, creating an electrochemical gradient ($\Delta\psi$) across MIM. This movement of electrons generates an alkaline matrix and an acidic IMS. The electrochemical proton gradient, known as proton motive force (Δp) helps protons to back flow through complex V (ATP synthase complex / F_1F_0-ATPase synthase), which utilizes the energy to drive phosphorylation of ADP to ATP.

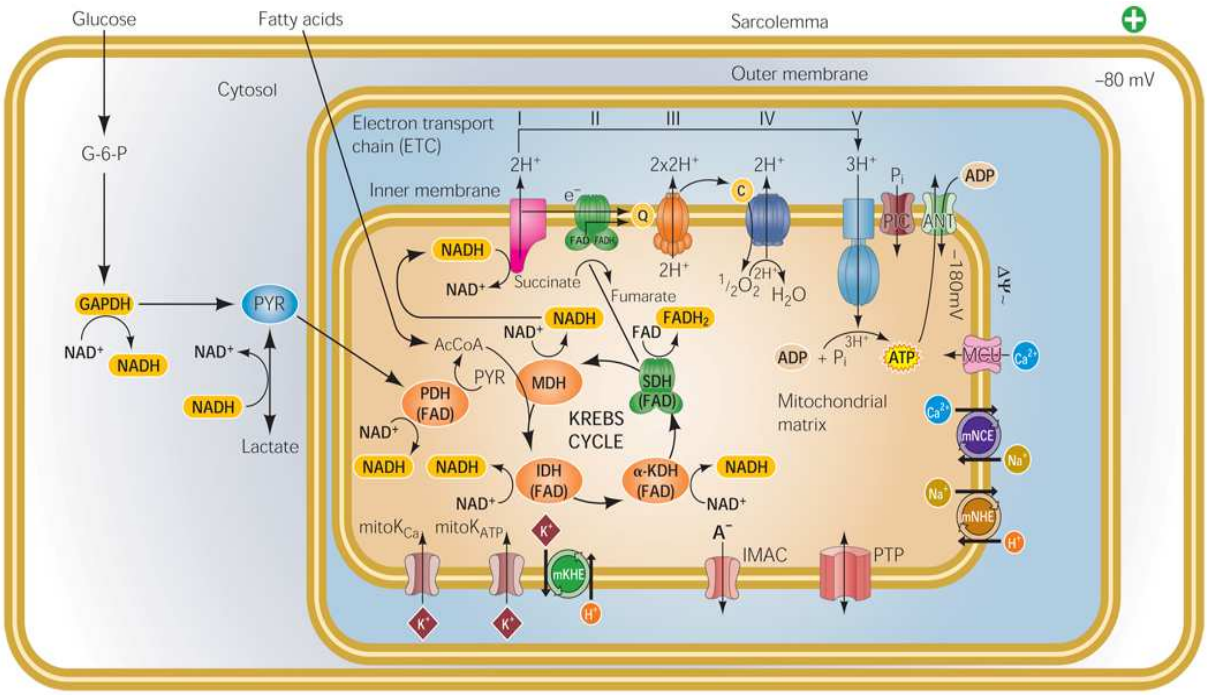

Figure 6. Oxidative phosphorylation in cardiac cells: the sequential oxidation of fuel (e.g. fatty acids and glucose) leads to the common substrate for the Krebs cycle, aceyl-CoA, which drives the production of the reducing equivalents NADH and $FADH_2$. Electrons are passed to the ETC, where coupled redox reactions mediate proton translocation across MIM to establish an electrical potential and pH gradient (Δp) that drives ATP synthesis by the mitochondrial ATP synthase. Ion-selective or nonselective mitochondrial channels dissipate energy and alter the ionc balance and volume of the mitochondrial matrix, which is patly compensated by antiporters coupled to H^+ movement.

Adenine nucleotide translocase (ANT), glucose-6-phosphate (G-6-P), inner-membrane anion channel (IMAC), mitochondrial Ca^{2+} uniporter (MCU), mitochondrial Ca^{2+}-activated K^+ channel ($mitoK_{Ca}$), mitochondrial ATP-sensitiveK^+ channel ($mitoK_{ATP}$), phosphate carrier (PIC), permeability transition pore (PTP), pyruvate (PYR), K^+/H^+ exchanger (KHE), Na^+H^+ exchanger (NHE), isocitrate dehydrogenase (IDH), α-ketoglutarate dehydrogenase (KDH), malate dehydrogenase (MDH), pyruvate dehydrogenase (PDH), succinate dehydrogenase (SDH). Taken from [14] with permission.

Complex I is a large enzyme, which contains a prosthetic flavinmononucleotide (FMN)-containing flavoprotein and six sulfur centers. It has an L-shape, one arm of the L being in the membrane and the other extending into the matrix. Complex I catalyzes two simultaneous and obligated coupled processes: the exergonic transfer to ubiquinone of a hydride ion from NADH and a proton from the matrix:

$NADH + H^+ + Q \rightarrow NAD^+ + QH_2$

and the endergonic transfer of four protons from the matrix to the IMS.

Complex II is a membrane-bound enzyme in the Krebs cycle, it contains flavin adenine dinucleotide (FAD) prosthetic groups and Fe-S centers. Complex II catalyzes the transfer of electrons from succinate via FAD and Fe-S centers to ubiquinone. The β-oxidation of fatty acids involves transfer of electrons from the substrate to the FAD of the dehydrogenase, and then to electron-transferring flavoprotein (ETF), which in turn passes its electrons to ETF:ubiquinone oxidoreductase. The effect of each of these electron-transferring enzymes is to contribute to the pool of reduced ubiquinone. Ubiquinol (QH_2) diffuses in the MIM, to be reoxidized by Complex III.

Complex III is a homodimer. Each dimer has with 11 different subunits and their functional core consist of: cytochrome *b* with two heme, the Rieske iron-sulfur protein with 2Fe-2S centers, and cytochrome c_1 with its heme. Complex III couples the transfer of electrons from QH_2 to cytochrome *c* with the transport of protons from the matrix to the IMS. The net equation of the Q cycle is

$QH_2 + 2\text{cyt } c_1 \text{ (oxidized)} + 2H^+_N \rightarrow Q + 2 \text{ cyt } c_1 \text{ (reduced)} + 4H^+_P$

Complex IV has 13 subunits and carries electrons from cytochrome *c* to molecular oxygen, reducing it to H_2O.

$4 \text{ Cytc (reduced)} + 8H^+_N + O_2 \rightarrow 4 \text{ cyt c (oxidized)} + 4H^+_N + 2H_2O$

The four-electron reduction of O_2 involves redox centers and occurs without the release of incompletely reduced intermediates (hydrogen peroxide or hydroxyl fee radical) that would damage cellular components.

Along the ETC/RC the redox potential increases gradually. The energy stored in the electrochemical potential of protons ($\Delta\mu_{H+}$) has two components: the chemical potential (ΔpH) energy and the mitochondrial electrical potential energy ($\Delta\psi_m$) [14]:

$$\Delta\mu_{H+} = 2.3RT * \Delta pH + \mathscr{F}\Delta\psi$$

The electrochemical energy inherent to the proton-motive force drives the synthesis of ATP as protons flow passively back into the matrix through ATP synthase. This is the chemiosmotic model proposed by Peter Mitchell:

$$\Delta p = \frac{\Delta \mu_{H+}}{\mathscr{F}} = \frac{2.3\ RT}{\mathscr{F}} * \Delta pH + \Delta \psi$$

The efficiency of oxidative phosphorylation is defined by the amount of inorganic phosphate incorporated into ATP per amount of molecule of oxygen consumed.

Pyruvate and acyl-CoA obtained by glycolysis and fatty acid oxidation, respectively, are transported across the mitochondrial membrane and oxidized in the mitochondrial matrix. Pyruvate transport is affected by the difference in pH through MIM, with mitochondrial NADH:NAD^+ ratio playing a key role in the control of β-oxidation.

2.4. ATP synthase

The ATP synthase (F_1F_o) is a large complex of the MIM that catalyzes the formation of ATP from ADP and P_i, accompanied by the flow of protons from the IMS to the matrix. The mitochondrial F_1 has nine subunits of five different types, with the composition $\alpha_3\beta_3\gamma\delta\varepsilon$. Each of the three β subunits has one catalytic site for ATP synthesis. The conformational difference among β subunits extend to differences in their ATP/ADP-binding sites (β-ATP, β-ADP and β-empty). The F_o complex that makes up the proton pore is composed of three subunits $ab_2c_{10\text{-}12}$.

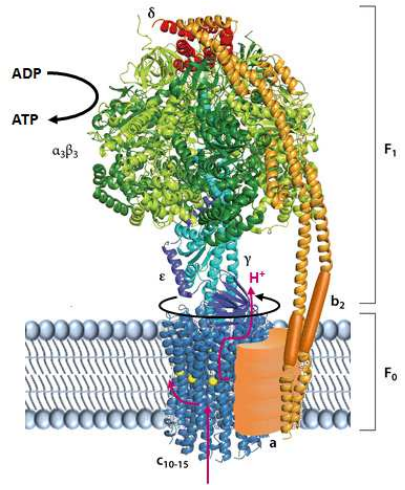

Figure 7. Mitochondrial ATP synthase: F_1 is peripherial domain, consisting of three α subunits and three β subunits, one δ, and a central shaft (the γ subunit). F_o is the integral portion has multiple copies of c, one a and two b subunits. F_o provides a transmembrane channel through which about four protons are pumped (pink arrows) for each ATP hydrolyzed on the β subunits of F_1. Its mechanism involves the rotation of F_o relative to F_1 (black arrow). Reprinted from [15] with permission.

The movement of protons (H^+) causes the rotation of the central shaft (γ subunit), which comes into contact with each αβ subunit pair in succession. This produces a cooperative conformational change in which the β-ATP site is converted to the β-empty conformation, and ATP dissociates; the β-ADP site is converted to the β-ATP conformation, which promotes condensation of bound ADP + P_i to form ATP; and the β-empty site becomes a β-ADP site , which loosely binds ADP + P_i, entering from the solvent.

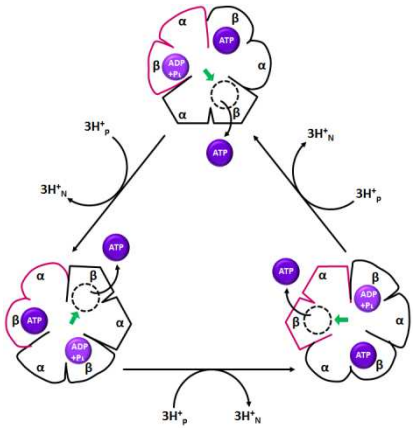

Figure 8. Mechanism of ATP synthase: the F_1 complex has three nonequivalent adenine nucleotide-binding sites, one for each pair of α and β subunits. One of these sites is in the β-ATP conformation (which binds ATP tightly), a second is in the β-ADP (loose-binding) conformation, and a third is in the β-empty (very-loose-binding). The proton-motive force causes rotation of the central shaft (the γ subunit -green arrow-) which comes into contact with each αβ subunit pair in succession. This produces a cooperative conformational change in which the β-ATP site is converted to the β-empty conformation, and ATP dissociates; the β-ADP site is converted to the β-ATP conformation, which promotes condensation of bound ADP + P_i to form ATP; and the β-empty site becomes a β-ADP site, which loosely binds ADP + P_i entering from the solvent. ATP cannot be released from one site unless and until ADP and P_i are bound at the other. Redrawn from [7].

Proposed by Paul Boyer, the rotational catalysis mechanism in which the three active sites of F_1 take turns catalyzing ATP synthesis. The conformational changes central to this mechanism are driven by the passage of protons through the F_o portion of ATP synthase.

2.5. Adenine nucleotide transporter.

The adenine nucleotide transporter (ANT) is an antiporter that moves ATP^{4-} out of the mitochondria for every ADP^{3-} moved in. Its activity is favored by the transmembrane electrochemical gradient, which gives the matrix a net negative charge; the proton movement drives ATP-ADP exchange [7]. Thus, the ATP synthesized inside of the mitochondrion through the oxidative phosphorylation is pumped out of the matrix into the cytosol, while ADP and P_i are moved in the opposite direction (*i.e*. from the cytosol to the matrix) [16].

Therefore, the electrochemical proton gradient across the MIM is used to drive the formation of ATP and the transport of metabolites across the membrane. The ATP pool is therefore used to drive cellular processes (*i.e*. contraction). The ANT adjusts ATP supply and the phosphorylation potential of ATP in accordance with cytosolic requirements.

Previous studies [17] have shown a direct cooperation of ATP synthase and ANT, such that entering ADP is handed over directly to the ATP synthase and released as ATP into the endogenous pool. Thereby, it has been proposed [18-21] that a functional micro-compartmentation must be viewed on the background of the physical organization of the IMS and the inner membrane into two sections: the inner cristae membrane surrounding and inner boundary membrane facing the outer membrane, provided by small tubular structures.

Oxidative phosphorylation rate is regulated by the ADP availability to ANT, and the affinity of ANT for ADP is very high with an apparent K_m(ADP) between 5 and 20 μM even in presence of ATP at physiological concentration (3-5 mM) [22].

3. MUSCLE CELL AND FUNCTIONING

3.1. Contractile module

The contractile machinery of striated muscles -skeletal and cardiac muscle (the myocytes)- is composed of sarcomeric units, which are joined into highly ordered myofibril structures [23]. Sarcomeres are comprised of thin (*i.e*. actin, tropomyosin -Tm- and troponin -Tn-) and thick (*i.e*. myosin) filaments and titin filaments highly ordered the I-band and A-band.

Contraction occurs when myosin heads of the thick filament attach to and exert force on actin molecules in the thin filament. This force causes the thin filament to slide over the thick filament, shortening the sarcomere and contracting the muscle fiber. Ca^{2+} binding to troponin (Tn) on the thin filament initiates the force-generating interaction of myosin and actin, and ATP hydrolysis provides the energy for the molecular changes that drive force generation and muscle shortening. Ca^{2+} regulation is mediated through changes in the thin filament, though modulation can occur through myosin [24].

The arrangement of thick and thin filaments originates the A and I bands. The I band contains the thin filaments and the A band stretches the length of the thick filaments and includes the region where parallel thick and thin filaments overlap. Furthermore, the actin filaments in the I band are limited by the Z lines in a very regular pattern, and the M line is found in the A band [7].

The titin proteins extend from the Z line to the M line, regulating the length of the sarcomere and preventing overextension of the muscle. It provides a third level of filaments organization and is responsible for the resting elasticity muscle. Titin contains multiple α-actinin binding sites on differentially spliced Z repeats, which tightly correlates to the number of α-actinin molecules and hence to Z line thickness. Slow oxidative muscles (*e.g.* soleus) have more Z lines than fast glycolytic muscles (*e.g.* extensor digitorum longus) [25]. Moreover, skeletal and cardiac muscles contain different titin isoforms that depend on the physiological demands of fibers type [26].

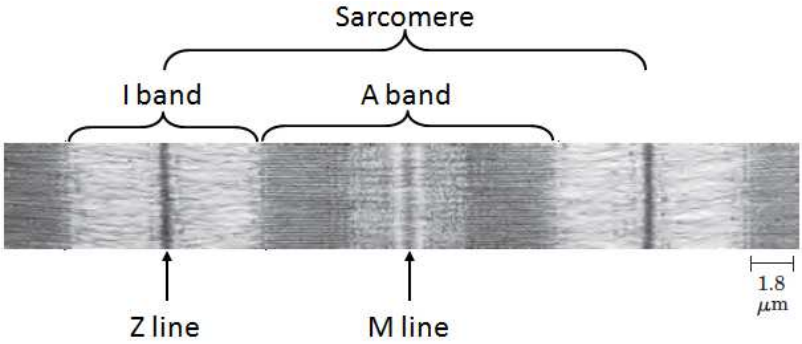

Figure 9. Electron microscopy of the myofibril organization: the sarcomere consists of thick filaments interleaved at either end with thin filaments. This electron micrograph shows the relaxed state of the muscle, I band, A band, Z line and M line. Taken from [7].

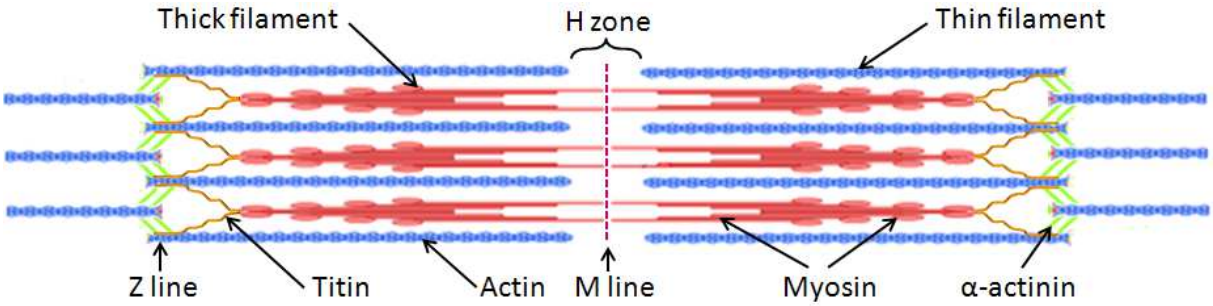

Figure 10. Major components of the thin and thick filaments in the myofibril: thick filament is composed of myosin and titin. Thin filaments consist of actin and tropomyosin. The Z line contains α-actinin. It also shows the M line and H zone.

Skeletal muscles consist of parallel bundles of muscle fibers which fuse together and often span the length of the muscle. Each fiber is made up of a single, very large, multinucleated cell with a diameter of 20-100 μm. In contrast, cardiac myofibers are composed of a series of cardiomyocytes that are joined together end-to-end by intercalated disks to form a functional syncitium. Cardiomyocytes' contractile apparatus consists of thin actin filaments and thick myosin filaments [8], when a contraction occurs actin and myosin are combined in the presence of ATP to produce the complex actomyosin [27].

Cardiac Z lines are considerably thicker due to more α-actinin cross-links, and consequently the lateral mechanical strength of cardiac myofibrils is 2-10 times higher than skeletal myofibrils in both the relaxed and the rigor state [28]. Meanwhile, titin protein is responsible for the increased tension of cardiac muscle related to an increase in the ventricular volume through modulation of the lattice

spacing between the filaments. In addition, it sets the slack length of cardiac myocytes on the ascending limb of the length-tension curve; this allows the heart to adapt to increased filling with a stronger contraction, a phenomenon called the Frank-Starling law [26].

3.2. Excitation-contraction coupling.

In striated muscle cells, myosin and actin are specialized to transform the chemical energy of ATP into motion. The binding and subsequent hydrolysis of ATP provides the energy that forces cyclic changes in the conformation of the myosin head. Actin-myosin interaction and ATP-hydrolysis are regulated by chemomechanical cross-bridge cycles, in skeletal and cardiac muscle. The contractile properties differ across types of muscle. Moreover, Ca^{2+} activation is needed for muscle contraction.

Biochemical and structural studies suggest the existence of three states of the thin filament which are in dynamic equilibrium [29]:

- Open conformation: myosin can strongly bind to actin.
- Closed state: where cross-bridges can weakly bind to actin.
- Blocked state: in the absence of Ca^{2+}, Tm "blocks" cross-bridge access to thin filament strong binding sites.

The force exerted by the muscle in the isometric state depends on the number of strongly attached cross-bridges and the force developed by each cross-bridge. This depends on the number of actin binding sites open for strong myosin binding.

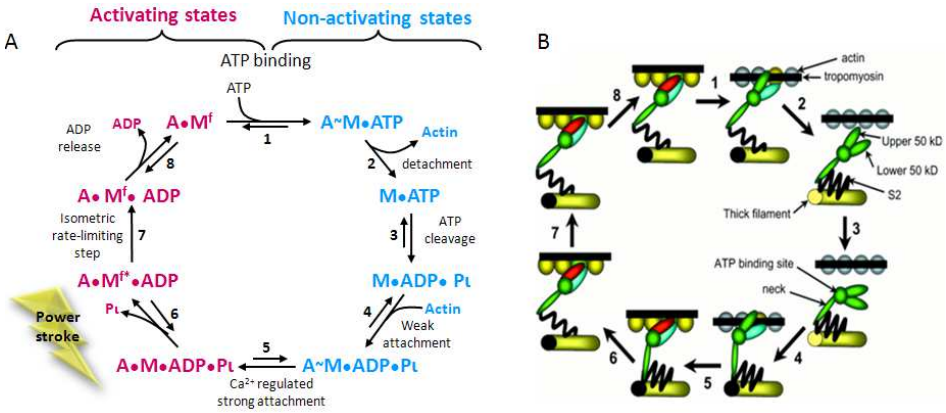

Figure 11. Mechanism of the cross-bridge cycle: formation of actin-myosin cross-bridges (AM) in terms of various reagents and products (A) and the corresponding structural changes (B).

Figure 11 A: actin; M: myosin; Pι: inorganic phosphate; f: cross-bridge exerting force; "•" is a strong connection; "~" is weak connection. Reprinted from [24] with permission.

ATP binding to myosin (step 1) is rapid and irreversible. The subsequent detachment of actin from the A~M·ATP complex (step 2) is similarly rapid and is caused by an opening between myosin's upper and lower regions like the "opening of jaws". Bending of myosin neck region accompanies step 3, the hydrolytic cleavage of ATP. Following ATP cleavage, myosin again bind weakly to actin at a high rate, but in the absence of Ca^{2+} Tm sterically blocks access of the myosin head to strong binding sites on actin. In step 5, Ca^{2+} is bound to TnC, Tnl detaches from actin, allowing the Tm/Tn complex to slide over the thin filament surface. This exposes weak binding sites on actin and transiently exposes strong binding sites on actin for binding to the complementary regions in myosin's domain. The greater the $[Ca^{2+}]$, the greater the fraction of time the Tm/Tn complex allows myosin access to strong binding sites on actin. Consequently, the rate of strong cross-bridge attachment, the flux through step 5, is dependent on $[Ca^{2+}]$ and Tm position. Strong binding of myosin to actin (Fig. B) is associated with movement of "closing the jaws". This movement may allow the neck region of myosin to extend, opening a pathway for inorganic phosphate release from the ATP binding pocket in myosin. Alternatively, closing the jaws might promote Pι release from the binding pocket, which then allows the extension of myosin's neck region. Step 6 involves myosin neck extension, which is the power stroke that in isometric muscle, stenches an elastic element (represented as S2) by some 10nm and produces a force of ~2pN/cross-bridge. In nonisometric conditions, shortening of the neck extension causes the thick and thin filaments to slide past each other. Step 7 is an irreversible isomerization and is strain sensitive. Finally, ADP is released from $A{\cdot}M^f{\cdot}ADP$ in the reversible step 8 to form the rigor state $A{\cdot}M^f$. cross-bridges attach and exert force constantly during steps 7, 8 and 1 during isometric contraction, and force drops to zero when the cross-bridges detach in step 2. During shortening contractions the filaments slide past each other, the strain on the cross-bridge is reduced,

and step 7 occurs more rapidly. This chemomechanical mechanism implies that during an isometric contraction, a cross-bridge remains strongly attached for a relatively long time (>100 ms/cycle). Strongly bound cross-bridges prevent Tm/Tn from returning to its blocked or closed position, maintaining the thin filament in a “switched on” position (Fig. B). In the absence of Ca^{2+}, cross-bridge detachment at the end of the cycle allows Tm/Tn to cover the strong myosin binding sites on actin and deactivate the thin filament (Fig. A).

Differentiation and maturation of adult mammalian muscle cells lead to specialization, allowing different muscle types to have highly variable contractile abilities. In adult muscle cells, subcellular functions are specifically localized within structural and functional compartments: energy consuming processes take place in the SR and myofibrillar compartments, whereas depending on muscle type, energy production occurs mainly within mitochondria or glycolytic complexes [30].

Experimental studies in muscle cell energetics by Nabuurs [31] showed that ATP and ADP in muscles are bound to macromolecules and that these results in a non-equilibrium state of the creatine kinase (CK) reaction. These data contribute to the explanation of the cellular mechanisms of ATP compartmentation [32]. The energy metabolism of muscle cells, including heart, the compartmentation of adenine nucleotides in the cells is closely related to the CK system role [33]. Diffusion restrictions result in compartmentation of adenine nucleotides, which may explain the need for energy transfer and metabolic signaling networks [22].

In addition, MgADP is an efficient competitive inhibitor of ATPases. Thus, MgADP accumulation in the vicinity of any ATPases slows down the contraction cycle and impairs the Frank-Starling mechanism. Consequently, intracellular energy and metabolic signaling phosphotransfer networks within a cellular structural organization have the potential to protect cells from the excess of cytosolic free Ca^{2+} and ADP, and regulate respiratory ATP production in close correspondence to ATP consumption.

4. INTEGRATED ENERGY METABOLISM

4.1. Intracellular diffusion and compartmentation phenomenon.

Dense cytoskeleton, sarcoplasmic reticulum (SR), myofibrillar networks and macromolecular traffic result in the presence of physical barriers. Therefore, the cell metabolism is organized in: micro- and macrocompartments, metabolic channeling and functional coupling [34]. Compartmentation refers to the heterogeneity of intracellular diffusion, inasmuch as diffusion of metabolites in an organized intracellular media showing a clear restriction. Local diffusion restrictions are microcompartmentation of metabolites and their channeling within organized multi-enzyme complexes [32].

For many decades, several models have been developed to explain these diffusion restrictions in cells originated by the specific organization of intracellular structures that causes heterogeneity of diffusion, metabolite compartmentation and metabolic channeling [35].

Because of cytoskeletal structures and macromolecular crowding (high concentration of macromolecules) in cells, there is a decrease in the available volume for free diffusion substrates. The mitochondrial matrix is much more viscous than the cytoplasm. In mitochondria more than 60% of the matrix volume is constituted by the high density of enzymes and other proteins [32].

The term of apparent diffusion coefficient used for the analysis of ADP and ATP diffusion is expressed as: $D^{app} = D_{Fx}D_0$; where D_0 is the diffusion coefficient in the bulk water phase, and D_{Fx} is a diffusion factor accounting for all intracellular mechanism locally restricting the particles movement [36-38]. The phenomenon of diffusion restriction studied by Ridgway [39] showed that the apparent coefficient might be decreased by an order of magnitude depending upon the size of the diffusing particles and occupied volume fraction.

Mathematical modeling of permeabilized cardiomyocytes, with a decreased affinity of mitochondria for exogenous ADP *in situ*, showed that ADP or ATP diffusion in cells is heterogeneous. Also, the apparent diffusion coefficient for ADP and ATP may be locally decreased by several orders of

magnitude [38]. Experimental evidence has shown the existence of distinct ATP pools in mitochondria, and how ATP utilization sites are connected by phosphotransfer networks, notably via Phosphocreatine-Creatine kinase pathway [35, 37].

Phosphotransfer networks function as a bypass and overcome the local restrictions of ATP or ADP diffusion, and hence perform the important task of energy supply and metabolic feedback regulation of respiration [32].

In the heart, the intracellular energy transfer networks are structurally organized. Macromolecules and organelles, surrounding a regular mitochondrial lattice, are involved in multiple structural and functional interactions.

5. ORGANIZATION OF MITOCHONDRIA IN CARDIAC CELLS

5.1. Mitochondrial functioning in cardiac myocytes.

Cells are open systems that operate far from thermodynamic equilibrium while exchanging energy and matter with the external environment. These structurally and functionally organized metabolic systems may be described as cellular metabolic dissipative structures. They have functional enzymatic associations that form a catalytic entity as a whole and carry out their activities relatively independent [40].

The structural and functional unit of striated cardiac muscle cells consisting of distinct mitochondria localized at the level of sarcomeres between z-lines and interacting with surrounding myofibrils, SR, cytoskeleton, and cytoplasmic enzymes, is referred to as intracellular energetic units (ICEUs) [40]. These complexes have specialized metabolic regulatory pathways of energy transfer and feedback, mediated by creatine kinase (CK) and adenylate kinase (AK). The ICEUs are metabolic dissipative structures that help to extract Gibbs free energy and negentropy from the environment [41].

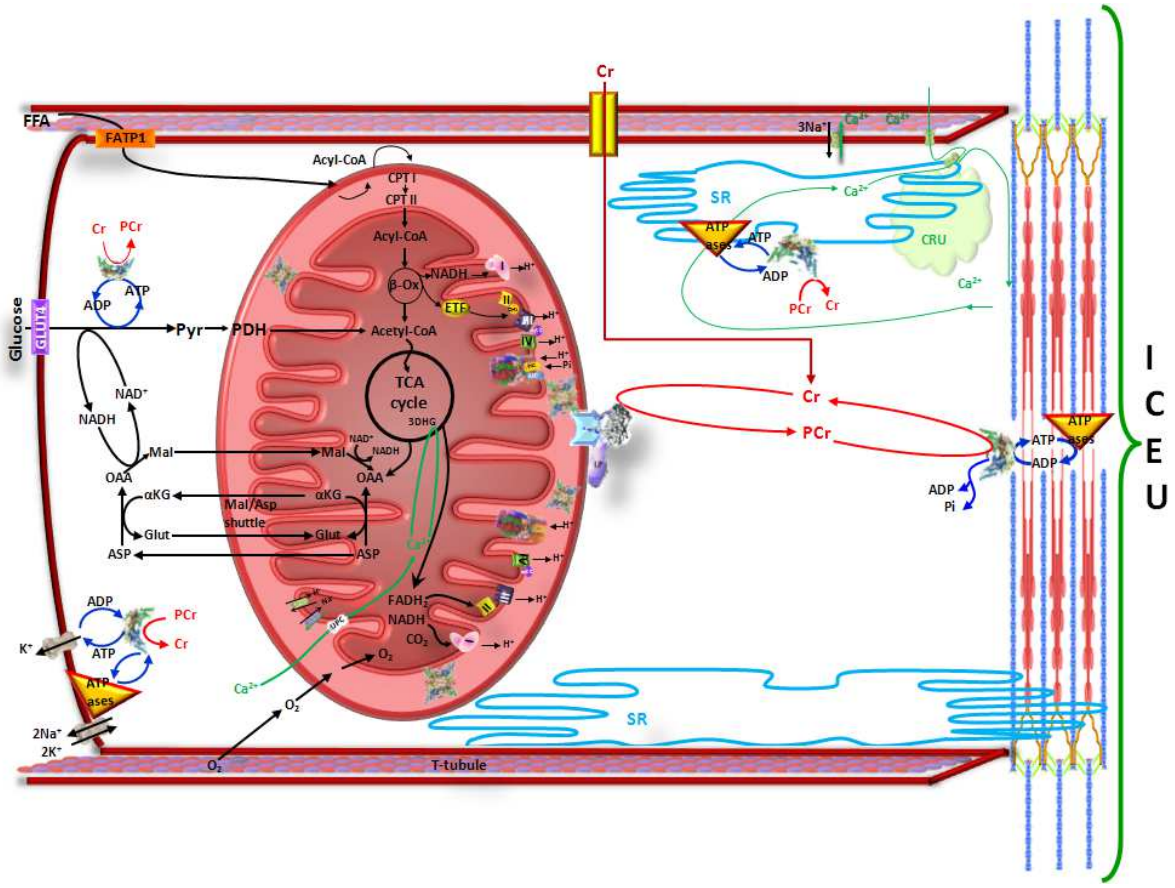

Figure 12. Intracellular Energy Unit (ICEU): structural organization of the energy transfer networks of coupled CK and AK reactions within an ICEU. By the interaction with cytoskeletal elements, mitochondrial and sarcoplasmic reticulum are precisely fixed in respect to the structure of the sarcomere of myofibrils between two Z lines and correspondingly between two t-tubules. Redrawn with permission [40].

The free fatty acids (FFA) are introduced in the cell by a family of plasma membrane proteins. Once in the ICEUs FFA are esterified to acyl-CoA. Acyl-CoAs enter in the β-fatty acids oxidation (β-FAO) pathway, producing acetyl-CoA. The electron-transferring flavoprotein (ETF)-ubiquinon oxidoreductase delivers the electrons produced by the β-FAO directly to the complex III of the respiratory chain (RC). The NADH produced by β-FAO is oxidized in the complex I of the RC, passing two electrons and two protons along. This contributes to the polarization of MIM.

In addition, the glucose is taken up by the glucose transporter-4 (GLUT-4) and oxidized. This oxidation produces pyruvate. Pyruvate dehydrogenase (PDH) complex catalyzes pyruvate into acetyl-CoA. The NADH redox potential from glycolysis enters into the mitochondrial matrix via the malate-

aspartate shuttle. Malate generated in the cytosol enters the matrix in exchange for α-ketoglutarate (αKG) and can be used to produce matrix NADH.

Matrix oxaloacetate returns to the cytosol by conversion to aspartate and glutamate exchange. Acetyl-CoA is oxidized to CO_2 in the tricarboxylic acids (TCA) cycle, generating NADH and $FADH_2$. Both, NADH and $FADH_2$ are further oxidized in the RC (complex I, II) with the final ATP synthesis. The glycolysis rate is decreased by G6P inhibition of HK.

The mitochondrial interactosome (MI) supercomplex that transfers energy from mitochondria to cytoplasm is composed of ATP synthase, ANT, phosphate carriers (PiC), MtCK and VDAC with bound cytoskeletal proteins. MtCK is responsible of creatine phosphorylation, producing phosphocreatine (PCr). PCr is used to regenerate local ATP by CK and ATPases (actomyosin ATPase, sarcoplasmic reticulum SERCA and ion pumps ATPases). The re-phosphorylation of ADP in MMCK reaction increases the Cr/PCr ratio, which is transferred towards MtCK via CK/PCr shuttle. Calcium released from local intracellular stores during excitation-contraction coupling through calcium-induced calcium release mechanism, 1) activates the contraction cycle by binding to troponin C in the troponin-tropomyosin complex of thin filaments and 2) enters the mitochondria mainly via the mitochondrial Ca^{2+} uniporter to activate Krebs cycle dehydrogenases: PDH, αKG, IDH.

Previous studies with electron microscopy and confirmed by confocal microscopy have shown that cardiac cells have a very regular arrangement of mitochondria, crystal-like, at the level of A-band of sarcomeres in myofibrils surrounded by the sarcoplasmic reticulum[42].

One component of the ICEUs is the MI, which is used to designate the complex make-up of:

- ATP synthasome: including ATP synthase, adenine nucleotide carrier (ANC) and inorganic phosphate carrier (PiC)
- Mitochondrial creatine kinase (MtCK),
- Voltage dependent anion channel (VDAC)

- Regulatory cytoskeletal proteins (such as tubulins and/or linker proteins (LP)).

The role of the MI is to regulate the mitochondrial adenine nucleotide flux and the cytoplasmatic Cr/PCr cycles in the IMS of the heart, skeletal muscle and brain cells. In addition, the MI strongly increases the efficiency of functional coupling between MtCK and the ATP synthasome [40]. The central mechanisms of energy transfer compartmentalization, is the functional coupling between the mitochondrial ATP/ADP translocase (ANT) and the mitochondrial creatine kinase (MtCK).

In addition, the MI functions in the non-equilibrium state caused by the dissipative enzymatic sub-networks (glycolysis, Krebs cycle, fatty acid oxidation, electrons transport chain, shuttles of creatine kinase/ phosphocreatine, malate/aspartate, etc.), structured and connected together by flows and regulating signals.

Therefore, the functional and structural role of MI is to increase the efficiency of the oxidative ATP synthesis and peripheral ATP hydrolysis, avoiding the waste of energy and fulfilling energy requirements. These can be achieved on one side by the ATP/ADP intramitochondrial circuit between ATP synthase and MtCK, through their functional coupling via ANT, and also by the Cr/PCr circuit through the different CK isotypes.

Creatine kinase (CK) has five different isotypes, three of which are cytosolic (dimeric) and two of which are mitochondrial (octameric): BCK, MCK, MB-CK, ubiquitous MtCK and sarcomeric MtCK, respectively [43]. The compartmentalized CK isotypes network is the main ICEUs phosphor-transfer circuit. MtCK was discovered in 1964 by Klingenberg's lab. It is bound to the outer surface of the MIM through electrostatic interactions involving positive charges of lysine residues and negative charges from cardiolipin which is also associated with the ANT. The ADP formed at the active site of MtCK is transferred into IMS. Then ADP may either return to the matrix via ANT or leave the mitochondria via VDAC.

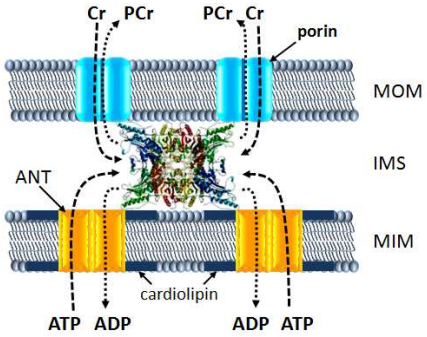

Figure 13. Mitochondrial creatine kinase functioning for high-energy metabolite channeling: ATP synthesis and ATP export through the MIM via ANT are tightly coupled to transphosphorylation of ATP to PCr by MtCK. PCr is exported into the cytosol by the outer membrane porin. Octameric MtCK binds to cardiolipin at the MIM. Redrawn from [44].

VDAC is the most abundant protein in MOM and is known to be primarily responsible for metabolites flux across the outer membrane [45]. VDAC is a monomeric β-barrel protein of 32 KDa and 2.5-3 nm-diameter. Three isoforms have been characterized in mammals: VDAC1, VDAC2 and VDAC3. VDAC has the ability to adopt fully open state and multiple states with smaller conductance, i.e. the "close states" that are impermeable to ATP but still permeable to small ions, including Ca^{2+} [46]. These conformational states are also influenced by the transmembrane voltage. Due to its limited permeability, VDAC and the entire MOM create a dynamic micro-compartmentation of metabolites in the IMS that contributes to MtCK-linked channeling and separate mitochondrial ATP and ADP pools [22].

Rostovtseva et al. [46] showed the role of tubulin as a possible regulator of VDAC. They demonstrated the functional interaction between the dimeric tubulin and VDAC. Cytosolic heterodimeric tubulins (αβ-tubulin) are in a dynamic equilibrium with the microtubular network. Furthermore, they proposed a model for tubulin-VDAC interaction, where the C-terminal tail (CTT) penetrates into the channel lumen potentially reaching though the channel. Because of the length of the CTT, tubulin interacts with the positively charged domain of VDAC. Besides regulating VDAC permeability, the apparent affinity of oxidative phosphorylation for cytoplasmic ADP can be modified by tubulin [47].

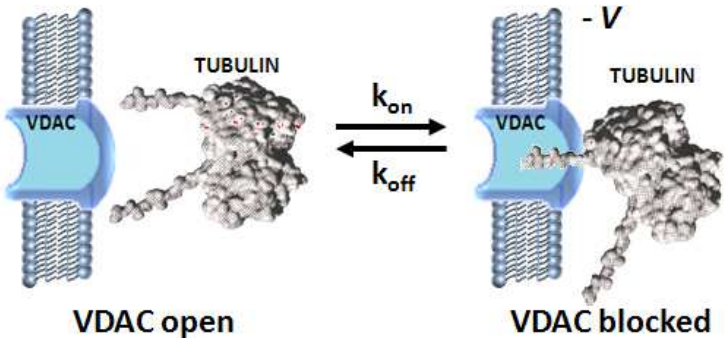

Figure 14. Possible regulation of VDAC by tubulin: One tubulin CTT partially blocks channel conductance by entering VDAC pore. Redrawn from [46].

The selective permeability of VDAC to ATP/ADP and Cr/PCr has an important influence over the control of respiration rate and energy fluxes displayed by the different components of the MI.

Experimental data showed that tubulin binding to VDAC restricts significantly the availability of ADP to oxidative phosphorylation. In isolated heart mitochondria, the low apparent KmADP increased from 10-20µM up to 169±52µM by the addition of 1µM of dimeric αβ-tubulin [46]. Hence, the VDAC-tubulin interaction participates in the regulation of mitochondrial functioning via the modulation of mitochondrial compartmentation of adenine nucleotides [44].

Accordingly, the structural organization of ICEUs results in local confinement of adenine nucleotides and Cr-PCr coupling in discrete dynamic energetic circuits between actomyosin ATPases and mitochondrial ATPsynthases. Mitochondrial respiration and ADP kinetics are effectively modulated by all these mitochondrial interactions with cytoskeletal elements [36].

ICEU functioning is based on the regulation of mitochondrial ATP synthesis by intracellular energy consuming processes. It adjusts energy extraction from nutrients, to energy used to perform cellular work.

5.2. Mitochondria and cytoskeletal interactions

The cardiomyocyte cytoskeleton is composed of rigid and elastic elements. It maintains the shape of the cell as an elongated cylinder with an elliptical cross-section, even during contraction-relaxation cycles. Proteins of the cardiomyocyte have been categorized into five different families:

- Contractile proteins: functional structural proteins, *i.e*. myosin, actin, tropomyosin and the troponins.
- Proteins which contribute to cell shape, mechanical resistance, signal transduction and morphological integrity: subdivided into their structural and functional properties
    - Sarcomeric skeleton: titin, myosin, binding protein C, α-actinin, myomesin, and M-protein.
    - True 'cytoskeletal' proteins: tubulin, desmin and actin.
    - Membrane-associated proteins: dystrophin, spectrin, talin, vinculin, ankyrin.
    - Proteins of the intercalated disc: desmosomes consisting of desmoplakin, desmocollin, desmoglein and desmin; adherens junctions with N-cadherin, the catenins and vinculin, and gap junctions with connexin [48].

The major constituent of microfilaments is actin. The microtubules are essentially composed of tubulin, and their assembly and function are regulated by microtubule associated proteins, such as the microtubule associated motors (kinesin, dynein, etc.) and the structurally associated proteins (tau, Microtuble Associated Protein MAPs). Both tubulin and actin exist in equilibrium between polymerized and depolymerised states [49]. Intermediate filaments, which are rather stable, are constituted by desmin and plectin.

The regular arrangement of mitochondria in cardiac cells is mediated by their association with three major cytoskeletal structures: microfilaments, microtubules (MT) and intermediate filaments. The microtubular network, intermediate filaments and microfilaments form specific structures which are vital during the contraction cycle and for the regulation of energy supply [40].

VDAC is not only the most abundant protein in MOM, but also one important element regulating substrates exchange between cytosol and mitochondria. It is known to be primarily responsible for ATP/ADP fluxes across the outer membrane. Previous studies have demonstrated that VDAC's closed states, impermeable to ATP, are still permeable to small ions including Ca^{2+}.

Several studies have shown that the cell's permeability depends on its preparation, meaning that a low permeability of the MOM (and hence VDAC) for ADP may be the result of the interaction of mitochondria with some cytoskeletal proteins. Therefore, high values of apparent K_m for ADP in permeabilized cells are related to decreased permeability of MOM, by the interaction with cytosolic proteins, such as tubulin [50].

5.3. Tubulins

Tubulin, the subunit protein MT, is an acidic heterodimer, composed of similar 50 kDa globular α and β subunits. Each subunit possess a strongly anionic, extended CTT of ~15 amino acids that represents (α=10, β=20) ~3% of the subunit mass and ~40% of the subunit charge. It binds to guanine nucleotides and polymerize into MT in a GTP-dependent manner. Tubulin is an abundant and stable protein, present in many cells.

The native structures of α- and β-tubulin consist of three domains: 2 globular domains comprising >90% of the protein, and an unstructured CTT. The globular domains consist of an N-terminal domain that binds GTP or GDP and represents about ½ of the protein, and a slightly smaller C-terminal globular domain to which the unstructured tail is grafted. These proteins have binding regions that facilitate longitudinal assembly of the protein into filaments consisting of heat-to-tail, single file alignments of the subunit protein. Moreover, additional binding sites allow the filaments to join together laterally to form sheets of filaments or closed cylinders of filaments called protofilaments [51].

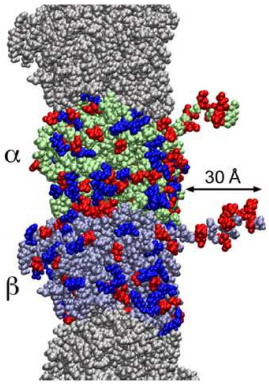

Figure 15. Tubulin dimer with C-terminal tails: a single dimer is highlighted, with non-charged residues colored in light green for α, and steel blue for β. Anionic (acidic) residues (Glu, Asp) are colored red and cationic (basic) residues (Lys, Arg) are colored blue. The C-terminal tails are shown on both subunits. Taken with permission from [51].

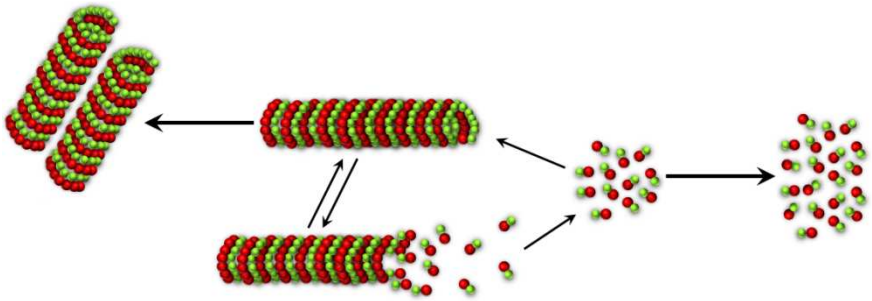

Figure 16. Tubulin portioning between dimers and polymers: in the nature tubulin can be present as a polymer (MT) or as dimers. GTP-tubulins are present as dimers. GDP-tubulins within MTs.

Tubulin sequence reveals a highly conserved polypeptide framework. Meanwhile, the CTT constitutes a major variable region domain for β-tubulin, and in a lesser extend for α-tubulin as well [52].

Isotype name (alternative name)	COOH-Terminal sequence
α1 A (α1)	^{401}KRAFVHWYVGEGMEEGEFSEAREDMAALE**K**DYEEVGVDSVEGEGEEEGEEY^{451}
α1 B (α2)	^{401}KRAFVHWYVGEGMEEGEFSEAREDMAALE**K**DYEEVGVDSVEGEGEEEGEEY^{451}
α1 C (α6)	^{401}KRAFVHWYVGEGMEEGEFSEAREDMAALE**K**DYEEVGADSAEGDDEGEEY^{450}
α3 A (α3)	^{401}KRAFVHWYVGEGMEEGEFSEAREDLAALE**K**DYEEVGVDSVEAEAEEGEEY^{451}
α3 B (α7)	^{401}KRAFVHWYVGEGMEEGEFSEAREDLAALE**K**DYEEVGVDSVEAEAEEGEEY^{451}
α4 A (α4)	^{401}1KRAFVHWYVGEGMEEGEFSEAREDMAALE**K**DYEEVGIDSYEDEDEGEE^{448}
α8 (α8)	^{401}KRAFVHWYVGEGMEEGEFSEAREDLAALE**K**DYEEVGTDSFEEENEGEEF^{449}
α-like3	^{401}KFDLMYAKKAFLHWYITEGMELGEFVEAREDLAALE**K**DYEEVGLSF^{451}
βI (β5)	^{391}R**K**AFLHWYTGEGMDEMEFTEAESNMNDLVSEYQQYQDATAEEEEDFGEEAEEEA^{444}
βII (β2A)	^{391}R**K**AFLHWYTGEGMDEMEFTEAESNMNDLVSEYQQYQDATADEQGEFEEEEGEDEA^{445}
βIII (β4)	^{391}R**K**AFLHWYTGEGMDEMEFTEAESNMNDLVSEYQQYQDATAEEEGEMYEDDDEESEAQGPK^{450}
βIVa (β4)	^{391}R**K**AFLHWYTGEGMDEMEFTEAESNMNDLVSEYQQYQDATAEEGEFEEEAEEEVA^{444}
βIVb (β2C)	^{391}R**K**AFLHWYTGEGMDEMEFTEAESNMNDLVSEYQQYQDATAEEEGEFEEEAEEEVA^{445}
βV (β6)	^{391}R**K**AFLHWFTGEGMDEMEFTEAESNMNDLVSEYQQYQDATVNDGEEAFEDEDEEEINE^{447}
βVI	^{391}RRAFVHWYTSEGMDISEFGEAESDIHDLVSEYQQFQDVRAGLEDSEEDVEEAEVEAEDKDH^{451}

Table 1: Sequence of rodent tubulin isotypes [53].

About 30% of total tubulin is present in αβ heterodimer (non-polymerized), and 70% in polymerized form [54]. The exact sequence that varies between species and isotypes is the CTT. Istoypes of α- and β-tubulin are expressed in multicellular organisms in a tissue- and stage-specific manner [55]. CTT structure can vary due to numerous post-translational modifications (PTM) and sequences differences. Acetylation, detyrosylation, tyrosination, phosphorylation, polyglutamylation, and polyglycalation are some of tubulin's PTMs. It has been shown that PTMs regulate many proteins binding to the microtubular surface [56].

Most of PTMs are concentrated in the C-terminal isotype-defining domain of α- and β-tubulins. Most of the PTMs are reversible and can act as switches for a fine regulation of microtubule functions within the cell [53].

Thus, mammalian tubulin proteins possess a very similar globular part but their CTT are quite different. This gives great variation in length and charge, including addition of many basic residues and acquisition of overall cationic character. Tubulin isotypes generate microtubules with distinct properties and functions [57]. Several groups have shown that there is a specific expression and localization of β-tubulin isotypes [58-60].

Many proteins interact with the tubulin dimer and/or MT surfaces. These proteins are known as Microtubule Associated Proteins (MAPs). They are divided into structural MAPs which bind to the MT surface and regulate MT stability, and motor proteins which use ATP hydrolysis to move cargo proteins along the MT surface. The binding of structural and motor MAPs to MT is dependent on or regulated by tubulin's CTT. Thus, MTs are important for mitochondrial localization, movement, fusion and fission, and are the main cytoskeletal fiber, while tubulin dimer interactions are found attached to the MOM and regulate VDAC activity and hence oxidative ADP phosphorylation.

In 1990 Sæterdal *et al*. [61] discovered the presence of a specific β-tubulin binding to the outer mitochondrial membrane, in adult isolated heart myocytes. This discovery suggested a role of cytoskeletal proteins in the regulation of these energy fluxes. Thereafter, Appaix *et al*. [62] showed

how cytoskeleton has an important intracellular factor involved in the metabolic regulation of mitochondrial respiration and energy fluxes, with their studies of mitochondrial structure disorganization by proteolytic treatment with trypsin in 2003. In addition, they proposed that this organization is a basis for effective cross-talk between different subcellular systems of energy conversion. Subsequently, Andrienko *et al*. [63] proposed that mitochondrial-cytoskeletal interactions effectively regulate cellular energetics.

More recently, Rostovtseva *et al.* [46] found tubulin binding to VDAC. They demonstrated that tubulin is in a tight complex with VDAC. Thus, the MOM controls through VDAC the ADP and ATP fluxes from the cytoplasm into or out of the mitochondria. They also showed that VDAC interaction with tubulin dimers' CTT is functionally significant since it causes reduction in the channel conductance and reduces the oxidative phosphorylation in functioning mitochondria.

Moreover, it has been proposed that tubulin increases the K_m of ADP by decreasing ATP/ADP permeability through MOM closure of VDAC. By this type of control, tubulin may selectively regulate metabolic fluxes between mitochondria and cytoplasm [22]. Cytoskeleton remodeling is observed in cardiac hypertrophy and cardiomyopathies, especially in the microtubular system [40].

6. REGULATION OF RESPIRATION IN HEART MITOCHONDRIA

6.1. Theories of regulation of mitochondrial respiration.

It has been found that there is a function-structure relationship between mitochondria, myofibrils and SR. Length-dependent activation of sarcomeres includes also changes of Ca^{2+} sensitivity by cardiac myofilaments. In adult cardiomyocytes mitochondria are arranged regularly in a longitudinal lattice at the level of A-band between the myofibrils and located within the limits of the sarcomeres.

Heart muscle has a regular rhythm of contraction and relaxation, and it has a completely aerobic metabolism at all times. The main fuel for the heart are free fatty acids, but it can also use glucose and ketone bodies. These fuels are oxidized via the citric acid cycle and oxidative phosphorylation to

generate ATP, obtaining its energy from oxidative phosphorylation. Moreover, it has small amounts of reserve energy in the form of phosphocreatine (PCr), enough for a few seconds of contraction [7].

Furthermore, Ca^{2+} has been proposed as a cellular mechanism regulating mitochondrial respiration in parallel with contraction activation [9, 64] . Mitochondrial Ca^{2+} cycle includes a calcium entry-and-export system that regulates Ca^{2+} concentration in the mitochondrial matrix, where Ca^{2+} is an important activator of the Krebs cycle dehydrogenases. Thus, it increases the capacity of oxidative phosphorylation, allows active regulation of compartmentalized cytoplasmic Ca^{2+} fluctuations and related signaling, and protects the mitochondria from Ca^{2+} overload [22].

Mitochondrial Ca^{2+} content above the optimal level inhibits ATP synthesis and causes the mitochondrial permeability transition pore (PTP) opening, which gives place to cell death. All these mitochondrial responses are worsened by reactive oxidative species (ROS) production within the respiratory chain [22].

6.2. The Frank-Starling law.

Starling discovered the ventricular capacity to vary its force of contraction as a function of preload. The heart maintains normal blood circulation under a wide range of workload. The cardiac performance increases with an increase at the end-diastolic ventricular volume.

Under normoxia, cardiac energy metabolism relies on aerobic oxidation of fatty acids and carbohydrate substrates in mitochondria, being ATP consumed mainly by contractile machinery and ion pumps. The heart maintains normal blood circulation under a wide range of workloads, a function governed by the Frank-Starling law [22].

The Frank-Starling law describes the contractile function of myocardium. It states that the force of contraction (active tension) increases if the pre-load (passive tension) increases. If the ventricular end-diastolic volume (ventricular filling - pre-load) is increased, the cardiac muscle length of the

sarcomere is increased. This produces an increased number of force-generating cross-bridges [65] and the amplification of muscle tension.

Frank showed that an increasing heart volume stimulated the ventricle to contract more rapidly and more forcefully. He highlighted that increasing the ventricular volume increases systolic pressure generation. Starling emphasized the role of the load on the heart in producing “maximal” dilation of the heart in the period of diastole [11].

Hibber and Jevell [66] discovered that the length-dependent activation of the sarcomere is the main cellular mechanism of the Frank-Starling law. If the ventricular end-diastolic volume (preload, ventricular filling) is increased, the length of the cardiac muscle sarcomere is increased. This results in an increased number of force generating cross-bridges [65] and an amplification of muscle tension. Thereby, cardiac output is directly related to venous return, the factor determining the most important pre-load [11, 22].

In addition, with a large body of experimental observations to explain the central problem of cardiac energetics, lead to the following conclusions: 1) Discovered by Neely [67] and confirmed by Balaban and others [68-70] was the metabolic stability or homeostasis, where in aerobic hearts an increase in cardiac work and mitochondrial respiration rate occur at unchanged cellular amount of both ATP and PCr. ^{31}P NMR experiments [31] showed that in muscle cells the major part of adenine nucleotides, ATP notably exists in an association state with macromolecules and free ADP may only be transiently present in the cytosol. 2) Multiple and detailed physiological experiments using optical methods for monitoring intracellular Ca^{2+} concentrations showed that workload and oxygen consumption changes induced by alteration of left ventricle filling had unchanged calcium transients [71].

6.3. The intracellular phosphotransfer network

CK and AK phosphotransfer networks are considered essential in the management of cellular energy metabolism. CK catalyzes the reversible transphosphorylation between PCr and ADP and AK catalyzes between ATP and AMP. CK and AK networks are conceived to exist as intracellular circuits of enzyme

molecules catalyzing sequential series of near-equilibrium reactions linking ATP consumption and generation sites [72].

Both CK- and AK-catalyzed reactions optimize mitochondrial respiration and myofibrillar contraction by dissipating intracellular nucleotide gradients, thus increasing the efficiency of muscle performance. Action of mitochondrial and cytosolic AK increases the rate and efficiency of energy transfer, whereas CK facilitates high-energy phosphoryl transfer between cellular compartments. Both CK and AK, cytosolic and mitochondrial channeling, have the same intracellular phosphotransfer systems. Even though they appear to cooperate within the cell, CK system it seems more efficient due to its near equilibrium reaction and high cytosolic content [30].

The major cellular energy transferring networks relies on the activity of CK isoenzymes which produce as 'high energy' intermediates. The MtCK utilizes ATP formed during oxidative phosphorylation to phosphorylate cratine which is exported in the cytosol towards the sites of energy utilization, and delivers ADP within the intermembrane space which can be immediately rephosphorylated by oxidative phosphorylation, and stimulates respiration [73]. This interaction induces a functional compartmentation of adenine nucleotides and favors mitochondrial respiration and the reversible CK reaction with a high ATP/ADP ratio in the IMS.

In general, CK catalyzes the reversible transfer of 'high energy' phosphoryl groups from PCr to ADP to generate ATP, or from ATP to Cr to generate PCr. CK acts as very sensitive ADP sensor. This enzyme is able to remove ADP *in situ* by re-phosphorylating it. ATP traps the large cellular PCr pool. ADP enters the matrix space to stimulate oxidative phosphorylation. ADP increases the mitochondrial recycling of specific pools of ATP and ADP. PCr is the primary 'high-energy' phosphoryl compound that leaves the mitochondria to enter the cytosol.

The CK-PCr system bypasses ATP and ADP diffusion restrictions in the cell. It represents an efficient regulator of energy flux, using metabolite channeling as a fine-tune device of local ATP levels. In addition, the role and contribution of individual phosphotransfer enzymes also depends on the

species, tissue, developmental state or physiological state, underlining the plasticity of the cellular energetic system in governing metabolic homeostasis.

CK, AK and other phosphotransfer isoenzymes in different intracellular compartments are 'pushed' or 'pulled' from the equilibrium in opposite directions, depending on the activity of an associated process which drives steady-state high-energy phosphoryl flux. Sarcomere stretching and cross-bridge cycling lead to increases in: the respiration rate, coupled mitochondrial PCr production, and energy flux via the CK-PCr system, while maintaining metabolic stability [74].

The dynamic interaction between CK, AK and glycolytic enzymes (pyruvate kinase -PK-) phosphotransfer relays determines the behavior of metabolic sensors such as the K_{ATP} channel, and subsequent cellular responses, such as excitability, hormone secretion, intracellular calcium homeostasis and vascular tone.

ATP consumed during myofibrillar contraction and Ca^{2+} pumping is rapidly replenished by CK, AK and glycolytic phosphotransfer relays, maintaining optimal local ATP/ADP ratios and free energy of ATP hydrolysis. These systems generate and translate to stimulate ATP production in the mitochondria and to convey information to energy demand sensors, such as K_{ATP} channels.

Phosphotransfer-mediated metabolic feedback and Ca^{2+} signaling are important components in regulated signal transmission and coordinated dehydrogenase activation. It produces an optimal mitochondrial response to increase cellular energy demands. The regulation of the sarcolemmal metabolic sensor (K_{ATP} channels, the CK-AK-glycolytic networks) affects the excitation-contraction process and thus the Ca^{2+} cycle of the cell.

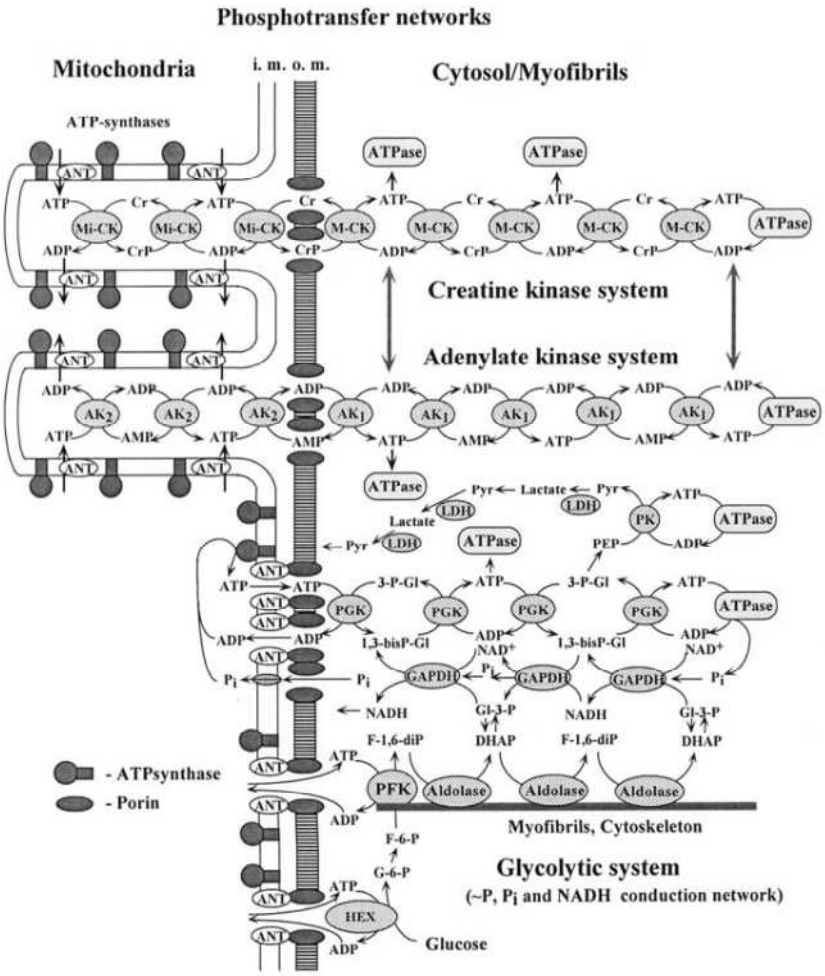

Figure 17. Proposed functional arrangement of the intracellular phosphotransfer network: MtCK isoforms and AK2 serve the spatially and diffusionally restricted intracristae and IMS to provide ADP for oxidative phosphorylation and to facilitate ATP export. Exported ATP molecules are relayed to ATPases through sequential chains of reactions catalyzed by the cytosolic isoforms MtCK and AK1. The glycolytic system could serve a similar intracellular energy transfer and signal communication function by transferring mitochondrially-produced high-energy phosphoryls through hexokinase (Hex), phosphofruktokinase (PFK), and near-equilibrium glyceraldehydes-3-phosphate dehydrogenase/3-phosphoglycerate kinase (GAPDH/PGK) enzymes, present in the vicinity or bound to the MOM, as well as by generating additional ATP molecules as a product of glycolysis. Near-equilibrium reactions catalyzed by GAPDH/PGK chains could also facilitate transfer of P_i and NADH from remote cellular locales to mitochondria. The glycolytic system, which is activated under stress conditions, is envisioned to have a more significant role in carrying-on phosphoryls directly from the high-throughput contact sites between mitochondrial membranes, thus by passing intracristae space. Binding of glycolytic enzymes to the cytoskeleton and clustering inside myofibrils can provide a scaffold for positioning of the glycolytic phosphotransfer network. Figure reproduced from [72] with permission.

These metabolic networks play a significant role in cellular life by distributing energy and providing metabolic signals required for coordination of processes in distinct intracellular compartments. Thus, ATP export could be facilitated by contact sites between the inner and outer mitochondrial membranes, rendering mitochondrially produced ATP readily available for cytosolic MCK catalyzed PCr generation [72].

In a highly structured cytosol, energy transfer and metabolic signaling networks are needed because of the local diffusion restrictions of adenine nucleotides. This results in compartmentation of adenine nucleotides and kinetic and thermodynamic inefficiency of energy-dependent processes. Energy is transferred towards the sites of energy consumption in form of PCr via the Cr/PCr shuttle [30, 35, 75]. The Cr/PCr circuit helps surpass the diffusion barriers in the cell [43, 76, 77], and avoids the dissipation of energy because of ATP transportation. Moreover, it helps to avoid ADP accumulation, thus inhibition of ATPases activity, and AMP accumulation due to the reaction of the AK [22, 72].

In healthy adult cardiac muscle cells, about 80-88% of high-energy phosphoryl transfer is provided by compartmentalized CK reactions and about 7-20% of the total ATP rate is supplied by compartmentalized AK reactions. The net rates of AK catalyzed phosphoryl transfer increased from the equivalent of 2-3% of the total flux in the resting muscle to 23% of the ADP produced in ATPase reaction during contraction [44].

Therefore, the generation of ATP mitochondria must be regulated effectively and expeditiously to meet the challenges in balancing energy demand and supply. In addition, mitochondria use Ca^{2+} as a key regulator for controlling their metabolic activities. During contraction the excitation-contraction cycles, mitochondria sequester a small amount of Ca^{2+} that activates several enzymes involving in the ATP generating machineries [10].

Under total ischemia conditions the PCr concentrations fall rapidly and the heart contraction ceases, but ATP concentration stays almost stable decreasing by 10% at the end of the first minute of ischemia. This can be explained by two mechanisms: adenine metabolite compartmentalization and

the transfer of high-energy phosphoryls between micro-compartments associated to a very effective communication by intracellular signals from myofibrils to mitochondria [44].

In mammal cells, ADP diffusion is restricted at the level of MOM. The apparent K_m for free ADP increases about 370.75 ± 90.57 µM. The respiration rate becomes almost linearly dependent on local ADP concentrations. In addition, endogenous ADP is an important regulator of respiration but only in the presence of creatine and activated MtCK. In contrast with NB HL-1 cells, mitochondrial phosphorylation displays a very high apparent affinity for exogenous ADP. It also has a high activity of hexokinase and creatine is unable to stimulate its respiration. All these suggest a different MI in NB HL-1 cells.

7. MITOCHONDRIAL DYNAMICS

7.1. Fusion and fission

Mitochondrial morphology varies highly between species, tissues and physiological conditions [78]. A large body of literature has shown the adaptation of mitochondrial distribution and morphology to the bioenergetic requirements in highly differentiated cells [79-82]. The cytoskeleton is the most prominent and ubiquitous system bringing organelles into the right position and provides a large and heterogeneous surface for associations with other structures and molecules [78].

Mitochondrial morphology and intracellular organization are tightly controlled by mitochondrial remodeling processes. These processes include continuous fission-fusion events and inner membrane/cristae transitions [83]. The fusion and fission phenomena occur in a careful balance in order to maintain proper mitochondrial dynamics, and both processes require GTP hydrolysis [10]. In addition, mitochondrial dynamics depends on their functional characteristics, on metabolic parameters -*i.e*. substrate and oxygen availability- and specific local cellular functions and demands [83].

Mitochondrial movement is highly dynamic and very important in cells. Cytoskeletal elements and motor proteins for mitochondrial dynamic motion and regulation vary greatly in different cell types. These give cell type-specific functions for particular physiological demands, and can serve to direct mitochondria to cellular regions of locally high ATP demand, providing energy and Ca^{2+} buffer capacity. Recent studies have shown that Ca^{2+} can regulate mitochondrial fission, fusion, and motility [10].

Depending on the cell type and physiological conditions, the interconnectivity and dynamics of the mitochondrial compartment are determined by cycles of fusion and fission [84]. Mitochondrial dynamics serve a variety of different functions. These include mitochondrial distribution and inheritance, remodeling of mitochondria during developmental processes and coordination of programmed cell death by release of pro-apoptotic factors from the IMS [84].

Mitochondria imaging in living cells has revealed that mitochondria are clustered or arranged in a highly organized, tissue-specific manner (*i.e*. adult rat cardiomyocytes, skeletal muscles, hepatocytes, etc.). This clustering may be associated with specific cellular demands and physiological roles. Mitochondria need to be localized at specific subcellular sites, providing ATP and participating in intracellular signaling. This specific mitochondrial distribution, involves mitochondrial intracellular transfer by means of a cytoskeleton-based transportation system and is highly coordinated in response to various cellular demands [83].

Mitochondrial fusion and fission are antagonist processes that predominate under different conditions to adapt mitochondrial morphology and dynamics to the bioenergetic requirements of the cell. Both processes actively participate in the processes of morphologic regulation, transmission of energy and Ca^{2+} signaling, cellular division, mitochondrial DNA inheritance, cell development, and also in the early stages of mitochondria-dependent apoptosis. Mitochondrial dynamics, shapes and spatial arrangement may be very heterogeneous in different cell-types.

Previous studies of mitochondrial dynamics in mammals have been performed with cultured cells. It has been found that many cultured cell lines produce ATP mainly by glycolysis and how they have different mitochondrial morphology (*i.e*. filamentous, interconnected and ramified). Available data point to a functional link between changes of energy metabolism and adaptations of mitochondrial morphology [84]. Fusion and fission events continuously change mitochondrial shape under physiological (*e.g*. cellular division) and pathophysiological (*e.g*. apoptosis) conditions. Disruption in the balance between fusion and fission influences not only mitochondrial morphology but also mitochondrial mobility and their distribution. This may lead to mitochondrial pathology and influences cell survival [85].

Mitochondrial fusion allows efficient mixing of mitochondrial content, and it generates extended mitochondrial networks. It engages the entire mitochondrial compartment in the respiration to maximize ATP synthesis [84]. Moreover, fusion is an essential step in certain developmental processes (*i.e*. embryonic development and spermatogenesis) [86] and has been associated with the dissipation of mitochondrial membrane potential ($\Delta\psi_m$) [87]. Mitochondrial fusion has essential GTPase proteins (*e.g*. Mfn1, Mfn2 and OPA1). In mammals, mitofusin 1 and 2 (Mfn1 and Mfn2) are found in MOM. OPA1 is an IMS protein closely associated with MIM. Mfns and OPA1 work together to promote mitochondrial fusion. In mitochondrial fusion, MOM and MIM should fuse simultaneously in order to maintain the organelle integrity. OPA1 has been suggested to play a role in cristae maintenance [10]. It has been proposed also that disruption of mitochondrial fusion results in mitochondrial dysfunction and loss of respiratory capacity [84]. In contrast, several reports emphasize the importance of mitochondrial fusion under conditions of high energy demand in mammals. It was shown that some cell stressors can trigger increased mitochondrial fusion, called stress-induced mitochondrial hyperfusion, in an Mfn1- and Opa1-dependent manner [88].

In contrast, mitochondrial fission is vital process in dividing cells to ensure a sufficient number of functional mitochondria and the inheritance of mitochondria in newly formed daughter [86]. It helps

in the partition and inheritance of organelles during cell division, release of cyt *c* and other IMS proteins during apoptosis, and generation of transportable mitochondrial units for movement along the cytoskeleton [84]. In mammals, Fis1 and dynamin-related protein 1 (Drp1) are the proteins required for mitochondrial fission. Drp1 is mostly distributed in the cytoplasm under physiological conditions. Mitochondrial fission results in the generation of two non-identical daughter mitochondria, one with a high membrane potential and the other with a low membrane potential. The mitochondrial fission machinery may be regulated by intramitochondrial Ca^{2+}, since it can occur rapidly and reversibly by an increase of Ca^{2+}, and it requires mitochondrial Ca^{2+} uptake [10]. Moreover, fission can be triggered by a decrease in the driving force for ATP synthesis (*i.e.* $\Delta\psi_m$ depolarization) [87].

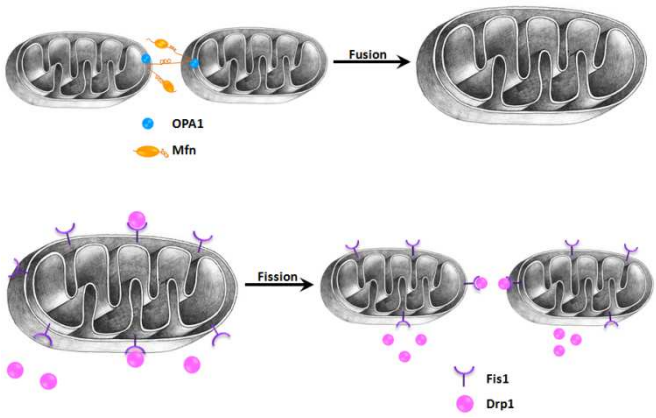

Figure 18. Proteins involved in fusion and fission: general scheme of mammal proteins involved in mitochondrial morphology. This balance can be changed in response to various stimuli (*e.g*. nutrients availability, stress conditions, cell development). OPA1 and Mfns proteins are involved in mitochondrial fusion. Mitochondrial fission requires Fis1 and Drp1 proteins.

Emerging evidences in mitochondrial fusion and fission regulation indicate that there are three main posttranslational modifications of mitochondria-related proteins *i.e*. phosphorylation, ubiquitination and SUMOlyation. These modifications also modulate protein-protein interactions, subcellular localization, and activation of signaling pathways [86]. Electron transport and regulation of apoptosis are affected by the disruption of molecules involved in mitochondrial fusion and fission. Defects in fusion frequently cause fragmentation of the mitochondria network, whereas fission incapacity results in excessive formation of elongated and interconnected organelles networks [86].

Several authors have concluded that mitochondrial fusion is necessary for normal mitochondrial functioning [84]. Thus, it has been proposed that mitochondrial morphology adapts depending on the respiratory activity. This model proposes that when respiratory activity is low, fragmented mitochondria are preferred morphological state, whereas under respiratory conditions mitochondria undergo frequent cycles of fusion and fission to allow spreading of metabolites and macromolecules throughout the entire compartment [84].

Fission events are associated with major changes in $\Delta\psi_m$ generating functionally divergent daughters; it is required for the removal of damaged and inactive organelles. While fusion mixes the content of the parent mitochondria, through the rapid diffusion of matrix proteins, with slower migration of inner and outer membrane components. Therefore, mitochondrial dynamics have an impact on mitochondrial turnover and thereby the bioenergetic efficiency of the mitochondria population within a cell. In addition, mitochondria differences in matrix density, crista structure and density may reflect different metabolic demands of cytoplasm [89] or degenerative processes [90]. Mutations in either processes cause human diseases (*e.g.* Alzheimer, Charcot-Marie-Tooth syndrome, autosomal-dominant optic atrophy).

It is well-known that cytoskeleton has many roles among which bringing organelles into the right position and providing a large and heterogeneous surface for associations with other structures and molecules are the most prominent and ubiquitous [78]. Therefore, neither the distribution nor the appearance of mitochondria might be at random and without control. Many previous studies using electron microscopy have shown the associations of mitochondria with the cytoskeleton. Intermediate filaments appear to play a role in mitochondrial positioning [82].

In muscle cells associations of mitochondria and desmin has been described long time ago [91], as well as in cardiomyocytes anchoring mitochondria to microtubule interactions [61]. Evidence of mitochondria associations with actin fibrils has been described [92]. Moreover, proteins bound to the mitochondrial outer membrane and to microtubules have been identified [78]. Another structure

that is associated with mitochondrial clusters is the SR. This cellular organelle structure forms a continuous network that surrounds myofibrils. SR is the primary calcium storage and source of the vast majority of the free cytosolic Ca^{2+} that drives sarcomeric contraction [79]. Additionally, it has been seen that intracellular positioning of mitochondria depends on the energy demand of muscle cells, *i.e*. mitochondria are embedded between the myofibrils along their entire length to provide ATP to the sarcomeres [93, 94]. It has been shown that there is an adaptation of mitochondria and morphology (*e.g*. insects flight muscles, neurons, and lymphocytes) to the bioenergetic requirements in high differentiated cells [84].

7.2. Mitochondria dynamics in different cardiac muscle cell phenotypes

In adult cardiomyocytes, the size, shape and metabolic activity of mitochondria also depend on intracellular localization. Three subpopulations of mitochondria have been identified in adult heart: interfibrillar, subsarcolemmal and perinuclear [95]. Interfibrillar mitochondria are aligned in longitudinal rows between myofibrils in close proximity to SR Ca^{2+} release sites. Subsarcolemmal and perinuclear mitochondria appear less organized and more variable in shape and size. Moreover, mitochondria need to be localized at specific subcellular sites for providing ATP and participating in intracellular signaling. Specific mitochondrial distribution involves mitochondrial intracellular transfer by means of a cytoskeleton-based transportation system and it is highly coordinated in response to various cellular demands [83].

Cardiomyocyte mitochondria are individually situated in pairs sandwiched between the contractile machinery of the sarcomere, longitudinally and radially. Thus, their shape represent the three-dimensional balance of forces extant at any given moment [96]. In adult rat cardiomyocytes, interfibrillar mitochondria are dynamic structures which are capable of undergoing rapid low-amplitude fluctuations, although they appear isolated with respect to electrical activity [97].

Segretain *et al*. showed the ultrastructure of cardiac muscle. These electron microscopy studies showed the three dimensional organization of mitochondria and SR. They presented a diagrammatic

representation of this arrangement in heart muscle fiber, showing how complex this organization is. Where a network of tubules forms like a mesh around mitochondria and at the level of all bands, *i.e.* H-band, A band, and I-band. Therefore, mitochondria are likely to be maintained in position by the SR, and the relationship among mitochondria, sarcoplasmic reticulum and T-tubule is constant [98].

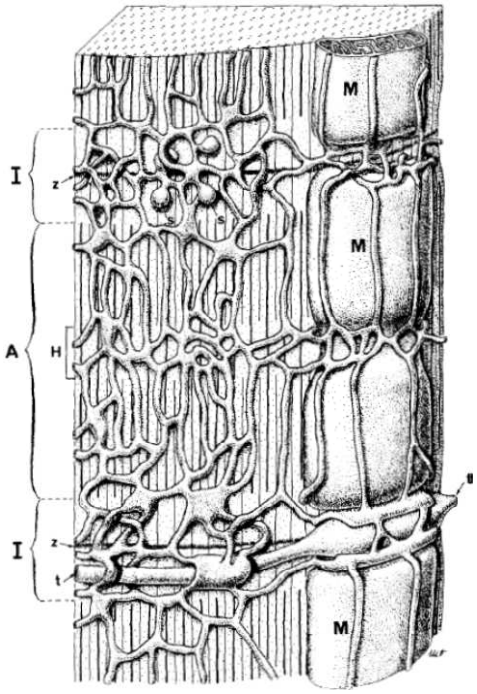

Figure 19. Representation of the three-dimensional organization of the sarcoplasmic reticulum (SR) as it is seen in a heart muscle fiber: At the H-band level (H), middle of the A band (A), the SR takes the appearance of a tight network of tubules. From this network, cisternae of SR are roughly parallel to the long axis of the myofibrils and extend in both directions toward the I-band level where they merge in large meshes over the A-I junction. Sometimes these longitudinal cisternae join together to give rise to flattened cisternae. Over the mitochondria (M), the longitudinal cisternae are more widely dispersed and a tight network is seen to face the depression of the mitochondria. At the I-band level (I), cisternae of SR from a 3-D network made up of large polygonal meshes anastomosed in all directions of space. In the absence of the T-tubule, this mesh-work simply extended across the I-band and showed some terminal bulbous swellings (S). In the presence of the T-tubule (t), SR were parallel on one or both. Over or below the T-tubule, some short tubular or flattened bridges of SR ensure longitudinal continuity. In the space between the tips of adjacent mitochondria and facing the I-band, in absence of the T-tubule (upper right), the SR form a loose three-dimensional network of tubules. In presence of the T-tubule (lower right), SR cisternae are arranged in a casing around the distended T-tubule (t) and are in continuity with longitudinally and transversally running SR cisternae. Reprinted from [98] with permission.

In contrast, neonatal rat cardiomyocytes possess an undeveloped SR and surface membrane system. Mitochondria in neonatal cardiac cells appear to be connected into a mitochondrial reticulum and its implications for control of energy metabolism are still unknown. The mitochondrial cristae of young myocytes are sparse, which indicates a lower amount of aerobic metabolism [12]. Therefore, mitochondrial dynamics may be more pronounced during the early development of cardiac muscle cells [10].

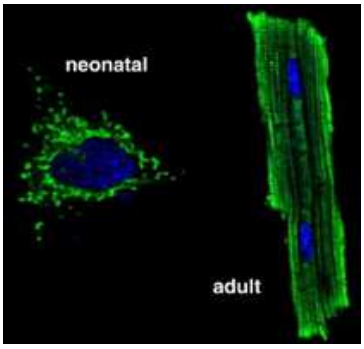

Figure 20. Distribution of mitochondria in adult and neonatal rat cardiomyocytes: developmental changes in the distribution of mitochondria (green) and nuclei (blue). Taken from [12] with permission.

Cardiac muscle has relatively homogeneous patterns of mitochondrial redox state, membrane potential and Ca^{2+}. It shows a typical regular mitochondrial arrangement [99]. In contrast, neither fusion nor fission phenomena have been seen under normal conditions, though the presence of essential proteins involved in these processes has been documented [100].

Under pathological conditions a remarkable remodeling of mitochondria has been seen. Therefore, mitochondrial fusion in the heart could be a sign of pathogenesis or cell death. In addition, previous studies [101] have shown that hypoxia may result in abnormal distribution of mitochondrial redox/electrical potential and Ca^{2+}, and the formation of gigantic mitochondria in ischemia reperfused hearts. Whereas mitochondrial fusion is induced as an endogenous protective mechanism from further hypoxic or ischemic insult in short non-lethal periods of hypoxia. Mitochondrial fusion may be an initial response to a low level of stress, which provides a protective response against a future insult.

It has been observed that under several pathological conditions, mitochondrial dynamics and functioning is altered. Heart failure is associated with reduced mitochondrial oxidative phosphorylation and the production of mitochondrial oxidative stress. Disorganized small mitochondria have been observed in a variety of cardiac conditions (*e.g.* dilated cardiomyopathy and myocardial hibernation). In addition, an induced mitochondrial fragmentation has been seen during hyperglycemia, which can be a major contributor linked to increased risk of cardiovascular disease in patients with diabetes mellitus where hyperglycemia-induced mitochondrial oxidative stress can induce cellular injury and dysfunction [95].

In skeletal muscles, different mitochondrial distribution may have important functional and physiological consequences. Mitochondria found in skeletal muscle have a highly heterogeneous oxidative state. Subsarcolemmal mitochondria are located close to the periphery, which may explain their more oxidized state and could potentially indicate a more active mitochondrial respiration [83].

In contrast, HL-1 cells and other carcinoma cell lines, show a clear heterogeneity, highly dynamic with fusion and fission events. Qualitative studies of imaging have shown that NB HL-1 cells possess randomly organized filamentous and dynamic mitochondria. Therefore in cancer cell lines, mitochondrial dynamics and metabolism differ from healthy mammal cells. Yet this type of cells may be a useful model for studying mitochondrial transitions, fragmentation and heterogeneity under normal and pathological conditions (*i.e*. hypoxia-reoxygenation, oxidative stress and apoptosis).

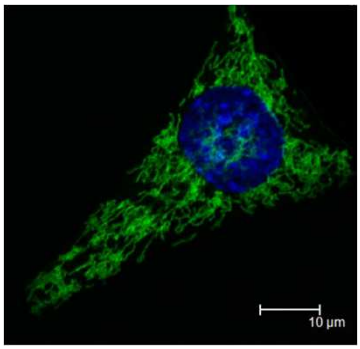

Figure 21. Mitochondrial distribution in NB HL-1 cells: reticular and fragmented network of mitochondria (green) and the nucleus (blue). Taken from [97] with permission.

Finally, in heart muscle mitochondrial dynamics could be an integral part of the regulation of cellular bioenergetics, redox signaling, Ca^{2+} homeostasis, differentiation, fatty acid and glucose metabolism, ROS generation, mitochondrial-dependent apoptosis and aging [8, 10].

7.3. Do fusion-fission events occur in all cells?

Notwithstanding over 30 years of research on mitochondrial dynamics has provided a good insight into mitochondrial morphology-function interaction, all these broad information have also brought many a controversy about these phenomena. However, it is highly risky to generalized these information since most of the studies have been perform in immortal cell-lines, *e.g.* HeLa, COS-7, CV1-4A, NB HL-1 cells, etc. and their dynamics strongly depend on the culturing conditions [102].

Many research groups claim the existence of fusion and fission phenomena in all type of mammalian cells, including healthy and pathological states. This belief is based on many studies where it is stated that mitochondria cannot be generated *de novo*, but rather derive from existing mitochondria through the division, synthesis and import of proteins and lipids [10].

Every mitochondrion contains several copies of mtDNA genome, which is maternally inherited. The mtDNA can be replicated multiple times during each cell cycle. Fusion between two or more mitochondria allows the mixing of mitochondrial matrix contents. A decrease in mitochondrial fusion activity results in decreased mitochondrial oxygen consumption and membrane potential, as well as a decrease of mtDNA [103].

Meanwhile fragmented mitochondria (fission) are thought to be easily transportable and allow rapid mitochondrial trafficking to energy-demanding regions of the cell [104]. Disruption of mitochondrial fission results in altered mitochondrial recruitment and location. In addition, it has been shown that mitochondrial fission is a necessary component for high glucose-induced respiration increase and ROS overproduction [105].

In cultured neonatal ventricular myocytes, inhibition of mitochondrial fission prevents over-production of reactive oxygen species (ROS), mitochondrial permeability transition pore formation and subsequent cell death under sustained high glucose condition. Despite variations in mitochondrial size and shape in individual myocytes, very little is known about mitochondrial dynamics in the adult heart disease [105].

Despite the contraction and relaxation cycles in cardiac muscle mitochondria, there are cytoskeletal proteins that do not allow these fusion and fission process. Mitochondria deform in three dimensions during cadiomyocyte contraction and relaxation. Mitochondria are distributed between, and are in dynamic force balance with, the cytoskeletal proteins. They expand asymmetrically along the width- and thick-axes during cell contraction. When mitochondria inside cardiomyocytes are compressed, it is assumed that the internal pressure of each mitochondrion increases as if it were a single compartment. Those small deformations are accompanied by effectively equivalent areas of surface contact with adjoining cytoskeletal structures (*i.e.* sarcomere, myofilaments) [96]. There are several conditions where cardiomyocytes morphology has been seen altered.

In the aging heart, there are changes in cardiomyocyte morphology with the overall length increasing without proportional changes in cell width and thickness. These changes may also be accompanied by alterations in the cytoskeleton. It has been shown that in failing hearts, mitochondria are small and fragmented compared with normal hearts, consistent with a decreased rate of fusion. However, in healthy cardiomyocytes, sarcomeric mitochondrial diameters returned to those at rest after transient sarcomere contraction [96].

Mitochondrial dysfunction is suggested to play a central role in metabolic and chronic diseases; under these conditions, accumulation of dysfunctional mitochondria leads to oxidative stress and impaired cellular functions. It plays a central role in metabolic (*e.g*. diabetes) and chronic (*e.g*. Alzheimer disease, Parkinson disease) diseases [105]. In cardiac disease, including end-stage dilated

cardiomyopathy, myocardial hibernation, cardiac rhabdomyoma, and ventricular-associated congenital heart diseases, mitochondria were found to be disorganized and abnormally small [10].

Disorders in mitochondrial organization and the presence of abnormally small and fragmented mitochondria have been noticed at the end-stage of dilated cardiomyopahty, myocardial hibernation and ventricular-associated congenital disease. Likewise, in failing rat hearts intra-mitochondrial structural changes including disorganized cristae and/or reduced cristae density have been seen [105]. Another condition that enhances fission phenomenon in cardiac mitochondria is copper deficiency, which results in cardiac hypertrophy with a dramatic increase in mitochondria, possibly as a compensatory mechanism for a reduction in cyt *c* oxidase and ATP synthase [8].

Several groups suggest that mitochondrial fusion is a complementary mechanism through which mitochondria compensate certain metabolic depletions by transferring soluble and membranous components. Therefore, fusion may lead to a functionally even distribution of components involved in respiration and the generation of dissimilar daughter mitochondria [87]. All together this information suggests that there is a relationship between mitochondrial morphology and the pathogenesis of cardiac disease.

Despite the fact that several groups have shown the existence of different mitochondrial dynamics depending on the type of cell, immortal cell-lines and mammalian cells, and its physiological state there are still some groups that claim mitochondrial fusion as a highly necessary event to support normal mitochondrial functions and respiratory activity [103, 106, 107]. In addition, it has been proposed by Westermann [84] how mitochondrial morphology is adapted to respiratory activity. His model suggests that fragment mitochondria, the preferred morphological state of mitochondria, have a low respiratory activity. Meanwhile, fusion causes a hyperfused network of mitochondria with a high respiratory activity. This state is favored when the bioenergetic state becomes critical, in order to optimize mitochondrial function. Therefore, it is important to clarify this model.

II. STUDY LIMITATIONS

Cardiac and skeletal muscle functional and metabolic regulation has been in the spotlight of many research groups over several decades. To approach a better understanding of this complex system, scientists have made use of systems biology to understand how these cells regulate their functional and metabolic roles.

An important element of functional and metabolic regulation of cardiac and skeletal muscle is the mitochondrion. Mitochondria have been under study since their discovery. It is well known that they are in charge of regulating the cell's energy status and of adjusting its functional activity under conditions of stress or other aspects of life.

Mitochondria display a tissue-specific distribution and energy consumption. In adult rat cardiomyocytes, mitochondria are arranged regularly in a longitudinal lattice at the level of A band between the myofibrils and located within the limits of the sarcomeres. A decade ago, Saks and Seppet [108, 109] established the functional role and importance of the intracellular energetic units (ICEUs).

ICEUs have specialized pathways of energy transfer and metabolic feedback regulation between mitochondria and ATPases, mediated by CK and AK; the mitochondrial interactosome (MI) is found within the ICEUs. The main role of MI is the regulation of the intracellular phosophotransfer networks.

Sæterdal [61] discovered the associations between beta-tubulin and mitochondria in adult isolated heart myocytes. This discovery suggested a role of cytoskeletal proteins in the regulation of these energy fluxes. This was complemented with Appaix's [62] studies of mitochondrial structure disorganization by proteolytic treatment with trypsin, and Andrienko's [63] proposition of cytoskeletal proteins interaction with effective regulation of cellular energetics. Recently, Rostovtseva [46] discovered that tubulin is the X factor regulating VDAC activity. Thus, all these

works have provided a better understanding of this complex structure-function relationship in regulation of compartmentalized energy metabolism.

Finally, taking in consideration Beraud's [97] observations to study in depth and have a better knowledge of cardiac mitochondria and regulation. This work has the intention to purvey a better understanding of this function-structure relationship in healthy adult rat cardiomyocytes, considering mitochondrial dynamics, cytoskeletal interactions and respiratory activity.

III. AIM OF THE STUDY

The aim of this study was to investigate the mechanism of control of energy fluxes and the role of structure-function relationship in the metabolic regulation in adult rat cardiomyocytes under physiological conditions *in vivo*.

To achieve this aim, the objectives of this study were.

1. Visualization of cytoskeletal proteins distribution and their co-localization with mitochondria in cardiac muscle: α-actinin and tubulin isotypes.
2. Role of tubulins in regulation of oxygen consumption.
3. Mitochondria dynamics by the *in vivo* transfection of GFP-α-actinin.

IV. METHODS

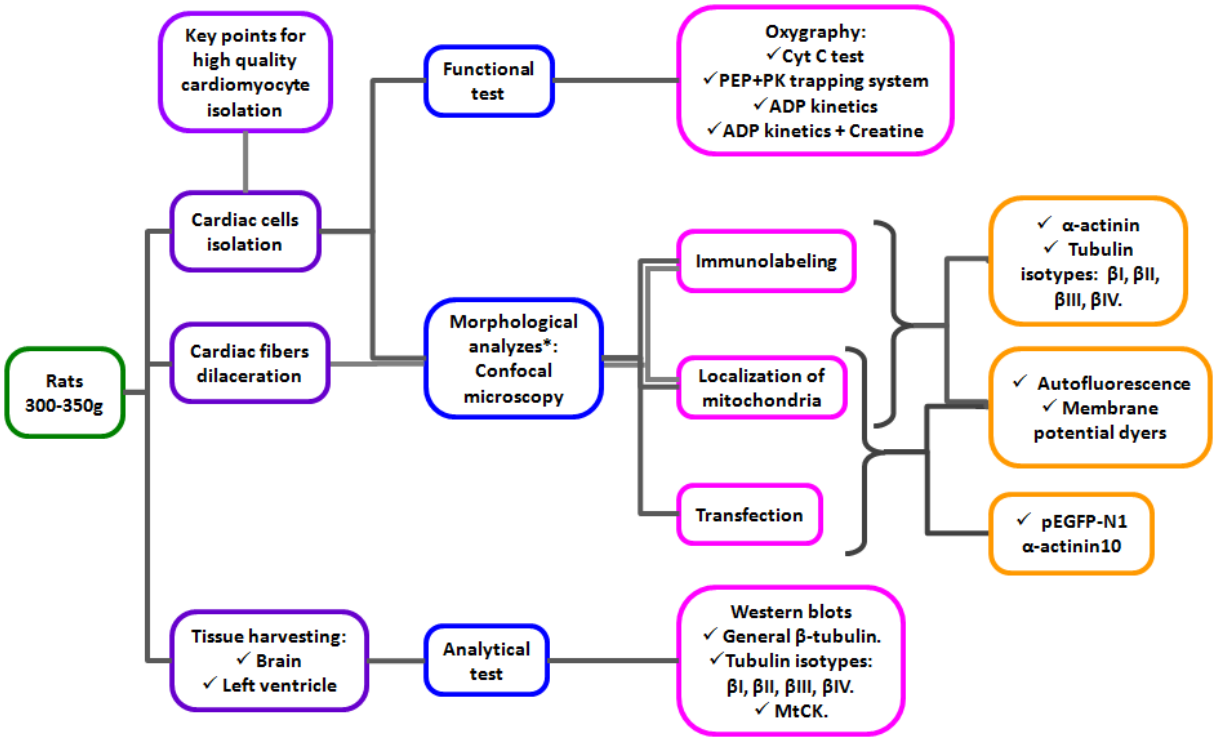

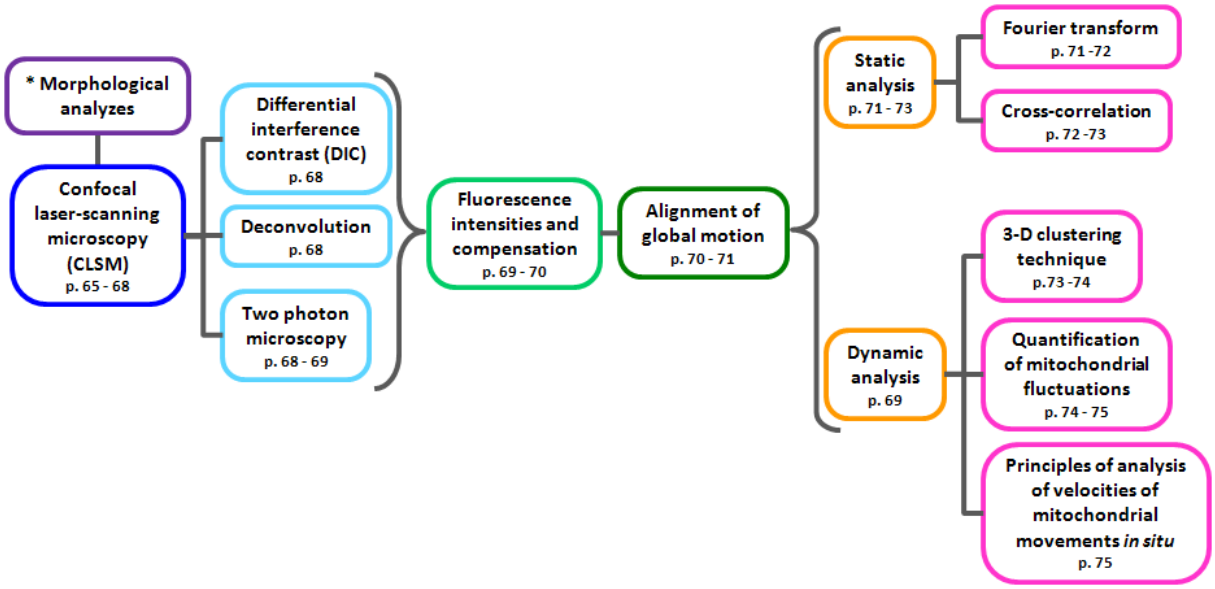

1. Animals:

Male wistar rats weighing 300-350g were used. The animals were housed at constant temperature and humidity with 12h light-dark cycles at the animal facility of the laboratory of fundamental and applied bioenergetics (LBFA) - INSERM U1055. Rats were provided with standard chow diet (Safe A04) and water was *ad libitum*. Animal procedures were approved by "Comité d'éthique pour

l'expérimentation animale, Comité d'éthique Cométh Grenoble" Comité National de Réflexion Ethique sur l'Expérimentation Animale sous le numéro 12: 33_LBFA-VS-01.

1.1. Cardiomyocytes isolation

Rats were anesthetized with pentobarbital (45 mg/kg) after half an hour of 500U of heparin injection, and the heart was quickly excised preserving a portion of the aorta and placed into a canula to perfuse with oxygenated isolation buffer (117mM NaCl, 5.7mM KCl, 4.4mM $NaHCO_3$, 1.5mM KH_2PO_4, 1.7mM $MgCl_2$, 11.7mM Glucose, 10 mM Creatine, 20mM Taurine, 10mM Phosphocreatine, 2mM Pyruvate, and 21.1mM HEPES, pH 7.2 [Materials - Table 3.a.]). After rinsing all blood from the heart, digestion solution (collagenase 0.03 U/mL, $CaCl_2$ 0.026mM, BSA 2mg/mL [Materials - Table 3.b.]) saturated with oxygen was poured into the perfusion system and the recirculation of the solution was started, the heart is digested ~30'. After digestion, the heart was detached from the canula and transferred into a petri dish containing sedimentation buffer (BSA 2mg/mL, $CaCl_2$ 0.026 mM, Soy trypsin inhibitor (STI) 0.42mM [Materials - Table 3.c.]).

Once in the petri dish, two or three cuts were made to the tissue and cardiomyocytes (CM) were dissociated by gentle pipette suction. Cells were suspended in sedimentation buffer and passed through a fine mesh (200µm opening) to remove all connective tissue. Thereafter, CM were centrifuged at 300 rpm for 5' and re-suspended in the respective sedimentation buffer, the supernatant is discarded and the pellet was re-suspended using the respective buffer. Rod-like shape CM were left to sediment within 3-5', then the supernatant containing the damaged-cells was discarded. This re-suspension-sedimentation cycle with calcium-tolerant cells was performed twice. After these cycles, cells were transferred gradually into the respective [Ca^{2+}] gradients solution buffers or Mitomed depending if CM were going to be used for oxygraphy, immunofluorescence or transfection.

2. Oxygraphy.

Once cells were in the sedimentation buffer, they were gradually transferred into free Ca^{2+} Mitomed solution (EGTA 0.5mM, $MgCl_2$ 95.21mM, K-Lactobionate 60mM, Taurine 20mM, KH_2PO_4 3mM, HEPES 20mM, Sucrose 110mM, DTT 0.5mM [Materials - Table 3.d.3.]). Isolated CM were stocked in 1-2mL volume containing 85-100% of rod-like shape cells that were observed under a light microscope and stored on ice during further experiments. The rod-like shape viability of cardiomyocytes depends on several key points described in detailed later (Table 2) and the different quality tests, specified in detail below, were performed in CM to ensure reliable results.

2.1. Measurements of oxygen consumption.

The respirometry is a method that allows measuring cell oxygen (O_2) consumption. Cardiomyocytes were permeabilized with saponin (25µg/mL). The saponin is a detergent with high affinity to cholesterol found in plasma membranes, being selective to the sarcolemma. Therefore, cells' permeabilization allowed studying the mitochondria *in situ* without endogenous substrates contained in the cells, which gave a better control of intracellular conditions during the protocol.

The rates of oxygen were determined with a high-resolution respirometer oxygraph-2K (OROBOROS Instruments, Austria) in Mitomed solution with 2mg/mL fatty acids free of BSA, and enriched with 5mM glutamate and 2mM malate as respiratory substrates. The measurements were carried out at 25° C; solubility of oxygen was taken as 240 nmol/mL [110]. The respiration rates were expressed in nmol of oxygen consumed per minute per nmol of cytochrome aa3.

It is important to consider the respiratory control ratio (RCR) that goes from 6 to 10. The RCR is a quality control for the permeabilized preparation. A high RCR indicates good function and a low RCR usually indicates mitochondrial dysfunction, particularly of the electron transport chain [111].

$$RCR = \frac{V_{ADPmax}}{V_0} = \frac{\text{maximal rate of respiration (state 3)}}{\text{sample's basal respiration}}.$$

2.1.a. Integrity of the outer membrane: Addition of saturated ADP (2mM) to CM induces high state 3 respiration rate. No effect on the state 3 of respiration after the addition of exogenous cyt *c*, helps to evaluate the integrity of MOM. Finally, with the addition of atractyloside (ATR) , the respiration rate went back to State 2 (V_0) level showing the integrity of MIM [112]. ATR is a powerful inhibitor of the oxidative phosphorylation that blocks adenoside nucleotides' transfer through the mitochondrial membrane. Addition of ATR shows that all ADP is imported into mitochondrial matrix via ANT (Materials - Table 1.a.).

2.1.b. PK-PEP trapping system: It helps to stimulate *in vivo* conditions in cells where the glycolytic pathway is present, competing with mitochondrial respiration through consuming ADP. Addition of MgATP (2mM) and Creatine (20mM) in saturation to CM activates respiration, the addition of PK (20 UI/mL) and PEP (5mM) has no effect in the PK-PEP system, indicating that it does not have any access to the intramitochondrial ADP, and therefore no effect on the oxidative phosphorylation inside mitochondria or respiration rate [113]. This protocol shows the role of the MOM in the control of MI (Materials - Table 1.b.1.).

2.1.c. Regulation of mitochondrial respiration by creatine in the presence of activated MtCK: Addition of MgATP (2mM) in saturation to CM induces an increase in the respiration rate. In the presence of PEP (5mM) the addition of PK (20 UI/mL) decreased this rate. Thereafter, titrated addition of creatine rapidly increased the respiration rate up to the maximal value, indicating that ADP produced by MtCK is not accessible for the PK-PEP system, thus, it is rapidly taken up by ANT into the mitochondrial matrix [114].

2.1.d. Regulation of respiration by exogenous ADP: Creatine significantly activates respiration and decreases the apparent Km for ADP, showing intracellular local restriction on diffusion of adenine nucleotides and metabolic feedback regulation of respiration via phosphotransfer networks that are related to the complex structural organization of cardiomyocytes [115]. A high K_m for exogenous ADP

reflects the local restriction of ADP and ATP diffusion, which in cardiac cells are bypassed by creatine kinase system [116].

1.2. Dilaceration of adult left-ventricle fibers

Adult rat heart fibers were isolated by dilacerations of the cardiac left-ventricle fibers [112]. Male Wistar rats (300-350g) were anesthetized and the heart was quickly excised and washed in Solution A (2.77mM CaK_2EGTA, 7.23mM K_2EGTA, 20mM Imidazole, 0.5mM DTT, 6.56mM $MgCl_2$, 53.3mM MES, 20mM Taurine, 5.3 Na_2ATP and 15mM Na_2PCr [Materials - Table 3.d.4.]). Fibers of left ventricle were carefully dilacerated in solution A. Dilacerated fibers were transferred to Mitomed solution. Fibers were incubated with 10µM Mitotracker® deep red for 30' at 37°C. Mitomed solution was removed. Thereafter, fibers were fixed as it is explained below.

3. Microscopy techniques

3.1. Immunofluorescence.

Freshly isolated cardiomyocytes were fixed using paraformaldehyde (PFA) 4% + Glutaraldehyde 0.1% solution for 1h on ice. Then cells were washed 3 times with PBS containing 2% of BSA. Thereafter, cardiac cells were permeabilized with 1% Triton X-100 during 30' at room temperature (25° C), followed by 3 washes with 2% BSA solution.

After fixation and permeabilization, cardiomyocytes were incubated with the 1^{st} antibody with 2% BSA in PBS, overnight. The next day cardiac cells were washed once with PBS containing 2% BSA and incubated with the chosen 2^{nd} antibody for 2 hours at room temperature. 1^{st} and 2^{nd} antibodies used are shown in Tables a and b (2. Immunofluorescence, confocal imaging).

For autofluorescence: Freshly isolated CM were incubated for 10' in a petri dish containing oxygen-saturated Mitomed and 5µM of rotenone to produce the oxidation of flavoproteins. Thereafter, cells were fixed as mentioned previously.

Removal of tubulins from CM: Freshly isolated CM were trypsinated with 0.05µM or 0.3µM (0.1-0.4 mg of trypsin/mg CM protein) for 10' at 25° C and then STI (0.02mM) was added to stop the trypsin action. Afterwards, CM were fixed as mentioned previously.

3.2. Transfection.

Isolated cardiomyocytes were sedimented with increasing gradient Ca^{2+}concentration (0.2mM, 0.7mM and 0.8mM) buffers containing BSA and Soy Trypsin Inhibitor (STI), at 37° C. After washing the cardiomyocytes wish the three gradient Ca^{2+}concentration, a final wash was performed with the recovery culture medium; then the whole medium was removed. 16µL of cardiomyocytes were placed in each well of 2-well lab-tek, containing 2mL of "recovery" culturing medium, and left in the incubator (37° C, 5% CO_2) for 4h. After this time, media was carefully removed from the wells trying not to disturb the cardiomyocytes, and the transfection culture medium containing the plasmid pEGFP-N1 alpha-actinin 1 and the transfection reagent (lipofectamine™) was added. Cells were left in the incubator overnight and up to 20-22h to find a positive transfection.

In order to localize mitochondria in transfected cardiomyocytes MitoTracker® Red FM (Molecular probes®, Invitrogen™) was used. It has an excitation/emission wavelenght of 581nm/644nm.

The pEGFP-N1 alpha-actinin is a high-copy mammalian non-viral plasmid with a size of 4700bp and an eGFP tag, resistant to kanamycin.

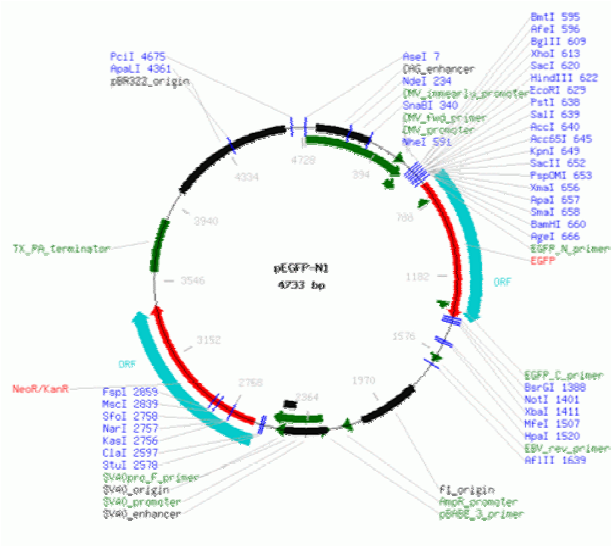

Figure 22. **pEGFP-N1 alpha-actinin map vector.**

Plasmids are circular DNA molecules that replicate separately from the host chromosome. Naturally occurring bacterial plasmids range in size from 5,000 to 400,000 bp. Plasmids usually carry antibiotics resistance genes, and contain a number of conveniently located restriction endonuclease sites into which foreign DNA can be inserted. Plasmid vectors can be used to clone DNA segments of no more than ~10Kb.

Transformation is the process by which the foreign DNA (plasmids) can be introduced into bacterial cells, expressing the specific gene(s) introduced [117].

Transfection is the process by which foreign nucleic acids are introduced into mammalian cells, usually followed by expression of one or more genes in the newly introduced DNA[118].

The bacteria containing the pEGFP-N1 alpha-actinin plasmid were grown in standard Luira Bertani (LB) medium to a cell density of ~3-4x10^9 cell/mL. LB medium contained Kanamycin at 0.1%. After overnight incubation (12-16h) at 37° C with vigorous shaking (~300 rpm), bacteria were harvested and centrifugated at 6000 x g for 15' at room temperature, thereafter QIAGEN protocol for QIAfilter plasmid purification was followed (available http://www.qiagen.com/products/plasmid/qiagenplasmidpurificationsystem/qiafilterplasmidmegakit.aspx#Tabs=t2).

Lipofectamine™ 2000 transfection reagent is a proprietary cationic lipid formulation that offers the highest transfection efficiencies and protein expression levels on the widest variety of adherent and suspension cell lines. To perform the transfection, Invitrogen's protocol was followed (available http://tools.invitrogen.com/content/sfs/manuals/lipofectamine2000_man.pdf).

3.3. Confocal imaging.

The fluorescence images were acquired with a Leica TCS SP2 AOBS inverted laser scanning confocal microscope (Leica, Heidelberg, Germany) equipped with a 63x water immersion objective (HCX PL APO 63.0x1.20 W Corr). Laser excitation was 488nm (green fluorescence) and 633nm (red fluorescence). Images were then analyzed using Volocity software (Improvision, France).

4. Principles of fluorescence imaging

4.a.) Electromagnetic spectrum of radiation (ESR): ESR extends from high-frequency gamma rays through X-rays, ultraviolet light, visible light, infrared radiation and microwaves to very low frequency long-wavelenghts radio waves. Visible light is a portion of the electromagnetic spectrum, corresponding to wavelengths from about 390 to 750 nm.

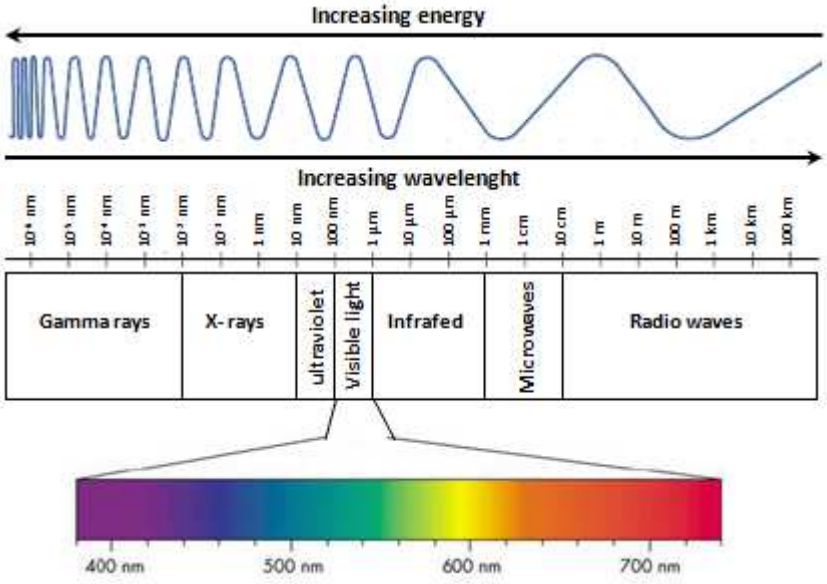

Figure 23. Electromagnetic spectrum of radiation: Different types of electromagnetic radiation by their wavelengths. An increasing wavelength belongs to a decreasing frequency.

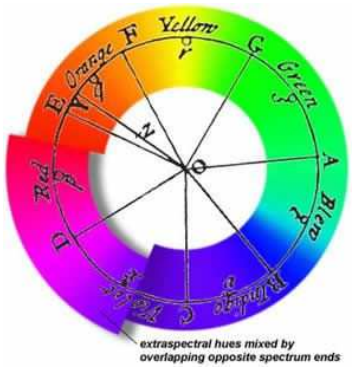

Figure 24. Newton's color circle: It shows the colors correlated with musical notes. The spectral colors from red to violet are divided by the notes of the musical scale, starting at D. The circle completes a full octave, from D to D. Newton's circle places red, at one end of the spectrum, next to violet, at the other. This reflects the fact that non-spectral purple colors are observed when red and violet light are mixed.

4.b.) Fluorescence: It is complex phenomenon where the absorbed light by molecules is emitted during the rapid relaxation of fluorescent molecules. The wavelength of emitted fluorescence is longer than the absorbed light wavelength [119].

Jablosnski energy diagrams: They represent the energy levels for a fluorescent molecule and several important transitions. The ground electronic state and the first singlet electronic state are represented by $\mathbf{S_0}$ and $\mathbf{S_1}$, respectively. The closely spaced states within each electronic level at each energy level (represented by the three lines at the S_0) represent vibrational energy levels of the molecule. Transitions between states are depicted by a sphere (representing an electron) followed by a vertical arrow that traverses the region between the ground and excited state. The electronic transitions are almost instantaneous in nature, often occurring in time frames ranging from nano to sub-pico seconds.

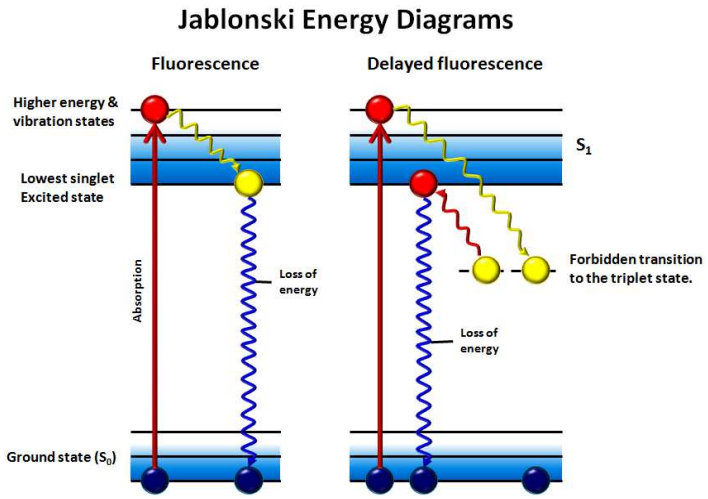

Figure 25. Jablonski energy diagrams: Illustrates the characteristic molecular states and relaxation processes involved in fluorescent emission. The states are arranged vertically by energy and grouped horizontally by spin multiplicity. The fluorescence diagram shows the lowest excited singlet state, the electrons are then able to "relax" back to the ground state with simultaneous emission of fluorescent light. The emitted light is always of longer wavelength than the excitation light and continues so long as the excitation illumination bathes the fluorescent specimen. If the exiting radiation is halted, the fluorescence ceases. The delayed fluorescence takes little longer than usual fluorescence. It is when the excited electrons may go from the triplet state back to the lowest excited singlet state and then return to the ground state, subsequently emitting fluorescent light.

At room temperature, a fluorescent molecule occupies the ground state S_0 of both energy levels: electronic and vibrational. Absorption, understood as an absorbed photon of energy, is required to excite a molecule. The amount of energy corresponding to the transition step of the absorbed photon will lift the molecule to a higher level of the electronic and vibrionic energy states. Following photon absorption, an excited molecule quickly relaxes to the lowest vibrational level of S_1. Fluorescence is generated when a molecule occupying the singlet electronic excited state relaxes to the ground state via spontaneous photon emission [120].

In addition, the energy of any photon emitted via fluorescence is less than the energy of the originally absorbed photon due to the energy lost to internal conversion. This explains the Stokes's shifts that refer to a longer wavelength and thus lower energy photons [120].

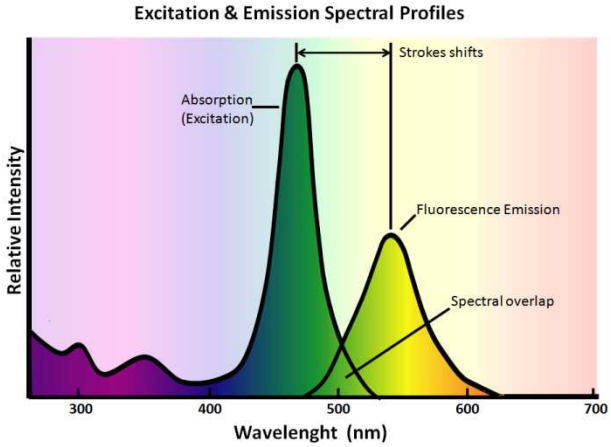

Figure 26. Excitation and emission spectral profiles: The emission spectrum of a particular fluorochrome, the wavelength of maximum absorption is determined and the fluorochrome is excited at that wavelength. The excitation spectrum of a given fluorochrome is determined in a similar manner by monitoring fluorescence emission at the wavelength of maximum intensity while the fluorophore is excited through a group of consecutive wavelengths. The strokes shift is the wavelength difference between their peaks and varies with the dye and its environment. The overlap of excitation and emission intensities and wavelengths must be eliminated.

Due to all this properties, fluorescence microscopy is highly used in biological and biomedical science where fluorescence probe specificity and sensitivity can provide important information regarding the biochemical, biophysical ad structural status of cells and tissues. One important aspect that has to be considered, while studying the different biological systems by fluorescence microscopy, is the use of the fluorescent probes; such as GFP vectors, organelle's specific dyers and immunofluorescence.

4.c.) NADH and flavoproteins autofluorescence: The endogenous compounds that act as hydrogen carriers, which ferry the protons and electrons from carbohydrates to the electron transport chain have fluorescent properties. Autofluorescence can be used as an indicator of changes in cellular metabolism, as its properties change when the carrier binds to electron.

The fluorescence of the pyridine nucleotide NADH is excited at 350 nm, in the ultraviolet (UV), and emits at 450nm [121]. The oxidized form, NAD^+, is not fluorescent. Thus, an increase in UV-induced blue fluorescence indicates an increase in the ratio of NADH to NAD^+ and a net shift in the pyridine nucleotide pool to the reduced state. The binding of NADH to membranes enhance the fluorescence

while enzymatic binding tends to quench the cytosolic fraction [120]. Any light above 390 nm is likely to excite flavoprotein fluorescence, also it is important to keep in mind that flavoproteins fluorescence changes inversely with the degree of reduction. The emission may be measured using a wide bandpass filter with a peak at 450 nm and a bandwidth from ± 20 to 40 nm. The fluorescence tends to bleach, and excessive illumination can cause photodamage to the cell.

Flavoprotein fluorescence has an excitation at 450nm and it is emitted at 550nm. A bandpass filter 550±40nm can be used for measuring emission. A decrease in flavoproteins autofluorescence reflects an increase in the ratio of reduced to oxidized flavoproteins, which is the inverse of the response of the pyridine nucleotides. It has been shown that in cardiomyocytes, which mitochondria may represent 40%-50% of the cell volume, and sensory neurons produce very robust signals.

5. Principle of confocal microscopy

The confocal scanning microscope was invented and built, in 1955, by Marvin Lee Minsky. The confocal microscope combines the ideas of point-by-point illumination of the specimen and rejection of out-of-focus light, thus confocal approach is the use of spatial filtering to eliminate out-of-focus light in specimens that are thicker than the plane of focus. Minsky's first design used a pinhole placed in front of a zirconium arc source as the point source of light. The light was focused by a microscope objective at the chosen focal plane in the specimen, and light that passed through was focused by a second objective lens at a second pinhole confocal to the first pinhole. Any light that traveled through the second pinhole struck a low-noise photomultiplier, which produced a signal that correlated to the intensity of the light from the specimen. The second pinhole barred light originated from above or below the plane of focus in the specimen from reaching at the photomultiplier. To build an image, the focused spot of light was scanned across the specimen. Minsky's writings also described a reflected light version of the microscope that used a single objective lens and a dichromatic mirror arrangement, which became the basis of the current systems.

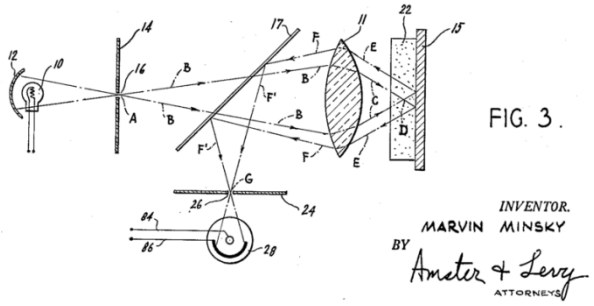

Figure 27. Confocal point sensor principle from Minsky's patent: Minsky patented the principle of confocal imaging in 1957. The optical path of a reflection confocal microscope.

Fluorescence microscopy relies on the properties of fluorochromes, which absorb the energy carried by photons in a given band of wavelengths and emits new photons in a longer band of wavelengths. The first fluorescence microscopes were based on a very simple design directly derived from classical transmission microscope. With the development of more accurate equipments and devices, fluorescence microscopes have evolved up to a highly specialized confocal microscopy. Modern confocal microscopes have kept Minsky's design: the pinhole apertures and point-by-point illumination of the specimen [122].

5.1. Confocal laser-scanning microscope (CLSM)

This imaging process is based on the use of a high intensity source of light, laser, limited in size to a single spot. Its fundamental idea is to prevent out-of-focus photons from ever contributing to the recorded image. This is achieved first by illuminating the specimen with diffraction-limited focused beams of laser, which are subsequently detected point by point with a photomultiplier tube (PMT) during the scanning of the sample. The images produced by scanning the specimen are called optical sections. Those photons coming from out-of-focus regions are prevented from reaching the detector by placing an imaging aperture in front of it [119]. Also it allows to control depth of field, elimination or reduction of background information away from the focal plane, and collects serial optical sections from thick specimens. In addition, a computer controls the scanning mirrors or other scanning devices to facilitate the collection and display of images.

Confocal microscopes provide a marginal improvement in both axial and lateral resolution, as well as high-quality images from both fixed and living cells and tissues, labeled with one or more fluorescent probes but it provides optical sectioning that greatly improves image readings. Moreover, confocal microscopy enables the automated collection of three-dimensional (z-series) data, and improves the specimen images using multiple labeling.

The lateral resolution is given by the Abbe equation ($r = 0.6\lambda / NA$), where λ is the wavelength and *NA* is the numerical aperture of the objective lens of the microscope. The numerical aperture is defined as $n \sin \alpha$, where n is the index of refraction of the object medium and α is the half angle of light collection of the objective.

The axial distance in the specimen space that is in focus in a single image is the depth of the field. The CLSM creates very thin optical slices through the specimen, such images reject light from out-of-focus planes almost completely; the smaller depth of field and the rejection of out-of-focus information achieved give a remarkable detail and quality images [120].

Light originating from the in-focus crossover point of illuminating light beam is focused to a small spot precisely at the pinhole, this in-focus light passes through the pinhole to a photomultiplier beyond. Light originated from above and below the focal plane forms crossover spots behind and in front of the pinhole, respectively. Therefore, light from planes above and below the plane of focus is spread out at the pinhole and selectively blocked. The pinhole placement in the objective image plane permits selective transmission of in-focus light with rejection of out-of focus light. This optical design is the basis for creating thin optical slices through thick specimens.

The diameter of the pinhole relative to the magnification and NA of the objective lens determines the axial resolution of a confocal microscope.

Moreover, confocal microscopes allow creating sharp optical sections that can be used to build 3D renditions of the specimen. Specimen recordings piled up from a series of optical sections, imaged at

short and regular intervals along the optical axis, can be used to create the 3D reconstruction. Many software available in the market combine the 2D images to create the 3D rendition.

Together, the laser, dichroic mirror, scan generator, objective lens, pinhole, photomultiplier, and computer form the essential elements of a laser scanning confocal microscope.

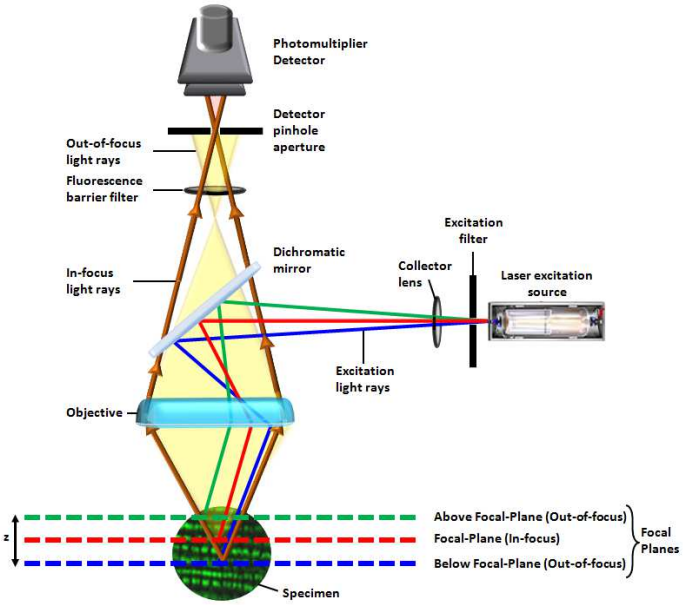

Figure 28. Mechanics of confocal microscopy: The laser beam passes through neutral density and barrier filters and is focused on a pinhole, which acts as a point source of light. The dichroic mirror reflects the laser beam through the x-y scan generator and objective lens onto the specimen. Fluoresced (or reflected) light passes back through the objective, scan generator, dichroic mirror, and emission barrier filter to be focused on a pinhole placed in the image plane. Light from the in-focus specimen plane passes through the pinhole to a photomultiplier. Light from out-of-focus planes is spread out at the pinhole and does not pass through to the photomultiplier. Photomultiplier output goes to a computer.

Despite of its high resolution images, confocal microscopy has inherent resolution limitation due to diffraction. The diffraction pattern resulting from a uniformly-illuminated circular aperture that has a bright region in the center is referred to as an Airy disk which together with the series of concentric bright rings around is called the Airy pattern and contains 84% of the luminous energy; an Airy disk size depends on the wavelength of the light source and the numerical aperture of the objective lens. The Airy disk limits the maximum resolution that can be attained with the confocal microscope. Resolution along the optical axis is also limited by diffraction effects, as in the lateral direction there is a periodic but elliptical distribution of intensity in the shape of an Airy disk [123]. The smaller the

Airy disks projected by an objective in forming the image, the more detail of the specimen that becomes appreciable. Objective lenses with higher numerical aperture are capable of producing smaller Airy disks.

Furthermore, the optical sectioning provided by confocal microscopes derives from having a pinhole that rejects out-of-focus light rays and the optical sectioning strength depends strongly on the size of the pinhole [123]. Thus, the pinhole prevents light originated from anywhere but the plane of focus from reaching the detector. The rule of thumb to obtain a desirable image is to make the pinhole about the size of the Airy disk.

In CLSM one important element to keep in mind, due to its sensitivity and noise behavior, is the photomultiplier tube (PMT), the most common detector, which captures light from the specimen. PMT sensitivity is characterized by the quantum efficiency, and is limited by Poisson statistics. That is, the accuracy of the measurement is improved by increasing the number of photons arriving at the detector; this is obtained by averaging data from many frames or by increasing the intensity of the fluorescence signal. Regarding the fluorescence, it can be increased by dyeing the specimen with a larger concentration of fluorophore molecule or by raising the intensity of the excitation light. Increasing fluorescence by increasing the excitation light intensity leads to an eventual saturation of the fluorophore. Higher intensities drive a larger fraction of fluorophore molecules into excited states, which in turn lead to a smaller fraction of ground state of molecules.

5.1.a.) Differential interference contrast (DIC): It is a technique used to enhance the contrast in unstained, transparent samples, works by separating a polarized light source into two orthogonally polarized mutually coherent parts which are spatially displaced at the sample plane, and recombined before observation. Adding an adjustable offset phase determining the interference at zero optical path difference in the sample, the contrast is proportional to the path length gradient along the shear direction, giving the appearance of a three-dimensional physical relief corresponding to the

variation of optical density of the sample, emphasizing lines and edges though not providing a topographically accurate image.

5.1.b.) Deconvolution: It is based on the reverse transform of convolution. The convolution transforms the distribution of a point light source in the object plane into a diffraction spot (Airy disk) in the image plane. 3-D deconvolution in confocal microscopy reduces the difference between lateral and axial resolution. To “deconvolve” confocal 3-D sets, it is necessary to measure the point spread function (PSF), which describes the relationship between a real object and its image formed in the microscope.

5.1.c.) Two photon microscopy: It uses the same scanning system as the LSCM, but does not require the pinhole aperture at the detector. The pinhole is dispensable because the laser excites the fluorochrome label only at the point of focus, eliminating the out of focus emission. Moreover, it naturally provides confocal imaging of planes much deeper in the sample, and with considerably higher light-gathering efficiency, as well with less fluorescence bleaching and specimen damage outside of the focal plane due to the reduced energy absorbed from the laser beam [123]. The fraction of the short wavelength excitation beam that reaches the focal plane is reduced by absorption in the intervening material. By focusing a pulse of very intense laser beam with twice the wavelength (half the frequency) of the standard short wavelength excitation beam, and with a period shorter than the fluorescence decay time of the fluorophore; the coherently interfering photons can excite molecules at half the wavelength of the long wavelength laser, and “selectively” in the focused spot. The output of an intense near-infrared (IR) laser induces fluorescence in a blue or UV excitable fluorophore at the focused spot where the coherent electromagnetic field strength is so high that it acts nonlinearly to excite the chromophores at twice the frequency if the IR field. The fluorophores in the cone of the illuminating light above and below focus do not experience the two-photon effect, and therefore, are not excited or damaged [123].

5.2. Dynascope prototype

It has two independent scanner groups LSM 7 Live DuoScan and LSM 7 DUO. This system gathers different imaging techniques such as two-photon and multiphoton laser, FLIM, FRAP, FRET, FCS, ICS, and live mode. This system allows processing and analyzing the images in 3D and 4D.

6. Principles for the dynamics analysis.

To analyze time series images a correction of the average level of fluorescence through time was performed, where an equal number of pixels in the final image have its available brightness of fluorescence. The shape of the transfer function can be straightforwardly determined from the brightness histogram of the original image. The method expands the contrast in regions of high gradients, so the details are easier to see [124]. Fluorescence correction of the images was done using the software ImageJ.

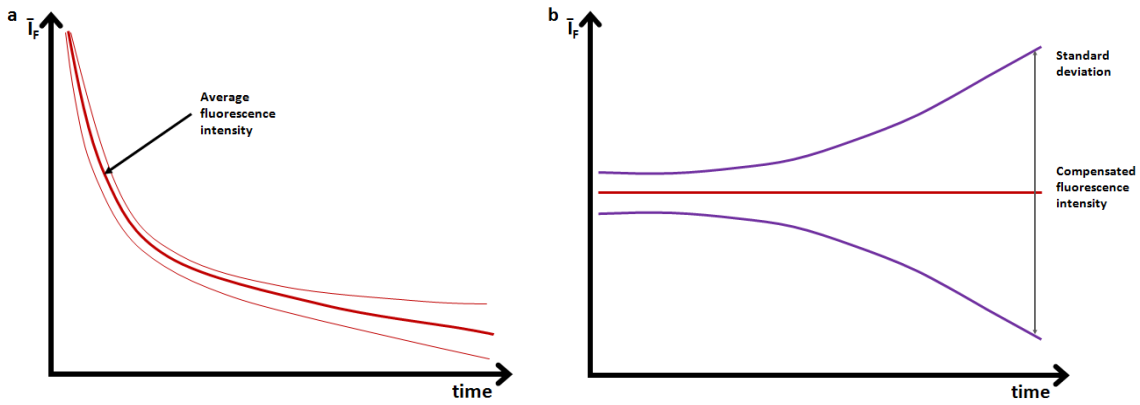

Figure 29. Plot of a) fluorescence intensity versus time and b) fluorescence compensation plot: a) It displays how fluorescence decays through the time, photobleaching. b) The corrected fluorescence intensity versus time shows how the background noise is increasing through time.

Once we obtained these values, we were able to do the Fourier transform for the intensity plots and its covariance, and dynamics analysis of the transfected cardiomyocytes.

Fourier-space is extremely useful in discussing optical imaging because the process of imaging can be modeled by simply multiplying the Fourier transform of the sample.

Most of the image processing and image analyzes were performed with the ImageJ public domain software using scripts and plug-ins especially developed for this work. The first part of the image processing was the correction of the average level of fluorescence through the time to compensate photobleaching (long time-series of 2000 to 3000 frames). Because the aim was to characterize the proper motion of mitochondria it was necessary to correct the frames for all global motions such as cell contraction and/or cell drift that may occur over long duration recordings. To achieve this goal, XT projections (for the z-line channel) and YT projections (for the mitochondria channel) were calculated for each time series. For example YT projection (Fig. 33) consisted in building a column of pixels for each frame in which each pixel correspond to the average intensity of the corresponding pixel row of the frame. Thus we built the YT projection by compiling the calculated columns in a single image where the horizontal axis accounted for time. This representation offered the advantage to summarize all the vertical motions during the recording. The next step consisted in calculating cross-correlation curves between each successive pair of columns and shifting up or down one frame with respect to the other by an amount depending on the maximum of cross-correlation. Using this method for both XT projection (horizontal motion) and YT projection (vertical motion), it was possible to cancel out most of the global motions due to cell drift and cell contraction.

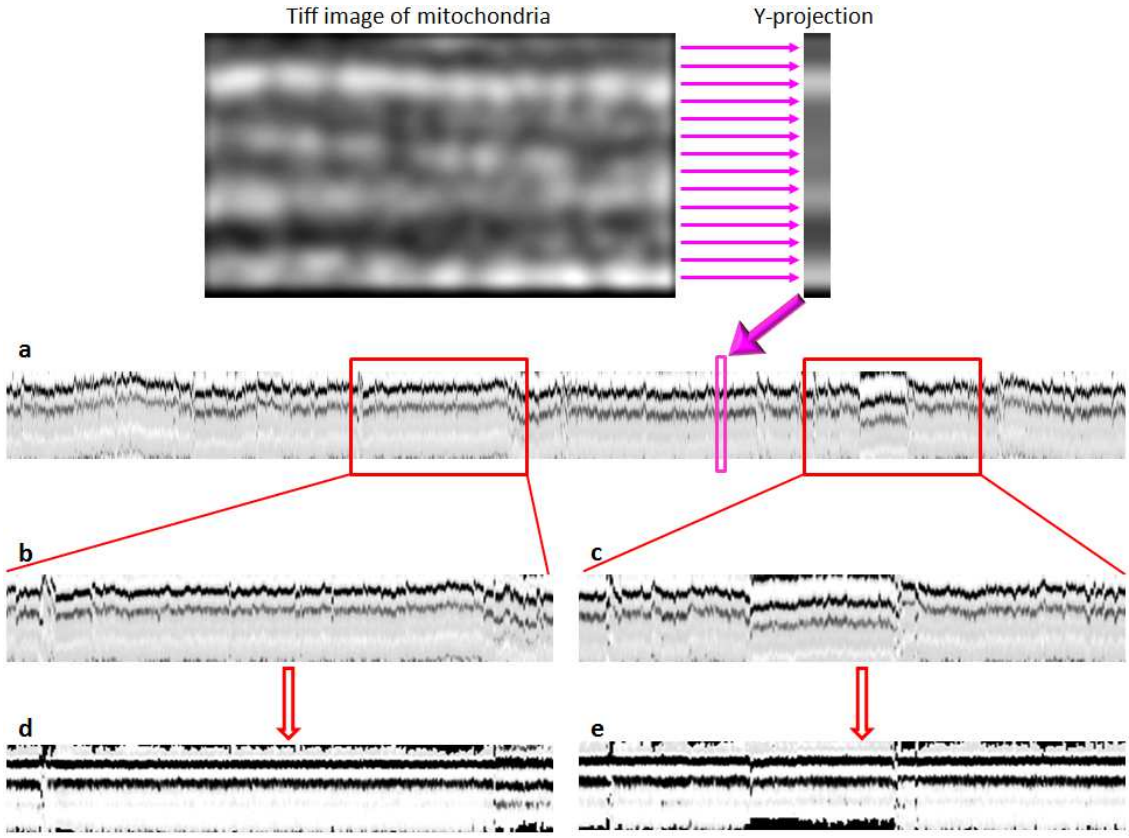

Figure 30. Alignment of global motion: An example (pink box) of how the tiff image of the mitochondria was taken to make the Y-projection at each pixel a) Raw results of the time series images (2000 frames)

b) and c) Zoom fragments of the raw time series images.

d) and e) Zoom fragments of the registered time series.

6.1. Fourier transform

It was used to characterize the spatial positioning and frequency of Z-lines and mitochondria. It is a mathematical operation that expresses a function of time or space as a function of frequency, known as its frequency spectrum. It is a major image processing tool which is used to decompose an image into a harmonic series of sine and cosine components. The input image is the spatial domain equivalent, while the output of the transformation represents the image in Fourier or frequency domain. In the Fourier domain image, each point represents a particular frequency contained in the spatial domain image.

The frequency domain is a space in which each image value at image position F represents the amount that the intensity values in image I vary over a specific distance related to F. In the frequency

domain, changes in image position correspond to changes in the spatial frequency are changing in the spatial domain image I.

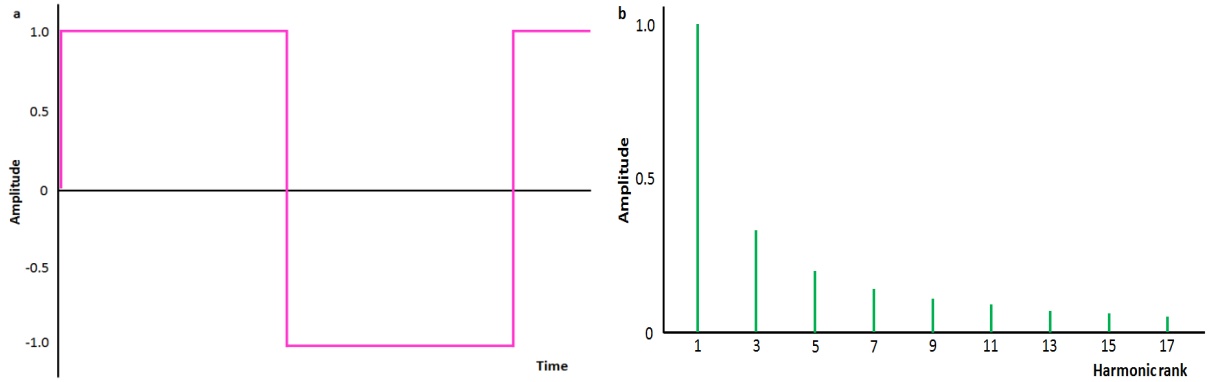

Figure 31. Plot of one dimensional Fourier transform a) of time signal and b) one spectrum of a square signal: a) It shows the original square wave of the signal.

b) It composed of odd harmonics, the amplitude of the harmonic is 1/(rank of harmonic).

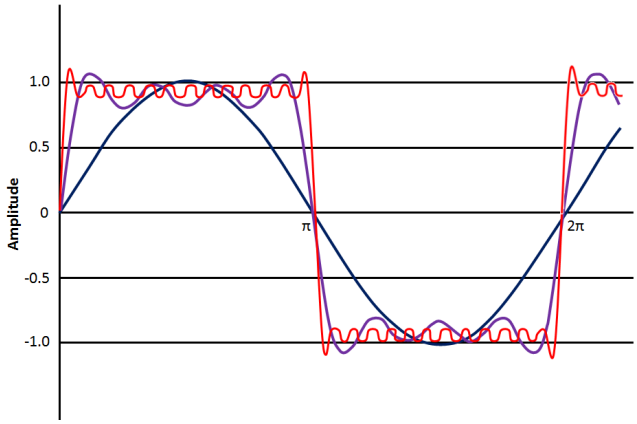

Figure 32. Plot of the Fourier expansion of sine waves: the three curves show the one term (dark blue line), four terms (purple line) and thirteen terms (red line).

6.2. Cross-correlation

To find if there was an association between z-lines and mitochondria, a cross-correlation analysis was done. It is a standard method of estimating the degree to which two time series are correlated. It considers two series - Z-lines (autofluorescence) and mitochondria (mitotracker red) -, providing the similarities and dissimilarities by shifting stepwise one reference to the other. It provided the value in a range between -1 and +1. A negative value means that both series are varying in opposite ways, hence they are alternating between them. Meanwhile a positive cross-correlation shows a strong superimposition of both series.

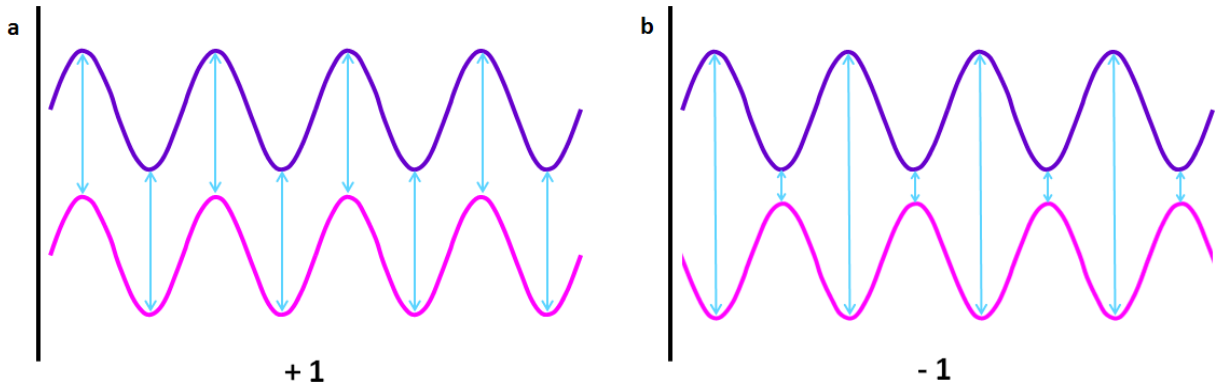

Figure 33. Cross-correlation schemes:

a) A positive cross-correlation has a strong superimposition of both fluorescent signals.

b) A negative cross-correlation shows an opposite variation of both fluorescent signals, thus alternating between them.

6.3. Image processing

6.3.a) Gradient clustering algorithm: To calculate automatically the number of mitochondria and the position of their fluorescence centers (virtual mass centers) a gradient clustering algorithm was used to calculate them automatically [125]. The algorithm relies on a physical analogy: where a fluorescent pixel is considered as a physical object characterized by a couple of coordinates *x* and *y* (i.e. the initial position on the image grid) and a weight (virtual mass) equal to the fluorescence intensity at this point. Virtual masses concentration (fluorescence intensities) in particular regions of the images (i.e. mitochondria) creates gravitational wells, attracting the neighboring points. Actually, the algorithm calculates local intensity gradients in order to aggregate in an iterative manner the points belonging to the same mitochondrion.

After a number of iterations these points will occupy a single position corresponding to the mass center of the mitochondrion, which acts as a gravitational attractor. Explained in a pragmatic way, at the beginning, all of the pixels images with a fluorescence intensity greater than a fixed threshold are converted into points defined by their coordinates (*x*, *y*) and an associated mass (*m*) which corresponds to the pixel intensity. On each image, the mass center within a fixed neighborhood is calculated. After one iteration step each point is translated toward the nearest mass center, traveling a fraction of the distance between its initial position and the mass center. The sum of all the resulting point motions is calculated and used as a criterion to monitor the clustering process. The process is

iterated until the sum falls under a pre-set threshold for which it is considered that the clustering process is achieved. To complete the algorithm, a merging procedure is applied where all the points with the same coordinates are merged into a unique point, which is considered as the mass center of a single mitochondrion.

Using this clustering technique and under the hypothesis of an invariant Point Spread Function, it was possible to obtain the location of the fluorescence centers with a better accuracy than the actual optical resolution. The positions of these fluorescence centers directly depend on the configuration of the inner mitochondrial membrane to which the fluorescent dye used is fixed.

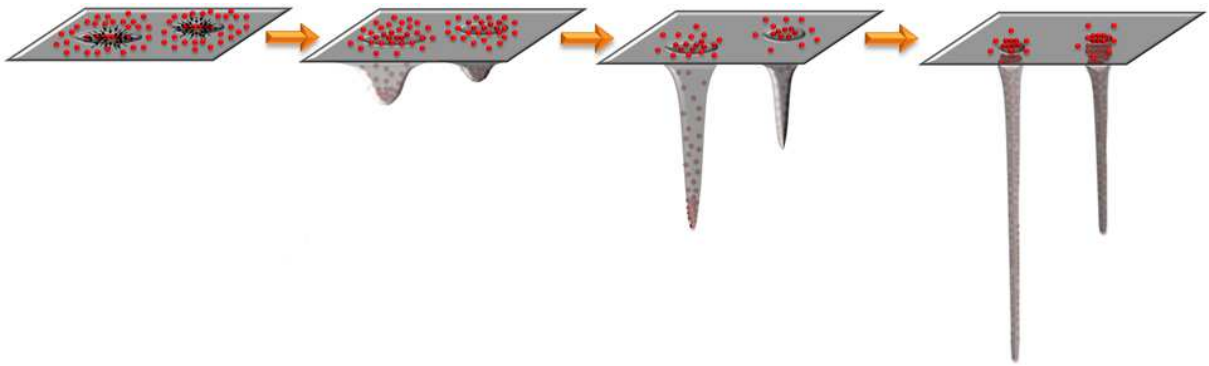

Figure 34. 3-D diagram of clustering technique in two mitochondria: It displays how the mitochondrial fluorescent centers were obtained. Red dots symbolize the pixels obtain in each image acquired. Dots are converging to find their fluorescent local centers.

6.3.b.) Quantification of mitochondrial fluctuations: The trajectories of the fluorescence centers were plotted as a function of time and the average scatters parallel to the long axis of the myocardial cells and to the short axis were calculated for each mitochondrion. In order to express the motion of mitochondrial fluorescence centers in terms of a random-walk movement process, similar to Brownian movement of particles [126], the average squared distances (d^2) as a function of time (t) were plotted using two models: second order polynomial or linear. The fitted mean second order polynomial curve ($d^2 = at^2 + bt + c$) models the motion behavior as combination of random walk and a translational process. In such model the a constant may be assimilated to the apparent velocity component, and the b constant relates with the apparent mobility constant D. The apparent mobility constant D is analogous to the apparent diffusion constant and was determined from the slope b of

the fitted mean square linear curve ($d^2 = bt + c$). In this expression, the parameter c is related to the initial coordinates of the mitochondrial centers studied. For $c = 0$ the expression can be reduced to the expression $d^2 = bt$, which may be taken equivalent to a general expression for random-walk mechanism based on the Einstein-Smoluchowski's equation [127, 128] for Brownian movement in two dimensions, $d^2 = 4Dt$, which gives the relationship among, diffusion coefficient (D) distance of displacement (d) and time (t) of this displacement t [129-132]. Thus, the apparent mobility constant D calculated from the slop b of the fitted mean squared linear curve ($d^2 = bt + c$) can be used as a quantitative measure of fluctuations of the fluorescence centers of mitochondria.

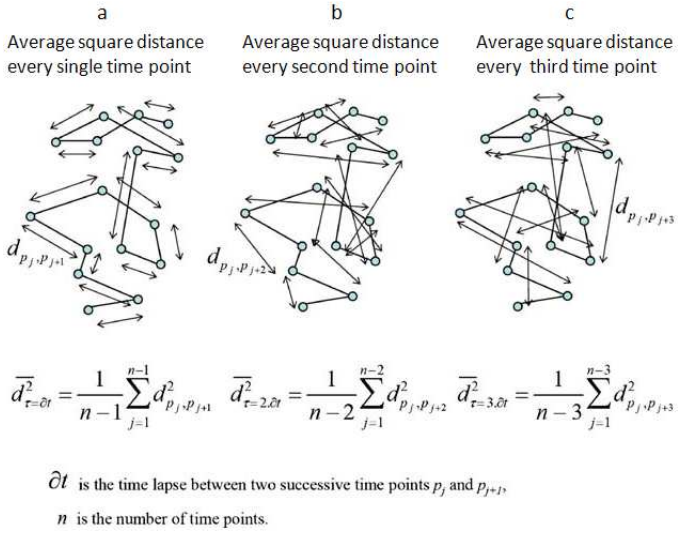

Figure 35. Principle of analysis of velocities of mitochondrial movements in cells *in situ*: a, b, and c) Analysis of the random walk (Brownian) movement at three consecutive times points of observations. Showing how the average square distances are calculated for a series of trajectory points. Reproduced with permission [97].

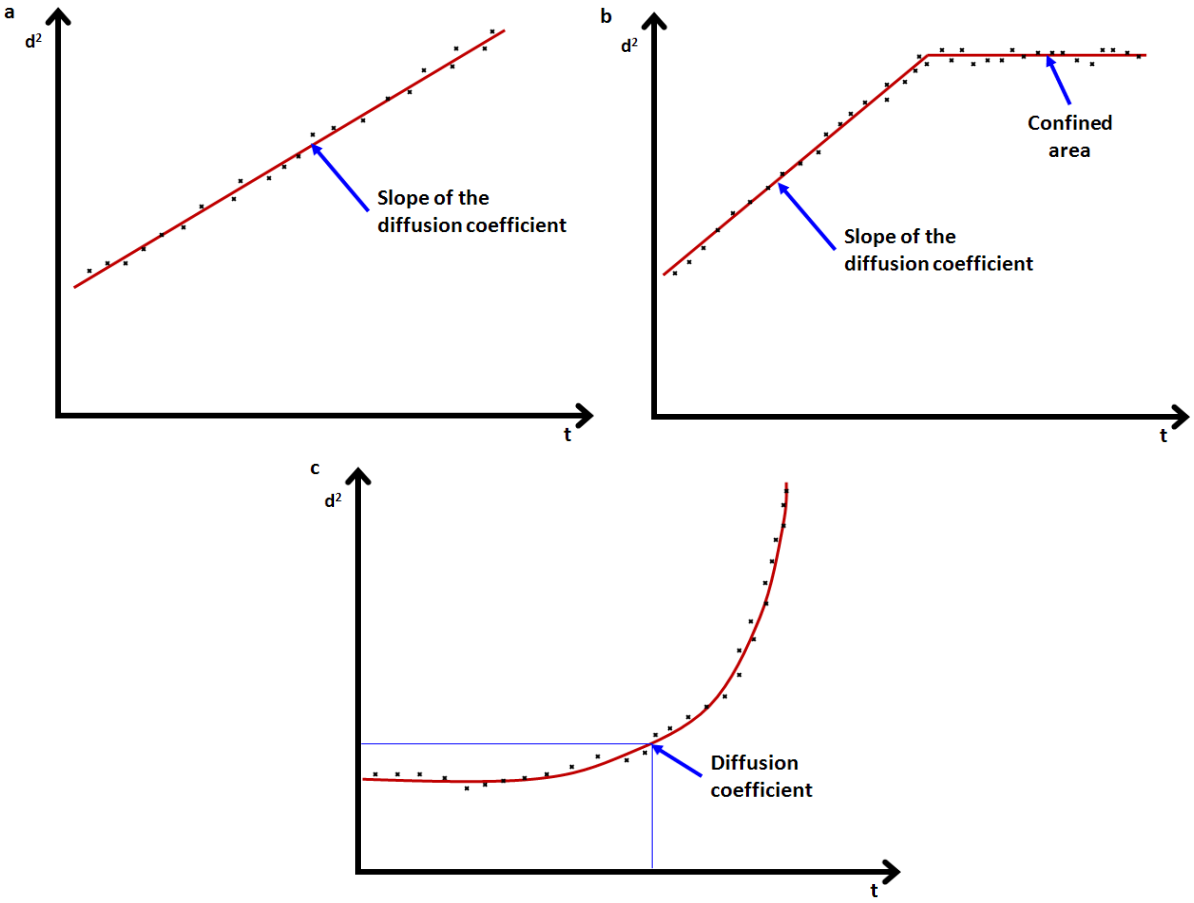

Figure 36. Example plots of the mean square distance vs time for:

a) Unlimited-random walk

b) Random walk in a confined space, and

c) Constant motion

V. RESULTS

1. DISCOVERY OF SPECIFIC β-TUBULIN ISOTYPES IN ADULT RAT CARDIAC CELLS

(Article 1)

This section shows the studies of distribution and possible functional roles of four β-tubulin isotypes in adult rat cardiac cells.

Cardiomyocytes structural-interactions of β-tubulin and MOM was discovered by Sætresdal in the early 90's [61], thereafter Rostovtseva in 2008 found how tubulin vastly increase VDAC sensitivity to voltage and proposed a tubulin-VDAC interaction through tubulin carboxyl-terminal tail (CTT) [46]. Therefore, to reveal the significance and possible role of β-tubulin isotypes, fixed adult rat cardiomyocytes were immunolabeled with anti-tubulin βI (gene TUBB or TUBB5), βII (gene TUBB2A and TUBB2B), BIII (gene TUBIII), and βIV (gene TUBB4).

Mitochondria of adult rat cardiac cells and HL-1 cells were visualized using Mitotracker™ Green and Red probes. Widely described by many groups [99, 114], figure 40 displays mitochondrial distribution in two different cell types. Cardiomyocyte mitochondria exhibited a highly organized "crystal-like" pattern whereas NB HL-1 cells displayed chaotic filament-like structures. These very different mitochondrial arrangements between cardiomyocytes and NB HL-1 cells confer very specific functional and enzymatic properties on each of them [133].

The specific arrangement of cardiac mitochondria is related to its complex interactions with cytoskeletal structures in the cells. Mammalian cardiac mitochondria are functionally coupled to multiple intracellular ATP-consuming processes by energy transfer and metabolic feedback signaling networks within highly organized energetic units [22]. In contrast, NB HL-1 cells are characterized by their randomly organized filamentous dynamic mitochondria, which are subject to fission and fusion transitions [114].

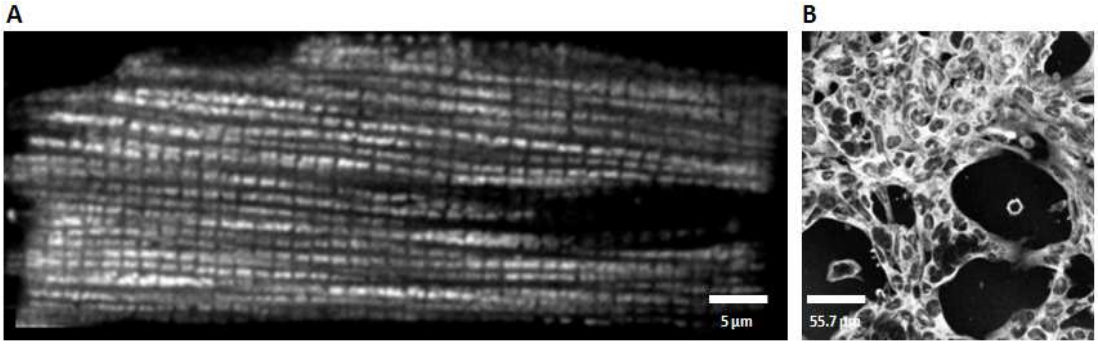

Figure 37. Fluorescent microscopy imaging of mitochondria fluoroprobes:

A. Cardiac mitochondria were visualized using 0.2 µM MitoTracker™ Green. Scale bar 5 µm.

B. Mitochondria in NB HL-1 cells were seen using 0.2 MitoTracker™ Red. Scale bar 55.7 µM.

Immunostaining of each tubulin β isotypes revealed a specific distribution of each one along the fixed cardiomyocytes. These suggested that each tubulin β isoform has a specific role in the adult rat cardiomyocytes. Results of general anti-β-tubulin are in agreement with previous observations [61, 62, 83]. General β-tubulin exhibited a longitudinally, obliquely and diffusely distributed tubulin, whereas tubulin βI labeled with Cy5 had a diffuse intracellular "dotted-like" pattern. Tubulin βIII displayed a prevalent arrangement in transversal lines that co-localized with sarcomeric Z lines. βIV-tubulin displayed polymerized longitudinal- and oblique-oriented microtubules.

Finally, the most remarkable tubulin isotype-arrangement was tubulin βII. To avoid any artifact, anti-βII-tubulin was labeled with FITC and Cy5. Tubulin βII immunolabeling revealed a very regular localized distribution in rows along the long-axis of the cell. This distribution resembles mitochondrial distribution. This result is considerably outstanding since it agreed with previous studies by Rostovtseva [46], where it was shown the role of tubulin in VDAC's regulation. This discovery may suggest that βII-tubulin association with MOM decreases VDAC permeability selectively, *i.e.* limiting MgATP and MgADP molecules.

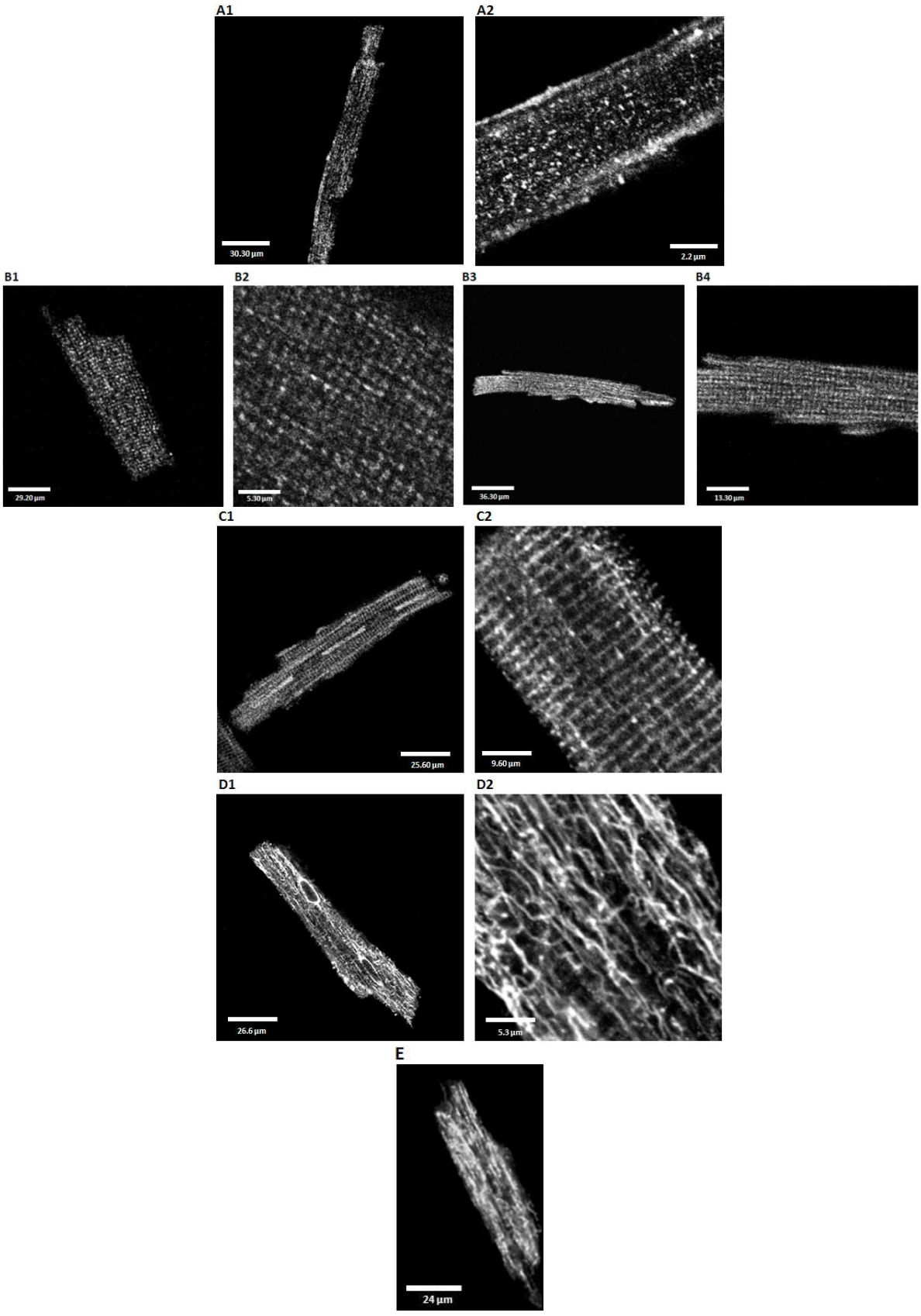

Figure 38. Immunofluorescent confocal microscopy imaging of β-tubulin isotypes in fixed cardiomyocytes:

A1. Diffusive intracellular distribution of tubulins labeled with anti-βI-tubulin antibody. Scale bar 30 µm.

A2. Zoom portion of tubulin βI. Scale bar 2.2µm.

B1 and B3. Tubulins labeled with anti-βII labeled with Cy5 (B1) and FITC (B3). Scale bar 29.2 µm and 36.3 µm, respectively.

B2 and B4. Zoom portion βII labeled with Cy5 (B2) and FITC (B4). Scale bar 5.3 µm 13.3 µm, respectively.

C1. Tubulin labeled with anti-βIII-tubulin antibody and FITC. Scale bar 25.6 µm.

C2. Zoom portion of tubulin βIII. Scale bar 9.60 µm.

D1. Tubulin labeled with anti-βIV-tubulin antibody and Cy5. Scale bar 26.6 µm.

D2. Zoom section of tubulin βIV. Scale bar 5.3 µm.

E1. Longitudinally, obliquely and diffusely total β-tubulins labeled with anti-β-tubulin antibody and FITC. Scale bar 24µm.

In contrast, immunolabeling of fixed HL-1 cells with tubulin isotypes showed a completely different distribution of tubulin isotypes in this cancer cell line. βI-tubulin labeling had a similar distribution as in adult cardiac cells, diffuse "dotted-like" pattern. Immunofluorescence revealed the absence of tubulin βII in this cancer cell-line. Tubulin βIII was evidently diffused and its presence were in agreement with previous studies, where patients with aggressive evolution of ovarian, lung, pancreas, breast cancer and melanoma, the overexpression of it had a valuable prognostic factor [134, 135]. This suggests some interdependence between intracellular βIII-tubulin distribution and cancer metastasis. Lastly, tubulin βIV displayed a filamentous, "bundle-like" arrangement; therefore, the absence of a polymerized microtubular network may explain why HL-1 cells acquire a spherical shape in suspension and a spread shape in culture.

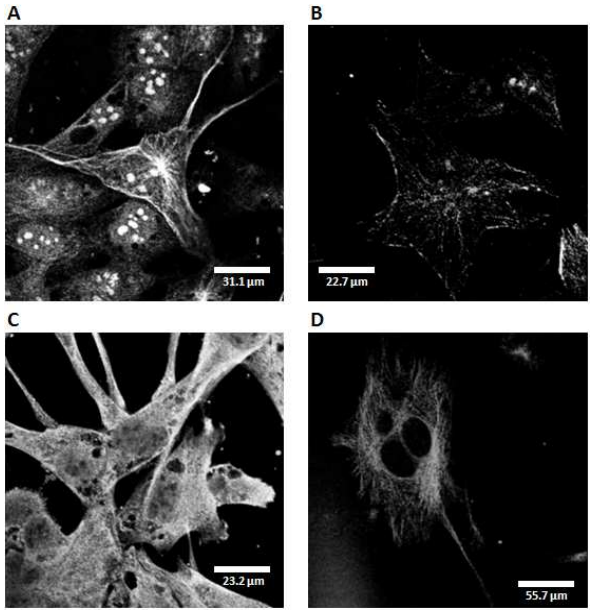

Figure 39. Immunofluorescent confocal microscopy imaging of β-tubulin isotypes in fixed HL-1 cells:

A. Tubulin labeled with anti-βI-tubulin antibody and Cy5. It had a diffuse distribution. Scale bar 31.1 µm

B. Tubulin label with anti-βII-tubulin antibody and Cy5. It is practically absent in this cancer cell line. Scale bar 22.7 µm

C. Tubulins labeled with anti-βIII-tubulin antibody and FITC. Scale bar 23.2 µm

D. Tubulin labeled with anti-βIV-tubulin antibody and Cy5. Filaments showed a radial distribution from the nucleus to cell periphery, creating also inter-connections among branches. Scale bar 55.7 µm

The following experiments were performed to confirm the specific distribution of tubulin βII isotype, once it was found its distribution. Z lines were immunolabeled using α-actinin -green- and mitochondria stained with MitoID -red-, figure 40 A and B, respectively. Figure 40C shows the absence of overlapping structure, therefore non evident mitochondrial fusion events can be appreciated. Images D and E displayed tubulin βII immunolabeling -red- and mitochondria autofluorescence, respectively. In figure 40F can be seen an overlap of tubulin βII with mitochondria which may suggest its possible role on VDAC's permeability. These results are in agreement with Sætersdal findings of β-tubulin association with mitochondrial membranes using immunogold labeling [61].

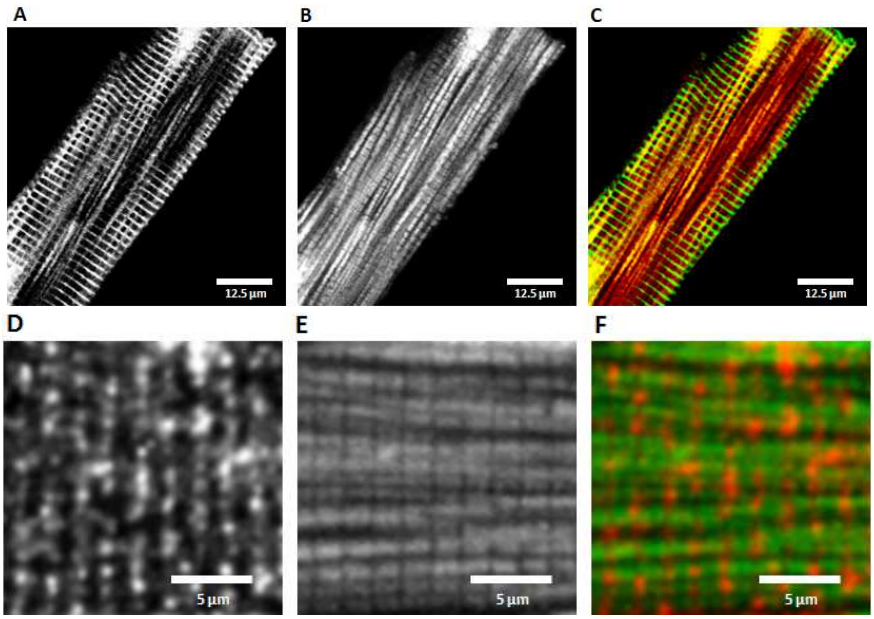

Figure 40. Immunofluorescent confocal microscopy imaging of α-actinin and βII-tubulin proteins, and fluorescent staining and autofluorescence of mitochondria in fixed cardiac cells:

A. Intensity fluorescence of FITC showed α-actinin positioning.

B. Intensity fluorescence of MitoID™ displayed mitochondrial arrangement.

C. Merged images of α-actinin (green) and mitochondria (red). Scale bars 12.5 µm

D. Intensity fluorescence of tubulin βII and Cy5. Fluorescent spots have a comparable arrangement to mitochondria.

E. Intensity fluorescence of autofluorescence displayed mitochondrial arrangement in cardiomyocytes.

F. Overlap images of tubulin βII (red) and mitochondria (green). Scale bars 5 µm.

Co-immunofluorescent labeling was done to get in depth of the possible role of the specific distribution of tubulin β isotypes in the structural arrangement of cardiomyocytes. α-actinin and tubulin βIII co-immunolabeling showed how these two proteins overlap. Figure 41A shows α-actinin, it had its pattern, situated in the characteristic sarcomeric transversal Z lines. It is in agreement with what has been previously well-established by several groups [25, 48, 136]. Image 41B displays βIII-tubulin distribution in the cardiac cell. These results suggest an interaction between α-actinin and tubulin βIII, which may also suggest a possible role of βIII-tubulin in the cardiomyocyte structural arrangement.

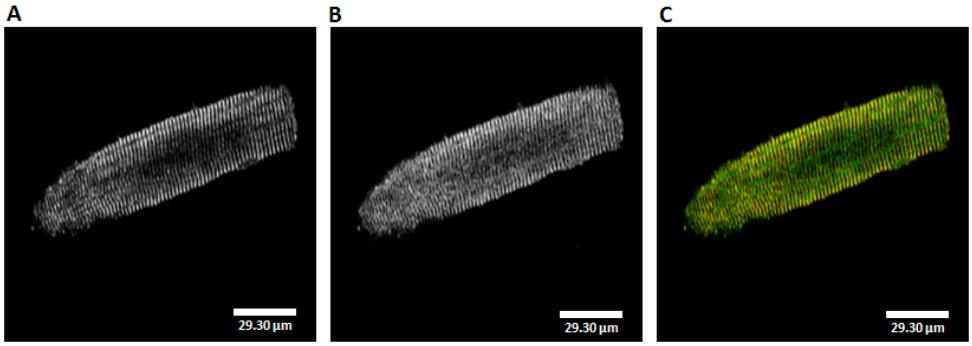

Figure 41. Co-immunofluorescent labeling of α-actinin and βIII-tubulin in fixed cardiomyocytes:

A. Fluorescence intensity of Cy5 showed α-actinin positioning.

B. Fluorescence intensity of FITC displayed tubulin βIII distribution.

C. Merged images of α-actinin (Red) and βIII-tubulin (Green). Scale bars 29.30 µm.

To complete these observations, isolated rat heart mitochondria were co-immunolabeled with tubulin βII -red- and VDAC -green-. Absence of tubulin βII can be explained by the fact that cytoskeletal proteins associated with mitochondria were removed during their isolation due to trypsin treatment. In contrast, the presence of VDAC was clearly detected.

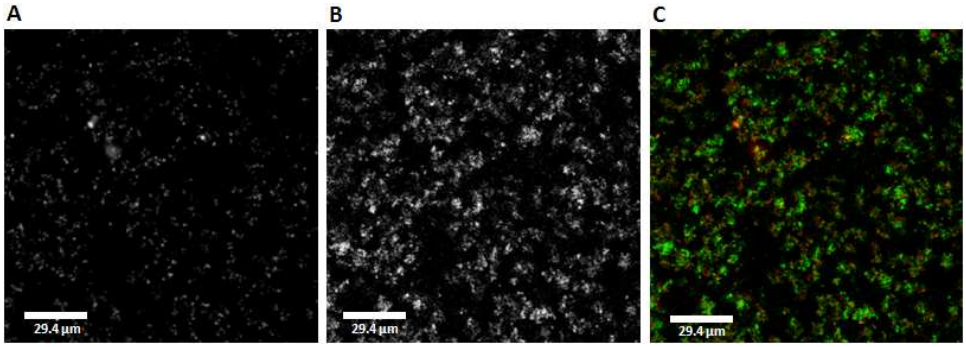

Figure 42. Co-immunostaining βII-tubulin and VDAC in isolated rat heart mitochondria:

A. Absence of tubulin βII in red fluorescence (Cy5).

B. VDAC in green fluorescence (FITC) in isolated heart mitochondria.

C. Overlap images of βII-tubulin and VDAC. Scale bar 29.4 µm.

Nonetheless, co-labeling of tubulin βII -green- and MitoID -red- in HL-1 cells showed the absence of tubulin βII. These observations are in conformity with Hiser findings [137], where βII-tubulin was found in only four cell lines and in very low abundance. This study was performed in 12 different human cancer cell lines.

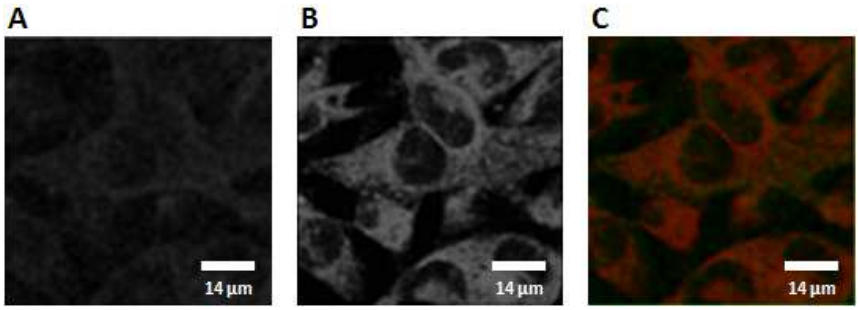

Figure 43. Co-immunofluorescent labeling of βII-tubulin and MitoID in fixed HL-1 cells:

A. Absence of βII-tubulin labeling.

B. Red fluorescence with Mito-ID™ shows distribution.

C. Merged images of βII-tubulin and MitoID. Scale bar 14 µm.

Confocal microscopy results were confirmed by Western blot analyzes of tubulin isoforms and MtCK, in different tissues and HL-1 cells. Purified total-brain-tubulin was used as a reference, which has a molecular mass of 55 KDa. The most outstanding result was the presence of MtCK and tubulin βII in heart left ventricle and their absence in HL-1 cells. These suggest us a different structural regulation

by tubulin βII and also enzymatically by MtCK, in healthy mammalian cells and immortal cell lines. These results are in agreement with previous studies by Patra [138], where they showed that MCK and sarcomeric MtCK progressively decreased as malignancy progressed, and they were virtually absent in full-grown tumors. All these results confirmed what was observed previously by confocal microscopy.

In contrast, the absence of MtCK in HL-1 cells is in agreement with previous observations by Eimre et al. [139], who showed that BCK is the only CK isoenzyme present in the NB HL-1 cells. In addition, these results were in agreement with functional tests (Fig. 48) where it is shown that creatine maximally activates the respiration in permeabilized cardiomyocytes but had no effect on the respiration of permeabilized HL-1 cells.

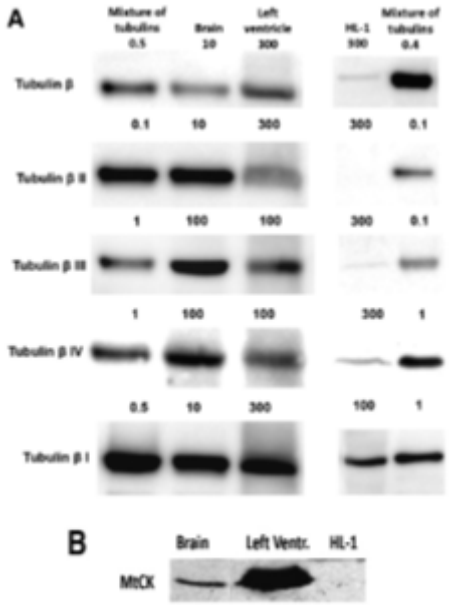

Figure 44. Western blots:

A. Various β-tubulin isotypes in different tissues and HL-1 cells.

B.MtCK in different tissues and HL-1 cells.

The effect and role of MtCK in cardiomyocytes were verified by functional respiratory test. Figure 45 displays the effect of creatine in cardiomyocytes and NB HL-1 cells. These results showed how

creatine maximally activates the respiration only in permeabilized cardiomyocytes and has no effect on permeabilized HL-1 cells.

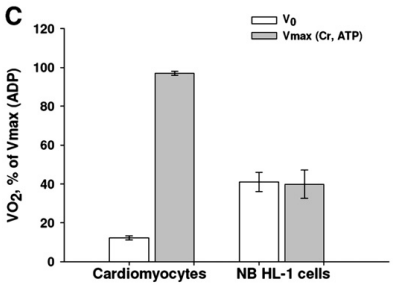

Figure 45. Creatine effect on the respiration of permeabilized cadiomyocytes and NB HL-1 cells: The rates are expressed as % of the maximal values (V_{max}) observed in the presence of ADP 2mM.

2. POSSIBLE ROLE OF STRUCTURAL PROTEINS (TUBULIN BETA II) IN THE REGULATION OF RESPIRATION

(Article 4)

The previous results of tubulin βII distribution had a very suggesting role, since its distribution was very akin to mitochondrial distribution. Therefore, a specificity test was an important aspect to verify the high affinity of the secondary antibody. Adult rat cardiac cells were labeled with secondary antibody Cy™ 5-conjugated AffiniPure goat anti-mouse IgG. Transmitted light was used to visualize the cardiomyocyte position. Figure 46A shows how cells incubated only with the secondary antibody did not label any intracellular structure.

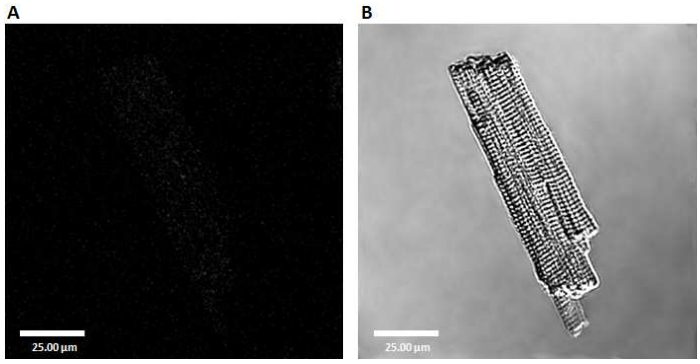

Figure 46. Specificity test for immunofluorescence Cy5-conjugated labeling:

A. Confocal image of isolated fixed and permeabilized cardiomyocytes with secondary antibody Cy5-conjugated AffiniPure goat anti-mouse IgG (Jackson Immunoresearch) without primary antibody.

B. Transmission image of the same cadiomyocyte. Scale bar 25 µm.

Figure 47 shows the distribution of tubulin βII in fresh-isolated fixed and trypsinated fixed adult rat cardiac cells. Fresh isolated adult rat cardiomyocytes fixed and incubated with tubulin βII, observed in figure 47A, showed a very regular distribution. This result goes in agreement with the previous results published by Guzun et al. [58], where it was proposed tubulin βII as the tubulin isotype in charge of VDAC's permeability.

In addition, structural-altered test by mild proteolysis (trypsin 0.05µM) was performed to show how βII-tubulin distribution was modified after trypsin treatment. Figure 47 shows how after a short proteolysis the fluorescence intensity decreased significantly and the regular arrangement of tubulin βII disappeared.

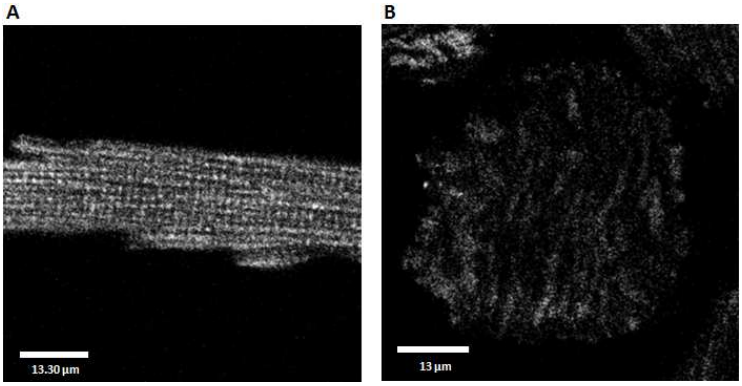

Figure 47. Immunofluorescence labeling of βII-tubulin with IgG-FITC:

A. Fixed and permeabilized cardiomyocyte without trypsin treatment.

B. Typsinated, fixed and permabilized cardiomyocyte. Scale bar 13 µm.

Due to autofluorescence of oxidized mitochondrial flavoproteins, previous results had to be confirmed by the use of red-fluorescence labeling. Therefore, tubulin βII distribution was observed using Cy5-conjugated AffiniPure as secondary antibody. Figure 48 shows the very regular distribution of tubulin-βII as previously observed with IgG-FITC -green fluorescence-. This highly specific

distribution completely matches with mitochondrial distribution. All these results highly suggested that βII-tubulin may be the tubulin isotype in charge of VDAC's permeability regulation.

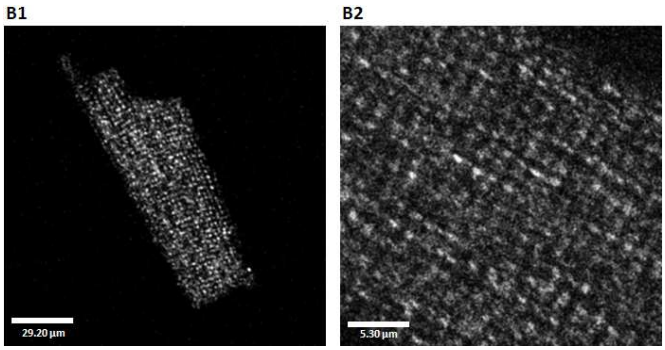

Figure 48. Immunofluorescence labeling of βII-tubulin with Cy5-conjugated AffiniPure.

Scale bars 25 µm (A) and 5.30 µm (B)

Proteolytic treatment before fixation of adult rat cardiomyocytes completely removed tubulin βII isotype. Figure 49 displays in red-immunofluorescence the complete removal of tubulin βII. In addition, proteolytic treatment changed the cell's shape due to the destruction of tubulin and cytoskeletal systems. These observations are in accordance with earlier observations of Vendelin and Beraud [62, 99], where it was showed the changes of intracellular arrangement of mitochondria from a regular distribution to an irregular-clustered distribution.

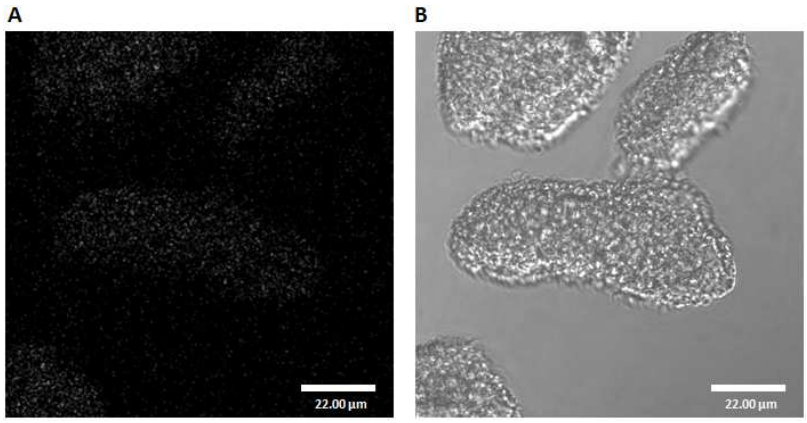

Figure 49. Immunofluorescence labeling of βII-tubulin with Cy5-conjugated AffiniPure after a short proteolysis treatment (trypsin 0.5µM) of permeabilized cardiomyocytes.

A. Confocal image of fixed and permeabilized trypsinated cardiomyocytes.

B. Transmission image of the same cells. Scale bar 22 µm

Figure 50 (A and E) displays the merged images of the intracellular distribution of α-actinin (Z line) and βII-tubulin with mitochondria. These results were obtained by the use of mitochondrial autofluorescence of flavoproteins, therefore adult rat cardiomyocytes were oxidized in an oxygen-saturated solution with rotenone before being fixed. Cells were permeabilized and immunolabeled with the respective antibody. Images were recorded by separated channels. The merged image (Fig. 50A) of immunostained cells with α-actinin showed a symmetrical interleaved distribution of mitochondria and Z lines. It should be noticed that mitochondrial autofluorescence by oxidized flavoproteins (green) was not detected in the Z line area. This confirms previous observations by Saks [41], where none mitochondrial fusion was observed in cardiomyocytes.

In contrast, merged image of immunolabeled βII-tubulin (Fig. 50E) showed a weaker fluorescence of both mitochondrial autofluorescence and tubulin βII, due to the overall staining of mitochondria. βII-tubulin was detected overall the cardiomyocyte including the Z line area. Therefore, tubulin βII seems to form network-like structures connecting mitochondria to other cytoskeletal structures. Images 50F and 50G confirmed with higher resolution previous observations of βII-tubulin co-localizing with mitochondria by Guzun et al. [58]. Although images had a resolution about 0.2µm, a better resolution is needed to obtain a more detailed analysis of protein localization at the submitochondrial level.

An interesting analysis that showed outstanding information regarding fusion-fission events were the intensity plots of α-actinin (Fig. 50D) and βII-tubulin (Fig. 50H). Intensity plots were done for the analysis of four mitochondria. The intensity plot of α-actinin and mitochondrial autofluorescence displayed the periodicity of Z lines between mitochondria. This confirmed previous observations by Beraud et al. [97], where it was demonstrated the absence of inter-mitochondrial connectivity in cardiomyocytes. Finally, both intensity plots (Fig. 50D and 50H) showed how the presence of tubulin βII on the mitochondria and α-actinin in Z lines makes a highly complex cytoskeletal organization of

cardiomyocytes. These analyzes suggest a highly ordered cytoskeleton that makes nearly impossible fusion and fission events.

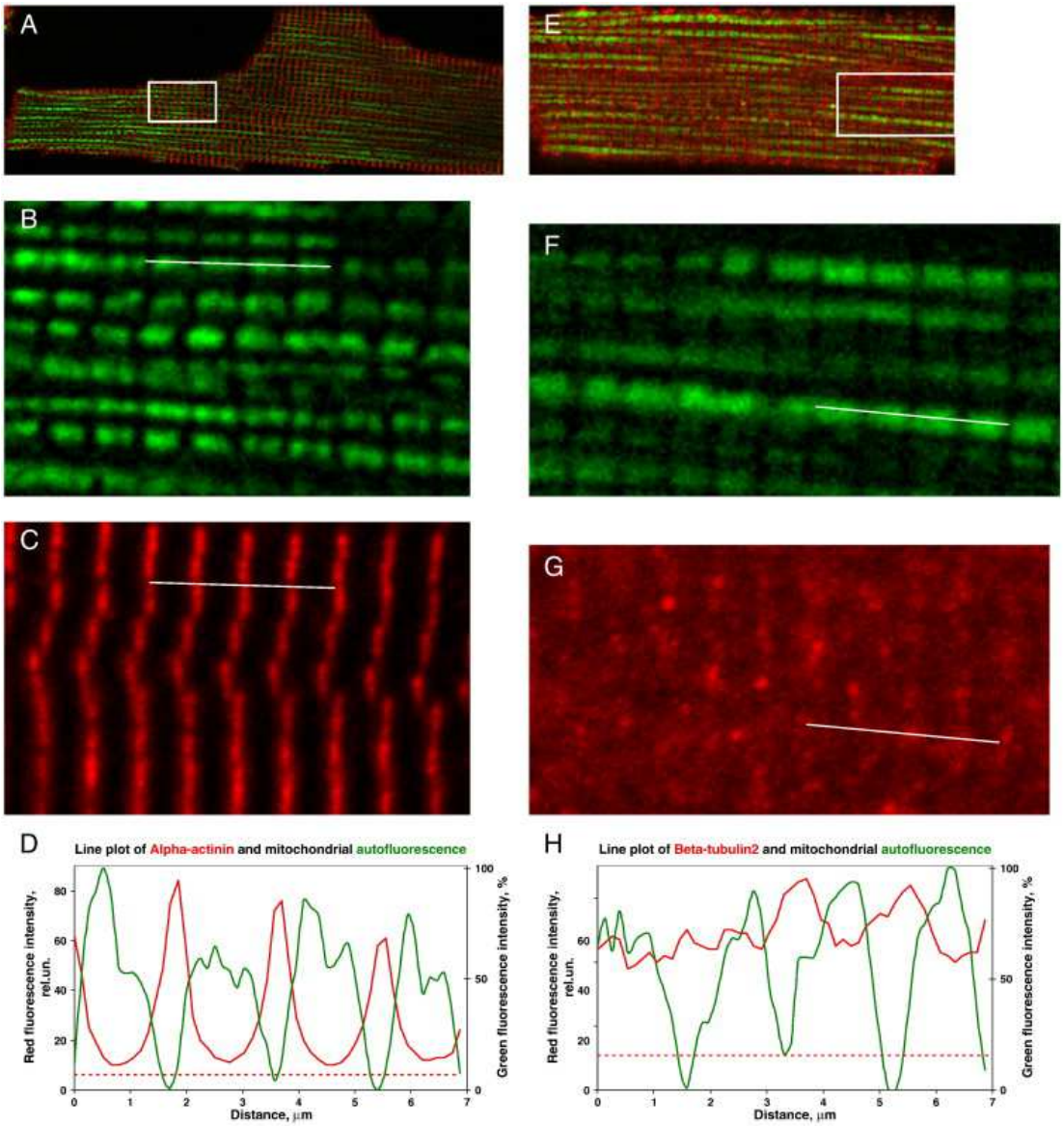

Figure 50. Comparison of the intracellular distribution of βII-tubulin, α-actinin, and mitochondria:

Confocal merged images of immunofluorescence labeling of α-actinin (A) or βII-tubulin (E).

Zoom regions of interest highlighted by the white rectangles in separated channels, panels B, C, F and G.

Green mitochondrial autofluorescence (B) and (F). Red immunofluorescence of α-actinin (C) or βII-tubulin (G).

D and H. intensity plots along the white lines drawn through representative sequences of 4 mitochondria (panels B, C, F, G).

dashed red lines indicate the background level of unspecific fluorescence staining measured in control experiments. Red plots are presented in relative units using the same scale for βII-tubulin and α-actinin. Green plots were normalized to the 100% of the maximal intensity of autofluorescence after the background substraction.

Figure 51 presents the effect of trypsin on the apparent Km for ADP of mitochondrial respiration in isolated permeabilized cardiomyocytes. This graph showed how the removal of βII-tubulin from mitochondrial membrane decreases the apparent Km for exogenous ADP in regulation of mitochondrial respiration. These results are in agreement with prior observations by Kuznetsov and Appaix [62, 140].

When tubulin βII is bound to MOM thus to VDAC, VDAC permeability is limited and ADP transfer to the matrix is increased via ANT. This enhances the functional coupling between ANT and MtCK, therefore, the functional coupling of adenine nucleotides within the cells is increased.

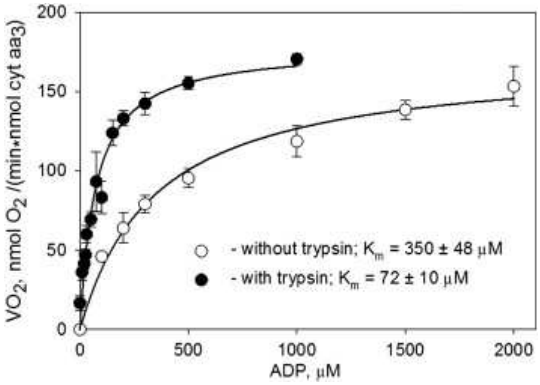

Figure 51. Effect of trypsin on apparent Km for ADP of mitochondrial respiration in isolated permeabilized cardiomyocytes: respiration rates without (°) and with (•) trypsin treatment. Proteolytic treatment with trypsin resulted in an increase in the affinity of respiration for free ADP due to the proteolytic removal of βII-tubulin.

Mean values and standard deviations of 9 experiments.

3. FUNCTIONAL ROLES OF STRUCTURAL PROTEINS IN THE ENERGY FLUXES

(Articles 3, 4, 5)

Functional test, through respiratory response analyzes, were used to evaluate mitochondrial intactness before and after trypsin treatment. In addition, respiratory response tests were performed -before and after trypsin treatment- to find the role of structural proteins in energy fluxes regulation.

Proteolytic treatment test of cardiomyocytes was performed to demonstrate how important it is the role of cytoskeletal proteins in the regulation of mitochondrial respiration. Permeabilized and, permeabilized and trypsinated adult rat cardiomyocytes were tested to evaluate mitochondrial outer membrane integrity. Tests were carried out at 25° C in a medium supplemented with fatty acids free BSA, 5mM glutamate and 2mM malate.

Mitochondrial respiration was activated by the addition of ADP. To assess the intactness of MOM, cytochrome C was added. Cytochrome C is a highly soluble hemoprotein of the respiratory chain, loosely associated with the outer side of MIM. If MOM is disrupted, cytochrome C leaves the mitochondria increasing the respiration rate. Finally, ATR addition inhibited ADP-stimulated respiration.

Both plots (Fig. 52) control and trypsinated cardiomyocytes, show how ADP increased the respiration rate more than 10 times and, how addition of cytochrome C did not change respiration rate. Cardiac cells in figure 52A showed that mitochondrial membranes endure completely intact even after being challenged to a short proteolytic treatment. These results are in agreement with previous data of isolated heart mitochondria studies by Appaix et al. [62, 141].

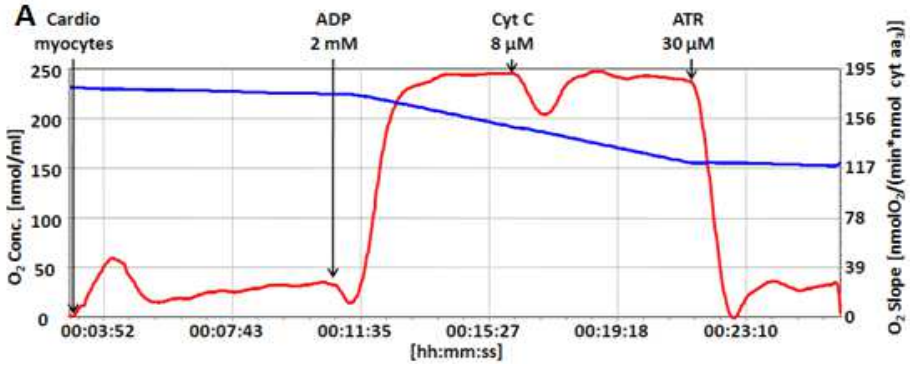

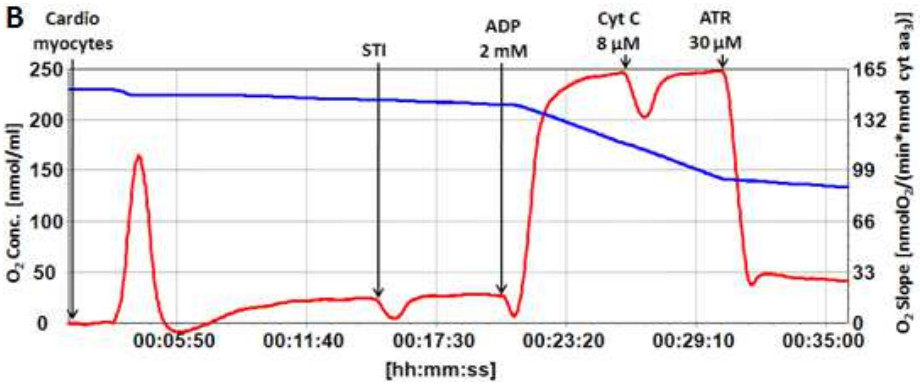

Figure 52. Respiration activated by 2mM of exogenous ADP, Cyt C test to show intactness of MOM, and ATR test to show the total control of ANT on respiration:

A. Representative respiration traces before trypsin treatment of permeabilized cardiomyocytes (CM).

B. Representative respiration traces after trypsin treatment (0.05 µM) for 10', then soybean trypsin inhibitor (STI) was added.

PK-PEP system test was performed to observe detailed changes in the regulation of mitochondrial respiration after the removal of βII-tubulin. To evaluate the regulation of mitochondrial respiration, MtCK was activated by the addition of creatine and MgATP. The ADP produced in the active site of MtCK is released into the mitochondrial IMS. ADP may either return to matrix via ANT or leave the mitochondria through VDAC. ADP flux distribution between ANT and VDAC depends on the channeling permeability for adenine nucleotides.

The figure 53 shows the results of intact permeabilized cardiomyocytes (more than 90% of rod-like cells), therefore, addition of PK-PEP system did not change the rate of respiration. Respiration rate is maintained at the maximal value even during MtCK activation within the mitochondrial interactosome, meaning that the MgADP produced by MtCK is not accessible for this system.

However after a short proteolysis treatment (Fig. 54), tubulin βII was removed from MOM. The removal of βII-tubulin caused a decrease in the respiration rate to half of its maximal value by the addition of PK-PEP system. This means that about 50% of MgADP produced by MtCK can leave the mitochondria through VDAC. This is due to an increased permeability of VDAC for MgADP.

Remarkably, the effect of PK-PEP system on mitochondrial respiration was also observed in not properly-isolated cardiomyocytes (Fig. 55), which means a preparation containing 50% rod-like intact cardiomyocytes and 50% round-shape cells without the use of trypsin. These results demonstrated the importance of PK-PEP test to verify the intactness of isolated cardiomyocytes inasmuch as VDAC permeability regulation. Assuming that tubulin βII is bound to MOM in intact permeabilized cardiomyocytes *in vivo*, VDAC channel permeability is limited by tubulin βII binding, thus it increases ADP transfer to the matrix via ANT.

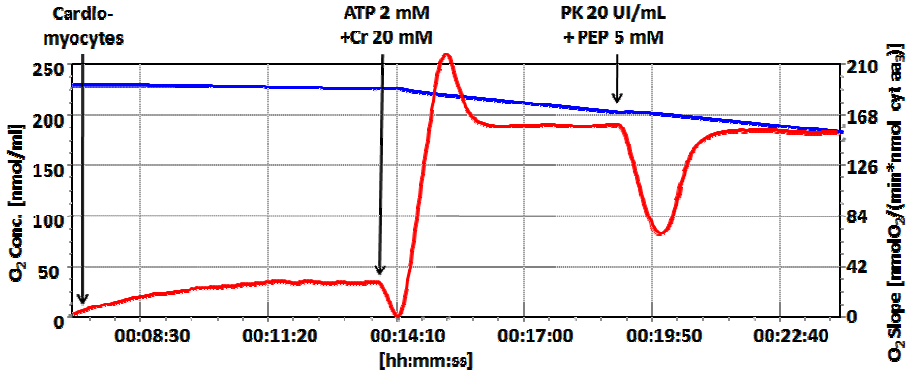

Figure 53. Respiration of permeabilized cardiomyocytes activated by MgATP (2mM) and creatine: Addition of PK-PEP system had no effect on the respiration.

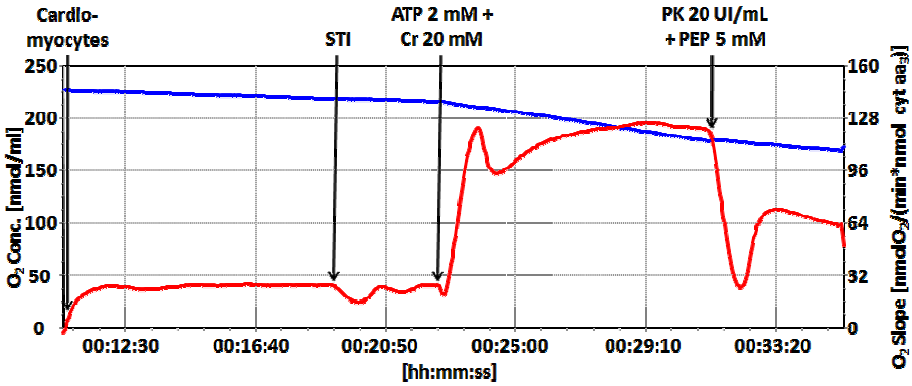

Figure 54. Respiration of permeabilized cardiomyocytes activated by MgATP (2mM) and creatine after short proteolysis: Respiration of trypsin-treated cardiomyocytes in the presence of 20mM Cr and 2mM ATP. Proteolytic treatment was inhibited by addition of soybean trypsin inhibitor (STI, 0.02mM).

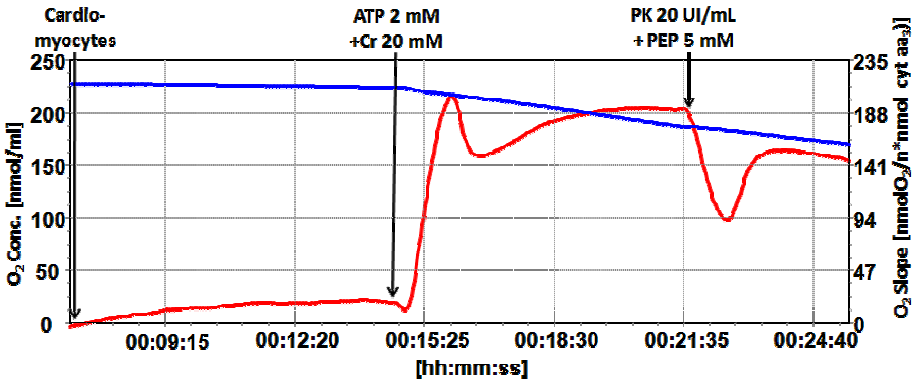

Figure 55. Respiration of about 50% of rod-like intact cells activated by MgATP (2mM) and creatine: Addition of PK-PEP system showed the accessibility of ADP to the PEP-PK.

Figure 56A shows that in intact permeabilized cardiomyocytes the MtCK reaction completely controlled the respiration rate even in the presence of cytoplasmic ADP trapping system. An increase in creatine concentration rapidly increased the respiration rate to its maximal value. In addition, oxidative phosphorylation was maintained by ADP regeneration and recycling within mitochondrial interactosome coupled to permanent creatine phosphorylation and phosphocreatine production with high PCr/O_2 ratio equal to about 6 [142]. Whereas, when βII-tubulin was removed from MOM by proteolytic treatment (Fig 56B), VDAC permeability was increased and adenine nucleotides exchange between mitochondria and cytoplasm was increased, hence MtCK partially controlled the respiration.

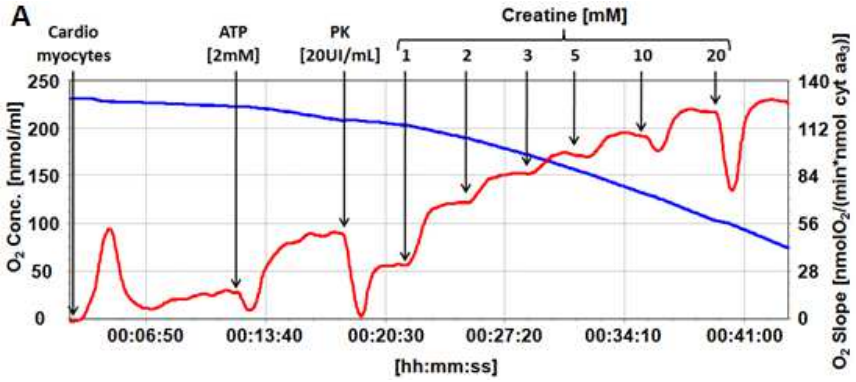

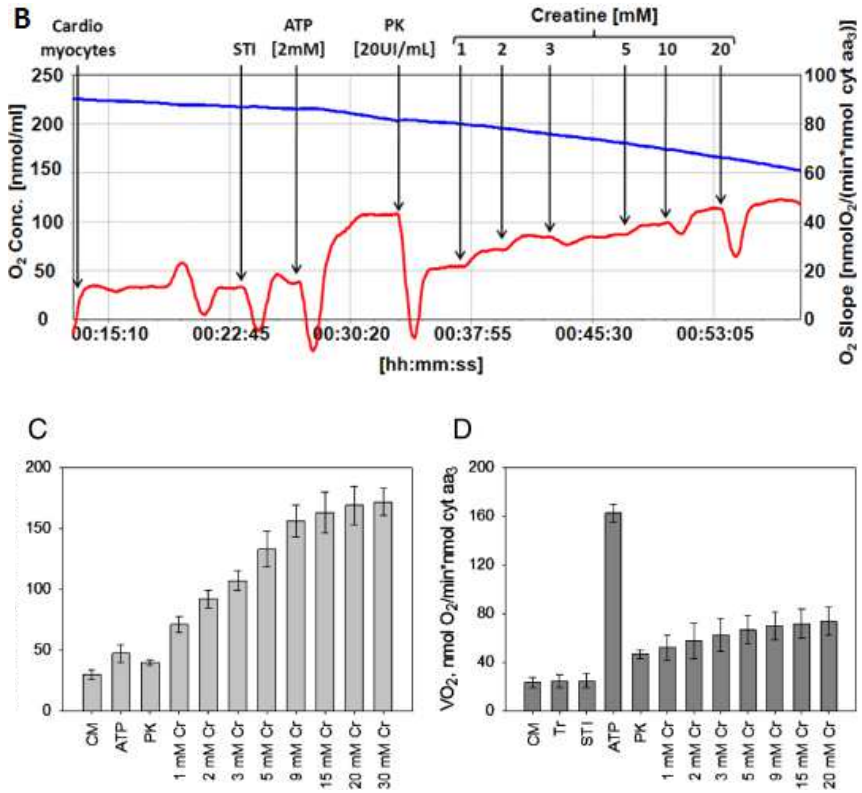

Figure 56. Regulation of mitochondrial respiration by creatine in the presence of activated MtCK in permeabilized cardiomyocytes, with and without short proteolysis: A. Permeabilized cardiomyocytes, state 2 respiration was recorded. MgATP was added to increase the respiration rate. Addition of PK and PEP decrease the respiration rate. Creatine titration increased the respiration rate up to maximal value.

B. The same protocol was followed by trypsin-treated cells, extramitochondrial ADP was more accessible to PEP-PK reaction due to the proteolytic treatment.

C. Mean values and standard errors for 7 experiments described in panels A and B, respectively.

4. FUSION-FISSION PROCESSES IN DIFFERENTIATED ADULT RAT CARDIAC CELLS

(Paper 6: In preparation)

Mitochondrial organization was observed by confocal microscopy in several fixed cardiac cells, showing the remarkable regular arrangement of mitochondria akin to “crystal-like” and Z lines, as it has been previously reported by other groups [59, 97, 99]. Whether or not fusion events were a common phenomenon in healthy adult cardiac cells, we observed the

arrangement of mitochondria and Z lines by the use of mitochondrial autofluorescence and immunolabeling of α-actinin (Z lines). Figure 57 shows six examples (A, B, C, D, E, an F) of the characteristic sarcomeric transversal Z lines and regular “crystal-like” arrangement of mitochondria.

These two dimensional (2-D) images were recorded sequentially in separate channels to avoid fluorescence bleedthrough between channels as well as possible FRET artifacts, and were done in different cells in order to obtain statistical significance. It can be appreciated in the examples of the merged images below how mitochondria and Z lines are well intercalated. Therefore, this highly reproducible arrangement of healthy adult cardiac cells makes us think about the very seldom possibility that fusion events happen, as it has been previously suggested by other authors [41, 97, 143, 144].

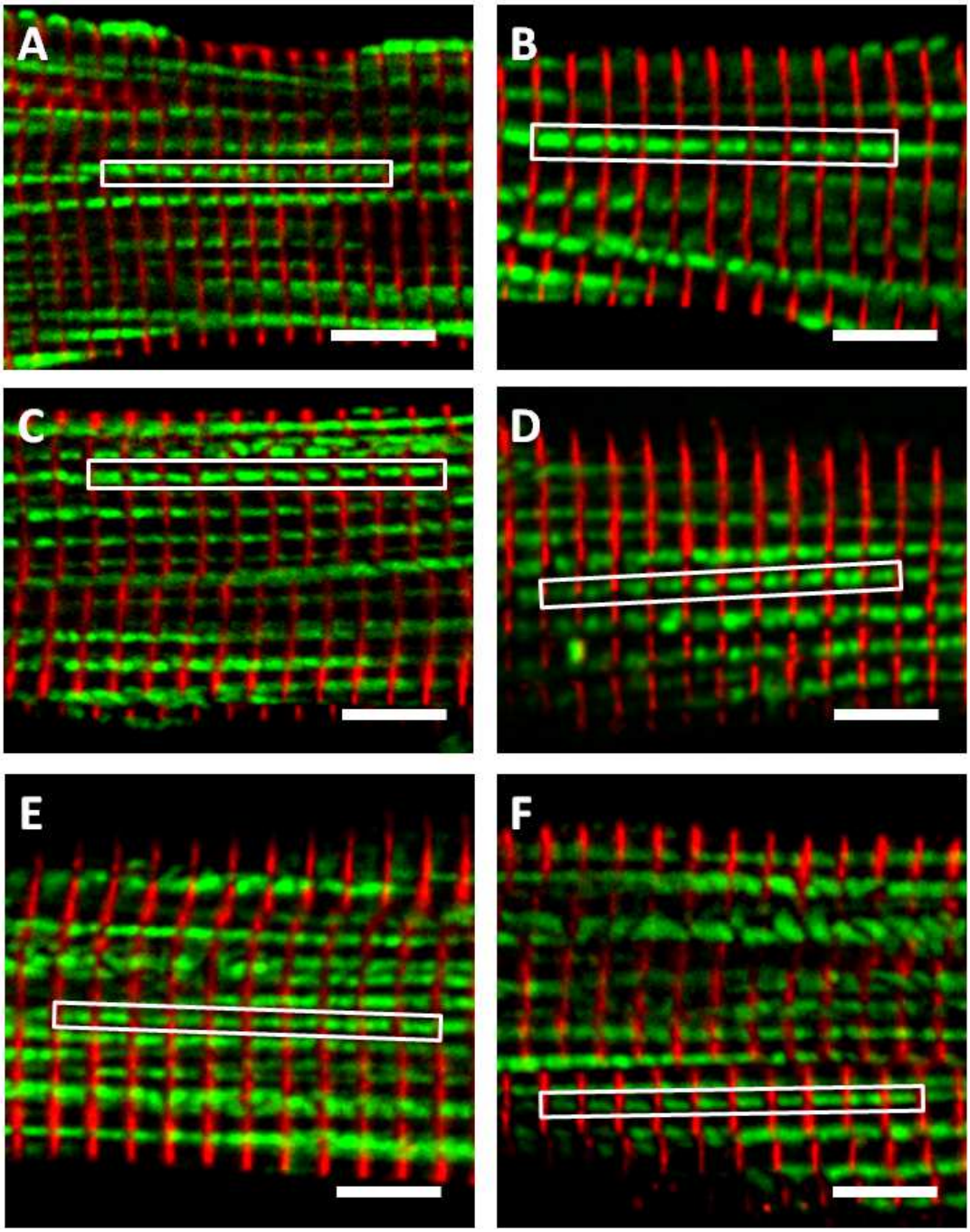

Figure 57. Examples of 6 different fixed cardiomyocytes: panels A, B, C, D, E, and F display a section of the confocal merged images of α-actinin (red) with Cy5 immunolabeling and autofluorescence of flavoproteins mitochondria (green) in adult rat cardiomyocytes. All panels show the intracellular distribution of Z lines (α-actinin) and mitochondria. The white box shown on each panel represents the area I focused my analysis on. White bars 5µm.

In addition, fixed isolated cardiac cells were analyzed to observe how reproducible this arrangement was. Figure 58 shows the different positional and mathematical analyzes were done in the different cardiac cells studied; the mitochondrial row of each cardiomyocyte analyzed is indicated in white boxes in Figure 57. Plots in figure 58 have the following organization, the lettering refers to figure 57, and the number corresponds to the analysis performed (1: Intensity profiles, 2: Fourier transform of the intensity profiles, and 3. Cross-correlation analysis of intensity profiles). Solid-lines represent mitochondrial autofluorescence and dashed-lines α-actinin immunofluorescence (Z lines).

The intensity profile analyzes give an overview of the trends of mitochondria and α-actinin over the length of the cardiomyocytes. As it can be seen in the intensity profile plots (A1, B1, C1, D1, E1, and F1) mitochondrial autofluorescence and α-actinin immunofluorescence had a regular periodicity among them, and it can be appreciated that mitochondria were interleaved with z-lines. These results are in good agreement with what it has been published before [59].

Fourier transform analyzes of each image analyzed are highly interesting. The Fourier transforms of mitochondrial autofluorescence (solid-line) and α-actinin immunofluorescence (dashed-line) -Z lines- revealed that both had a spatial frequency of 0.55 μm^{-1}, this corresponds to a periodicity of 1.82 μm.

Finally, mitochondrial autofluorescence and α-actinin immunofluorescence were analyzed by the covariance analysis of intensity profiles. This analysis allowed measuring both profiles as a function of a spatial-lag. All plots displayed a negative cross-correlation (-1) for no spatial shift (lag) while a strong positive cross-correlation was obtained for a 0.9 μm shift that is roughly half periodicity given by Fourier analyzes. These results confirmed the visual

interpretation of the images (Fig. 57) and by the intensity profiles plots (Fig. 58 - A1, B1, C1, D1, E1, and F1), which means that mitochondria were perfectly interleaved with Z lines.

Figure 58. Analysis of intensity profiles in fixed adult rat cardiac cells: Plots, Fourier transform and Covariance analyzes of intensity profiles: from panels A, B, C, D, E, and F refer to the respective case shown in Fig. 57.

1. Intensity profiles of immunolabeled α-actinin (dashed-line) with Cy5 and flavoproteins autofluorescence of mitochondria (solid-line), of the selected area.

2. Fourier transforms of the intensity profiles, mitochondria (solid-line) and α-actinin (dashed-line).

3. Covariance analysis of the intensity profiles (mitochondria and α-actinin).

A.1.

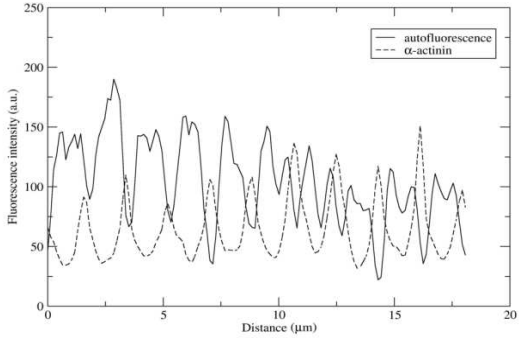

A.2.

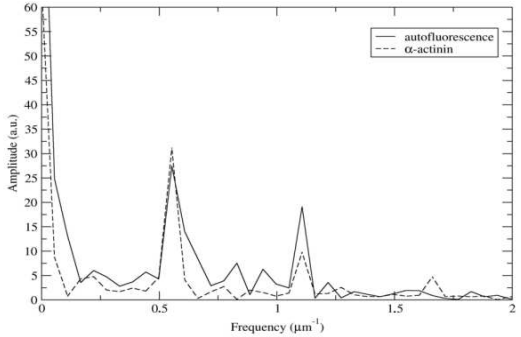

A.3.

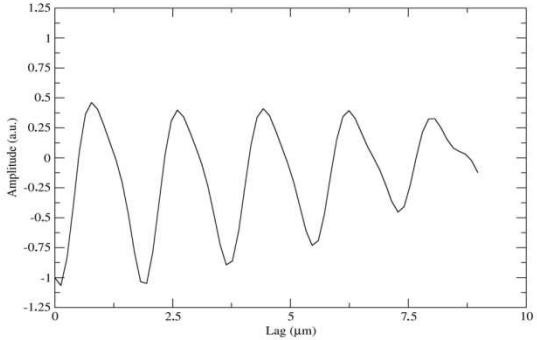

B.1.

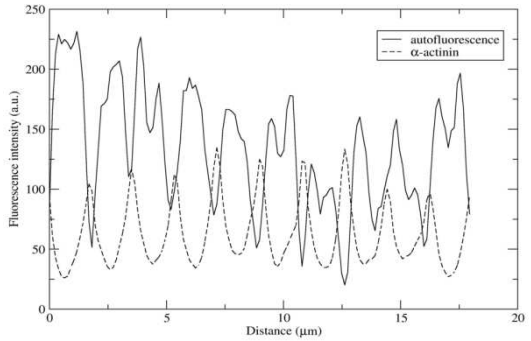

B.2.

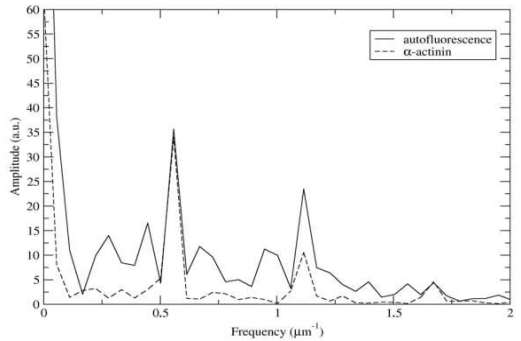

B.3.

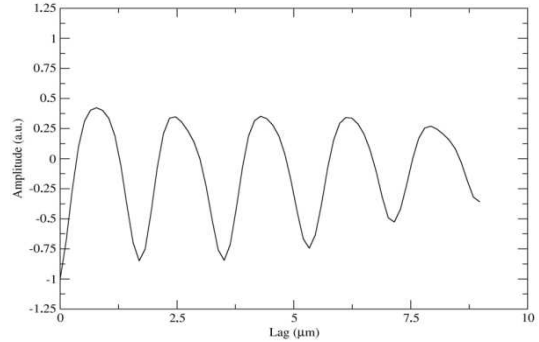

C.1.

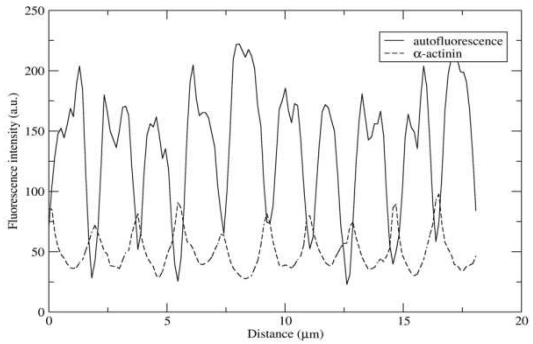

C.2.

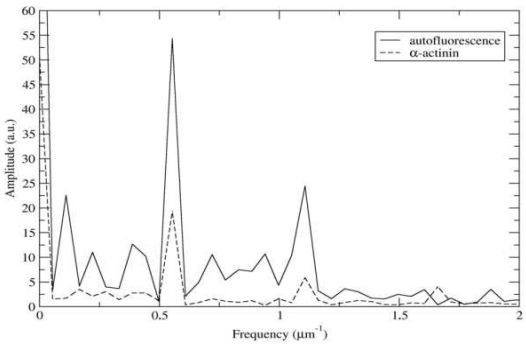

C.3.

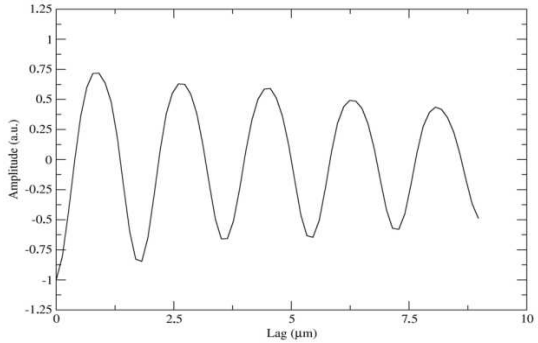

D.1. Intensity profiles in cardiac cells

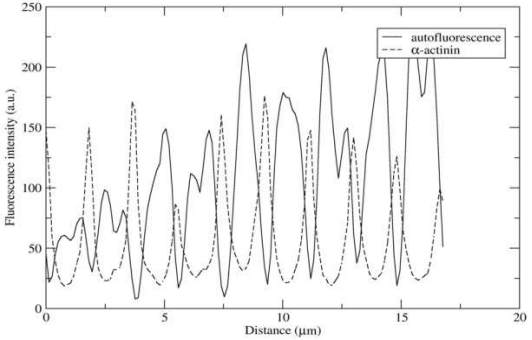

D.2. Fourier transform of intensity profiles

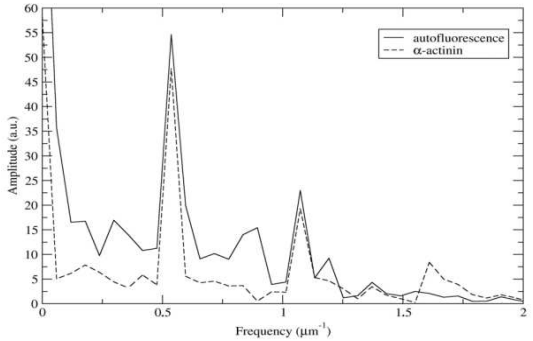

D.3. Covariance analysis of intensity profiles

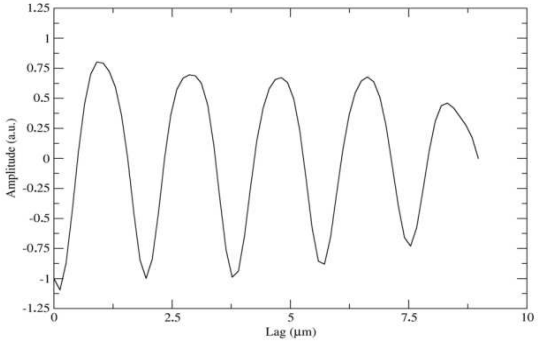

E.1. Intensity profiles in cardiac cells

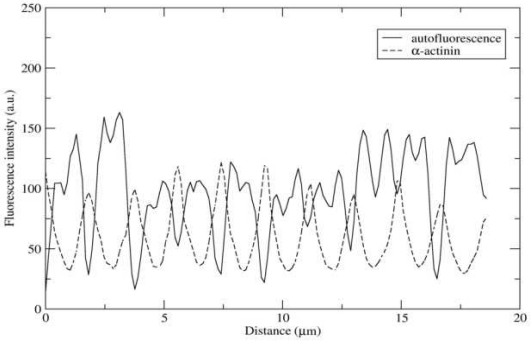

E.2. Fourier transform of intensity profiles

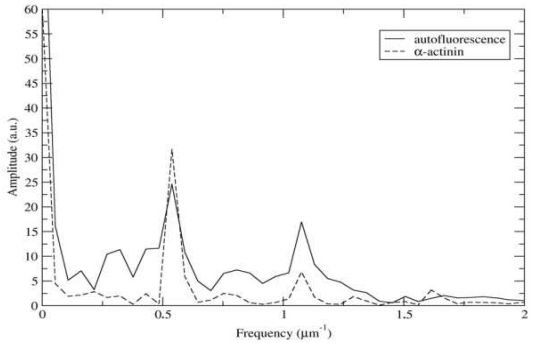

E.3. Covariance analysis of intensity profiles

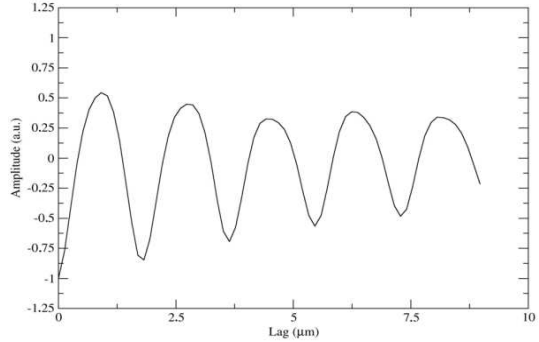

F.1. Intensity profiles in cardiac cells

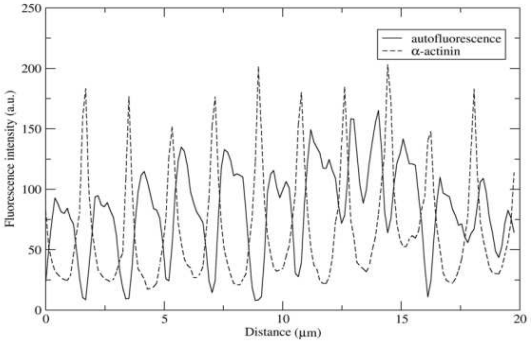

F.2. Fourier transform of intensity profiles

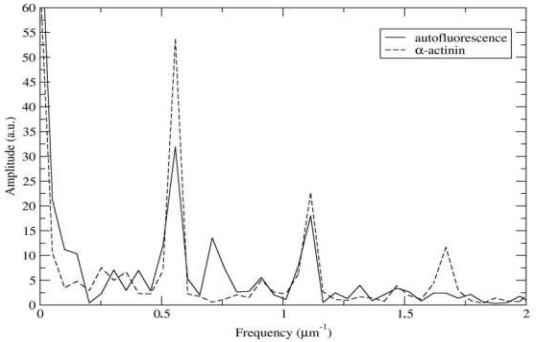

F.3. Covariance analysis of intensity profiles

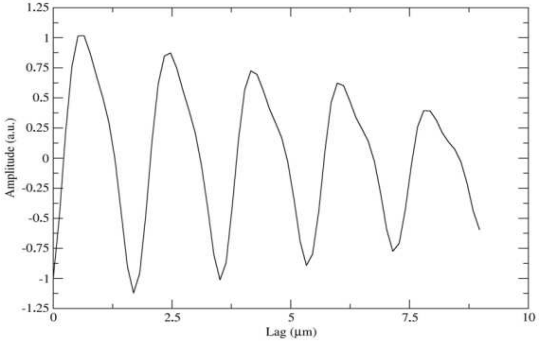

Previous observations in adult healthy isolated-fixed cardiac cells were confirmed by analyzing dilacerated cardiac fibers. The analysis of cardiac fibers also allowed us to observe if fusion events occur in cardiac cells in a more physiological state. Dilacerated cardiac fibers were stained with MitoTracker® deep red FM, thereafter fixed and immunolabeled with α-actinin.

Figure 59 shows a picture of the dilacerated cardiac fiber used to make the three-dimensional (3-D) image (Supplementary video). A 3-D analysis was highly necessary to make, in order to confirm previous observations of the absence of interfibrillar mitochondrial fusion. The 3-D image was re-constructed from 12 optical slices (2.2 µm) and it showed the characteristic sarcomeric Z lines and crystal-like arrangement of interfibrillar mitochondria within the fiber.

Figure 59 displays mitochondria in red (stained with MitoTracker® deep red FM) and α-actinin in green (immunolabeled with FITC). White lines (a, b, c, and d) represent the selected areas for further analysis.

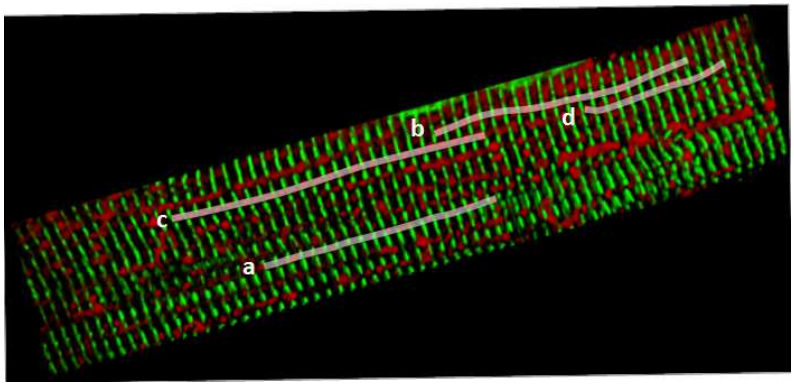

Figure 59. Image of three dimensional structure of a cardiac fiber: It shows the intracellular distribution of Z lines (α-actinin) and mitochondria. Mitochondria (red) were stained with MitoTracker® deep red FM and Z lines were visualized by immunolabeling of anti-α-actinin (green). White lines display the areas analyzed. The 3-D movie of adult rat cardiac fiber was built from the confocal sections (12 optical slices) with a total thickness of 2.2 µm. (3-D movie included in supplementary data).

The dilacerated fibers were also studied by positional and mathematical analyzes (Fig.60). Figure 59 displays the areas (white lines) used for positional and mathematical analyzes. In addition, all analyzes were done from 5 optical slices (0.2 µm each slice). The 5 optical sections, accounting for approximately 1 µm thickness, were used for these analyzes taking in consideration the thickness of a mitochondrial layer. This restrictive choice makes the analyzes more precise and informative than taking in consideration the whole stack acquired.

Once more, each plot of the selected row of mitochondria was identified by lower-case letter (a, b, c, and d) and next to a number, which indicates the analysis done (1: Intensity profiles, 2: Fourier transform of the intensity profiles, and 3. Covariance analysis of intensity profiles). Solid-lines represent MitoTracker® Red fluorescence signal (mitochondria) and dashed-lines α-actinin immunofluorescence (Z lines).

The intensity profile plots (Fig. 60 - a1, b1, c1, and d1) give an overview of the patterns of mitochondria and α-actinin over the length of the cardiac fiber. As it can be appreciated in the intensity profile plots, MitoTracker® Red fluorescence and α-actinin immunofluorescence had a regular periodicity among them, and mitochondria were interleaved with z-lines. These results are in good agreement with what it was shown previously and with what it has been published before [59].

The Fourier transforms of MitoTracker® Red fluorescence - solid-line - (mitochondria) and α-actinin immunofluorescence - dashed-line - (Z lines) revealed that both had a spatial frequency of 0.5 μm^{-1}, this corresponds to a periodicity of 2 µm. This periodicity was reproducible in all analyzes of cardiac fibers and the ~0.2 µm difference between isolated fixed cardiac cells and dilacerated cardiac fibers depended on their contraction state, as previously described by Yaniv *et al*. [96]. Moreover, these analyzes disclosed that

mitochondria present most of the times two close fluorescent peaks, which usually were found in all acquired images.

Furthermore, MitoTracker® Red fluorescence and α-actinin immunofluorescence were analyzed by the covariance analysis of the intensity profiles (Fig. 60 - a3, b3, c3, and d3). This crossed-correlation allowed measuring both waveforms as a function of a time-lag variables and all results displayed a negative crossed-correlation (-1). These results confirmed what it was seen in the intensity profiles plots (Fig. 60 - a1, b1, c1 and d1). A negative cross-correlation of -1 means, that mitochondria were perfectly interleaved with Z lines. These results in dilacerated fibers confirmed our previous observations in isolated cardiac cells.

Finally, isolated, cultured and transfected adult cardiomyocytes were used to confirm whether or not fusion events occur in adult healthy mammalian cardiac cells. Figure 61 shows just an example of how *in vivo* transfected-cardiomyocytes looked like. Part of their rod-like shape was lost due to the long time of incubation. However, as it has been shown in previous studies and in the present work, the arrangement of mitochondria is also very regular in the transfected GFP-α-actinin cardiac cells.

Transfection of isolated cardiac cells was done to see whether mitochondria undergo to any fusion event, fast speed scanning recordings of transfected cells showed (Supplementary video) the constant presence of Z lines between mitochondria during the acquisition of the frames (3000 frames) of a selected area (14.0µm x 7.6µm) which were used for the dynamical studies.

a.1. Intensity profiles in cardiac fibres

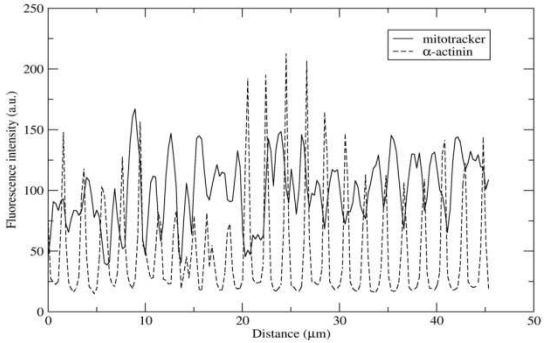

a.2. Fourier transform of the intensity profiles

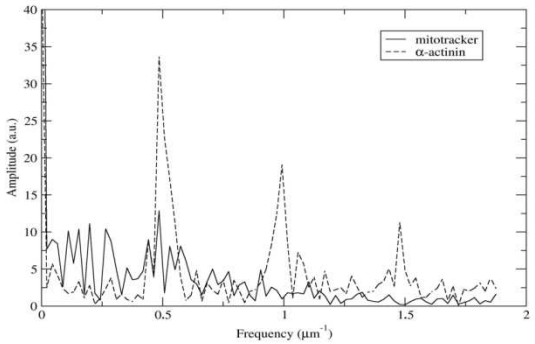

a.3. Covariance analysis of the intensity profiles

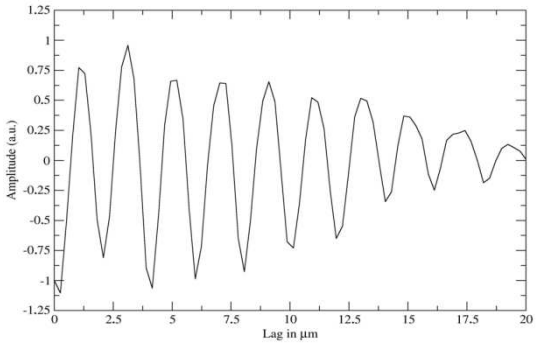

b.1. Intensity profiles in cardiac fibers

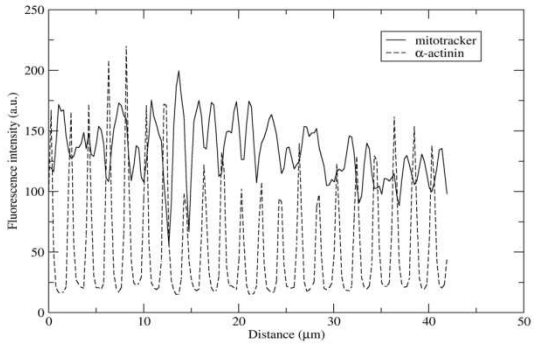

b.2. Fourier transform intensity profiles

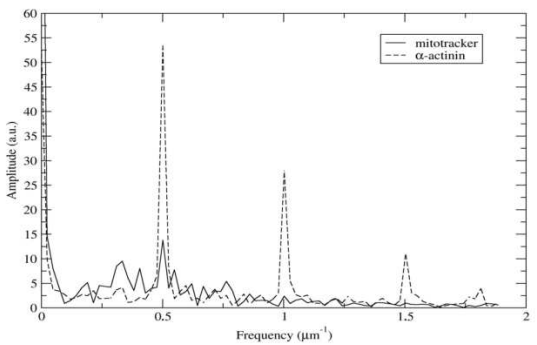

b.3. Covariance analysis of the intensity profiles

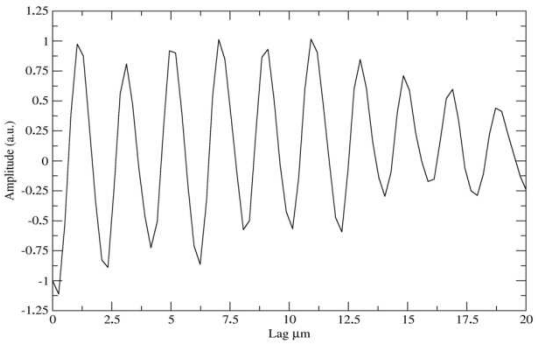

c.1. Intensity profiles in cardiac fibers

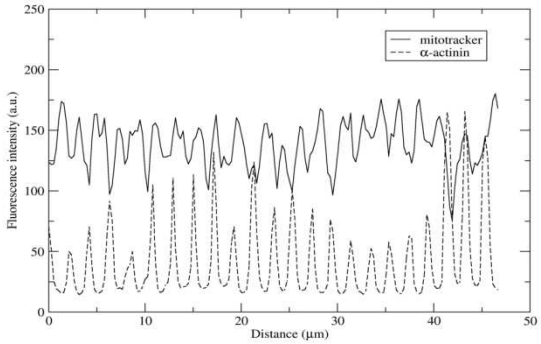

c.2. Fourier transform intensity profiles

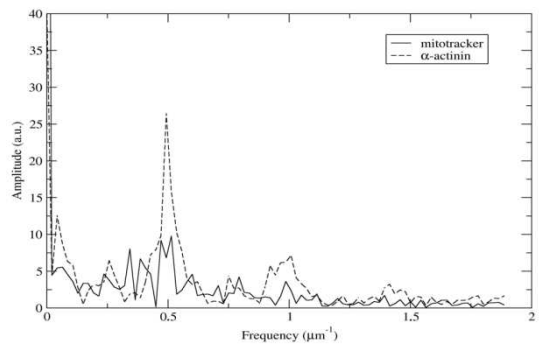

c.3. Covariance analysis of the intensity profiles

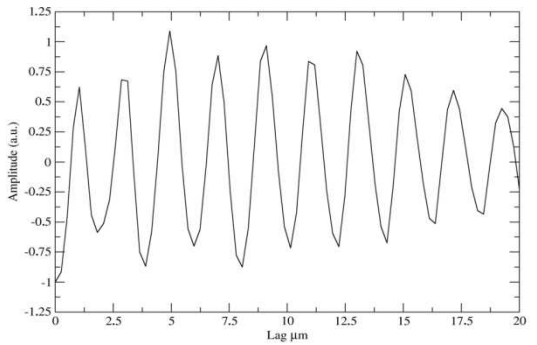

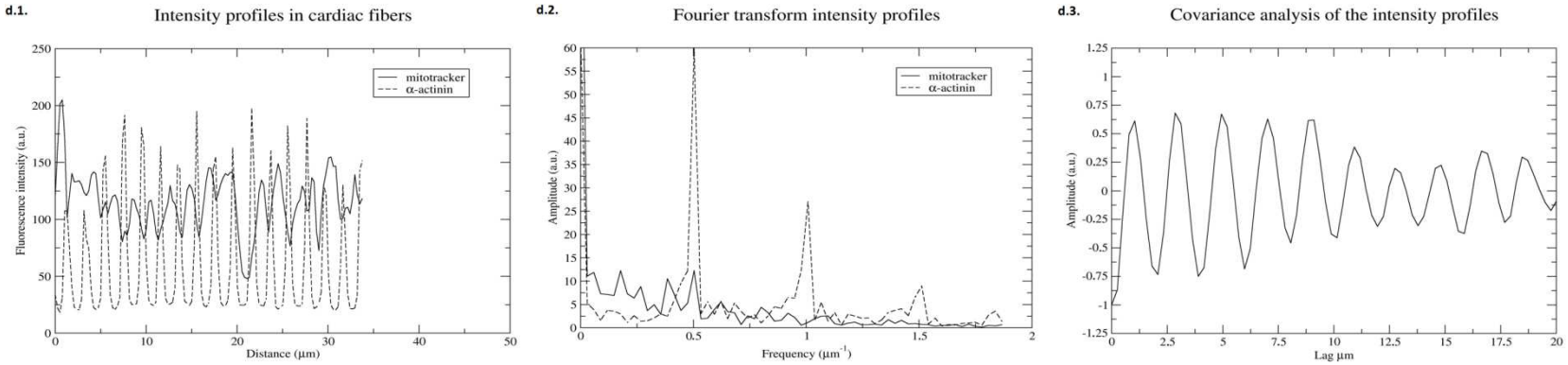

Figure 60. Plots of Intensity profiles, Fourier transforms of intensity profiles and Covariance analyzes of intensity profiles in fixed adult rat cardiac fibers: from lines drew in figure 59 a, b, c, and d different analysis of the intracellular distribution of mitochondria and Z-lines were done. To visualized mitochondria MitoTracker® deep red FM was used and for Z-lines α-actinin immunolabeling was used. Analyzes were done in 1µm (5 optical sections) thick, this corresponds to the thickness of one layer of mitochondria.

1. Intensity profiles of immunolabeled α-actinin (dashed-line) with Cy5 and flavoproteins autofluorescence of mitochondria (solid-line), of the selected area.

2. Fourier transforms of the intensity profiles, mitochondria (solid-line) and α-actinin (dashed-line).

3. Covariance analysis of the intensity profiles (mitochondria and α-actinin).

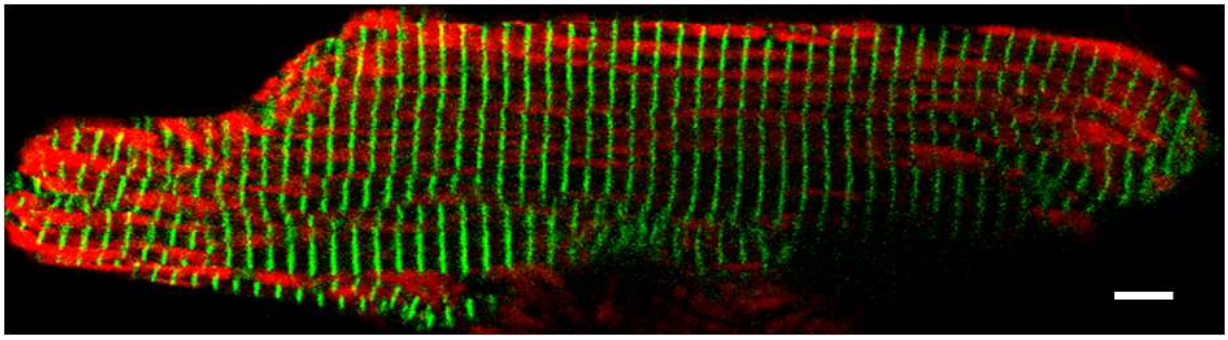

Figure 61. Example of a transfected cardiomyocytes with pEGFP-N1 α-actinin and MitoTracker® red FM: Image of a cultured-transfected adult cardiac cell with pEGFP-N1 α-actinin (green) and stain mitochondria (red). Positive-transfected cells were visualized 20-22h after its transfection. A selected area of the transfected cells was recorded by high speed scanning to observe mitochondrial fluctuations of position in their fluorescent centers. White bar 5µm.

Figure 62 shows how the area analyzed by the clustering algorithm (explained in methods) looked like after the image processing. The studies of mitochondrial dynamics, required an increased scanning speed to achieve a pixel dwell time close to 0.64µs and intervals between images of 200ms (Supplementary video). At this scanning speed mitochondrial fluorescent centers and alignment of Z lines were monitored. The position of these fluorescent centers depended on both, the precise localization of mitochondria in the cells and the configuration of their inner membrane. On the other side, fluorescence alignment of Z lines depended on their localization between mitochondria.

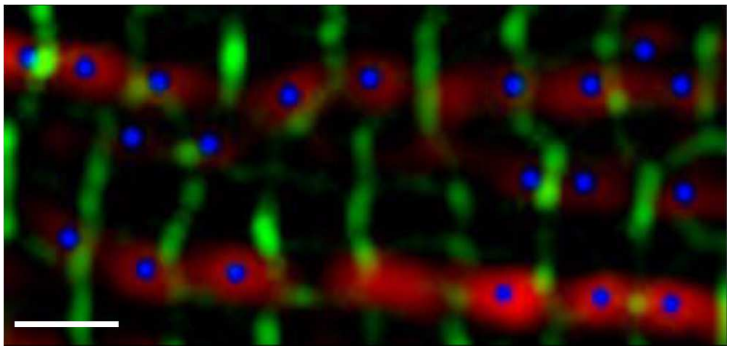

Figure 62. Example the clustering technique applied in isolated cardiomyocytes transfected with pEGFP-N1 α-actinin and labeled with MitoTracker® red FM: It displays Z-lines (green), mitochondria (red), and mitochondrial fluorescent centers (blue). (Mitochondrial fluctuations movie is included in supplementary data). White bar 2µm.

Finally, the mitochondrial upper row of the recorded mitochondria (Fig. 62) was studied once again by positional and mathematical analyzes (Fig. 63). Once again, the following plots the solid lines represent the MitoTracker® red fluorescent signal (mitochondria) and dashed-lines are the GFP-α-actinin fluorescence (Z lines).

The intensity profile plot (Fig. 63) shows a general outlook of the patterns of mitochondria and α-actinin over the length of the area selected. As it can be appreciated in the intensity profile plots, MitoTracker® Red fluorescence and GFP-α-actinin fluorescence, both fluorescent signals had a regular periodicity among them. As it is observed, mitochondria were interleaved with z-lines. These results in isolated, cultured and transfected cardiac cells are in good agreement with what it was shown previously in the isolated fixed cardiac cells and the dilacerated fixed cardiac fibers.

The Fourier transforms (Fig. 63) of MitoTracker® Red fluorescence - solid-line - (mitochondria) and α-actinin immunofluorescence - dashed-line - (Z lines) revealed that both had a spatial frequency of 0.55 μm^{-1}, this corresponds to a periodicity of 1.82 μm. This periodicity was reproducible in other analyzes of transfected cardiac cells (results not shown). Once again, these analyzes disclosed that mitochondria present most of the times two close fluorescent peaks, which usually were found in all acquired images from fixed isolated and dilacerated cardiac cells and fibers, respectively.

The analysis of isolated, cultured and transfected cardiomyocytes were completed by the covariance analysis of the intensity profiles (Fig. 63). The cross-correlation allowed measuring both profiles as a function of a time-lag variables and displaying a negative cross-correlation (-1). These results confirmed what it was seen in the intensity profiles plot, how mitochondria were interleaved with Z lines. A negative cross-correlation of -1 means, that mitochondria were perfectly interleaved with Z lines. These results in isolated, cultured and

transfected adult cardiomyocytes confirmed our previous observations in isolated-fixed cardiac cells and dilacerated-fixed cardiac fibers.

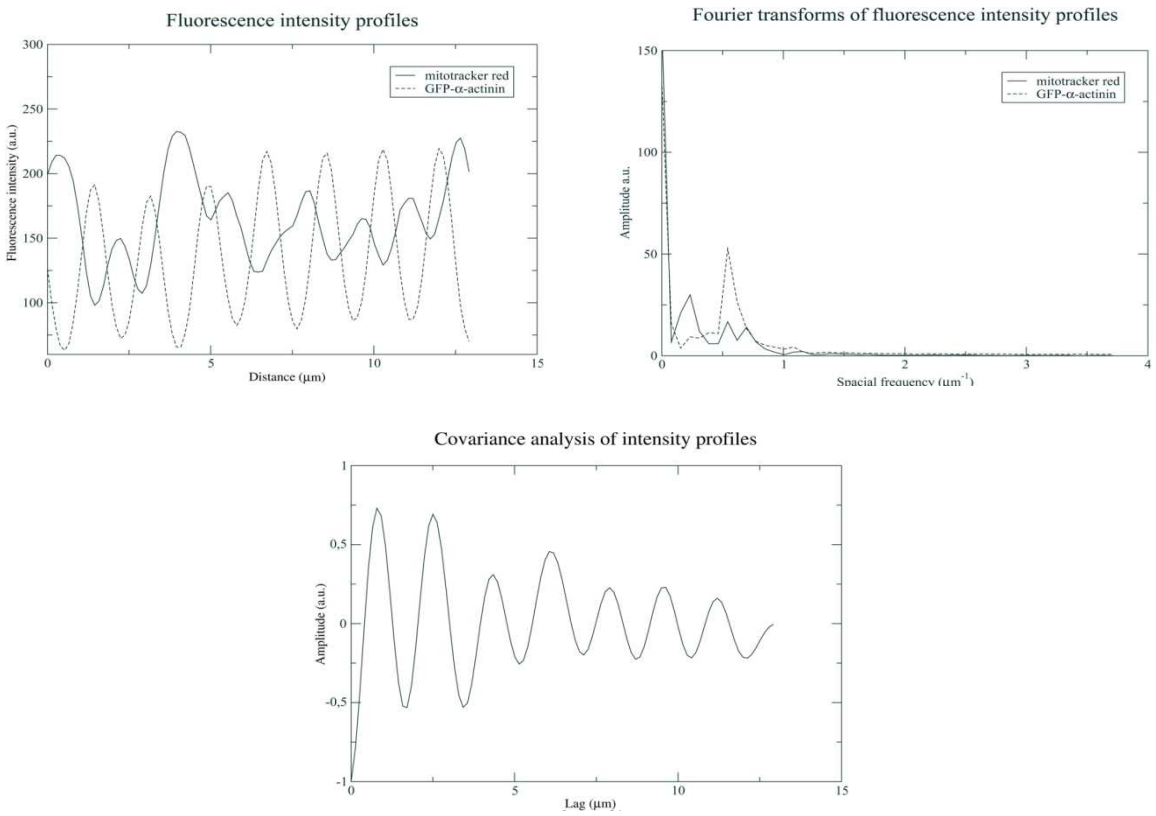

Figure 63. Plots of Intensity profiles, Fourier transforms of intensity profiles and Covariance analyzes of intensity profiles in cultured transfected adult rat cardiac cells: Analyzes were done from the selected area taken by confocal microscopy high speed scanning.

1. Intensity profiles of α-actinin (dashed-line) and mitotracker (solid-line) of the selected area.

2. Fourier transforms of the intensity profiles, mitotracker (solid-line) and α-actinin (dashed-line).

3. Covariance analysis of the intensity profiles (mitochondria and α-actinin).

VI. DISCUSSION

The results of my work show a detailed comparative analysis of the structure-function relationship of energy fluxes in adult cardiomyocytes, described in previous works [41, 114, 139, 145]. In addition, my studies provided a better insight of mitochondria-cytoskeletal interactions in shaping the specific pathway of energy transfer by creatine kinase network in cardiac cells, as well as how these interactions have a role in the intracellular arrangement of mitochondria which prevents from their fusion in healthy adult cardiomyocytes. In heart cells, the discovery of the specific distribution of β-tubulin isotypes provided a better understanding of how cytoskeletal interactions have an important role in the regulation of heart energy fluxes and mitochondrial respiration. Moreover, the surprising discovery was the distribution of βII-tubulin that it seemed to be co-localized with mitochondria. Therefore, tubulin βII is the tubulin isotype connected to the mitochondrial outer membrane through VDAC. The analysis of mitochondrial dynamics, to complete these studies of mitochondria - cytoskeletal interactions, was achieved by the transfection of α-actinin. These high speed scanning results revealed that fusion events scarcely occur in healthy adult cardiac cells.

Cytoskeletal interactions: role of tubulins.

Tubulin isotypes are just one component of the highly structured cytoskeleton of adult cardiomyocytes. Tubulin is one of the most representative proteins of cytoskeleton. Besides its structural role, it has been seen a direct role of tubulin βII in energy metabolism through the intracellular micro-compartments, formation of dissipative metabolic structures and, hence in the regulation of metabolic fluxes. Under *in vivo* conditions αβ-tubulin heterodimer is a highly dynamic protein that has a rapid assembly/disassembly turnover by exchange of subunits. In cardiomyocytes, about 70% of total tubulin is found in its polymerized form (microtubules) and 30% is present as a non-polymerized cytosolic heterodimers [54]. In higher vertebrates, eight α-tubulin and seven β-tubulin isotypes encoded by different genes have been identified [53]. The major differences among tubulin isotypes are found in the last 15 amino acids of the carboxyl-terminal tail. The C-terminal

residues are often target of numerous microtubule-associated proteins (MAPs) and post-translational modification (PTMs), such as acetylation, detyrolation, tyrosination, phosphorylation, polyglutamylation, and polyglycalation [56]. The C-terminal composition determines the nature of PTM and affects their interactions with different cellular factors and their distribution, as it has been shown in this work.

More than two decades ago, Kummel [146] with other laboratories [41, 74, 147] discovered the differences in mitochondrial respiration behavior *in vitro* and in permeabilized cardiomyocytes *in situ*: being the apparent K_m for exogenous ADP 20-30 times higher in permeabilized cardiomyocytes than in isolated mitochondria. On the other side, Sætersdal *et al*. [61] demonstrated the presence of tubulin at the mitochondrial outer membrane of cardiomyocytes and myofibers, through electron microscopy by immunogold anti-β-tubulin labeling. Recently, Rostovtseva *et al.* [46] have proposed a mechanism of interaction between tubulin and VDAC, this involves the interaction of the negative carboxyl-terminal tail (CTT) of tubulin with the positive charged domain of VDAC channel. Although, my immunolabeling results showed that it may be highly possible that the negatively charged CTT of βII-tubulin is located on the surface of the mitochondrial outer membrane (MOM). Tubulin βII interaction with MOM may likewise prevent significantly the association of pro-apoptotic proteins to MOM [148]. This may explain why apoptosis is unusual in healthy human hearts [149]. Alterations of mitochondria-tubulin interactions in dilated and ischemic cardiomyopathies may explain why the rate of apoptosis can increase several hundred-folds in these diseases [149]. All these results lead to conclude that in cardiac cells this phenomenon is related to tight interactions between mitochondria and cytoskeleton, and to propose that some cytoskeletal components may control the permeability of the VDAC channel in the MOM and controls its permeability [74, 147].

From the functional analyses performed in this work, it was found that the presence of βII-tubulin at the outer mitochondrial membrane explains the very high value of apparent K_m for free exogenous ADP in adult permeabilized cardiomyocytes which is an order of magnitude higher than in isolated

mitochondria (370 µM and 10-15 µM, respectively), and also higher than in NB HL-1 cells (7-10 µM) [41, 62, 140, 146, 150, 151]. In addition, these analyses showed the importance of mitochondrial arrangement. It was seen that respiratory activity of the highly arranged intermyofibrillar-mitochondria in permeabilized isolated cardiomyocytes greatly differed from isolated cardiac mitochondria and NB HL-1 cells. These results suggest that mitochondrial dynamics have an important role in the regulation of respiratory activity. Isolated mitochondria have none structural arrangement given by cytoskeletal proteins and mitochondrial arrangement in NB HL-1 cells forms a dense reticulum of elongated mitochondrial threads surrounding nuclei; both mitochondrial arrangements have an impact on their respiratory activity. Thus, structural organization and mitochondrial disposition and dynamics, *i.e*. fusion and fission, have an important role in the regulation of energy fluxes in cells.

Additional kinetic analyzes of respiration regulation by mitochondrial creatine kinase (MtCK) reaction in permeabilized cardiomyocytes confirmed previous results about tubulin binding to VDAC [46, 152, 153]. Thus, the results showed a significant decrease of the apparent affinity for extramitochondrial ATP of MtCK localized on the intermembrane space *in vivo*, in comparison with isolated mitochondria. This appears to be due to the diffusion restrictions created by interactions of VDAC in MOM with the αβ-tubulin heterodimer [46, 142, 154].

These results also showed that high apparent K_m for exogenous ADP and expression of MtCK correlate with the expression of βII-tubulin. In comparison, the absence of tubulin βII in isolated mitochondria and NB HL-1 cells results in an increase of the apparent affinity of oxidative phosphorylation for free ADP. This observation is consistent with the assumption that the binding of βII-tubulin to VDAC limits ADP/ATP diffusion through MOM and the important role of cytoskeleton.

Therefore, the restricted permeability for ADP and ATP favors their recycling in the coupled MtCK-ATP synthasome, called “Mitochondrial Interactosome” (MI) [41, 142]. My results and previous data suggest that the MI is composed of ATP synthasome, MtCK and mitochondrial βII-tubulin. A key

structure of phosphocreatine pathway of intracellular energy transfer [155]. In addition, a limited permeability of VDAC to ADP has an important physiological function. It prevents from rapid saturation of ANT by its substrates and, hence making possible the metabolic feedback regulation of mitochondrial respiration during workload changes [22, 41, 156, 157]. I confirmed the importance of the intactness of MI structure while testing its functioning, in adult cardiomyocytes. This was assessed by PK/PEP system test that is the most sensitive and covering test to evaluate the intactness of the whole MI system, including the regulatory proteins at MOM. This test is based on the use of an external PEP-PK system to trap ADP and thus competing with ANT for the substrate, this method was developed by Gellerich *et al.* and Guzun *et al.* [44, 142, 158, 159]. In addition, this competitive enzymatic system is able to decrease 50% of Cr-stimulated respiration in isolated cardiac mitochondria, showing a fairly effective channeling of ADP from MtCK to the medium [154, 158]. This protocol is very helpful to elucidate the role of the MOM in controlling the MI function. Nevertheless, under pathological conditions, when the MOM is broken or tubulin is lost from the MI a direct transfer of ATP is observed.

An outstanding result presented in this work shows that any disturbance in MOM permeability regulation, either a mild proteolytic treatment or an insufficient (<95 %) intact rod like cardiac cells, results in an ADP leakage, hence a remarkable decrease of respiration.

Cytoskeletal proteins interactions and mitochondrial dynamics

The well-established arrangement of mitochondria in cardiac cells, together with the discovery of specific tubulin-distribution and how various cytoskeletal proteins play an important role in the energy metabolism and morphology provided us a better insight of previous studies. The normal shape of cardiomyocytes is maintained by proteins such as tubulins, plectin, desmin, among others [48, 49, 160-163]. Although when cells are permeabilized with saponin, mitochondria retain their crystal-like pattern along with relative slow fluctuations around their position [97, 99]. In Beraud's *et*

al. [97] work, it was proposed that these fluctuations reflect the configurational changes of mitochondrial matrix between two classical condensed and orthodox states.

The observations of Beraud *et al*. showed in adult cardiac cells that under normal conditions, mitochondria remain in rather fixed positions with low amplitude fluctuations in their fluorescent centers within the range of less than a mitochondrion diameter (~20%). Moreover, this study showed that the position of mitochondrial fluorescent centers depend on the precise localization of mitochondria in cells, and on the configuration of their inner membrane. Therefore, the rapid low amplitude changes in the position of fluorescent centers may reflect frequent and continuous transitions in the configuration of the cristae in the inner mitochondrial membrane [97]. In addition, she showed the absence of inter-mitochondrial connectivity, hence no electrical connectivity among adult cardiac mitochondria.

Finally, with all previous studies and my observations, it was important to have a better understanding of mitochondrial dynamics -*i.e*. fusion events- in healthy adult cardiac cells. The cytoskeletal protein α-actinin was used to observe its regular distribution in Z lines that confines mitochondrion to a specific area in cardiac cells. Therefore, fusion events may be possible in perinuclear-mitochondria. Perinuclear mitochondrial clusters display a different spatial conformation compared to interfibrillar-mitochondria which have a regular crystal-like arrangement.

The last dynamic studies show the fluctuations of mitochondrial fluorescent centers, nevertheless Z lines are constant during the recordings. These confirm previous observations by Beraud *et al*. and indicate that mitochondrial fusion is scarcely occurring in healthy adult interfibrillar-mitochondria cardiomyocytes. However, further studies may be needed to understand fusion-fission phenomena in adult cardiomyocytes in respect to interfibrillar- and perinuclear-mitochondria. Moreover, it is important to mention that these final observations of the cardiac mitochondrial dynamics have to consider that this highly structure cells include many other cytoskeletal proteins, such as tubulins, plectin, desmin, microfilaments, myotubules, etc. All these cytoskeletal proteins were not possible to

observe during *in vivo - in situ* studies, due its complexity and proximity, but all these proteins are involved in some degree to give the well-established crystal-like pattern of adult cardiac mitochondria, that also goes in complete agreement with the previous three-dimensional electron microscopy observations by Hayashi *et al*. [164] where it was well shown this T-tubule arrangement between mitochondria.

Thus, the present work provides a further insight into the structure-function relationship of energy fluxes in adult cardiac cells and how these mitochondria-cytoskeletal interactions are directly involved in the energy fluxes and mitochondrial respiration. Besides, a more impressive discovery was the specific distribution of tubulin βII that seems to be the tubulin isotype in charge of VDAC permeability, therefore, the protein in charge of the regulation of ATP/ADP fluxes across MOM. Furthermore, dynamic studies show us that mitochondrial fusion phenomenon hardly occurs in adult healthy cardiac cells due in part to all cytoskeletal proteins that have distinct roles in the heart physiology, but also have a morphological role that confine mitochondria into a very specific area of the cardiomyocytes.

«Our conclusion from the results shown above is that there is still no direct evidence of the existence of mitochondrial reticulum in heart cells. This conclusion is consistent with the results of many earlier electron microscopic studies [8, 98, 165] and recent observations by confocal microscopy [58, 83, 99]. Most interestingly, however, the question of mitochondrial morphology and arrangement in cardiac cells was unequivocally and with absolute clarity solved in a recent excellent electron tomographic study by Hayashi *et al*. of membrane structures involved in calcium cycling in heart cells [164]. This advanced technology allowed achieving 5-8 nm resolution 3D microscopic analyses across multiple sarcomeres in mammalian cardiac muscle [164]. This excellent study and others [166, 167] invalidate one of main arguments used by Westermann to develop his hypothesis that in muscle cells, mitochondrial filaments connect a dense layer of mitochondria in the oxygen-rich cell periphery with mitochondria in the oxygen-poor core of the muscle fiber, thereby forming a continuous network that dissipates the membrane potential generated in the cell periphery over a large area and uses it to produce ATP in remote parts of the cell [84]. This is not needed, and even not possible because

of the fine spatial structure of extensions of sarcolemma into the cell interior, called T-tubular system. It is an elaborate network of transversal-axial tubules located at the level of Z lines or between these lines of each sarcomere in close contact with sarcoplasmic reticulum and mitochondria. This makes possible the direct supply of calcium, substrates and oxygen from extracellular medium into the cell to each mitochondria in these local areas, it also prevents from mitochondrial fusion. This technique and information were not available when the original hypothesis was proposed [104, 168, 169].

Calcium release units.

Calcium cycling is the mechanism of the excitation – contraction coupling which regulates the contraction of striated muscle cells [170, 171]. In the heart, small amounts of calcium enter into the cell from extracellular medium during depolarization phase of action potential through sarcolemmal calcium channels called also dyhydropyridine receptors (DHPR) and releases larger amounts of calcium from sarcoplasmic reticulum (calcium induced calcium release, CICR) through the channels called ryanodine receptors (RyR). Calcium cycle is terminated by re-accumulation of calcium within sarcoplasmic reticulum (SR) through Ca-dependent ATPase (SERCA) and part of calcium is exported into extracellular medium via Na-Ca exchanger in the sarcolemmal membrane [171]. The elementary event in calcium cycle is a Ca spark: localized Ca-release events, due to random and collective opening of RyR channels clustered in the local areas, called calcium release units (CRU). Each CRU contains about 10 sarcolemmal Ca channels and several hundred RyR [172-175]. Different CRU form diffusively coupled networks in cardiomyocytes [174]. Total number of CRUs in one cardiomyocyte has been found to be of the order of 10^4 [174, 175].

The calcium is released in the all diffusively connected CRU that activates sarcomere contraction, by binding to troponin complex on thin actin filaments and by making possible the myosin-actin interaction, thus a contraction cycle [170, 176]. The force of contraction and cardiac work are regulated also by changes in sarcomere length [176]. This is the length-dependent mechanism of muscle contraction regulation, explaining Frank-Starling law of the heart - the dependence of cardiac performance on left venticular filling [22, 40].

Mitochondrial arrangement into Intracellular Energetic Units, ICEUs, and respiration regulation.

Mitochondria take part in the calcium cycle, importing calcium by the calcium uniport transporter and exporting it through the Na-Ca exchanger [170, 177]. In mitochondria, calcium is needed to maintain Krebs cycle dehydrogenases in active state [177]. Mitochondrial respiration and ATP production are dependent both

upon calcium entry into mitochondria from CRUs and metabolic signaling from myofibrillar ATPases in sarcomeres, meanwhile contraction is regulated by Ca and sarcomere length-dependent mechanism [22, 177].

About 50 % of DHPR are located in the T-tubular system, which in the cells is localized transversely and axially [167] close to Z-lines in vicinity of junctional cisterns of SR (jSR) and mitochondria. Hayashi et al. studied the morphology and distribution of T-tubular system, jSR and mitochondria in cardiomyocytes with the use of high resolution electron tomography [164]. The most interesting results of this excellent work are reproduced in Figure 6 of the last paper (Karu-Varikmma *et al*. submitted). Figure 6A shows individual mitochondria localized at the level of A-band of sarcomeres. Figure 6B shows that at the Z-line mitochondria are in close contacts with jSR and T-tubular system forming CRUs, which also separate mitochondria from each other, thus making their fusion impossible. Figure 6C shows the 3D image of separate mitochondria in another volume that crosscuts of most of myofilaments. Again, one sees individual mitochondria separated from each other by cellular structures. These results are in concord with earlier 3D electron microscopic studies of cardiac cell structures by Segretain reproduced in Figure 7 (Karu-Varikmma *et al*. submitted)[98]. Figure 7A shows the crossection of cardiomyocyte at H-band level where separate mitochondria are regularly surrounded by myofibrils. In cross-section taken at Z-line level no mitochondria are seen but T-tubular system and SR (Figure 7B). Figure 7C shows again that at Z-line level mitochondria are separated by T-tubular system and SR, those taking part in CRU.

Finally, Figure 7D shows the 3D reconstruction of T-tubular system in cardiac cell [44]. This is the very elaborated and effective system of Ca supply, substrates and oxygen from extracellular medium into cardiomyocytes. It plays an important role in cellular structural organization, metabolism and mitochondrial arrangement [164, 166, 167]. The discovery of this elaborated cellular architecture about 12 year ago profoundly changed our knowledge of heart cell structure and mechanisms of regulation of its metabolism [167]. Beraud *et al*. by using rapid scanning confocal microscopy showed that high frequency oscillations of the mitochondrial fluorescent centers occur only in the limited space between Z lines [97]. This is in concord with all structural data described above. It has also been shown in many laboratories that there is no electrical conductivity between individual mitochondria in cardiomyocytes [83, 175, 178-180]. Yaniv *et al*. [96] measured simultaneously the sarcomere and mitochondrial dimensions *in situ* along the long-axis in isolated cardiomyocytes by registering variations in transmitted light intensity and directly observed mitochondria as micron-sized spheres localized between sarcomeres and distributed throughout the cell in a crystal-like lattice

without any fusion. In this organized lattice, transient depolarizations of single mitochondria, known as flickers, due to ROS-induced opening of anion channels in the mitochondrial inner membranes may propagate in cells as depolarization waves [175, 180]. Cardiomyocytes were found to contain about 5000 – 10 000 single mitochondria regularly arranged in the cell [175].

All these data lead to the conclusion that the respiration of mitochondria is dependent on the events in the limited area of their localization in the vicinity of sarcomeres, SR and T-tubules. These structurally organized functional domains are called Intracellular Energetic Units, ICEUs [40, 41, 108] (Figure 8 - Karu-Varikmma *et al*. submitted). Due to elaborated structure of T-tubular system, mitochondria in ICEUs are in contact both with myofibrils and sarcolemma, and therefore we cannot distinct between subsarcolemmal or intermyofibrillar populations of mitochondria.

In the heart almost all ATP is synthesized by oxidative phosphorylation, and the linear relationship between heart workload (ATP hydrolysis) and oxygen consumption indicates very effective feedback regulation of mitochondrial respiratory activity in ICEUs [22, 40, 41]. Furthermore, the large range of changes of ATP turnover rate that may increase 20 times from resting state to maximal physiological workloads [181], is seen in the presence of stable intracellular levels of such energy metabolites as the ADP, Pi, ATP and PCr (metabolic stability or homeostasis) [67, 181, 182]. Several mechanisms of regulation of mitochondrial ATP synthesis matching intracellular ATP needs were proposed to explain heart bioenergetics under conditions of metabolic stability. Among them are above discussed Ca-dependent activation of Krebs cycle dehydrogenases [177, 182] and the control of oxidative phosphorylation on beat to beat basis by the complex signal consisting of creatine/PCr ratio as well as the ADP, Pi and AMP small-scale local fluctuations within contraction cycle (my). It was demonstrated by Dzeja and Terzic groups with using ^{18}O tracer method that about 80% of mitochondrial ATP is used for phosphocreatine (PCr) production in the mitochondrial creatine kinase (MtCK) reaction, the PCr flux carrying energy to all cites of ATP regeneration for ATPases within ICEUs (Figure 8 - Karu-Varikmma *et al*. submitted) [75, 183]. Metabolic control analysis of mitochondrial respiration regulation in cardiomyocytes has shown that by the mechanism of effective recycling of ADP-ATP in mitochondria, the MtCK reaction of PCr production coupled to oxidative phosphorylation is an effective amplifier of metabolic signals within ICEUs [40, 184]. Glancy and Balaban have recently also concluded that "a possibility for the observed metabolic homeostasis in intact tissues is the compartmentation of metabolic intermediates in the

cytosol much like that demonstrated for Ca^{2+} . The basic concept is that regional changes in ADP, Pi, and creatine in the regions around the mitochondria are major factors in driving mitochondrial ATP production" [177].

Thus, matching of ATP synthesis to ATP hydrolysis for cellular work is the result of compartmentation of integrated metabolic processes, created by the interaction between cellular membranes, cytoskeletal proteins and organelles in the limited space of ICEUs [40]. To overcome the restricted diffusion of metabolites in the structurally organized intracellular medium, the most effective mechanism of functioning of organized metabolic pathways is the metabolic channeling of reaction intermediates within supercomplexes - metabolons [5, 32, 43, 97, 185]. An example of such a processes is the intracellular glycolytic metabolon, mitochondrial TCA metabolon, β-fatty acids oxidation complex in mitochondrial matrix, PDH complex and even the formation of electron transport chain supercomplexes [186].These reactions occur in ICEUs in closely associated CRUs [40] (Figure 8 - Karu-Varikmma *et al*. submitted). A mitochondrial substrate such as pyruvate (final product of anaerobic glycolysis) is directly transferred through the integrated within MIM PDH enzymes complex giving acetyl CoA. The transfer of fatty acids towards the matrix is also dependent on the membrane enzymes: acetyl coenzyme-A synthetase and carnitine palmitoyl transferase (CPT1) in the outer, and CPT2 in the inner membrane. Released into the matrix acyl coenzyme-A enters directly the β-fatty acids oxidation (β-FAO) pathway giving acetyl CoA. Once acetyl CoA is formed, the Krebs cycle begins. Krebs cycle is a big metabolon attached to MIM and forming eight steps of enzymatic transformation of acetyl into $NADH,H^+$, $FADH_2$ and CO_2. All attempts to disrupt this metabolon will slow down formation of the reducing equivalents for the respiratory chain [187]. The electron transfer complexes ANT, Phosphate Carrier (PC) are incorporated into large assemblies, called supercomplexes [188, 189].

Mixing the contents of all mitochondria into one reticulum may be expected only to destroy all these effective metabolic complexes, increasing diffusion time for intermediates and thus decreasing the energy fluxes (as seen in HL-1 cells), but not elevating the respiration rates, as proposed by Westermann [84, 190].

This, if fusion-fission cycle occurs in heart cells, it is a very infrequent phenomenon and does not include the formation of continuous mitochondrial reticulum. It is not excluded that some fusion may occur in the perinuclear mitochondrial clusters. Two main indirect evidences are used for mitochondrial fusion-fission dynamics in cardiac muscle cells [79]. One of them is the presence of fusion-fission proteins in heart muscle and another one consists in pathological remodeling of cardiac cells induced by abrogation of these proteins

by genetic manipulations [79]. However, fusion is not an exclusively mitochondrial feature. It is typical for such membranous intracellular structures as the sarcoplasmic reticulum, Golgi apparatus and intracellular vesiculs. Koshiba's et al., have shown that mitochondrial fusions, like other intracellular membrane fusion events, proceeds through a tethering step mediated by heptad repeat region (HR2) [191]. In normal adult cardiac cells fusion proteins may be tethering regularly arranged individual mitochondria to the surrounding membranous structures such as T-tubules and sarcoplasmic reticulum as shown in Scorrano's laboratory [192], rather than to induce fusion. In recent work, Chen Y et al have also shown that Mfn2 is essential for tethering mitochondria to sarcoplasmic reticulum [193].

Moreover, the fusion-fission mitochondrial dynamics becomes evident for cardiac cells under pathological conditions such as the ischemia-reperfusion [79]. It is interesting that in all these situations mitochondrial fusion-fission is associated with the remodeling of sarcomeres and T-tubules. Cardiac failure *in vivo* due to the loss of fusongenic proteins associated with fragmentation of cardiac mitochondria into small heterogeneous conglomerates [194] can be due to the disorganization of cell structure and metabolic compartmentation (remodeling of mitochondria-associated membrane interactions), impairment of intramitochondrial energy conversion, intracellular distribution of energy fluxes and controlling signals. In conclusion, one cannot extend knowledge experimentally obtained for one cell-type to all others. For every cell type integrative structural and functional studies should be performed separately for revealing the mechanisms of regulation of their metabolism and energy fluxes». (Taken from Minna Karu-Varikmaa, Marcela González-Granillo, Alexei Grichine, Yves Usson, François Boucher, Tuuli Kaambre, Rita Guzun and Valdur Saks. Matter of the heart in bioenergetics: mitochondrial fusion into continuous reticulum is not needed for maximal respiration activity. Submitted for revision to: BBA-Bioenergetics, July 13th).

Therefore, Westermann's proposal about how fragmented mitochondria have a low respiratory activity and hyperfused mitochondria have a high respiratory activity [84], goes completely against what it was demonstrated in cardiac cells and even with what it has been previously seen [40, 97, 142, 145, 152, 154].

VII. CONCLUSIONS

The present work shows by different measurements the existence of a structure-function relationship that regulates the energy fluxes. The very regular arrangement of mitochondria observed in adult healthy cardiac cells is supported by cytoskeletal proteins, such as the tubulin system and α-actinin, among others. An outstanding feature of the present work is the specific distribution of tubulin isotypes in adult cardiac cells. The Mitochondrial Interactosome (MI) is composed of ATP synthasome, mitochondrial creatine kinase (MtCK), voltage dependent anion channel (VDAC) in the outer membrane and regulatory proteins associated to VDAC. Therefore, the results presented in this work highly suggest that tubulin-βII is the tubulin isotype bound to VDAC that controls the ATP/ADP diffusion into mitochondrial intermembrane space in adult cardiomyocytes.

Mitochondrial organization of adult cardiac cells and of the cancerous cardiac phenotype HL-1 cells differs greatly from each other. Meanwhile, tubulin-βII and MtCK are co-expressed in adult cardiomyocytes, both proteins lack in HL-1 cells. Therefore, the structure of the MI in healthy mammalian cells differs from the immortal cancerous cardiac cell lines.

None of the analyzed samples, isolated cardiomyocytes and cardiac fibers, displayed the presence of a mitochondrial tubular network or any fusion event in interfibrillar mitochondria within the interval time of our observations. Our studies of mitochondrial dynamics showed that interfibrillar mitochondria are confined in a specific area, surrounded by sarcomeres and the tubular system. Therefore, fusion events were absent in adult healthy cardiac cells, and fusion is not needed for maximal respiratory activity as it was proposed by other authors. However, a fused or fragmented state of mitochondria evidently has an effect on the respiratory activity, but still none of the present results showed a direct evidence of a mitochondrial reticulum in heart cells.

VIII. FUTURE PERSPECTIVES

The results obtained in the present work showed that there is a structure-function relationship that regulates the energy fluxes in healthy adult cardiac cells. To have a better understanding of this fine regulation, it would be important to study if there is a specific pairing of each β-tubulin isotype, with the still unknown distribution of α-tubulin isotypes.

Regarding this structure-function relationship it would be interesting to elucidate in skeletal muscle due to their metabolic variability, on one side to show the distribution of cytoskeletal proteins and on the other side if this structure-function relationship regulates their metabolic activity *i.e*. glycolytic and oxidative.

Moreover, it would be interesting to see in mammalian cardiac cells how this relationship is modified under pathological conditions, such as ischemia and metabolic diseases. If the specific distribution of β-tubulin isotypes is still kept during pathological states or if there is any re-arrangement of these cytoskeletal proteins and how these modifications are involved in the respiratory activity.

Finally, it would be highly interesting to observe under pathological states whether mitochondrial dynamics present a reorganization of interfibrillar mitochondria, having a higher presence of fusion or fission phenomena and how this modifies the maximal respiratory activity.

IX. REFERENCES

1. Kohl, P., et al., *Systems biology: an approach.* Clin Pharmacol Ther. **88**(1): p. 25-33.
2. Watson, J.D. and F.H. Crick, *Molecular structure of nucleic acids; a structure for deoxyribose nucleic acid.* Nature, 1953. **171**(4356): p. 737-8.
3. Noble, D., *The music of life : biology beyond the genome*. 2006, Oxford: Oxford University Press.
4. Noble, D., *Claude Bernard, the first systems biologist, and the future of physiology.* Exp Physiol, 2008. **93**(1): p. 16-26.
5. Saks, V., C. Monge, and R. Guzun, *Philosophical basis and some historical aspects of systems biology: from Hegel to Noble - applications for bioenergetic research.* Int J Mol Sci, 2009. **10**(3): p. 1161-92.
6. Xavier M. Leverve, N.T., Roland Favier, Cécile Batandier, Dominique Detaille, Anne Devin, Eric Fontaine, and Michel Rigoulet *Molecular System Bioenergetics: Basic Principles, Organization, and Dynamics of Cellular Energetics*, in *Molecular System Bioenergetics: energy for life*, P.V. Saks, Editor. 2007, Wiley-VCH Verlag GmbH & Co. KGaA: Grenoble Cedex 9. p. 11-27.
7. Lehninger, A.L., D.L. Nelson, and M.M. Cox, *Lehninger principles of biochemistry*. 4th ed. 2005, New York: W.H. Freeman. 1 v. (various pagings).
8. Hoppel, C.L., et al., *Dynamic organization of mitochondria in human heart and in myocardial disease.* Int J Biochem Cell Biol, 2009. **41**(10): p. 1949-56.
9. Brookes, P.S., et al., *Calcium, ATP, and ROS: a mitochondrial love-hate triangle.* Am J Physiol Cell Physiol, 2004. **287**(4): p. C817-33.
10. Hom, J. and S.S. Sheu, *Morphological dynamics of mitochondria--a special emphasis on cardiac muscle cells.* J Mol Cell Cardiol, 2009. **46**(6): p. 811-20.
11. Opie, L.H., *The heart : physiology, metabolism, pharmacology, and therapy*. 1984, London ; Orlando: Grune & Stratton. xii, 392 p.
12. Griffiths, E.J., D. Balaska, and W.H. Cheng, *The ups and downs of mitochondrial calcium signalling in the heart.* Biochim Biophys Acta. **1797**(6-7): p. 856-64.
13. Svensson, O.L., *Mitochondria : structure, functions, and dysfunctions*, Hauppauge, N.Y.: Nova Biomedical Books.
14. O'Rourke, B., S. Cortassa, and M.A. Aon, *Mitochondrial ion channels: gatekeepers of life and death.* Physiology (Bethesda), 2005. **20**: p. 303-15.
15. von Ballmoos, C., A. Wiedenmann, and P. Dimroth, *Essentials for ATP synthesis by F1F0 ATP synthases.* Annu Rev Biochem, 2009. **78**: p. 649-72.
16. Alberts, B., J.H. Wilson, and T. Hunt, *Molecular biology of the cell*. 5th ed. 2008, New York: Garland Science. xxxiii, 1601, [90] p.
17. Vignais, P.V., P.M. Vignais, and J. Doussiere, *Functional relationship between the ADP/ATP-carrier and the F1-ATPase in mitochondria.* Biochim Biophys Acta, 1975. **376**(2): p. 219-30.
18. Saks, V.A., et al., *Role of creatine phosphokinase in cellular function and metabolism.* Can J Physiol Pharmacol, 1978. **56**(5): p. 691-706.
19. Dolder, M., S. Wendt, and T. Wallimann, *Mitochondrial creatine kinase in contact sites: interaction with porin and adenine nucleotide translocase, role in permeability transition and sensitivity to oxidative damage.* Biol Signals Recept, 2001. **10**(1-2): p. 93-111.
20. Colombini, M., *Voltage gating in the mitochondrial channel, VDAC.* J Membr Biol, 1989. **111**(2): p. 103-11.
21. Mannella, C.A., et al., *The internal compartmentation of rat-liver mitochondria: tomographic study using the high-voltage transmission electron microscope.* Microsc Res Tech, 1994. **27**(4): p. 278-83.
22. Saks, V., et al., *Cardiac system bioenergetics: metabolic basis of the Frank-Starling law.* J Physiol, 2006. **571**(Pt 2): p. 253-73.

23. Gautel, T.B.M., *Transcriptional mechanisms regulating skeletal muscle differentiation, growth and homeostasis.* Nature Reviws Molecular Cell Biology, 2011. **12**: p. 349-61.
24. Gordon, A.M., M. Regnier, and E. Homsher, *Skeletal and cardiac muscle contractile activation: tropomyosin "rocks and rolls".* News Physiol Sci, 2001. **16**: p. 49-55.
25. Gautel, M., *The sarcomeric cytoskeleton: who picks up the strain?* Curr Opin Cell Biol. **23**(1): p. 39-46.
26. Horowits, R., *The physiological role of titin in striated muscle.* Rev Physiol Biochem Pharmacol, 1999. **138**: p. 57-96.
27. Page, E., *The Actions of Cardiac Glycosides on Heart Muscle Cells.* Circulation, 1964. **30**: p. 237-51.
28. Akiyama, N., et al., *Transverse stiffness of myofibrils of skeletal and cardiac muscles studied by atomic force microscopy.* J Physiol Sci, 2006. **56**(2): p. 145-51.
29. McKillop, D.F. and M.A. Geeves, *Regulation of the interaction between actin and myosin subfragment 1: evidence for three states of the thin filament.* Biophys J, 1993. **65**(2): p. 693-701.
30. Ventura-Clapier, R., A. Kaasik, and V. Veksler, *Structural and functional adaptations of striated muscles to CK deficiency.* Mol Cell Biochem, 2004. **256-257**(1-2): p. 29-41.
31. Nabuurs, C., et al., *31P saturation transfer spectroscopy predicts differential intracellular macromolecular association of ATP and ADP in skeletal muscle.* J Biol Chem. **285**(51): p. 39588-96.
32. Saks, V., N. Beraud, and T. Wallimann, *Metabolic compartmentation - a system level property of muscle cells: real problems of diffusion in living cells.* Int J Mol Sci, 2008. **9**(5): p. 751-67.
33. Aliev, M., et al., *Molecular System Bioenergics of the Heart: Experimental Studies of Metabolic Compartmentation and Energy Fluxes versus Computer Modeling.* Int J Mol Sci. **12**(12): p. 9296-331.
34. de Duve, C., *The origin of eukaryotes: a reappraisal.* Nat Rev Genet, 2007. **8**(5): p. 395-403.
35. Theo Wallimann, M.T.-S., Dietbert Neumann, Richard M. Epand, Raquel F. Epand, Robert H. Andres, Hans Rudolf Widmer, Thorsten Hornemann, Valdur Saks, Irina Agarkova, Uwe Schlattner, *The Phosphocratine Circuit: Molecular and Cellular Physiology of Creatine Kinases, Sensitivity to Free Radicals, and Enhancement by Creatine Supplementation*, in *Molecular System Bioenegetics: Energy for Life*, V. Saks, Editor. 2007, WILEY-VCH Verlag GmbH & Co. KGaA. p. 195-240.
36. Saks, V., et al., *Heterogeneity of ADP diffusion and regulation of respiration in cardiac cells.* Biophys J, 2003. **84**(5): p. 3436-56.
37. Saks, V., et al., *The creatine kinase phosphotransfer network: thermodynamic and kinetic considerations, the impact of the mitochondrial outer membrane and modelling approaches.* Subcell Biochem, 2007. **46**: p. 27-65.
38. Vendelin, M., et al., *Intracellular diffusion of adenosine phosphates is locally restricted in cardiac muscle.* Mol Cell Biochem, 2004. **256-257**(1-2): p. 229-41.
39. Ridgway, D., et al., *Coarse-grained molecular simulation of diffusion and reaction kinetics in a crowded virtual cytoplasm.* Biophys J, 2008. **94**(10): p. 3748-59.
40. Saks, V., et al., *Intracellular Energetic Units regulate metabolism in cardiac cells.* J Mol Cell Cardiol. **52**(2): p. 419-36.
41. Saks, V., et al., *Structure-function relationships in feedback regulation of energy fluxes in vivo in health and disease: mitochondrial interactosome.* Biochim Biophys Acta. **1797**(6-7): p. 678-97.
42. Fozzard, H.A., *The heart and cardiovascular system : scientific foundations*. 1986, New York, N.Y.: Raven.
43. Wallimann, T., et al., *Intracellular compartmentation, structure and function of creatine kinase isoenzymes in tissues with high and fluctuating energy demands: the 'phosphocreatine circuit' for cellular energy homeostasis.* Biochem J, 1992. **281 (Pt 1)**: p. 21-40.

44. Guzun, R., et al., *Regulation of respiration in muscle cells in vivo by VDAC through interaction with the cytoskeleton and MtCK within Mitochondrial Interactosome.* Biochim Biophys Acta.
45. Colombini, M., *VDAC structure, selectivity, and dynamics.* Biochim Biophys Acta.
46. Rostovtseva, T.K., et al., *Tubulin binding blocks mitochondrial voltage-dependent anion channel and regulates respiration.* Proc Natl Acad Sci U S A, 2008. **105**(48): p. 18746-51.
47. Colombini, M., *VDAC: the channel at the interface between mitochondria and the cytosol.* Mol Cell Biochem, 2004. **256-257**(1-2): p. 107-15.
48. Kostin, S., et al., *The cytoskeleton and related proteins in the human failing heart.* Heart Fail Rev, 2000. **5**(3): p. 271-80.
49. Rappaport, L., P. Oliviero, and J.L. Samuel, *Cytoskeleton and mitochondrial morphology and function.* Mol Cell Biochem, 1998. **184**(1-2): p. 101-5.
50. Lemasters, J.J. and E. Holmuhamedov, *Voltage-dependent anion channel (VDAC) as mitochondrial governator--thinking outside the box.* Biochim Biophys Acta, 2006. **1762**(2): p. 181-90.
51. Sackett, D.L., *Evolution and coevolution of tubulin's carboxyl-terminal tails and mitochondria*, in *Mitochondria: Structure, Functions and Dysfunctions*, O.L. Svensson, Editor. 2010, Nova Science: New York. p. 789-810.
52. Cleveland, D.W., *The multitubulin hypothesis revisited: what have we learned?* J Cell Biol, 1987. **104**(3): p. 381-3.
53. Redeker, V., *Mass spectrometry analysis of C-terminal posttranslational modifications of tubulins.* Methods Cell Biol. **95**: p. 77-103.
54. Tagawa, H., et al., *Cytoskeletal role in the transition from compensated to decompensated hypertrophy during adult canine left ventricular pressure overloading.* Circ Res, 1998. **82**(7): p. 751-61.
55. Luduena, R.F., *Multiple forms of tubulin: different gene products and covalent modifications.* Int Rev Cytol, 1998. **178**: p. 207-75.
56. Tuszynski, J.A., et al., *The evolution of the structure of tubulin and its potential consequences for the role and function of microtubules in cells and embryos.* Int J Dev Biol, 2006. **50**(2-3): p. 341-58.
57. Janke, C. and J.C. Bulinski, *Post-translational regulation of the microtubule cytoskeleton: mechanisms and functions.* Nat Rev Mol Cell Biol. **12**(12): p. 773-86.
58. Guzun, R., et al., *Mitochondria-cytoskeleton interaction: distribution of beta-tubulins in cardiomyocytes and HL-1 cells.* Biochim Biophys Acta. **1807**(4): p. 458-69.
59. Gonzalez-Granillo, M., et al., *Studies of the role of tubulin beta II isotype in regulation of mitochondrial respiration in intracellular energetic units in cardiac cells.* J Mol Cell Cardiol. **52**(2): p. 437-47.
60. Joshi, H.C. and D.W. Cleveland, *Differential utilization of beta-tubulin isotypes in differentiating neurites.* J Cell Biol, 1989. **109**(2): p. 663-73.
61. Saetersdal, T., G. Greve, and H. Dalen, *Associations between beta-tubulin and mitochondria in adult isolated heart myocytes as shown by immunofluorescence and immunoelectron microscopy.* Histochemistry, 1990. **95**(1): p. 1-10.
62. Appaix, F., et al., *Possible role of cytoskeleton in intracellular arrangement and regulation of mitochondria.* Exp Physiol, 2003. **88**(1): p. 175-90.
63. Andrienko, T., et al., *Metabolic consequences of functional complexes of mitochondria, myofibrils and sarcoplasmic reticulum in muscle cells.* J Exp Biol, 2003. **206**(Pt 12): p. 2059-72.
64. Gunter, T.E., et al., *Calcium and mitochondria.* FEBS Lett, 2004. **567**(1): p. 96-102.
65. Gordon, A.M., E. Homsher, and M. Regnier, *Regulation of contraction in striated muscle.* Physiol Rev, 2000. **80**(2): p. 853-924.
66. Hibberd, M.G. and B.R. Jewell, *Calcium- and length-dependent force production in rat ventricular muscle.* J Physiol, 1982. **329**: p. 527-40.
67. Neely, J.R., et al., *The effects of increased heart work on the tricarboxylate cycle and its interactions with glycolysis in the perfused rat heart.* Biochem J, 1972. **128**(1): p. 147-59.

68. Balaban, R.S., et al., *Relation between work and phosphate metabolite in the in vivo paced mammalian heart.* Science, 1986. **232**(4754): p. 1121-3.
69. Wan, B., et al., *Effects of cardiac work on electrical potential gradient across mitochondrial membrane in perfused rat hearts.* Am J Physiol, 1993. **265**(2 Pt 2): p. H453-60.
70. Hassinen, I.E. and K. Hiltunen, *Respiratory control in isolated perfused rat heart. Role of the equilibrium relations between the mitochondrial electron carriers and the adenylate system.* Biochim Biophys Acta, 1975. **408**(3): p. 319-30.
71. Shimizu, J., K. Todaka, and D. Burkhoff, *Load dependence of ventricular performance explained by model of calcium-myofilament interactions.* Am J Physiol Heart Circ Physiol, 2002. **282**(3): p. H1081-91.
72. Dzeja, P.P., A. Terzic, and B. Wieringa, *Phosphotransfer dynamics in skeletal muscle from creatine kinase gene-deleted mice.* Mol Cell Biochem, 2004. **256-257**(1-2): p. 13-27.
73. Kay, L., et al., *Direct evidence for the control of mitochondrial respiration by mitochondrial creatine kinase in oxidative muscle cells in situ.* J Biol Chem, 2000. **275**(10): p. 6937-44.
74. Saks, V.A., et al., *Metabolic compartmentation and substrate channelling in muscle cells. Role of coupled creatine kinases in in vivo regulation of cellular respiration--a synthesis.* Mol Cell Biochem, 1994. **133-134**: p. 155-92.
75. Dzeja, P.P. and A. Terzic, *Phosphotransfer networks and cellular energetics.* J Exp Biol, 2003. **206**(Pt 12): p. 2039-47.
76. Saks, V.A., et al., *Functional coupling as a basic mechanism of feedback regulation of cardiac energy metabolism.* Mol Cell Biochem, 2004. **256-257**(1-2): p. 185-99.
77. Vendelin, M., M. Lemba, and V.A. Saks, *Analysis of functional coupling: mitochondrial creatine kinase and adenine nucleotide translocase.* Biophys J, 2004. **87**(1): p. 696-713.
78. Bereiter-Hahn, J. and M. Voth, *Dynamics of mitochondria in living cells: shape changes, dislocations, fusion, and fission of mitochondria.* Microsc Res Tech, 1994. **27**(3): p. 198-219.
79. Dorn, G.W., 2nd, *Mitochondrial dynamics in heart disease.* Biochim Biophys Acta.
80. Duchen, M.R., *Mitochondria in health and disease: perspectives on a new mitochondrial biology.* Mol Aspects Med, 2004. **25**(4): p. 365-451.
81. Kane, L.A. and R.J. Youle, *Mitochondrial fission and fusion and their roles in the heart.* J Mol Med (Berl). **88**(10): p. 971-9.
82. Yaffe, M.P., *The machinery of mitochondrial inheritance and behavior.* Science, 1999. **283**(5407): p. 1493-7.
83. Kuznetsov, A.V., et al., *The cell-type specificity of mitochondrial dynamics.* Int J Biochem Cell Biol, 2009. **41**(10): p. 1928-39.
84. Westermann, B., *Bioenergetic role of mitochondrial fusion and fission.* Biochim Biophys Acta.
85. Chen, H. and D.C. Chan, *Emerging functions of mammalian mitochondrial fusion and fission.* Hum Mol Genet, 2005. **14 Spec No. 2**: p. R283-9.
86. Han, X.J., et al., *Regulation of mitochondrial dynamics and neurodegenerative diseases.* Acta Med Okayama. **65**(1): p. 1-10.
87. Twig, G., B. Hyde, and O.S. Shirihai, *Mitochondrial fusion, fission and autophagy as a quality control axis: the bioenergetic view.* Biochim Biophys Acta, 2008. **1777**(9): p. 1092-7.
88. Chan, D.C., *Mitochondria: dynamic organelles in disease, aging, and development.* Cell, 2006. **125**(7): p. 1241-52.
89. Ord, M.J., *The effects of chemicals and radiations within the cell: an ultrastructural and micrurgical study using Amoeba proteus as a single-cell model.* Int Rev Cytol, 1979. **61**: p. 229-81.
90. Brunner, A., Jr., J.A. Bilotta, and D.D. Morena, *Mitochondria, hemosomes and hemoglobin biosynthesis.* Cell Tissue Res, 1983. **233**(1): p. 215-25.
91. Stromer, M.H. and M. Bendayan, *Immunocytochemical identification of cytoskeletal linkages to smooth muscle cell nuclei and mitochondria.* Cell Motil Cytoskeleton, 1990. **17**(1): p. 11-8.
92. Kuznetsov, S.A., G.M. Langford, and D.G. Weiss, *Actin-dependent organelle movement in squid axoplasm.* Nature, 1992. **356**(6371): p. 722-5.

93. Ogata, T. and Y. Yamasaki, *Scanning electron-microscopic studies on the three-dimensional structure of sarcoplasmic reticulum in the mammalian red, white and intermediate muscle fibers.* Cell Tissue Res, 1985. **242**(3): p. 461-7.
94. Ogata, T. and F. Murata, *Cytological features of three fiber types in human striated muscle.* Tohoku J Exp Med, 1969. **99**(3): p. 225-45.
95. Ong, S.B. and D.J. Hausenloy, *Mitochondrial morphology and cardiovascular disease.* Cardiovasc Res. **88**(1): p. 16-29.
96. Yaniv, Y., et al., *Analysis of mitochondrial 3D-deformation in cardiomyocytes during active contraction reveals passive structural anisotropy of orthogonal short axes.* PLoS One. **6**(7): p. e21985.
97. Beraud, N., et al., *Mitochondrial dynamics in heart cells: very low amplitude high frequency fluctuations in adult cardiomyocytes and flow motion in non beating Hl-1 cells.* J Bioenerg Biomembr, 2009. **41**(2): p. 195-214.
98. Segretain, D., A. Rambourg, and Y. Clermont, *Three dimensional arrangement of mitochondria and endoplasmic reticulum in the heart muscle fiber of the rat.* Anat Rec, 1981. **200**(2): p. 139-51.
99. Vendelin, M., et al., *Mitochondrial regular arrangement in muscle cells: a "crystal-like" pattern.* Am J Physiol Cell Physiol, 2005. **288**(3): p. C757-67.
100. Shen, T., et al., *Mitofusin-2 is a major determinant of oxidative stress-mediated heart muscle cell apoptosis.* J Biol Chem, 2007. **282**(32): p. 23354-61.
101. Kuznetsov, A.V., et al., *Functional heterogeneity of mitochondria after cardiac cold ischemia and reperfusion revealed by confocal imaging.* Transplantation, 2004. **77**(5): p. 754-6.
102. Sauvanet, C., et al., *Energetic requirements and bioenergetic modulation of mitochondrial morphology and dynamics.* Semin Cell Dev Biol. **21**(6): p. 558-65.
103. Chen, H., A. Chomyn, and D.C. Chan, *Disruption of fusion results in mitochondrial heterogeneity and dysfunction.* J Biol Chem, 2005. **280**(28): p. 26185-92.
104. Skulachev, V.P., *Mitochondrial filaments and clusters as intracellular power-transmitting cables.* Trends Biochem Sci, 2001. **26**(1): p. 23-9.
105. Palaniyandi, S.S., et al., *Regulation of mitochondrial processes: a target for heart failure.* Drug Discov Today Dis Mech. **7**(2): p. e95-e102.
106. Rapaport, D., et al., *Fzo1p is a mitochondrial outer membrane protein essential for the biogenesis of functional mitochondria in Saccharomyces cerevisiae.* J Biol Chem, 1998. **273**(32): p. 20150-5.
107. Hermann, G.J., et al., *Mitochondrial fusion in yeast requires the transmembrane GTPase Fzo1p.* J Cell Biol, 1998. **143**(2): p. 359-73.
108. Saks, V.A., et al., *Intracellular energetic units in red muscle cells.* Biochem J, 2001. **356**(Pt 2): p. 643-57.
109. Seppet, E.K., et al., *Functional complexes of mitochondria with Ca,MgATPases of myofibrils and sarcoplasmic reticulum in muscle cells.* Biochim Biophys Acta, 2001. **1504**(2-3): p. 379-95.
110. Gnaiger, E., *Oxygen solubility in experimental media*, in *Oroboros Bioenergetics Newsletter*. 2001. p. 1-6.
111. Brand, M.D. and D.G. Nicholls, *Assessing mitochondrial dysfunction in cells.* Biochem J. **435**(2): p. 297-312.
112. Kuznetsov, A.V., et al., *Analysis of mitochondrial function in situ in permeabilized muscle fibers, tissues and cells.* Nat Protoc, 2008. **3**(6): p. 965-76.
113. Gonzalez-Granillo, M., et al., *Studies of the role of tubulin beta II isotype in regulation of mitochondrial respiration in intracellular energetic units in cardiac cells.* J Mol Cell Cardiol.
114. Anmann, T., et al., *Different kinetics of the regulation of respiration in permeabilized cardiomyocytes and in HL-1 cardiac cells. Importance of cell structure/organization for respiration regulation.* Biochim Biophys Acta, 2006. **1757**(12): p. 1597-606.
115. Valdur Saks, C.M., Tiia Anmann, and Petras P. Dzeja., *Integrated and organized cellular energetic systems: theories of cell energetics, compartmentation, and metabolic channeling*,

in *Molecular System Bioenergetics: Energy for Life*, P.V. Saks, Editor. 2007, Wiley-VCH Verlag GmbH & Co. KGaA: Grenoble Cedex 9. p. 59-109.
116. Nikolaev, V.O. and M.J. Lohse, *Monitoring of cAMP synthesis and degradation in living cells.* Physiology (Bethesda), 2006. **21**: p. 86-92.
117. Donald Voet, J.G.V., Charlotte W. Pratt, *Nucleotides, nucleic acids, and genetic information*, in *Fundamentals of Biochemistry: Life at the molecular level*. 2008, John Wiley & Sons, Inc. p. 39-73.
118. Bruce Alberts, A.J., Julian Lewis, Martin Raff, Keith Roberts, and Peter Walter, *Manipulating proteins, DNA, and RNA*, in *Molecular biology of the cell*. 2008, Harland Science, Taylor & Francis Group, LLC: New York. p. 501-578.
119. Ronot, X. and Y. Usson, *Imaging of nucleic acids and quantitation in photonic microscopy*. Methods in visualization. 2001, Boca Raton, FL: CRC Press. xv, 164 p.
120. Periasamy, A. and American Physiological Society (1887-). *Methods in cellular imaging*. The American Physiological Society methods in physiology series. 2001, Oxford ; New York: Published for the American Physiological Society by Oxford University Press. xiv, 434 p.
121. Saks, V.A., et al., *Permeabilized cell and skinned fiber techniques in studies of mitochondrial function in vivo.* Mol Cell Biochem, 1998. **184**(1-2): p. 81-100.
122. Semwogerere, D.W., E.R., *Confocal microscopy*, in *Encyclopedia of biomaterials and biomedical engineering*, T. Francis, Editor. 2005: Atlanta, Georgia. p. 10.
123. Pawley, J.B., *Handbook of biological confocal microscopy*. 3rd ed. 2006, New York, NY: Springer. xxviii, 985 p.
124. Russ, J.C., *Computer-assisted microscopy : the measurement and analysis of images*. 1990: Plenum Press.
125. Fukanga, K.a.H., Larry, *The Estimation of the Gradient of a Density function, with applications in Pattern Recognition.* IEEE Transactions of information theory, 1975. **IT-21**(1): p. 32-40.
126. Codling, E.A., M.J. Plank, and S. Benhamou, *Random walk models in biology.* J R Soc Interface, 2008. **5**(25): p. 813-34.
127. Einstein, A., *Von der molerulärkinetichen theorie der wärmegefordete bewegung von in ruhenden flüssigkeiten suspendiertenteilchen.* Ann Phys (Leipzig), 1905(17): p. 549-60.
128. Smoluchowski, M.v., *Zur kinetishen Theorie der Brownschen Molekularbewegung und der Suspensionen.* Ann. Physik, 1906(21): p. 756-80.
129. Philbert, J., *One and a half century of diffusion: Fick, Einstein, before and beyond.* Diffusion Fundam, 2006. **4**(6): p. 1-19.
130. Islam, M.A., *Einstein-Smoluchowski diffusion equation: a discussion.* Physica Scripta, 2004. **70**: p. 120-5.
131. Agutter, P.S., P.C. Malone, and D.N. Wheatley, *Intracellular transport mechanisms: a critique of diffusion theory.* J Theor Biol, 1995. **176**(2): p. 261-72.
132. Agutter, P.S., P.C. Malone, and D.N. Wheatley, *Diffusion theory in biology: a relic of mechanistic materialism.* J Hist Biol, 2000. **33**(1): p. 71-111.
133. Kuznetsov, A.V., et al., *Mitochondrial subpopulations and heterogeneity revealed by confocal imaging: possible physiological role?* Biochim Biophys Acta, 2006. **1757**(5-6): p. 686-91.
134. Mariani, M., et al., *Class III beta-tubulin (TUBB3): more than a biomarker in solid tumors?* Curr Mol Med. **11**(9): p. 726-31.
135. Dumontet, C., M.A. Jordan, and F.F. Lee, *Ixabepilone: targeting betaIII-tubulin expression in taxane-resistant malignancies.* Mol Cancer Ther, 2009. **8**(1): p. 17-25.
136. Sjoblom, B., A. Salmazo, and K. Djinovic-Carugo, *Alpha-actinin structure and regulation.* Cell Mol Life Sci, 2008. **65**(17): p. 2688-701.
137. Hiser, L., et al., *Comparison of beta-tubulin mRNA and protein levels in 12 human cancer cell lines.* Cell Motil Cytoskeleton, 2006. **63**(1): p. 41-52.
138. Patra, S., et al., *Progressive decrease of phosphocreatine, creatine and creatine kinase in skeletal muscle upon transformation to sarcoma.* FEBS J, 2008. **275**(12): p. 3236-47.

139. Eimre, M., et al., *Distinct organization of energy metabolism in HL-1 cardiac cell line and cardiomyocytes.* Biochim Biophys Acta, 2008. **1777**(6): p. 514-24.
140. Kuznetsov, A.V., et al., *Striking differences between the kinetics of regulation of respiration by ADP in slow-twitch and fast-twitch muscles in vivo.* Eur J Biochem, 1996. **241**(3): p. 909-15.
141. Appaix, F., et al., *Bax and heart mitochondria: uncoupling and inhibition of respiration without permeability transition.* Biochim Biophys Acta, 2002. **1556**(2-3): p. 155-67.
142. Timohhina, N., et al., *Direct measurement of energy fluxes from mitochondria into cytoplasm in permeabilized cardiac cells in situ: some evidence for Mitochondrial Interactosome.* J Bioenerg Biomembr, 2009. **41**(3): p. 259-75.
143. Aon, M.A., S. Cortassa, and B. O'Rourke, *Percolation and criticality in a mitochondrial network.* Proc Natl Acad Sci U S A, 2004. **101**(13): p. 4447-52.
144. Aon, M.A., et al., *Synchronized whole cell oscillations in mitochondrial metabolism triggered by a local release of reactive oxygen species in cardiac myocytes.* J Biol Chem, 2003. **278**(45): p. 44735-44.
145. Monge, C., et al., *Comparative analysis of the bioenergetics of adult cardiomyocytes and nonbeating HL-1 cells: respiratory chain activities, glycolytic enzyme profiles, and metabolic fluxes.* Can J Physiol Pharmacol, 2009. **87**(4): p. 318-26.
146. Kummel, L., *Ca, Mg-ATPase activity of permeabilised rat heart cells and its functional coupling to oxidative phosphorylation of the cells.* Cardiovasc Res, 1988. **22**(5): p. 359-67.
147. Saks, V.A., et al., *Control of cellular respiration in vivo by mitochondrial outer membrane and by creatine kinase. A new speculative hypothesis: possible involvement of mitochondrial-cytoskeleton interactions.* J Mol Cell Cardiol, 1995. **27**(1): p. 625-45.
148. Antonsson, B., *Mitochondria and the Bcl-2 family proteins in apoptosis signaling pathways.* Mol Cell Biochem, 2004. **256-257**(1-2): p. 141-55.
149. Dorn, G.W., 2nd, *Apoptotic and non-apoptotic programmed cardiomyocyte death in ventricular remodelling.* Cardiovasc Res, 2009. **81**(3): p. 465-73.
150. Saks, V.A., Y.O. Belikova, and A.V. Kuznetsov, *In vivo regulation of mitochondrial respiration in cardiomyocytes: specific restrictions for intracellular diffusion of ADP.* Biochim Biophys Acta, 1991. **1074**(2): p. 302-11.
151. Saks, V.A., et al., *Retarded diffusion of ADP in cardiomyocytes: possible role of mitochondrial outer membrane and creatine kinase in cellular regulation of oxidative phosphorylation.* Biochim Biophys Acta, 1993. **1144**(2): p. 134-48.
152. Monge, C., et al., *Regulation of respiration in brain mitochondria and synaptosomes: restrictions of ADP diffusion in situ, roles of tubulin, and mitochondrial creatine kinase.* Mol Cell Biochem, 2008. **318**(1-2): p. 147-65.
153. Rostovtseva, T.K. and S.M. Bezrukov, *VDAC regulation: role of cytosolic proteins and mitochondrial lipids.* J Bioenerg Biomembr, 2008. **40**(3): p. 163-70.
154. Guzun, R., et al., *Regulation of respiration controlled by mitochondrial creatine kinase in permeabilized cardiac cells in situ. Importance of system level properties.* Biochim Biophys Acta, 2009. **1787**(9): p. 1089-105.
155. Bessman, S.P. and C.L. Carpenter, *The creatine-creatine phosphate energy shuttle.* Annu Rev Biochem, 1985. **54**: p. 831-62.
156. Saks, V., *Molecular system bioenergetics-new aspects of metabolic research.* International journal of molecular sciences, 2009. **10**(8): p. 3655-7.
157. Guzun, R. and V. Saks, *Application of the principles of systems biology and Wiener's cybernetics for analysis of regulation of energy fluxes in muscle cells in vivo.* Int J Mol Sci. **11**(3): p. 982-1019.
158. Gellerich, F. and V.A. Saks, *Control of heart mitochondrial oxygen consumption by creatine kinase: the importance of enzyme localization.* Biochem Biophys Res Commun, 1982. **105**(4): p. 1473-81.

159. Guzun, R., et al., *Systems bioenergetics of creatine kinase networks: physiological roles of creatine and phosphocreatine in regulation of cardiac cell function.* Amino Acids. **40**(5): p. 1333-48.
160. Capetanaki, Y., et al., *Muscle intermediate filaments and their links to membranes and membranous organelles.* Exp Cell Res, 2007. **313**(10): p. 2063-76.
161. Ball, E.H. and S.J. Singer, *Mitochondria are associated with microtubules and not with intermediate filaments in cultured fibroblasts.* Proc Natl Acad Sci U S A, 1982. **79**(1): p. 123-6.
162. Anesti, V. and L. Scorrano, *The relationship between mitochondrial shape and function and the cytoskeleton.* Biochim Biophys Acta, 2006. **1757**(5-6): p. 692-9.
163. Aon, M.A. and S. Cortassa, *Coherent and robust modulation of a metabolic network by cytoskeletal organization and dynamics.* Biophys Chem, 2002. **97**(2-3): p. 213-31.
164. Hayashi, T., et al., *Three-dimensional electron microscopy reveals new details of membrane systems for Ca2+ signaling in the heart.* J Cell Sci, 2009. **122**(Pt 7): p. 1005-13.
165. Fawcett, D.W. and N.S. McNutt, *The ultrastructure of the cat myocardium. I. Ventricular papillary muscle.* J Cell Biol, 1969. **42**(1): p. 1-45.
166. Nivala, M., et al., *Computational modeling and numerical methods for spatiotemporal calcium cycling in ventricular myocytes.* Front Physiol. **3**: p. 114.
167. Soeller, C. and M.B. Cannell, *Examination of the transverse tubular system in living cardiac rat myocytes by 2-photon microscopy and digital image-processing techniques.* Circ Res, 1999. **84**(3): p. 266-75.
168. Bakeeva, L.E., S. Chentsov Yu, and V.P. Skulachev, *Mitochondrial framework (reticulum mitochondriale) in rat diaphragm muscle.* Biochim Biophys Acta, 1978. **501**(3): p. 349-69.
169. Amchenkova, A.A., et al., *Coupling membranes as energy-transmitting cables. I. Filamentous mitochondria in fibroblasts and mitochondrial clusters in cardiomyocytes.* J Cell Biol, 1988. **107**(2): p. 481-95.
170. Bers, D.M., *Cardiac excitation-contraction coupling.* Nature, 2002. **415**(6868): p. 198-205.
171. Bers, D.M. and K.S. Ginsburg, *Na:Ca stoichiometry and cytosolic Ca-dependent activation of NCX in intact cardiomyocytes.* Ann N Y Acad Sci, 2007. **1099**: p. 326-38.
172. Wang, S.Q., et al., *Imaging microdomain Ca2+ in muscle cells.* Circ Res, 2004. **94**(8): p. 1011-22.
173. Soeller, C., et al., *Three-dimensional high-resolution imaging of cardiac proteins to construct models of intracellular Ca2+ signalling in rat ventricular myocytes.* Exp Physiol, 2009. **94**(5): p. 496-508.
174. Nivala, M., et al., *Criticality in intracellular calcium signaling in cardiac myocytes.* Biophys J. **102**(11): p. 2433-42.
175. Nivala, M., et al., *Linking flickering to waves and whole-cell oscillations in a mitochondrial network model.* Biophys J. **101**(9): p. 2102-11.
176. Schneider, N.S., et al., *Mechanism of the Frank-Starling law--a simulation study with a novel cardiac muscle contraction model that includes titin and troponin I.* J Mol Cell Cardiol, 2006. **41**(3): p. 522-36.
177. Glancy, B. and R.S. Balaban, *Role of mitochondrial Ca2+ in the regulation of cellular energetics.* Biochemistry. **51**(14): p. 2959-73.
178. Zorov, D.B., et al., *Reactive oxygen species (ROS)-induced ROS release: a new phenomenon accompanying induction of the mitochondrial permeability transition in cardiac myocytes.* J Exp Med, 2000. **192**(7): p. 1001-14.
179. Collins, T.J. and M.D. Bootman, *Mitochondria are morphologically heterogeneous within cells.* J Exp Biol, 2003. **206**(Pt 12): p. 1993-2000.
180. Zhou, L., et al., *Dynamic modulation of Ca2+ sparks by mitochondrial oscillations in isolated guinea pig cardiomyocytes under oxidative stress.* J Mol Cell Cardiol. **51**(5): p. 632-9.
181. Williamson, J.R., et al., *Coordination of citric acid cycle activity with electron transport flux.* Circ Res, 1976. **38**(5 Suppl 1): p. I39-51.

182. Balaban, R.S., *Cardiac energy metabolism homeostasis: role of cytosolic calcium.* J Mol Cell Cardiol, 2002. **34**(10): p. 1259-71.
183. Dzeja, P.P., et al., *Rearrangement of energetic and substrate utilization networks compensate for chronic myocardial creatine kinase deficiency.* J Physiol. **589**(Pt 21): p. 5193-211.
184. Tepp, K., et al., *High efficiency of energy flux controls within mitochondrial interactosome in cardiac intracellular energetic units.* Biochim Biophys Acta. **1807**(12): p. 1549-61.
185. Ovadi, J. and P.A. Srere, *Macromolecular compartmentation and channeling.* Int Rev Cytol, 2000. **192**: p. 255-80.
186. Lenaz, G. and M.L. Genova, *Supramolecular organisation of the mitochondrial respiratory chain: a new challenge for the mechanism and control of oxidative phosphorylation.* Adv Exp Med Biol. **748**: p. 107-44.
187. Saks, V., et al., *Molecular system bioenergetics: regulation of substrate supply in response to heart energy demands.* J Physiol, 2006. **577**(Pt 3): p. 769-77.
188. Acin-Perez, R., et al., *Respiratory active mitochondrial supercomplexes.* Mol Cell, 2008. **32**(4): p. 529-39.
189. Ko, Y.H., et al., *Mitochondrial ATP synthasome. Cristae-enriched membranes and a multiwell detergent screening assay yield dispersed single complexes containing the ATP synthase and carriers for Pi and ADP/ATP.* J Biol Chem, 2003. **278**(14): p. 12305-9.
190. Westermann, B., *Mitochondrial fusion and fission in cell life and death.* Nat Rev Mol Cell Biol. **11**(12): p. 872-84.
191. Koshiba, T., et al., *Structural basis of mitochondrial tethering by mitofusin complexes.* Science, 2004. **305**(5685): p. 858-62.
192. de Brito, O.M. and L. Scorrano, *Mitofusin 2 tethers endoplasmic reticulum to mitochondria.* Nature, 2008. **456**(7222): p. 605-10.
193. Chen, Y., et al., *Mitofusin 2-Containing Mitochondrial-Reticular Microdomains Direct Rapid Cardiomyocyte Bioenergetic Responses via Inter-Organelle Ca2+ Crosstalk.* Circ Res.
194. Chen, Y., Y. Liu, and G.W. Dorn, 2nd, *Mitochondrial fusion is essential for organelle function and cardiac homeostasis.* Circ Res. **109**(12): p. 1327-31.

X. ANNEXES

MATERIALS

1. Functional tests, oxygraphy.

a. Integrity of the outer membrane

Product	Final concentration	Volume to add from stock solutions	Stock solution [mM]
Mitomed		2145 µL	
Glutamate	5 mM	22 µL	500 mM
Malate	2 mM	22 µL	200 mM
BSA	0.2%	22 µL	20%
Add cells or fibers into the chamber			
ADP	2 mM	40 µL	100 mM
Cytochrome C	8 µM	16 µL	1 mM
Atractyloside	30 µM	60 µL	1 mM

b. PK+PEP trapping system

b.1.) Regulation of mitochondrial respiration by creatine in the presence of activated MtCK.

Product	Final concentration	Volume to add from stock solutions	Stock solution [mM]
Mitomed		1910 µL	
Glutamate	5 mM	22 µL	500 mM
Malate	2 mM	22 µL	200 mM
PEP	5 mM	50 µL	200 mM
BSA	0.2%	22 µL	20%
Add cells or fibers into the chamber			
ATP	2 mM	40 µL	100 mM
PK	20 IU/mL	40 µL	1000 IU/mL
Creatine	1 mM	10 µL	200 mM
	2 mM	10 µL	
	3 mM	10 µL	
	5 mM	20 µL	
	10 mM	50 µL	
	20 mM	100 µL	
PCr	2 mM	4 µL	1 mM
	5 mM	6 µL	
	10 mM	10 µL	
	20 mM	20 µL	

c. ADP kinetics.

Product	Final concentration	Volume to add from stock solutions	Stock solution [mM]
Mitomed		2167 µL	

Glutamate	5 mM	22 µL	500 M
Malate	2 mM	22 µL	200 mM
BSA	0.2%	22 µL	20%
Add cells or fibers into the chamber			
ADP	0.05 mM	10 µL	100 mM
	0.1 mM	10 µL	10 mM
	0.3 mM	4 µL	
	0.5 mM	4 µL	100 mM
	0.75 mM	5 µL	
	1 mM	5 µL	
	2 mM	20 µL	
Cytochrome C	8 µM	16 µL	1 mM
Atractyloside	30 µM	60 µL	1mM

d. ADP kinetics + Creatine.

Product	**Final concentration**	**Volume to add from stock solutions**	**Stock solution [mM]**
Mitomed		2155 µL	
Glutamate	5 mM	22 µL	1 mM
Malate	2 mM	22 µL	200 mM
BSA	0.2%	22 µL	20%
Creatine	20 mM	200 µL	200 mM
Add cells or fibers into the chamber			
ADP	0.05 mM	10 µL	10 mM
	0.1 mM	10 µL	
	0.3 mM	4 µL	100 mM
	0.5 mM	4 µL	
	0.75 mM	5 µL	
	1 mM	5 µL	
	2 mM	20 µL	
Cytochrome C	8 µM	16 µL	1 mM
Atractiloside	30 µM	60 µL	1mM

2. Immunofluorescence, confocal imaging

a. 1st Antibodies

Antibody (commercial name)	**Dilution**	**Immunogen**
Mouse monoclonal [SAP.4G5] to beta I tubulin (Abcam, ab11312)	1/1000	Peptide corresponding to the C-terminal sequence
Mouse monoclonal [6B1] to beta II tubulin (Abcam, ab28036)	1/1000	Amino acids CEEEEGEDEA at the C terminus
Rabbit monoclonal [EP1331Y] to beta III tubulin (Abcam , ab52901)	1/100	Peptide corresponding to the C-terminal sequence
Mouse monoclonal [ONS.1A6] to beta IV tubulin (Abcam, ab11315)	1/1000	Peptide corresponding to the C-terminal sequence
Anti-alpha Actinin antibody [SA-20] (Abcam, ab82247)	1/100	Rabbit skeletal alpha actinin

VDAC (home-made) TATIANA	1/10000	
Anti-VDAC/Porin antibody - Mitochondrial marker (Abcam, ab61273)		MAVPPTYADL GKSARDVFTK GYGFGLIKLD LKTKSENGLE FTSSGSANTE TTKVTGSLET KYRWTEYGLT FTEKWNTDNT LGTEITVEDQ LARGLKLTFD , corresponding to amino acids 1-100 of Human VDAC1 / Porin
Anti-VDAC2 antibody (Abcam, ab37985)		C-GHKVGLALELEA, corresponding to C terminal amino acids 283-294 of Human VDAC2
VDAC3 antibody (Novus, NB100-74561)		

b. 2nd Antibodies

Antibody (commercial name)	Dilution
Cy™ 5-conjugated Affini-Pure goat anti-mouse IgG (Jackson Immunoresearch 115-175-146)	1/100
DyLight 488, Goat anti-mouse IgG, Fcγ fragment specific ML (Jackson Immunoresearch 115-485-008)	1/100
Anti-Rabbit IgG (H&L) goat Antibody DyLight™ 649 conjugated (Rockland 611-143-122)	1/100
Goat anti-rabbit IgG, $F(ab')_2$-FITC (Santa Cruz sc3839)	1/100

c. Mitochondrial membrane potential dependent dyers

Commercial names	Concentration used
Mitotracker Green	200 nM
Mitotracker Red or Far Red	200 nM
TMRM (Tetramethyl rhodamine methyl ester)	50 nM

3. Buffers, solutions and media

a. Isolation buffer:

Reagent	Final concentration [mM]	MW (g/mol)	Reference	1000 mL ddH_2O	100 mL ddH_2O
NaCl	117	58.44	Sigma Aldrich S9625	6.837 g	0.684
KCl	5.7	74.55	Sigma Aldrich P4504	0.425 g	0.043
KH_2PO_4	1.5	136.09	Sigma Aldrich 60218	0.204 g	0.02
$NaHCO_3$	4.4	84.01	Sigma Aldrich S8875	0.37 g	0.037
$MgCl_2$ solution	1.7	95.21	Sigma	1.7 mL	170 µL

1 M			Aldrich 63069		
HEPES	21.1	238.30	Sigma Aldrich H3375	5.028 g	0.503 g
Glucose	11.7	180.16	Sigma Aldrich G8270	2.108 g	0.211 g
Creatine	10	131.13	Sigma Aldrich C0780	1.311 g	0.131 g
Taurine	20	125.15	Sigma Aldrich T0625	2.503 g	0.25 g
Phosphocreatine	10	255.08	Sigma-Aldrich P7936	2.551	0.255 g
Pyruvate sodium salt	2	110.04	Sigma Aldrich 15990	0.22	0.022 g

pH 7.2 with NaOH at 25° C

b. Digestion solution:

Reagent	Final concentration	To prepare 50 mL	Reference
Isolation buffer		50 mL	
Collagenase A	0.03 U/mL	30-35 mg	Roche 11088793001
$CaCl_2$	0.026 mM	13 µL	Sigma-Aldrich C1016
BSA	2 mg/mL	0.1 g	Roche 10775835001

c. Sedimentation buffers

c.1.) Sedimentation buffer for oxygraphy

Reagent	Final concentration	To prepare 33 mL	Reference
Isolation buffer		33 mL	
BSA	2 mg/mL	0.066 g	Roche 10775835001
$CaCl_2$	0.2 mM	66 µL	Sigma-Aldrich C1016
STI Soy Trypsin Inhibitor	0.42 mM	0.014 g	Roth 5279.6
Leupeptin	10 µM	33 µL	Roche 11529048001

c.2.) Ca^{2+} gradient buffers for culturing:

Prepare them with 25mL of isolation buffer.

Ca^{2+} gradients	**[Ca^{2+}] µL**	**BSA (g)**	**STI (g)**
1st Gradient [0.2mM]	50	0.25	0.014
2nd Gradient [0.4mM]	100	0.50	0.014
3rd Gradient [0.8mM]	200	1	0.014

100mM Ca^{2+} stock solution

c.3.) Ca^{2+} stock solution

Reagent	**Final concentration [mM]**	**MW (g/mol)**	**Reference**	**100 mL ddH_2O**
$CaCl_2$	100	110.98	Sigma-Aldrich C1016	1.11 g

d. Culturing media

d.1.) Recovery medium

Medium 199 HEPES modified: With Earle's salts, sodium bicarbonate and 25 mM HEPES.

Reagent	**Final concentration [mM]**	**MW (g/mol)**	**Reference**	**50 mL**
Medium 199 HEPES modified			Sigma-Aldrich M7528	50 mL
Creatine	5	131.1	Sigma-Aldrich C0780	0.033 g
L-Carnitine	2	197.66	Sigma-Aldrich C0283	100 µL
Taurine	5	125.15	Sigma-Aldrich T0625	0.031 g
Antibiotic + L-Glutamine	2	[200 mM] solution	PAN BIOTECH GmbH P06-19100	50 µL
Fetal Bovine Serum (FBS)	10 %		PAN BIOTECH GmbH P30-0601	5 mL

d.2.) Transfection medium

Medium 199 HEPES modified: With Earle's salts, sodium bicarbonate and 25 mM HEPES.

Reagent	**Final concentration [mM]**	**MW (g/mol)**	**Reference**	**15 mL**
Medium 199 HEPES modified			Sigma-Aldrich M7528	15 mL
Creatine	5	131.1	Sigma Aldrich C0780	0.01 g
L-Carnitine	2	197.66	Sigma Aldrich C0283	0.01
Taurine	5	125.15	Sigma Aldrich T0625	0.0094 g

L-Glutamine	2	[200 mM] solution	PAN BIOTECH GmbH P04-80100	15 µL

d.3.) Mitomed without Ca^{+2} solution

Reagent	Final concentration [mM]	MW (g/mol)	Reference	1000 mL ddH_2O	100 mL ddH_2O
EGTA Ethylene glycol-bis(2-aminoethylether)-*N,N,N',N'*-tetraacetic acid	0.5	380.35	Sigma Aldrich 03778	0.19 g	0.019 g
$MgCl_2$ solution 1 M	3	95.21	Sigma Aldrich 63069	0.286 g	0. 029 g
K-Lactobionate*	60	358.3	Sigma Aldrich 61321	120 mL	12 mL
Taurine	20	125.15	Sigma Aldrich T0625	2.503 g	0.25 g
KH_2PO_4 Potassium phosphate monobasic	3	136.09	Sigma Aldrich 60218	0.408 g	0.041 g
HEPES 4-(2-Hydroxyethyl) piperazine-1-ethanesulfonic acid	20	238.31	Sigma Aldrich H3375	4.766 g	0.477 g
Sucrose	110	342.3	Sigma Aldrich S9378	37.65 g	3.765 g
DTT (+4°C) DL-Dithiothreitol	0.5	154.25	Sigma Aldrich 43815	0.077 g	0.008 g

pH 7.1 with NaOH at 25° C

*K-Lactobionate: Because of its very low pH, it has to be prepared separately and added as a solution.

d.3.1.) K-Lactobionate solution

Reagent	Final concentration [mM]	MW (g/mol)	Reference	120 mL	24 mL
Lactobionic acid	500	358.3	Sigma Aldrich 61321	21.5 g	4.3 g

pH 7.1 with KOH; with solid KOH approach pH 6.5, thereafter with 1 M KOH solution.

d.3.2.) BSA 20%

Reagent	Final concentration	To prepare 1mL	Reference
BSA	1 g/L	0.2 g	Roche 10735094001
Mitomed solution		1 mL	

d.3.3.) Saponin

Reagent	Final concentration	To prepare 1mL	Reference
Saponin		0.003 g	Sigma Aldrich S7900
Solution A / Mitomed		1 mL	

d.4.) Solution A for fibers.

Reagent	Final concentration [mM]	MW (g/mol)	Reference	1000 mL	100 mL
CaK_2EGTA*	2.77	-	-	27.7 mL	2.77 mL
K_2EGTA*	7.23	-	.	72.3 mL	7.23 mL
Imidazole	20	68.08	Sigma Aldrich 56748	1.362 g	0.136 g
DTT (+4°C) DL-Dithiothreitol	0.5	154.25	Sigma Aldrich 43815	0.077 g	0.008
$MgCl_2$ solution 1 M	6.56	95.21	Sigma Aldrich 63069	6.56 mL	0.656 µL
MES 2-(N-Morpholino) ethanesulfonic acid	53.3	213.25	Sigma Aldrich 69889	11.366	1.137 g
Taurine	20	125.15	Sigma Aldrich T0625	2.503	0.25 g
Na_2ATP (+4° C) Adenosine-5'-triphosphate disodium salt	5.3	605.2	Roche 10127531001	3.208 g	0.321 g
Na_2PCr (-20° C) Phosphocreatine disodium salt hydrate	15	255.1	Sigma Aldrich P7936	3.827 g	0.383 g

pH 7.1 with KOH at 25° C

*Because of their pH, solutions were prepared aside.

d.4.1.) CaK_2EGTA

Reagent	Final concentration [mM]	MW (g/mol)	Reference	200 mL	100 mL
EGTA Ethylene glycol-bis(2-aminoethylether)-*N,N,N',N'*-tetraacetic acid	100	380.25	Sigma Aldrich 03778	7.605 g	0.761 g

$CaCO_3$	100	100.09	Sigma Aldrich 21061	2 g	0.2 g
To dilute $CaCO_3$ place the solution into a water-bath (80° C) and wait until it reaches 25° C to add the KOH					
KOH	200	56.11	Sigma Aldrich 60368	2.244 g	0.224 g

pH 7.1 with NaOH

d.4.2.) K_2EGTA

Reagent	Final concentration [mM]	MW (g/mol)	Reference	200 mL	100 mL
EGTA Ethylene glycol-bis(2-aminoethylether)-*N,N,N',N'*-tetraacetic acid	100	380.25	Sigma Aldrich 03778	7.605 g	0.761 g
KOH	200	56.11	Sigma Aldrich 60368	2.244 g	0.224 g

pH 7.1 with NaOH

e. Stock substrate solutions for oxygraphy

e.1.) Creatine

Reagent	Final concentration	To prepare 5mL	Reference	MW
Creatine	200 mM	0.1310 g	Sigma Aldrich C0780	131.13
Mitomed solution		5 mL		

Dissolve it in water bath (50° C)

e.2.) Glutamate

Reagent	Final concentration	To prepare 10mL	Reference	MW
L-Glutamic acid	500 mM	0.7355 g	Sigma Aldrich G1251	147.13
Mitomed solution		10 mL		

pH 7.1 with KOH at 25° C, once the pH has been reached adjust the final volume

e.3.) Malate

Reagent	Final concentration	To prepare 5mL	Reference	MW
L-Malic acid	200 mM	0.3634 g	Sigma Aldrich	178.05

disodium salt			M9138	
Mitomed solution		10 mL		

pH 7.1 with KOH

e.4.) Cytochrome C

Reagent	Final concentration	To prepare 1mL	Reference	MW
Cytochrome C (-20 °C)	1 mM	0.0123 g	Sigma Aldrich C2506	123
Mitomed solution		1 mL		

e.5.) Atractyloside

Reagent	Final concentration	To prepare 1mL	Reference	MW
Atractyloside potassium salt	1 mM	0.0.08 g	Sigma Aldrich A6882	802.99
ddH_2O		5 mL		
Ethanol 70%		5 mL		

e.6.) Sodium pyruvate

Reagent	Final concentration	To prepare 10mL	Reference	MW
Sodium pyruvate (4° C)	500 mM	0.055 g	Sigma Aldrich 15990	110.04
Mitomed solution		10 mL		

e.7.) Phosphoenolpyruvate (PEP)

Reagent	Final concentration	To prepare 5mL	Reference	MW
PEP (-20° C) Phospho(enol)pyruvic acid trisodium salt hydrate	200 mM	0.234 g	Sigma-Aldrich P7002	233.99
Mitomed solution		5 mL		

e.8.) NADH

Reagent	Final concentration	To prepare 5mL	Reference	MW
NADH-Na_2 (4° C)	15 mM	0.053 g	Roche 10107735001	665.4
Mitomed solution		5 mL		

e.9.) Pyruvate kinase (PK)

Reagent	Final concentration	To prepare 5mL	Reference	MW
PK (-20° C) Pyruvate Kinase	1000 U/mL	0.0225 g	Sigma-Aldrich P9136	350 - 600 U/mg protein
Mitomed solution		5 mL		

Verify the concentration by spectrometry.

e.10.) Lactate dehydrogenase (LDH)

Reagent	Final concentration	To prepare 5mL	Reference	MW
LDH (-20° C) L-Lactic Dehydrogenase	1000 U/mL	0.0052 g / 0.0047 g	Sigma-Aldrich L1254	700 - 1,200 U/mg protein
Mitomed solution		5 mL		

Verify the concentration by spectrometry.

e.11.) ATP-Na_2

Reagent	Final concentration	To prepare 5mL	Reference	MW
ATP (4° C)	10 mM	0.0605 g	Roche 10833835	605.2
	100 mM	0.6052 g		
Mitomed solution		10 mL		

pH 7.1 with KOH

e.12.) ADP

Reagent	Final concentration	To prepare 5mL	Reference	MW
ADP (-20° C)	10 mM	0.0471	Roche 10129062103	427.2
	100 mM	0.4712		
Mitomed solution		10 mL		

pH 7.1 with KOH

e.13.) 2% BSA solution

Reagent	Quantity	Reference
PBS (Phosphate buffered saline)	100 mL	Insitut de biotechnologies Jacques Boy SSA0402
BSA (Bovine Serum Albumin)	2g	Roche 10735094001

f. Fixation solutions

f.1.) PFA 4% solution

Reagent	Quantity	Reference
PBS (Phosphate buffered saline)	100 mL	Insitut de biotechnologies Jacques Boy SSA0402
PFA (Paraformaldehyde)	4g	Electron Microscopy Sciences 15714

Dissolve PFA < 60°C

f.2.) Glutaraldehyde 25%

Reagent	Quantity	Reference
Destillated water	75 mL	
Glutaraldehyde)	25 mL	Electron Microscopy Sciences 16100

f.3.) PFA 4% + Glutaraldehyde 0.1% solution

Reagent	Quantity
PFA 4%	100 mL
Glutaraldehyde 25%	320 µL

f.4.) 1% Triton

Reagent	Quantity
PBS (Phosphate buffered saline)	50 mL
Triton	500 µL

Steps	Problems	Possible reasons	Solutions
Heart dissection and hanging to start perfusion	Improper or too high flow rate, see below.	Damage of the wall of aorta or aortic valve	Discard this heart. For dissection of the heart holding this between fingers, gently stretch the aorta and cut it to get long aorta to preserve aortic valve from damage.
Initial perfusion (80 cm H_2O)	Perfusion pressure too high (>69 mm Hg), coronary flow rate too low (≤15 mL/min).	Aorta partially clogged up	I. Wait for some minutes, small embolus might flow out II. Remove heart and hang up once again, otherwise discard the heart
	Coronary flow>25 mL/min, abnormally low perfusion pressure.	Leak of perfusate due to improper hanging, see above	Hang up the heart once again, otherwise discard the heart
Collagenase perfusion	Perfusion pressure >10-15 mm Hg after 50 min perfusion.	Protease concentration too low Enzyme inactivation Perfusion temperature is too low Protease concentration too high	Increase the concentration of the collagenase preparation Check storage conditions and the enzyme activity Verify temperature Decrease the concentration of the collagenase preparation
	Too rapid drop perfusion pressure down to zero (in 10–15 min). Stained heart surface	Uneven perfusate flow in the heart body due to clogging in some capillaries. Ischemic regions in the heart	Discard the heart, otherwise the yield will be low and quality doubtful
Preparing and washing of the cells	Too low cell sedimentation rate	Substantial amounts of damaged cells present	Normal intact cells sediment in 2–4 min. Elongation of sedimentation time in an attempt to improve the yield could exclusively result in collecting damaged cells
	Low cell viability and yield	Mechanical force for heart dissection is too excessive	Reduce shear force and use the pipette more gently
Saponin treatment	Too low activation of respiration by exogenous ADP	Incomplete permeabilization of sarcolemma	Cell permeabilization has to be checked in the oxygraph cells by addition of the saponin stock solution, the activation of respiration should be complete in ca. 10 min. and the final oxygen consumption rate remain unaltered at least for 20 min, otherwise the saponin concentration should be adjusted
Stirring	Gradual decay in the oxygen consumption rate	Cell damaging due to too vigorous stirring	Decrease in the stirring rate to sufficiently low value

Table 2: Key points for high quality cardiomyocyte isolation

XI. ACKNOWLEDGEMENTS

Esta tesis está dedicada a mi familia y mi amado México (CONACYT beca 211959) por su apoyo, comprensión y por siempre ser y estar.

Je souhaite remercier les membres du jury pour l'intérêt qu'ils ont porté à ce travail et pour le temps qu'ils ont consacré à le juger :

Pr. Pierre Dos Santos et Pr. Yves Tourneur pour avoir accepté d'être rapporteurs de cette thèse. Je suis consciente de l'effort que cela implique et espère sincèrement que vous aurez trouvé ce manuscrit intéressant.

Dr. Anne Cantereau, Pr. François Boucher, Pr. Andrey Kuznetsov et Pr. Uwe Schlattner pour l'intérêt qu'ils ont porté à cette étude en acceptant d'examiner ces travaux. De plus, je remercie tout particulièrement le Pr. Uwe Schlattner de m'avoir accueillie au sein du LBFA pour effectuer mon doctorat.

I owe the deepest thanks to my academic supervisor Professor Valdur Saks for his support, advices and optimism. Thanks for all the things you taught me and for letting me be part of your group.

Je souhaite remercier mon co-directeur, le Dr. Yves Usson, pour son soutien, ses conseils et sa gentillesse.

Thank you to Valdur Saks' team and collaborations in France: Rita Guzun, Lauriane Michel, Alexei Grichine and Charles Auffray. For your time, advices and help during these years.

Je remercie l'ANR pour le soutien apporté lors de ma thèse.

Je tiens à remercier tous les membres du LBFA : Abder, Brigitte, Cécile B., Cécile C., Christiane, Eric, Fayçal, Florance, Fred, Guillaume, Hervé, Jose, Karine, Laurence, Malgorzata, Serge B, Valerie.
Merci de m'avoir accueilli chaleureusement. Je remercie plus particulièrement ceux qui garantissent le bon fonctionnement au quotidien: Joëlle, Cindy, Sarah, Gérard, Mado et Régis.
Thank you to all students, for all those ups and downs, cheering, sharing and hard moments… thank you for everything, just keep in mind how great you are and I am quite sure you will become great scientists… Evi, Farida, Marie, Martin, Sarah, Shuijie.

Merci à tous ceux que je n'aurais pas nommés, chacun d'entre vous m'a apporté, scientifiquement et /ou humainement, durant ces presque trois dernières années et je vous en suis très reconnaissante.

I wish to thank to all my colleagues and co-authors in Tallin, at the Laboratory of Bioenergetics of the National Institute of Chemical Physics and Biophysics: Tuuli Kaambre, Minna Karu-Varikmaa, Kersti Tepp, Natalja Timohhina, Madis Metsis and Merle Saaremäe.

XII. LIST OF PUBLICATIONS

Guzun R, Karu-Varikmaa M, **Gonzalez-Granillo M**, Kuznetsov AV, Michel L, Cottet-Rousselle C, Saaremäe M, Kaambre T, Metsis M, Grimm M, Auffray C, Saks V. Mitochondria-cytoskeleton interaction: distribution of β-tubulins in cardiomyocytes and HL-1 cells. Biochim Biophys Acta. 2011 Apr;1807(4):458-69.

Guzun R, Timohhina N, Tepp K, **Gonzalez-Granillo M**, Shevchuk I, Chekulayev V, Kuznetsov AV, Kaambre T, Saks VA. Systems bioenergetics of creatine kinase networks: physiological roles of creatine and phosphocreatine in regulation of cardiac cell function. Amino Acids. 2011 May;40(5):1333-48.

Saks V, Kuznetsov AV, **Gonzalez-Granillo M**, Tepp K, Timohhina N, Karu-Varikmaa M, Kaambre T, Dos Santos P, Boucher F, Guzun R. Intracellular Energetic Units regulate metabolism in cardiac cells. J Mol Cell Cardiol. 2012 Feb;52(2):419-36.

Gonzalez-Granillo M, Grichine A, Guzun R, Usson Y, Tepp K, Chekulayev V, Shevchuk I, Karu-Varikmaa M, Kuznetsov AV, Grimm M, Saks V, Kaambre T. Studies of the role of tubulin beta II isotype in regulation of mitochondrial respiration in intracellular energetic units in cardiac cells. J Mol Cell Cardiol. 2012 Feb;52(2):437-47.

Guzun R, **Gonzalez-Granillo M**, Karu-Varikmaa M, Grichine A, Usson Y, Kaambre T, Guerrero-Roesch K, Kuznetsov A, Schlattner U, Saks V. Regulation of respiration in muscle cells in vivo by VDAC through interaction with the cytoskeleton and MtCK within Mitochondrial Interactosome. Biochim Biophys Acta. 2012 Jun;1818(6):1545-54

Marcela Gonzalez-Granillo, Alexeï Grichine, Valdur Saks and Yves Usson. Mitochondrial arrangement and dynamics in intact cardyomyocytes tansfected with pegp-n1 alpha-actinin. Biophysical Journal, *in preparation*.

Minna Karu-Varikmaa, **Marcela Gonzalez-Granillo**, Alexei Grichine, Yves Usson, François Boucher, Tuuli Kaambre, Rita Guzun and Valdur Saks. Matters of the heart in bioenergetics: *mitochondrial fusion into continuous reticulum is not needed for maximal respiratory activity*. Biochimica et Biophysica Acta, Submitted 2012

Biochimica et Biophysica Acta 1807 (2011) 458–469

Contents lists available at ScienceDirect

Biochimica et Biophysica Acta

journal homepage: www.elsevier.com/locate/bbabio

Mitochondria–cytoskeleton interaction: Distribution of β-tubulins in cardiomyocytes and HL-1 cells

Rita Guzun [a], Minna Karu-Varikmaa [b], Marcela Gonzalez-Granillo [a], Andrey V. Kuznetsov [c], Lauriane Michel [a], Cécile Cottet-Rousselle [a], Merle Saaremäe [b], Tuuli Kaambre [b], Madis Metsis [b], Michael Grimm [c], Charles Auffray [a,d], Valdur Saks [a,b,*]

[a] INSERM U884, Laboratory of Fundamental and Applied Bioenergetics, Joseph Fourier University, Grenoble, France
[b] Laboratory of Bioenergetics, National Institute of Chemical Physics and Biophysics, Tallinn, Estonia
[c] Cardiac Surgery Research Laboratory, Department of Heart Surgery, Innsbruck Medical University, Innsbruck, Austria
[d] Functional Genomics and Systems Biology for Health, CNRS Institute of Biological Sciences, Villejuif, France

ARTICLE INFO

Article history:
Received 30 November 2010
Received in revised form 13 January 2011
Accepted 31 January 2011
Available online 4 February 2011

Keywords:
Cardiomyocytes
Creatine kinase
HL-1 cells
Mitochondrial interactosome
β-tubulin isotypes
Warburg effect

ABSTRACT

Mitochondria–cytoskeleton interactions were analyzed in adult rat cardiomyocytes and in cancerous non-beating HL-1 cells of cardiac phenotype. We show that in adult cardiomyocytes βII-tubulin is associated with mitochondrial outer membrane (MOM). βI-tubulin demonstrates diffused intracellular distribution, βIII-tubulin is colocalized with Z-lines and βIV-tubulin forms microtubular network. HL-1 cells are characterized by the absence of βII-tubulin, by the presence of bundles of filamentous βIV-tubulin and diffusely distributed βI- and βIII-tubulins. Mitochondrial isoform of creatine kinase (MtCK), highly expressed in cardiomyocytes, is absent in HL-1 cells. Our results show that high apparent K_m for exogenous ADP in regulation of respiration and high expression of MtCK both correlate with the expression of βII-tubulin. The absence of βII-tubulin isotype in isolated mitochondria and in HL-1 cells results in increased apparent affinity of oxidative phosphorylation for exogenous ADP. This observation is consistent with the assumption that the binding of βII-tubulin to mitochondria limits ADP/ATP diffusion through voltage-dependent anion channel of MOM and thus shifts energy transfer via the phosphocreatine pathway. On the other hand, absence of both βII-tubulin and MtCK in HL-1 cells can be associated with their more glycolysis-dependent energy metabolism which is typical for cancer cells (Warburg effect).

1. Introduction

Recent advances in studies of cellular energetics show that the mechanisms of regulation of energy fluxes and respiration in cells *in vivo* can be understood only in the framework of molecular system bioenergetics, which considers energy metabolism not only as a network of biochemical reactions, but also takes into account the spatial organization and temporal dynamics of intracellular interactions [1–4]. Interactions between cellular components result in appearance of new, system level properties such as macro- and micro-compartmentation of metabolites, metabolic channeling and functional coupling [3–7]. Thus, they give rise to specific mechanisms, such as energy transfer from the mitochondria to the cytoplasm through phosphotransfer networks [3–9].

Among the factors, most important for regulation of mitochondrial function in the cells *in vivo*, are the interactions of these organelles with other cellular structures, such as the cytoskeleton [10–13]. Among the cytoskeleton structures, one of the most important roles is attributed to the tubulin–microtubular system. Interactions of mitochondria with tubulin have been observed by many authors [14–18]. The most detailed and pioneering study of the structural interactions performed by Saetersdal et al. in 1990 demonstrated the presence of immunogold anti-β-tubulin labeling at the mitochondrial outer membrane (MOM) in cardiomyocytes, as well as in fibers in close apposition to this membrane [18]. For 20 years, this important observation was left almost unnoticed and unexplained. A possible functional role of this mitochondria-associated tubulin was found in extensive studies of the respiration regulation in permeabilized cells (i.e. *in situ* mitochondria [19]), when it has been shown that the apparent K_m for ADP in oxidative muscle cells (cardiomyocytes, skeletal m. soleus) is 20–30 times higher than in isolated mitochondria [8,20–23]. In addition, the high apparent K_m for ADP was found to be decreased by addition of creatine to activate MtCK [21,22], or by proteolytic treatment [23]. The apparent K_m for exogenous ADP is indicative of the availability of ADP for the adenine nucleotide translocase (ANT) in the mitochondrial inner membrane (MIM) and was proposed to be dependent on the permeability of the voltage-dependent anion channel (VDAC) located in the (MOM) [11,12]. The

* Corresponding author at: Laboratory of Bioenergetics, Joseph Fourier University, 2280, Rue de la Piscine, BP53X-38041, Grenoble Cedex 9, France.
E-mail address: Valdur.Saks@ujf-grenoble.fr (V. Saks).

0005-2728/$ – see front matter © 2011 Elsevier B.V. All rights reserved.
doi:10.1016/j.bbabio.2011.01.010

strong decrease of the apparent K_m for exogenous ADP induced by trypsin pointed to the possible involvement of some cytoskeleton-related protein(s) in the control of the VDAC permeability originally referred to as "factor X" [11,12,24]. Using immunofluorescence confocal microscopy Appaix et al. showed that tubulin and plectin are among cytoskeletal proteins sensitive to the proteolytic treatment [24]. The first established candidate for the role of "factor X" proved to be αβ heterodimeric tubulin, which strongly modulated the VDAC conductance upon binding to channel's protein reconstructed into a planar lipid membrane [17]. Reconstitution experiments indicated that the addition of the heterodimeric tubulin to isolated mitochondria strongly increased the apparent K_m for ADP [16].

The results of these experimental studies led to the assumption that oxidative phosphorylation in cardiomyocytes is effectively regulated by the mitochondrial interactosome (MI), a supercomplex consisting of the ATP synthasome, mitochondrial creatine kinase (MtCK), VDAC, tubulin controlling VDAC permeability, and possible linker proteins localized in the contact sites of two mitochondrial membranes [8,25,26].

Pedersen et al. have shown the existence of a similar supercomplex in cancer cells containing the ATP synthasome-VDAC-Hexokinase 2 [27–29]. In contrast to the highly oxidative phenotype of metabolism characteristic for adult cardiomyocytes, cancer cells have a glycolytic phenotype characterized by the increased lactic acid production even in the presence of sufficient amounts of oxygen to support mitochondrial function [30–32]. This common metabolic hallmark of malignant tumors was discovered by Otto Warburg and is known as the "Warburg effect" [33,34]. Our earlier studies of mouse cancerous HL-1 cells of cardiac phenotype have shown that the apparent K_m for exogenous ADP is very low and creatine has no effect on their respiration [35,36]. These functional properties of HL-1 cells appear related to alterations in the structure of the mitochondrial interactosome [8,36,37].

In the present work, we continue this direction of research by comparative study of the intracellular distribution of different isotypes of tubulin in normal adult cardiomyocytes and HL-1 cells, using confocal fluorescence and immunofluorescence microscopy and Western blotting. We show that the localization and functional role of β-tubulin isotypes are different in oxidative muscle tissues and HL-1 cells. Most importantly, in adult cardiomyocytes we identified an isotype of tubulin which is associated with mitochondria–βII-tubulin. The absence of this isotype in cancer cells appears to allow binding of hexokinase 2 to VDAC and to be directly involved in development of the Warburg effect.

2. Materials and methods

2.1. Cells preparation

For this study we used freshly isolated adult rat cardiomyocytes, isolated rat heart mitochondria and non-beating cancerous HL-1 cells of cardiac phenotype developed in Dr. W.C. Claycomb laboratory (Louisiana State University Health Science Center, New Orleans, LA, USA).

2.2. Isolation of adult cardiac myocytes

Adult cardiomyocytes were isolated after perfusion of the rat heart with collagenase using modified technique described previously [21]. Wistar male rats (300–350 g) were anaesthetized with pentobarbital and blood was protected against coagulation by injection of 500 U of heparin. The heart was quickly excised preserving a part of the aorta and placed into isolation medium (IM) of the following composition: 117 mM NaCl, 5.7 mM KCl, 4.4 mM $NaHCO_3$, 1.5 mM KH_2PO_4, 1.7 mM $MgCl_2$, 11.7 mM glucose, 10 mM creatine, 20 mM taurine, 10 mM PCr, 2 mM pyruvate and 21 mM HEPES, pH 7.1. The excised rat heart was cannulated by the aorta and suspended in a Langendorf system for perfusion and washed for 5 min with a flow rate of 15–20 ml/min. The collagenase treatment was performed by switching the perfusion to circulating isolation medium supplemented with 0.03 mg/ml collagenase (Roche) and BSA 2 mg/ml at the flow rate of 5 ml/min for 20–30 min. The end of the digestion was determined following the decrease in perfusion pressure measured by a manometer. After the digestion, the heart was washed with IM for 2–3 min and transferred into IM containing 20 μM $CaCl_2$, 10 μM leupeptin, 2 μM soybean trypsin inhibitor (STI) and 2 mg/ml fatty acid free BSA. The cardiomyocytes were then gently dissociated using forceps and pipette suction. Cell suspension was filtered through a crude net to remove tissue remnants and let to settle for 3–4 min at room temperature. After 3–4 min the initial supernatant was discarded, pellet of cardiomyocytes resuspended in 10 ml of IM containing 20 μM $CaCl_2$ and the protease inhibitors. This resuspension–sedimentation cycle with calcium-tolerant cells was performed twice, after that cardiomyocytes were gradually transferred from 20 μM Ca^{2+} IM into free calcium Mitomed (supplemented with protease inhibitors and BSA) and washed 5 times. Each time, slightly turbid supernatant was removed after 4–5 min of the cells' sedimentation. Isolated cells were re-suspended in 1–2 ml of Mitomed solution [19] for the labeling with MitoTracker fluorophore or in paraformaldehyde 4 % for fixation.

2.3. Isolation of mitochondria from cardiac muscle

Heart mitochondria were isolated from adult white Wistar rats 300 g body weight, as described by Saks et al. 1975 [58]. The rats were anesthetized with intraperitoneal injection of Pentobarbital (50 mg/kg body weight). Hearts were removed and placed into ice-cold isolation medium containing 300 mM sucrose, 10 mM HEPES, pH 7.2, and 0.2 mM EDTA. Atriums and vessels were cut off and the ventricles finely minced by scissors. After a brief mild homogenization in a glass potter with teflon pestle (clearance 0.7–0.8) at 200 rpm, during 30 sec, tissue underwent proteolytic digestion in the presence of 0.125 mg/ml trypsin for 15 min at 4 °C. The proteolysis was stopped by addition of 0.5 mg/ml soybean trypsin inhibitor (STI). The sample was carefully and briefly homogenized in a glass-teflon homogenizer (clearance 0.7–0.8) at 250 rpm and 4 °C. This homogenization was followed by a second one (300 rpm, 4 °C) using the potter with smaller clearance. After, the homogenate was centrifuged at 1250*g* for 10 min at 4 °C. The supernatant was carefully separated and centrifuged at 6300*g* for 10 min at 4 °C. Mitochondrial pellet obtained was re-suspended in 15 ml of ice-cold extraction medium, supplemented with 1 mg/ml fatty acid free bovine serum albumin, BSA, and washed three times applying the principle of differential centrifugation (3800*g* at 4 °C for 10 min each time), always carefully removing the upper layer of light fraction of damaged mitochondria in the pellet if it was present [38]. The final pellet containing mitochondria was re-suspended in 1 ml of the same isolation medium.

2.4. Cell culture

Cardiac muscle cell line, designated as HL-1 cells were derived in the Claycomb laboratory from the AT-1 mouse atrial cardiomyocyte tumor lineage [35–37]. Non-beating HL-1 cells (NB HL-1) were obtained from the HL-1 line developed by W. Claycomb by growing them up in different serum (Gibco fetal bovine serum) [35–37]. NB HL-1 cells do not beat spontaneously. These cells maintain cardiac properties characterized by immunolabeling actin, tubulin, desmin, connexin 43, myosin (developmental isoform), dihydropyridine receptors, by the presence of a sodium–calcium exchanger [36,37]. These cells are devoid of sarcomere structures and possess randomly organized filamentous dynamic mitochondria. NB HL-1 possess the electrophysiological characteristics and ionic currents of cardiac cells

(cardiac potassium current), but do not display electrical pacemaker activity and do not show spontaneous depolarization [36].

HL-1 cells were cultured in fibronectin (12.5 mg/l)–gelatine (0.02%) coated flasks containing Claycomb medium (Sigma) supplemented with 10% foetal bovine serum (PAN Biotech GmbH), 2 mM L-glutamine (PAN Biotech GmbH), 0.1 mM norepinephrine (Sigma), ascorbic acid 0.3 mM (Sigma), 100 U/ml penicillin and 100 μg/ml streptomycin (Sigma) in a humid atmosphere of 5% CO2 / 95% air at 37 °C. Cells were cultured in Lab-Tek® chambered coverglass, chamber volume 0.5 ml.

2.5. Sample preparation for Western blot analysis

Male Wistar rats (300–350 g) were anesthetized with pentobarbital, de-coagulated using 500 U heparin and decapitated. Approximately 50 mg samples of the brain tissue were quickly removed, weighed in cryovials and frozen in liquid nitrogen. At the same time, heart was quickly excited, ca. 50 mg samples of the left ventricle weighed and frozen. The samples were stored at −80 °C for not more than 1 month. For the sample preparation the tissues were crashed in liquid nitrogen, calculated amount (10 μl per mg tissue) of the buffer (10 mM Tris, 1 mM $MgCl_2$, 1 mM EDTA, 0.2 μM STI, 2 μM leupeptin, pH 7.4) added, homogenized at room temperature for 1 h with short shaking (Vortex in every 10–15 min, centrifuged at 15,000*g* for 4 min and the solid residual discarded. The obtained homogenate was supplemented by one-half (50 μl per 100 μl) of the sample buffer (0.2 M tris, 16% SDS, 1% DDT, 0.04% bromophenol blue, pH 6.8) and one-half of 50 % glycerol and incubated at 95 °C for 5 min. The HL-1 nonbeating cells were washed three times with 1 ml ice-cold phosphate buffered saline (PBS, 0.1 M KH_2PO_4, 0.15 M NaCl, pH 7.2) and lysed on ice with the Tris/Triton X-100 buffer (10 mM tris, 100 mM NaCl, 1 mM EDTA, 1 mM EGTA, 1% Triton X-100, 10% glycerol, 0.1% SDS, 0.5% sodium deoxycholate, pH 7.4), concentrated on 500 μl Vivaspin (10 000 MWCO PES) columns (Sartorius Stedim Biotech S.A.) up to approximately 100 μl, and supplemented by the sample buffer and treated as described above.

The protein concentration was routinely determined using the Pierce BCA Protein Kit as suggested by the manufacturer. Heating of the samples was performed at 60 °C for 30 min.

2.6. Western blotting

Electrophoresis was performed on the Mini Protean II from BioRad on 10% polyacrylamide gels in the Tris-tricine buffer solution developed by Schrägger and von Jagow [39] by applying of 0.5 μg (tubulin mixture) up to 300 μg of the tissue protein (tissue and cell lysates) as described in Fig. 1. The gels were fixed in 40% methanol and 5% phosphoric acid and, if required, stained with colloidal Coomassie G-250.

Blotting of the unstained gels was performed on the Trans-Blot SD Semi-Dry Transfer Cell (BioRad) using PVDF membranes (Millipore) according to the manufacturer's instructions. The blotting buffer contained 48 mM Tris, 39 mM glycine, 1% SDS and 20% methanol. The membranes were blocked for 1 hr with the skimmed milk/TBS solution (0.2 M Tris, 1.5 M NaCl, 0.1% Tween-20, 5% skimmed milk, pH 7.5) with gentle shaking and washed three times for 10 min with the same solution (without skimmed milk) and once in TBS solution lacking both the skimmed milk and Tween-20. Primary antibodies were diluted in the skimmed milk/TBS solution. Primary antibodies and used dalutions are shown in Table 1. Secondary antibodies were IgG and HRP-conjugated preparations. The membranes were exposed using the CL-X Posure film and SuperSignal West Dura Extended Duration substrate (SuperSignal West Dura Stable Peroxide Buffer and SuperSignal West Dura Luminol/Enhancer Solution).

Rabbit α-actinin antibody was obtained from Abcam (Abcam, ab82247). Mouse α-actinin antibody was obtained from Sigma

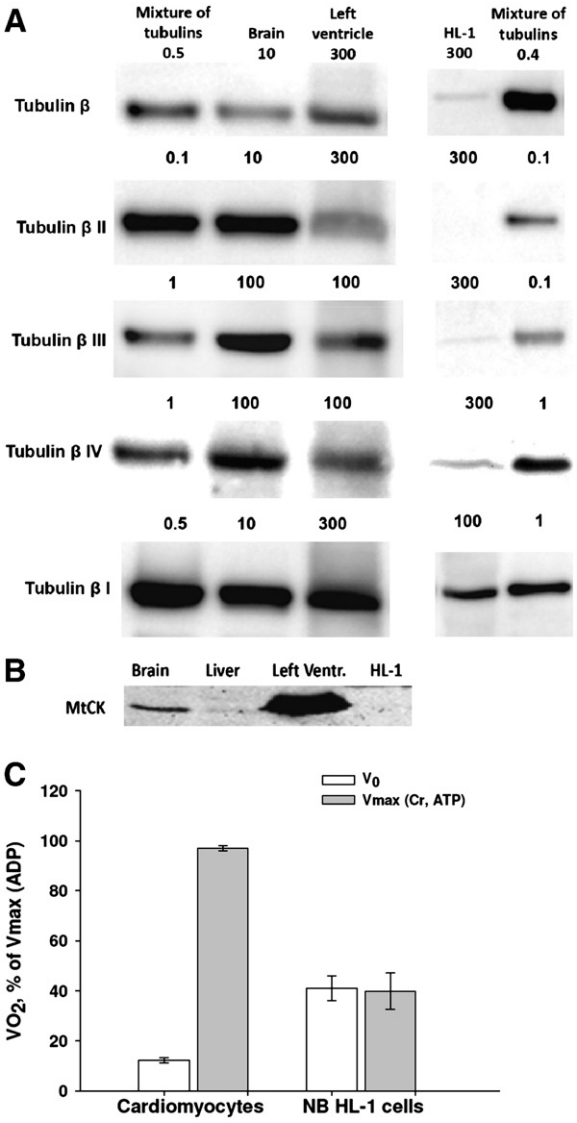

Fig. 1. Western Blot analysis of various tubulin isotypes (A) and MtCK (B) in different cells and tissues. LV—rat heart left ventricle. Numbers above the gel images show the amount of added total protein (in μg). Mixture of purified tubulins obtained from brain was used as a reference. The tubulin bands in reference samples correspond to the molecular mass of 55 kDa. (C) Creatine effect on the respiration of permeabilized cardiomyocytes and non-beating HL-1 cells. The rates are expressed as % of the maximal values (V_{max}) observed in the presence of ADP, 2 mM.

(A7811). VDAC antibody was obtained from the Laboratory of Physics and Structural Biology, National Institute of Child Health and Human Development, National Institute of Health, USA. Purified mixture of tubulin obtained as described before [16] was used as reference. They were kindly supplied by D. Sackett, Laboratory of Integrative and Medical Biophysics, Eunice Kennedy Shriver National Institute of Child Health and Human Development, National Institutes of Health, Bethesda, USA

2.7. Immunofluorescence

Freshly isolated cardiomyocytes and cultured cells were fixed in 4% paraformaldehyde at 37 °C for 15 min. After rinsing with PBS solution containing 2% BSA (bovine serum albumin) cells were permeabilized with 1% Triton X-100 at 25 °C for 30 min. Finally cells were rinsed repeatedly and incubated with primary antibody as described above for immunoblotting using concentrations indicated into the Table 1 (in 2% BSA containing PBS solution). The next day

Table 1
Primary antibodies.

Commercial name	Dilution for Western blot	Dilution for immunofluorescence	Immunogen
Mouse monoclonal βI Tubulin antibody, (Abcam ab11312)	1/20000	1/1000	Peptide corresponding to the C-terminal sequence
anti-tubulin βII(β2), (Abcam ab28036)	1/1000	1/1000	Amino acids CEEEEGEDEA at the C terminus
Rabbit polyclonal TUBB2A antibody, (Abnova PAB0379)		5 μg/ml	Amino acids DLVSEYQQYQDATADEQGE (417–435) at the C terminus
Rabbit monoclonal βIII Tubulin antibody, 5 (Abcam, ab52901	1/1000	1/50	Peptide corresponding to the C-terminal sequence
Mouse monoclonal βIV Tubulin antibody, (Abcam ab11315)	1/400	1/1000	Peptide corresponding to the C-terminal sequence
Rabbit polyclonal β Tubulin antibody, (Cell signalling 2146)	1/1000	1/50	Recognizes all tubulin isotypes

samples were rinsed and stained for 30 min at room temperature with secondary antibody. Secondary antibodies: Cy™ 5-conjugated Affini-Pure goat anti-mouse IgG (Jackson Immunoresearch 115-175-146), Goat polyclonal secondary antibody to mouse IgG-FITC (Abcam ab6785), goat anti-rabbit IgG, F(ab′)$_2$-FITC (Santa Cruz sc3839) were used respecting concentrations recommended by the providers. For co-staining the sequential protocol was applied. Two primary antibodies (one overnight at 4 °C and another for 2 h at room temperature) and two secondary antibodies were used to stain fixed samples with repeated rinsing procedures between every staining step. When the immunofluorescence was supplemented with mitochondria labeling, the fixed and immunostained cells (with primary and secondary antibodies) were incubated for 30 min at 37 °C in the presence of 2500 fold dilution of Mito-ID™ Red detection reagent (Mito-ID™ Red detection kit Enabling Discovery in Life Science, Enz-51007-500). For sharper image these cells were visualized immediately after labeling.

For the study of mitochondria arrangement in cardiomyocytes and HL-1 cells, freshly isolated or cultured cells were preloaded with mitochondria-specific fluorescent probe 0.2 μM MitoTracker Red™ and Green™ (Molecular Probes, Eugene, OR) for 2 h at 4 °C for cardiomyocytes and 15 min at 37° for HL-1 cells. Images were then analyzed using Volocity softwere (Improvision, France)

2.8. Confocal imaging

The fluorescence images were acquired with a Leica TCS SP2 AOBS inverted laser scanning confocal microscope (Leica, Heidelberg, Germany) equipped with a 63× water immersion objective (HCX PL APO 63.0×1.20 W Corr). Laser excitation was 488 nm for FITC and MitoTracker™ Green, 543 nm for Mito-ID™, and 633 nm for Cy 5, MitoTracker™ Red.

2.9. Measurements of oxygen consumption

The rates of oxygen uptake were determined with high-resolution respirometer Oxygraph-2K (OROBOROS Instruments, Austria) in Mitomed solution [25] containing 0.5 mM EGTA, 3 mM $MgCl_2$, 60 mM K-lactobionate, 3 mM KH_2PO_4, 20 mM taurine, 20 mM HEPES, 110 mM sucrose, 0.5 mM dithiothreitol (DTT), pH 7.1, 2 mg/ml fatty acid free BSA, complemented with 5 mM glutamate and 2 mM malate as respiratory substrates. Respiration was activated by addition of creatine to final concentration of 10 mM in the presence of ATP (2 mM). Maximal respiration rate was measured in the presence of ADP, 2 mM. Measurements were carried out at 25 °C; solubility of oxygen was taken as 240 nmol/ml [25].

2.10. Data analysis

The experiments were carried out independently in two different laboratories by using cardiomyocytes isolated from 10 animals. Functional data were expressed as means ± SE.

3. Results

In this study we analyze the distribution and possible functional roles of four isotypes of β-tubulins: βI (gene TUBB or TUBB5), βII (gene TUBB2A and TUBB2B), βIII (gene TUBIII), and βIV (gene TUBB4 and TUBB2C) in adult rat cardiomyocytes and mouse HL-1 cells (the classification of tubulin isotypes is based on recommended official names (http://www.ncbi.nlm.nih.gov/gene). Brain tissue samples and a mixture of tubulins purified from brain were used as a reference for each separate Western blot. Purified tubulins were obtained as described before (see Materials and methods) and were earlier used in the reconstitution experiments with isolated mitochondria [16]. Western blot analysis revealed the presence of all studied β-tubulin isotypes in rat left ventricular muscle tissue, as well as in brain and the reference mixture sample; in contrast, βII-tubulin was not detected in HL-1 cells (Fig. 1A). The distribution of the sarcomeric isoform of MtCK follows the same pattern of significant abundance in left ventricular muscle tissue and complete absence in cancer cells (Fig. 1B). This result is consistent with earlier data by Eimre et al. [36] who showed that in non-beating HL-1 cells the creatine kinase is presented by BB isozyme only. These results are in agreement with the observation that creatine maximally activates the respiration only

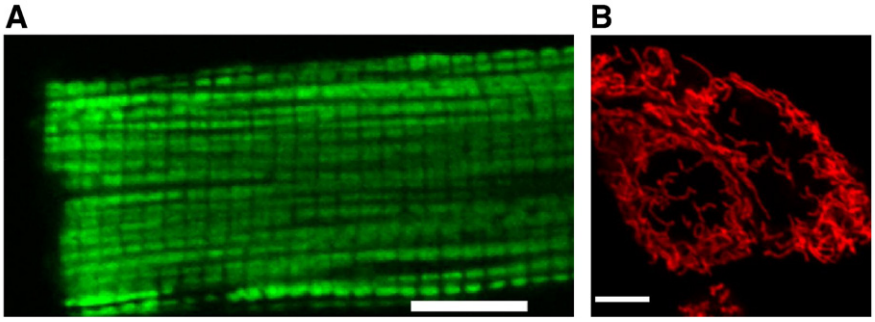

Fig. 2. Fluorescent microscopy imaging of mitochondria fluoroprobes, respectively. A: Mitochondria in cardiomyocytes visualized by fluorescent probe 0.2 μM MitoTracker™ Green shows separated individual organelles arranged in the regular lines. Scale bar 10 μm. B: Mitochondria in HL-1 cells 0.2 μM MitoTracker™ Red shows disorganized, filamentous mitochondrial network. Scale bar 6 μm.

in permeabilized cardiomyocytes and has no effect on respiration in permeabilized HL-1 cells (Fig. 1C).

The regular arrangement of individual mitochondria in adult cardiomyocytes imaged by MitoTracker green (Fig. 2A) dramatically contrasts with the disorganized thread-like mitochondrial reticulum of continuously dividing cancerous, highly glycolytic HL-1 cells (Mitotracker red, Fig. 2B). The striking differences observed in mitochondrial arrangement can obviously be related to the specific structural organization and mitochondria–cytoskeleton interactions in these cells [40].

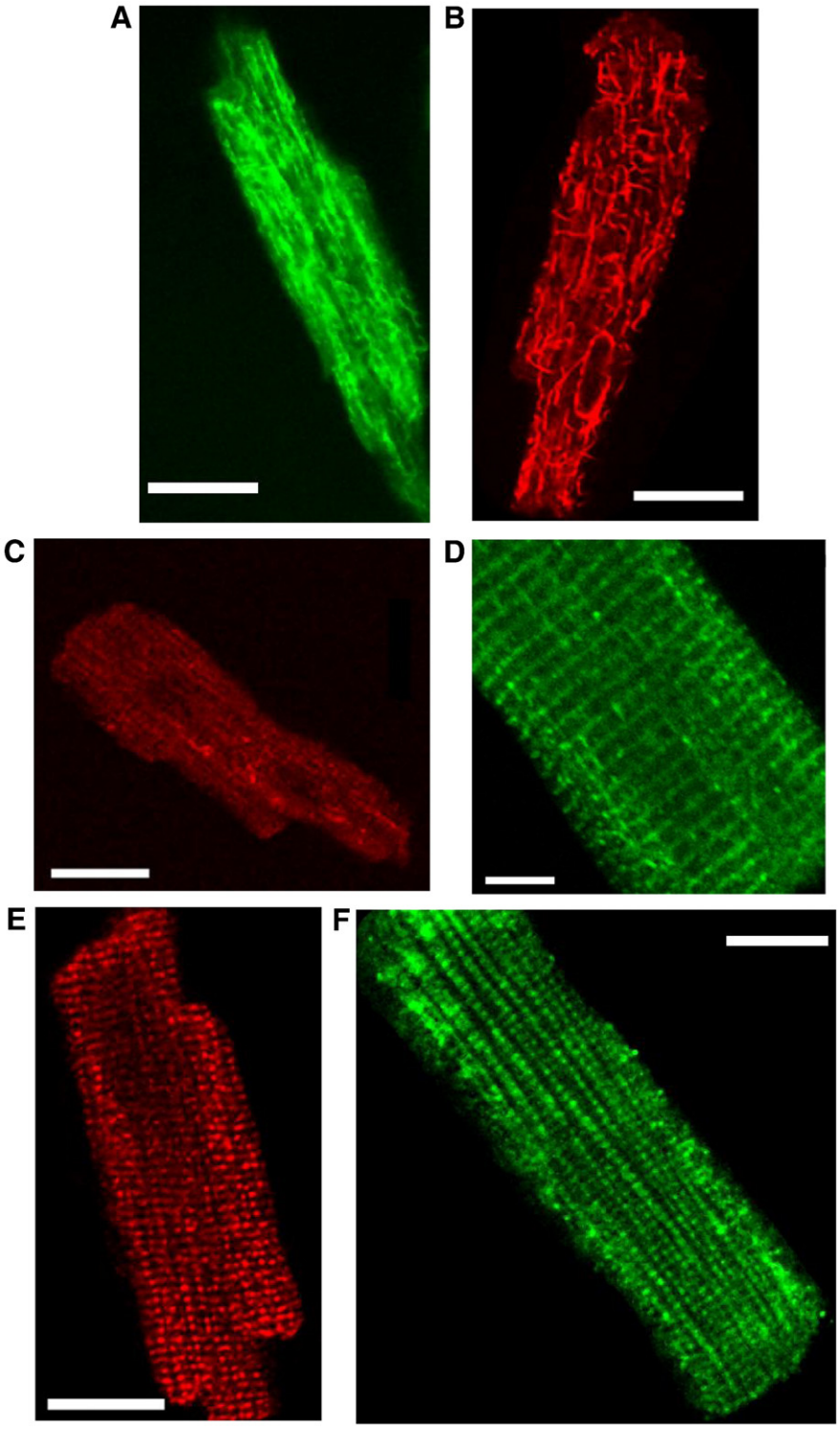

Fig. 3. Immunofluorescent confocal microscopy imaging of various β-tubulin isotypes in fixed cardiomyocytes. A: Longitudinally, obliquely and diffusely distributed total β-tubulins labeled with anti-β-tubulin antibody and FITC. Scale bar 24 μm. B: Tubulin labeled with anti-βIV-tubulin antibody and Cy5. βIV-tubulin shows polymerised longitudinally and obliquely oriented microtubules. Scale bar 21 μm. C: Diffusive intracellular distribution of tubulins labeled with anti-βI-tubulin antibody. Scale bar 10 μm. D: Tubulin labeled with anti-βIII-tubulin antibody and FITC demonstrates clearly distinguishable prevalent arrangement in transversal lines colocalized with sarcomeric Z-lines. Scale bar 6 μm. E: and F: Regularly arranged tubulins labeled with anti-βII-tubulin antibody and secondary antibodies: Cy5 (E) and FITC (F). In both cases, separate fluorescent spots organized in distinct longitudinally oriented parallel lines similarly to the mitochondrial arrangement (see Fig. 2A) in cardiomyocytes. Scale bar 14 μm (E) and scale bar 12 μm (F).

In order to further analyze the localization of β-tubulin isotypes, fixed cells were labeled first with primary antibodies against the proteins studied and then with fluorescent secondary antibodies (described in Materials and methods) and visualized by fluorescent confocal microscopy (Fig. 3). In control experiments without specific primary antibodies no binding of secondary fluorescent antibodies was seen (results not shown). Total β-tubulin forms tortuous microtubular structure with longitudinally and obliquely orientated crossed filaments in adult cardiomyocytes (Fig. 3A). The contribution of each individual tubulin isotype to these structures was analyzed by isotype-specific immunolabeling (Fig. 3B–F). The characteristic structure of β-tubulin appears to be mainly formed by polymerization of βIV-tubulin (Fig. 3B), whereas βI-tubulin is associated with a rather scattered distribution of fluorescent spots typical of its usual short polymerized fragments (Fig. 3C). βIII-tubulin is characteristically arranged in transversal lines demonstrating colocalization with sarcomeric Z-lines (Fig. 3D). This is very similar to earlier observation made using the immunogold labeling technique [18]. Thus both βIV-tubulin and βIII-tubulin appear at least partially responsible for the formation of the typical rod-like shape of adult cardiomyocytes.

The most interesting and exciting results of this study are related to the arrangement of βII-tubulin as revealed by differential immunofluorescent labeling (Cy5, Fig. 3E and FITC, Fig. 3F). In both cases, βII-tubulin is very regularly localized in rows along the long axis of the cell in an arrangement which is very similar to that of mitochondria (Fig. 2A). This observation is in a good agreement with the earlier findings of an association of β-tubulin with mitochondrial membranes using immunogold labeling [18]. Double-staining with anti-βII-tubulin and an anti-VDAC antibody against epitope 102–120, involved in the protein binding site, revealed an incomplete overlap of fluorescence (results not shown). This can be explained by the difficulties in immunolabeling VDAC, most probably due to presence of the bound tubulin resulting in a low accessibility of VDAC in cardiomyocytes.

Importantly, immunofluorescent labeling detects only traces of β-tubulin II in isolated mitochondria (Fig. 4A) in contrast to immunolabeled VDAC which is clearly detected in isolated mitochondria (Fig. 4B). This apparent contradiction can be explained by the fact that all cytoskeleton proteins associated with mitochondria are removed through trypsin proteolysis during their isolation.

By contrast with the results observed in cardiomyocytes, fluorescent immunolabeling of fixed HL-1 cells revealed the absence of βII-tubulin (Fig. 5A), confirming the results of Western blot analyses (Fig. 1). The clear colocalization of βIII-tubulin with α-actinin in Z-lines in cardiomyocytes is replaced by a rather diffusive distribution in HL-1 cells (Fig. 5B), which can be explained by the absence of the sarcomere structure in HL-1 cells. It is well known that overexpression of βIII-tubulin represents a valuable prognostic factor for the patients with aggressive evolution of ovarian, lung, pancreas, breast cancer and melanoma, and, at the same time, a poor probability of benefiting from the standard first-line platinum/taxane chemotherapy [41,42]. This suggests some interdependence between intracellular βIII-tubulin distribution and cancer metastasis. In addition, βI-tubulin labeling appears similar in cancerous HL-1 cells as in adult cardiac cells (Fig. 5C). The filamentous, bundle-like arrangement of βIV-tubulin in cancerous HL-1 cells (Fig. 5D) and the absence of a polymerized microtubular network could explain that they acquire a spherical shape in suspension and spread in culture.

The intracellular localization of βII-tubulin and βIII-tubulin isotypes was investigated by direct colocalization with Z-lines and mitochondria (Figs. 6 and 7). The Z-lines were labeled by α-actinin antibodies (Figs. 6A and 7A) for imaging of the sarcomere limits in cardiomyocytes. Labeling α-actinin with red fluorescence (Fig. 6A) and βIII-tubulin with green fluorescence (Fig. 6B) revealed significantly overlapping structures (Fig. 6C), suggesting that the previously observed specific transversal localization of β-tubulin is due to βIII-tubulin binding close to the Z-lines of the sarcomere.

Co-staining of α-actinin, labeled this time with a green fluorescence antibody (Fig. 7A) and mitochondria labeled by a specific red fluorescence probe Mito-ID™ (Fig. 7B) shows that mitochondria are localized very regularly between Z lines at the level of sarcomeres (see merged image in Fig. 7C). The absence of overlap of α-actinin at Z-lines and mitochondria-specific fluorescence reflects the absence of mitochondrial fusion. βII-tubulin labeling with green fluorescent antibodies shows its very regular localization in rows parallel to the long axis of the cell (Fig. 7D) orientated perpendicularly to Z-lines, an arrangement similar to that of mitochondria (Fig. 7E), and their full colocalization in cardiomyocytes (Fig. 7F). Comparison of the results displayed in Fig. 3E and F, and Fig. 7D and F indicates that all mitochondria are covered by βII-tubulin, which can therefore be used as an excellent natural intrinsic mitochondrial marker in adult cardiomyocytes.

In contrast, double labeling of HL-1 cells with antibodies against βII-tubulin (Fig. 8A) and with Mito-ID™ (Fig. 8B) as well as their overlap (Fig. 8C) clearly demonstrates the complete lack of βII-tubulin in cancerous HL-1 cells.

4. Discussion

Detailed comparative analysis of structure-function relationship in the regulation of energy fluxes in adult cardiomyocytes and cancerous HL-1 cells of cardiac phenotype described in our previous works [8,35–37] and in this study have yielded a wealth of information concerning the role of mitochondria–cytoskeleton interactions in shaping the specific pathway of energy transfer by the creatine kinase network in heart cells, as well as about the intracellular arrangement of mitochondria and complete prevention of their fusion in adult cardiomyocytes. These studies also show alteration of the mitochondrial dynamics, energy transfer pathways and metabolic phenotype in

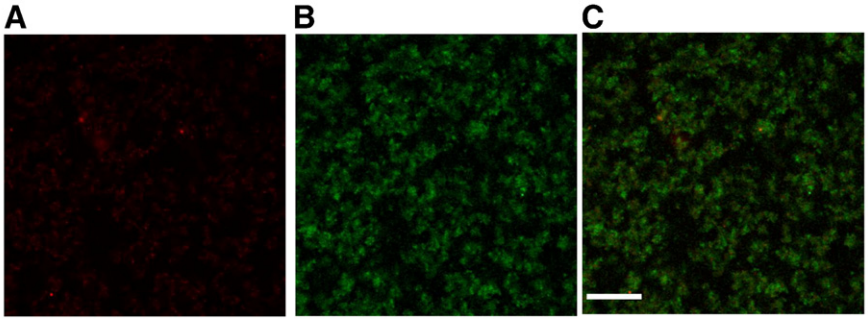

Fig. 4. Immunofluorescent confocal microscopy imaging of βII-tubulin and VDAC co-immunolabeling in isolated rat heart mitochondria. A: Absence of immunolabeling by anti-βII-tubulin (and Cy5) antibodies in isolated mitochondria. B: Strong immunofluorescent labeling of VDAC in isolated heart mitochondria (the interaction of mitochondria with βII-tubulin is removed by proteolysis with trypsin). C: The overlap of co-immunolabeling (βII-tubulin and VDAC). Scale bar 29 μm.

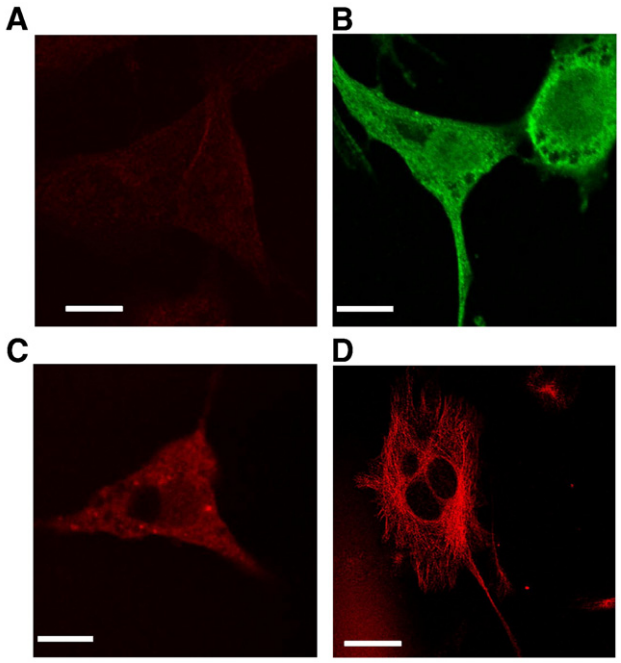

Fig. 5. Immunofluorescent confocal microscopy imaging of β-tubulin isotypes in fixed HL-1 cells. A: Tubulins labeled with mouse anti-βII-tubulin antibody and Cy5 are practically absent in HL-1 cells. Scale bar 14 μm. B: Tubulins labeled with anti-βIII-tubulin antibody and C: diffuse distribution of tubulins labeled with anti-βI-tubulin antibody. Scale bar 10 μm. D: Immunofluorescence imaging of polymerized tubulin microtubules labeled with anti-βIV-tubulin antibody and Cy5. The filaments show radial distribution from nucleus to cell periphery, creating also inter-connections between branches. Scale bar 18 μm.

cancerous cells that may help to understand the mechanism of the Warburg effect. In this study we found that different isotypes of tubulin have different intracellular distribution and therefore may play different roles in the control of energy fluxes and mitochondrial respiration in cardiac muscle cells. We have identified in adult cardiomyocytes the isotype of tubulin which is colocalized with mitochondria and is connected to the mitochondrial outer membrane–βII-tubulin. It is co-expressed with MtCK and by structural interactions with VDAC and ATP synthasome they form the mitochondrial interactosome [8,25,26]. This supercomplex, localized at contact sites of two mitochondrial membranes, is a key structure of a specific pathway of energy transport from mitochondria into the cytoplasm by phosphotransfer networks which effectively supply energy for contraction and ion pumps by local regeneration of ATP pools in myofibrils and at cellular membranes [8,25]. This prevents from wasting mitochondrial ATP in glycolytic reactions in spite of the presence of hexokinase-2 in the cytoplasm. βII-tubulin binding to the MOM may also protect the heart from apoptosis. On the contrary, in cancer cells of cardiac phenotype structural changes in the mitochondrial interactosome—lack of βII-tubulin, which is replaced by hexokinase-2, and lack of MtCK contribute to the mechanism of the Warburg effect by making possible the direct utilization of mitochondrial ATP for increased glucose phosphorylation and lactic acid production under aerobic conditions.

4.1. βII-tubulin isotypes in oxidative cardiomyocytes and glycolytic cancer HL-1 cells

Tubulin is one of the most representative proteins of cytoskeleton which among its other functions has a direct role in energy metabolism participating in the structuring of intracellular micro-compartments, formation of dissipative metabolic structures [43,44] and thus in the regulation of metabolic fluxes [45–49]. Under *in vivo* conditions cytoskeletal protein tubulin is highly dynamic and undergo rapid assembly/disassembly turnover by exchange of subunits. Building block of microtubules is a αβ-tubulin heterodimer [50]. In cardiomyocytes, about 70% of total tubulin is present in the polymerized form as microtubules whereas 30% occurs as non-polymerized cytosolic heterodimeric protein [51–54]. Interestingly, after complete dissociation of microtubular system by colchicine tubulin is still present in permeabilized cardiomyocytes, obviously because of its association with other cellular structures [55]. In higher vertebrates there are eight α-tubulin and seven β-tubulins encoded by different genes [50]. The majority of differences between tubulin isotypes are concentrated within the last 15 residues of the C-terminal (also called as isotype defining region) which is a main site for various alterations by post-translational modifications (PTMs) including tyrosinylation, acetylation, phosphorylation, polyglutamylation, and polyglycylation. In addition to that, C-terminal end has been identified to be a main target for numerous microtubule-associated proteins (MAPs) [56–58]. Differences in the C-terminal composition of tubulin isotypes determine the nature of PTM and affect their interactions with different cellular factors and the pattern of localization, thus explaining observations of this study. Recently, Rostovtseva et al. have proposed a mechanism of interaction between tubulin and VDAC, according to which the negatively charged carboxy-terminal tail (CTT) of tubulin penetrates into the cannel lumen interacting with a positively charged domain of VDAC [17,59]. For our experiments we used anti-βII-tubulin antibody against the CEEEEGEDEA amino acids of the CTT. The labeling of all mitochondria by this antibody shows that the negatively charged CTT of βII-tubulin is located on the outer mitochondrial membrane surface, very probably in close contact with positively charged region of the VDAC also located on this surface when it is in the closed conformation [60,61]. This explains also the decreased permeability of this channel for adenine nucleotides, as described below.

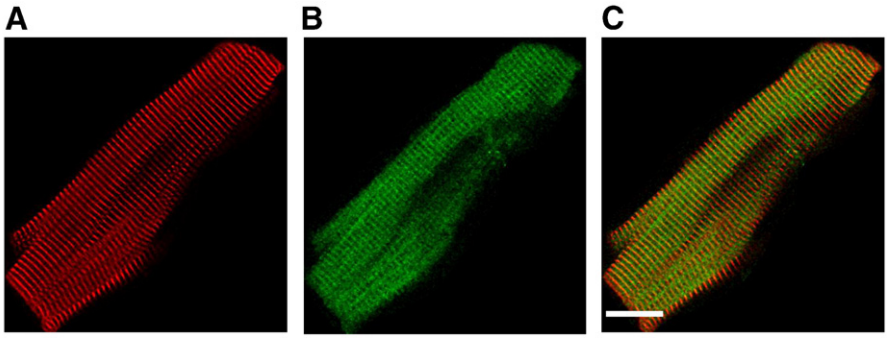

Fig. 6. Co-immunofluorescent labeling of α-actinin and βIII-tubulin in fixed cardiomyocytes. A: Characteristic sarcomeric transversal Z-lines labeled with anti-α-actinin antibody and Cy5. B: Tubulins labeled with anti-βIII-tubulin antibody and FITC. C: The overlap of α-actinin and βIII-tubulin. Both proteins are arranged at Z-lines. Scale bar 18 μm.

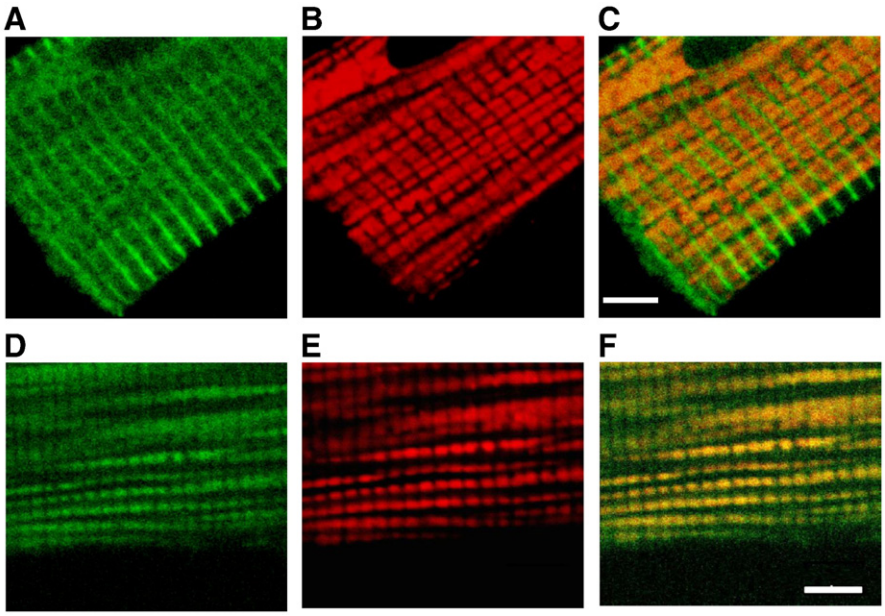

Fig. 7. Immunofluorescent imaging of α-actinin, β-tubulin II proteins and fluorescent staining of mitochondria. A: Green immunofluorescence of proteins labeled with anti-α-actinin antibody and FITC, demonstrating the characteristic sarcomeric transversal Z-lines. B: Typical regular arrangement of mitochondria labeled with Mito-ID™ Red. C: Merge image of A and B. Mitochondria (red) are localized exclusively between Z-lines (green). Scale bar 5 μm. D: Tubulins labeled with anti-βII-tubulin antibody and FITC. Fluorescent spots are regularly arranged (similarly to mitochondria). E: Mito-ID™ Red labeled mitochondria in cardiomyocyte. F: The overlap of D and E. β-tubulin class II (green) is arranged between Z-lines and fully co-localised with mitochondria. Scale bar 5 μm.

In contrast, we did not find βII-tubulin in cancer HL-1 cells of cardiac phenotype (Fig. 8). This observation matches well with previous finding of Hiser et al. [62]. Authors reported the absence of β-tubulin class II protein in 8 from 12 studied human cancer cell lines.

Mitochondria–cytoskeletal interactions, particularly the connection of βII-tubulin to the MOM may also prevent in significant degree the association of pro-apoptotic proteins to this membrane [63]. This may explain why apoptosis is rare in normal human hearts [64]. Possible alteration of mitochondria–tubulin interactions in dilated and ischemic cardiomyopathies may explain why the rate of apoptosis can increase several hundred folds in these diseases [64]. This is one of interesting problems for further study.

The presence of βII-tubulin at the outer mitochondrial membrane explains the very high value of apparent K_m for free exogenous ADP in adult permeabilized cardiomyocytes which is an order of magnitude higher than in isolated mitochondria (370 μM compared to 10–15 μM, respectively) [8,20–25]. Complete kinetic analysis of regulation of respiration by mitochondrial creatine kinase (MtCK) reaction in permeabilized cardiomyocytes confirmed the conclusions made in experiments with tubulin binding to VDAC [16,17,59] and uncovered specific restrictions of VDAC permeability by tubulin [25]. These experiments showed significant decrease of the apparent affinity for extramitochondrial ATP of MtCK localized on the outer surface of inner mitochondrial membrane in the intermembrane space in vivo in comparison with isolated mitochondria. This appears to be due to the diffusion restrictions created by interactions of VDAC in MOM with the tubulin αβ heterodimer [17,25,26,59]. Direct measurements of energy fluxes in permeabilized cardiomyocytes and in perfused hearts using the ^{18}O isotope tracer coupled with ^{31}P-NMR spectrometry showed that the ratio of the rates of PCr production to oxygen consumption ($VPCr/VO_2$) is close to 6, meaning that almost all energy is carried out of mitochondria by phosphocreatine molecules [26,65]. The results of these experimental studies showed that oxidative phosphorylation in cardiomyocytes is effectively regulated by creatine via MtCK in the mitochondrial interactosome (MI) [8,26].

In cancer HL-1 cells the apparent K_m for exogenous ADP was found to be in the range of 8–20 μM, which is similar to that of isolated mitochondria [35]. Moreover, in cancer cells creatine did not induce change of the respiration rates due to the absence of MtCK [35,36], but it was increased in cancer HL-1 cells in response to the addition of glucose showing its phosphorylation by hexokinase 2 [36].

Previous observations and results of the present study show that the two events—high apparent K_m for exogenous ADP and expression of MtCK correlate with the expression of βII-tubulin. The absence of

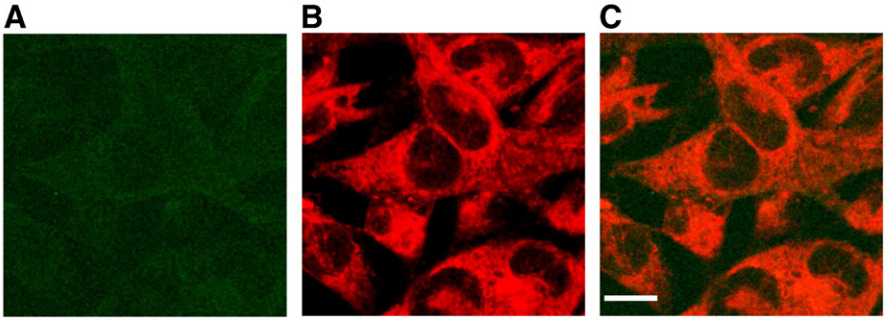

Fig. 8. The immunofluorescence of anti-βII-tubulin antibody (A) of rabbit source (and FITC) and mitochondria labeled with Mito-ID™ Red fluoroprobe (B) in HL-1 cells. Image A and merge image (C) shows the absence βII-tubulin labeling in HL-1 cells, scale bar 14 μm.

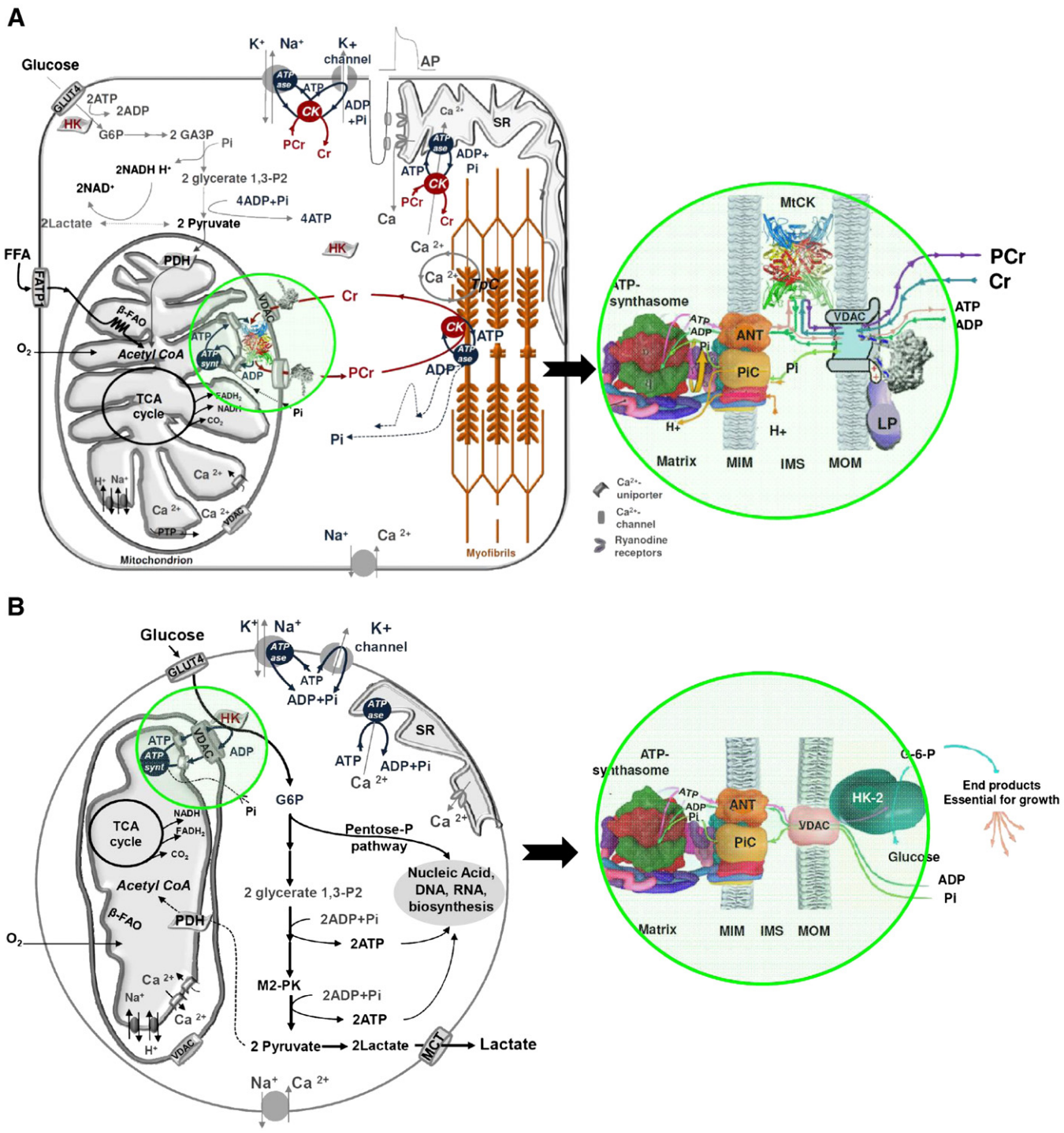

Fig. 9. Different pathways of intracellular energy transfer from mitochondria to cytoplasm in adult cardiomyocytes and HL-1 cells. A: Bessman–Wallimann–Saks pathway of energy transfer via creatine kinase phosphotransfer network in normal adult cardiomyocytes. Tubulin βII isotype is co-expressed with MtCK in Mitochondrial Interactosome and energy is channelled into cytoplasm by PCr which regenerate the local pools of ATP (phosphocreatine shuttle). Figure A represents adult cardiac cell (scheme at the left). Free fatty acids (FFA) are taken up by a family of plasma membrane proteins (FATP1), esterified to acyl-CoA which enters the β-oxidation pathway resulting in acetyl-CoA production. Glucose (GLU) is taken up by glucose transporter-4 (GLUT-4) and via the phosphorylation by hexokinase (HK) (depicted as soluble enzyme) with production of glucose-6-phosphate (G6P), enters the Embden–Meyerhof pathway. Pyruvate produced from glucose oxidation is transformed by the pyruvate dehydrogenise complex (PDH) into acetyl-CoA. G6P inhibits HK decreasing the rate of glucolysis. Acetyl-CoA is further oxidized to CO_2 in the tricarboxylic acids (TCA) cycle with the concomitant generation of NADH and $FADH_2$ which are oxidized in the respiratory chain (complexes I, II, III and IV) with final ATP synthesis. These pathways occur under aerobic conditions. Under anaerobic conditions, pyruvate can be converted to lactate. The insert shown in right panel illustrates functioning of Mitochondrial Interactosome (MI), a key system in energy transfer from mitochondria to cytoplasm. MI a supercomplex, formed by ATP synthase, adenine nucleotides translocase (ANT), phosphate carriers (PIC), mitochondrial creatine kinase (MtCK), voltage-dependent anion channel (VDAC) and bound cytoskeleton protein tubulin (specifically β-tubulin II selectively controlling VDAC permeability) and some linker proteins (LP), is responsible for recycling of ATP and ADP within mitochondria coupled to direct phosphorylation of creatine (Cr) into phosphocreatine (PCr). PCr is then transferred via cytosolic Cr/PCr shuttle to be used by functionally coupled CK with ATPases (acto-myosin ATPase and ion pumps) for regeneration of local ATP pools. B: Warburg–Pedersen pathway of energy transfer in cancer cells. Structure of mitochondrial interactosome is significantly modified: protein β-tubulin class II is replaced by HK, and the absence of MtCK allows all oxidative ATP to be exported directly from mitochondria. As the result, VDAC-bound HK is protected from the Glucose-6-P product inhibition, and uses mitochondrially produced ATP for phosphorylation of glucose and stimulation of glycolytic lactate production. The Glucose-6-P and glycolytic ATP synthesized during lactate production are used in biosynthetic pathways for cell growth and proliferation.

the βII-tubulin isotype both in isolated mitochondria and in HL-1 cells results in increase of the apparent affinity of oxidative phosphorylation for free ADP. This observation is consistent with the assumption that the binding of βII-tubulin to VDAC limits ADP/ATP diffusion through MOM.

The increased restriction of diffusion of adenine nucleotides through the MOM and the presence of MtCK functionally coupled to ANT in the MI are the most important mechanisms in the pathway of intracellular energy transport by phosphoryl transfer via the creatine kinase–phosphocreatine (PCr) network [3,8,9,66]. The system of compartmentalized creatine kinase isoenzymes and notably mitochondrial CK (MtCK) is the prerequisite condition for the efficient intracellular phosphotransfer [3]. The functioning of MI and its role in the energy transfer from mitochondria into the cytoplasm in cardiomyocytes with respiratory phenotype are represented schematically in Fig. 9A. In these cells, energy is transferred from mitochondria by the phosphotransfer PCr-CK circuit or shuttle. This pathway of energy transfer was in details described in Bessman [67,68], Wallimann [9,66] and Saks [3–8,21–26] laboratories and many others. In order to acknowledge the contribution of these three laboratories in the identification of energy transfer via creatine kinase phosphotransfer network it is named the Bessman–Wallimann–Saks pathway.

Analysis of the compartmentalized energy transfer by mathematical modelling [69] showed, in agreement with experimental data, that not more that 6–10% of ATP formed in oxidative phosphorylation is directly transferred out of mitochondria [70]. This, by maintaining local ATP pools, prevents the wasteful use of mitochondrial ATP for glucose phosphorylation by hexokinase-2, and ensures availability of an energy supply matching the specific cell needs (see Fig. 9A).

4.2. The lack of βII-tubulin and increased hexokinase-2 open the way to the Warburg effect

One of possible mechanisms triggering the Warburg effect is overexpression of hexokinase-2 [28,29,32,71–73]. In cancer cells, hexokinase-2 is bound to the VDAC and this interaction enhances its affinity for ATP by ~5-fold, and protects the enzyme from the inhibition by its byproduct glucose-6 phosphate [74]. In HL-1 cells hexokinase-2 is also overexpressed and its activity is increased by a factor of 5 in comparison with that observed in adult cardiomyocytes [36,37]. Thus, according to Pedersen's explanation of the Warburg mechanism, hexokinase-2 bound to VDAC actively phosphorylates glucose using mitochondrially synthesized ATP, redirecting it actively through the glycolytic pathway [28,75].

Hexokinase-2 is also prevalent in cardiac muscle cells [36,37,76]. However, it is only in cancer HL-1 cells which lack βII-tubulin, that hexokinase-2 binds to VDAC, altering cellular metabolism. Thus, binding of βII-tubulin to VDAC in normal cells prevents the wasting of mitochondrial ATP for increased lactate production that occurs in cancers cells through its binding of hexokinase-2 made possible by the absence of βII-tubulin. A comparative study of enzyme profiles in HL-1 cells and cardiomyocytes showed an increased activity of several glycolytic enzymes, particularly hexokinase-2 in HL-1 cells [37]. The decrease or absence of MtCK and the downregulation of its mRNA were previously reported in human sarcoma, gastric and colonic adenocarcinoma [77], indicating that these cells are unable to retain their intracellular creatine pool in the form of phosphocreatine because of the intrinsic low level of MtCK [77].

Thus, the mitochondrial interactosome in cancer HL-1 cells of cardiac phenotype is lacking of βII-tubulin and MtCK and significantly differs from that of healthy adult cardiac muscle cells incorporating ATP synthase, ANT, PiC, VDAC and HK-2 bound to VDAC. The absence of βII-tubulin and MtCK in the MI of HL-1 cells allows hexokinase-2 to bind to VDAC through its N-terminal hydrophobic domain [73]. The functioning of the MI in HL-1 cells is represented schematically in Fig. 9B. This pathway of energy transfer may be called the Warburg–Pedersen pathway to recognize the contribution of these distinguished investigators in its identification. In the absence of MtCK, mitochondrial ATP is directly carried out from mitochondria and used by VDAC-bound hexokinase-2 for glucose phosphorylation. Glucose-6P produced in this reaction enters the glycolytic and pentose-phosphate pathways, sustaining cellular growth and proliferation.

In conclusion, the remodelling of MI, namely the lack of βII-tubulin protein that makes possible hexokinase binding may be considered as the structural basis of the Warburg effect, explaining the switch from the energy transfer supporting the respiratory phenotype in normal cardiac cells to the more glycolytic phenotype of cancerous cells (see Fig. 9A and B). To verify this hypothesis, detailed further studies of distribution of hexokinase and tubulin isoforms in different cancer cells are needed.

Acknowledgments

The authors thank Dan L. Sackett, Laboratory of Integrative and Medical Biophysics, Eunice Kennedy Shriver National Institute of Child Health and Human Development, National Institutes of Health, Bethesda, USA, for reading this manuscript and for very helpful critical discussion. The authors thank Anu Nutt, National Institute of Chemical Physics and Biophysics, Tallinn, Estonia, for skilful technical assistance. This work was supported by INSERM, France, by Agence Nationale de la Recherche, project ANR-07-BLAN-0086-01 France, by grant No. 7823 from the Estonian Science Foundation, SF0180114Bs08 from Estonia Ministry of Education and Science, by National Council of Science and Technology of Mexico (CONACYT) and by a research grant from the Austrian Science Fund (FWF): [P 22080-B20].

References

[1] H.V. Westerhoff, A. Kolodkin, R. Conradie, S.J. Wilkinson, F.J. Bruggeman, K. Krab, J.H. van Schuppen, H. Hardin, B.M. Bakker, M.J. Mone, K.N. Rybakova, M. Eijken, H.J. van Leeuwen, J.L. Snoep, Systems biology towards life in silico: mathematics of the control of living cells, J. Math. Biol. 58 (2009) 7–34.
[2] R. Ramzan, K. Staniek, B. Kadenbach, S. Vogt, Mitochondrial respiration and membrane potential are regulated by the allosteric ATP-inhibition of cytochrome c oxidase, Biochim. Biophys. Acta 1797 (2010) 1672–1680.
[3] Molecular System Bioenergetics, in: V. Saks (Ed.), Energy for Life, Wiley-VCH: Weinheim, Gmbh, Germany, 2007.
[4] V. Saks, C. Monge, R. Guzun, Philosophical basis and some historical aspects of systems biology: from Hegel to Noble—applications for bioenergetic research, Int. J. Mol. Sci. 10 (2009) 1161–1192.
[5] V. Saks, The phosphocreatine-creatine kinase system helps to shape muscle cells and keep them healthy and alive, J. Physiol. 586 (2008) 2817–2818.
[6] V. Saks, T. Anmann, R. Guzun, T. Kaambre, P. Sikk, U. Schlattner, T. Wallimann, M. Aliev, M. Vendelin, The Creatine Kinase Phosphotransfer Network: Thermodynamic and Kinetic Considerations, the Impact of the Mitochondrial Outer Membrane and Modelling Approaches, in: M. Wyss, G. Salomons (Eds.), Creatine and Creatine Kinase in Health and Disease, Springer, Dordrecht, 2007, pp. 27–66.
[7] V. Saks, N. Beraud, T. Wallimann, Metabolic compartmentation—a system level property of muscle cells: real problems of diffusion in living cells, Int. J. Mol. Sci. 9 (2008) 751–767.
[8] V. Saks, R. Guzun, N. Timohhina, K. Tepp, M. Varikmaa, C. Monge, N. Beraud, T. Kaambre, A. Kuznetsov, L. Kadaja, M. Eimre, E. Seppet, Structure-function relationships in feedback regulation of energy fluxes in vivo in health and disease: mitochondrial interactosome, Biochim. Biophys. Acta 1797 (2010) 678–697.
[9] T. Wallimann, M. Wyss, D. Brdiczka, K. Nicolay, H.M. Eppenberger, Intracellular compartmentation, structure and function of creatine kinase isoenzymes in tissues with high and fluctuating energy demands: the "phosphocreatine circuit" for cellular energy homeostasis, Biochem. J. 281 (Pt 1) (1992) 21–40.
[10] Y. Capetanaki, R.J. Bloch, A. Kouloumenta, M. Mavroidis, S. Psarras, Muscle intermediate filaments and their links to membranes and membranous organelles, Exp. Cell Res. 313 (2007) 2063–2076.
[11] V.A. Saks, Z.A. Khuchua, E.V. Vasilyeva, O. Belikova, A.V. Kuznetsov, Metabolic compartmentation and substrate channelling in muscle cells. Role of coupled creatine kinases in in vivo regulation of cellular respiration—a synthesis, Mol Cell Biochem 133–134 (1994) 155–92.
[12] V.A. Saks, A.V. Kuznetsov, Z.A. Khuchua, E.V. Vasilyeva, J.O. Belikova, T. Kesvatera, T. Tiivel, Control of cellular respiration in vivo by mitochondrial outer membrane and by creatine kinase. A new speculative hypothesis: possible involvement of mitochondrial–cytoskeleton interactions, J. Mol. Cell. Cardiol. 27 (1995) 625–645.

[13] L. Winter, C. Abrahamsberg, G. Wiche, Plectin isoform 1b mediates mitochondrion-intermediate filament network linkage and controls organelle shape, J. Cell Biol. 181 (2008) 903–911.
[14] F. Bernier-Valentin, B. Rousset, Interaction of tubulin with rat liver mitochondria, J. Biol. Chem. 257 (1982) 7092–7099.
[15] M. Carre, N. Andre, G. Carles, H. Borghi, L. Brichese, C. Briand, D. Braguer, Tubulin is an inherent component of mitochondrial membranes that interacts with the voltage-dependent anion channel, J. Biol. Chem. 277 (2002) 33664–33669.
[16] C. Monge, N. Beraud, A.V. Kuznetsov, T. Rostovtseva, D. Sackett, U. Schlattner, M. Vendelin, V.A. Saks, Regulation of respiration in brain mitochondria and synaptosomes: restrictions of ADP diffusion in situ, roles of tubulin, and mitochondrial creatine kinase, Mol. Cell. Biochem. 318 (2008) 147–165.
[17] T.K. Rostovtseva, K.L. Sheldon, E. Hassanzadeh, C. Monge, V. Saks, S.M. Bezrukov, D.L. Sackett, Tubulin binding blocks mitochondrial voltage-dependent anion channel and regulates respiration, Proc. Natl. Acad. Sci. U. S. A. 105 (2008) 18746–18751.
[18] T. Saetersdal, G. Greve, H. Dalen, Associations between beta-tubulin and mitochondria in adult isolated heart myocytes as shown by immunofluorescence and immunoelectron microscopy, Histochemistry 95 (1990) 1–10.
[19] A.V. Kuznetsov, V. Veksler, F.N. Gellerich, V. Saks, R. Margreiter, W.S. Kunz, Analysis of mitochondrial function in situ in permeabilized muscle fibers, tissues and cells, Nat. Protoc. 3 (2008) 965–976.
[20] L. Kummel, Ca Mg-ATPase activity of permeabilised rat heart cells and its functional coupling to oxidative phosphorylation of the cells, Cardiovasc. Res. 22 (1988) 359–367.
[21] V.A. Saks, Y.O. Belikova, A.V. Kuznetsov, In vivo regulation of mitochondrial respiration in cardiomyocytes: specific restrictions for intracellular diffusion of ADP, Biochim. Biophys. Acta 1074 (1991) 302–311.
[22] V.A. Saks, E.V. Vassilyeva, Yu.O. Belikova, A.V. Kuznetsov, A. Lyapina, L. Petrova, N.A. Perov, Retarded diffusion of ADP in cardiomyocytes: possible role of outer mitochondrial membrane and creatine kinase in cellular regulation of oxidative phosphorylation, Biochim. Biophys. Acta 1144 (1993) 134–148.
[23] A.V. Kuznetsov, T. Tiivel, P. Sikk, T. Kaambre, L. Kay, Z. Daneshrad, A. Rossi, L. Kadaja, N. Peet, E. Seppet, V.A. Saks, Striking differences between the kinetics of regulation of respiration by ADP in slow-twitch and fast-twitch muscles in vivo, Eur. J. Biochem. 241 (1996) 909–915.
[24] F. Appaix, A.V. Kuznetsov, Y. Usson, L. Kay, T. Andrienko, J. Olivares, T. Kaambre, P. Sikk, R. Margreiter, V. Saks, Possible role of cytoskeleton in intracellular arrangement and regulation of mitochondria, Exp. Physiol. 88 (2003) 175–190.
[25] R. Guzun, N. Timohhina, K. Tepp, C. Monge, T. Kaambre, P. Sikk, A.V. Kuznetsov, C. Pison, V. Saks, Regulation of respiration controlled by mitochondrial creatine kinase in permeabilized cardiac cells in situ. Importance of system level properties, Biochim. Biophys. Acta 1787 (2009) 1089–1105.
[26] N. Timohhina, R. Guzun, K. Tepp, C. Monge, M. Varikmaa, H. Vija, P. Sikk, T. Kaambre, D. Sackett, V. Saks, Direct measurement of energy fluxes from mitochondria into cytoplasm in permeabilized cardiac cells in situ: some evidence for mitochondrial interactosome, J. Bioenerg. Biomembr. 41 (2009) 259–275.
[27] C. Chen, Y. Ko, M. Delannoy, S.J. Ludtke, W. Chiu, P.L. Pedersen, Mitochondrial ATP synthasome: three-dimensional structure by electron microscopy of the ATP synthase in complex formation with carriers for Pi and ADP/ATP, J. Biol. Chem. 279 (2004) 31761–31768.
[28] P.L. Pedersen, Warburg, me and Hexokinase 2: multiple discoveries of key molecular events underlying one of cancers' most common phenotypes, the "Warburg Effect," i.e., elevated glycolysis in the presence of oxygen, J. Bioenerg. Biomembr. 39 (2007) 211–222.
[29] P.L. Pedersen, Voltage dependent anion channels (VDACs): a brief introduction with a focus on the outer mitochondrial compartment's roles together with hexokinase-2 in the "Warburg effect" in cancer, J. Bioenerg. Biomembr. 40 (2008) 123–126.
[30] V. Gogvadze, B. Zhivotovsky, S. Orrenius, The Warburg effect and mitochondrial stability in cancer cells, Mol. Aspects Med. 31 (2010) 60–74.
[31] G. Kroemer, J. Pouyssegur, Tumor cell metabolism: cancer's Achilles' heel, Cancer Cell 13 (2008) 472–482.
[32] P.L. Pedersen, The cancer cell's "power plants" as promising therapeutic targets: an overview, J. Bioenerg. Biomembr. 39 (2007) 1–12.
[33] O. Warburg, On respiratory impairment in cancer cells, Science 124 (1956) 269–270.
[34] O. Warburg, K. Poesener, E. Negelein, Über den Stoffwechsel der Tumoren, Biochem. Z. 152 (1924) 319–344.
[35] T. Anmann, R. Guzun, N. Beraud, S. Pelloux, A.V. Kuznetsov, L. Kogerman, T. Kaambre, P. Sikk, K. Paju, N. Peet, E. Seppet, C. Ojeda, Y. Tourneur, V. Saks, Different kinetics of the regulation of respiration in permeabilized cardiomyocytes and in HL-1 cardiac cells. Importance of cell structure/organization for respiration regulation, Biochim. Biophys. Acta 1757 (2006) 1597–1606.
[36] M. Eimre, K. Paju, S. Pelloux, N. Beraud, M. Roosimaa, L. Kadaja, M. Gruno, N. Peet, E. Orlova, R. Remmelkoor, A. Piirsoo, V. Saks, E. Seppet, Distinct organization of energy metabolism in HL-1 cardiac cell line and cardiomyocytes, Biochim. Biophys. Acta 1777 (2008) 514–524.
[37] C. Monge, N. Beraud, K. Tepp, S. Pelloux, S. Chahboun, T. Kaambre, L. Kadaja, M. Roosimaa, A. Piirsoo, Y. Tourneur, A.V. Kuznetsov, V. Saks, E. Seppet, Comparative analysis of the bioenergetics of adult cardiomyocytes and nonbeating HL-1 cells: respiratory chain activities, glycolytic enzyme profiles, and metabolic fluxes, Can. J. Physiol. Pharmacol. 87 (2009) 318–326.
[38] V.A. Saks, G.B. Chernousova, D.E. Gukovsky, V.N. Smirnov, E.I. Chazov, Studies of energy transport in heart cells. Mitochondrial isoenzyme of creatine phosphokinase: kinetic properties and regulatory action of Mg2+ ions, Eur. J. Biochem. 57 (1975) 273–290.
[39] H. Schrägger, G. von Jagow, Tricine-sodium dodecyl-sulfate-polyacrylamide gel electrophoresis for the separation of proteins in the range from 1 to 100 kDa, Anal. Biochem. 166 (1987) 368–379.
[40] A.V. Kuznetsov, M. Hermann, J. Troppmair, R. Margreiter, P. Hengster, Complex patterns of mitochondrial dynamics in human pancreatic cells revealed by fluorescent confocal imaging, J. Cell. Mol. Med. (2009).
[41] K. Akasaka, C. Maesawa, M. Shibazaki, F. Maeda, K. Takahashi, T. Akasaka, T. Masuda, Loss of class III beta-tubulin induced by histone deacetylation is associated with chemosensitivity to paclitaxel in malignant melanoma cells, J. Invest. Dermatol. 129 (2009) 1516–1526.
[42] G. Raspaglio, I. De Maria, F. Filippetti, E. Martinelli, G.F. Zannoni, S. Prislei, G. Ferrandina, S. Shahabi, G. Scambia, C. Ferlini, HuR regulates beta-tubulin isotype expression in ovarian cancer, Cancer Res. 70 (2010) 5891–5900.
[43] I.M. de la Fuente, Quantitative analysis of cellular metabolic dissipative, self-organized structures, Int. J. Mol. Sci. 11 (2010) 3540–3599.
[44] I.M. De La Fuente, L. Martinez, A.L. Perez-Samartin, L. Ormaetxea, C. Amezaga, A. Vera-Lopez, Global self-organization of the cellular metabolic structure, PLoS ONE 3 (2008) e3100.
[45] M.A. Aon, S. Cortassa, Coherent and robust modulation of a metabolic network by cytoskeletal organization and dynamics, Biophys. Chem. 97 (2002) 213–231.
[46] M.A. Aon, B. O'Rourke, S. Cortassa, The fractal architecture of cytoplasmic organization: scaling, kinetics and emergence in metabolic networks, Mol. Cell. Biochem. 256–257 (2004) 169–184.
[47] L.M. Huff, D.L. Sackett, M.S. Poruchynsky, T. Fojo, Microtubule-disrupting chemotherapeutics result in enhanced proteasome-mediated degradation and disappearance of tubulin in neural cells, Cancer Res. 70 (2010) 5870–5879.
[48] B.G. Vertessy, F. Orosz, J. Kovacs, J. Ovadi, Alternative binding of two sequential glycolytic enzymes to microtubules. Molecular studies in the phosphofructokinase/aldolase/microtubule system, J. Biol. Chem. 272 (1997) 25542–25546.
[49] V. Saks, P. Dzeja, U. Schlattner, M. Vendelin, A. Terzic, T. Wallimann, Cardiac system bioenergetics: metabolic basis of the Frank–Starling law, J. Physiol. 571 (2006) 253–273.
[50] V. Redeker, Mass spectrometry analysis of C-terminal posttranslational modifications of tubulins, Methods Cell. Biol. 95 (2010) 77–103.
[51] S. Kostin, S. Hein, E. Arnon, D. Scholz, J. Schaper, The cytoskeleton and related proteins in the human failing heart, Heart Fail. Rev. 5 (2000) 271–280.
[52] J. Schaper, S. Kostin, S. Hein, A. Elsasser, E. Arnon, R. Zimmermann, Structural remodelling in heart failure, Exp. Clin. Cardiol. 7 (2002) 64–68.
[53] S. Hein, S. Kostin, A. Heling, Y. Maeno, J. Schaper, The role of the cytoskeleton in heart failure, Cardiovasc. Res. 45 (2000) 273–278.
[54] H. Tagawa, M. Koide, H. Sato, M.R. Zile, B.A. Carabello, G.T. Cooper, Cytoskeletal role in the transition from compensated to decompensated hypertrophy during adult canine left ventricular pressure overloading, Circ. Res. 82 (1998) 751–761.
[55] K. Guerrero, C. Monge, A. Bruckner, U. Puurand, L. Kadaja, T. Kaambre, E. Seppet, V. Saks, Study of possible interactions of tubulin, microtubular network, and STOP protein with mitochondria in muscle cells, Mol. Cell. Biochem. 337 (2010) 239–249.
[56] C. Janke, M. Kneussel, Tubulin post-translational modifications: encoding functions on the neuronal microtubule cytoskeleton, Trends Neurosci. 33 (2010) 362–372.
[57] R.F. Luduena, Multiple forms of tubulin: different gene products and covalent modifications, Int. Rev. Cytol. 178 (1998) 207–275.
[58] K.J. Verhey, J. Gaertig, The tubulin code, Cell Cycle 6 (2007) 2152–2160.
[59] T.K. Rostovtseva, S.M. Bezrukov, VDAC regulation: role of cytosolic proteins and mitochondrial lipids, J. Bioenerg. Biomembr. 40 (2008) 163–170.
[60] M. Colombini, VDAC: the channel at the interface between mitochondria and the cytosol, Mol. Cell. Biochem. 256–257 (2004) 107–115.
[61] M. Colombini, The published 3D structure of the VDAC channel: native or not? Trends Biochem. Sci. 34 (2009) 382–389.
[62] L. Hiser, A. Aggarwal, R. Young, A. Frankfurter, A. Spano, J.J. Correia, S. Lobert, Comparison of beta-tubulin mRNA and protein levels in 12 human cancer cell lines, Cell Motil. Cytoskeleton 63 (2006) 41–52.
[63] B. Antonsson, Mitochondria and the Bcl-2 family proteins in apoptosis signaling pathways, Mol. Cell. Biochem. 256–257 (2004) 141–155.
[64] G.W. Dorn II, Apoptotic and non-apoptotic programmed cardiomyocyte death in ventricular remodelling, Cardiovasc. Res. 81 (2009) 465–473.
[65] V. Saks, R. Favier, R. Guzun, U. Schlattner, T. Wallimann, Molecular system bioenergetics: regulation of substrate supply in response to heart energy demands, J. Physiol. 577 (2006) 769–777.
[66] T. Wallimann, M. Tokarska-Schlattner, D. Neumann, R.F. Epand, R.H. Andres, H.R. Widmer, T. Hornemann, V. Saks, I. Agarkova, U. Schlattner, The Phosphocreatine Circuit: Molecular and Cellular Physiology of Creatine Kinases, Sensitivity to Free Radicals, and Enhancement by Creatine Supplementation, in: V. Saks (Ed.), Molecular System Bioenergetics. Energy for Life, Wiley-VCH: Weinheim, GmbH, Germany, 2007, pp. 195–264.
[67] S.P. Bessman, C.L. Carpenter, The creatine–creatine phosphate energy shuttle, Annu. Rev. Biochem. 54 (1985) 831–862.
[68] S.P. Bessman, P.J. Geiger, Transport of energy in muscle: the phosphorylcreatine shuttle, Science 211 (1981) 448–452.
[69] M.K. Aliev, V.A. Saks, Compartmentalized energy transfer in cardiomyocytes: use of mathematical modeling for analysis of in vivo regulation of respiration, Biophys. J. 73 (1997) 428–445.
[70] R. Guzun, V. Saks, Application of the principles of systems biology and Wiener's cybernetics for analysis of regulation of energy fluxes in muscle cells in vivo, Int. J. Mol. Sci. 11 (2010) 982–1019.

[71] P.L. Pedersen, Transport ATPases into the year 2008: a brief overview related to types, structures, functions and roles in health and disease, J. Bioenerg. Biomembr. 39 (2007) 349–355.
[72] P.L. Pedersen, Y.H. Ko, S. Hong, ATP synthases in the year 2000: evolving views about the structures of these remarkable enzyme complexes, J. Bioenerg. Biomembr. 32 (2000) 325–332.
[73] P.L. Pedersen, S. Mathupala, A. Rempel, J.F. Geschwind, Y.H. Ko, Mitochondrial bound type II hexokinase: a key player in the growth and survival of many cancers and an ideal prospect for therapeutic intervention, Biochim. Biophys. Acta 1555 (2002) 14–20.
[74] E. Bustamante, H.P. Morris, P.L. Pedersen, Energy metabolism of tumor cells. Requirement for a form of hexokinase with a propensity for mitochondrial binding, J. Biol. Chem. 256 (1981) 8699–8704.
[75] S.P. Mathupala, Y.H. Ko, P.L. Pedersen, Hexokinase-2 bound to mitochondria: cancer's stygian link to the "Warburg Effect" and a pivotal target for effective therapy, Semin. Cancer Biol. 19 (2009) 17–24.
[76] J.E. Wilson, Hexokinases, Rev. Physiol. Biochem. Pharmacol. 126 (1995) 65–198.
[77] S. Patra, S. Bera, S. SinhaRoy, S. Ghoshal, S. Ray, A. Basu, U. Schlattner, T. Wallimann, M. Ray, Progressive decrease of phosphocreatine, creatine and creatine kinase in skeletal muscle upon transformation to sarcoma, FEBS J. 275 (2008) 3236–3247.

Amino Acids (2011) 40:1333–1348
DOI 10.1007/s00726-011-0854-x

REVIEW ARTICLE

Systems bioenergetics of creatine kinase networks: physiological roles of creatine and phosphocreatine in regulation of cardiac cell function

R. Guzun · N. Timohhina · K. Tepp · M. Gonzalez-Granillo · I. Shevchuk · V. Chekulayev · A. V. Kuznetsov · T. Kaambre · V. A. Saks

Received: 10 July 2010 / Accepted: 10 November 2010 / Published online: 10 March 2011

Abstract Physiological role of creatine (Cr) became first evident in the experiments of Belitzer and Tsybakova in 1939, who showed that oxygen consumption in a well-washed skeletal muscle homogenate increases strongly in the presence of creatine and with this results in phosphocreatine (PCr) production with PCr/O_2 ratio of about 5–6. This was the beginning of quantitative analysis in bioenergetics. It was also observed in many physiological experiments that the contractile force changes in parallel with the alteration in the PCr content. On the other hand, it was shown that when heart function is governed by Frank–Starling law, work performance and oxygen consumption rate increase in parallel without any changes in PCr and ATP tissue contents (metabolic homeostasis). Studies of cellular mechanisms of all these important phenomena helped in shaping new approach to bioenergetics, Molecular System Bioenergetics, a part of Systems Biology. This approach takes into consideration intracellular interactions that lead to novel mechanisms of regulation of energy fluxes. In particular, interactions between mitochondria and cytoskeleton resulting in selective restriction of permeability of outer mitochondrial membrane anion channel (VDAC) for adenine nucleotides and thus their recycling in mitochondria coupled to effective synthesis of PCr by mitochondrial creatine kinase, MtCK. Therefore, Cr concentration and the PCr/Cr ratio became important kinetic parameters in the regulation of respiration and energy fluxes in muscle cells. Decrease in the intracellular contents of Cr and PCr results in a hypodynamic state of muscle and muscle pathology. Many experimental studies have revealed that PCr may play two important roles in the regulation of muscle energetics: first by maintaining local ATP pools via compartmentalized creatine kinase reactions, and secondly by stabilizing cellular membranes due to electrostatic interactions with phospholipids. The second mechanism decreases the production of lysophosphoglycerides in hypoxic heart, protects the cardiac cells sarcolemma against ischemic damage, decreases the frequency of arrhythmias and increases the post-ischemic recovery of contractile function. PCr is used as a pharmacological product Neoton in cardiac surgery as one of the components of cardioplegic solutions for protection of the heart against intraoperational injury and injected intravenously in acute myocardial ischemic conditions for improving the hemodynamic response and clinical conditions of patients with heart failure.

Keywords Creatine · Phosphotransfer networks · Mitochondria · Respiration · Regulation · Systems biology

R. Guzun · M. Gonzalez-Granillo · V. A. Saks (✉)
Laboratory of Fundamental and Applied Bioenergetics, INSERM U884, Joseph Fourier University, 2280, Rue de la Piscine, BP53X-38041 Grenoble Cedex 9, France
e-mail: Valdur.Saks@ujf-grenoble.fr

N. Timohhina · K. Tepp · I. Shevchuk · V. Chekulayev · T. Kaambre · V. A. Saks
Laboratory of Bioenergetics, National Institute of Chemical Physics and Biophysics, Tallinn, Estonia

A. V. Kuznetsov
Cardiac Research Laboratory, Department of Cardiac Surgery, Innsbruck Medical University, Innsbruck, Austria

Introduction: historical note

Creatine was discovered 175 years ago by the French scientist Michel Eugene Chevreul. Almost one century later Otto Meyerhoff and Archibald Hill studied the energetics of carbohydrate catabolism in skeletal muscles, for which

they subsequently received the Nobel Prize (Hill et al. 1924; Kresge et al. 2005). Meyerhoff focused on the study of glycolytic pathways demonstrating that in the absence of oxygen glycolysis leads to production of lactic acid. Archibald Hill used these theoretical bases to explain mechanisms of transformation of energy liberated during metabolism into mechanical work of muscles. Hill and Meyerhoff hypothesized that muscle contraction is fuelled by the energy released from glycogen conversion into lactic acid. The role of oxygen in their theory was limited to the removal of lactic acid during the resting period. The worldwide recognized lactic acid theory of contraction (Mommaerts 1969; Ivanov et al. 1997) was ruled out by the very simple experiment performed by Lundsgaard, in 1930. Lundsgaard inhibited glycolysis in contracting frog muscle by iodoacetate and observed that despite inhibition of glycolysis, frog's muscle continued to contract during some time under hypoxic conditions (Lundsgaard 1930). By that time, a new compound in which phosphate is linked to creatine through a phosphoamide bond, the phosphagen (later named phosphocreatine, PCr), was already discovered by Grace and Philip Eggleton and by Fiske and Subbarow (Eggleton and Eggleton 1927; Fiske and Subbarao 1927). Lundsgaard observed that after a series of contractions under anaerobic conditions in the iodoacetate-injected muscle, the lactic acid content was similar to that of resting muscle and the phosphocreatine content was completely used up. In the control muscle contracting under the conditions of Hill's experiment (glycolysis and anoxia), the increase in lactic acid concentration was associated with only slight decrease in phosphocreatine content. In this way, Lundsgaard hypothesized that in muscle poisoned with iodoacetate the immediate energy source of muscle contraction was phosphocreatine. Poisoned cardiac muscle stopped its work in anoxic conditions after a few minutes of contraction and continued to contract for 1.5–2 h in the presence of oxygen even under very high concentrations of iodoacetate. Lohmann, in 1934, described the creatine kinase (CK) reaction which links PCr with ATP. In 1939, Belitzer and Tsybakova measured the phosphagene (PCr) production and oxygen consumption in pigeon's pectoral muscles homogenate stimulated by creatine without the addition of adenine nucleotides. These authors were the first to show that creatine stimulates respiration and that PCr production was associated with P/O_2 ratio between 5.7 and 7 (Belitzer and Tsybakova 1939). During the same time period, Frank and Starling discovered the basic law of the heart functioning—parallel increase in respiration and cardiac work with increase in left ventricle filling (Starling and Visscher 1926; Saks et al. 2006).

It took about 80 years to identify the cellular mechanisms of these important phenomena, which are all related to the physiological role of creatine and creatine kinase system in heart cells (Bessman and Geiger 1981; Bessman and Carpenter 1985; Wallimann et al. 1992, 2007; Saks 2007). The central role of Cr, PCr and CK (Cr/PCr/CK) system in cardiac cells is shown in Fig. 1. Their central role is based on the intracellular distribution of different isoforms of CK in muscle cells that has been previously described in great details elsewhere (Wallimann et al. 1992, 2007).

The aim of this review article is to describe the key mechanisms of the functioning of the Cr/PCr/CK system in the heart that has been revealed in functional and kinetic studies. Central among these mechanisms is the functioning of a supercomplex, mitochondrial interactosome (Timohhina et al. 2009). These mechanisms result from complex interactions in structurally highly organized cells and are therefore best understood using the approaches developed in Systems Biology (Saks 2007). The central role of the Cr/PCr/CK system in muscle and brain cells' energetics makes it an important target for understanding of the mechanisms of pathogenesis of many muscular and neuromuscular diseases and their possible treatment.

Mitochondrial interactosome

Evidence for functional coupling between MtCK and ANT in isolated heart mitochondria

The mitochondrial isoform of CK was discovered in 1964 in the Klingenberg's laboratory (Klingenberg 1970). Sarcomeric (sMtCK) is present in muscle cells and ubiquitous (uMtCK) is present in other tissues (Wallimann et al. 1992). Bessman and Fonyo (1966) and Jacobus and Lehninger (1973) showed that creatine stimulates respiration of isolated mitochondria in State 4 (when ADP is completely used up) up to State 3 (corresponding to maximal level of ADP-stimulated respiration) (Bessman and Fonyo 1966; Jacobus and Lehninger 1973). This and other similar experiments led to conclusion that MtCK controls the oxidative phosphorylation. Under respiring conditions, the MtCK reaction is influenced by its coupling with oxidative phosphorylation via adenine nucleotide translocase (ANT). Jacobus and Saks (1982) evaluated the kinetic properties of MtCK in isolated heart mitochondria under conditions of the ATP supply either by activated oxidative phosphorylation or by the exogenous addition (in the presence of inhibited oxidative phosphorylation (Jacobus and Saks 1982). In the first case, the MtCK reaction rate was evaluated by measuring oxygen consumption (process functionally coupled to the PCr production) while in the second case by measuring ADP production and subsequent NADH oxidation in phosphoenolpyruvate–pyruvate kinase–lactate dehydrogenase (PEP–PK–LDH) enzymes system (Fig. 2a). The results

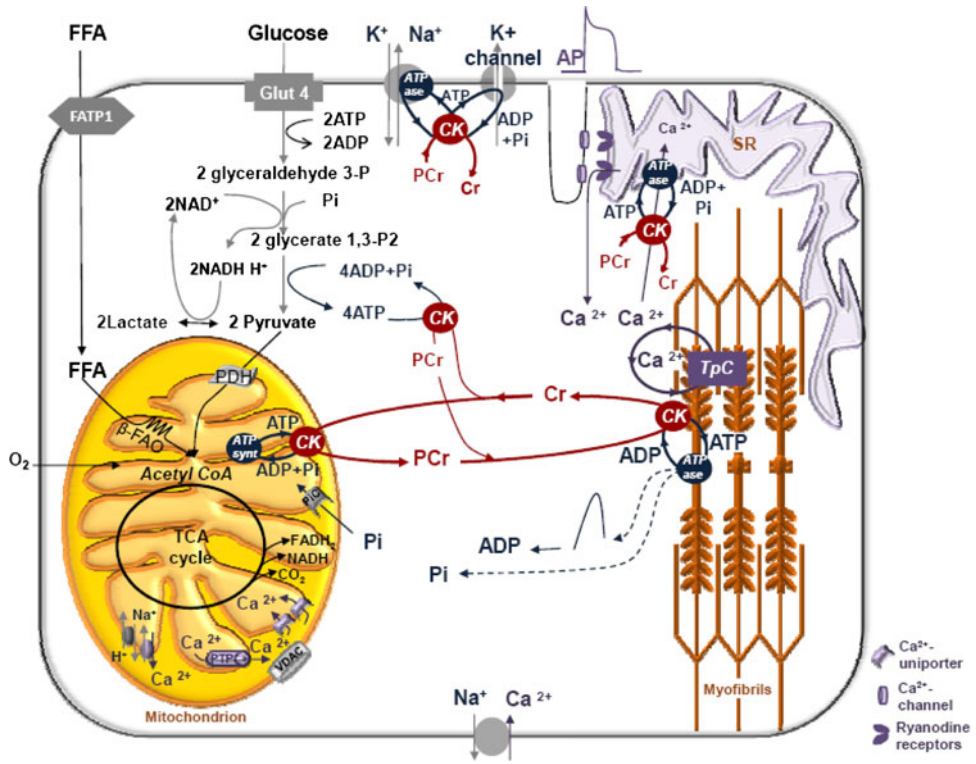

Fig. 1 Scheme of energy metabolism in heart and skeletal muscle cells. Two sources of ATP re-synthesis, mitochondrial oxidative phosphorylation and glycolysis, are interconnected with sites of ATP hydrolysis via the phosphocreatine/creatine kinase (PCr/CK) shuttle. *GLUT4* glucose transporter, *FATP1* fatty acid transport protein, *β-FAO* beta-oxidation of fatty acids, *PHD* pyruvate dehydrogenase, *PTP* permeability transition pore, *VDAC* voltage-dependent anion channel, *TpC* troponin C, *AP* action potential. The isoforms of the creatine kinase (CK) present in different subcellular compartments are coupled with both ATP producing (mitochondrial and glycolytic) and ATP consuming (contraction, ions pumping) processes. In muscle cells sarcomeric mitochondrial CK (MtCK) functionally coupled to ATP synthase via adenine nucleotide translocase (ANT) and cytosolic isoforms of CK (MMCK and MBCK) coupled to glycolytic enzymes (phosphoglycerate kinase (PGK) and pyruvate kinase (PK) catalyse forward reaction of phosphocreatine (PCr) synthesis from mitochondrial or glycolytic ATP and creatine). The MMCK functionally coupled to myosin ATPases, sarcoplasmic reticulum ATPases or ions-pumping-ATPases catalyse reverse reaction of ATP regeneration from PCr and locally produced ADP. The prevalence of one of the ways of PCr production is tissue specific. In cardiac and oxidative muscle cells PCr used for muscle contraction is produced mainly from mitochondrial ATP, while in fast twitch glycolytic muscle it is produced from ATP supplied by glycolysis

showed that the oxidative phosphorylation strongly increases the rate of PCr production (Fig. 2b). The explanation of this observation was given by a complete kinetic analysis of the creatine kinase reaction in isolated heart mitochondria which follows the Bi Bi random type quasi equilibrium mechanism (Jacobus and Saks 1982):

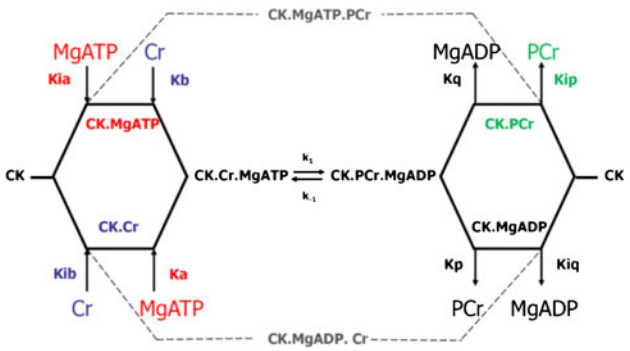

The apparent constant K_a of dissociation of MgATP from the ternary enzyme–substrates complex, CK.Cr.MgATP, decreased by an order of magnitude when ATP was supplied to MtCK from oxidative phosphorylation (Fig. 2c; Table 1). This was explained by the direct transfer of adenine nucleotides between MtCK and ANT. It was shown that MtCK and ANT are present in cardiac mitochondria in the 1:1 molar ratio (Kuznetsov and Saks 1986) and linked to each other by cardiolipin molecules (Schlattner et al. 2004). The results shown in Fig. 2b describe the increase in the rate of PCr production by oxidative phosphorylation that cannot be explained by the assumption of free ATP diffusion in the intermembrane space. Free diffusion of molecules by Brownian movement (Fig. 2d) is described by the Einstein–Smoluchowski equation: $D = \lambda^2/2t$, where D is diffusion coefficient, λ is the distance of displacement for a given time t (Saks et al. 2008). Employing this equation and knowing that the distance between two mitochondrial membranes is

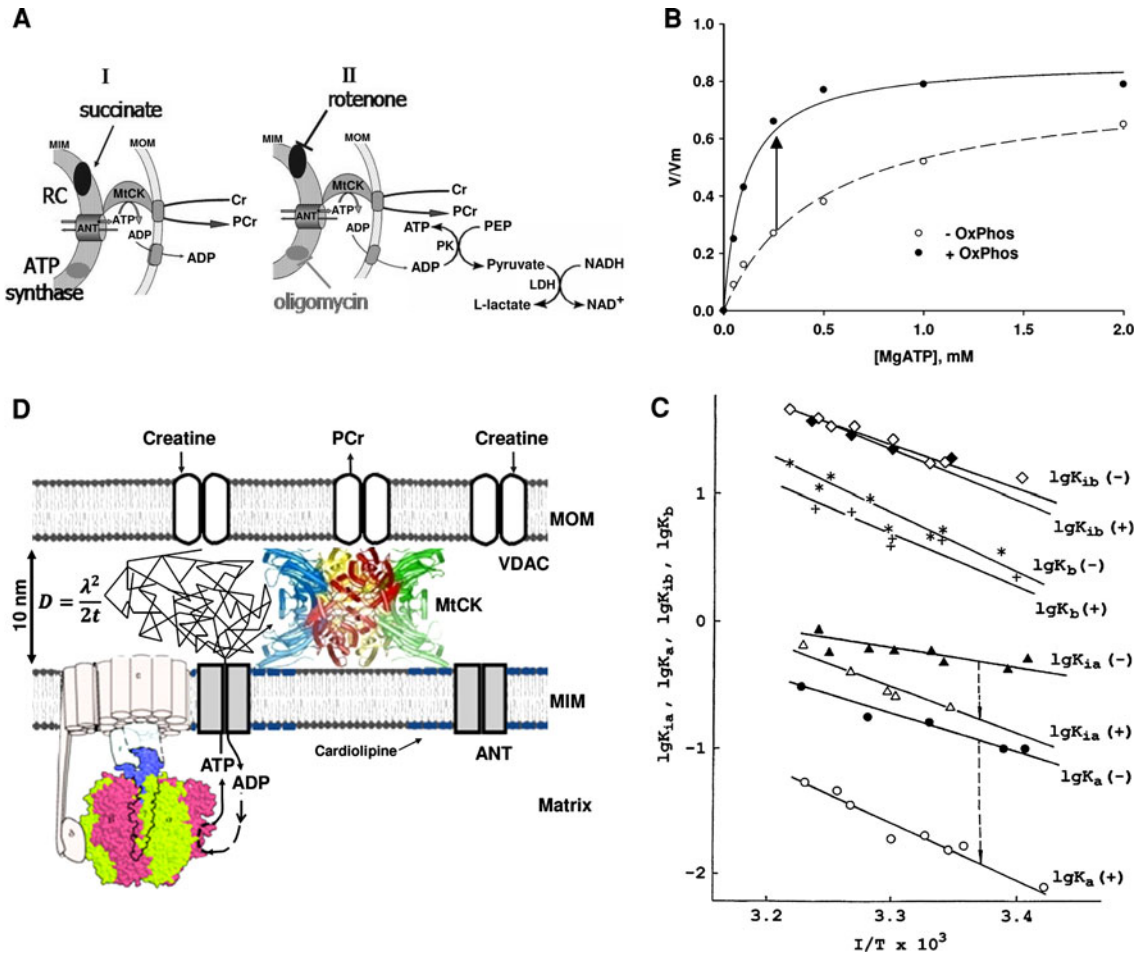

Fig. 2 **a** Scheme of experiments performed to study the kinetic properties of creatine kinase (CK) in isolated heart mitochondria. In the presence of oxidative phosphorylation (I), the measurement of reaction rates was carried out by recording the oxygen uptake in the presence of activated respiratory chain (by succinate). In the second experiment (II), the disappearance of NADH in pyruvate–lactate dehydrogenase reactions (LDH) was followed spectrophotometcally in the presence of inhibited respiratory chain by rotenone and oligomycin. *MIM* Mitochondrial inner membrane, *MOM* mitochondrial outer membrane, *RC* respiratory chain, *ANT* adenine nucleotide translocase, *MtCK* mitochondrial creatine kinase, *Cr* creatine, *PCr* phosphocreatine. **b** Michaelis–Menten representation of relative rates of MtCK reaction (V/V_m) in isolated heart mitochondria as a function of MgATP concentrations measured in the presence of 10 mM creatine and inhibited (*empty circles*) or activated oxidative phosphorylation (*filled circles*) (adapted from). **c** Complete kinetic analysis of the forward MtCK reaction in heart mitochondria. The temperature dependencies of the kinetic constants are shown at a semi-logarithmic scale in the presence (+) and absence (−) of oxidative phosphorylation. The dissociation constants were expressed in mM. Only K_a (dissociation constant of MgATP from ternary enzyme–substrate complex) is changed by oxidative phosphorylation by an order of magnitude; smaller changes are seen for Ki_a, but practically no changes are seen for the dissociation constant of creatine (reproduced from Saks et al. 1998] with permission). **d** Scheme of the microcompartment of adenine nucleotides in mitochondrial intermembrane space created by proteolipid complexes of MtCK with VDAC and ANT, and limited by mitochondrial outer membrane (MOM). This complex allows the direct exchange-metabolite channelling, depicted by *arrows*. This *figure* represents also schematically hypothesis of free diffusion of adenine nucleotides molecules within mitochondrial intermembrane space, which can be described by Einstein–Smoluchowski diffusion equation. The inconsistently of this hypothesis is argued in the text

about 0.01 μm, and admitting that the coefficient of ATP diffusion in water is 200 $\mu m^2/s$ (Saks et al. 2008), the time during which the molecule of ATP will cross this distance by free diffusion will be 0.25×10^{-6} s. Given that the turnover number (TN) of MtCK reaction in direction of PCr production is equal to 33–41 s^{-1} (Engelborghs et al. 1975), the time τ needed for MtCK to transfer the phosphoryl group from ATP to creatine, $\tau = 1/TN$ will be, respectively, 0.03–0.024 s, any theoretical attempt to explain the functional coupling of MtCK with ANT by the simple diffusion becomes futile: very rapid diffusion should equilibrate ATP concentration in intermembrane space and surrounding medium. The real apparent constant of ATP diffusion in (or from) the microcompartment between octameric MtCK and ANT, taking into consideration the above given values for λ, τ and Einstein–Smoluchowski diffusion equation, has to be

in the range of 10^{-3} $\mu m^2/s$ and not 200 $\mu m^2/s$ as it was supposed to be in a homogenous water bulk solution (Saks et al. 2008). Most probably, there is a vectorial movement of ATP molecules (channelling) directly from ANT to MtCK due to their close proximity without liberation into intermembrane space (Saks et al. 2007a, b). The molecular details of this channelling need to be revealed. After the utilisation of this ATP in the MtCK reaction for creatine phosphorylation, ADP may be channelled back to ANT, or liberated into intermembrane space and into the surrounding medium, if the voltage-dependent anion channel (VDAC) in the mitochondrial outer membrane is open. Thus, the functional coupling between ANT and MtCK is finally depending on the state of VDAC in the outer mitochondrial membrane, MOM.

Control of outer mitochondrial membrane permeability in cardiac cells in situ

Cells' permeabilisation technique revealed a remarkable decrease in affinity of oxidative phosphorylation for free ADP in permeabilized cardiac cells in situ (Fig. 3a) in comparison with isolated heart mitochondria (the apparent K_m for free ADP is respectively $\sim$350 and $\sim$10 μM) (Saks et al. 1995, 1998). The analysis of this data led to the conclusion of the restriction of movement of adenine nucleotides across the MOM in permeabilized cardiomyocytes, this resulting in increase in the functional coupling within MtCK-oxidative phosphorylation system, thereby increasing the role of the Cr/PCr/CK system in energy transfer (Aliev and Saks 1997). The restriction of ADP diffusion can be clearly seen in experiments in which the ADP-trapping system, pyruvate kinase-phosphoenolpyruvate (PK-PEP), proposed previously by F. Gellerich for isolated mitochondria (Gellerich and Saks 1982), is added to permeabilized cardiomyocytes in the presence of activated MtCK (by the addition of ATP and creatine). Under these conditions, the PEP–PK system allows us in detecting the possible leak of ADP produced by MtCK from the mitochondrial intermembrane space (Fig. 3b, c). As it is shown in Fig. 4a, the PK–PEP system cannot inhibit the respiration of permeabilized cardiomyocytes in contrast to that of isolated heart mitochondria where respiration rate is decreased by this system by about 50% (Gellerich and Saks 1982). The ADP produced locally in the MtCK reaction of permeabilized cardiomyocyte is returned entirely into the matrix without any leak of mitochondrial ADP towards intracellular milieu.

Recently, it was shown that the selective permeability of MOM for adenine nucleotides is due to the control of VDAC by certain cytoskeleton proteins, specifically by $\alpha\beta$-tubulin (Rostovtseva and Bezrukov 2008; Rostovtseva et al. 2008). Reconstructing purified VDAC into planar phospholipid membranes, author showed that dimeric tubulin (which in nanomolar concentration is insufficient for polymerization in the absence of GTP and Mg^{2+}) induced the reversible voltage-dependent partial block of the channel. The addition of dimeric tubulin to isolated heart mitochondria induced the decrease in the affinity of oxidative phosphorylation for free ADP (i.e. the increase in the apparent K_m for free ADP) (Fig. 4b). Rostovtseva et al. proposed the model for the control of the VDAC permeability by tubulin which is based on the interaction of positively charged domain of VDAC with negatively charged C-terminal tail of tubulin (Fig. 4c) (Rostovtseva and Bezrukov 2008; Rostovtseva et al. 2008). This model is in concord with the results of our recent immunolabelling studies on localization of tubulin isoforms in permeabilized heart cells which directly shows the connection of beta II tubulin with mitochondria (Fig. 4d).

By continuously removing extramitochondrial MgADP, the PEP–PK system allows us to avoid its stimulatory effect on respiration (Fig. 3c). Under these conditions, the MtCK reaction activated by MgATP and creatine controls oxidative phosphorylation via the MgADP produced inside the mitochondrial intermembrane space. We applied this protocol for investigation of the MtCK kinetic properties in permeabilized cardiac cells in situ. A series of experiments were performed in the presence of different fixed concentrations of MgATP and stepwise raised concentrations of creatine, to allow us to estimate kinetics parameters of the

Table 1 Complete kinetic analysis of the forward MtCK reaction in heart mitochondria

	K_{ia}^{app}MgATP (mM)	K_{a}^{app}MgATP (mM)	K_{ib}^{app}Cr (mM)	K_{b}^{app}Cr (mM)	K_{ip}^{app} PCr (mM)
Mitochondria in vitro					
−OxPhos	0.92 ± 0.09	0.15 ± 0.023	30 ± 4.5	5.2 ± 0.3	
+OxPhos	0.44 ± 0.08	0.016 ± 0.01	28 ± 7	5 ± 1.2	0.84 ± 0.22
Mitochondria in situ (with PEP–PK)	1.94 ± 0.86	2.04 ± 0.14	2.12 ± 0.21	2.17 ± 0.40	0.89 ± 0.17

The decrease by about order of magnitude of the apparent constant of dissociation of MgATP from its ternary complex with MtCK under conditions when MgATP is regenerated by oxidative phosphorylation (OxPhos) in isolated mitochondria point on the presence of functional coupling of MtCK with OxPhos controlling MgATP direct transfer

In permeabilized cardiomyocytes in situ this constant is increased by two orders of magnitude, showing selective limitation of the permeability of the outer mitochondrial membrane for ATP

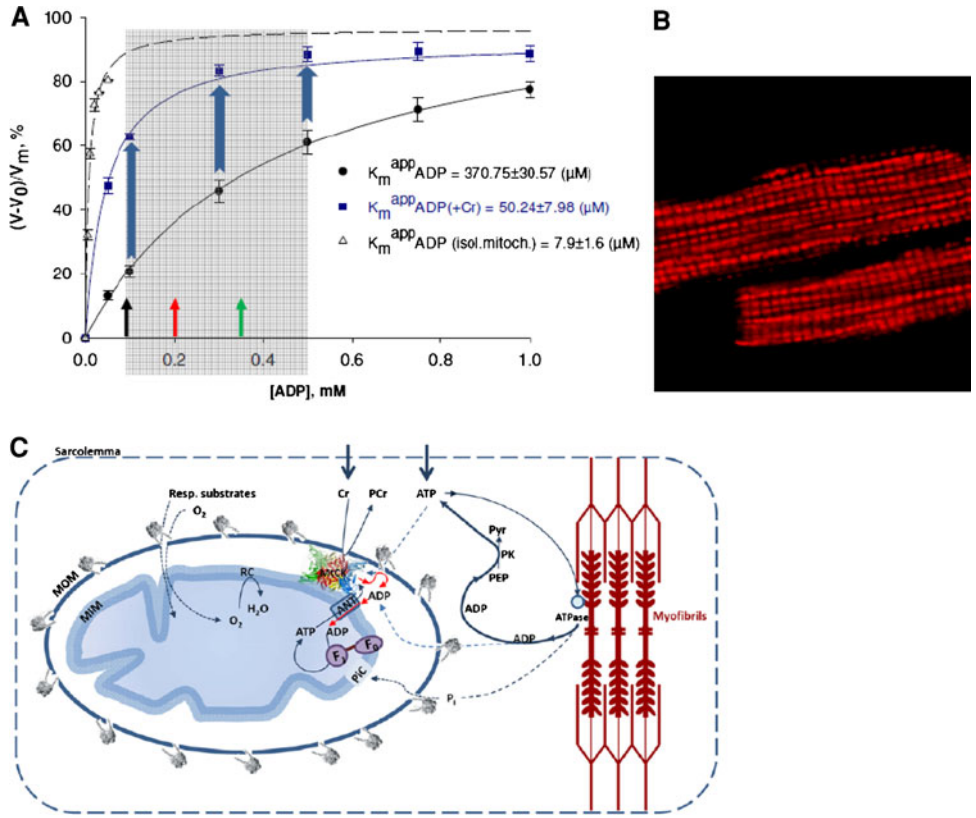

Fig. 3 **a** Michaelis–Menten representation of ADP-stimulated respiration of isolated heart mitochondria (*empty triangles*) and permeabilized cardiomyocytes measured under conditions of the absence (*full circles*) and presence of creatine (*full squares*). *Colour arrows* correspond to the fluctuations of ADP concentrations subsequent to different heart workloads. The *gray rectangle* delimits area of physiological cytosolic ADP concentration. Outer membrane of isolated mitochondria being highly permeable for adenine nucleotides limits the respiration regulation by free ADP. The maximal respiration rate is achieved by minimal ADP concentrations equivalent to the minimal workload. When the ADP diffusion is restricted at the level of MOM, as in mitochondria in situ, the respiration rates become linearly dependent on ADP concentrations. This linear dependence under physiological conditions can be amplified by creatine in the presence of activated MtCK. So, this *graph* explains the role of MOM permeability in feedback regulation. If there is no restriction of diffusion, there is no regulation (adapted from Guzun et al. 2009). **b** Confocal image of isolated rat cardiomyocyte. Mitochondrial labelling with MitoTracker Red. **c** Protocol of the method used to study interaction between mitochondrial and glycolytic systems in competition for endogenous ADP. Exogenous ATP is hydrolyzed by cellular ATPases into endogenous extramitochondrial ADP and inorganic phosphate (Pi). Mitochondrial (MtCK) and non-mitochondrial creatine kinases in myofibrils and at membrane of sarcoplasmic reticulum in the presence of creatine and ATP produce endogenous intra- and extramitochondrial ADP. Phosphoenolpyruvate (PEP) and pyruvate kinase (PK) system removes extramitochondrial ADP produced by intracellular ATP consuming reactions and continuously regenerate extramitochondrial ATP. Endogenous intramitochondrial ADP produced by MtCK forms microcompartments within the mitochondrial intermembrane space (IMS) and is re-imported into the matrix via adenine nucleotide translocase (ANT) due to its functional coupling with MtCK

MtCK reaction in the cells in situ (Guzun et al. 2009). These results are also shown in Fig. 5a and Table 1. Figure 5a shows rapid activation of respiration by creatine under these conditions. Figure 5b shows that this is directly related to the control of the mitochondrial membrane potential. On the other hand, the remarkable decrease in affinity for MgATP, seen as an increase in the apparent constant of dissociation for MgATP from ternary enzyme–substrates complex (MtCK.Cr.MgAT) (Table 1) is due to the restriction of MgATP diffusion at the level of mitochondrial outer membrane (MOM) in permeabilized cardiomyocytes in comparison with isolated mitochondria. Significant decrease in ATP diffusion through MOM results in the energy export out of the mitochondria almost exclusively by PCr. Concomitant measurements of PCr production and oxygen consumption through the experiment in which the respiration is stimulated by creatine in the presence of activated MtCK and removed extramitochondrial ADP, showed that the P/O ratio is close to theoretical value ~6 (Fig. 5c) allowing us to assume that PCr is the main energy flux exported from cardiac mitochondria (Timohhina et al. 2009). These experimental results fit and

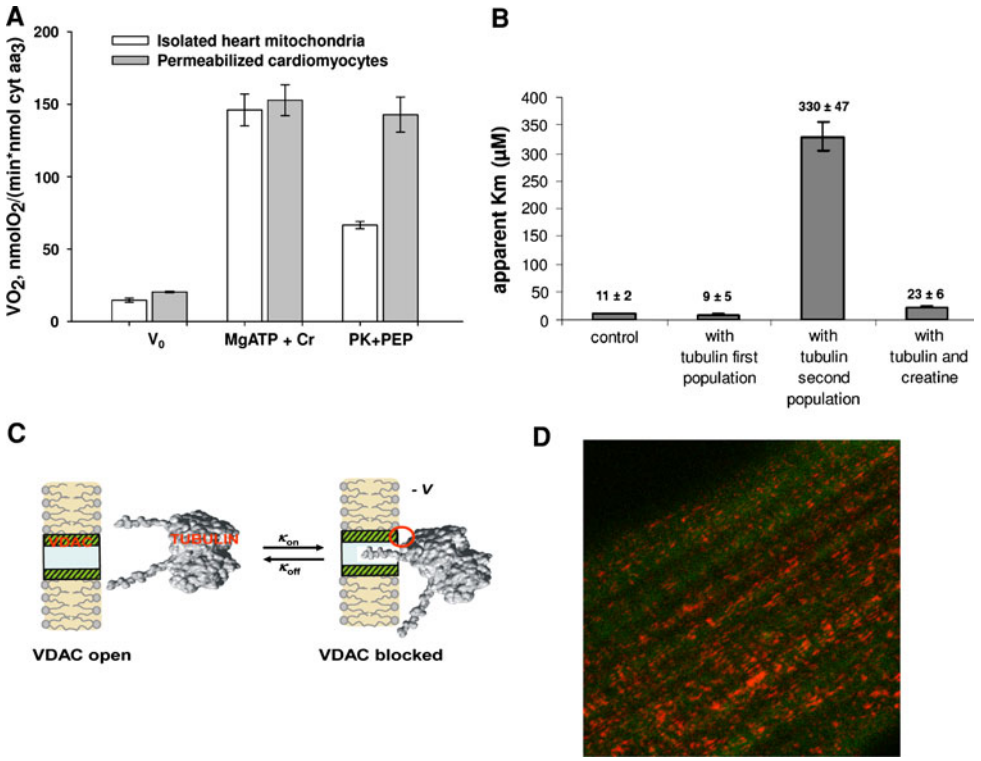

Fig. 4 **a** Full compartmentalization of intramitochondrial ADP produced by MtCK in the intermembrane space of mitochondria in permeabilized cardiomyocytes in situ. Respiration was activated by addition of MgATP (5 mM) and creatine (20 mM). Stable and maximal respiration rates are supported by MtCK activity in the presence of ATP and creatine. Under these conditions, approximately 50% of ADP, produced in the intermembrane space, can be trapped by the powerful PEP–PK system in the case of isolated heart mitochondria. The respiration is not completely inhibited because of the presence of direct ADP transfer from MtCK to ANT. In permeabilized cardiomyocytes in situ when mitochondrial respiration is controlled by the MtCK reaction, the powerful PEP–PK system is not able to inhibit respiration. The permeability of VDAC for ADP seems strongly decreased. **b** Tubulin dramatically increases apparent K_m for ADP in regulation of respiration of isolated brain mitochondria. In the presence of creatine, the apparent K_m for ADP is again decreased. These effects reproduce the observations on permeabilized cardiomyocytes shown in Fig. 3a (adapted from Rostovtseva et al. 2008). **c** Model of tubulin–VDAC interaction. One tubulin C-terminal tail partially blocks channel conductance by entering VDAC pore. This process is voltage dependent and could be described by the first-order reaction of one-to-one binding of tubulin to VDAC. Some additional interaction between tubulin globular body and VDAC may be involved (adapted from). **d** Confocal image of immunofluorescent labeling of tubulin βII co-localisation with VDAC in fixed cardiomyocytes. The anti-tubulin βII antibody (Abcam, ab28036) with the Cy5 (Jackson Immunoresearch 115-175-146) antibody (*red color*) were used to label tubulin βII isoform, and the anti-VDAC1/2/3/ antibody IgG-FITC (*green color* Santa Cruz Biotechnology; sc-98708) were used to label VDAC. As we can see in a part tubulin βII co-localizes with VDAC

explain perfectly the earlier observation by Belitzer and Tsybakova (1939).

Thus, the apparent kinetic parameters of the MtCK reaction, its direction, velocity of reaction and the ability to function in non-equilibrium steady state are in a tight dependency upon the functional interaction of MtCK with ANT and VDAC due to the orchestrated functioning of oxidative phosphorylation/ANT/MtCK/VDAC selective permeability of which is governed by tubulin. All they may be grouped into structure–functional unit, a supercomplex that we called mitochondrial interactosome (MI) (Fig. 6a). The following complexes were integrated into the mitochondrial interactosome: ATP synthasome (Chen et al. 2004; Pedersen 2007, 2000), the functional complexes formed by MtCK, ANT, VDAC and tubulin (Saks 2007; Wallimann et al. 1992; Dolder et al. 2003; Timohhina et al. 2009) (Fig. 6a). This unit can also include the super complex formed by the respiratory chain (Lenaz and Genova 2007; Vonck 2009). The role of interactosome is to ensure the cycling of adenine nucleotides in mitochondria, coupled to PCr synthesis and facilitate the export of the free energy of mitochondrial ATP phosphorylation potential as energy of PCr fluxes. Functioning of MI is effectively controlled by creatine concentration and PC/Cr ratio. Interestingly, this supercomplex is significantly altered in cancerous HL-1 cells of cardiac phenotype (Fig. 6b). The analysis of mechanisms of energy metabolism regulation and MI

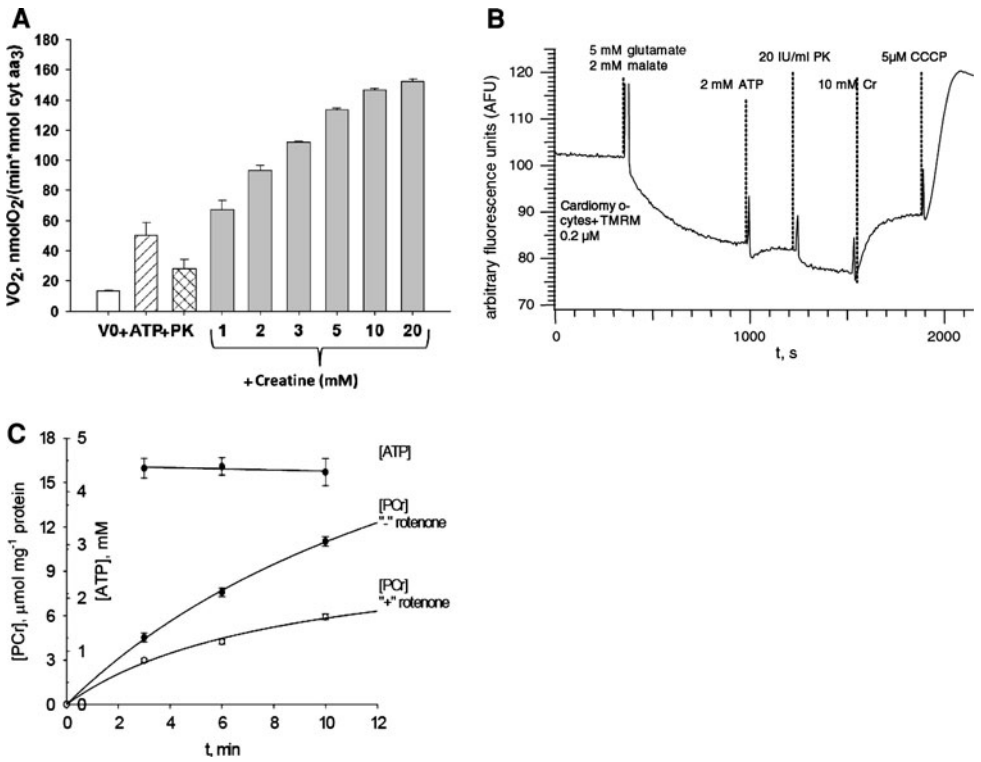

Fig. 5 **a** High efficiency of creatine in the control of respiration of permeabilized cardiomyocytes. The addition of 2 mM MgATP activates respiration due to production of endogenous MgADP in ATPase reaction. Pyruvate kinase (PK) and phosphoenolpyruvate (PEP) added to experimental milieu remove the extramitochondrial MgADP and thus inhibit respiration. Creatine under these conditions rapidly activates mitochondrial creatine kinase (MtCK) reaction and subsequently local MgADP recycling and oxygen consumption rate to the maximal values. **b** Measurement of mitochondrial membrane potential by using the fluorescence of TMRM (0.2 μM). The protocol described in Fig. 5a was applied in this experiment. The addition of 5 mM glutamate and 2 mM malate caused a decrease in fluorescence indicating the accumulation of TMRM in mitochondrial matrix. 2 mM ATP produced a small change in mitochondrial membrane potential, activation of MtCK and mitochondrial respiration by the addition of 10 mM creatine decreased membrane potential to a lower steady state level. The uncoupling agent CCCP 5 μM was used to dissipate the membrane potential. **c** The rate of phosphocreatine production by mitochondrial and cytoplasmic creatine kinases in permeabilized cardiomyocytes was measured using ion pair HPLC/UPLC during the experiment described in Fig. 5a. Experiments were performed under conditions of activated (*full circles*) and inhibited (*empty circles*) complex I of the respiratory chain and with addition of creatine in concentration of 20 mM. The ATP level, continuously regenerated by the PEP–PK system, was stable during the experiment. The between VO_2 (measured by oxygraphy represented in Fig. 5a) and VPCr was about 5.7. Adapted from Timohhina et al. (2009)

structure of tumour cardiac cells (NB HL-1 cells line) confirms this hypothesis. Mitochondria of NB HL-1, cells in comparison with adult cardiomyocytes, are filamentous and in a continuous fusion/fission (Pelloux et al. 2006; Beraud et al. 2009). The affinity of oxidative phosphorylation for free ADP is high (K_m^{app} ADP = 25 ± 4 μM) and identical to that of isolated heart mitochondria surrounded by a homogeneous medium (Anmann et al. 2006). The high affinity for free ADP indicates the important permeability of MOM for adenine nucleotides. Respiration of NB HL-1 cells cannot be stimulated by the addition of creatine. Eimre et al. (2008) and Monge et al. (2009) showed that NB HL-1 cells have a glycolytic metabolic profile characterized by a low activity of the total creatine kinase and a high activity of hexokinase II (Eimre et al. 2008; Monge et al. 2009). These properties are characteristic to energy metabolism of cancer cells, described by Otto Warburg in 1956, and more recently elucidated in Pedersen's work (Warburg 1956; Pedersen 2007).

Metabolic control analysis: increased flux control coefficients in mitochondrial interactosome

Both theoretically and experimentally, the most effective quantitative method for identification of the regulatory mechanisms in the complex metabolic systems is metabolic control analysis developed about 35 years ago by Heinrich and Rapoport and Kacser and Burns (Kholodenko et al. 1995). In this approach, the relative changes of total flux J through a metabolic system is studied in dependence of the fractional change in activity of the given enzyme *k*, and the role of the latter in flux regulation is quantitatively described by its flux control coefficient:

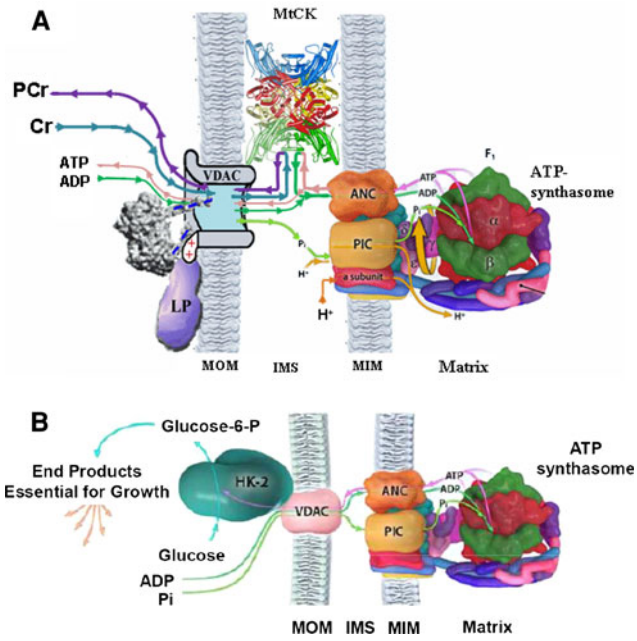

Fig. 6 **a** Mitochondrial interactosome of adult cardiomyocyte consists of functionally coupled supercomplex of ATP synthasome (formed by the ATP synthase, adenine nucleotides carrier, ANC, and phosphate carrier (PIC) Pedersen 2007, 2000), mitochondrial creatine kinase and VDAC with bound protein (tubulin and/or linker protein, LP) (Timohhina et al. 2009). MtCK transfer the phosphate group from mitochondrial ATP to creatine producing PCr and recycling ADP. Recycled ADP is returned to ATP synthasome due to its functional coupling with MtCK. PCr leaves mitochondria as a main energy flux due to high selective permeability of VDAC for this compound. **b** In HL-1 cancer cells of cardiac phenotype MtCK is absent and ATP synthesized by ATP synthasome leaves mitochondria. This ATP is used by HK-II, interacting with the VDAC in the outer mitochondrial membrane (effect Warburg) Pedersen (2007)

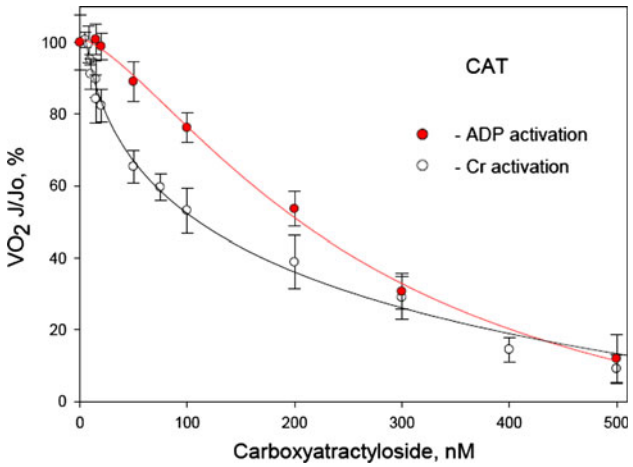

Fig. 7 The effect of functional coupling of mitochondrial CK and local ADP regeneration in the vicinity of adenine nucleotide translocase (ANT) on the flux control coefficient of the ANT. Inhibitor titration experiments were performed with a specific and irreversible inhibitor ANT carboxyatractyloside (CAT). Two titrations with carboxyatractyloside are shown, one under conditions of simple ADP activation of respiration by externally added ADP, at its saturating concentration (1 mM) (*filled circles*, *red curve*) and one under conditions of CK-ANT coupling and local ADP recycling, in the presence of activated CK (added creatine) and PK-PEP ADP trapping system (*open circle*, *black curve*). At similar rates of respiration, the same amount of carboxyatractyloside had a dramatically more pronounced inhibitory effect in coupled system, when compared with maximal respiration activated by externally added 1 mM ADP. This indicates that the flux control coefficient of ANT is significantly larger in the presence of functionally coupled CK. In both cases, values of the flux control coefficients for ANT were determined experimentally and calculated with the graphical method (Gellerich et al. 1990) from the initial slopes of the titration curves of respiration with CAT, estimated by linear regression of the first titration points

$$C_k^j = \frac{v_k}{J_j}\frac{\delta J_j}{\delta v_k}$$

For mitochondria in vivo, the total flux is the rate of respiration, VO_2, and the activities of different complexes of mitochondrial interactosome can be changed by using their irreversible inhibitors (Gellerich et al. 1990). Figure 7 shows the results of experimental determination of the flux control coefficients for ANT which was inhibited by increasing the concentration of carboxyatractyloside (CAT), for two different conditions: for direct activation of respiration by ADP in saturating concentration of 2 mM (ADP activation), and for conditions when respiration is controlled by the MtCK reaction in the presence of MgATP (2 mM), creatine (10 mM) and PK–PEP system. In the latter case, adenine nucleotides ADP and ATP are being continuously recycled in the mitochondria in the functionally coupled system within mitochondrial interactosome. Theoretical analysis control theory of metabolic channeling performed by Kholodenko, Cascante and Westerhoff some years ago revealed that in the system with metabolic channeling and functional coupling the control coefficients should be increased (Kholodenko et al. 1995). This is exactly what we see in Fig. 7: for direct activation of respiration by ADP the flux control coefficient for ANT is 0.21, and for the MtCK-activated respiration the flux control coefficient increases to 0.93 (unpublished results). Thus, the functional coupling between MtCK and ANT in MI strongly increases the efficiency of the control of mitochondrial oxidative phosphorylation by intracellular metabolic factors. Recycling of ADP in MI is controlled much more effectively than direct supply of ADP via ANT. The rate of this recycling of adenine nucleotides is controlled by creatine via MtCK reaction. It has also been shown that such a recycling of ADP and ATP in MI decreases the rate of reactive oxygen species (ROS) production (Meyer et al. 2006) and PTP opening (Dolder et al. 2003).

Systems biology of the creatine kinase pathway in the heart: feedback mechanism of regulation of energy fluxes

Localization of cytosolic MM creatine kinase in myofibrils and at the membranes of sarcoplasmic reticulum and sarcolemma has been described in details in previous studies (Wallimann et al. 1992, 2007; Saks et al. 2007a, b). These creatine kinases catalyze the reaction in the opposite direction, when compared with mitochondria: the use of PCr for rapid regeneration of local ATP (Guzun et al. 2009). Thus, in the creatine kinase pathway creatine kinases operate in mitochondria and at the sites of ATP utilization in the opposite direction in the non-equilibrium state (Guzun et al. 2009). In cardiac cells, the mitochondria and the whole phosphocreatine pathway are organized into regularly arranged intracellular energetic units (Saks et al. 2001) (Fig. 1). These units including phosphocreatine pathway are the results of specific interactions in the cells and best described by Systems Biology approaches in Molecular System Bioenergetics (Saks 2007). These specific interactions result in new, system level properties which do not exist if the system components are isolated (Saks 2007). Examples of these important new properties are compartmentalization of metabolites and enzymes, including creatine kinases in the cells, metabolic channeling and functional coupling—all characteristic for the PCr/CK pathway of energy transfer. One of the results of application of this approach is description of the cellular mechanisms of metabolic aspects of Frank–Starling law of the heart (Starling and Visscher 1926; Saks et al. 2006). Systems Biology approach relies on the use of mathematical models for description of complex phenomena (Saks 2007). Compartimentalized energy transfer by the creatine kinase system has been described mathematically by Vendelin–Aliev–Saks (VAS) model using enzyme localization data and their kinetics, metabolic channeling, functional coupling and limitation of MOM permeability (Aliev and Saks 1997; Vendelin et al. 2000, 2004; Dos Santos et al. 2000). The model describes well the Frank–Starling phenomenon under conditions of metabolic stability (Saks et al. 2006). According to the VAS model and the results of in vivo studies of heart energy metabolism using nuclear magnetic resonance spectroscopy by ^{31}P (Honda et al. 2002; Spindler et al. 2001), the ATP hydrolyzed in ATPase reactions during cyclic contractions is associated with cyclic oscillations of ADP, PCr/Cr ratio, Pi and proton concentrations in myofibrils (Fig. 8). The Pi is not consumed in the MMCK reaction, but diffuses freely and enters mitochondrial matrix via its carrier (PIC). The local impulse of ADP concentration is used up mainly in the MMCK reaction, due to its non-equilibrium state, and at the same time forms a gradient of ADP concentration transmitted towards the mitochondrial matrix. The rephosphorylation of ADP in the MMCK reaction using PCr changes the PCr/Cr ratio in the direction of the increase of creatine concentration. These signals are transferred towards MtCK via CK/PCr shuttle. ADP signal reaches mitochondria and increases ATP regeneration. Regenerated ATP, due to the MtCK-ANT functional coupling, supplies the MtCK reaction (which is also in non-equilibrium steady state). Thus, the cytosolic ADP signal is transformed into a PCr amplified energy flux which is maintained by the MtCK reaction due to its non-equilibrium steady-state, local turnover of ATP/ADP between ATPsynthase and MtCK within mitochondrial interactosome. The efficiency of PCr production by MtCK in cardiomyocytes is close to the maximum efficiency of oxidation phosphorylation ($PCr/O_2 = 5.7 \pm 0.7$) (Timohhina et al. 2009; Guzun et al. 2009). By applying the general principle of feedback regulation proposed by Norbert Wiener (1947), one can represent the mechanism of adjustment of intracellular ATP requirement to mitochondrial ATP regeneration through feedback signalling fluxes (cytosolic Cr/PCr, ADP, Pi) and energy fluxes (PCr) transformed in non-equilibrium steady-state compartmentalized CK reactions and ATPases reactions (Saks et al. 2007a, b; Guzun et al. 2009). The mechanism of feedback regulation of mitochondrial ATP regeneration tends to maintain the fundamental property of living system, intracellular metabolic stability (Dos Santos et al. 2000; Balaban et al. 1986; Williamson et al. 1976).

Mitochondrial interactosome in pathology, clinical effects of phosphocreatine (Neoton)

In myocardial infarction and in heart failure, rapid decrease in PCr content occurs due to lack of oxygen supply and pathological changes in the creatine kinase system (Neubauer 2007; Neubauer et al. 1997; Wyss and Kaddurah-Daouk 2000; Wallimann et al. 2007; Saks et al. 2007a, b). Total ATP content usually changes very slowly and its changes, as well as changes in the free energy of ATP hydrolysis calculated from total metabolites' contents, are dissociated from the rapid fall of the cardiac contractile force (Neely et al. 1973; Kammermeier et al. 1990), total depletion of ATP resulting in contracture of heart muscle (Koretsune and Marban 1990). Rapid decline in heart contractile function in hypoxia and ischemia are most likely to be related to changes in compartmentalized energy transfer systems, leading to decreased regeneration of ATP in functionally important cellular compartments, as shown in Fig. 1. First, rapid decline in ATP regeneration in subsarcolemmal area results in changes in ion currents across this membrane and thus in shortening of action potential (Dzeja et al. 2007; Saks et al. 2007a), and secondly, rapid

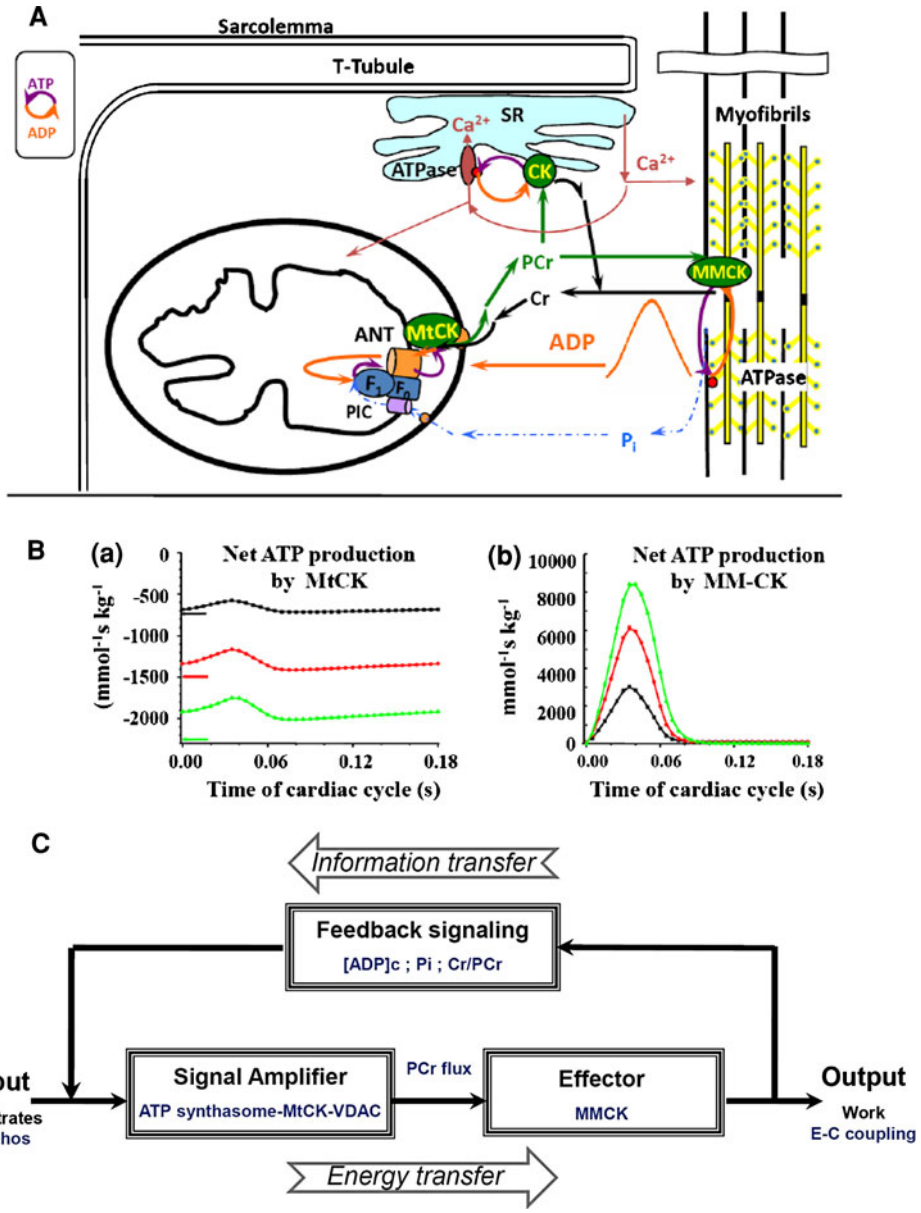

Fig. 8 **a** Intracellular energy unit of cardiomyocytes in which the sites of ATP utilization (ATPases of sarcoplasmic reticulum, of myosin, of Na^+/K^+ pumps) are connected to the site of ATP regeneration (F_0F_1 represents oxidative phosphorylation) by the phosphotransfer shuttle (CK/PCr). **b** The ATP hydrolysis during muscle contraction produces a fluctuation of ADP concentrations (Fig. 8 **b**-*b*) associated with the release of Pi. A part of released ADP is rephosphorylated by MMCK using PCr. Produced creatine serves as a feedback metabolic signal for mitochondrial respiration. Another part of ADP creates a concentration gradient from the core of myofibril toward mitochondrion, and is used to regenerate the mitochondrial ATP while entering the matrix via the ANT. Regenerated ATP supply MtCK reaction increasing local ATP/ADP turnover between ATP synthasome and MtCK with continuous PCr production (Fig. 8 **b**-*a*). **c** Feedback regulation of mitochondrial respiration within intracellular energy units in vivo. In this scheme, the ATP consumption to complete cellular work, marked as output, and ATP regeneration are interconnected via the feedback signalling through cytosolic ADP, Pi and Cr/PCr. PCr produced in MtCK reaction from mitochondrial ATP is exported towards intracellular milieu as energy flux and is used for the local ATP regeneration by myofibrillar MMCK [adapted from Guzun et al. (2009)]

decline in ATP regeneration in myofibrillar microcompartments due to lack of phosphocreatine slows down the contraction cycle (Saks et al. 2007a, b). Similar but slower changes are observed in chronic cardiac and skeletal muscle diseases (Nascimben et al. 1996; Ingwall 2004, 2006, 2009; Shen et al. 2005; Tian and Ingwall 1996; Weiss et al. 2005; Mettauer et al. 2006; Ventura-Clapier et al. 2002; De Sousa et al. 2000). In concord with this conclusion are the results published by Weiss et al. (2005) showing that cardiac ATP flux through CK is reduced by 50% in cases of human heart failure in the absence of reduction of ATP stores. Local phosphotransfer networks

in the subsarcolemmal area are an important part of the membrane sensors of the cellular energy state also in brain cells (Wallimann et al. 2007; Andres et al. 2008; Burklen et al. 2006; Adhihetty and Beal 2008), this explaining the dependence of functional state of these cells on phosphocreatine supply, and thus the central importance of the PCr/Cr system. In brain cells, ubiquitous mitochondrial creatine kinase is co-expressed with cytosolic BB isoenzyme localized both in cytoplasm and at the cell membrane. Alterations of these systems are observed in many neurodegenerative diseases (Andres et al. 2008; Burklen et al. 2006).

Both in experiments on frog hearts (Saks et al. 1976, 1978) and in patients with heart diseases (Nascimben et al. 1996) the significant decrease in intracellular creatine level resulting in decreased content of PCr has been shown to result in the hypodynamic state characterized by decreased contractility. In experiments, restorations of the intracellular Cr level by its inclusion into perfusate allowed completely normalize the PCr content and the contractile force (Saks et al. 1976).

All these results are in concord with the very early observation by Lundsgaard that intracellular PCr is one of the important factors of regulation of the force of muscle contraction (Lundsgaards 1930).

Intensive and numerous studies have been carried out on transgenic mice with knockout of different CK isoenzymes, or enzymes responsible for creatine metabolism and transport (Ingwall 2009; Ventura-Clapier et al. 2002; ten Hove et al. 2005). Despite multiple adaptive mechanisms—activation of alternative phosphotransfer pathways, such as adenylate kinase shuttle (Ventura-Clapier et al. 2002; Dzeja et al. 1996), structural changes in the cells and increase in oxidative capacity of skeletal muscle (Ingwall 2004; Ventura-Clapier et al. 2002), and many others (Ingwall and Weiss 2004), significant functional and metabolic changes especially related to calcium metabolism and contractile performance have been observed in these experiments (Ingwall and Weiss 2004; Momken et al. 2005; Spindler et al. 2004; Nahrendorf et al. 2006; ten Hove et al. 2005). Thus, Momken et al. (2005) have reported that double knockout of MtCK and MM CK very significantly impairs voluntary running capacity of mice. Knockout of enzymes of creatine biosynthesis in mice resulted in significantly reduced responses to inotropic stimulation (ten Hove et al. 2005). Similarly, hearts of rats treated with guanidinopropionic acid performed much less pressure–volume work (Kapelko et al. 1989). Most interestingly, recent works from Neubauer's laboratory have shown that overexpression of creatine transporter and supernormal myocardial creatine contents lead to heart failure (Phillips 2009; Wallis et al. 2005). In these hearts, creatine content is increased by more than a factor of 2 (Phillips 2009). Most interestingly, these experiments put into evidence the importance of the PCr shuttle: the heart failure may be due to the formation of dead-end complex CK.MgADP.Cr formation (Morrison and James 1965) and inhibition of PCr utilization for local ATP regeneration.

In summary, data obtained in experiments with CK knockout mice are in concord with our conclusion made in this work and before (Saks et al. 2006; Saks 2007; Wallimann et al. 1992; Saks et al. 2007a) that muscle (and other) cells are viable without MtCK and other CK isoenzymes, as HL-1 cells, but PCr-CK and other phosphotransfer pathways are necessary for effective energy transfer and metabolic regulation at higher energy demand, and thus for survival under stress conditions. An important observation is that exercise training results in cytoskeleton remodelling, including changes in Mitochondrial Interactosome and increased efficiency of energy transfer via PCr- CK pathway (Zoll et al. 2002; Walsh et al. 2001; Guerrero et al. 2005).

An important clinical study was performed by Neubauer's group in United Kingdom (Neubauer 2007; Neubauer et al. 1997). Using ^{31}P-NMR spectroscopy in combination with imaging for investigation of cardiac muscle energy metabolism in patients, the authors showed that in patients with cardiac disease—dilated cardiomyopathy (DCM) the decreased PCr/ATP ratio (lower than 1.6) is very clear and strong diagnostic index of increased mortality. In the heart of patients with DCM the ATP content remained the same as in healthy control patients, but PCr decreased by 70% as compared to control. This shows the vital importance of the phosphocreatine—creatine kinase energy transfer network for the cardiac muscle normal function and life (Neubauer 2007; Neubauer et al. 1997).

Thus, the PCr/ATP ratio is an important diagnostic parameter of heart disease, as is the total creatine content. Low PCr concentrations and low PCr/ATP ratios mean decreased regeneration of ATP by the PCr/CK system in microdomains (compartments) which are critically important for the function of the heart, skeletal muscle and brain. These microdomains are localised in myofibrils, near the sarcolemma and the membrane of sarcoplasmic reticulum in muscle cells and near cellular membrane in brain cells (see Fig. 1). There is a general consensus now among the researchers in muscle and brain energy metabolism that the further challenge and urgent need is to develop better bioprobes to image metabolic microdomains of ATP and functional proteomics to identify physical interactions between key proteins responsible for their formation (Neubauer 2007; Saks et al. 2007a, b; Weiss et al. 2005).

In addition to its important role in supporting regeneration of local ATP pools as a substrate for MM–CK reactions in myofibrils and cellular membranes, the PCr molecule appears to have another very useful property—membrane stabilizing action (Fig. 9c). This was revealed in

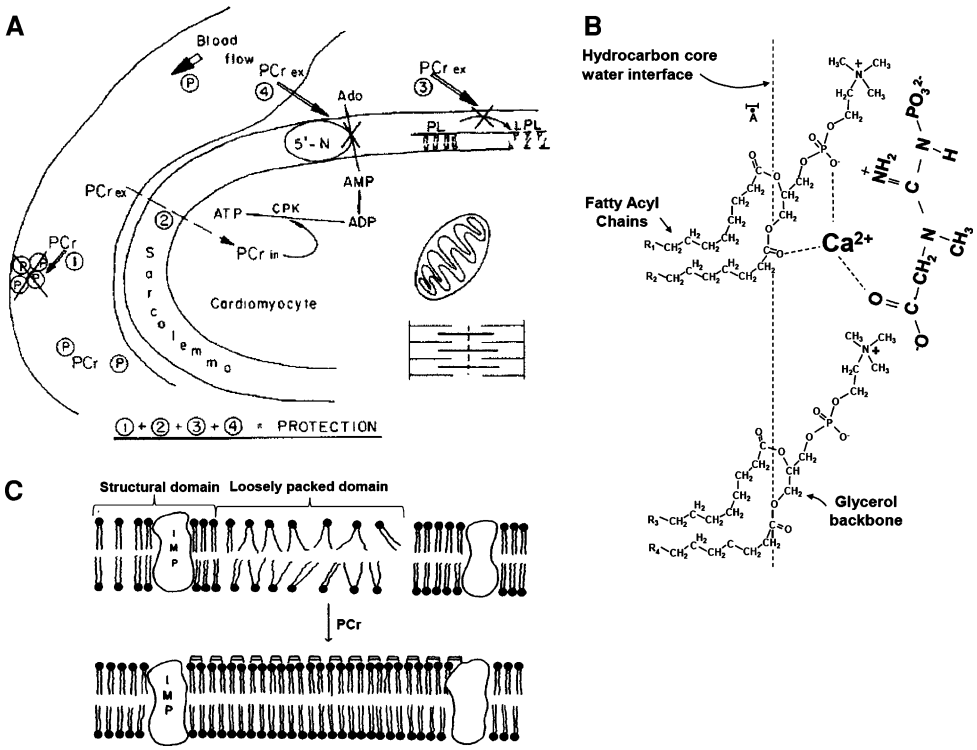

Fig. 9 **a** Scheme of the mechanisms of PCr protective action in cardiac ischemia. These mechanisms include *1* inhibition of platelet aggregation, extracellular mechanism, *2* possible penetration into the cells and participation in intracellular energy transfer (intracellular mechanism), *3* inhibition of accumulation of lysophosphoglycerides, *4* inhibition of 5′-nucleotidase of sarcolemma (adapted from). **b** Zwitterionic interaction of phosphocreatine with bipolar heads of phospholipid molecules in the membrane surface interphase. **c** Stabilization of the phospholipid bilayer by PCr molecules [adapted from Saks and Strumia (1993)]

long series of clinical use of extracellular phosphocreatine injection with clear protective effect on ischemic myocardium, and in detailed experimental studies (Semenovsky et al. 1987; Ruda et al. 1988; Robinson et al. 1984; Woo et al. 2005). In all these studies, extracellular phosphocreatine was used and shown to decrease the ischemic damage of heart muscle by multiple mechanisms (Fig. 9). Among others, there is clear membrane stabilizing effect of PCr (Saks and Strumia 1993) which may be explained by interaction of its zwitterionic molecule carrying positive and negative charges with opposite charges of phospholipids polar heads in the membrane surface interphase (Fig. 9b) that resulting in the transition of the mobile domain (fluid phase) of membranes into a structured domain (gel phase) as shown in Fig. 9c, leading to the decrease of the rate of phospholipids degradation into lysophospholipids and lipid peroxidation (Saks and Strumia 1993). Rapid fall of the intracellular PCr pool in hypoxia and ischemia may thus be a significant factor of destabilization of cellular membranes.

In conclusion, the PCr–CK pathway is as an efficient highway connecting ATP production and consumption sites. Without this highway, cells have to find other ways of ATP and energy transfer, but the efficiency of communication and regulation is lost and energy may be wasted (as in HL-1 cells). Under these conditions, muscle and brain cells degrade into a pathological state.

Acknowledgments This work was supported INSERM, and by a grant from Agence Nationale de la Recherche, France, project ANR-07-BLAN-0086-01 and by grants N 7117 and 7823 from Estonian Science Foundation. The authors thank Irina Guzun for improving the English of this manuscript.

References

Adhihetty PJ, Beal MF (2008) Creatine and its potential therapeutic value for targeting cellular energy impairment in neurodegenerative diseases. Neuromol Med 10:275–290

Aliev MK, Saks VA (1997) Compartmentalized energy transfer in cardiomyocytes: use of mathematical modeling for analysis of in vivo regulation of respiration. Biophys J 73(1):428–445

Andres RH, Ducray AD, Schlattner U, Wallimann T, Widmer HR (2008) Functions and effects of creatine in the central nervous system. Brain Res Bull 76:329–343

Anmann T, Guzun R, Beraud N, Pelloux S, Kuznetsov AV, Kogerman L, Kaambre T, Sikk P, Paju K, Peet N, Seppet E, Ojeda C, Tourneur Y, Saks V (2006) Different kinetics of the regulation of respiration in permeabilized cardiomyocytes and in HL-1 cardiac cells. Importance of cell structure/organization for respiration regulation. Biochim Biophys Acta 1757:1597–1606

Balaban RS, Kantor HL, Katz LA, Briggs RW (1986) Relation between work and phosphate metabolite in the in vivo paced mammalian heart. Science 232:1121–1123

Belitzer V, Tsybakova E (1939) About mechanism of phosphorylation, respiratory coupling. Biochimia 4:516–533

Beraud N, Pelloux S, Usson Y, Kuznetsov AV, Ronot X, Tourneur Y, Saks V (2009) Mitochondrial dynamics in heart cells: very low amplitude high frequency fluctuations in adult cardiomyocytes and flow motion in non beating Hl-1 cells. J Bioenerg Biomembr 41:195–214

Bessman SP, Carpenter CL (1985) The creatine-creatine phosphate energy shuttle. Annu Rev Biochem 54:831–862

Bessman SP, Fonyo A (1966) The possible role of the mitochondrial bound creatine kinase in regulation of mitochondrial respiration. Biochem Biophys Res Commun 22(5):597–602

Bessman SP, Geiger PJ (1981) Transport of energy in muscle: the phosphorylcreatine shuttle. Science 211:448–452

Burklen TS, Schlattner U, Homayouni R, Gough K, Rak M, Szeghalmi A, Wallimann T (2006) The creatine kinase/creatine connection to Alzheimer's disease: CK inactivation, APP–CK complexes and focal creatine deposits. J Biomed Biotechnol 2006(3)35936

Chen C, Ko Y, Delannoy M, Ludtke SJ, Chiu W, Pedersen PL (2004) Mitochondrial ATP synthasome: three-dimensional structure by electron microscopy of the ATP synthase in complex formation with carriers for Pi and ADP/ATP. J Biol Chem 279:31761–31768

De Sousa E, Veksler V, Bigard X, Mateo P, Ventura-Clapier R (2000) Heart failure affects mitochondrial but not myofibrillar intrinsic properties of skeletal muscle. Circulation 102:1847–1853

Dolder M, Walzel B, Speer O, Schlattner U, Wallimann T (2003) Inhibition of the mitochondrial permeability transition by creatine kinase substrates. Requirement for microcompartmentation. J Biol Chem 278:17760–17766

Dos Santos P, Aliev MK, Diolez P, Duclos F, Besse P, Bonoron-Adele S, Sikk P, Canioni P, Saks VA (2000) Metabolic control of contractile performance in isolated perfused rat heart. Analysis of experimental data by reaction: diffusion mathematical model. J Mol Cell Cardiol 32:1703–1734

Dzeja PP, Zeleznikar RJ, Goldberg ND (1996) Suppression of creatine kinase catalyzed phosphotransfer results in increased phosphoryl transfer by adenylate kinase in intact skeletal muscle. J Biol Chem 271:12847–12851

Dzeja P, Chung S, Terzic A (2007) Integration of adenylate kinase and glycolytic and glycogenolytic circuits in cellular energetic. In: Saks V (ed) Molecular system bioenergetics. Energy for life. Wiley-VCH, Germany, pp 195–264

Eggleton P, Eggleton GP (1927) The inorganic phosphate and a labile form of organic phosphate in the gastrocnemius of the frog. Biochem J 21(1):190–195

Eimre M, Paju K, Pelloux S, Beraud N, Roosimaa M, Kadaja L, Gruno M, Peet N, Orlova E, Remmelkoor R, Piirsoo A, Saks V, Seppet E (2008) Distinct organization of energy metabolism in HL-1 cardiac cell line and cardiomyocytes. Biochim Biophys Acta 1777:514–524

Engelborghs Y, Marsh A, Gutfreund H (1975) A quenched-flow study of the reaction catalysed by creatine kinase. Biochem J 151(1):47–50

Fiske CH, Subbarao Y (1927) The nature of the 'inorganic phosphate' in voluntary muscle. Science 65(1686):401–403

Gellerich F, Saks VA (1982) Control of heart mitochondrial oxygen consumption by creatine kinase: the importance of enzyme localization. Biochem Biophys Res Commun 105(4):1473–1481

Gellerich FN, Kunz WS, Bohnensack R (1990) Estimation of flux control coefficients from inhibitor titrations by non-linear regression. FEBS Lett 274:167–170

Guerrero K, Wuyam B, Mezin P, Vivodtzev I, Vendelin M, Borel JC, Hacini R, Chavanon O, Imbeaud S, Saks V, Pison C (2005) Functional coupling of adenine nucleotide translocase and mitochondrial creatine kinase is enhanced after exercise training in lung transplant skeletal muscle. Am J Physiol Regul Integr Comp Physiol 289:R1144–R1154

Guzun R, Saks V (2010) Review: application of the principles of systems biology and wiener's cybernetics for analysis of regulation of energy fluxes in muscle cells in vivo. Int J Mol Sci 11(3):982–1019

Guzun R, Timohhina N, Tepp K, Monge C, Kaambre T, Sikk P, Kuznetsov AV, Pison C, Saks V (2009) Regulation of respiration controlled by mitochondrial creatine kinase in permeabilized cardiac cells in situ. Importance of system level properties. Biochim Biophys Acta 1787:1089–1105

Hill AV, Long CNH, Lupton H (1924) Muscular exercise, lactic acid, and the supply and utilization of oxygen. Proc R Soc Lond B Biol Sci 16:84–137

Honda H, Tanaka K, Akita N, Haneda T (2002) Cyclical changes in high-energy phosphates during the cardiac cycle by pacing-gated 31P nuclear magnetic resonance. Circ J 66:80–86

Ingwall JS (2004) Transgenesis and cardiac energetics: new insights into cardiac metabolism. J Mol Cell Cardiol 37:613–623

Ingwall JS (2006) On the hypothesis that the failing heart is energy starved: lessons learned from the metabolism of ATP and creatine. Curr Hypertens Rep 8:457–464

Ingwall JS (2009) Energy metabolism in heart failure and remodelling. Cardiovasc Res 81:412–419

Ingwall JS, Weiss RG (2004) Is the failing heart energy starved? On using chemical energy to support cardiac function. Circ Res 95:135–145

Ivanov II, Korovkin BF, Pinaev GP (1997) Biochemistry of muscles. Meditsina, Moscow

Jacobus WE, Lehninger AL (1973) Creatine kinase of rat heart mitochondria. Coupling of creatine phosphorylation to electron transport. J Biol Chem 248(13):4803–4810

Jacobus WE, Saks VA (1982) Creatine kinase of heart mitochondria: changes in its kinetic properties induced by coupling to oxidative phosphorylation. Arch Biochem Biophys 219(1):167–178

Kammermeier H, Roeb E, Jungling E, Meyer B (1990) Regulation of systolic force and control of free energy of ATP-hydrolysis in hypoxic hearts. J Mol Cell Cardiol 22:707–713

Kapelko VI, Saks VA, Novikova NA, Golikov MA, Kupriyanov VV, Popovich MI (1989) Adaptation of cardiac contractile function to conditions of chronic energy deficiency. J Mol Cell Cardiol 21:79–83

Kholodenko BN, Cascante M, Westerhoff HV (1995) Control theory of metabolic channelling. Mol Cell Biochem 143(2):151–168

Klingenberg M (1970) Mitochondria metabolite transport. FEBS Lett 6(3):145–154

Koretsune Y, Marban E (1990) Mechanism of ischemic contracture in ferret hearts: relative roles of $[Ca^{2+}]i$ elevation and ATP depletion. Am J Physiol 258:H9–H16

Kresge N, Simoni RD, Hill RL (2005) Otto Fritz Meyerhof and the elucidation of the glycolytic pathway. J Biol Chem 280(4):e3

Kuznetsov AV, Saks VA (1986) Affinity modification of creatine kinase and ATP-ADP translocase in heart mitochondria: determination of their molar stoichiometry. Biochem Biophys Res Commun 134(1):359–366

Lenaz G, Genova ML (2007) Kinetics of integrated electron transfer in the mitochondrial respiratory chain: random collisions vs. solid state electron channelling. Am J Physiol Cell Physiol 292:C1221–C1239

Lundsgaard E (1930) Untersuhungen uber Muskelkontraktionen ohne Milchsaurebildung. Biochem Z 217:162–177

Mettauer B, Zoll J, Garnier A, Ventura-Clapier R (2006) Heart failure: a model of cardiac and skeletal muscle energetic failure. Pflugers Arch 452:653–666

Meyer LE, Machado LB, Santiago AP, da-Silva WS, De Felice FG, Holub O, Oliveira MF, Galina A (2006) Mitochondrial creatine kinase activity prevents reactive oxygen species generation: antioxidant role of mitochondrial kinase-dependent ADP re-cycling activity. J Biol Chem 281(49):37361–37371

Momken I, Lechene P, Koulmann N, Fortin D, Mateo P, Doan BT, Hoerter J, Bigard X, Veksler V, Ventura-Clapier R (2005)

Impaired voluntary running capacity of creatine kinase-deficient mice. J Physiol 565:951–964
Mommaerts WF (1969) Energetics of muscular contraction. Physiol Rev 49:427–508
Monge C, Beraud N, Tepp K, Pelloux S, Chahboun S, Kaambre T, Kadaja L, Roosimaa M, Piirsoo A, Tourneur Y, Kuznetsov AV, Saks V, Seppet E (2009) Comparative analysis of the bioenergetics of adult cardiomyocytes and nonbeating HL-1 cells: respiratory chain activities, glycolytic enzyme profiles, and metabolic fluxes. Can J Physiol Pharmacol 87:318–326
Morrison JF, James E (1965) The mechanism of the reaction catalysed by adenosine triphosphate-creatine phosphotransferase. Biochem J 97:37–52
Nahrendorf M, Streif JU, Hiller KH, Hu K, Nordbeck P, Ritter O, Sosnovik D, Bauer L, Neubauer S, Jakob PM, Ertl G, Spindler M, Bauer WR (2006) Multimodal functional cardiac MRI in creatine kinase-deficient mice reveals subtle abnormalities in myocardial perfusion and mechanics. Am J Physiol Heart Circ Physiol 290:H2516–H2521
Nascimben L, Ingwall JS, Pauletto P, Friedrich J, Gwathmey JK, Saks V, Pessina AC, Allen PD (1996) Creatine kinase system in failing and nonfailing human myocardium. Circulation 94:1894–1901
Neely JR, Rovetto MJ, Whitmer JT, Morgan HE (1973) Effects of ischemia on function and metabolism of the isolated working rat heart. Am J Physiol 225:651–658
Neubauer S (2007) The failing heart—an engine out of fuel. N Engl J Med 356:1140–1151
Neubauer S, Horn M, Cramer M, Harre K, Newell JB, Peters W, Pabst T, Ertl G, Hahn D, Ingwall JS, Kochsiek K (1997) Myocardial phosphocreatine-to-ATP ratio is a predictor of mortality in patients with dilated cardiomyopathy. Circulation 96:2190–2196
Pedersen PL (2007) Warburg, me and hexokinase 2: multiple discoveries of key molecular events underlying one of cancers' most common phenotypes, the "Warburg effect", i.e., elevated glycolysis in the presence of oxygen. J Bioenerg Biomembr 39:211–222
Pedersen PL, Ko YH, Hong S (2000) ATP synthases in the year 2000: evolving views about the structures of these remarkable enzyme complexes. J Bioenerg Biomembr 32:325–332
Pelloux S, Robillard J, Ferrera R, Bilbaut A, Ojeda C, Saks V, Ovize M, Tourneur Y (2006) Non-beating HL-1 cells for confocal microscopy: application to mitochondrial functions during cardiac preconditioning. Prog Biophys Mol Biol 90:270–298
Phillips D, Ten Hove M, Schneider JE, Wu CO, Sebag-Montefiore L, Aponte AM, Lygate CA, Wallis J, Clarke K, Watkins H, Balaban RS, Neubauer S (2009) Mice over-expressing the myocardial creatine transporter develop progressive heart failure and show decreased glycolytic capacity. J Mol Cell Cardiol
Robinson LA, Braimbridge MV, Hearse DJ (1984) Creatine phosphate: an additive myocardial protective and antiarrhythmic agent in cardioplegia. J Thorac Cardiovasc Surg 87:190–200
Rostovtseva TK, Bezrukov SM (2008) VDAC regulation: role of cytosolic proteins and mitochondrial lipids. J Bioenerg Biomembr 40:163–170
Rostovtseva TK, Sheldon KL, Hassanzadeh E, Monge C, Saks V, Bezrukov SM, Sackett DL (2008) Tubulin binding blocks mitochondrial voltage-dependent anion channel and regulates respiration. Proc Natl Acad Sci USA 105:18746–18751
Ruda M, Samarenko MB, Afonskaya NI, Saks VA (1988) Reduction of ventricular arrhythmias by phosphocreatine (Neoton) in patients with acute myocardial infarction. Am Heart J 116:393–397
Saks V (ed) (2007) Molecular system bioenergetics. Energy for life. Wiley-VCH, Germany
Saks V, Strumia E (1993) Phosphocreatine: molecular and cellular aspects of the mechanism of cardioprotective action. Curr Therapeut Res 53:565–598
Saks VA, Rosenshtraukh LV, Undrovinas AI, Smirnov VN, Chazov EI (1976) Studies of energy transport in heart cells. Intracellular creatine content as a regulatory factor of frog heart energetic and force of contraction. Biochem Med 16:21–36
Saks VA, Rosenshtraukh LV, Smirnov VN, Chazov EI (1978) Role of creatine phosphokinase in cellular function and metabolism. Can J Physiol Pharmacol 56:691–706
Saks V, Belikova Y, Vasilyeva E, Kuznetsov A, Fontaine E, Keriel C, Leverve X (1995) Correlation between degree of rupture of outer mitochondrial membrane and changes of kinetics of regulation of respiration by ADP in permeabilized heart and liver cells. Biochem Biophys Res Commun 208(3):919–926
Saks VA, Veksler VI, Kuznetsov AV, Kay L, Sikk P, Tiivel T, Tranqui L, Olivares J, Winkler K, Wiedemann F, Kunz WS (1998) Permeabilized cell and skinned fiber techniques in studies of mitochondrial function in vivo. Mol Cell Biochem 184(1–2):81–100
Saks VA, Kaambre T, Sikk P, Eimre M, Orlova E, Paju K, Piirsoo A, Appaix F, Kay L, Regitz-Zagrosek V, Fleck E, Seppet E (2001) Intracellular energetic units in red muscle cells. Biochem J 356:643–657
Saks V, Dzeja P, Schlattner U, Vendelin M, Terzic A, Wallimann T (2006) Cardiac system bioenergetics: metabolic basis of the Frank–Starling law. J Physiol 571:253–273
Saks V, Monge C, Anmann T, Dzeja P (2007a) Integrated and organized cellular energetic systems: theories of cell energetics, compartmentation and metabolic channelling. In: Saks V (ed) Molecular system bioenergetics. Energy for life. Wiley-VCH, Germany, pp 59–110
Saks VA, Dzeja P, Guzun R, Aliev MK, Vendelin M, Terzic A, Wallimann T (2007b) System analysis of cardiac energetics–excitation–contraction coupling: integration of mitochondrial respiration, phosphotransfer pathways, metabolic pacing and substrate supply in the heart. In: Saks V (ed) Molecular system bioenergetics. Energy for life. Wiley-VCH, Germany, pp 367–405
Saks V, Beraud N, Wallimann T (2008) Metabolic compartmentation—a system level property of muscle cells. Int J Mol Sci 9:751–767
Schlattner U, Gehring F, Vernoux N, Tokarska-Schlattner M, Neumann D, Marcillat O, Vial C, Wallimann T (2004) C-terminal lysines determine phospholipid interaction of sarcomeric mitochondrial creatine kinase. J Biol Chem 279:24334–24342
Semenovsky ML, Shumakov VI, Sharov VG, Mogilevsky GM, Asmolovsky AV, Makhotina LA, Saks VA (1987) Protection of ischemic myocardium by exogenous phosphocreatine. J Thoracic Cardiovasc Surg 94:762–769
Shen W, Spindler M, Higgins MA, Jin N, Gill RM, Bloem LJ, Ryan TP, Ingwall JS (2005) The fall in creatine levels and creatine kinase isozyme changes in the failing heart are reversible: complex post-transcriptional regulation of the components of the CK system. J Mol Cell Cardiol 39:537–544
Spindler M, Illing B, Horn M, de Groot M, Ertl G, Neubauer S (2001) Temporal fluctuations of myocardia high-energy phosphate metabolite with the cardiac cycle. Basic Res Cardiol 96:553–556
Spindler M, Meyer K, Stromer H, Leupold A, Boehm E, Wagner H, Neubauer S (2004) Creatine kinase-deficient hearts exhibit increased susceptibility to ischemia–reperfusion injury and impaired calcium homeostasis. Am J Physiol Heart Circ Physiol 287:H1039–H1045
Starling E, Visscher HMB (1926) The regulation of the energy output of the heart. J Physiol 62(3):243–261

ten Hove M, Lygate CA, Fischer A, Schneider JE, Sang AE, Hulbert K, Sebag-Montefiore L, Watkins H, Clarke K, Isbrandt D, Wallis J, Neubauer S (2005) Reduced inotropic reserve and increased susceptibility to cardiac ischemia/reperfusion injury in phosphocreatine-deficient guanidinoacetate-*N*-methyltransferase knockout mice. Circulation 111:2477–2485

Tian R, Ingwall JS (1996) Energetic basis for reduced contractile reserve in isolated rat hearts. Am J Physiol 270:H1207–H1216

Timohhina N, Guzun R, Tepp K, Monge C, Varikmaa M, Vija H, Sikk P, Kaambre T, Sackett D, Saks V (2009) Direct measurement of energy fluxes from mitochondria into cytoplasm in permeabilized cardiac cells in situ: some evidence for mitochondrial interactosome. J Bioenerg Biomembr 41(3):259–275

Vendelin M, Kongas O, Saks V (2000) Regulation of mitochondrial respiration in heart cells analyzed by reaction-diffusion model of energy transfer. Am J Physiol Cell Physiol 278:C747–C764

Vendelin M, Lemba M, Saks VA (2004) Analysis of functional coupling: mitochondrial creatine kinase and adenine nucleotide translocase. Biophys J 87:696–713

Ventura-Clapier R, De Sousa E, Veksler V (2002) Metabolic myopathy in heart failure. News Physiol Sci 17:191–196

Vonck J, Schafer E (2009) Supramolecular organization of protein complexes in the mitochondrial inner membrane. Biochim Biophys Acta 1793:117–124

Wallimann T, Wyss M, Brdiczka D, Nicolay K, Eppenberger HM (1992) Intracellular compartmentation, structure and function of creatine kinase isoenzymes in tissues with high and fluctuating energy demands: the 'phosphocreatine circuit' for cellular energy homeostasis. Biochem J 281(Pt 1):21–40

Wallimann T, Tokarska-Schlattner M, Neumann D, Epand RF, Andres RH, Widmer HR, Hornemann T, Saks V, Agarkova I, Schlattner U (2007) The phosphocreatine circuit: molecular and cellular physiology of creatine kinases, sensitivity to free radicals, and enhancement by creatine supplementation. In: Saks V (ed) Molecular system bioenergetics. Energy for life. Wiley-VCH, Germany, pp 195–264

Wallis J, Lygate CA, Fischer A, ten Hove M, Schneider JE, Sebag-Montefiore L, Dawson D, Hulbert K, Zhang W, Zhang MH, Watkins H, Clarke K, Neubauer S (2005) Supranormal myocardial creatine and phosphocreatine concentrations lead to cardiac hypertrophy and heart failure: insights from creatine ransporteroverexpressing transgenic mice. Circulation 112:3131–3139

Walsh B, Tonkonogi M, Sahlin K (2001) Effect of endurance training on oxidative and antioxidative function in human permeabilized muscle fibres. Pflugers Arch 442:420–425

Warburg O (1956) On respiratory impairment in cancer cells. Science (New York) 124:269–270

Weiss RG, Gerstenblith G, Bottomley PA (2005) ATP flux through creatine kinase in the normal, stressed, and failing human heart. Proc Natl Acad Sci USA 102:808–813

Williamson JR, Ford C, Illingworth J, Safer B (1976) Coordination of citric acid cycle activity with electron transport flux. Circ Res 38:S139–S151

Woo YJ, Grand TJ, Zentko S, Cohen JE, Hsu V, Atluri P, Berry MF, Taylor MD, Moise MA, Fisher O, Kolakowski S (2005) Creatine phosphate administration preserves myocardial function in a model of off-pump coronary revascularization. J Cardiovasc Surg (Torino) 46:297–305

Wyss M, Kaddurah-Daouk R (2000) Creatine and creatinine metabolism. Physiol Rev 80:1107–1213

Ventura-Clapier R, Garnier A, Veksler V Energy metabolism in heart failure. J Physiol 555:1–13

Zoll J, Sanchez H, N'Guessan B, Ribera F, Lampert E, Bigard X, Serrurier B, Fortin D, Geny B, Veksler V, Ventura-Clapier R, Mettauer B (2002) Physical activity changes the regulation of mitochondrial respiration in human skeletal muscle. J Physiol 543:191–200

Journal of Molecular and Cellular Cardiology 52 (2012) 419–436

Contents lists available at ScienceDirect

Journal of Molecular and Cellular Cardiology

journal homepage: www.elsevier.com/locate/yjmcc

Review article

Intracellular Energetic Units regulate metabolism in cardiac cells

Valdur Saks [a,b,*], Andrey V. Kuznetsov [c], Marcela Gonzalez-Granillo [b], Kersti Tepp [a], Natalja Timohhina [a], Minna Karu-Varikmaa [a], Tuuli Kaambre [a], Pierre Dos Santos [d], François Boucher [e], Rita Guzun [b]

[a] Laboratory of Bioenergetics, National Institute of Chemical Physics and Biophysics, Tallinn, Estonia
[b] INSERM U1055, Laboratory of Fundamental and Applied Bioenergetics, Joseph Fourier University, Grenoble, France
[c] Cardiac Surgery Research Laboratory, Department of Heart Surgery, Innsbruck Medical University, Innsbruck, Austria
[d] INSERM U1034, Bordeaux Segalen University, Bordeaux, France
[e] Experimental, Theoretical and Applied Cardio-Respiratory Physiology, Laboratory TIMC-IMAG, Joseph Fourier University, Grenoble, France

ARTICLE INFO

Article history:
Received 24 March 2011
Received in revised form 20 June 2011
Accepted 18 July 2011
Available online 26 July 2011

Keywords:
Cardiomyocytes
Mitochondria
Respiration
Regulation
Tubulin
Systems Biology

ABSTRACT

This review describes developments in historical perspective as well as recent results of investigations of cellular mechanisms of regulation of energy fluxes and mitochondrial respiration by cardiac work — the metabolic aspect of the Frank–Starling law of the heart. A Systems Biology solution to this problem needs the integration of physiological and biochemical mechanisms that take into account intracellular interactions of mitochondria with other cellular systems, in particular with cytoskeleton components. Recent data show that different tubulin isotypes are involved in the regular arrangement exhibited by mitochondria and ATP-consuming systems into Intracellular Energetic Units (ICEUs). Beta II tubulin association with the mitochondrial outer membrane, when co-expressed with mitochondrial creatine kinase (MtCK) specifically limits the permeability of voltage-dependent anion channel for adenine nucleotides. In the MtCK reaction this interaction changes the regulatory kinetics of respiration through a decrease in the affinity for adenine nucleotides and an increase in the affinity for creatine. Metabolic Control Analysis of the coupled MtCK–ATP Synthasome in permeabilized cardiomyocytes showed a significant increase in flux control by steps involved in ADP recycling. Mathematical modeling of compartmentalized energy transfer represented by ICEUs shows that cyclic changes in local ADP, Pi, phosphocreatine and creatine concentrations during contraction cycle represent effective metabolic feedback signals when amplified in the coupled non-equilibrium MtCK–ATP Synthasome reactions in mitochondria. This mechanism explains the regulation of respiration on beat to beat basis during workload changes under conditions of metabolic stability. This article is part of a Special Issue entitled "Local Signaling in Myocytes."

Contents

* Corresponding author at: Laboratory of Bioenergetics, Joseph Fourier University, 2280, Rue de la Piscine, BP53X-38041, Grenoble Cedex 9, France. Tel.: +33 4 76 63 56 27; fax: +33 4 76 51 42 18.
E-mail address: Valdur.Saks@ujf-grenoble.fr (V. Saks).

0022-2828/$ – see front matter © 2011 Elsevier Ltd. All rights reserved.
doi:10.1016/j.yjmcc.2011.07.015

"The essential thing in integrated metabolism is that the organism succeeds in freeing itself from all entropy it cannot help producing while alive". E. Schrödinger "What is life?" Cambridge, 1944

1. Introduction

In this work we describe application of Systems Biology and Molecular System Bioenergetics for solution of fundamental problems of cardiac energetics and metabolism. A Systems Biology solution needs the integration of physiological and biochemical mechanisms that take into account intracellular interactions of mitochondria with other cellular systems [1–10], in particular with cytoskeleton components [5]. This approach needs both experimental studies and computer analyses [6–10], and it takes into account the wealth of knowledge acquired during earlier periods of studies of these important problems [3,8,10], thus avoiding the limitations of narrowly focused reductionist studies [10]. The history of research is an important part of Systems Biology [8,10], and accordingly, we begin this review with short description of the history of studies of cardiac energy metabolism.

1.1. Historical background: oxygen consumption and substrate selection by the heart

Research in the area of energy metabolism of mammalian cells goes back to 1783 when Lavoisier and Laplace discovered biological oxidation. They showed that oxygen is consumed during respiration and CO_2 produced in animals, and concluded that "respiration is a process analogous to burning of coal" that gives energy to live [11]. About 150 years later, Ernest Starling applied this knowledge in his classical studies of cardiac function by using isolated heart and lung preparations, accepting that "rate of oxygen consumption is taken as a measure of the total energy set free in the heart during its activity" [12]. In these studies Starling discovered the capacity of the intact ventricle to vary its contraction force on a beat-to-beat basis as a function of its preload, generally referred to as the Frank–Starling law of the heart [13]. This law states that cardiac function, quantitatively characterized as work performance, is a function of ventricular filling, which in turn depends on pre- or afterload [13–15]. We know now that an increase in the length of sarcomeres of striated cardiac muscle results in changes in the overlapping between thin and thick filaments, alteration in myofilament lattice spacing, increased thin filament cooperativity and, consequently, in the number of force-generating cross-bridges [16]. Length-dependent activation of sarcomeres includes also changes of calcium sensitivity by cardiac myofilaments, which is of major importance particularly for low sarcomere length values [16]. A diminished functional response of the heart to changes in ventricle filling is observed in heart failure [14,15]. Furthermore, Starling et al. discovered the linear dependence of the rate of oxygen consumption upon cardiac work — this is the metabolic aspect of Frank–Starling law of the heart [12].Coupling of ATP synthesis to oxygen consumption was shown by Engelhard and Kalckar [17]. In 1939 Belitzer and Tsybakova found that oxygen uptake in the homogenate of the pectoral muscle of a pigeon was activated by creatine without addition of exogenous ADP (trace amounts of endogenous adenine nucleotides present were sufficient to catalyze coupling of the mitochondrial creatine kinase reaction and oxidative phosphorylation), and resulted in phosphocreatine (PCr) production with PCr/O_2 ratio equal to 5.2–7 [18]. These pioneering studies opened the way for a rapid development of bioenergetics and detailed description of the mechanism of ATP synthesis coupled to respiration in mitochondria [11,19,20], which in cardiac cell occupy about 30% of volume [21]. Mitochondrial respiration and ATP synthesis are coupled to phosphorylation of creatine and synthesis of phosphocreatine (PCr) by the mitochondrial creatine kinase (MtCK), a key component of the cellular system of creatine kinases [22–34].

Cardiac work determines not only the rate of oxygen consumption, as discovered by Starling, but also substrate uptake and fuel selection [15,35–37]. Major substrates used by the heart are carbohydrates (glucose, lactate, glycogen) and fatty acids [5,35–37]. Oxidation of carbohydrates accounts for not more than 20% of the oxygen consumed (or ATP produced) by the heart [15,35–37]. During the 1950s, Richard Bing initiated intensive research on metabolism of the human heart, and observed that the preferred substrates are fatty acids [38,39]. This phenomenon and the mechanisms of regulation of substrate uptake by the heart and skeletal muscle were studied and described in detail by Randle, Newsholm and their colleagues in Cambridge, UK [40–43]. They discovered the glucose–fatty acid cycle, now known as Randle cycle, which describes the cellular mechanisms by which fatty acid oxidation inhibits glycolysis [40,41,44,45]. The reason for natural selection of fatty acids by oxidative muscle as preferred substrates for energy metabolism was well explained by Newsholme [43]. The content of free energy per gram of mass that can be released during oxidation and converted into chemical energy in the form of ATP, is much higher for fatty acids than for carbohydrates due to the much higher content of nonoxidized-C—C— and —C—H chemical bonds; depending on the amount of bound water the difference in carbohydrates can range from 3- to 9-fold. Neely, Morgan and Williamson et al. investigated the regulation of the Randle cycle, *via* changes in Krebs cycle intermediates as a function of workload in isolated-perfused working heart [46–51]. This technique allows a precise examination of the Frank–Starling law by achieving high workloads and respiration rates [37,46–51]. Both carbohydrates and fatty acids are oxidized in mitochondria *via* Krebs cycle after formation of acetyl-CoA (see Fig. 1), the main difference being the amount of reducing equivalents produced by both fuels [36,44]. Formation of pyruvate from carbohydrates occurs in the cytoplasm through glycolysis. It is associated with NADH production, which enters rather slowly the mitochondria only *via* malate–aspartate shuttle (Fig. 1), and may limit the rate of glycolysis, particularly under high energy demand [46,52]. On the contrary, β-oxidation of fatty acids occurs in the mitochondrial matrix within an enzymatic supercomplex (metabolon) that appear to operate without rate limitations [53–55]. Therefore, fatty acid oxidation is free from kinetic limitation by the malate–aspartate shuttle, especially at high workloads when malonyl-CoA is decreased due to diminished acetyl-CoA concentration arising from Krebs cycle activation [56]. Malonyl-CoA is an effective inhibitor of the carnitine palmitoyltransferase I (CPT I), and thus of the transfer of acyl-groups into mitochondria for beta-oxidation [35,36,44,57]. It is produced from acetyl-CoA through the acetyl-CoA carboxylase (ACC) reaction, and in the malonyl-CoA decarboxylase (MCD) reaction converted back into acetyl-CoA (reviewed in references [36,44,56,57]). Among the metabolic changes in the heart at high workloads is a decrease of the content of acetyl-CoA, that as a consequence is leaving ACC with much less substrate and thus resulting in a significant decrease of malonyl-CoA in the presence of active MCD. Alterations in malonyl-CoA are the consequence of the increased fatty acid oxidation at elevated workloads, when the level of

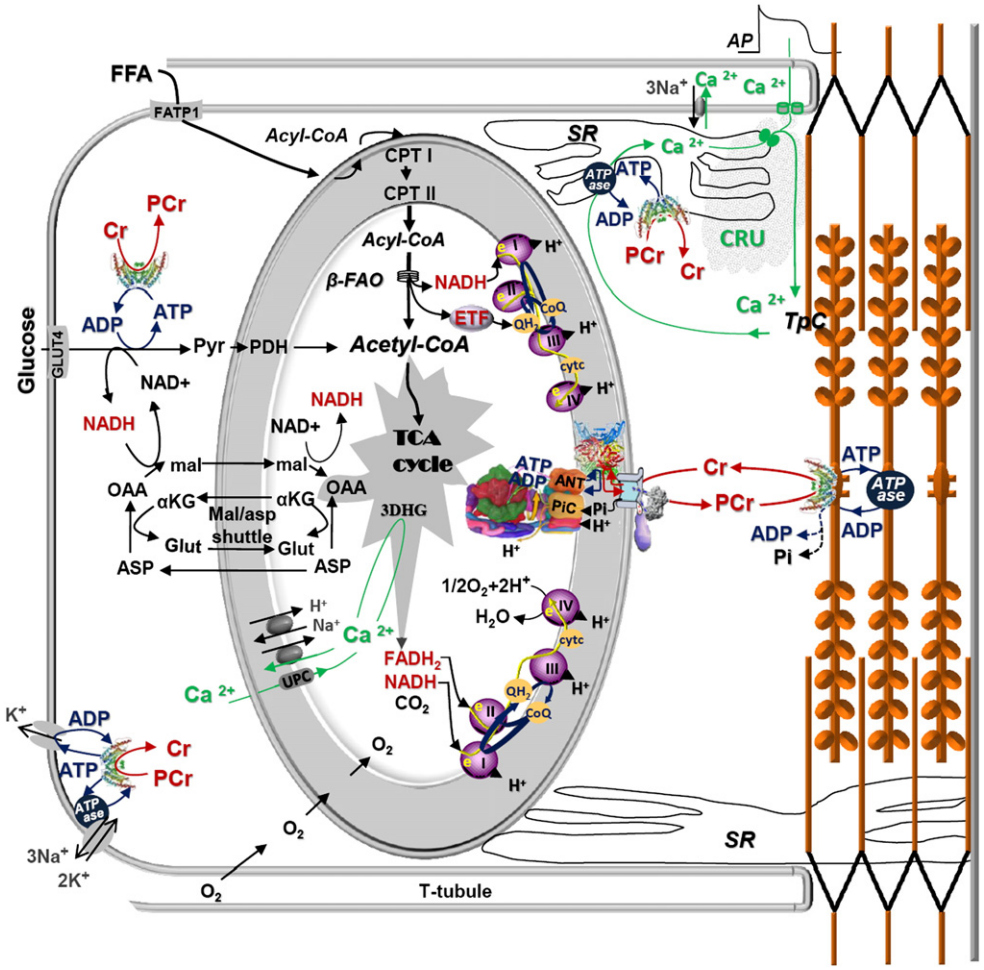

Fig. 1. Functional scheme of the Intracellular Energetic Units of adult cardiac muscle cell. Free fatty acids (FFA) taken up by a family of plasma membrane proteins (FATP1), are esterified to acyl-CoA which entering further the β-fatty acids oxidation (β-FAO) pathway which results in acetyl-CoA production. CPT I and CPT II — carnitine palmitoyltransferases I and II, respectively. Electron-transferring flavoprotein (ETF)-ubiquinone oxidoreductase delivers electrons from β-FAO *directly* to complex III of the respiratory chain (RC). NADH produced by β-FAO is oxidized in the complex I of the RC passing along two electrons and two protons which contribute to the polarization of mitochondrial inner membrane (MIM). Glucose (GLU) is taken up by glucose transporter-4 (GLUT-4) and oxidized via Embden–Meyerhof pathway. Pyruvate produced from glucose oxidation is transformed by the pyruvate dehydrogenise complex (PDH) into acetyl-CoA. The NADH redox potential resulted from glycolysis enters mitochondrial matrix via malate–aspartate shuttle. Malate generated in the cytosol enters the matrix in exchange for α-ketoglutarate (αKG) and can be used to produce matrix NADH. Matrix oxaloacetate (OAA) is returned to the cytosol by conversion to aspartate (ASP) and exchange with glutamate (Glut). Acetyl-CoA is oxidized to CO_2 in the tricarboxylic acids (TCA) cycle generating NADH and $FADH_2$ which are further oxidized in the RC (complexes I, II) with final ATP synthesis. G6P inhibits HK decreasing the rate of glucolysis. The key system in energy transfer from mitochondria to cytoplasm is Mitochondrial Interactosome (MI). MI is a supercomplex, formed by ATP synthase, adenine nucleotides translocase (ANT), phosphate carriers (PIC), mitochondrial creatine kinase (MtCK), voltage-dependent anion channel (VDAC) with bound cytoskeleton proteins (specifically βII-tubulin). MI is responsible for the narrow coupling of ATP/ADP intramitochondria turnover with phosphorylation of creatine (Cr) into phosphocreatine (PCr). PCr is then used to regenerate ATP locally by CK with ATPases (actomyosin ATPase, sarcoplasmic reticulum SERCA and ion pumps ATPases). The rephosphorylation of ADP in MMCK reaction increases the Cr/PCr ratio which is transferred towards MtCK via CK/PCr shuttle. A small part of ADP issued from ATP hydrolysis creates gradient of concentration transmitted towards the matrix. The shaded area in the upper right corner shows the Calcium Release Unit [87–89]. Calcium liberated from local intracellular stores during excitation–contraction coupling through calcium-induced calcium release mechanism, (1) activates contraction cycle by binding to troponin C in the troponin–tropomyosin complex of thin filaments and (2) enters the mitochondria mainly via the mitochondrial Ca^{2+} uniporter (UPC) to activate 3 Krebs cycle dehydrogenases: PDH, αKG, isocitrate dehydrogenase.

acetyl-CoA decreases due to shifts in the kinetics of the Krebs cycle [56]. This makes malonyl-CoA a negative metabolic feedback regulator that allows acyl-CoA entry into mitochondrial matrix space only when it is needed [56]. While all electrons from NADH, and thus from glycolysis, enter the respiratory chain *via* complex I, those obtained from β-oxidation are transferred *via* electron transferring flavoprotein (ETF) and complex III (Fig. 1), resulting in lower ATP/O ratio [36,44,57]. Under aerobic conditions, however, oxygen supply is not a limiting factor for ATP production and differences in ATP/O ratios are only of minor importance. Therefore, the increase in workload is more adequately supported by increase in fatty acid oxidation due to much more favorable kinetics of mass transfer and substrate supply, allowing maximal respiration rates of 160 μmol O_2/min/gdw in working hearts perfused with octanoate as a substrate [47] (Fig. 2A). Only under hypoxic or ischemic conditions, reduction or cessation of mitochondrial respiration results in the decrease or cessation of fatty acid oxidation, while that of carbohydrates is increased [37]. Under these conditions, glucose oxidation provides a potential advantage compared to that of fatty acids.

These classical mechanisms explain well the failure of recent attempts to metabolically modulate heart contractility by reducing fatty acid oxidation and increasing carbohydrate utilization (see [36,58]).

1.2. Cellular bioenergetics in the framework of Systems Biology: Molecular System Bioenergetics

In spite of the brilliant achievements of membrane bioenergetics in explaining the mechanism of ATP synthesis in mitochondrial oxidative phosphorylation [20], the central question of cardiac metabolism – how

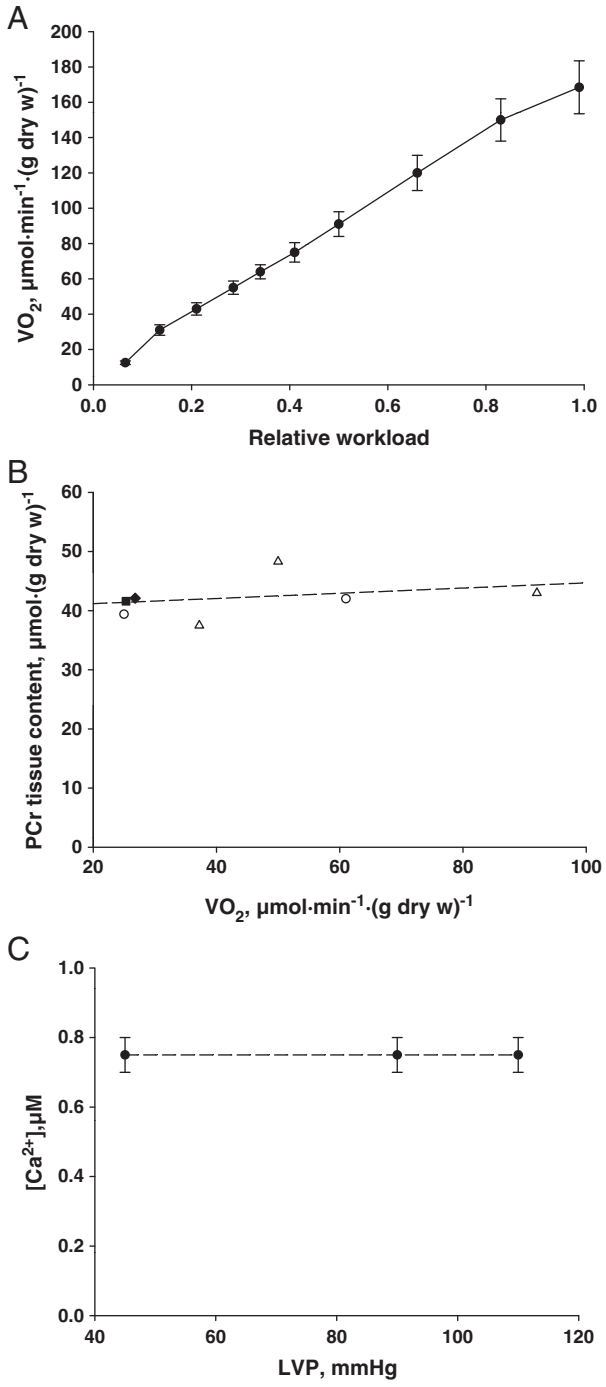

Fig. 2. Metabolic aspect of the Frank–Starling's low of the heart and the mystery of cardiac metabolism. A. Linear increase of oxygen consumption rates as a function of increased relative workload (which is a fraction of maximal workload). Experimental data are taken from [47]. B. Cardiac intracellular PCr homeostasis for different increasing respiration rates. Experimental data were summarized from different studies [48,64,65]. C. Intracellular calcium homeostasis: stable calcium transients for different heart workloads (different left ventricular pressure, LVP) of canine's heart. Experimental data are adapted from [72].

and by which mechanism cardiac work regulates energy fluxes, mitochondrial respiration and substrate uptake – remains to be elucidated despite 80 years of intense research effort. Fig. 2 shows the apparent puzzle of cardiac energy metabolism. For isolated mitochondria, control of respiration by ADP and Pi is indisputable [20,59,60]. Also, activation of Krebs cycle dehydrogenases by Ca^{2+} ions has been well established [61,62]. Although the experimental data obtained with isolated mitochondria and other cellular structures are valuable, they are not sufficient to explain the central problem of cardiac energetics. Two main observations lead us to this conclusion.

1. In aerobic hearts, increase of cardiac work and mitochondrial respiration rate occur at unchanged cellular amount of both ATP and PCr. This phenomenon, discovered by Neely et al. [48] and later confirmed by Balaban and others [63–66], is called metabolic stability or homeostasis (Fig. 2B). This initial set of key observations was interpreted to exclude any explanation of workload dependence of cardiac oxygen consumption upon a mechanism involving the control of mitochondrial respiration by ADP or Pi [67–70]. The basis of that interpretation is the assumption that these metabolites are related through equilibrium relationships [67–70]. The popular assumption of the creatine kinase equilibrium is, however, unnecessary limitation in contradiction with very many experimental data [27,29,31], including recent high resolution ^{31}P NMR experiments [71], showing that the major part of adenine nucleotides, notably ATP in muscle cells exists in the state of association with macromolecules and free ADP may be only transiently be present is cytosol [71].
2. Multiple and detailed physiological experiments using optical methods for monitoring intracellular Ca^{2+} concentrations showed that workload and oxygen consumption changes induced by alteration of left ventricle filling – referred to as the Frank–Starling phenomenon – are observed at unchanged calcium transients [16,72] (Fig. 2C). This crucial observation excludes any explanation involving a mechanism of control of mitochondrial respiration by intracellular calcium, as it has been proposed by several authors ([73], reviewed in [74]). A calcium-mediated mechanism may be important only in the case of adrenergic activation of the heart [75]).

O'Rourke proposed the two main conditions that need to be fulfilled by a metabolic signal regulating respiration *in vivo*: 1) its change must correlate with workload; and 2) it must be able to regulate ATP synthesis [76]. Obviously, the two popular hypotheses described above do not meet these criteria and leave the mechanism underlying the metabolic aspect of the Starling law unexplained.

Manifestly, the problem of regulation of oxygen consumption and substrate uptake by cardiac work demands the use of methods developed in the framework of Systems Biology for its solution. The aim is to explain the physiological phenomena observed by investigating intracellular interactions and resulting regulatory mechanisms, using both experimental and computer modeling methods [1–10,27,29–31]. This approach is rooted in the work of Claude Bernard [8–10] and has been intensively developed during the last decade [1–10,29–31,33]. Revealing the mechanisms of regulation of integrated energy metabolism *in vivo* in the framework of Systems Biology is the objective of Molecular System Bioenergetics [5,10,27]. This research area aims at studying system level properties arising from intracellular interactions, such as metabolic compartmentation, channeling and functional coupling [5,10,26–33]. In this review, we show that the mechanism of feedback regulation in cellular metabolism, linking the cardiac work with mitochondrial respiration under conditions of metabolic stability, can be analyzed quantitatively from experimental data describing intracellular interactions, structure–function relationships, and steady state kinetics of non-equilibrium reactions in cardiac cells.

2. Intracellular Energetic Units (ICEUs): organization of mitochondria by the cytoskeleton and control of mitochondrial morphodynamics

Cells are open systems that operate far from thermodynamic equilibrium while exchanging energy and matter with the external environment [77–84]. Therefore, the intracellular processes are best

described by using the methods of non-equilibrium thermodynamics [79–84] and non-equilibrium steady state kinetics [78].A part of the energy inflow is used to lower entropy as reflected by the emergence of highly ordered intracellular structures which exhibit functionally complex dynamic behavior as a result of collective spatio-temporal organization [79–84]. These structurally and functionally organized metabolic systems may be described as cellular metabolic dissipative structures, representing functional enzymatic associations that form a catalytic entity as a whole and carry out their activities relatively independently [80–84].

In the heart cell, Intracellular Energetic Units, ICEUs [5,10,26–34,85,86] can be interpreted as metabolic dissipative structures. The concept of ICEUs (Fig. 1) was developed on the basis of information of cardiac cell structure and experimental data obtained in the studies of permeabilized cardiac cells and fibers. These studies revealed the major importance of structure–function relationships in the regulation of cardiac cell metabolism [26–34]. As shown in Fig. 1, an ICEU is a structural and functional unit of striated muscle cells consisting of distinct mitochondria localized at the level of sarcomeres between Z-lines and interacting with surrounding myofibrils, sarcoplasmic reticulum, cytoskeleton and cytoplasmic enzymes [5,10,26–34]. In adult cardiomyocytes, ICEUs interact with other dissipative metabolic structures such as calcium release units, CRUs (Fig. 1, shaded area at the upper right corner)[87–89]. Electron microscopic studies have always shown very regular arrangement of mitochondria in cardiomyocytes at the level of A-bands of sarcomeres in myofibrils in turn surrounded by the sarcoplasmic reticulum, a network on its own [90–92] . These results were later confirmed in studies with confocal microscopy [93,94] which also revealed crystal-like arrangement of mitochondria in cardic cells, as illustrated in Fig. 3A. The green fluorescence of antibodies against α-actinin at Z-lines does not colocalize with mitochondria (Figs. 3B and C). Thus, mitochondria are very regularly localized in the space between Z-lines as separate entities in close connection to sarcomeres and sarcoplasmic reticulum to form ICEUs. This conclusion was further confirmed by results of rapid scanning confocal microscopy shown in Fig. 3D, and by direct evidence of the absence of electrical connectivity between adjacent mitochondria (Fig. 3E). High speed scanning (1 frame per 400 ms) revealed very rapid position fluctuations of fluorescence centers of mitochondria labeled with MitoTracker® Green. No mitochondrial fusion or fission was observed in adult cardiomyocytes in contrast to cancerous HL-1 cells of cardiac phenotype [94]. Electrical discontinuity of mitochondria in adult cardiomyocytes has been reported by many authors [95–101]. It has been shown that laser irradiation resulted in the collapse of the membrane potential of individual mitochondria due to local ROS production and permeability transition (Fig. 3E; see also refs. [97,99–105]. These results show the presence of closely located but differentially energized mitochondria. This may have important physiological consequences. Depolarization and functional damage of distinct mitochondria under various pathological conditions like apoptosis will not translate to other mitochondria thus collapsing the entire cell energetics. In addition, mitochondrial discontinuity can prevent propagation of calcium or ROS signals. These results do not support the increasingly popular point of view that mitochondrial fusion is necessary for their normal functional activity [105–110]. Fusion becomes characteristic of mitochondria under pathophysiological states of cardiac cells, and is usually observed in continuously dividing tumor-like cells in culture [94,97,99,111–115].

2.1. Role of the microtubular system and β-tubulin isotypes in mitochondrial arrangement into ICEUs

Regular arrangement of mitochondria in cardiac cells is mediated by their association with three major cytoskeletal structures: microfilaments, microtubules and intermediate filaments [116–122]. It is well known that the cytoskeleton is most important for mitochondria, cell morphology and motility, intracellular traffic and mitosis [121,122]. By its nature, the contraction process needs very precise structural organization of sarcomeres and also mitochondria [123] which in muscle cells is maintained by cytoskeletal proteins. Among them, tubulin [124–126] is one of the most prominent components of the cytoskeleton that, among other functions, plays a role in energy metabolism. By establishing the boundaries of intracellular micro-compartments and of dissipative metabolic structures [127,128] it may intervene in the regulation of metabolic fluxes. In cardiac cells, the microtubular network together with intermediate filaments (plectin, desmin) and microfilaments (actin), form specific structures that represent a vital organization during the contraction cycle, and for regulation of energy supply [129–134]. About 30% of total tubulin is present in the form of αβ heterodimer, and 70% in polymerized form [135]. Remodeling of cytoskeleton, in particular of the microtubular system, is observed in cardiac hypertrophy and cardiomyopathies [132–134].

Most interestingly, already 20 years ago Saetersdal et al. discovered the association of tubulin with the mitochondrial outer membrane (MOM) by immunogold labeling and electron microscopy in cardiac cells [136]. Some of these results are reproduced in Fig. 4B. More recent investigations using immunofluorescence confocal microscopy allowed identifying the beta II isoform of tubulin interacting with MOM (Fig. 4C). This tubulin isotype exhibits a different distribution as compared with other β isotypes in cardiac cells [34]. Similarly to βII-tubulin, we have found that βIII- and βIV-tubulin were present in the left ventricular muscle and adult cardiac cells (Figs. 4D and E). Immunofluorescent labeling allowed us to show that βIV-tubulin is polymerized forming a characteristic microtubular network, and that βIII-tubulin colocalizes with Z-lines [34]. Thus, it appears that the main role of βIV-tubulin is to support the whole cellular morphology. The arrangement of βIV-tubulin in cardiac cancer cells (HL-1) is very different from that in adult cardiomyocytes. This observation may explain their different morphology together with the fact that HL-1 cells completely lack βII-tubulin [34].

The intracellular distribution of β-tubulin isotypes and the dense and complementary distributed system of polymerized and depolymerized tubulin isotypes, contribute to the very regular arrangement of distinct mitochondria into ICEUs in cardiomyocytes. Thus, βII tubulin fixes mitochondria concomitantly controlling their functioning and anchoring them to clusters exhibiting 3D structuring of βIII and βIV-tubulins. Under pathological conditions, such as in cancerous cardiac HL-1 cells, when the β-tubulin isotypes IV and II are absent, and βIII tubulin is diffusely distributed, mitochondria form a dynamic filamentous reticulum characterized by continuous fusion/fission movements (speed of mitochondrial movement ~90 nm/s) [34,94].

In these works described above the immunostaining by antibodies against C-terminal tail of the tubulin βII has been used to study their localization in permeabilized cardiomyocytes [34]. However, the tubulin exists in forms of non-polymerized or polymerized αβ-heterodimers [124–126], and there are several isotypes of both subunits which differ mostly by the structure of C-terminal tail [124,126]. Further intensive studies by immunocoprecipitation, mutagenesis and use of chemical inhibitors are needed to find out why only βII-tubulin is associated with mitochondria, what is the possible role of the α isotype and how they both interact with VDAC in the mitochondrial outer membrane. Also, the role of different VDAC isoforms in the interaction with cytoskeletal proteins in muscle cells is of interest, and how these interactions are influenced by other membrane-bound proteins [124–126].

The proper cyto-architecture and positioning of other cellular structures in adult cardiomyocytes are also dependent on the cytoskeletal proteins plectin and desmin [137–141]. Importantly, mutations of the human plectin gene showed that pathological disorganization of the intermediate filament cytoskeleton can be associated with severe mitochondrial dysfunction. Moreover, plectin deficiency in mice results in significantly decreased mitochondrial number and function [139–142]. Among many known isoforms of plectin, skeletal and cardiac muscle are characterized by high expression

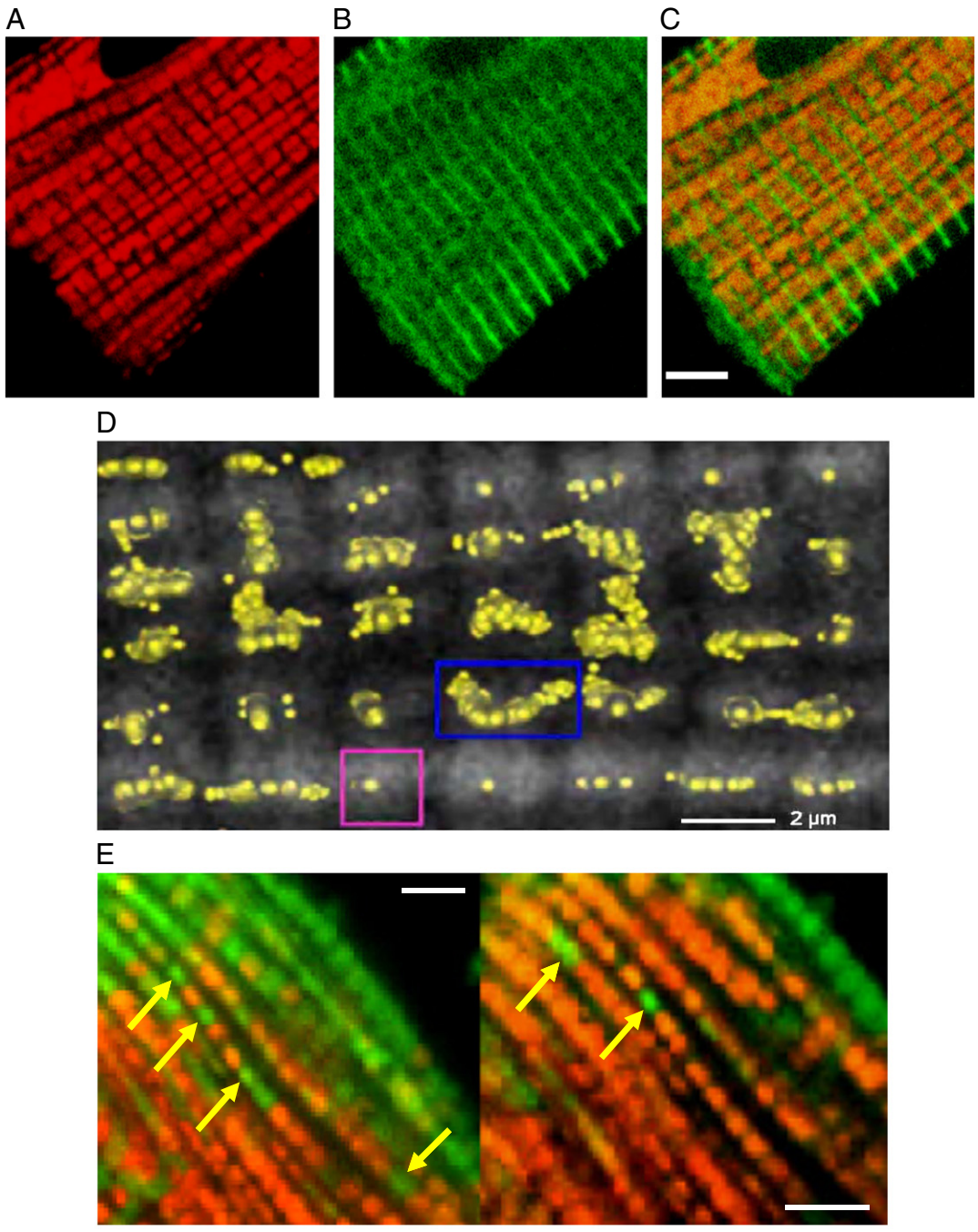

Fig. 3. A. Confocal image of regularly arranged mitochondria in fixed cardiomyocytes labeled by Mito-ID. B. Immunofluorescence labeling of α-actinin showing its specific localization at Z-lines (second antibody with FITC). C. Superposition of A and B shows clearly that mitochondria are localized between Z-lines (green fluorescence) without any fusion processes. Scale bar 5 μm. Reproduced from [34] with permission from Elsevier. D. Visualization of the positions of mitochondrial fluorescent (mass) centers in a cardiomyocyte over a long time (total duration 100 s) of rapid scanning: movements of fluorescence centers are limited within internal space of mitochondria. These fluorescence centers (which are assimilated to the center of mitochondria in cardiomyocytes) are shown as small yellow spheres. The position of fluorescent centers were superimposed with a reference confocal image of MitoTracker® Green fluorescence (in gray) showing mitochondrial localization. Note that the fluorescence centers are observed always within the space inside the mitochondria, but from mitochondrion to mitochondrion the motion pattern may differ from very low amplitude motions (pink frame) to wider motions distributed over significant space but always within the internal space of a mitochondrion (blue frame). Reproduced from [94] with permission from Springer. E. Imaging of double-labeled cardiomyocytes mitochondria with ΔΨ-sensitive probe TMRM (red) and MitoTracker™ Green. Representative merge images of MitoTracker Green and TMRM fluorescence show very closely located normally energized and fully depolarized mitochondria (indicated by arrows), demonstrating their electrical disconnectivity. Scale bar 5 μm.

of plectins 1, 1b, 1d, and 1f isoforms [140,141]. Plectin 1d is specifically associated with Z-disks, whereas plectin 1b is shown to colocalize with mitochondria [139–142]. Plectin 1b is inserted into the MOM with the exon 1b-encoded N-terminal sequence serving as a target to mitochondria and anchoring signal that may also directly interact with the voltage-dependent anion channel (VDAC) [142]. Notably, in addition to its anchoring function, plectin 1b may participate also in promoting proper mitochondrial shape, since plectin 1b-deficient fibroblasts and myoblasts exhibit remarkably elongated mitochondria.

Likely, association of βII-tubulin and plectin with MOM may prevent binding of proteins both pro-apoptotic and those inducing mitochondrial fission or fusion.

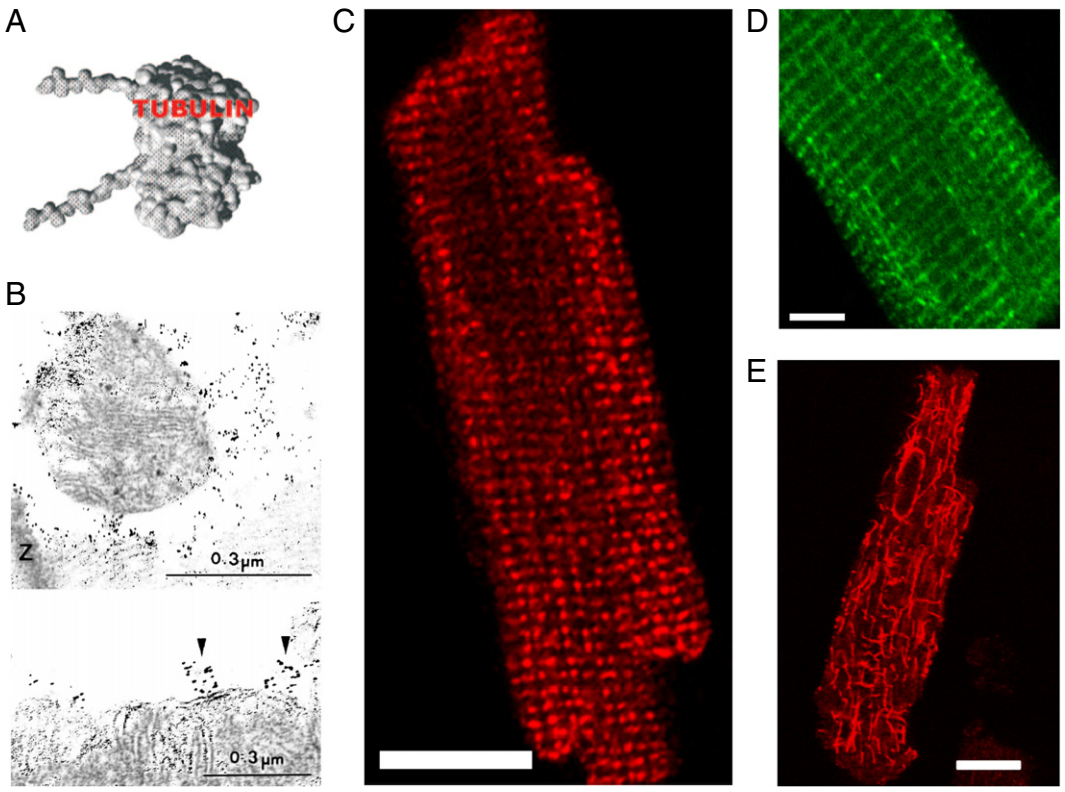

Fig. 4. A. Tubulin αβ-dimer with C-terminal tails. Adapted from [153]. B. Immunogold electron micrography showing the presence of β-tubulin in close proximity to mitochondria in freshly isolated cardiomyocytes. Figure reproduced from [136] with permission from Springer. C. Regularly arranged proteins labeled with anti-βII-tubulin antibody and Cy5 Separate fluorescent spots are organized in distinct longitudinally oriented parallel lines repeating mitochondrial arrangement in cardiomyocytes. Scale bar 14 μm. D. Tubulin labeled with anti-βIII-tubulin antibody and FITC demonstrates clearly distinguishable prevalent arrangement in transversal lines co-localized with sarcomeric Z-lines. Scale bar 6 μm. E. Tubulin labeled with anti-βIV-tubulin antibody and Cy5. βIV-tubulins form polymerised longitudinally and obliquely oriented microtubules. Scale bar 21 μm. Reproduced from [34] with permission from Elsevier.

2.2. Mitochondrial functional properties in ICEUs — selective control of outer membrane permeability by tubulin, Mitochondrial Interactosome

2.2.1. Role of cytoskeleton

Comparative studies of permeabilized adult cardiomyocytes with cancerous, cardiac-like non-beating HL-1 cells [26,27] showed that tubulin βII isotype co-expresses with MtCK in adult cardiomyocytes, while they are both absent in NB HL-1 cells (Fig. 5A). Non-beating (NB) HL-1 cells are derived from tumoral atrial cardiac myocytes (HL-1 cell line) grown up in Clycomb's laboratory [143]. These cells express cardiac proteins connexin 43, desmin, developmental myosin, cardiac isoforms of dihydropyridin receptors and are devoid of sarcomere structures [144]. NB HL-1e cells are characterized by the presence of sodium–calcium exchanger, the rapid delayed potassium current, but not pacemaker current. The spontaneous depolarization also was not observed. They possess randomly organized filamentous dynamic mitochondria. [34,94,144]. Fusion or fission was seen only in cancerous NB HL-1 cells but not in adult cardiomyocytes [94]. The differences observed in mitochondrial dynamics are related to distinct specific structural organization and mitochondria–cytoskeleton interactions in these cells [29] In contrast to adult cardiomyocytes, the NB HL-1 cells lack MtCK and βII-tubulin [34]. Thus, co-expression of MtCK and βII-tubulin correlate with contractile function in cardiac cells. The initial observation by Saertesdal et al. showing the association of tubulin with MOM in cardiac cells [136] remained unnoticed for a long time. A possible explanation of the functional role of βII-tubulin, however, became evident from studies of regulation of mitochondrial respiration in permeabilized cardiac cells and muscle fibers in many laboratories during the last two decades [145–151] (reviewed in [5,29]). In these studies, the apparent affinity of oxidative phosphorylation for exogenous ADP was characterized by an apparent Km of an order of magnitude lower in permeabilized cardiomyocytes than in isolated mitochondria. The apparent Km decreases after proteolytic treatment with trypsin [148] or addition of creatine (Fig. 5B, see ref. [29] for review). This effect of trypsin on mitochondrial respiration regulation *in situ* suggested that cytoskeletal proteins, then called Factor X, could be involved in the control of MOM permeability [149,150]. Appaix et al. showed in permeabilized cardiomyocytes that tubulin and plectin are very sensitive to proteolytic digestion [152]. Finally, Rostovtseva et al. showed direct interaction of tubulin with VDAC while reconstitution experiments by Monge et al. indicated that association with tubulin increased the apparent Km for ADP in isolated mitochondria [153–155]. F. Bernier-Valentin, B. Rousset and Carre et al. have shown association of tubulin with mitochondria from liver and several other type of cells [156,157]. Association of βII-tubulin with mitochondria in adult cardiomyocytes (Fig. 4) and its absence in HL-1 cells with very low apparent Km for ADP (Fig. 5B) further supported the idea that this tubulin isotype likely is Factor X, which controls VDAC permeability in the MOM [158–160].

Association of βII-tubulin with VDAC and its coexpression with MtCK has fundamental consequences for the regulation of metabolite and energy fluxes between mitochondria and cytoplasm in cardiac cells. One of them is that it strongly increases the functional compartmentation of adenine nucleotides in mitochondria while shifting the energy transfer via the phosphocreatine pathway [26–34]. These proteins were supposed to form a supercomplex, dubbed the Mitochondrial Interactosome (MI) in contact sites of the inner and outer mitochondrial membranes [29,33,34,161]. MI represents a key structure of regulation

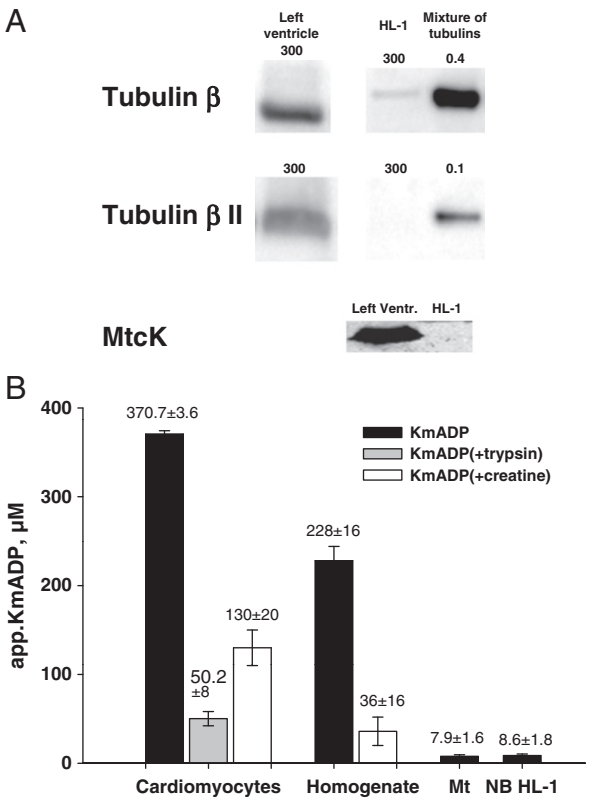

Fig. 5. A. Western Blot analysis of β and βII-tubulin isotypes, and MtCK in rat heart left ventricle and non beatting HL-1 cancer cells of cardiac phenotype. Numbers above the gel images show the amount of added total protein (in μg). Mixture of purified tubulins from brain was used as a reference [34]. Studied proteins are absent in HL-1 cells. B. Regulation of mitochondrial respiration by exogenous ADP in permeabilized muscle cells and fibers. High apparent Km for ADP in permeabilized cardiomyocytes and cardiac muscle homogenate decreases after trypsin proteolysis showing the increase of mitochondrial outer membrane (MOM) permeability for ADP. Increase of MOM permeability is caused by the proteolytic remove of βII-tubulin and other linker proteins from VDAC's protein-binding site. Isolated mitochondria and non beating HL-1 cells are characterized by very low KmADP and very high MOM permeability for ADP, respectively. This high permeability is caused by the absence of βII-tubulin (see Western blot). Creatine regulates respiration of permeabilized cardiomyocytes (decrease of the app. KmADP in the presence of creatine) and has no effect on the respiration of non-beating HL-1 cells because of the absence of MtCK (see Western blot). Data are taken from references [29,32,158,159].

of energy fluxes in ICEUs that strongly increases the efficiency of functional coupling between MtCK and the ATPSynthasome (Fig. 6). The MI supercomplex includes βII tubulin, VDAC, MtCK and ATPsynthasome, consisting of structurally bound ATPsynthase, ANT and PIC [29,33,34,161]; in the cristae membranes, there are only functionally coupled MtCK and ATP synthasome (Fig. 6B). The latter system is also present in isolated mitochondria (Fig. 6A) which have lost tubulin and therefore VDAC permeability is high (low apparent KmADP).

2.2.2. Kinetics of respiration regulation within MI

MtCK is present in mitochondria in octameric form [24,25] and bound to the outer surface of the inner membrane through electrostatic interactions involving positive charges of lysine residues and negative charges from cardiolipin which is also associated with the ANT [162,163]. The ANT carries ATP out of the mitochondrial matrix in exchange for ADP [164]. Due to its close proximity with MtCK, ATP is directly channeled to the active cite of MtCK and effectively used for PCr production if creatine is present (Fig. 6A). Such functional coupling of ANT and MtCK by direct channeling of ATP is well documented in many experimental studies with isolated mitochondria [165–171]. ADP formed at the active site of MtCK is released into intermembraine space (IMS) and may either return to the matrix via ANT or leave mitochondria via VDAC [172,173]. The flux distribution between these two routes depends upon VDAC permeability for adenine nucleotides. Binding of βII-tubulin to the MOM in cardiomyocytes limits this permeability further enhancing functional coupling between ANT and MtCK while increasing ADP transfer to the matrix *via* ANT. The overall effect of this structural–functional coupling is to increase the functional compartmentation of adenine nucleotides in the cell (Fig. 6B). Most remarkably, interaction of βII tubulin with VDAC significantly changes the kinetics of respiration by the MtCK reaction within MI [32,33].

It is important to notice that in permeabilized cardiomyocytes, mitochondria in all ICEUs have similar functional characteristics, as revealed by the kinetic analysis of respiration regulation by exogenous ADP (Figs. 6D–F). First, as it is shown in Table 1 and in Fig. 6D, the maximal ADP-dependent respiration rates when calculated per nmol of cytochromes aa3, are equal in isolated mitochondria (isolated with the use of trypsin) and in permeabilized cardiomyocytes, that meaning that in the permeabilized cells the activities of the whole mitochondrial population were measured. Second, the kinetic curves of the dependence of the respiration rates on ADP concentration are always represented by one hyperbolic curve (both in the absence and presence of creatine) (Fig. 6E), which are linearized by one straight line in double-reciprocal plots (Fig. 6F). Thus, there is no difference in the kinetic behavior of subsarcolemmal and intermyofibrillar mitochondria in permeabilized cardiomyocytes. In the intact non-permeabilized cells, subsarcolemmal ICEUs include both myofibrillar and sarcolemmal ATP consuming systems (Fig. 1), while in the cell interior mitochondria interact with ATP consuming systems of adjacent sarcomeres and sarcoplasmic reticulum (calcium release units, CRU). In all cases the permeability of MOM seems to be controlled by tubulin and possibly other cytoskeletal proteins.

The experimental protocol utilized to study MtCK properties *in situ* in permeabilized cardiomyocytes is schematically represented in Fig. 6C, and illustrated by oxygraph recordings shown in Fig. 6G. In this experimental setting, the kinetics of regulation of respiration is stimulated by endogenous ADP, in turn produced by MtCK in mitochondrial intermembrane space (MIM). The influence of extra-mitochondrial ADP is ruled out by adding exogenous pyruvate kinase (PK)–phosphoenolpyruvate (PEP) which are used to trap ADP outside the mitochondria [26,29,32,174]. Addition of MgATP activated ADP synthesis by MgATPases and stimulated respiration. Subsequent addition of PK + PEP decreased the respiration rate, which was rapidly increased again by stepwise addition of creatine. The maximal respiration rate achieved by activation of MtCK is equal to the State 3 rate [29,32] (Fig. 6G and Table 1). These results are in agreement with the idea that all ADP produced by the MtCK in the intermembrane space is not accessible for external PK–PEP system but is continuously recycled within MI, maintaining high rates of respiration and coupled PCr production [26,28–30,32]. In isolated mitochondria in the absence of bound βII tubulin, PK–PEP decreased the respiration rate by 50% as a result of the open state of VDAC (Table 1) [32,174]. The efficiency of intramitochondrial ATP/ADP turnover in the ATP synthasome [175] coupled to the MtCK reaction is confirmed by the high ratio of PCr production over oxygen consumption (P/O_2 ~5.98) [29,32,161]. This ratio is close to the theoretical value of P/O for mitochondrial oxidative phosphorylation [20], thus indicating the high efficiency of MI function within ICEUs in cardiac muscle cells [161]. As a result, almost all mitochondrial ATP is dephosphorylated by MtCK within MI and the free energy of phosphoryl bonds transferred to the cytoplasm through the PCr/Cr pathway [24–34].

This conclusion is further strengthening by the results of experiments shown in Fig. 6H. Since one of the enzymes which may be associated with the mitochondrial outer membrane may be hexokinase [176], we compared the effects of glucose and creatine on the respiration rate of permeabilized cardiomyocytes in the presence of MgATP and PK–PEP system. Glucose addition had only

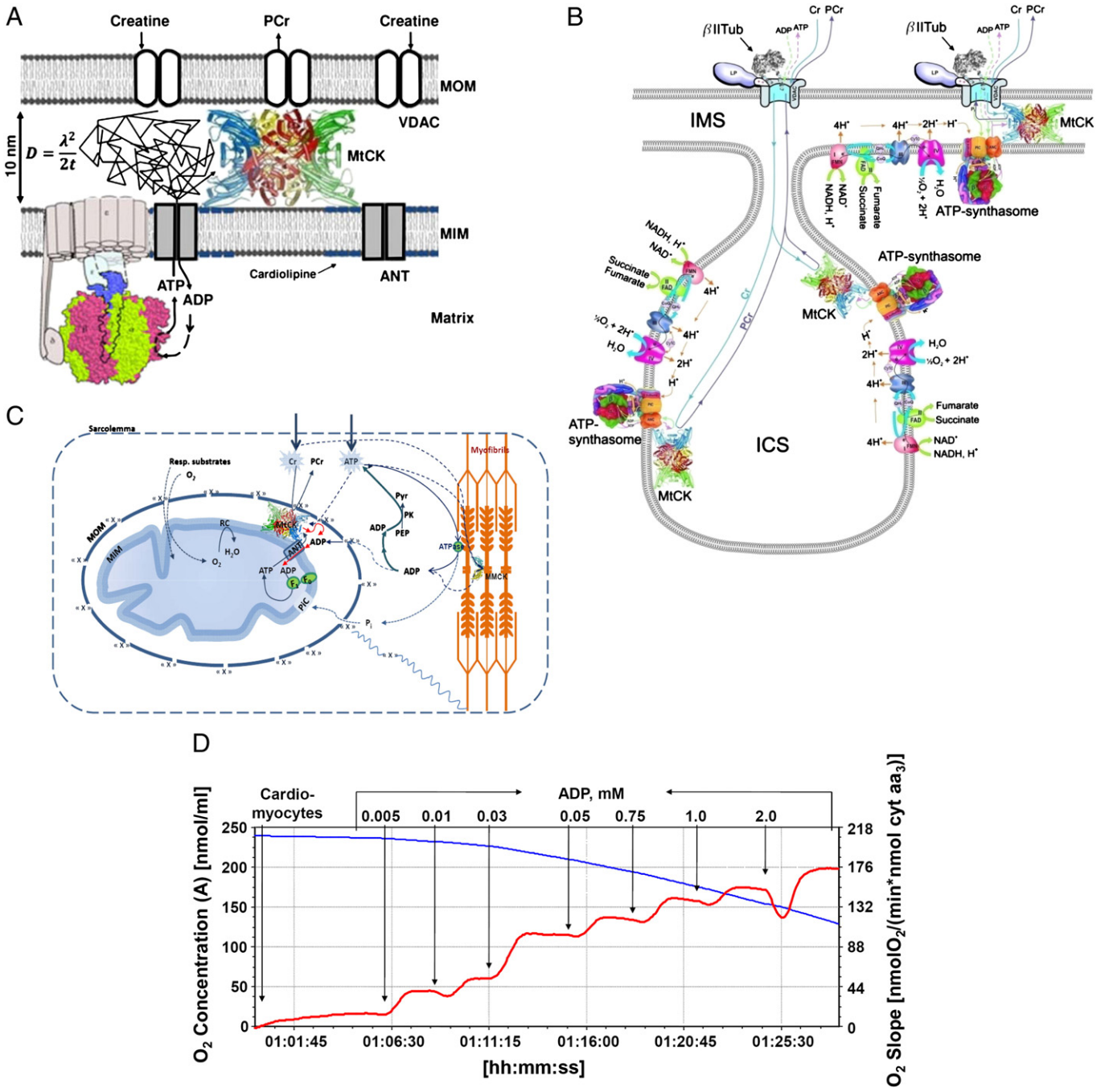

Fig. 6. A and B: Scheme of the microcompartment of adenine nucleotides in mitochondrial intermembrane space created by proteolipid complexes of MtCK with VDAC and ANT, and limited by mitochondrial outer membrane (MOM). LP – still unknown cytoskeletal linker protein which may help tubuli binding to VDAC. This complex allows the direct exchange — metabolite channeling, depicted by arrows. This figure represents also schematically hypothesis of free diffusion of adenine nucleotides molecules within mitochondrial intermembrane space, which can be described by Einstein–Smoluchowski diffusion equation. C shows the protocol of studies of the kinetics of the respiration rate regulation by ADP produced by MtCK in permeabilized cardiomyocytes. D. Oxygraph recording of oxygen consumption by permeabilized cardiomyocytes during titration with increased concentrations of ADP (from 0.05 to 2 mM) in the presence of 5 mM glutamate, 2 mM malate. The blue slope and left y-axes correspond to O_2 concentration; the red slope and right y-axes correspond to O_2 flux. E. Graphical presentation of experimental data of respiration rates as a function of ADP concentrations. This dependence is described by Henri–Michaelis–Menten equation. Empty bullets correspond to experiments performed in the presence of 20 mM creatine. F. Analyses of experimental data by linearization of dependences from panel E in double reciprocal plot of $1/VO_2$ as a function of 1/[ADP]. This plot gives value of the apparent Km for ADP (the abscise intercept corresponds to −1/Km). G. Experimental oxygraph recording of the respiration rate regulated by ADP produced by MtCK in permeabilized cardiomyocytes. First, the basal rate of respiration (V_0) of permeabilized cardiomyocytes (25 μg/mL saponin, 10 min, 25 °C) was recorded in the presence of respiratory substrates for complex I (5 mM glutamate and 2 mM malate). After that, respiration was activated by the addition of 2 mM MgATP which is hydrolyzed by myofibrillar ATPases releasing endogenous MgADP, inorganic phosphate (Pi) and proton. On the oxygraph trace this step is seen as an increase in oxygen consumption stimulated by endogenous MgADP. Next, extramitochondrial MgADP was removed by the addition of phosphoenolpyruvate (PEP, 5 mM) and pyruvate kinase (PK, 20 IU/mL) [32]. The PEP dephosphorylation catalyzed by PK uses ADP to regenerat extramitochondrial pool of ATP. This step is seen on oxygraph trace as an inhibition of respiration. Finally, stepwise creatine in the presence of MgATP activates MtCK and in thus MgADP and PCr production from MgATP and creatine. Respiration rate rapidly increases to its maximal value (Table 1), this showing that MgADP produced by MtCK behind the MOM is not accessible for PK + PEP system [29,32]. H. Comparison of the regulation of mitochondrial respiration by glucose and creatine in presence of MgATP and PK–PEP system in permeabilized cardiomyocytes (CM). Cardiomyocytes were permeabilized by saponin and State 2 respiration recorded. MgATP was added to a 2 mM final concentration to stimulate MgATPases, increasing the respiration rate. This rate was decreased by the addition of PK (20 U/mL) in the presence of PEP (5 mM). Thereafter, no effect on respiration rate was seen after the addition of glucose (10 mM). Subsequent addition of creatine (20 mM) rapidly increased the respiration rate up to maximal value. ADP produced by MtCK is not accessible for the PK–PEP system and is rapidly taken up by ANT into mitochondrial matrix.

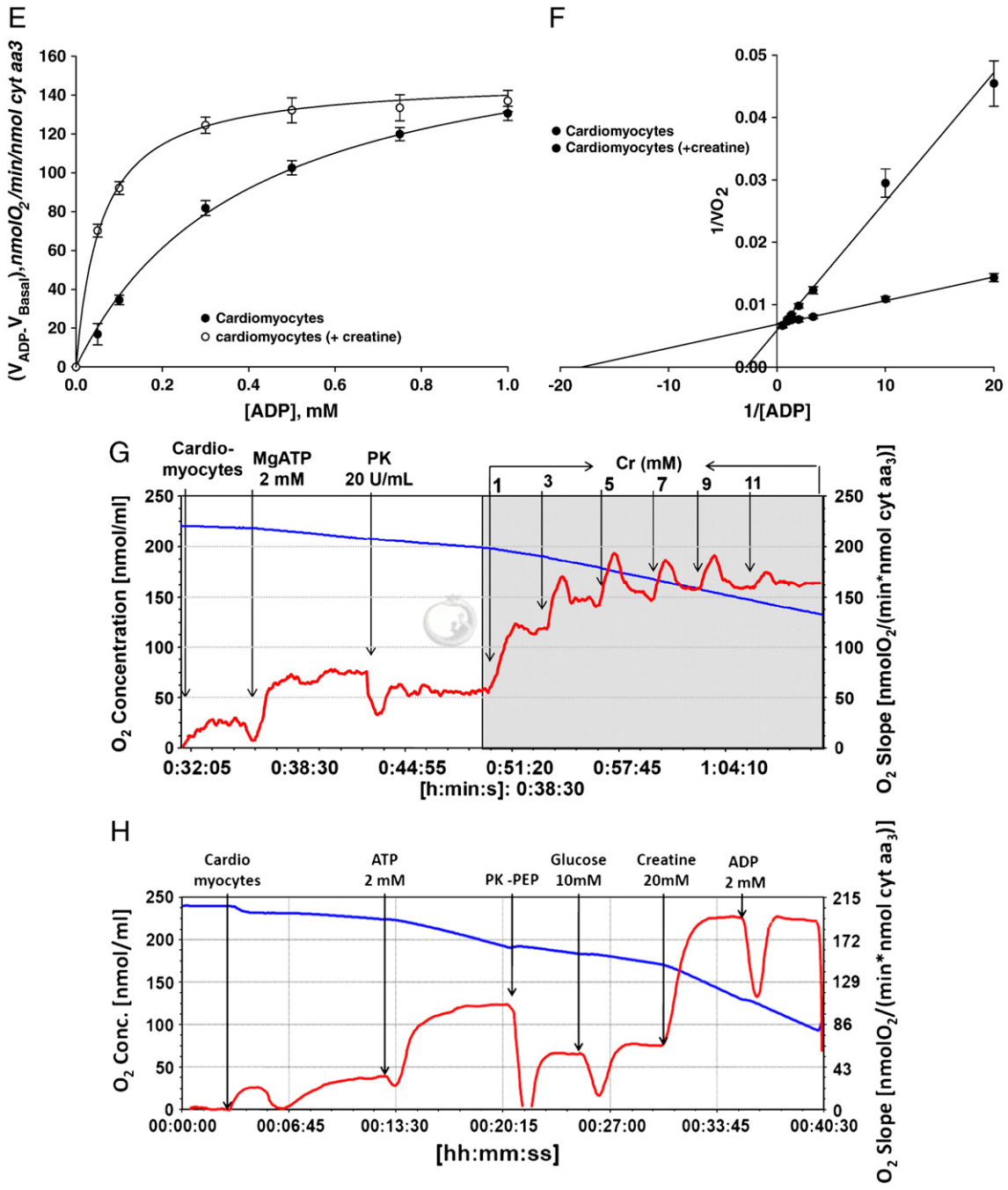

Fig. 6 (*continued*).

minor effect on the respiration rate, while creatine maximally activated the respiration. This shows that MgADP produced by hexokinase is accessible for PK–PEP system, while MgADP produced by MtCK is not accessible and is only recycling in coupled reactions in mitochondria resulting in PCr production.

As compared to isolated mitochondria, complete kinetic analyses of MtCK-controlled respiration performed in permeabilized cardiomyocytes using the protocol shown in Fig. 6C revealed significant changes in the kinetics of MtCK as a result of molecular interactions within MI [32]. The MtCK reaction follows a BiBi quasi-equilibrium random type mechanism, according to Cleland's classification [165]. The constants Kia, Ka, Kib and Kb are dissociation constants, showing the affinity of the free enzyme or its binary complexes for MgATP and creatine (see Table 2). When the MtCK reaction is coupled to the ATP synthasome, these constants reflect apparent affinities of the whole system to these substrates. Table 2 shows that while in isolated mitochondria coupling of MtCK to oxidative phosphorylation decreases both Kia and Ka for MgATP due to recycling of adenine nucleotides [165–171], in permeabilized cardiomyocytes these constants are much higher; the apparent Ka is increased by a factor of 100. At the same time, dissociation constants for creatine are decreased, resulting in the increased apparent affinity for this substrate by MtCK within MI [32]. These results show that βII-tubulin association with MOM decreases VDAC permeability selectively, *i.e.* limiting for MgATP and MgADP but not for creatine and PCr. To explain the observed specific increase of the apparent dissociation constants for MgATP in

Table 1
Basic respiration parameters of isolated rat heart mitochondria and of mitochondria *in situ* in permeabilized cardiomyocytes. V_3 — respiration rate in the presence of 2 mM ADP, $V_{Cr,ATP}$ — respiration rate in the presence of activated MtCK by 2 mM ATP and 20 mM Creatine; $V_{Cr,ATP+PK,PEP}$ — respiration rate in the presence of activated MtCK by 2 mM ATP and 20 mM Creatine in the presence of 20 IU/mL PK and 5 mM PEP. Data from [29,32].

Parameter	Mitochondria *in vitro*	Mitochondria *in situ* (permeabilized cardiomyocytes)
V_0, nmol O_2 min^{-1} mg $prot^{-1}$	26.37 ± 7.93	7.53 ± 1.61
V_3 (2 mM ADP), nmol O_2 min^{-1} mg $prot^{-1}$	187.94 ± 40.68	84.45 ± 13.85
[Cyt aa_3], nmol mg $prot^{-1}$	1.00 ± 0.04	0.46 ± 0.09
V_3 (2 mM ADP), nmolO_2 min^{-1}cyt aa_3^{-1}	187.94 ± 40.68	178.23 ± 33.96
$V_{Cr,ATP}$, nmol O_2 min^{-1} cyt aa_3^{-1}	197.90 ± 31.86	162.63 ± 26.87
$V_{Cr,ATP+PK,\ PEP}$, nmol O_2 min^{-1} cyt aa_3^{-1}	82.1 ± 10.5	160.45 ± 26.87

the MtCK reaction in permeabilized cardiomyocytes (Table 2) and apparent Km for exogenous ADP in respiration rate regulation (Fig. 6D–F) we may refer to the specific voltage gating mechanism of the VDAC channel. VDAC has a mobile and positively charged domain that forms part of the wall of the channel, according to Colombini's functional model [172,173,177]. It was proposed that the channel undergoes significant structural rearrangements upon voltage-gating when a positively charged voltage sensor domain translocates across the membrane towards one of the membrane interfaces depending on the sign of the applied voltage under conditions when purified VDAC is integrated into the phospholipid membrane [177]. Its conformational change results in a channel with reduced pore size. The metabolic anions (such as ATP) that moved easily through the open state face a barrier to flow through the closed state. Under *in vivo* conditions the conformational state and permeability of VDAC can be modified by its interaction with proteins from the intracellular environment, such as tubulin. At the same time, the absence of significant change in the apparent affinity of MtCK for creatine and PCr is in accordance with findings that VDAC in so called "closed" states are still permeable to small ions including [177].

Thus, the role of Mitochondrial Interactosome is to ensure continuous recycling of adenine nucleotides in mitochondria, their transphosphorylation and metabolic channeling of ATP via ANT to MtCK, and back ADP, resulting in the export of free energy from mitochondria into cytoplasm as flux of PCr. The functioning of this complex structure is best explained by the theory of vectorial metabolism and the vectorial ligand conduction, proposed by P. Mitchell [178]. Initially, this theory was developed to explain the organization of enzymes in supercomplexes allowing the scalar transport of electrons and the vectorial conduction of protons through the mitochondrial inner membrane to create the electrochemical potential [178]. This theory corresponds to the increasing amount of experimental data showing that in the living systems proteins function in concentrated and complicated environments [5,10,27,29,179] within organized metabolic dissipative structures [79–84] and metabolic networks [4]. Vectorial metabolism by ligand conduction within multienzyme complexes allows overcoming the diffusion problems for metabolites including ATP, the major part of which has been found to be associated with proteins in muscle cells [71].

2.2.3. MI as an amplifier of metabolic signals from cytoplasm

Fig. 7A shows that as a result of these kinetic features MI is a powerful amplifier of the effects of ADP in regulating mitochondrial respiration [29–34,161]. The role of extra- and intra-mitochondrial ADP in respiration regulation was studied by MgATP titration in the presence of creatine, *i.e.*, activated MtCK [32,161]. The influence of intramitochondrial ADP alone on respiration was estimated by removing extramitochondrial ADP according to the method described above (PEP–PK system mimicking glycolytic ADP consumption). We can see from Fig. 7A that the extra-mitochondrial ADP producing system alone cannot effectively activate respiration. The high apparent Km for exogenous MgATP (157.8 ± 40.1 μM) corresponds to the apparent Km of myofibrillar ATPase reaction for MgATP. When oxidative phosphorylation is stimulated by both extra- and intra-mitochondrial ADP (in the presence of creatine to activate MtCK), the respiration rate increases rapidly up to maximal values and the apparent Km for ATP decreases from 157.8 ± 40.1 μM to 24.9 ± 0.8 μM. Removal of extra-mitochondrial ADP by PEP–

Table 2
Kinetic properties of MtCK *in situ* in cardiomyocytes.

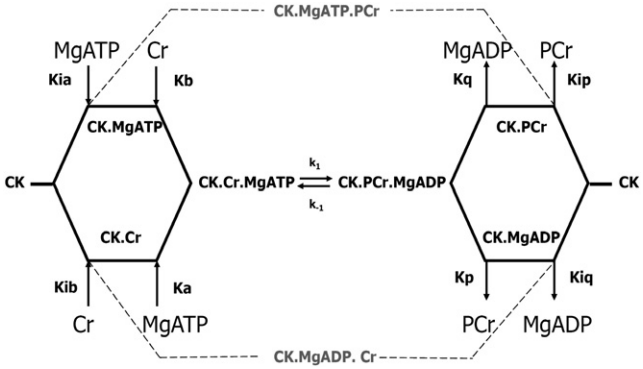

		K_{ia} (MgATP), mM	K_a (MgATP), mM	K_{ib} (Cr), mM	K_b (Cr), mM	K_{ip} (PCr), mM
Isolated mitoch.	− OxPhosph	0.92 ± 0.09	0.15 ± 0.023	30 ± 4.5	5.2 ± 0.3	
	+ OxPhosph	0.44 ± 0.08	0.016 ± 0.01	28 ± 7	5 ± 1.2	0.84 ± 0.22
Mitoch. *in situ* (*PEP-PK*)		1.94 ± 0.86	2.04 ± 0.14	2.12 ± 0.21	2.17 ± 0.40	0.89 ± 0.17

Values of constants for isolated mitochondria are taken from [165]. In isolated mitochondria the oxidative phosphorylation decreases dissociation constants of MgATP from MtCK–substrates complexes suggesting the privileged up-take of all ATP by MtCK [32,33,165–171]. In mitochondria *in situ* in permeabilized cardiomyocytes the increase of apparent constants of dissociation of MgATP compared with *in vitro* mitochondria shows the decrease of apparent affinity of MtCK *in situ* for extramitochondrial MgATP. The decrease of apparent constants of dissociation of creatine from MtCK–substrates complexes suggests the increase of the apparent affinity of MtCK for creatine *in situ*. The apparent constant of dissociation for PCr did not change *in situ* compared with isolated mitochondria. Reproduced from [29,32] with permission from Elsevier.

PK provokes the increase of Km for MgATP up to 2.04 ± 0.10 mM. These results show that endogenous ADP is an important regulator of respiration but only in the presence of creatine and activated MtCK. The stimulatory effect of respiration by endogenous ADP is strongly amplified by functional coupling of MtCK with ANT that increases adenine nucleotides recycling within the MI [29–34,161].

2.2.4. Metabolic control analysis of mitochondrial interactosome

In order to characterize quantitatively the role of each MI component in the control regulation of respiration within ICEUs, Metabolic Control Analysis was utilized [180]. Permeabilized cardiomyocytes were utilized under two conditions: i) direct activation of respiration by ADP (without MtCK), ii) and activation of respiration via MtCK, using the protocol described in Fig. 7B. Specific inhibitors of the MI components were used to titrate the respiratory flux in order to calculate flux control coefficients under both conditions [180]. The results obtained show high flux control by ANT and the ATP synthasome, both involved in ADP/ATP cycling. Interestingly, the flux control coefficient is increased in the presence of creatine also for the Complex I, probably due to the possible differences in red-ox state of its components. In both cases the Pi carrier PIC has been found to play only a minor role in the control of energy fluxes (Fig. 7B). The sum of flux control coefficients in the case of MtCK activation is close to 4, while in the case of ADP activation is close to one, as previously described [180]. Earlier theoretical work by Kholodenko et al. [181,182] showed that the sum of flux control coefficients may exceed unity in metabolic pathways exhibiting channeling as in the case of the ADP/ATP recycling exerted by MtCK. These results are in agreement with the notion that the MI is rate-controlling of respiration, conveying local metabolic signals in the ICEUs [180–182].

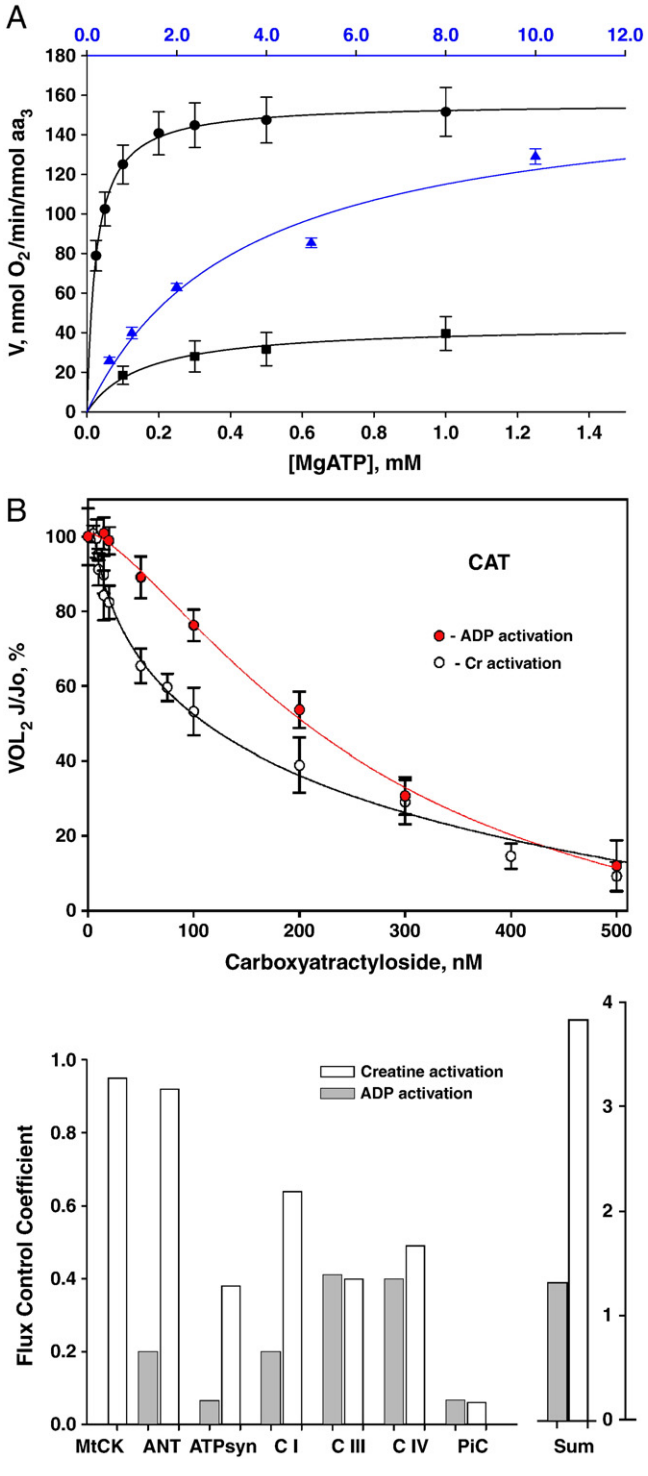

Fig. 7. Amplification of the metabolic signals by Mitochondrial Interactosome. A. Dependence of the rate of respiration in permeabilized cardiomyocytes on the concentration of MgATP added into the medium. This graphical representation reveals the role of endogenous ADP produced by MtCK within mitochondrial intermembrane space for the respiration regulation. (■) — respiration regulation by extramitochondrial MgADP issued from MgATP hydrolysis in MgATP reactions (experiment performed without ADP trapping system (PEP-PK) and in the absence of creatine); (●) — respiration regulation by extramitochondrial and intramitochondrial ADP produced by activated MtCK reaction (experiment performed without PEP–PK system but in the presence of 20 mM creatine); (▲) — respiration regulation by intramitochondrial ADP produced by activated MtCK only (experiment performed in the presence of both trapping system for free ADP and 20 mM creatine). Reproduced with permission from the reference 162. B. Metabolic Control Analysis of the MI. Flux control coefficients were measured as described in [169] under conditions of direct activation of respiration by ADP (2 mM), or by activation of MtCK by ATP (2 mM) and creatine (20 mM) in the presence of PK (20 IU/mL) and PEP (5 mM). A. Changes in the respiration rates in permeabilized cardiomyocytes during inhibition by carboxyatractyloside. B. Flux control coefficients for MtCK, adenine nucleotide translocase (ANT), ATP synthasome (ATPsyn), respiratory complexes I (C I), III (C III), IV (C IV), and inorganic phosphate carrier (PiC). The right panel shows the sum of flux control coefficients.

3. Feedback metabolic regulation within ICEUs

Fig. 2 depicts the riddle of cardiac metabolism: the manifold increase in the rate of myocardial oxygen consumption in response to elevated workload, which is induced by increased left ventricle filling (Starling's law) at apparently constant level of energy metabolites and calcium transients. Setting aside trivial explanations of this puzzle, what we need is to analyze experimental data obtained in studies of intracellular interactions in permeabilized cardiomyocytes described above with an adequate mathematic model, in combination with more detailed analyses of metabolic changes during the cardiac contraction cycle. This analysis will also help to understand the physiological meaning of VDAC interaction with βII-tubulin that restricts permeability of the outer mitochondrial membrane to adenine nucleotides.

Several authors have recorded cyclic changes of main metabolite concentrations during the cardiac cycle [183–185]. Fig. 8A reproduces experimental results of Wikman-Coffelt et al. in 1983 [183], Honda et al. in 2002 [184] and Spindler et al. in 2001 [185] showing the slight (8–12%) oscillations of PCr and Cr concentrations during 1 cycle. These cyclic changes were reproduced by the mathematical model of compartmentalized energy transfer corresponding to the concept of ICEUs, including the restriction of VDAC permeability [186–189]. This model was initially proposed by Aliev and Saks [186,187] and further developed by Vendelin et al. [188,189]. Mathematical modeling shows that not more than 10% of free energy is transported out of mitochondria by ATP flux needed to equilibrate the information-carrying flux of ADP into mitochondria [186]. According to this model,

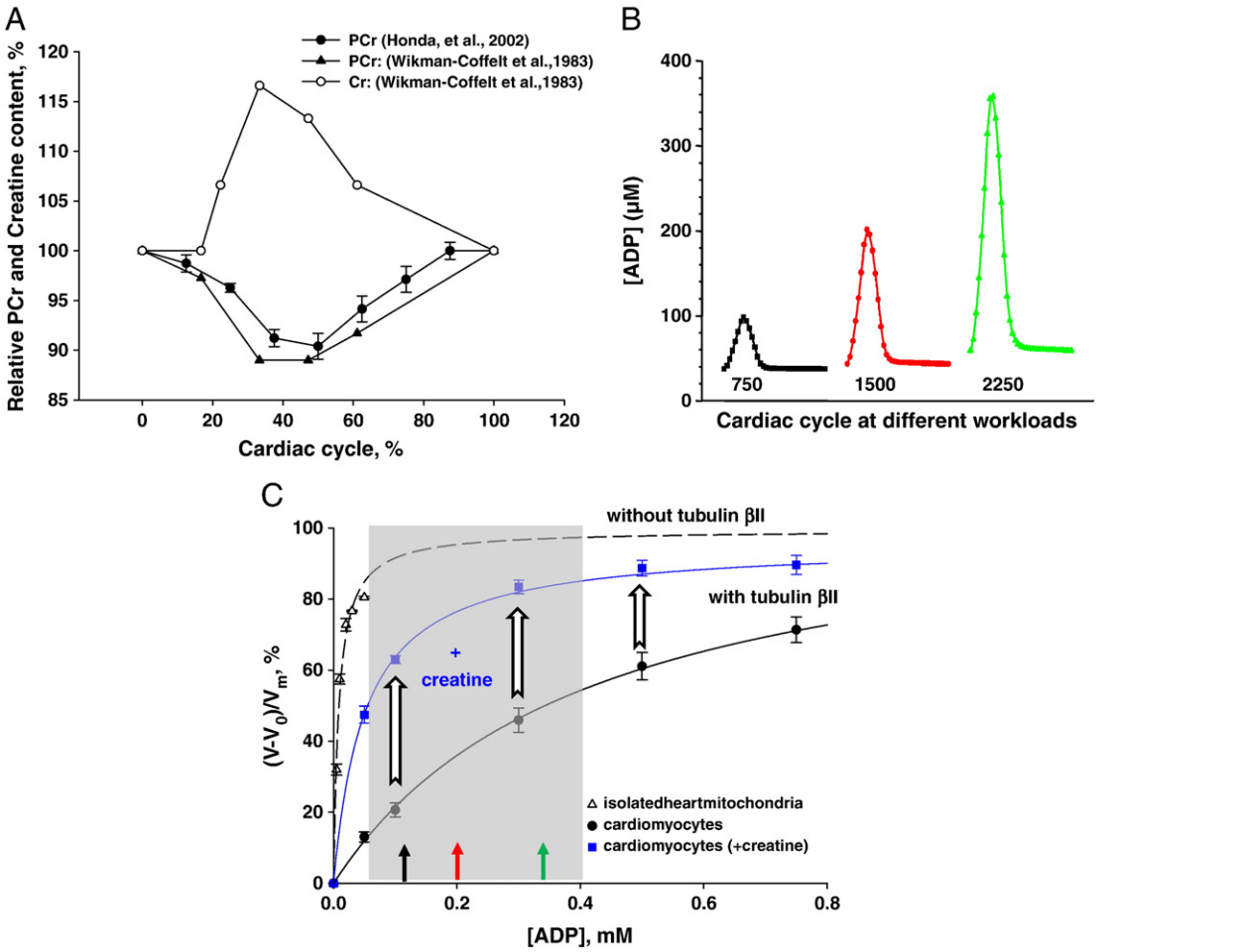

Fig. 8. Oscillations of PCr and creatine concentrations during cardiac cycle in perfused rat heart under conditions of metabolic stability. Experimental data adapted from Honda et al., 2002 [184] from gate-pacing ^{31}PMRS measurements and Wikman-Coffelt et al., 1983 [183] from rapid freeze clamp experiments. B. Mathematically modeled oscillations of ADP concentrations in the core of myofibrils over cardiac cycle at workloads equivalent to 750 (black), 1500 (red) and 2250 (green) μmol ATP s^{-1} kg^{-1}. Reproduced from [28] with permission. C. Graphical Michaelis–Menten representation of the dependence of mitochondrial respiration rate on the concentration of ADP. Colored arrows on X-axes show ADP concentrations corresponding to increased workloads from panel B. For explanation see the text.

ADP released from actomyosin crossbridges stimulates the local MMCK reaction in myofibrillar space of ICEUs and at the same time forms a gradient of concentration transmitted towards the mitochondria [186–188], Figs. 8B and C). The amplitude of displacement of MMCK from equilibrium, as well as cyclic changes of ADP are proportionally increased with workload (Fig. 8B) [28,29,31,186–188]. The rephosphorylation of ADP in MMCK reaction increases locally the Cr/PCr ratio which is transferred towards MtCK via CK/PCr shuttle [186]. The amplitude of ADP concentration changes during contraction are to our knowledge the only variables that meet the requirements for a metabolic signal formulated by O'Rourke (see above). Fig. 8C shows that the regulation of VDAC permeability by βII-tubulin is needed to induce linear responses of mitochondrial respiration to these local signals within ICEUs. When the mitochondrial outer membrane is permeable, as in isolated mitochondria, the regulation of respiration is impossible because of saturating concentrations in intracellular ADP. The latter exceeds manifold the apparent affinity of oxidative phosphorylation for free ADP ($K_m^{app}ADP = 7.9 \pm 1.6$ μM), even in diastolic phase (about 40 μM). On the contrary, when ADP diffusion is restricted at the level of MOM, as in mitochondria *in situ*, the apparent Km for free ADP increases to about 370.75 ± 30.57 μM and the respiration rate becomes almost linearly dependent on local ADP concentrations. Under these conditions, the initial rate of the hyberbolic curve can be approximated by linear dependence within the range of values corresponding to the increase in workload (Fig. 8B). Thus, cyclic changes in local ADP concentrations within the myofibrillar space of ICEUs become an effective regulatory signal due to: *i*) the non-equilibrium state of CK reactions, *ii*) the restricted VDAC permeability to metabolites elicited by association with βII-tubulin, and *iii)* the presence of creatine. When these conditions are fulfilled, activation of the coupled MtCK with MI by creatine, induces ADP/ATP recycling, increases respiration rate and displaces this linear dependence upward and to the left as shown in Fig. 8C, thus amplifying the effect of cytoplasmic ADP; and the apparent Km for ADP becomes equal to 50.24 ± 7.98 μM. These data suggest that regulation of respiration by local changes in ADP concentration, under condition of restriction of adenine nucleotides diffusion across mitochondrial membrane, is mediated by the specific structure of the MI. According to this view, the MtCK reaction amplifies the ADP signal due to its functional coupling with ATP Synthasome, thus increasing the steady state rate of adenine nucleotides recycling in mitochondria and the rate of respiration. The coupled reactions of muscle type MM CK in myofibrils and MtCK in mitochondria perform under non-equilibrium conditions and proceed in opposite directions (Fig. 9A and B) [24–34]. This mode of function results in separation of energy fluxes (mass and energy transfer by PCr) and signaling (information transfer by oscillations of cytosolic ADP concentrations, Pi and PCr/Cr ratio) which is amplified

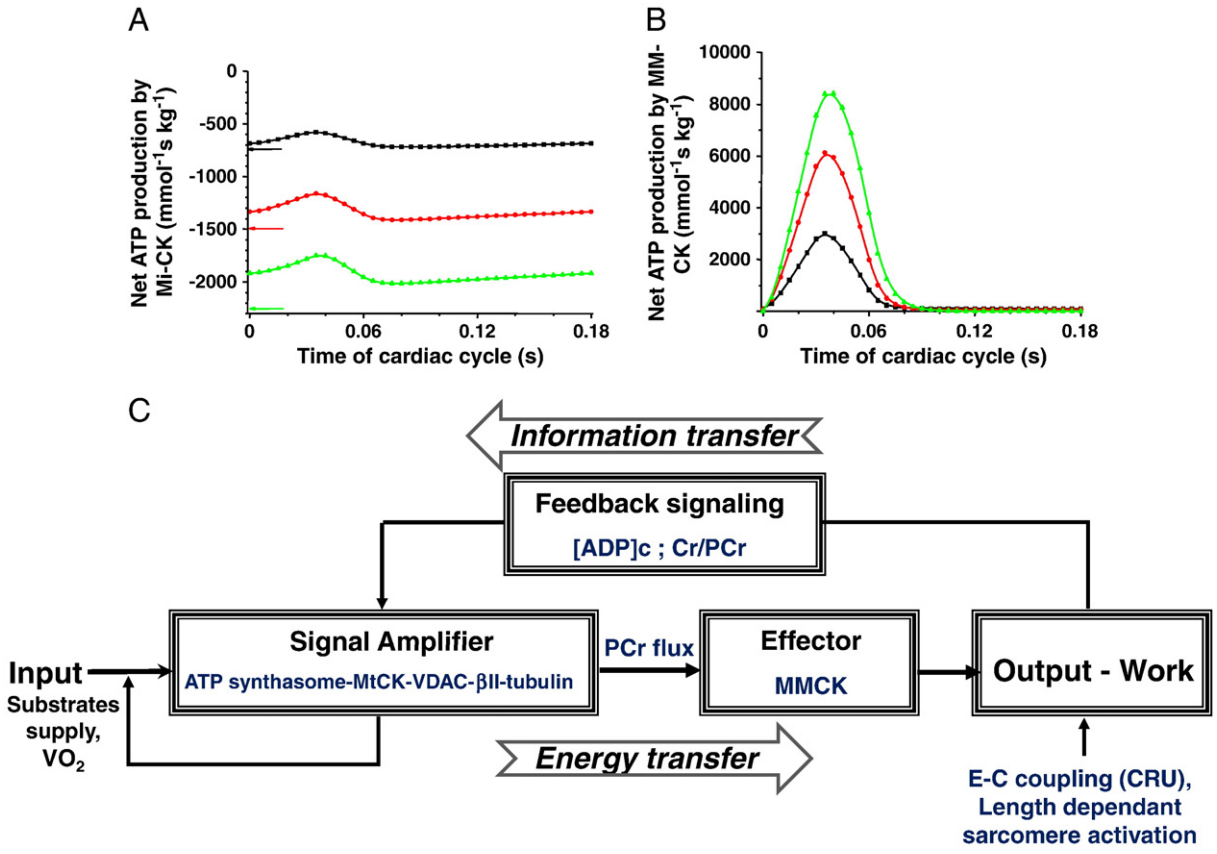

Fig. 9. A and B. Calculated net PCr production rates in non-equilibrium steady state MtCK reaction and cyclic changes in rates of ATP regeneration in non-equilibrium myofibrillar MMCK reaction during contraction cycles at different workloads correspond to oscillations of [ADP]c described in Fig. 8B (Reproduced from [28] with permission from Wiley & Sons). C. General presentation of the feedback metabolic signaling in regulation of energy metabolism within Intracellular Energetic Units in cardiac cells. Due to the non-equilibrium steady-state MtCK and non-equilibrium cyclic MMCK reactions intracellular ATP utilization (marked as output) and mitochondrial ATP regeneration (marked as input) are interconnected via the cyclic fluctuations of cytosolic ADP and Cr/PCr. For explanation see the text.

within the MI. As a result, reactions catalyzed by different isoforms of compartmentalized CK tend to maintain the intracellular metabolic stability.

The separation of energy and information transfer is illustrated by the scheme depicted in Fig. 9C. This Scheme shows feedback regulation of respiration *in vivo* corresponding to the Norbert Wiener's cybernetic principles [29,31,190]: the usage of ATP (or release of free energy of ATP hydrolysis, ΔG_{ATP}, to perform work (marked as output) and the ATP regeneration (or extraction of ΔG_{ATP} from substrates by oxidative phosphorylation; corresponding to input) are interconnected via the feedback signaling through oscillations of cytosolic concentrations in ADP, Pi and Cr/PCr amplified within MI. In this framework, the role of βII-tubulin association with MOM in cardiomyocytes would be to induce the linear response of mitochondrial respiration to workload-dependent metabolic signals. This elegant feedback mechanism of regulation of respiration on a beat-to beat basis ensures metabolic stability necessary for normal heart function, and explains well the metabolic aspect of the Frank–Starling's law of the heart, *i.e.* the linear dependence of respiration rate upon workload [12,13,28–30,186,188]. Importantly, recycling of adenine nucleotides within MI when coupled to PCr production significantly decreases also ROS levels ensuring maximal efficiency of free energy transduction in mitochondria and inhibits permeability transition pore opening [191–193], thus protecting the heart under stress conditions.

Interaction of βII-tubulin with VDAC within MI may be modified by phosphorylation [194], cytoskeletal remodeling or by structural rearrangements during the contraction cycle [195]. Most interestingly, if tubulin connects MOM to some structural elements in sarcomere, length-dependent activation of the latter may also change mitochondrial sensitivity to metabolic signaling.

4. Conclusions, perspectives and clinical significance

It is clear from the data presented in this review that the tubulin system plays important role in organizing mitochondria into Intracellular Energetic Units in cardiac cells and in the control of their functional properties. However, molecular mechanisms of the interaction of tubulin β II isotype with VDAC needs detailed further studies. In order to further verify *in vivo* some of the findings described throughout this work, we need to develop fluorescent or bioluminescent probes sensitive to ATP and ADP to monitor ICEUs function and the molecular interactions involved in the MI using FRET, fluorescence correlation spectroscopy and other techniques. Similarly to the discoveries of localized calcium domains (sparks) within CRUs [87–89], this will be most important for a quantitative description of localized mechanisms of regulation of energy fluxes in the heart. Very significant information about metabolic compartmentation of adenine nucleotides, their turnover and interaction with cellular structures can be obtained also by analysis of ^{31}P relaxation properties by NMR saturation transfer spectroscopy [71]. Numerous studies have shown that knock-out of creatine kinase isozymes or replacement of creatine by its analogs results in very significant structural and functional changes in muscle cell, a significant loss of contractile force, and perturbation of calcium metabolism (reviewed in [29,33]). In these cases, regulatory properties and the role of MI in information transfer are lost. The increase in energy transfer by other phosphotransfer pathways is another potential compensatory mechanism [196].

The results described in this review are in agreement with important clinical observations performed by Neubauer's group [197], showing that in patients with dilated cardiomyopathy a decreased PCr/ATP ratio is a strong predictor of increased mortality. In myocardial infarction and in heart failure, rapid decrease of PCr content and heart function occur, possibly due to lack of oxygen supply and pathological changes in the creatine kinase system. A significant decrease of Cr and PCr content is observed in chronic cardiac and skeletal muscle diseases [198]. Data published by Weiss et al. [199] showing that cardiac ATP flux through CK is reduced by 50% in human heart failure in the absence of reduction of ATP stores, is also in agreement with the key role played by the CK/PCr system. The links between alterations in the CK/PCr system and cardiac pathology have been extensively reviewed elsewhere [200–204]. Finally, lack of βII-tubulin and MtCK in HL-1 cells may be helpful for explaining the Warburg mechanism in cancer cells [29,33,34].

Acknowledgments

The authors are very grateful to one of anonymous reviewers of this work for correcting English of the manuscript. This work was supported by INSERM and Agence Nationale de la Recherche programme SYBECAR, France, by grant No. 7823 from the Estonian Science Foundation, SF0180114Bs08 from Estonia Ministry of Education and Science and by a research grant from the Austrian Science Fund (FWF): [P 22080-B20]. The skillful technical assistance by Igor Shevchuk, Vladimir Chekulaev and Merle Saaremäe (Tallinn, Estonia) is gratefully acknowledged. This work was presented as an invited lecture at the Bioenergetics Subgroup Symposium at the 55th Annual Meeting of the Biophysical Society (Baltimore, USA, March 5–9, 2011).

References

[1] Kitano H. Systems biology: a brief overview. Science 2002;295:1662–4.
[2] Noble D. Modeling the heart—from genes to cells to the whole organ. Science 2002;295:1678–82.
[3] Noble D. The music of life. Biology beyond the genome. Oxford, UK: Oxford University Press; 2006.
[4] Weiss JN, Yang L, Qu Z. Systems biology approaches to metabolic and cardiovascular disorders: network perspectives of cardiovascular metabolism. J Lipid Res 2006;47:2355–66.
[5] Molecular system bioenergetics. Energy for life. In: Saks V, editor. Weinheim, Germany: Wiley-VCH, Gmbh; 2007.
[6] Kohl P, Crampin EJ, Quinn TA, Noble D. Systems biology: an approach. Clin Pharmacol Ther 2010;88:25–33.
[7] Westerhoff HV, Kolodkin A, Conradie R, Wilkinson SJ, Bruggeman FJ, Krab K, et al. Systems biology towards life in silico: mathematics of the control of living cells. J Math Biol 2009;58:7–34.
[8] Noble D. Claude Bernard, the first systems biologist, and the future of physiology. Exp Physiol 2008;93:16–26.
[9] Auffray C, Nottale L. Scale relativity theory and integrative systems biology: 1. Founding principles and scale laws. Prog Biophys Mol Biol 2008;97:79–114.
[10] Saks V, Monge C, Guzun R. Philosophical basis and some historical aspects of systems biology: from Hegel to Noble — applications for bioenergetic research. Int J Mol Sci 2009;10:1161–92.
[11] Vignais P. La biologie des origines à nos jours. Les Ulis, France: EDP Sciences; 2001.
[12] Starling EH, Visscher MB. The regulation of the energy output of the heart. J Physiol 1927;62:243–61.
[13] Patterson SW, Piper H, Starling EH. The regulation of the heart beat. J Physiol 1914;48:465–513.
[14] Katz AM. Ernest Henry Starling, his predecessors, and the "Law of the Heart". Circulation 2002;106:2986–92.
[15] Opie L. The heart. Physiology, from cell to circulation. Philadelphia: Lippincott-Raven Publishers; 1998. p. 43–63.
[16] Shiels HA, White E. The Frank–Starling mechanism in vertebrate cardiac myocytes. J Exp Biol 2008;211:2005–13.
[17] Engelhardt WA. Life and science. Annu Rev Biochem 1982;51:1–19.
[18] Belitzer VA, Tsybakova ET. About mechanism of phosphorylation, respiratory coupling. Biokhimiya 1939;4:516–34.
[19] Vignais P. Science expérimentale et connaissance du vivant. La méthode et les concepts. Les Ulis, France: EDP Sciences; 2006.
[20] Nicholls DG, Ferguson SJ. Bioenergetics 3. 3 ed. New York: London Academic Press; 2002.
[21] Barth E, Stammler G, Speiser B, Schaper J. Ultrastructural quantitation of mitochondria and myofilaments in cardiac muscle from 10 different animal species including man. J Mol Cell Cardiol 1992;24:669–81.
[22] Bessman SP, Geiger PJ. Transport of energy in muscle: the phosphorylcreatine shuttle. Science 1981;211:448–52.
[23] Bessman SP, Carpenter CL. The creatine–creatine phosphate energy shuttle. Annu Rev Biochem 1985;54:831–62.
[24] Wallimann T, Wyss M, Brdiczka D, Nicolay K, Eppenberger HM. Intracellular compartmentation, structure and function of creatine kinase isoenzymes in tissues with high and fluctuating energy demands: the 'phosphocreatine circuit' for cellular energy homeostasis. Biochem J 1992;281:21–40.
[25] Wallimann T, Tokarska-Schlattner M, Neumann D, Epand RF, Andres RH, Widmer HR, et al. The phosphocreatine circuit: molecular and cellular physiology of creatine kinases, sensitivity to free radicals, and enhancement by creatine supplementation. In: Saks V, editor. Molecular system bioenergetics energy for life. Weinheim, Germany: Wiley-VCH, GmbH; 2007. p. 195–264.
[26] Saks V, Anmann T, Guzun R, Kaambre T, Sikk P, Schlattner U, et al. The creatine kinase phosphotransfer network: thermodynamic and kinetic considerations, the impact of the mitochondrial outer membrane and modelling approaches. In: Wyss M, Salomons G, editors. Creatine and Creatine Kinase in Health and Disease. Dordrecht: Springer; 2007. p. 27–66.
[27] Saks V, Beraud N, Wallimann T. Metabolic compartmentation — a system level property of muscle cells: real problems of diffusion in living cells. Int J Mol Sci 2008;9:751–67.
[28] Saks V, Dzeja P, Schlattner U, Vendelin M, Terzic A, Wallimann T. Cardiac system bioenergetics: metabolic basis of the Frank—Starling law. J Physiol 2006;571:253–73.
[29] Saks V, Guzun R, Timohhina N, Tepp K, Varikmaa M, Monge C, et al. Structure–function relationships in feedback regulation of energy fluxes in vivo in health and disease: mitochondrial interactosome. Biochim Biophys Acta 2010;1797:678–97.
[30] Saks V, Monge C, Anmann T, Dzeja P. Integrated and organized cellular energetic systems: theories of cell energetics, compartmentation and metabolic channeling. In: Saks V, editor. Molecular system bioenergetics energy for life. Weinheim, Germany: Wiley-VCH, GmbH; 2007. p. 59–110.
[31] Guzun R, Saks V. Application of the principles of systems biology and Wiener's cybernetics for analysis of regulation of energy fluxes in muscle cells in vivo. Int J Mol Sci 2010;11:982–1019.
[32] Guzun R, Timohhina N, Tepp K, Monge C, Kaambre T, Sikk P, et al. Regulation of respiration controlled by mitochondrial creatine kinase in permeabilized cardiac cells in situ. Importance of system level properties. Biochim Biophys Acta 2009;1787:1089–105.
[33] Guzun R, Timohhina N, Tepp K, Gonzalez-Granillo M, Shevchuk I, Chekulayev V, et al. Systems bioenergetics of creatine kinase networks: physiological roles of creatine and phosphocreatine in regulation of cardiac cell function. Amino Acids 2011;40:1333–48.
[34] Guzun R, Karu-Varikmaa M, Gonzalez-Granillo M, Kuznetsov AV, Michel L, Cottet-Rousselle C, et al. Mitochondria–cytoskeleton interaction: distribution of beta-tubulins in cardiomyocytes and HL-1 cells. Biochim Biophys Acta 2011;1807:458–69.
[35] Lopaschuk GD, Ussher JR, Folmes CD, Jaswal JS, Stanley WC. Myocardial fatty acid metabolism in health and disease. Physiol Rev 2010;90:207–58.
[36] Jaswal JS, Keung W, Wang W, Ussher JR, Lopaschuk GD. Targeting fatty acid and carbohydrate oxidation—a novel therapeutic intervention in the ischemic and failing heart. Biochim Biophys Acta 2011;1813:1333–50.
[37] Neely J, Morgan H. Relationship between carbohydrate and lipid metabolism and the energy balance of heart muscle. Annu Rev Physiol 1974;36:413–59.
[38] Bing RJ. Cardiac metabolism. Physiol Rev 1965;45:171–213.
[39] Bing RJ, Siegel A, Ungar I, Gilbert M. Metabolism of the human heart. II. Studies on fat, ketone and amino acid metabolism. Am J Med 1954;16:504–15.
[40] Randle PJ. Regulatory interactions between lipids and carbohydrates: the glucose fatty acid cycle after 35 years. Diabetes Metab Rev 1998;14:263–83.
[41] Randle PJ, Garland PB, Hales CN, Newsholme EA. The glucose fatty-acid cycle. Its role in insulin sensitivity and the metabolic disturbances of diabetes mellitus. Lancet 1963;1:785–9.
[42] Newsholme EA, Randle PJ. Regulation of glucose uptake by muscle. 6. Fructose 1,6-diphosphatase activity of rat heart and rat diaphragm. Biochem J 1962;83:387–92.
[43] Newsholme EA, Start C. Regulation in metabolism. London–New York–Sydney–Toronto: John Wiley&Sons Ltd.; 1973.
[44] Hue L, Taegtmeyer H. The Randle cycle revisited: a new head for an old hat. Am J Physiol Endocrinol Metab 2009;297:E578–91.
[45] Sugden MC. In appreciation of Sir Philip Randle: the glucose–fatty acid cycle. Br J Nutr 2007;97:809–13.
[46] Williamson JR. Mitochondrial function in the heart. Annu Rev Physiol 1979;41:485–506.
[47] Williamson JR, Ford C, Illingworth J, Safer B. Coordination of citric acid cycle activity with electron transport flux. Circ Res 1976;38(Suppl 1):I39–51.
[48] Neely JR, Denton RM, England PJ, Randle PJ. The effects of increased heart work on the tricarboxylate cycle and its interactions with glycolysis in the perfused rat heart. Biochem J 1972;128:147–59.
[49] Neely JR, Grotyohann LW. Role of glycolytic products in damage to ischemic myocardium. Dissociation of adenosine triphosphate levels and recovery of function of reperfused ischemic hearts. Circ Res 1984;55:816–24.
[50] Neely JR, Rovetto MJ, Oram JF. Myocardial utilization of carbohydrate and lipids. Prog Cardiovasc Dis 1972;15:289–329.
[51] Neely JR, Rovetto MJ, Whitmer JT, Morgan HE. Effects of ischemia on function and metabolism of the isolated working rat heart. Am J Physiol 1973;225:651–8.
[52] Kobayashi K, Neely JR. Control of maximum rates of glycolysis in rat cardiac muscle. Circ Res 1979;44:166–75.
[53] Sumegi B, Srere PA. Binding of the enzymes of fatty acid beta-oxidation and some related enzymes to pig heart inner mitochondrial membrane. J Biol Chem 1984;259:8748–52.

[54] Parker A, Engel PC. Preliminary evidence for the existence of specific functional assemblies between enzymes of the beta-oxidation pathway and the respiratory chain. Biochem J 2000;345:429–35.
[55] Wang Y, Mohsen AW, Mihalik SJ, Goetzman ES, Vockley J. Evidence for physical association of mitochondrial fatty acid oxidation and oxidative phosphorylation complexes. J Biol Chem 2010;285:29834–41.
[56] Saks V, Favier R, Guzun R, Schlattner U, Wallimann T. Molecular system bioenergetics: regulation of substrate supply in response to heart energy demands. J Physiol 2006;577:769–77.
[57] Camara AK, Bienengraeber M, Stowe DF. Mitochondrial approaches to protect against cardiac ischemia and reperfusion injury. Front Physiol 2011;2:13.
[58] Ashrafian H, Neubauer S. Metabolic modulation in heart failure: high time for a definitive clinical trial. Heart (British Cardiac Society) 2011;97:267–8.
[59] Lardy HA, Wellman H. Oxidative phosphorylations; role of inorganic phosphate and acceptor systems in control of metabolic rates. J Biol Chem 1952;195: 215–24.
[60] Chance B, Williams GR. A method for the localization of sites for oxidative phosphorylation. Nature 1955;176:250–4.
[61] Hansford RG, Zorov D. Role of mitochondrial calcium transport in the control of substrate oxidation. Mol Cell Biochem 1998;184:359–69.
[62] McCormack JG, Halestrap AP, Denton RM. Role of calcium ions in regulation of mammalian intramitochondrial metabolism. Physiol Rev 1990;70:391–425.
[63] Balaban RS, Kantor HL, Katz LA, Briggs RW. Relation between work and phosphate metabolite in the in vivo paced mammalian heart. Science 1986;232:1121–3.
[64] From AH, Zimmer SD, Michurski SP, Mohanakrishnan P, Ulstad VK, Thoma WJ, et al. Regulation of the oxidative phosphorylation rate in the intact cell. Biochemistry 1990;29:3731–43.
[65] Wan B, Dounen C, Duszynsky J, Salama G, Vary TC KFL. Effect of cardiac work on electrical potential gradient across mitochondrial membrane in perfused hearts. Am J Physiol Cell Physiol 1993;265:H453–60.
[66] Hassinen IE, Hiltunen K. Respiratory control in isolated perfused rat heart. Role of the equilibrium relations between the mitochondrial electron carriers and the adenylate system. Biochim Biophys Acta 1975;408:319–30.
[67] Beard DA. A biophysical model of the mitochondrial respiratory system and oxidative phosphorylation. PLoS Comput Biol 2005;1:e36.
[68] Beard DA. Modeling of oxygen transport and cellular energetics explains observations on in vivo cardiac energy metabolism. PLoS Comput Biol 2006;2:e107.
[69] Beard DA, Kushmerick MJ. Strong inference for systems biology. PLoS Comput Biol 2009;5:e1000459.
[70] Wu F, Beard DA. Roles of the creatine kinase system and myoglobin in maintaining energetic state in the working heart. BMC Syst Biol 2009;3:22.
[71] Nabuurs C, Huijbregts B, Wieringa B, Hibers CW, Heerschap A. ^{31} P saturation transfer spectroscopy predicts differential intracellular association of ATP and ADP in skeletal muscle. J Biol Chem 2010;285:39588–96.
[72] Shimizu J, Todaka K, Burkhoff D. Load dependence of ventricular performance explained by model of calcium–myofilament interactions. Am J Physiol Heart Circ Physiol 2002;282:H1081–91.
[73] Balaban RS. Cardiac energy metabolism homeostasis: role of cytosolic calcium. J Mol Cell Cardiol 2002;34:1259–71.
[74] Yaniv Y, Juhaszova M, Nuss HB, Wang S, Zorov DB, Lakatta EG, et al. Matching ATP supply and demand in mammalian heart: in vivo, in vitro, and in silico perspectives. Ann N Y Acad Sci 2010;1188:133–42.
[75] Griffiths EJ, Rutter GA. Mitochondrial calcium as a key regulator of mitochondrial ATP production in mammalian cells. Biochim Biophys Acta 2009;1787:1324–33.
[76] Liu T, O'Rourke B. Regulation of mitochondrial Ca(2+) and its effects on energetics and redox balance in normal and failing heart. J Bioenerg Biomembr 2009;41:127–32.
[77] Schrödinger E. What is life? The physical aspect of the living cell. Cambridge, UK: Cambridge University Press; 1944.
[78] Qian H. Open-system non-equilibrium steady state: statistical thermodynamics, fluctuations, and chemical oscillations. J Phys Chem 2006;110:15063–74.
[79] Prigogine I, Nicolis G. Self-organization in nonequilibrium systems: from dissipative structures to order through fluctuations. New York: John Wiley & Sons Inc.; 1977.
[80] de la Fuente IM. Quantitative analysis of cellular metabolic dissipative, self-organized structures. Int J Mol Sci 2010;11:3540–99.
[81] de la Fuente IM. Quantitative analysis of cellular metabolic dissipative, self-organized structures. Int J Mol Sci 2011;11:3540–99.
[82] De La Fuente IM, Martinez L, Perez-Samartin AL, Ormaetxea L, Amezaga C, Vera-Lopez A. Global self-organization of the cellular metabolic structure. PLoS One 2008;3:e3100.
[83] Aon MA, Cortassa S. Dynamic biological organization. Fundamentals as applied to cellular systems. London: Chapman & Hall; 1997.
[84] Cortassa S, Aon MA, Iglesias AA, Lloyd D. An introduction to metabolic and cellular engineering. Singapore: World Scientific; 2002. p. 248.
[85] Saks VA, Kaambre T, Sikk P, Eimre M, Orlova E, Paju K, et al. Intracellular energetic units in red muscle cells. Biochem J 2001;356:643–57.
[86] Seppet EK, Kaambre T, Sikk P, Tiivel T, Vija H, Tonkonogi M, et al. Functional complexes of mitochondria with Ca, MgATPases of myofibrils and sarcoplasmic reticulum in muscle cells. Biochim Biophys Acta 2001;1504:379–95.
[87] Wang SQ, Wei C, Zhao G, Brochet DX, Shen J, Song LS, et al. Imaging microdomain Ca^{2+} in muscle cells. Circ Res 2004;94:1011–22.
[88] Maltsev AV, Maltsev VA, Mikheev M, Maltseva LA, Sirenko SG, Lakatta EG, et al. Synchronization of stochastic Ca^{2+} release units creates a rhythmic Ca^{2+} clock in cardiac pacemaker cells. Biophys J 2011;100:271–83.
[89] Rovetti R, Cui X, Garfinkel A, Weiss JN, Qu Z. Spark-induced sparks as a mechanism of intracellular calcium alternans in cardiac myocytes. Circ Res 2010;106:1582–91.
[90] Sommer J, Jennings R. Ultrastructure of cardiac muscle. In: Fozzard H, Haber E, Jennings R, Katz A, Morgan H, editors. The heart and cardiovascular system. New York: Raven; 1986. p. 61–100.
[91] Fawcett DW, McNutt NS. The ultrastructure of the cat myocardium. I. Ventricular papillary muscle. J Cell Biol 1969;42:1–45.
[92] Forbes MS. Ultrastructure of mammalian cardiac muscle. Boston: Nijhoff; 1984.
[93] Vendelin M, Beraud N, Guerrero K, Andrienko T, Kuznetsov AV, Olivares J, et al. Mitochondrial regular arrangement in muscle cells: a "crystal-like" pattern. Am J Physiol Cell Physiol 2005;288:C757–67.
[94] Beraud N, Pelloux S, Usson Y, Kuznetsov AV, Ronot X, Tourneur Y, et al. Mitochondrial dynamics in heart cells: very low amplitude high frequency fluctuations in adult cardiomyocytes and flow motion in non beating Hl-1 cells. J Bioenerg Biomembr 2009;41:195–214.
[95] Collins TJ, Berridge MJ, Lipp P, Bootman MD. Mitochondria are morphologically and functionally heterogeneous within cells. EMBO J 2002;21:1616–27.
[96] Collins TJ, Bootman MD. Mitochondria are morphologically heterogeneous within cells. J Exp Biol 2003;206:1993–2000.
[97] Rizzuto R, Pinton P, Carrington W, Fay FS, Fogarty KE, Lifshitz LM, et al. Close contacts with the endoplasmic reticulum as determinants of mitochondrial Ca^{2+} responses. Science 1998;280:1763–6.
[98] Kuznetsov AV, Hermann M, Troppmair J, Margreiter R, Hengster P. Complex patterns of mitochondrial dynamics in human pancreatic cells revealed by fluorescent confocal imaging. J Cell Mol Med 2010;14:417–25.
[99] Zorov DB, Filburn CR, Klotz LO, Zweier JL, Sollott SJ. Reactive oxygen species (ROS)-induced ROS release: a new phenomenon accompanying induction of the mitochondrial permeability transition in cardiac myocytes. J Exp Med 2000;192: 1001–14.
[100] Kuznetsov AV, Margreiter R. Heterogeneity of mitochondria and mitochondrial function within cells as another level of mitochondrial complexity. Int J Mol Sci 2009;10:1911–29.
[101] Cortassa S, Aon MA, Winslow RL, O'Rourke B. A mitochondrial oscillator dependent on reactive oxygen species. Biophys J 2004;87:2060–73.
[102] Knight MM, Roberts SR, Lee DA, Bader DL. Live cell imaging using confocal microscopy induces intracellular calcium transients and cell death. Am J Physiol Cell Physiol 2003;284:C1083–9.
[103] Wang W, Fang H, Groom L, Cheng A, Zhang W, Liu J, et al. Superoxide flashes in single mitochondria. Cell 2008;134:279–90.
[104] Kuznetsov AV, Troppmair J, Sucher R, Hermann M, Saks V, Margreiter R. Mitochondrial subpopulations and heterogeneity revealed by confocal imaging: possible physiological role? Biochim Biophys Acta 2006;1757:686–91.
[105] Chan DC. Mitochondria: dynamic organelles in disease, aging, and development. Cell 2006;125:1241–52.
[106] Chen H, Chan DC. Emerging functions of mammalian mitochondrial fusion and fission. Spec No. 2Hum Mol Genet 2005;14:R283–9.
[107] Chen H, Chomyn A, Chan DC. Disruption of fusion results in mitochondrial heterogeneity and dysfunction. J Biol Chem 2005;280:26185–92.
[108] Frank S, Gaume B, Bergmann-Leitner ES, Leitner WW, Robert EG, Catez F, et al. The role of dynamin-related protein 1, a mediator of mitochondrial fission, in apoptosis. Dev Cell 2001;1:515–25.
[109] Parra V, Verdejo H, Del Campo A, Pennanen C, Kuzmici J, Iglewski M, et al. The complex interplay between mitochondrial dynamics and cardiac metabolism. J Bioenerg Biomembr 2011;43:47–51.
[110] Kane LA, Youle RJ. Mitochondrial fission and fusion and their roles in the heart. J Mol Med (Berlin, Germany) 2010;88:971–9.
[111] Jezek P, Plecita-Hlavata L, Smolkova K, Rossignol R. Distinctions and similarities of cell bioenergetics and the role of mitochondria in hypoxia, cancer, and embryonic development. Int J Biochem Cell Biol 2010;42:604–22.
[112] Skulachev VP, Bakeeva LE, Chernyak BV, Domnina LV, Minin AA, Pletjushkina OY, et al. Thread–grain transition of mitochondrial reticulum as a step of mitoptosis and apoptosis. Mol Cell Biochem 2004;256–257:341–58.
[113] Karbowski M, Youle RJ. Dynamics of mitochondrial morphology in healthy cells and during apoptosis. Cell Death Differ 2003;10:870–80.
[114] Sun CN, Dhalla NS, Olson RE. Formation of gigantic mitochondria in hypoxic isolated perfused rat hearts. Experientia 1969;25:763–4.
[115] Shen T, Zheng M, Cao C, Chen C, Tang J, Zhang W, et al. Mitofusin-2 is a major determinant of oxidative stress-mediated heart muscle cell apoptosis. J Biol Chem 2007;282:23354–61.
[116] Capetanaki Y, Bloch RJ, Kouloumenta A, Mavroidis M, Psarras S. Muscle intermediate filaments and their links to membranes and membranous organelles. Exp Cell Res 2007;313:2063–76.
[117] Ball EH, Singer SJ. Mitochondria are associated with microtubules and not with intermediate filaments in cultured fibroblasts. Proc Natl Acad Sci USA 1982;79: 123–6.
[118] Mose-Larsen P, Bravo R, Fey SJ, Small JV, Celis JE. Putative association of mitochondria with a subpopulation of intermediate-sized filaments in cultured human skin fibroblasts. Cell 1982;31:681–92.
[119] Hirokawa N. Cross-linker system between neurofilaments, microtubules, and membranous organelles in frog axons revealed by the quick-freeze, deep-etching method. J Cell Biol 1982;94:129–42.
[120] Heggeness MH, Simon M, Singer SJ. Association of mitochondria with microtubules in cultured cells. Proc Natl Acad Sci USA 1978;75:3863–6.
[121] Rappaport L, Oliviero P, Samuel JL. Cytoskeleton and mitochondrial morphology and function. Mol Cell Biochem 1998;184:101–5.

[122] Anesti V, Scorrano L. The relationship between mitochondrial shape and function and the cytoskeleton. Biochim Biophys Acta 2006;1757:692–9.
[123] Gordon AM, Homsher E, Regnier M. Regulation of contraction in striated muscle. Physiol Rev 2000;80:853–924.
[124] Redeker V. Mass spectrometry analysis of C-terminal posttranslational modifications of tubulins. Methods Cell Biol 2010;95:77–103.
[125] Luduena RF. Multiple forms of tubulin: different gene products and covalent modifications. Int Rev Cytol 1998;178:207–75.
[126] Sackett DL. Evolution and coevolution of tubulin's carboxy-terminal tails and mitochondria. In: Svensson OL, editor. Mitochondria: structure, functions and dysfunctions. USA: Nova Science Publishers; 2010. p. 441–70.
[127] Aon MA, Cortassa S. Coherent and robust modulation of a metabolic network by cytoskeletal organization and dynamics. Biophys Chem 2002;97:213–31.
[128] Aon MA, O'Rourke B, Cortassa S. The fractal architecture of cytoplasmic organization: scaling, kinetics and emergence in metabolic networks. Mol Cell Biochem 2004;256–257:169–84.
[129] Guerrero K, Monge C, Bruckner A, Puurand U, Kadaja L, Kaambre T, et al. Study of possible interactions of tubulin, microtubular network, and STOP protein with mitochondria in muscle cells. Mol Cell Biochem 2010;337:239–49.
[130] Vertessy BG, Orosz F, Kovacs J, Ovadi J. Alternative binding of two sequential glycolytic enzymes to microtubules. Molecular studies in the phosphofructokinase/aldolase/microtubule system. J Biol Chem 1997;272:25542–6.
[131] Wolff J. Plasma membrane tubulin. Biochim Biophys Acta 2009;1788:1415–33.
[132] Kostin S, Hein S, Arnon E, Scholz D, Schaper J. The cytoskeleton and related proteins in the human failing heart. Heart Fail Rev 2000;5:271–80.
[133] Schaper J, Kostin S, Hein S, Elsasser A, Arnon E, Zimmermann R. Structural remodelling in heart failure. Exp Clin Cardiol 2002;7:64–8.
[134] Eckel J, Reinauer H. Effects of microtubule-disrupting agents on insulin binding and degradation in isolated cardiocytes from adult rat. Hoppe Seylers Z Physiol Chem 1983;364:845–50.
[135] Tagawa H, Koide M, Sato H, Zile MR, Carabello BA, Cooper Gt. Cytoskeletal role in the transition from compensated to decompensated hypertrophy during adult canine left ventricular pressure overloading. Circ Res 1998;82:751–61.
[136] Saetersdal T, Greve G, Dalen H. Associations between beta-tubulin and mitochondria in adult isolated heart myocytes as shown by immunofluorescence and immunoelectron microscopy. Histochemistry 1990;95:1–10.
[137] Schroder R, Kunz WS, Rouan F, Pfendner E, Tolksdorf K, Kappes-Horn K, et al. Disorganization of the desmin cytoskeleton and mitochondrial dysfunction in plectin-related epidermolysis bullosa simplex with muscular dystrophy. J Neuropathol Exp Neurol 2002;61:520–30.
[138] Konieczny P, Fuchs P, Reipert S, Kunz WS, Zeold A, Fischer I, et al. Myofiber integrity depends on desmin network targeting to Z-disks and costameres via distinct plectin isoforms. J Cell Biol 2008;181:667–81.
[139] Konieczny P, Wiche G. Muscular integrity—a matter of interlinking distinct structures via plectin. Adv Exp Med Biol 2008;642:165–75.
[140] Rezniczek GA, Abrahamsberg C, Fuchs P, Spazierer D, Wiche G. Plectin 5′-transcript diversity: short alternative sequences determine stability of gene products, initiation of translation and subcellular localization of isoforms. Hum Mol Genet 2003;12:3181–94.
[141] Rezniczek GA, Konieczny P, Nikolic B, Reipert S, Schneller D, Abrahamsberg C, et al. Plectin 1f scaffolding at the sarcolemma of dystrophic (mdx) muscle fibers through multiple interactions with beta-dystroglycan. J Cell Biol 2007;176:965–77.
[142] Winter L, Abrahamsberg C, Wiche G. Plectin isoform 1b mediates mitochondrion-intermediate filament network linkage and controls organelle shape. J Cell Biol 2008;181:903–11.
[143] Claycomb WC, Lanson NA, Stallworth BS, Egeland DB, Delcaprio A, Bahinski A, et al. HL-1 cells: a cardiac muscle cell line that contracts and retains phenotypic characteristics of the adult cardiomyocyte. Proc Natl Acad Sci USA 1998;95:2979–84.
[144] Pelloux S, Robillard J, Ferrera R, Bilbaut A, Ojeda C, Saks V, et al. Non beating HL-1 cells for confocal microscopy. Application to mitochondrial functions during cardiac preconditioning. Prog Biophys Mol Biol 2006;90:270–98.
[145] Kummel L. Ca, Mg-ATPase activity of permeabilised rat heart cells and its functional coupling to oxidative phosphorylation of the cells. Cardiovasc Res 1988;22:359–67.
[146] Saks VA, Belikova YO, Kuznetsov AV. In vivo regulation of mitochondrial respiration in cardiomyocytes: specific restrictions for intracellular diffusion of ADP. Biochim Biophys Acta 1991;1074:302–11.
[147] Saks VA, Vasil'eva E, Belikova Yu O, Kuznetsov AV, Lyapina S, Petrova L, et al. Retarded diffusion of ADP in cardiomyocytes: possible role of mitochondrial outer membrane and creatine kinase in cellular regulation of oxidative phosphorylation. Biochim Biophys Acta 1993;1144:134–48.
[148] Kuznetsov AV, Tiivel T, Sikk P, Kaambre T, Kay L, Daneshrad Z, et al. Striking differences between the kinetics of regulation of respiration by ADP in slow-twitch and fast-twitch muscles in vivo. Eur J Biochem/FEBS 1996;241:909–15.
[149] Saks VA, Khuchua ZA, Vasilyeva EV, Belikova O, Kuznetsov AV. Metabolic compartmentation and substrate channelling in muscle cells. Role of coupled creatine kinases in in vivo regulation of cellular respiration — a synthesis. Mol Cell Biochem 1994;133–134:155–92.
[150] Saks VA, Kuznetsov AV, Khuchua ZA, Vasilyeva EV, Belikova JO, Kesvatera T, et al. Control of cellular respiration in vivo by mitochondrial outer membrane and by creatine kinase. A new speculative hypothesis: possible involvement of mitochondrial–cytoskeleton interactions. J Mol Cell Cardiol 1995;27:625–45.
[151] Kuznetsov AV, Veksler V, Gellerich FN, Saks V, Margreiter R, Kunz WS. Analysis of mitochondrial function in situ in permeabilized muscle fibers, tissues and cells. Nat Protoc 2008;3:965–76.
[152] Appaix F, Kuznetsov AV, Usson Y, Kay L, Andrienko T, Olivares J, et al. Possible role of cytoskeleton in intracellular arrangement and regulation of mitochondria. Exp Physiol 2003;88:175–90.
[153] Rostovtseva TK, Sheldon KL, Hassanzadeh E, Monge C, Saks V, Bezrukov SM, et al. Tubulin binding blocks mitochondrial voltage-dependent anion channel and regulates respiration. Proc Natl Acad Sci USA 2008;105:18746–51.
[154] Rostovtseva TK, Bezrukov SM. VDAC regulation: role of cytosolic proteins and mitochondrial lipids. J Bioenerg Biomembr 2008;40:163–70.
[155] Monge C, Beraud N, Kuznetsov AV, Rostovtseva T, Sackett D, Schlattner U, et al. Regulation of respiration in brain mitochondria and synaptosomes: restrictions of ADP diffusion in situ, roles of tubulin, and mitochondrial creatine kinase. Mol Cell Biochem 2008;318:147–65.
[156] Bernier-Valentin F, Rousset B. Interaction of tubulin with rat liver mitochondria. J Biol Chem 1982;257:7092–9.
[157] Carre M, Andre N, Carles G, Borghi H, Brichese L, Briand C, et al. Tubulin is an inherent component of mitochondrial membranes that interacts with the voltage-dependent anion channel. J Biol Chem 2002;277:33664–9.
[158] Anmann T, Guzun R, Beraud N, Pelloux S, Kuznetsov AV, Kogerman L, et al. Different kinetics of the regulation of respiration in permeabilized cardiomyocytes and in HL-1 cardiac cells. Importance of cell structure/organization for respiration regulation. Biochim Biophys Acta 2006;1757:1597–606.
[159] Eimre M, Paju K, Pelloux S, Beraud N, Roosimaa M, Kadaja L, et al. Distinct organization of energy metabolism in HL-1 cardiac cell line and cardiomyocytes. Biochim Biophys Acta 2008;1777:514–24.
[160] Monge C, Beraud N, Tepp K, Pelloux S, Chahboun S, Kaambre T, et al. Comparative analysis of the bioenergetics of adult cardiomyocytes and nonbeating HL-1 cells: respiratory chain activities, glycolytic enzyme profiles, and metabolic fluxes. Can J Physiol Pharmacol 2009;87:318–26.
[161] Timohhina N, Guzun R, Tepp K, Monge C, Varikmaa M, Vija H, et al. Direct measurement of energy fluxes from mitochondria into cytoplasm in permeabilized cardiac cells in situ: some evidence for Mitochondrial Interactosome. J Bioenerg Biomembr 2009;41:259–75.
[162] Schlattner U, Wallimann T. Metabolite channeling: creatine kinase microcompartments. In: Lennarz WJ, Lane MD, editors. Encyclopedia of biological chemistry. New York, USA: Academic Press; 2004. p. 646–51.
[163] Schlattner U, Tokarska-Schlattner M, Wallimann T. Mitochondrial creatine kinase in human health and disease. Biochim Biophys Acta Feb 2006;1762(2):164–80.
[164] Klingenberg M. The ADP and ATP transport in mitochondria and its carrier. Biochim Biophys Acta 2008;1778:1978–2021.
[165] Saks VA, Chernousova GB, Gukovsky DE, Smirnov VN, Chazov EI. Studies of energy transport in heart cells. Mitochondrial isoenzyme of creatine phosphokinase: kinetic properties and regulatory action of Mg^{2+} ions. FEBS 1975;57:273–90.
[166] Jacobus WE, Saks VA. Creatine kinase of heart mitochondria: changes in its kinetic properties induced by coupling to oxidative phosphorylation. Arch Biochem Biophys 1982;219:167–78.
[167] Kuznetsov AV, Khuchua ZA, Vassil'eva EV, Medved'eva NV, Saks VA. Heart mitochondrial creatine kinase revisited: the outer mitochondrial membrane is not important for coupling of phosphocreatine production to oxidative phosphorylation. Arch Biochem Biophys 1989;268:176–90.
[168] Saks VA, Vendelin M, Aliev MK, Kekelidze T, Engelbrecht J. Mechanisms and modeling of energy transfer between and among intracellular compartments. In: Dienel G, Gibson G, editors. Handbook of neurochemistry and molecular neurobiology. 3rd ed. New York–Boston, USA: Springer Science and Business Media; 2007. p. 815–60.
[169] Barbour RL, Ribaudo J, Chan SH. Effect of creatine kinase activity on mitochondrial ADP/ATP transport. Evidence for a functional interaction. J Biol Chem 1984;259:8246–51.
[170] Saks VA, Khuchua ZA, Kuznetsov AV. Specific inhibition of ATP-ADP translocase in cardiac mitoplasts by antibodies against mitochondrial creatine kinase. Biochim Biophys Acta 1987;891:138–44.
[171] Kim IH, Lee HJ. Oxidative phosphorylation of creatine by respiring pig heart mitochondria in the absence of added adenine nucleotides. Biochem Int 1987;14:103–10.
[172] Colombini M. VDAC: the channel at the interface between mitochondria and the cytosol. Mol Cell Biochem 2004;256–257:107–15.
[173] Colombini M. The published 3D structure of the VDAC channel: native or not? Trends Biochem Sci 2009;34:382–9.
[174] Gellerich F, Saks VA. Control of heart mitochondrial oxygen consumption by creatine kinase: the importance of enzyme localization. Biochem Biophys Res Commun 1982;105:1473–81.
[175] Chen C, Ko Y, Delannoy M, Ludtke SJ, Chiu W, Pedersen PL. Mitochondrial ATP synthasome: three-dimensional structure by electron microscopy of the ATP synthase in complex formation with carriers for Pi and ADP/ATP. J Biol Chem 2004;279:31761–8.
[176] Brdiszka D. Mitochondrial VDAC and its complexes. In: Saks V, editor. Molecular system bioenergetics energy for life. Weinheim, Germany: Wiley-VCH, GmbH; 2007. p. 165–94.
[177] Song J, Midson C, Blachly-Dyson E, Forte M, Colombini M. The sensor regions of VDAC are translocated from within the membrane to the surface during gating processes. Biophys J 1998;74:2926–44.
[178] Mitchell P. Compartmentation and communication in living cells. Ligand conduction: a general catalytic principal in chemical, osmotic and chemiosmotic reaction systems. Eur J Biochem 1979;95:1–20.
[179] Laue T, Demeler B. A postreductionist framework for protein biochemistry. Nat Chem Biol 2011;7:331–4.

[180] Tepp K, Timohhina N, Chekulayev V, Shevchuk I, Kaambre T, Saks V. Metabolic control analysis of integrated energy metabolism in permeabilized cardiomyocytes — experimental study. Acta Biochim Pol 2010;57:421–30.
[181] Kholodenko BN, Rohwer JM, Cascante M, Westerhoff HV. Subtleties in control by metabolic channelling and enzyme organization. Mol Cell Biochem 1998;184: 311–20.
[182] Kholodenko BN, Westerhoff HV. Metabolic channelling and control of the flux. FEBS Lett 1993;320:71–4.
[183] Wikman-Coffelt J, Sievers R, Coffelt RJ, Parmley WW. The cardiac cycle: regulation and energy oscillations. Am J Physiol 1983;245:H354–62.
[184] Honda H, Tanaka K, Akita N, Haneda T. Cyclical changes in high-energy phosphates during the cardiac cycle by pacing-Gated 31P nuclear magnetic resonance. Circ J 2002;66:80–6.
[185] Spindler M, Illing B, Horn M, de Groot M, Ertl G, Neubauer S. Temporal fluctuations of myocardia high-energy phosphate metabolite with the cardiac cycle. Basic Res Cardiol 2001;96:553–6.
[186] Aliev MK, Saks VA. Compartmentalized energy transfer in cardiomyocytes: use of mathematical modeling for analysis of in vivo regulation of respiration. Biophys J 1997;73:428–45.
[187] Saks VA, Ventura-Clapier R, Aliev MK. Metabolic control and metabolic capacity: two aspects of creatine kinase functioning in the cells. Biochim Biophys Acta 1996;1274:81–8.
[188] Vendelin M, Kongas O, Saks V. Regulation of mitochondrial respiration in heart cells analyzed by reaction-diffusion model of energy transfer. Am J Physiol Cell Physiol 2000;278:C747–64.
[189] Saks VA, Kongas O, Vendelin M, Kay L. Role of the creatine/phosphocreatine system in the regulation of mitochondrial respiration. Acta Physiol Scand 2000;168:635–41.
[190] Wiener N. Cybernetics or control and communication in the animal and the machine. Second Edition. Cambridge, Massachussets: The MIT Press; 1965.
[191] Meyer LE, Machado LB, Santiago AP, da-Silva WS, De Felice FG, Holub O, et al. Mitochondrial creatine kinase activity prevents reactive oxygen species generation: antioxidant role of mitochondrial kinase-dependent ADP re-cycling activity. J Biol Chem 2006;281:37361–71.
[192] Dolder M, Walzel B, Speer O, Schlattner U, Wallimann T. Inhibition of the mitochondrial permeability transition by creatine kinase substrates. Requirement for microcompartmentation. J Biol Chem 2003;278:17760–6.
[193] Aon MA, Cortassa S, O'Rourke B. Redox-optimized ROS balance: a unifying hypothesis. Biochim Biophys Acta 2010;1797:865–77.
[194] Sheldon L, Bezrukov SM TKR. VDAC phosphorylation regulates interaction with tubulin. Biophysical Meeting, 3824. San Francisco Poster; 2010.
[195] Fuchs F, Smith SH. Calcium, cross-bridges, and the Frank–Starling relationship. News Physiol Sci 2001;16:5–10.
[196] Dzeja P, Chung S, Terzic A. Integration of adenylate kinase and glycolytic and clycogenolytic circuits in cellular energetics. In: Saks V, editor. Molecular system bioenergetics energy for life. Weinheim, Germany: Wiley-VCH, GmbH; 2007. p. 195–264.
[197] Neubauer S. The failing heart—an engine out of fuel. N Engl J Med 2007;356: 1140–51.
[198] Nascimben L, Ingwall JS, Pauletto P, Friedrich J, Gwathmey JK, Saks V, et al. Creatine kinase system in failing and nonfailing human myocardium. Circulation 1996;94:1894–901.
[199] Weiss RG, Gerstenblith G, Bottomley PA. ATP flux through creatine kinase in the normal, stressed, and failing human heart. Proc Natl Acad Sci USA 2005;102: 808–13.
[200] Ingwall JS. On the hypothesis that the failing heart is energy starved: lessons learned from the metabolism of ATP and creatine. Curr Hypertens Rep 2006;8: 457–64.
[201] Ingwall JS, Weiss RG. Is the failing heart energy starved? On using chemical energy to support cardiac function. Circ Res 2004;95:135–45.
[202] Ventura-Clapier R, Garnier A, Veksler V. Energy metabolism in heart failure. J Physiol 2004;555:1–13.
[203] Ventura-Clapier R. Exercise training, energy metabolism, and heart failure. Applied physiology, nutrition, and metabolism. Physiologie Appliquee, Nutrition et Metabolisme 2009;34:336–9.
[204] Ventura-Clapier R, De Sousa E, Veksler V. Metabolic myopathy in heart failure. News Physiol Sci 2002;17:191–6.

Journal of Molecular and Cellular Cardiology 52 (2012) 437–447

Contents lists available at ScienceDirect

Journal of Molecular and Cellular Cardiology

journal homepage: www.elsevier.com/locate/yjmcc

Original article

Studies of the role of tubulin beta II isotype in regulation of mitochondrial respiration in intracellular energetic units in cardiac cells

Marcela Gonzalez-Granillo [a], Alexei Grichine [b], Rita Guzun [a], Yves Usson [b], Kersti Tepp [c], Vladimir Chekulayev [c], Igor Shevchuk [c], Minna Karu-Varikmaa [c], Andrey V. Kuznetsov [d], Michael Grimm [d], Valdur Saks [a,c,*], Tuuli Kaambre [c]

[a] INSERM U1055, Laboratory of Fundamental and Applied Bioenergetics, Joseph Fourier University, Grenoble, France
[b] Life science imaging —in vitro platform, IAB CRI U823 Inserm/Joseph Fourier University, France
[c] Laboratory of Bioenergetics, National Institute of Chemical Physics and Biophysics, Tallinn, Estonia
[d] Cardiac Surgery Research Laboratory, Department of Heart Surgery, Innsbruck Medical University, Innsbruck, Austria

ARTICLE INFO

Article history:
Received 2 June 2011
Received in revised form 5 July 2011
Accepted 28 July 2011
Available online 5 August 2011

Keywords:
Cardiomyocytes
Cytoskeleton
Mitochondria
Tubulin
Regulation of respiration
Energy fluxes

ABSTRACT

The aim of this study was to investigate the possible role of tubulin βII, a cytoskeletal protein, in regulation of mitochondrial oxidative phosphorylation and energy fluxes in heart cells. This isotype of tubulin is closely associated with mitochondria and co-expressed with mitochondrial creatine kinase (MtCK). It can be rapidly removed by mild proteolytic treatment of permeabilized cardiomyocytes in the absence of stimulatory effect of cytochrome c, that demonstrating the intactness of the outer mitochondrial membrane. Contrary to isolated mitochondria, in permeabilized cardiomyocytes (*in situ* mitochondria) the addition of pyruvate kinase (PK) and phosphoenolpyruvate (PEP) in the presence of creatine had no effect on the rate of respiration controlled by activated MtCK, showing limited permeability of voltage-dependent anion channel (VDAC) in mitochondrial outer membrane (MOM) for ADP regenerated by MtCK. Under normal conditions, this effect can be considered as one of the most sensitive tests of the intactness of cardiomyocytes and controlled permeability of MOM for adenine nucleotides. However, proteolytic treatment of permeabilized cardiomyocytes with trypsin, by removing mitochondrial βII tubulin, induces high sensitivity of MtCK-regulated respiration to PK–PEP, significantly changes its kinetics and the affinity to exogenous ADP. MtCK coupled to ATP synthasome and to VDAC controlled by tubulin βII provides functional compartmentation of ATP in mitochondria and energy channeling into cytoplasm via phosphotransfer network. Therefore, direct transfer of mitochondrially produced ATP to sites of its utilization is largely avoided under physiological conditions, but may occur in pathology when mitochondria are damaged. This article is part of a Special Issue entitled "Local Signaling in Myocytes".

1. Introduction

Experimental studies of the mechanisms of regulation of mitochondrial function by feedback metabolic signaling *in vivo*[1–15] need the use of the permeabilized cells or fibers technique [16–24] and methods of *in vivo* kinetic studies [4–7]. Intensive investigations during the last two decades with use of these techniques have shown that the regulation of mitochondrial function *in vivo* is very different from that *in vitro*: the apparent Km for exogenous ADP in regulation of respiration is 20–30 times higher in the permeabilized cells than in isolated mitochondria *in vitro*[8–24]. This high apparent Km for ADP can be decreased by addition of creatine that activates mitochondrial creatine kinase, MtCK [8,13,19,20], or by the controlled proteolytic treatment [21–24]. The apparent Km for exogenous ADP shows the availability of ADP for the adenine nucleotide translocase (ANT) in mitochondrial inner membrane (MIM) and was proposed to be dependent on the permeability of the mitochondrial outer membrane's (MOM) voltage-dependent anion channel (VDAC) [22,23]. A strong decrease of the apparent Km for exogenous ADP produced by trypsin treatment pointed to the possible involvement of some cytoskeleton-related protein(s) in the control of the VDAC permeability originally referred to as "factor X" [22,23]. Appaix et al. [24] have shown that among cytoskeletal proteins sensitive to short

Abbreviations: ANT, adenine nucleotide translocase; BSA, bovine serum albumin; ATR, atractyloside; CK, creatine kinase; Cr, creatine; DTT, dithiothreitol; IM, isolation medium; IMS, mitochondrial intermembrane space; MI, Mitochondrial Interactosome; MIM, mitochondrial inner membrane; MOM, mitochondrial outer membrane; MtCK, mitochondrial creatine kinase; PCr, phosphocreatine; PBS, phosphate buffer solution; PEP, phosphoenolpyruvate; PK, pyruvate kinase; STI, soybean trypsin inhibitor; VDAC, voltage-dependent anion channel; WS, washing solution.

* Corresponding author at: Laboratory of Bioenergetics, National Institute of Chemical Physics and Biophysics, Akadeemia tee 23, Tallinn, Estonia. Tel.: +372 33 4 76 63 56 27; fax: +372 33 4 76 51 42 18.
E-mail address: valdur.saks@ujf-grenoble.fr (V. Saks).

0022-2828/$ – see front matter © 2011 Elsevier Ltd. All rights reserved.
doi:10.1016/j.yjmcc.2011.07.027

proteolytic treatment are tubulin and plectin. Rostovtseva et al. [25,26] established that the first candidate for the role of "factor X" is αβ heterodimeric tubulin, which upon binding to VDAC reconstructed into a planar lipid membrane strongly modulated the channel's conductance. Reconstitution experiments indicated that the addition of the heterodimeric tubulin to isolated mitochondria strongly increased the apparent Km for ADP [27]. Recent immunofluorescence confocal microscopic studies allowed to identify the tubulin associated with mitochondrial outer membrane in cardiomyocytes as its βII isotype [14]. The aim of this study was to investigate further the role of this tubulin-βII isotype in the regulation of respiration in cardiac cells. We show by immunofluorescence confocal microscopy and respirometry that short proteolytic treatment of permeabilized cardiomyocytes removes tubulin-βII from MOM. This significantly increases the MOM permeability for ADP as measured by activation of the MtCK located in the outer surface of inner mitochondrial membrane with trapping of extramitochondrial ADP by the pyruvate kinase (PK) – phosphoenolpyruvate (PEP) system. In accurately prepared permeabilized cardiomyocytes PK–PEP system has no effect on respiration, while in damaged cardiomyocytes and after proteolytic treatment MOM permeability is increased and respiration rate decreased due to ADP tapping by PK–PEP. This permeability test of MOM controlled by tubulin-βII can be used as the most sensitive quality control for intactness of mitochondria in permeabilized cardiomyocytes. Removal of tubulin-βII by proteolytic treatment does not damage the outer mitochondrial membrane itself (as shown by cytochrome c test), but significantly decreases the apparent Km for ADP via an increase of the permeability of VDAC.

2. Materials and methods

2.1. Isolation of cardiac myocytes with perfect rod-like shape, description of various troubleshooting

Adult cardiomyocytes were isolated by adaptation of the technique described previously [19]. Male Wistar rats (300–350 g) were anesthetized and the heart was quickly excised preserving a part of aorta and placed into washing solution (WS) (117 mM NaCl, 5.7 mM KCl, 4.4 mM $NaHCO_3$, 1.5 mM KH_2PO_4, 1.7 mM $MgCl_2$, 11.7 mM glucose, 120 mM sucrose, 10 mM Cr, 20 mM taurine, and 21 mM BES, pH 7.1). All solutions used during the procedure of isolation were saturated with oxygen. The heart was cannulated and washed with WS at a flow rate of 15–20 mL/min for 5 min. At that, the coronary flow should exceed ca. 20 mL/min; otherwise the heart has to be discarded. The collagenase treatment was performed by switching the perfusion to recirculation isolation medium (IM), (117 mM NaCl, 5.7 mM KCl, 4.4 mM $NaHCO_3$, 1.5 mM KH_2PO_4, 1.7 mM $MgCl_2$, 11.7 mM glucose, 10 mM creatine (Cr), 20 mM taurine, 10 mM PCr, 2 mM pyruvate, and 21 mM HEPES, pH 7.1), supplemented by collagenase (0.75 mg/mL) at a flow rate of 5 mL/min for 50 min at 37 °C. After the collagenase treatment the system was switched to the initial solution WS for 1–2 min and then the heart was transferred into the IM supplemented with 20 μM $CaCl_2$, 10 μM leupeptin, 2 μM soybean trypsin inhibitor (STI), and 5 mg/mL bovine serum albumin (BSA). The cardiomyocytes were then gently dissociated by pipette suction. The cell suspension was filtered and transferred into a test tube for sedimentation where the calcium-tolerant cells were allowed to freely sediment. After 3–4 min the initial supernatant was discarded and the pellet of cardiomyocytes resuspended in IM containing 20 μM $CaCl_2$, STI and leupeptine. The rod shaped intact cells sedimentated within 2–3 min and the supernatant with damaged cells was discarded. This resuspension–sedimentation cycle with calcium-tolerant cells was performed twice and after that cardiomyocytes were gradually transferred from calcium containing solution into calcium-free Mitomed [17]. Then, the cardiomyocytes were washed 5 times with the Mitomed containing 5 mg/mL BSA, 10 μM leupeptin, and 2 μM STI. Isolated cells were stocked in 1–2 mL volume and stored on ice during further experiments. Isolated cardiomyocytes contained 85–100% of rod-like cells when observed under a light microscope. Final quality of isolated rat cardiomyocytes was found to depend on a number of minor variations in different isolation steps beginning from the severing of the aorta, removal of the heart from the thorax and initial heart perfusion in order to remove Ca^{2+} and the remainder of blood before the collagenase treatment. It is also advisable to perform this operation in ≤1 min to avoid oxygen deficiency and hypoxia. The choice of the collagenase type is the next crucial step; to our experience, collagenase A (Roche) or Liberase Blendzyme 1 (Roche, similar to the new product Liberase DL Research Grade), an artificial mixture of purified enzymes with carefully controlled specific activities (Roche), results in satisfactory results. Caution should be taken in an attempt to reduce duration of the collagenase perfusion time at the expense of the increase in the enzymes activity. For every lot of collagenase the time of dissociation, enzyme ratios, and enzyme concentration affect tissue dissociation outcomes. The perfusion should be performed at controlled rate by pumping and, advisably, under manometric control in order to follow a decrease in the developed pressure from 55 to 60 mm Hg (which corresponds to ≈80 cm H_2O) to that less than 10 mm Hg. Collagenase solution should be washed out in the presence of the mixture of strong inhibitors of serine and thiol proteases and further operations also performed in the presence of these inhibitors. STI is capable of binding to different serine proteases, and leupeptin is the best choice for thiol proteases.

Usually, the obtained preparation is stable enough during 4–5 h needed for measurements. Used saponin concentration and permeabilization time should also be carefully adjusted by studies of the extent of permeabilization by respirometry.

An alternative to isolation of cardiomyocytes is the use of skinned cardiac fibers isolated according to the method described by Kuznetsov et al. and Saks et al. [17,18]. When correctly used, both methods allow obtaining identical results in studies of respiration regulation after cell or fiber permeabilization [8,9,16–24]. In both cases, it is important to avoid artifacts of cell or fiber isolation resulting in misleading and incorrect experimental data, sometimes reported in the literature, when permeabilized cells and fibers have very different properties [28]. The method of preparation of skinned fibers was in details described by Kuznetsov et al.[17]. To isolate high quality cardiomyocytes needed for functional studies it is equally important to avoid multiple errors, which are listed below in the Table 1.

2.2. . Cell preparation for confocal microscopy

Freshly isolated cardiomyocytes and cultured cells were fixed in 4% paraformaldehyde at 37 °C for 15 min. After rinsing with phosphate buffer solution (PBS, containing 2% BSA) cells were permeabilized with 1% Triton X-100 at 25 °C for 30 min. Finally, cells were rinsed repeatedly and incubated with primary antibody as described above for immunoblotting using concentrations indicated in the Table 1 (in 2% BSA containing PBS solution). The next day samples were rinsed and stained for 30 min at room temperature with secondary antibody. Secondary antibodies: Cy™ 5-conjugated AffiniPure goat anti-mouse IgG (Jackson Immunoresearch 115-175-146), goat polyclonal secondary antibody to mouse IgG-FITC (Abcam ab6785), were used respecting concentrations recommended by the providers (Table 2).

The same proceeding was done during trypsinization of cells but before being fixed, cells were trypsinized by 0.05 or 0.3 μM (0.1–4 mg

Table 1
Useful advises for high quality cardiomyocyte isolation.

Steps	Problems	Possible reasons	Solutions
Heart dissection and hanging to start perfusion	Improper or too high flow rate, see below	Damage of the wall of aorta or aortic valve	Discard this heart. For dissection of the heart holding this between fingers, gently stretch the aorta and cut it to get long aorta to preserve aortic valve from damage
Initial perfusion (80 cm H_2O)	Perfusion pressure too high (>69 mm Hg), coronary flow rate too low (≤15 mL/min)	Aorta partially clogged up	i. Wait for some minutes, small embolus might flow out ii. Remove heart and hang up once again, otherwise discard the heart
	Coronary flow>25 mL/min, abnormally low perfusion pressure	Leak of perfusate due to improper hanging, see above	Hang up the heart once again, otherwise discard the heart
Collagenase perfusion	Perfusion pressure >10–15 mm Hg after 50 min perfusion	Protease concentration too low	Increase the concentration of the collagenase preparation
		Enzyme inactivation	Check storage conditions and the enzyme activity
		Perfusion temperature is too low	Verify temperature
	Too rapid drop perfusion pressure down to zero (in 10–15 min)	Protease concentration too high	Decrease the concentration of the collagenase preparation
	Stained heart surface	Uneven perfusate flow in the heart body due to clogging in some capillaries. Ischemic regions in the heart	Discard the heart, otherwise the yield will be low and quality doubtful
Preparing and washing of the cells	Too low cell sedimentation rate	Substantial amounts of damaged cells present	Normal intact cells sediment in 2–4 min. Elongation of sedimentation time in an attempt to improve the yield could exclusively result in collecting damaged cells
	Low cell viability and yield	Mechanical force for heart dissection is too excessive	Reduce shear force and use the pipette more gently
Saponin treatment	Too low activation of respiration by exogenous ADP	Incomplete permeabilization of sarcolemma	Cell permeabilization has to be checked in the oxygraph cells by addition of the saponin stock solution, the activation of respiration should be complete in ca. 10 min. and the final oxygen consumption rate remain unaltered at least for 20 min, otherwise the saponin concentration should be adjusted
Stirring	Gradual decay in the oxygen consumption rate	Cell damaging due to too vigorous stirring	Decrease in the stirring rate to sufficiently low value

of TR/mg cardiomyocytes protein) for 10 min at 25 °C and then STI, up to a final concentration of 0.02 mM, was added.

2.3. Confocal imaging

The fluorescence images were acquired with a Leica TCS SP2 AOBS inverted laser scanning confocal microscope (Leika, Heidleberg, Germany) equipped with a 63× water immersion objective (HCX PL APO 63.0×1.20 W Corr). Laser excitation was 488 nm for FITC (green fluorescence) and 633 nm for Cy 5 (red fluorescence). Images were then analyzed using Volocity softwere (Improvision, France).

2.4. Colocalization studies

α-actinin and βII-tubulin were immunostained with Cy5-labeled antibody according to the protocol described elsewhere [14]. They were imaged using the 63×/1.4 oil immersion Plan Apo objective, 633 nm HeNe laser and 638–747 nm detection of LSM710NLO confocal microscope (Carl Zeiss). The pinhole value was set to 1 Airy unit. Optical slices closest to the glass surface were analyzed in order to minimize the optical distortions in cardiomyocytes. Mitochondria distribution in fixed cardiomyocytes was visualized using flavoprotein autofluorescence signal excited with the two-photon laser at 720 nm and integrated between 408 and 546 nm. For increasing the autofluorecence of flavoproteins and improving the imaging of mitochondria, the permeabilized cells were treated before fixation with 10 μM rotenone for 10 min under aerobic conditions and washed twice in Mitomed solution described in the next section. The choice of this label-free imaging of mitochondria allowed one to avoid any possible spectral bleed-through to the near-infrared detection channel for α-actinin or βII tubulin immunofluorescence. Indeed, no cell specific background was detected in this channel in unlabelled cardiomyocytes. The very low background signal was detected in case of nonspecific control with the Cy5-labeled secondary antibody. The signal to noise was improved using 16 line scan repetitions and 6 μs pixel dwell time. Overall photobleaching with the used laser intensities did not exceed 1%. The red channel images were not treated for the sake of intensity comparison; the green channel images were processed with a Top-hat square shape filter to improve the contrast of rectangular mitochondria pattern (MetaMorph, Universal Imaging).

Table 2
List of antibodies used.

Commercial name	Dilution for immunofluorescence	Immunogen
Primary antibodies:		
mouse anti-tubulin βII(β2),(Abcam ab28036)	1/1000	Amino acids CEEEEGEDEA at the C terminus
alpha-actinin rabbit (Abcam, ab82247)	1/100	
Secondary antibodies:		
a) Cy™ 5-conjugated AffiniPure goat anti-mouse IgG (Jackson Immunoresearch 115-175-146)	1/100	
b) goat anti- mouse polyclonal secondary antibody IgG-FITC (Abcam ab6785)	1/800	

2.5. Measurements of oxygen consumption

The rates of oxygen uptake were determined with high-resolution respirometer Oxygraph-2K (OROBOROS Instruments, Austria) in Mitomed solution [17] containing 0.5 mM EGTA, 3 mM $MgCl_2$, 60 mM K-lactobionate, 3 mM KH_2PO_4, 20 mM taurine, 20 mM HEPES (pH 7.1), 110 mM sucrose, 0.5 mM dithiothreitol (DTT), 2 mg/mL fatty

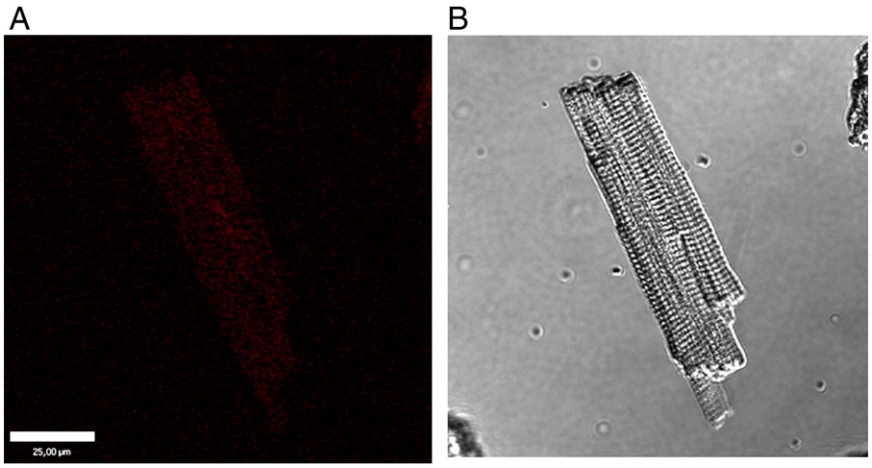

Fig. 1. Specificity test for immunofluorescence labeling of tubulin in cardiomyocytes. A. Confocal image of isolated cardiomyocytes after labeling with secondary antibodies Cy™ 5-conjugated AffiniPure goat anti-mouse IgG (Jackson Immunoresearch) without primary antibodies. B. Transmission image of the same cardiomyocyte.

acids free BSA, complemented with 5 mM glutamate and 2 mM malate as respiratory substrates. Respiration was activated by addition of creatine to a final concentration of 20 mM in the presence of 2 mM ATP. Maximal respiration rate was measured in the presence of 2 mM ADP. The measurements were carried out at 25 °C; solubility of oxygen was taken as 240 nmoL/mL [17].

2.6. Data analysis

The experiments were carried out independently in two different laboratories. The apparent Km for ADP or ATP was estimated from a linear regression of double-reciprocal plots or by non-linear least-squares.

3. Results

3.1. Confocal immunofluorescence imaging of tubulin-βII in permeabilized cardiomyocytes

Our recent study showed regular localization of βII-tubulin in cardiac cells [14], similar to the "crystal-like" arrangement of mitochondria [29–33]. Therefore, in this work we further investigated the correlation between localization of tubulin-βII close to the outer mitochondrial membrane in adult cardiomyocytes with several important parameters of regulation of mitochondrial respiration in permeabilized cardiac cells *in situ*. The second aim of this study was to describe the necessary quality tests of the intactness of mitochondria in permeabilized cardiomyocytes, required for the proper studies of the interaction of mitochondria with cytoskeleton *in situ*. A short-time proteolysis of permeabilized cells was optimized and used to remove tubulin-βII from the cells, since our earlier studies have shown that tubulin is one of the most sensitive proteins to this kind of treatment [24]. Trypsin treatment is also routinely used for isolation of intact mitochondria from heart muscle [12,24]. The localization of tubulin--βII in fixed cardiac cells was visualized by immunofluorescence confocal microscopy (Figs. 1–4). Fig. 1 shows the high selectivity of this method, demonstrating that incubation of cells with only secondary antibodies does not result in any labeling of intracellular structures. Only after incubation of the fixed and permeabilized cells with primary antibodies against C-terminal tail of tubulin-βII and subsequent incubation with secondary fluorescent antibodies intensive immunofluorescence labeling of tubulin-βII associated with mitochondria can be seen (Figs. 2 and 3). Fig. 2A shows the very regular immunofluorescence labeling of tubulin-βII by using secondary antibodies with green fluorescence before trypsin treatment. Fig. 2B shows that after short proteolysis the fluorescence intensity decreases significantly and regular arrangement of tubulin disappears. Since green fluorescence seen in Fig. 2A and B may be influenced by the autofluorescence of oxidized mitochondrial flavoproteins [18], localization of tubulin-βII was studied also by using secondary antibodies with red fluorescence (Fig. 3). Again, very regular labeling of mitochondria was seen. Similar to the results

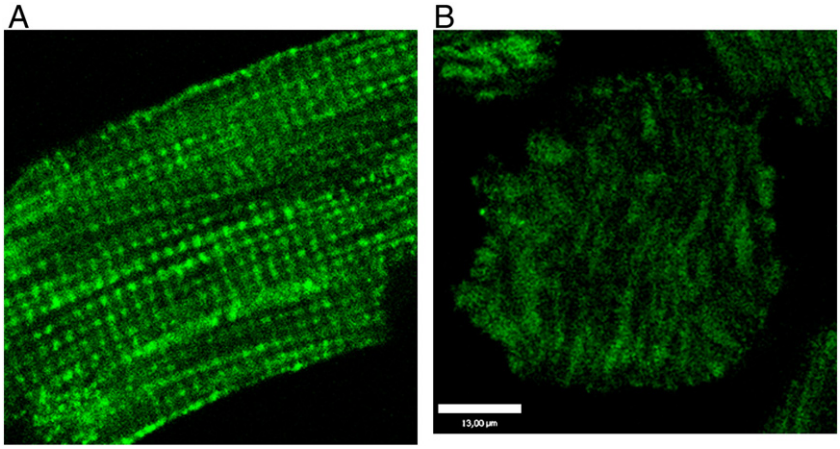

Fig. 2. Immunofluorescence labeling of βII-tubulin before and after trypsin treatment. Labeling with primary antibody and goat anti-mouse polyclonal secondary antibody IgG-FITC (Abcam ab6785). A. Before trypsin treatment. B. After trypsin (0.05 µM) treatment.

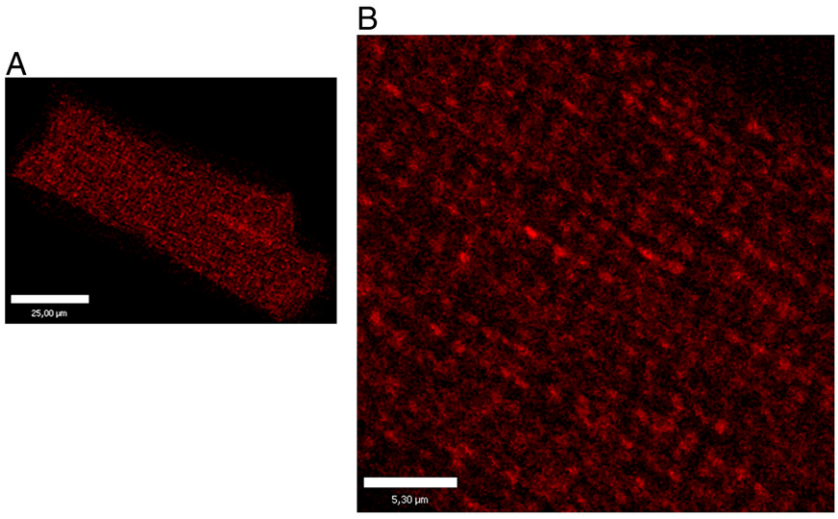

Fig. 3. Immunofluorescence labeling of βII-tubulin in isolated cardiomyocytes with primary and Cy™ 5-conjugated AffiniPure goat secondary anti-mouse IgG (Jackson Immunoresearch). Labeling of mitochondria in parallel rows parallel to long axis of the cell is seen. For further details see Ref. [14].

presented on Figs. 2B, Fig. 4 shows again that short treatment of permeabilized cardiomyocytes with trypsin completely removes the tubulin-βII, also changing the cell shape due to destruction of tubulin and other cytoskeletal systems, and changes intracellular arrangement of mitochondria from regular into irregular clustered one, in accordance with our earlier observations [24,32].

3.2. Colocalization of mitochondria and tubulin βII

To answer the question whether and how tubulin-βII is colocalized with mitochondria in cardiac cells, α-actinin in the Z-lines (Figs. 5A, C) and tubulin-βII (Figs. 5E, G) were immunostained with Cy5-labeled secondary antibody and mitochondrial localization was detected by imaging of the autofluorescence of mitochondrial flavoproteins in oxidized state. Figs. 5A and E show merged images, Figs. 5B, C and F, G show images recorded by separate channels. Figs. 5D and H show the results of quantitative analysis of these images — the fluorescence intensity plots along white lines drawn through representative sequences of 4 mitochondria (see panels B, C and F, G). The very low background signal (dashed lines in Figs. 5D, H) was detected in case of nonspecific control with only the Cy5-labeled secondary antibody. The amplitude of Cy5 fluorescence signal of α-actinin is strongly modulated along a mitochondrial chaplet with the period equal to that of mitochodria but with the inversed phase, indicating essential localisation of α-actinin on Z-lines (Figs. 5A–D). Remarkably, mitochondrial green autofluorescence was not detected in the Z-line area (Fig. 5D), showing the absence of mitochondrial fusion in cardiomyocytes, confirming our previous observation [8]. Contrary to the α-actinin staining, the tubulin-βII fluorescence amplitude modulation is very weak along the line of mitochondrial localization, showing the overall staining of the mitochondria (Figs. 5E–H). Since tubulin βII was detected also in the Z-line area, it seems to form a network-like structures connecting mitochondria to the other cytoskeletal structures. Thus, Figs. 3 and 5 confirm with higher resolution our earlier observations of colocalization of tubulin-βII with mitochondria. However, the resolution limit of confocal microscope (about 0.2 µm) does not allow more detailed analysis of protein localisation on the submitochondrial level (which can be done in the future by using FRET approach).

3.3. Alteration of parameters of respiratory regulation after removal of tubulin βII

The common tests of mitochondrial intactness, which include activation of mitochondrial respiration by ADP, are the cytochrome c test of intactness of the outer membrane of mitochondria and

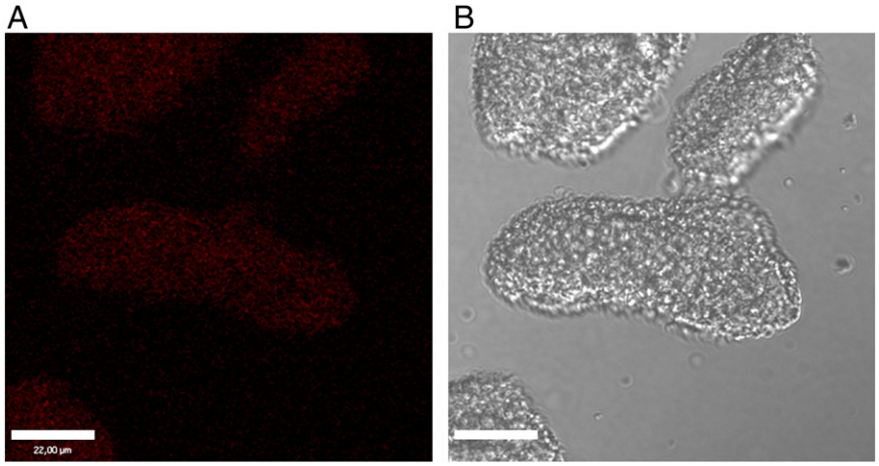

Fig. 4. Immunofluorescence labeling of βII-tubulin after short proteolysis of permeabilized cardiomyocytes with 0.05 µM trypsin before fixation (see Materials and methods). Cy™ 5-conjugated AffiniPure goat anti-mouse IgG (Jackson Immunoresearch 115-175-146) was used. A. Confocal image. B. Transmission image of the same cells.

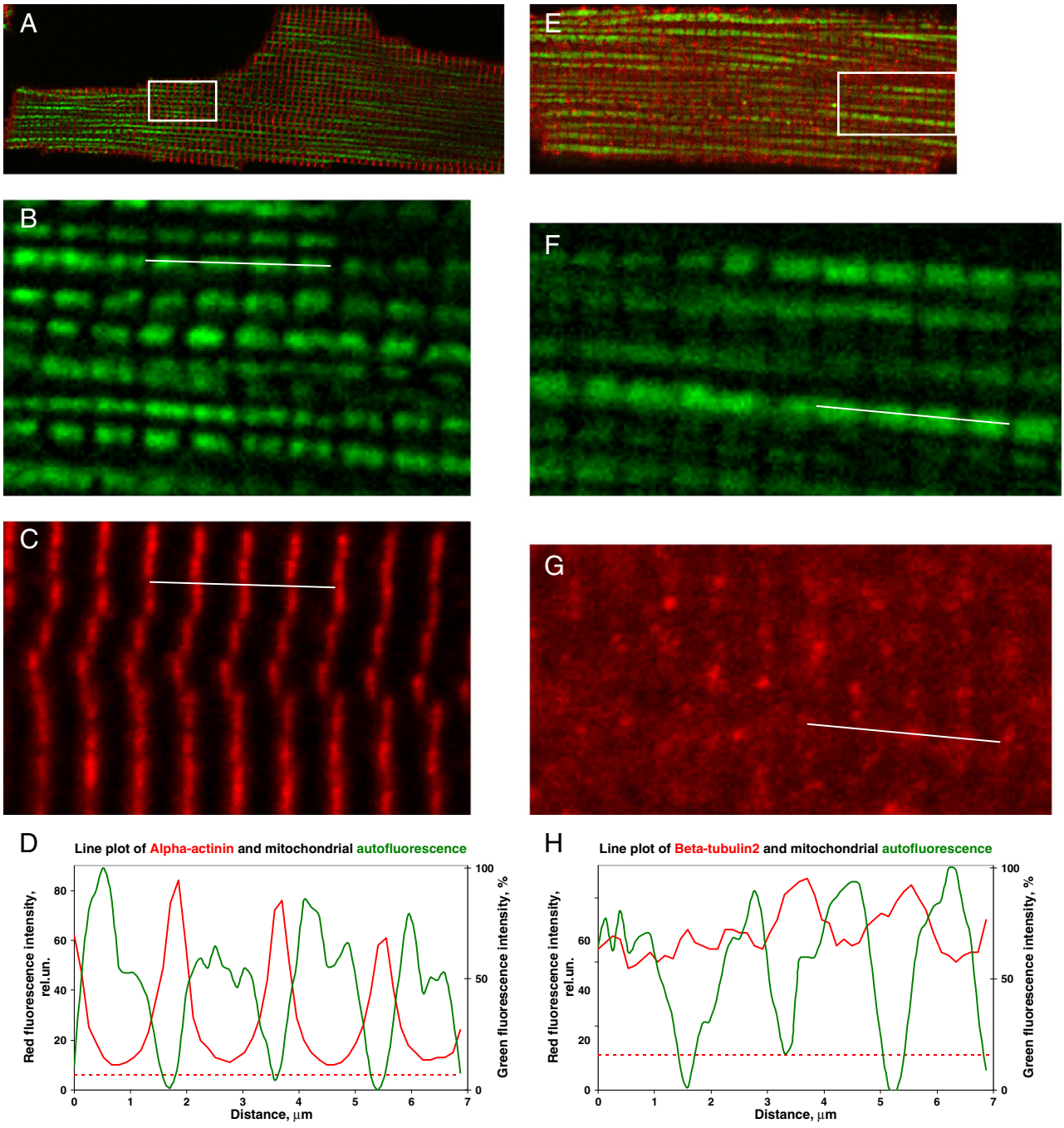

Fig. 5. Comparison of the intracellular distribution of βII-tubulin, α-actinine, a « Z-line label », and mitochondria. Confocal merged images of immunofluorescence labeling of α-actinin (A) or βII-tubulin (E), red color and mitochondrial autofluorescence, green color. B, C ,F, G — zoom in regions of interest highlighted by the white rectangles in the panels A and E, separated channels. D, H — intensity plots along white lines drawn through representative sequences of 4 mitochondria (panels B, C, F, G).Dashed red lines indicate the background level of unspecific fluorescence staining measured in control experiments. Red plots are presented in relative units using the same scale for βII-tubulin and α-actinin. Green plots were normalized to the 100% of the maximal intensity of autofluorescence after the background subtraction.

inhibition of ADP-stimulated respiration by atractyloside (ATR); they are shown in Fig. 6. In permeabilized cardiomyocytes ADP (2 mM) increases respiration rate more than 10 times and this rate is not changed by addition of cytochrome c (Fig. 6A). Cytochrome c, a highly soluble hemoprotein of the respiratory chain is loosely associated with the outer side of the inner membrane of the mitochondria. If the outer membrane is disrupted, cytochrome c leaves mitochondria, and in this situation addition of the protein increases respiration rate [34]. Thus, the cytochrome c test (Fig. 6A) shows that in permeabilized cardiomyocytes mitochondrial outer membrane is entirely intact. ATR completely inhibits ADP-activated respiration, showing that all ADP is imported into mitochondrial matrix *via* ANT [35]. Remarkably, all these parameters are not changed after treatment of permeabilized cardiomyocytes by trypsin (Fig. 6B) that showing that short proteolytic treatment leaves mitochondrial membranes completely intact, in accordance with all earlier data of studies of isolated heart mitochondria [24,34].

More sensitive test which shows clear changes in parameters of regulation of mitochondrial respiration after removal of βII-tubulin by short proteolysis is shown in Fig. 7. This Figure shows the parameters

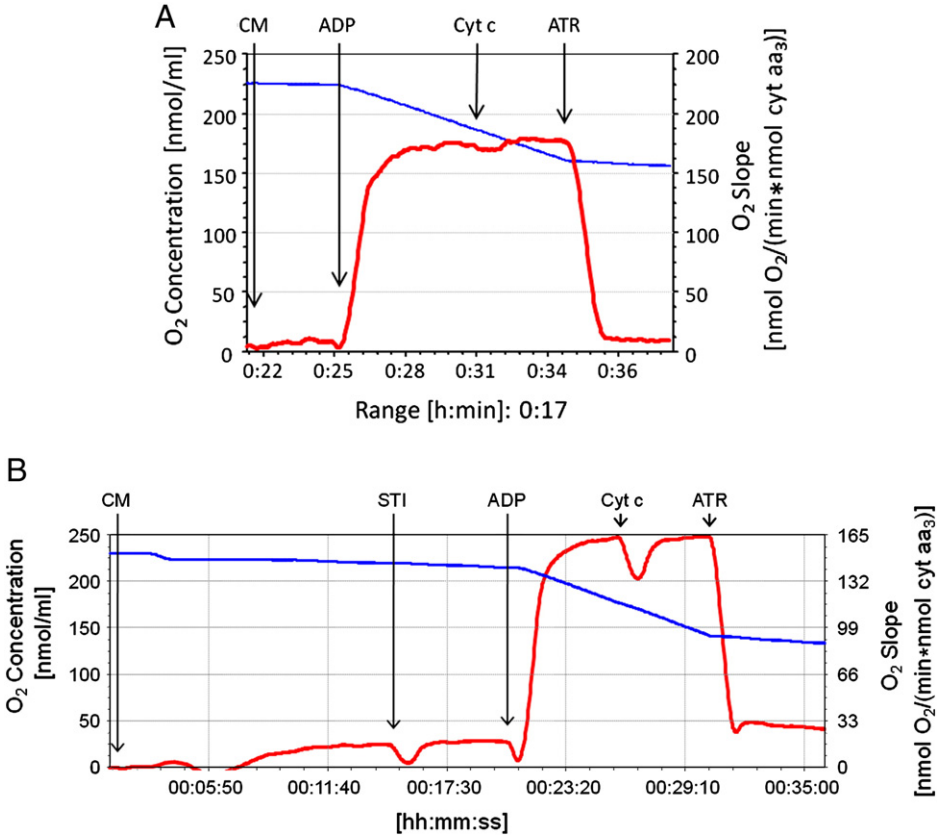

Fig. 6. Representative respiration traces before trypsin treatment of permeabilized cardiomyocytes (CM). A. Respiration is activated with 2 mM exogenous ADP. Cytochrome c (Cyt c) test (10 μM cytochrome) shows the intactness of MOM. Atractyloside (ATR, 0.1 mM) test shows that respiration is totally controlled by ANT. B. The same as A, but after treatment with trypsin at 0.05 μM for 10 min, then soybean trypsin inhibitor (STI) was added.

of regulation of mitochondrial respiration by MtCK activated by addition of creatine and MgATP. MtCK is located at the outer surface of mitochondrial inner membrane in close vicinity of ANT [2,3,36,37] and produces MgADP behind the outer mitochondrial membrane (Fig. 7A). This ADP formed in the active site of MtCK is released into intermembrane space of mitochondria and may either return to matrix *via* ANT or leave mitochondria through VDAC [38,39], the flux distribution between these two routes depending on the permeability of this channel for adenine nucleotides. The ADP flux distribution can be easily revealed by addition of exogenous ADP trapping system consisting of PK (20 U/mL) and PEP (5 mM) (Fig. 7B). Fig. 7C shows that in intact permeabilized cardiomyocytes (more than 90% of rod-like cells) addition of PK–PEP system does not change the rate of respiration, which is maintained at the maximal value by activated MtCK within mitochondrial interactosome. However after short proteolysis, removing βII-tubulin from MOM, addition of PK–PEP system decreases the respiration rate to half of its maximal value (Fig. 7D), as observed for isolated mitochondria before [8,12,40]. That means that about 50% of MgADP produced by MtCK can leave now mitochondria *via* VDAC which permeability for MgADP is increased. Remarkably, the effect of PK–PEP system on the respiration was also seen when the preparation of isolated cardiomyocytes contained, without use of trypsin, about 50% of rod-like intact cardiomyocytes and 50% of round-shape cells, probably due to some damaging factors listed in Table 1 (Fig. 7E). Thus, the PK–PEP test is an important quality control which has to be used in such studies to demonstrate intactness of isolated cardiomyocytes (see in details in Materials and methods section).

Fig. 8 shows that removal of βII-tubulin from mitochondrial membrane decreases the apparent Km for exogenous ADP in regulation of mitochondrial of mitochondrial respiration. This is in good agreement with earlier observation of Kuznetsov et al. and Appaix [21,24]. The results shown in Figs. 7 and 8 support the assumption that βII-tubulin bound to MOM in intact permeabilized cardiomyocytes *in vivo* limits the permeability of VDAC channel and increases ADP transfer to matrix *via* ANT, further enhancing the functional coupling between ANT and MtCK [5,7] and thus increases the functional compartmentation of adenine nucleotides within mitochondria in the cells (Fig. 7B). Under these conditions, the MtCK reaction completely controls the respiration rate even in the presence of cytoplasmic ADP trapping system: increase in creatine concentration rapidly increases the respiration rate to its maximal value (Figs. 9A, C). Under these conditions oxidative phosphorylation is maintained by ADP regeneration and recycling within mitochondrial interactosome coupled to permanent creatine phosphorylation and phosphocreatine production with high PCr/O_2 ratio equal to about 6 [41]. When the βII-tubulin is removed from MOM by proteolytic treatment and the VDAC permeability increased, exchange of adenine nucleotides between mitochondria and medium is increased and MtCK only partially controls the respiration (Figs. 9B, D).

4. Discussion

The results of this work are consistent with an assumption that βII-tubulin is one of the cytoskeletal proteins in heart cells which are able to control selectively the VDAC permeability in mitochondrial outer membrane for adenine nucleotides [14]. This restricted permeability for ADP and ATP favors their recycling in the coupled MtCK–ATP synthasome reactions in mitochondria connecting oxidative phosphorylation to PCr synthesis within a supercomplex, which we called “Mitochondrial Interactosome” [8,41], a key structure of phosphocreatine pathway of intracellular energy transfer [1–15]. Also, limited permeability of VDAC for ADP

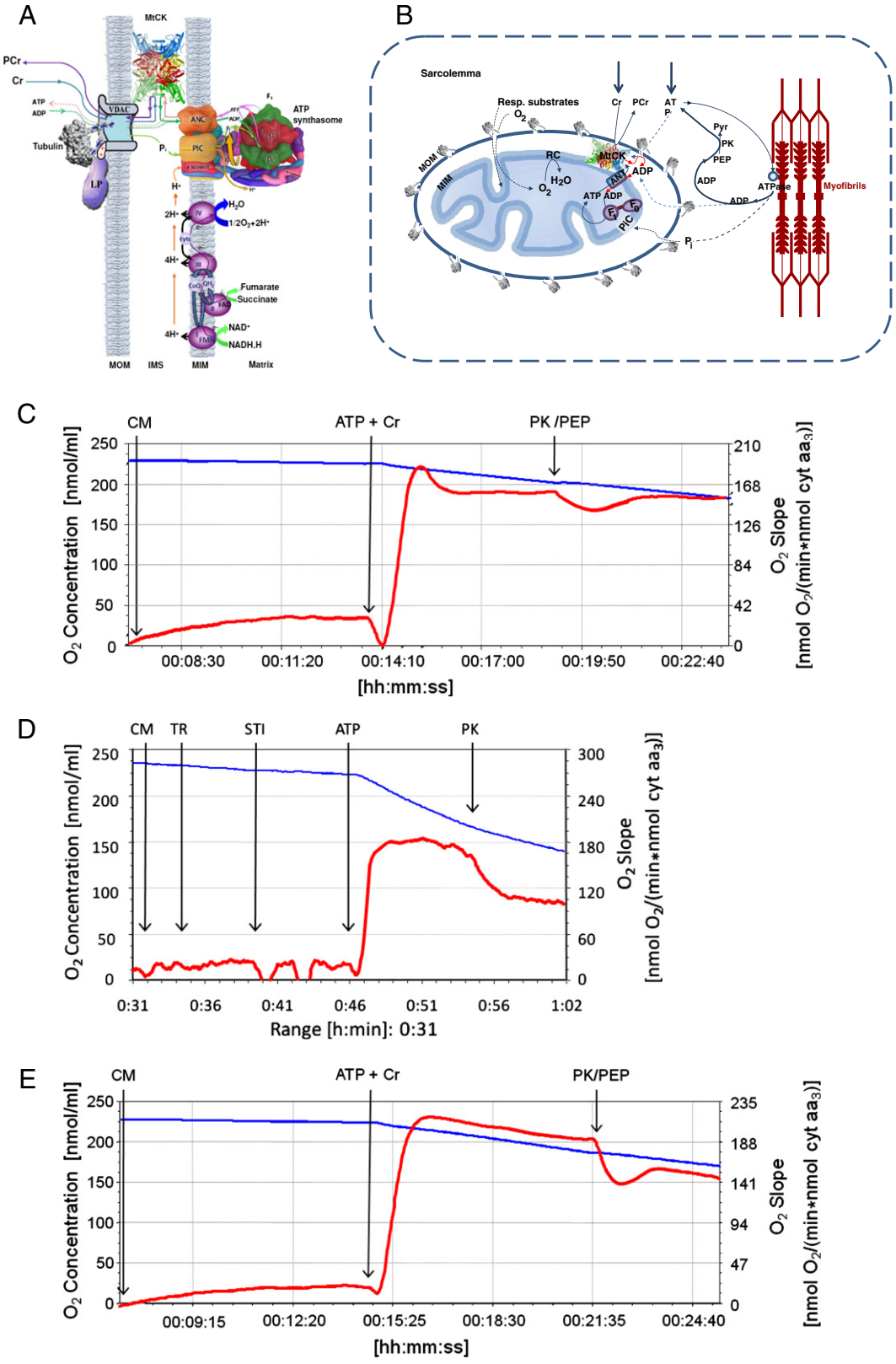

Fig. 7. A. The structure of mitochondrial interactosome showing the localization of MtCK coupled to ATP synthasome in cardiac cells. Adapted from [8,41]. B. The principle of the protocol of the study of ADP fluxes in permeabilized cells by PK–PEP system. C. Respiration of permeabilized cardiomyocytes (CM) was activated by MgATP (2 mM) and creatine (Cr, 20 mM). No effect of the addition of PK–PEP system on the respiration is seen, showing that the MgADP produced by MtCK is not accessible for this system. D. Respiration of trypsin (TR) treated cardiomyocytes in the presence of 20 mM Cr and 2 mM ATP. The oxygen uptake expressed in nmoL O_2/(min∗nmol cyt aa_3). Proteolytic treatment inhibited by addition of soybean trypsin inhibitor (STI, 0.02 mM) and BSA (5 mg/mL). Even after treatment of isolated cardiomyocytes with very low trypsin concentration (0.05 μM) ADP becomes accessible to the PEP–PK trapping system (PK 20 U/mL, PEP 5 mM). E. The effect of PK–PEP system on respiration of permeabilized cardiomyocytes which contained only about 50% of rod-like intact cells.

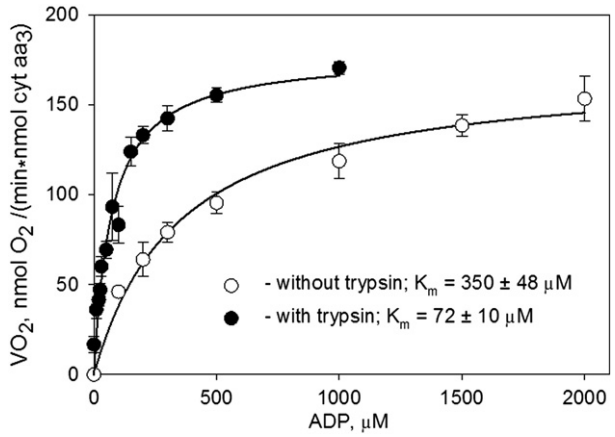

Fig. 8. Effect of trypsin on apparent Km for ADP of mitochondrial respiration in isolated permeabilized cardiomyocytes: respiration rates without (○) and with (●) trypsin treatment. Proteolytic treatment with trypsin resulted in an increase in the affinity of respiration for free ADP due to the proteolytic removal of βII-tubulin. Mean values and standard deviations for 9 experiments are shown.

has an important physiological function preventing from rapid saturation of ANT by this substrate and thus making possible the feedback metabolic regulation of mitochondrial respiration during workload changes [4,7,8,11,13]. Revealing the nature of interaction of tubulins with VDAC needs however further studies by using more selective methods than proteolysis.

Two decades ago two important observations were made almost simultaneously in the studies of cardiac cell bioenergetics. Using electron microscopy, Saetersdal et al. [42] have demonstrated in 1990 the presence of the immunogold anti-β-tubulin labeling at the outer mitochondrial membrane in cardiomyocytes, as well as in myofibers in close opposition to this membrane. This observation rested almost unnoticed and its importance unexplained for these two decades. In parallel, first Kummel in 1988 [16] and then many other investigators in different laboratories ([17–24], reviewed in Ref. [8,9]) discovered the differences in mitochondrial behavior *in vitro* and in permeabilized cardiomyocytes *in situ*: apparent Km for exogenous ADP in regulation of mitochondrial respiration was shown to be 20–30 times higher in the latter case than in isolated mitochondria [8,9]. Detailed investigation of this phenomenon in our laboratories led to conclusion that this phenomenon is related to the tight interactions between mitochondria and cytoskeleton in cardiac cells [22,23]. It was proposed that some components of cytoskeleton may control the permeability of the VDAC channel in the outer mitochondrial membrane in cardiac cells *in vivo*[22,23]. The results of the present and several other recent investigations confirm this suggestion and demonstrate directly that there is a specific isotype of tubulin-βII which is attached to the outer mitochondrial membrane and controls its permeability [14]. Mitochondrial βII-tubulin is co-expressed with MtCK and together with ATP Synthasome they were assumed to form a Mitochondrial Interactosome (MI), a key structure of the phosphotransfer pathway of energy transport into cytoplasm [14]. Evidently, this shows the important role of mitochondrial tubulin, discovered by Saetersdal et al. [42] in 1990.

Nevertheless, many questions still remain unanswered. Tubulin in non-polymerized form exists as αβ-heterodimer [43–45], and there are several isotypes of both subunits which differ mostly by the structure of C-terminal tail [43]. The questions that remain unanswered are: 1) why only βII-tubulin is associated with mitochondria; 2) which is the α isotype; 3) how they both interact with VDAC; and 4) what kind of other cytoskeletal proteins may be involved.

In this work we describe also the very simple and effective tests for investigation of the intactness of MI structure and function, energy fluxes from mitochondria into cytoplasm and functioning of MI which can be used as important quality controls for preparations of cardiac cells or myocardial fibers. Among other methods the cytochrome c test (Fig. 6) is first of them to be used for the detection of intactness of MOM in isolated mitochondria as well as in skinned fibers and permeabilized cardiomyocytes [17,18,34]. The loss of relatively weekly bound cytochrome c from MIM (as an important component of respiratory chain), especially at elevated ionic strength is accompanied by a significant decrease of the oxygen consumption and ATP synthesis [34]. Addition of saturating amount of exogenous cytochrome c to cytochrome c depleted mitochondria in cells or fibers in respiration medium results in restoration of the oxygen consumption and ATP synthesis from exogenous ADP, thus enabling to estimate the degree of damage and an amount of mitochondria with disrupted MOM. However, this effect does not allow estimating the state and quality of MI intactness, functioning and regulation of ATP/PCr synthesis. Inhibition of ANT by CAT [17,35] is another useful tool to check intactness of MIM, since increased rate in the residual oxygen consumption after inhibition by CAT is indicative for bypass of ADP–ATP and thus damage of MIM.

Some indication of functionally coupled MtCK could be observed from the creatine effect on the cellular respiration under conditions of externally added ADP, where creatine added to the experimental medium switches on the MtCK activity, resulting in a substantial decrease in Km(ADP) from values >300 μM down to 80–100 μM due to recycling of ADP in intermembrane space [19,24].

The use of the PK/PEP system is the most sensitive and comprehensive test for intactness of the whole MI system including the regulations at MOM. This simple and effective competitive enzyme method for studying the functional coupling phenomenon, namely the pathway of ADP movement from MtCK back to mitochondria or into the medium, was developed by Gellerich et al. and Guzun et al. [12,13,40,41]. These authors used an external PEP–PK system to trap ADP and thus to compete with ANT for this substrate. This competitive enzyme system was able to suppress 50% of Cr-stimulated respiration in isolated heart mitochondria, thereby showing the rather effective channeling of ADP from MtCK to the medium [12,40]. However, in permeabilized cardiomyocytes when MI is activated with 20 mMCr, PK/PEP system does not have any access to the intramitochondrial ADP and it is not affecting oxidative phosphorylation inside mitochondria and respiration rate. This protocol is excellent to elucidate the role of the mitochondrial outer membrane in the control of MI function, and foresaw many important functional aspects of the control of mitochondrial function *in vivo*. All these tests show that there is practically no measurable direct flux of ATP from mitochondria when MI is actively functioning. Direct transfer of ATP is observed under pathological conditions when the MOM is broken or tubulin lost from MI.

Any disturbances in MOM permeability regulation, including mild protease treatment, result in leakage of ADP and its competing trapping by the excessive PK/PEP and, finally, in a remarkable decrease of respiration. Only in the case of high cell quality (more than 95% intact rod like cells) cell respiration shows absence of the PK/PEP system effect.

The normal shape of the cardiac cells and mitochondrial arrangement are maintained by cytoskeletal structures, including tubulins, plectin, desmin and others [46–58]. In normal adult saponin-skinned fibers intermyofibrillar mitochondria retain their crystal-like pattern along with a relatively slow fluctuations around their position [32,33]. It has been supposed [33] that these fluctuations reflect the configurational changes of mitochondrial matrix between two classical condensed and orthodox

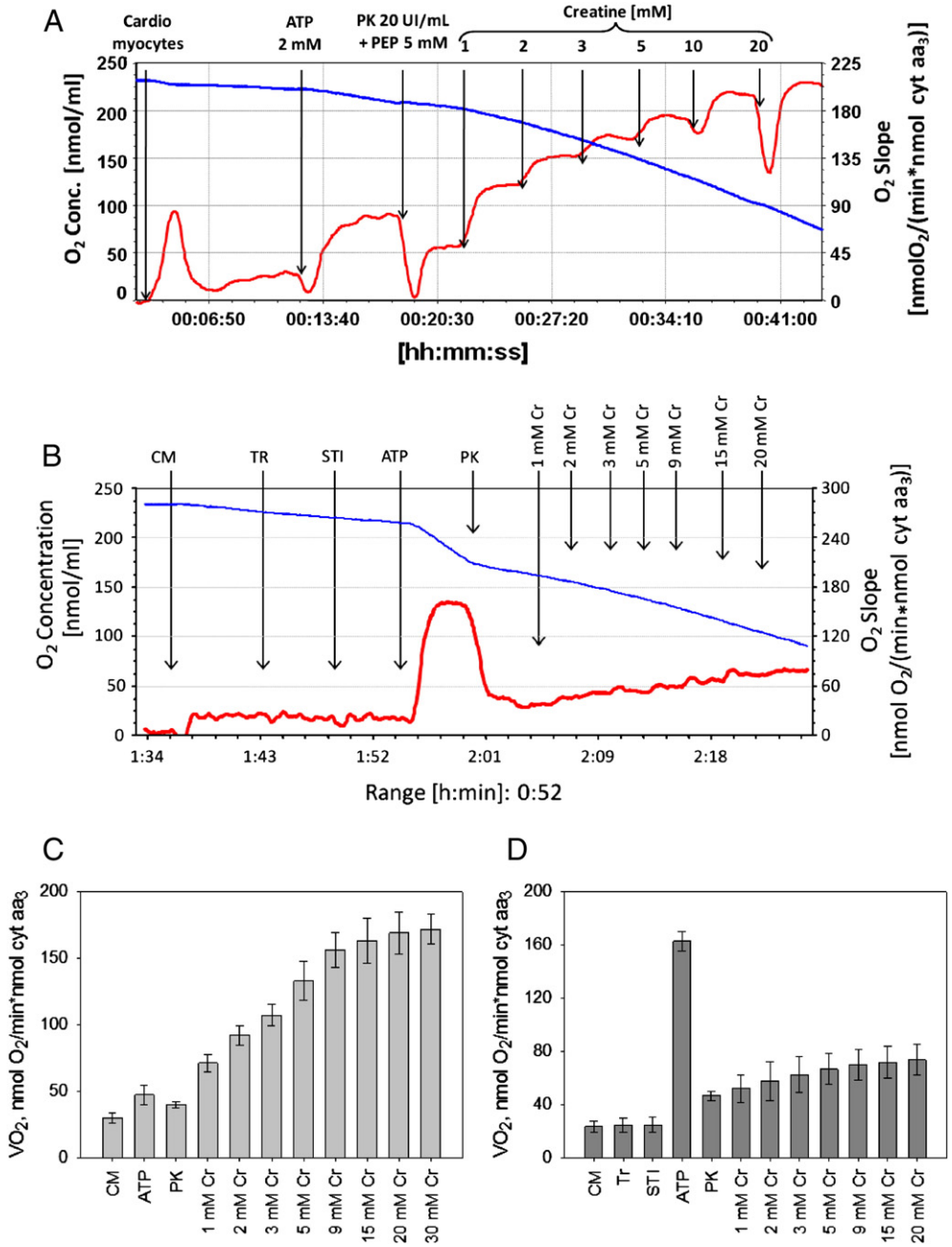

Fig. 9. Regulation of mitochondrial respiration by creatine (Cr) in the presence of activated MtCK, in cardiomyocytes (CM) non-treated and treated with trypsin. A. Cardiomyocytes were permeabilized by saponin and State 2 respiration recorded. MgATP was added to 5 mM final concentration to stimulate MgATPases, this increasing the respiration rate. This rate was decreased by addition of PK (20 U/mL) in the presence of PEP (5 mM). Subsequent addition of creatine rapidly increased the respiration rate up to maximal value. ADP produced by MtCK is not accessible for the PK–PEP system and is rapidly taken up by ANT into mitochondrial matrix. B. The same protocol after trypsin treatment: extramitochondrial ADP is more accessible to the PEP–PK reaction due to the proteolytic treatment, which destroys cytoskeletal proteins involved to the regulation of MOM. C. Mean values and standard errors for 7 experiments described in panel A. D. Mean values and standard errors for 7 experiments described in panel B.

states. Mitochondrial fusion and fission were not seen in adult intact cardiomyocytes [33]. This conclusion is confirmed by the results shown in Fig. 5D in this study.

Acknowledgments

This work was supported by INSERM and CNRS, by Agence National de la Recherche project SYBECAR France, by grant no. 7823 from the Estonian Science Foundation, SF0180114Bs08 from Estonia Ministry of Education and Science, by a research grant from the Austrian Science Fund (FWF): [P 22080-B20], and by National Council of Science and Technology of Mexico (CONACYT). The authors thank: Charles Auffray, Functional Genomics and Systems Biology for Health, CNRS; Institute of Biological Sciences (Villejuif, France) for continuous support of this work; Cécile Cottet-Rousselle, J. Fourier University, Grenoble; Peeter Sikk and Maire Peitel, Laboratory of Bioenergetics, National Institute of Chemical Physics and Biophysics (Tallinn, Estonia) for skillful technical assistance.

Disclosure statement

None.

References

[1] Bessman SP, Carpenter CL. The creatine–creatine phosphate energy shuttle. Annu Rev Biochem 1985;54:831–62.
[2] Wallimann T, Wyss M, Brdiczka D, Nicolay K, Eppenberger HM. Intracellular compartmentation, structure and function of creatine kinase isoenzymes in tissues with high and fluctuating energy demands: the 'phosphocreatine circuit' for cellular energy homeostasis. Biochem J 1992;281:21–40.
[3] Wallimann T, Tokarska-Schlattner M, Neumann D, Epand RF, Andres RH, Widmer HR, et al. The phosphocreatine circuit: molecular and cellular physiology of creatine kinases, sensitivity to free radicals, and enhancement by creatine supplementation. In: Saks V, editor. Molecular system bioenergetics energy for life. GmbH, Germany. Weinheim: Wiley-VCH; 2007. p. 195–264.
[4] Molecular system bioenergetics. In: Saks V, editor. Energy for life. Gmbh, Germany. Weinheim: Wiley-VCH; 2007.
[5] Saks V, Anmann T, Guzun R, Kaambre T, Sikk P, Schlattner U, et al. The creatine kinase phosphotransfer network: thermodynamic and kinetic considerations, the impact of the mitochondrial outer membrane and modelling approaches. In: Wyss M, Salomons G, editors. Creatine and creatine kinase in health and disease. Dordrecht: Springer; 2007. p. 27–66.
[6] Saks V, Beraud N, Wallimann T. Metabolic compartmentation — a system level property of muscle cells: real problems of diffusion in living cells. Int J Mol Sci 2008;9:751–67.
[7] Saks V, Dzeja P, Schlattner U, Vendelin M, Terzic A, Wallimann T. Cardiac system bioenergetics: metabolic basis of the Frank-Starling law. J Physiol 2006;571:253–73.
[8] Saks V, Guzun R, Timohhina N, Tepp K, Varikmaa M, Monge C, et al. Structure–function relationships in feedback regulation of energy fluxes in vivo in health and disease: mitochondrial interactosome. Biochim Biophys Acta 2010;1797:678–97.
[9] Saks V, Monge C, Anmann T, Dzeja P. Integrated and organized cellular energetic systems: theories of cell energetics, compartmentation and metabolic channeling. In: Saks V, editor. Molecular system bioenergetics energy for life. GmbH, Germany. Weinheim: Wiley-VCH; 2007. p. 59–110.
[10] Saks V, Monge C, Guzun R. Philosophical basis and some historical aspects of systems biology: from Hegel to Noble — applications for bioenergetic research. Int J Mol Sci 2009;10:1161–92.
[11] Guzun R, Saks V. Application of the principles of systems biology and Wiener's cybernetics for analysis of regulation of energy fluxes in muscle cells in vivo. Int J Mol Sci 2010;11:982–1019.
[12] Guzun R, Timohhina N, Tepp K, Monge C, Kaambre T, Sikk P, et al. Regulation of respiration controlled by mitochondrial creatine kinase in permeabilized cardiac cells in situ. Importance of system level properties. Biochim Biophys Acta 2009;1787:1089–105.
[13] Guzun R, Timohhina N, Tepp K, Gonzalez-Granillo M, Shevchuk I, Chekulayev V, et al. Systems bioenergetics of creatine kinase networks: physiological roles of creatine and phosphocreatine in regulation of cardiac cell function. Amino Acids 2011;40:1333–48.
[14] Guzun R, Karu-Varikmaa M, Gonzalez-Granillo M, Kuznetsov AV, Michel L, Cottet-Rousselle C, et al. Mitochondria–cytoskeleton interaction: distribution of beta-tubulins in cardiomyocytes and HL-1 cells. Biochim Biophys Acta 2011;1807:458–69.
[15] Saks VA, Kaambre T, Sikk P, Eimre M, Orlova E, Paju K, et al. Intracellular energetic units in red muscle cells. Biochem J 2001;356:643–57.
[16] Kummel L. Ca, Mg-ATPase activity of permeabilised rat heart cells and its functional coupling to oxidative phosphorylation of the cells. Cardiovasc Res 1988;22:359–67.
[17] Kuznetsov AV, Veksler V, Gellerich FN, Saks V, Margreiter R, Kunz WS. Analysis of mitochondrial function in situ in permeabilized muscle fibers, tissues and cells. Nat Protoc 2008;3:965–76.
[18] Saks VA, Veksler VI, Kuznetsov AV, Kay L, Sikk P, Tiivel T, et al. Permeabilized cell and skinned fiber techniques in studies of mitochondrial function in vivo. Mol Cell Biochem 1998;184:81–100.
[19] Saks VA, Belikova YO, Kuznetsov AV. In vivo regulation of mitochondrial respiration in cardiomyocytes: specific restrictions for intracellular diffusion of ADP. Biochim Biophys Acta 1991;1074:302–11.
[20] Saks VA, Vasil'eva E, Belikova Yu O, Kuznetsov AV, Lyapina S, Petrova L, et al. Retarded diffusion of ADP in cardiomyocytes: possible role of mitochondrial outer membrane and creatine kinase in cellular regulation of oxidative phosphorylation. Biochim Biophys Acta 1993;1144:134–48.
[21] Kuznetsov AV, Tiivel T, Sikk P, Kaambre T, Kay L, Daneshrad Z, et al. Striking differences between the kinetics of regulation of respiration by ADP in slow-twitch and fast-twitch muscles in vivo. Eur J Biochem 1996;241:909–15.
[22] Saks VA, Khuchua ZA, Vasilyeva EV, Belikova O, Kuznetsov AV. Metabolic compartmentation and substrate channelling in muscle cells. Role of coupled creatine kinases in in vivo regulation of cellular respiration — a synthesis. Mol Cell Biochem 1994;133–134:155–92.
[23] Saks VA, Kuznetsov AV, Khuchua ZA, Vasilyeva EV, Belikova JO, Kesvatera T, et al. Control of cellular respiration in vivo by mitochondrial outer membrane and by creatine kinase. A new speculative hypothesis: possible involvement of mitochondrial–cytoskeleton interactions. J Mol Cell Cardiol 1995;27:625–45.
[24] Appaix F, Kuznetsov AV, Usson Y, Kay L, Andrienko T, Olivares J, et al. Possible role of cytoskeleton in intracellular arrangement and regulation of mitochondria. Exp Physiol 2003;88:175–90.
[25] Rostovtseva TK, Sheldon KL, Hassanzadeh E, Monge C, Saks V, Bezrukov SM, et al. Tubulin binding blocks mitochondrial voltage-dependent anion channel and regulates respiration. Proc Natl Acad Sci USA 2008;105:18746–51.
[26] Rostovtseva TK, Bezrukov SM. VDAC regulation: role of cytosolic proteins and mitochondrial lipids. J Bioenerg Biomembr 2008;40:163–70.
[27] Monge C, Beraud N, Kuznetsov AV, Rostovtseva T, Sackett D, Schlattner U, et al. Regulation of respiration in brain mitochondria and synaptosomes: restrictions of ADP diffusion in situ, roles of tubulin, and mitochondrial creatine kinase. Mol Cell Biochem 2008;318:147–65.
[28] Sokolova N, Vendelin M, Birkedal R. Intracellular diffusion restrictions in isolated cardiomyocytes from rainbow trout. BMC Cell Biol 2009;10:90.
[29] Sommer J, Jennings R. Ultrastructure of cardiac muscle. In: Fozzard H, Haber E, Jennings R, Katz A, Morgan H, editors. The heart and cardiovascular system. New York: Raven; 1986. p. 61–100.
[30] Fawcett DW, McNutt NS. The ultrastructure of the cat myocardium. I. Ventricular papillary muscle. J Cell Biol 1969;42:1–45.
[31] Ultrastructure of mammalian cardiac muscle. In: Forbes MS, N.S., editors. Boston: Nijhoff; 1984.
[32] Vendelin M, Beraud N, Guerrero K, Andrienko T, Kuznetsov AV, Olivares J, et al. Mitochondrial regular arrangement in muscle cells: a "crystal-like" pattern. Am J Physiol Cell Physiol 2005;288:C757–67.
[33] Beraud N, Pelloux S, Usson Y, Kuznetsov AV, Ronot X, Tourneur Y, et al. Mitochondrial dynamics in heart cells: very low amplitude high frequency fluctuations in adult cardiomyocytes and flow motion in non beating Hl-1 cells. J Bioenerg Biomembr 2009;41:195–214.
[34] Appaix F, Guerrero K, Rampal D, Izziki M, Kaambre T, Sikk P, et al. Bax and heart mitochondria: uncoupling and inhibition of oxidative phosphorylation without permeability transition. Biochim Biophys Acta 2002;1556:155–67.
[35] Klingenberg M. The A.D.P. and ATP transport in mitochondria and its carrier. Biochim Biophys Acta 2008;1778:1978–2021.
[36] Schlattner U, Wallimann T. Metabolite channeling: creatine kinase microcompartments. In: Lennarz WJ, Lane MD, editors. In Encyclopedia of Biological Chemistry. New York, USA: Academic Press; 2004. p. 646–51.
[37] Schlattner U, Tokarska-Schlattner M, Wallimann T. Mitochondrial creatine kinase in human health and disease. Biochim Biophys Acta 2006 Feb;1762(2):164–80.
[38] Colombini M. VDAC: the channel at the interface between mitochondria and the cytosol. Mol Cell Biochem 2004;256–257:107–15.
[39] Colombini M. The published 3D structure of the VDAC channel: native or not? Trends Biochem Sci 2009;34:382–9.
[40] Gellerich F, Saks VA. Control of heart mitochondrial oxygen consumption by creatine kinase: the importance of enzyme localization. Biochem Biophys Res Commun 1982;105:1473–81.
[41] Timohhina N, Guzun R, Tepp K, Monge C, Varikmaa M, Vija H, et al. Direct measurement of energy fluxes from mitochondria into cytoplasm in permeabilized cardiac cells in situ: some evidence for mitochondrial interactosome. J Bioenerg Biomembr 2009;41:259–75.
[42] Saetersdal T, Greve G, Dalen H. Associations between beta-tubulin and mitochondria in adult isolated heart myocytes as shown by immunofluorescence and immunoelectron microscopy. Histochemistry 1990;95:1–10.
[43] Redeker V. Mass spectrometry analysis of C-terminal posttranslational modifications of tubulins. Methods Cell Biol 2010;95:77–103.
[44] Luduena RF. Multiple forms of tubulin: different gene products and covalent modifications. Int Rev Cytol 1998;178:207–75.
[45] Sackett DL. Evolution and coevolution of tubulin's carboxy-terminal tails and mitochonsdria. In: Svensson OL, editor. Mitochondria: structure, functions and dysfunctions. USA: Nova Science Publishers; 2010. p. 441–70.
[46] Capetanaki Y, Bloch RJ, Kouloumenta A, Mavroidis M, Psarras S. Muscle intermediate filaments and their links to membranes and membranous organelles. Exp Cell Res 2007;313:2063–76.
[47] Ball EH, Singer SJ. Mitochondria are associated with microtubules and not with intermediate filaments in cultured fibroblasts. Proc Natl Acad Sci USA 1982;79:123–6.
[48] Heggeness MH, Simon M, Singer SJ. Association of mitochondria with microtubules in cultured cells. Proc Natl Acad Sci USA 1978;75:3863–6.
[49] Rappaport L, Oliviero P, Samuel JL. Cytoskeleton and mitochondrial morphology and function. Mol Cell Biochem 1998;184:101–5.
[50] Anesti V, Scorrano L. The relationship between mitochondrial shape and function and the cytoskeleton. Biochim Biophys Acta 2006;1757:692–9.
[51] Aon MA, Cortassa S. Coherent and robust modulation of a metabolic network by cytoskeletal organization and dynamics. Biophys Chem 2002;97:213–31.
[52] Aon MA, O'Rourke B, Cortassa S. The fractal architecture of cytoplasmic organization: scaling, kinetics and emergence in metabolic networks. Mol Cell Biochem 2004;256–257:169–84.
[53] Guerrero K, Monge C, Bruckner A, Puurand U, Kadaja L, Kaambre T, et al. Study of possible interactions of tubulin, microtubular network, and STOP protein with mitochondria in muscle cells. Mol Cell Biochem 2010;337:239–49.
[54] Wolff J. Plasma membrane tubulin. Biochim Biophys Acta 2009;1788:1415–33.
[55] Kostin S, Hein S, Arnon E, Scholz D, Schaper J. The cytoskeleton and related proteins in the human failing heart. Heart Fail Rev 2000;5:271–80.
[56] Schaper J, Kostin S, Hein S, Elsasser A, Arnon E, Zimmermann R. Structural remodelling in heart failure. Exp Clin Cardiol 2002;7:64–8.
[57] Tagawa H, Koide M, Sato H, Zile MR, Carabello BA, Cooper Gt. Cytoskeletal role in the transition from compensated to decompensated hypertrophy during adult canine left ventricular pressure overloading. Circ Res 1998;82:751–61.
[58] Winter L, Abrahamsberg C, Wiche G. Plectin isoform 1b mediates mitochondrion-intermediate filament network linkage and controls organelle shape. J Cell Biol 2008;181:903–11.

MITOCHONDRIAL ARRANGEMENT AND DYNAMICS IN INTACT CARDYOMYOCYTES TANSFECTED WITH pEGP-N1 ALPHA-ACTININ 1

Marcela Gonzalez-Granillo [1], Alexeï Grichine [2], Valdur Saks [1,3] and Yves Usson[2].

[1] INSERM U1055, Laboratory of Fundamental and Applied Bioenergetics, Joseph Fourier University, Grenoble, France

[2] Optical microscopy - Cell imaging, IAB CRI U823 Institut Albert Bonniot/Joseph Fourier University, France

[3] Laboratory of Bioenergetics,

National Institute of Chemical Physics and Biophysics, Tallinn, Estonia

ABSTRACT

Mitochondria are dynamic organelles, capable of changing their shape and morphology. Their fusion and fission have been found to be important events in a wide variety of rapidly dividing cells, both under physiological and pathophysiological conditions. Nonetheless, fusion and fission processes are not seen in all cell types, including adult cardiac cells. The aim of this work was to analyze mitochondrial arrangement and dynamics in living adult cardiac cells transfected with EGFP-N1 α-actinin plasmid to localize Z-lines. Mitochondria were stained with membrane potential sensitive dye MitoTracker Red and the cells were studied by fluorescent confocal microscopy. High speed scanning (one image every 200ms) revealed very rapid fluctuations of positions of fluorescence centers of mitochondria. These fluctuation were restricted to the organelle aea between neighboring Z-lines. Confocal analysis of autofluorescence of mitochondrial flavoproteins in fixed cardiac cells in which Z-lines were labeled with fluorescent anti-actinin antibodies also showed that separate mitochondria are localized regularly at the level of A-band of sarcomeres without fusion. These results show that mitochondria are dynamic structures which move only in a confined area. In addition, these results indicate that the structural organization of cardiac cells and mitochondria - cytoskeletal interactions prevent from fusion-fission phenomena in adult rat cardiomyocytes. If fusion of mitochondria occurs in adult normal cardiomyocytes. If mitochondrial fusion occurs in adult normal cardiac cells, it is a very infrequent phenomenon and it may be possible in perinuclear mitochondrial clusters.

INTRODUCTION

Mitochondria are organelles with a large variety of functions, such as respiration, ATP production via oxidative phosphorylation, thermogenesis, cellular differentiation, calcium signaling, and cell death, also they can change their morphology. In the heart mitochondria occupy about 30% of cell volume [1] and are tightly packed either either between the myofibrils (interfibrillar) or between the myofibrils and the cell membrane (subsarcolemmal mitochondria). Electron microscopy studies carried out in many laboratories have consistently shown that most of mitochondria in heart cells are localized at the level of A-band of sarcomeres. Segretain *et al*. [2] studied the three-dimensional arrangement of mitochondria and sarcoplasmic reticulum (SR) in cardiac muscle by electron-microscopy. The SR forms a continuous network that surrounds myofibrils. It is the primary calcium storage and source of the vast majority of the free cytosolic Ca^{2+} that drives sarcomeric contraction [3]. Segretain *et al*. concluded that the relationship among mitochondria, endoplasmic reticulum and T-tubule are constant [2]. These results were confirmed by confocal microscopy, which have shown very regular, crystal-like arrangement of separate mitochondria in heart cells [4, 5]. Confocal microscopic studies with the use of membrane potential-sensitive probes showed also the absence of electrical contact between separate mitochondria [6]. These and many other electron-microscopy studies have shown that mitochondria in adult cardiac cells do not form large mitochondrial networks [6-10], which are present in some cell types [6, 11, 12]. These structural data and studies of kinectics of respiration regulation in permeabilized cardiomyocytes showed that each sarcomere -where ATP is used- has its own mitochondrion -where ATP is synthesized-, and together with the phosphotransfer system and the feedback metabolic signaling form the intracellular energetic units (ICEU) [13]. Thus, the highly regular arrangement of mitochondria is

explained by their involvement in the ICEUs, which are the structural and functional unit of striated cardiac muscle consisting of distinct mitochondria localized at the level of sarcomeres between z-lines, and interacting with surrounding myofibrils, SR, cytoskeletal and cytoplasmic enzymes [14]. Formation of ICEUs is based on mitochondria-cytoskeletal interactions [15-17]. It is well-known hat cytoskeleton has many roles among which bringing organelles into the right position and providing a large and heterogeneous surface for associations with other structures and molecules are the most prominent and ubiquitous [18]. Therefore, neither the distribution not the appearance of mitochondria might be at random and without control. Recent studies using confocal immunofluorescence microscopy have shown different association of tubulin isotypes with mitochondria and sarcomere structures [19]. Also, intermediate filaments appear to play a role in mitochondrial positioning [17]. In muscle cells associations of mitochondria with desmin and plectin that has been described long time ago [15, 16]. Moreover, proteins which bind to the mitochondrial outer membrane and to microtubules have been identified [20]

On the other side, pioneering studies with the use of optical microscopy by Bereiter-Hahn showed that mitochondrial morphology is highly dynamic and variable between species, tissues and physiological conditions [20]. Many authors have proposed that there are a functional link between changes of energy metabolism and adaptations of mitochondrial morphology in mammalian cells [21]. These entail dynamic remodeling processes of mitochondria, through the fusion and fission phenomena. These opposite events are essential for normal mitochondrial function and participate in fundamental processes, including development, apoptosis, and ageing [18]. Therefore, mitochondrial dynamics has a physiological role in cell homeostasis. Several authors have concluded that mitochondrial fusion is necessary for normal mitochondrial functioning [21]. Thus, it has been proposed

that mitochondrial morphology adapts depending on the respiratory activity [21]. This model proposes that when respiratory activity is low, fragmented mitochondria are the preferred morphological state; whereas under respiratory conditions mitochondria undergo frequent cycles of fusion and fission to allow spreading of metabolites and macromolecules throughout the entire compartment [21]. Fission events are associated with major changes in $\Delta\psi_m$ generating functionally divergent daughters; it is required for the removal of damaged and inactive organelles. While fusion mixes the content of the parent mitochondria, through the rapid diffusion of matrix proteins, with slower migration of inner and outer membrane components. Therefore, it is proposed that mitochondrial dynamics have an impact on mitochondrial turnover and thereby the bioenergetic efficiency of the mitochondrial population within a cell. In addition, mitochondria differences in matrix density, crista structure and density may reflect different metabolic demands of cytoplasm [22] or degenerative processes [23]. Mitochondrial fusion allows efficient mixing of mitochondrial content, and it generates extended mitochondrial networks. Mitochondrial fusion has essential GTPases proteins, e.g. Mfn1, Mfn2 and OPA1. In mammals, mitofusin 1 and 2 (Mfn1 and Mfn2) are found in MOM. OPA1 is a protein found in the intermembrane space closely associated with MIM and it has been suggested to play a role in cristae maintenance [24], and its activity is dependent on the bioenegetic state of mitochondria, *i.e*. mitochondrial membrane potential-dependent [21] . Mfns and OPA1 work together to promote mitochondrial fusion. In mitochondrial fusion, MOM and MIM should fuse simultaneously in order to maintain the organelle integrity. It has been proposed also that disruption of mitochondrial fusion results in mitochondrial dysfunction and loss of respiratory capacity [21]. In contrast, several reports emphasize the importance of mitochondrial fusion under conditions of high energy demand in mammals [21, 24]. It was

shown that some cell stressors can trigger increased mitochondrial fusion, called stress-induced mitochondrial hyperfusion, in an Mfn1- and Opa1-dependent manner [18].

While I has been shown that neonatal cardiac myocytes and cultured cells lines have highly dynamic mitochondria [6, 11], crystal-like arrangement of separate mitochondria in adult cardiomyocytes and their involvement in ICEUs described above contradicts the increasingly popular proposal that formation of reticular mitochondria network by fusion of separate mitochondria is needed their normal functional activity [21, 25]. In addition, mechanism and roles of proteins involved in fusion and fission of mitochondria are not fully understood. Notwithstanding over 30 years of research on mitochondrial dynamics have provided a good insight into mitochondrial morphology-function interaction, all these broad information have also brought many a controversy about these phenomena. Moreover, it is highly risky to generalized, thus most of the studies have been perform in immortal cell-lines, e.g. HeLa, COS-7, CV1-4A, NB HL-1 cells, etc. and these strongly depend on culturing conditions [12]. Mitochondrial dysfunction is suggested to play a central role in metabolic and chronic diseases; under these conditions, accumulation of dysfunctional mitochondria leads to oxidative and impaired cellular functions.

Previous studies by Beraud *et al*. [6] from our laboratories by using high speed scanning fluorescent confocal microscopy revealed that the local mitochondrial dynamics and fluctuations of their fluorescence centers. The aim of study was to use this highly informative method to analyze in healthy adult cardiac cells the mitochondrial positioning and dynamics through the visualization of mitochondria by autofluorescence or MitoTracker Red to reveal very precisely the mitochondrial positions with respect to the sarcomere Z-line. To visualize the Z-line of sarcomeres, we used immunolabeling or *in vivo* transfection of

α-actinin, respectively. This gives us the possibility to describe correctly how mitochondria are arranged in the heart cells and to find whether mitochondrial fusion occurs, and how frequent, in healthy adult cardiomyocytes.

MATERIALS AND METHODS

Isolation of adult cardiac myocytes:

Adult rat cardiomyocytes were isolated by adaptation of the technique described previously [26]. Male Wistar rats (300-350g) were anesthetized and the heart was quickly excised preserving a portion of the aorta and placed into a canula to perfuse with continuously oxygenated isolation buffer (IB) containing: 117mM NaCl, 5.7mM KCl, 4.4mM $NaHCO_3$, 1.5mM KH_2PO_4, 1.7mM $MgCl_2$, 11.7mM Glucose, 10 mM Creatine, 20mM Taurine, 10mM Phosphocreatine, 2mM Pyruvate, and 21.1mM HEPES, pH 7.2. For the first 5 minutes the heart was washed with oxygen-saturated IB with a flow rate of 15-20 mL/min. The heart was digested using IB containing collagenase type II (0.03 U/mL), $CaCl_2$ (0.026mM), and BSA (2mg/mL). After digestion, the heart was wash with IB containing: BSA (2mg/mL), $CaCl_2$ (0.026 mM), Soy trypsin inhibitor (STI) (0.42mM). Cells were suspended in sedimentation buffer and passed through a fine mesh (200µm opening) to remove all connective tissue. Rod-like shape CM were left to sediment within 3-5', then the supernatant containing the damaged-cells was discarded. This re-suspension-sedimentation cycle with calcium-tolerant cells was performed twice. After these cycles, cells were transferred gradually into the respective [Ca^{2+}] gradients solution buffers or Mitomed depending if CM were going to be used for immunofluorescence or transfection. Animal procedures were approved by "Comité d'éthique pour l'expérimentation animale, Comité d'éthique Cométh Grenoble" Comité National de Réflexion Ethique sur l'Expérimentation Animale sous le numéro 12: 33_LBFA-VS-01.

Isolation of adult left-ventricle fibers:

Adult rat heart fibers were isolated by dilacerations of the cardiac left-ventricle fibers [27]. Male Wistar rats (300-350g) were anesthetized and the heart was quickly excised and washed in Solution A (2.77mM CaK_2EGTA, 7.23mM K_2EGTA, 20mM Imidazole, 0.5mM DTT, 6.56mM $MgCl_2$, 53.3mM MES, 20mM Taurine, 5.3 Na_2ATP and 15mM Na_2PCr). Fibers of left ventricle were carefully dilacerated in solution A. Dilacerated fibers were transferred to Mitomed solution. Fibers were incubated with 10µM Mitotracker® deep red for 30' at 37°C. Mitomed solution was removed. Thereafter, fibers were fixed as it is explained below.

Cell preparation for confocal microscopy.

Autofluorescence: Freshly isolated CM were incubated for 10' in a petri dish containing oxygen-saturated Mitomed and 5µM of rotenone to produce the oxidation of flavoproteins. This was done to improve the imaging of mitochondria autofluorescence. Thereafter, cells were fixed as it is described below.

Immunofluorescence: Isolated cardiomyocytes and cardiac fibers were fixed using paraformaldehyde (PFA) 4% + Glutaraldehyde 0.1% solution for 1h on ice. Then cells were washed 3 times with PBS containing 2% of BSA. Thereafter, cardiac cells were permeabilized with 1% Triton X-100 during 30' at room temperature (25° C), followed by 3 washes with 2% BSA solution. After fixation and permeabilization, cardiomyocytes were incubated with the 1^{st} antibody (Anti-alpha actinin antibody [SA-20] – abcam, ab82247) with 2% BSA in PBS, overnight. The next day cardiac cells were washed once with PBS containing 2% BSA and incubated with the chosen 2^{nd} antibody (Cy™ 5-conjugated Afini-Pure goat anti mouse IgG - Jackson Immunoresearch 115-175-146, or DyLight 488 goat anti-mouse IgG, Fcγ fragment specific ML – Jackson Immuno research 115-485-008)for 2 hours at room temperature.

Transfection: Isolated cardiomyocytes were sedimented with increasing gradient Ca^{2+}concentration (0.2mM, 0.7mM and 0.8mM) buffers containing BSA and Soy Trypsin Inhibitor (STI), at 37° C. After washing the cardiomyocytes with the three gradients Ca^{2+} concentration, a final wash was performed with the recovery culture medium; then all the medium was removed. 16µL of cardiomyocytes were placed in each well of 2-well lab-tek, containing 2mL of "recovery" culturing medium, and left in the incubator (37° C, 5% CO_2) for 4h. After this time, media was carefully removed from the wells trying not to disturb the cardiomyocytes, and the transfection culture medium containing the plasmid pEGFP-N1 alpha-actinin 1 and the transfection reagent (lipofectamine™) was added. Cells were left in the incubator overnight and up to 20-22h to have a positive transfection. In order to localize mitochondria in transfected cardiomyocytes MitoTrcker Red was used. MitoTracker Red stains mitochondria in live cells and its accumulation is dependent upon membrane potential with an excitation/emission wavelenght of 581nm/644nm. The pEGFP-N1 alpha-actinin is a high-copy mammalian non-viral plasmid with a size of 4700bp and an eGFP tag, resistant to kanamycin.

Confocal imaging fixed cells

The fluorescence images were acquired with a Leica TCS SP2 AOBS inverted laser scanning confocal microscope (Leica, Heidelberg, Germany) equipped with a 63x water immersion objective (HCX PL APO 63.0x1.20 W Corr). Laser excitation was 488nm (green fluorescence) and 633nm (red fluorescence). Images were then analyzed using Volocity software (Improvision, France).

Colocalization studies

For fixed and immunolabeled cells: α-actinin was immunostained with Cy5-labeled antibody according to the protocol describe elsewhere [19]. They were imaged using the 63x/1.4 oil immersion Plan Apo objective, 633 nm HeNe laser and 638-747 nm detection of LSM710NLO confocal microscope (Carl Zeiss). The pinhole value was set to 1 Airy unit. Optical slices closest to the glass surface were analyzed in order to minimize the optical distortions in cardiomyocytes. Mitochondria distribution in fixed cardiomyocytes was visualized using flavoprotein autofluorescence signal excited with the two-photon laser at 720 nm and integrated between 408 and 546 nm. The choice of this label-free imaging of mitochondria allowed one to avoid any possible spectral bleed-though to the near-infrared detection channel for α-actinin. The very low background signal was detected in case of nonspecific control with the Cy5-labeled secondary antibody. The signal to noise was improved using 16 line scan repetitions and 6μs pixel dwell time. Overall photobleaching with the used laser intensities did not exceed 1%. The red channel images were not treated for the sake of intensity comparison; the green channel images were processed with a Top-hat square shape filter to improve the contrast of rectangular mitochondria pattern (MetaMorph, Universal Imaging).

Confocal imaging of mitochondria dynamics in living transfected cells

Cells were transfected with pEGFP-N1 alpha-actinin as described previously to localize Z-lines. For mitochondrial imaging (localization) cells were loaded with 0.2μM mitochondrial specific probe MitoTracker® Red FM (Molecular probes®, Invitrogen™). Cardiomyocytes were imaged using the 63x/1.20 W Corr water immersion C-Apochromat objective, z-lines were excited with 488 nm Ar laser and 500-540 nm detection and mitochondria were observed with 561 nm DPSS laser and 580-650 detection of LSM710NLO confocal

microscope (Carl Zeiss). The pinhole value was set 1 Airy unit. The acquisition parameters of time series images were: 3000 frames, image size 106x58 pixels, and pixel dwell time 0.64 µs. Images were analyzed as follows:

Image analysis

Image processing: most of the image processing and image analyzes were performed with the ImageJ public domain software using scripts and plugins especially developed for this work. The first part of the image processing was the correction of the average level of fluorescence through the time to compensate photobleaching (long time-series of 2000 to 3000 frames). Because the aim was to characterize the proper motion of mitochondria it was necessary to correct the frames for all global motions such as cell contraction and/or cell drift that may occur over long duration recordings. To achieve this goal, XT projections (for the z-line channel) and YT projections (for the mitochondria channel) were calculated for each time series. For example YT projection (Fig. 1) consisted in building a column of pixels for each frame in which each pixel corresponds to the average intensity of the corresponding pixel row of the frame. Thus we built the YT projection by compiling the calculated columns in a single image where the horizontal axis accounted for time. This representation offered the advantage to summarize all the vertical motions during the recording. The next step consisted in calculating cross-correlation curves between each successive pair of columns and shifting up or down one frame with respect to the other by an amount depending on the maximum of cross-correlation. Using this method for both XT projection (horizontal motion) and YT projection (vertical motion), it was possible to cancel out most of the global motions due to cell drift and cell contraction.

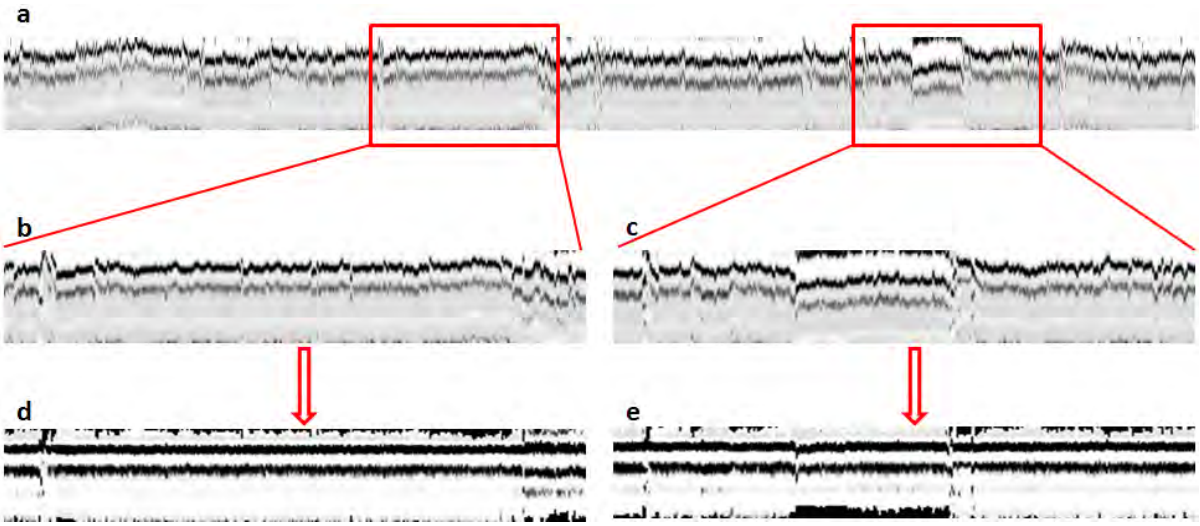

Figure 1. Cancellation of global motion: a) YT projection (horizontal axis: time, vertical axis: average intensity along frame rows) of a time series images (2000 frames), the first box illustrate the cell drift, the second box illustrate cell displacement between contractions.

b) and c) Zoom fragments of the raw time series images.

d) and e) Zoom fragments after registration by mean column to column intercorrelation.

Thereafter, the analysis of mitochondrial fluctuations (*i.e*. number of mitochondria and position of their fluorescence centers of gravity) in adult cardiomyocytes was done using the gradient clustering algorithm method as described in detail in Beraud *et al*. [6]. Briefly, this algorithm use a physical analogy where a fluorescent pixel is considered as a physical object characterized by a couple of coordinates *x* and *y* (i.e. the initial position on the image grid) and a weight or virtual mass, equal to the fluorescence intensity at this point. The concentration of virtual masses (fluorescence intensities) in particular regions of the image (*i.e*. mitochondria and z-lines) creates “gravitational wells” attracting the neighboring points. In fact, the algorithm calculates local intensity gradients in order to aggregate in an iterative manner the points belonging to the same mitochondrion or z-line. After a number of iterations these points will occupy a single position corresponding to the mass center of the mitochondrion, which acts as a gravitational attractor. To complete the algorithm, a merging procedure is applied where all the points with the same coordinates are merged into a unique point or line, which is considered as the mass center of a single mitochondrion or the

z-line. Using this clustering technique and under the hypothesis of an invariant Point Spread Function, it was possible to obtain the actual optical resolution. The positions of these fluorescent centers directly depend on the configuration of the mitochondrial inner membrane to which the fluorescent dye used is fixed, or the position of Z-lines where the eGFP α-actinin has been expressed.

In addition, mitochondrial fluctuations were quantified. The trajectories of the fluorescence gravity centers were plotted as a function of time and the average scatters parallel to the long and the short axes of the myocardial cells were calculated for each mitochondrion. The motion behavior of mitochondrial fluorescence centers was expressed in terms of a random walk movement process, akin to Brownian movement process. All mathematical equations and analysis can be found in detail Beraud *et al*. [6].

RESULTS

1. Mitochondrial organization in fixed cardiomyocytes: confocal immunofluorescence imaging.

a) 2-D imaging of fixed cardiac cells

Mitochondrial organization was observed by confocal microscopy in several fixed cardiac cells, showing the remarkable regular arrangement of mitochondria akin to “crystal-like” and Z-lines, as it has been previously reported by other groups [4, 6, 9]. To study whether or not fuision events were a common phenomenon in healthy adult cardiac cells, we observed the arrangement of mitochondria and Z-lines by the use of mitochondrial autofluorescence and immunolabeling of α-actinin (Z-lines). Figure 2 shows six examples (A, B, C, D, E, an F) of the characteristic sarcomeric transversal Z lines and regular “crystal-like” arrangement of mitochondria. These two dimensional (2-D) images were recorded in separate channels to avoid the misinterpretation of information and were done in different cells in order to obtain statistical information. It can be appreciated in the examples of the merged images below how mitochondria and Z lines are well intercalated. Therefore, this highly reproducible arrangement of healthy adult cardiac cells makes us think about the very seldom possibility that fusion events happen, as it has been previously suggested by other authors [6, 7, 28, 29].

In addition, fixed isolated cardiac cells were analyzed to observe how reproducible this arrangement was. Figure 3 shows the different positional and mathematical analyzes done in the different cardiac cells studied; the mitochondrial arrow of each cardiomyocyte analyzed is indicated in white boxes in Figure 2. Plots of figure 3 have the following organization, the letter belongs to figure 2, and the number corresponds to the analysis performed (1: Intensity profiles, 2: Fourier transform of the intensity profiles, and 3. Covariance analysis of

intensity profiles). Solid-lines represent mitochondrial autofluorescence and dashed-lines α-actinin immunofluorescence (Z lines).

The intensity profile analyzes give an overview of the trends of mitochondria and α-actinin over the length of the cardiomyocytes. As it can be seen in the intensity profile plots (A1, B1, C1, D1, E1, and F1) mitochondrial autofluorescence and α-actinin immunofluorescence had a regular periodicity among them, and it can be appreciated that mitochondria were interleaved with z-lines. These results are in good agreement with what it has been published before [9].

Fourier transform analyzes of each image analyzed are highly interesting. The Fourier transforms of mitochondrial autofluorescence - solid-line - and α-actinin immunofluorescence - dashed-line - (Z lines) revealed that both had a spatial frequency of 0.55 μm^{-1}, this corresponds to a periodicity of 1.82 μm.

Finally, mitochondrial autofluorescence and α-actinin immunofluorescence were analyzed by the covariance analysis of intensity profiles. This analysis allowed measuring both waveforms as a function of a time-lag variables. All plots displayed a negative crossed-correlation (-1), these results confirmed us what it was seen in the images (Fig. 2) and by the intensity profiles plots (Fig. 61 - A1, B1, C1, D1, E1, and F1), which means that mitochondria were perfectly interleaved with Z lines.

b) 3-D analysis of mitochondrial arrangement in fixed cardiac fibers

Previous observations in adult healthy isolated-fixed cardiac cells were confirmed by analyzing dilacerated cardiac fibers. The analysis of cardiac fibers also allowed us to observe if fusion events happen in cardiac cells in a more physiological state. Dilacerated cardiac

fibers were stained with MitoTracker® deep red FM, thereafter fixed and immunolabeled with α-actinin.

Figure 4 shows a picture of the dilacerated cardiac fiber used to make the three-dimensional (3-D) image (Supplementary video). In order to confirm previous observations of the absence of interfibrillar mitochondrial fusion, a 3-D analysis was highly necessary to make. The 3-D image was re-constructed from 12 optical slices (2.2 µm) and it showed the characteristic sarcomeric Z lines and crystal-like arrangement of interfibrillar mitochondria within the fiber.

Figure 4 displays mitochondria in red (stained with MitoTracker® deep red FM) and α-actinin in green (immunolabeled with FITC). White lines (a, b, c, and d) represent the selected areas for further analysis.

The dilacerated fibers were also studied by positional and mathematical analyzes (Fig. 5). Figure 4 displays the areas (white lines) used for positional and mathematical analyzes. In addition, all analyzes were done from 5 optical slices (0.2 µm each slice). The 5 optical sections, approximately 1 µm thickness, were used for these analyzes taking in consideration the thickness of a mitochondrial layer. This restrictive choice makes the analyzes more precise and informative than taking in consideration the whole stack acquired.

Once more, each plot of the selected arrow of mitochondria was identified by lower-case letter (a, b, c, and d) and next to a number, which indicates the analysis done (1: Intensity profiles, 2: Fourier transform of the intensity profiles, and 3. Covariance analysis of intensity profiles). Solid-lines represent MitoTracker® Red fluorescence signal (mitochondria) and dashed-lines α-actinin immunofluorescence (Z lines).

The intensity profile plots (Fig. 5 - a1, b1, c1, and d1) give an overview of the patterns of mitochondria and α-actinin over the length of the cardiac fiber. As it can be appreciated in

the intensity profile plots, MitoTracker® Red fluorescence and α-actinin immunofluorescence had a regular periodicity among them, and mitochondria were interleaved with z-lines. These results are in good agreement with what it was shown previously and with what it has been published before [9].

Fourier transform analyzes of each image analyzed results highly interesting. The Fourier transforms of MitoTracker® Red fluorescence - solid-line - (mitochondria) and α-actinin immunofluorescence - dashed-line - (Z lines) revealed that both had a spatial frequency of 0.5 μm^{-1}, this corresponds to a periodicity of 2 μm. This periodicity was reproducible in all analyzes of cardiac fibers and the ~0.2μm difference between isolated fixed cardiac cells and dilacerated cardiac fibers depended on the contraction state of them, as previously described by Yaniv et al. [10]. Moreover, these analyzes disclosed that mitochondria present most of the times two close fluorescent peaks, which usually were found in all acquired images.

Furthermore, MitoTracker® Red fluorescence and α-actinin immunofluorescence were analyzed by the covariance analysis of the intensity profiles (Fig.5 - a3, b3, c3, and d3). This crossed-correlation allowed measuring both waveforms as a function of a time-lag variables and all results displayed a negative crossed-correlation (-1). These results confirmed what it was seen in the intensity profiles plots (Fig. 5 - a1, b1, c1 and d1). A negative cross-correlation of -1 means, that mitochondria were perfectly interleaved with Z lines. These results in dilacerated fibers confirmed our previous observations in isolated cardiac cells.

2. Mitochondrial dynamics in non-fixed transfected cells.

Finally, isolated, cultured and transfected adult cardiomyocytes were used to confirm whether or not fusion events occur in adult healthy mammalian cardiac cells. Figure 6 shows just an example of how *in vivo* transfected-cardiomyocytes looked like. Part of their rod-like shape was lost due to the time of incubation. However, as it has been shown in previous studies and in the present work, the arrangement of mitochondria is also very regular in the transfected GFP-α-actinin cardiac cells.

Transfection of isolated cardiac cells was done to see whether mitochondria undergo to any fusion event, fast speed scanning recordings of transfected cells showed (Supplementary video) the constant presence of Z lines between mitochondria during the acquisition of the frames (3000 frames) of a selected area (14.01µm x 7.65µm) which were used for the dynamical studies.

Figure 7 shows how the area analyzed by the clustering algorithm (explained in methods) looked like after the image processing. The studies of mitochondrial dynamics, required an increased speed scanning to achieve the pixel dwell time close to 0.64µs and intervals between images of 200ms (Supplementary video). At this speed scanning mitochondrial fluorescent centers and alignment of Z lines were monitored. The position of these fluorescent centers depended on both, the precise localization of mitochondria in the cells and the configuration of their inner membrane. Moreover, the observation of fluorescent centers (blue dots, Figure 7) is due to individual mitochondrial bodies. If mitochondria were connected with each other assembling a network, we would not have been able to see fluorescent centers. Instead we would have seen a line along the fused mitochondria. On the

other side, fluorescence alignment of Z lines depended on their localization between mitochondria.

Finally, the mitochondrial upper arrow of the recorded mitochondria (Fig 7) was studied once again by positional and mathematical analyzes (Fig. 8). Once again, the following plots the solid lines represent the MitoTracker® red fluorescent signal (mitochondria) and dashed-lines are the GFP-α-actinin fluorescence (Z lines).

The intensity profile plot (Fig. 8) shows a general outlook of the patterns of mitochondria and α-actinin over the length of the area selected. As it can be appreciated in the intensity profile plots, MitoTracker® Red fluorescence and GFP-α-actinin fluorescence, both fluorescent signals had a regular periodicity among them. As it is observed, mitochondria were interleaved with z-lines. These results in isolated, cultured and transfected cardiac cells are in good agreement with what it was shown previously in the isolated fixed cardiac cells and the dilacerated fixed cardiac fibers.

The Fourier transforms (Fig. 8) of MitoTracker® Red fluorescence - solid-line - (mitochondria) and α-actinin immunofluorescence - dashed-line - (Z lines) revealed that both had a spatial frequency of 0.55 μm^{-1}, this corresponds to a periodicity of 1.82 μm. This periodicity was reproducible in other analyzes of transfected cardiac cells (results not shown). Once again, these analyzes disclosed that mitochondria present most of the times two close fluorescent peaks, which usually were found in all acquired images from fixed isolated and dilacerated cardiac cells and fibers, respectively.

The analysis of isolated, cultured and transfected cardiomyocytes were completed by the covariance analysis of the intensity profiles (Fig. 8). The crossed-correlation allowed measuring both waveforms as a function of a time-lag variables and displaying a negative crossed-correlation (-1). These results confirmed what it was seen in the intensity profiles

plot, how mitochondria were interleaved with Z lines. A negative cross-correlation of -1 means, that mitochondria were perfectly interleaved with Z lines. These results in dilacerated fibers confirmed our previous observations in isolated cardiac cells.

DISCUSSION

All our present and earlier results and observations show the absence of any link between respiratory activity and mitochondrial fusion-fission cycles in cardiac cells. None of analyzed samples, isolated cardiomyocytes and cardiac fibers, displayed the presence of a mitochondrial tubular network neither any fusion event in interfibrillar mitochondria within time interval of our observations, as it has been seen in previous studies [6, 9]. Fixed isolated cardiac cells and fixed cardiac fibers showed that the Z-lines labeled with fluorescent α-actinin antibodies are regularly interleaved with mitochondria. Our observations in non-fixed cardiomyocytes revealed that the distribution of mitochondria is interleaved with z-lines and both have a regular periodicity of 1.8 μm in isolated cardiac cells and 2 μm in cardiac fibers. In addition, it was observed that interfibrillar mitochondria are confined in a specific area, surrounded by sarcomeres and the tubular system. Isolated-fixed, transfected cardiomyocytes, and dilacerated-fixed fibers displayed the same structural organization. The present results are consistent with previous observations obtained with use of both electron and confocal microscopy [4, 5], where it was shown that in adult cardiac cells and fibers, separate mitochondria are very regularly arranged in fixed positions by cytoskeletal proteins.

Direct measurements of oxygen consumption rates showed that in permeabilized cardiomyocytes these very regularly arranged separate mitochondria show maximal ADP-dependent respiration rates corresponding to the maximal rate of oxygen uptake by intact hearts, and this maximal respiration rate is equally seen in isolated mitochondrial preparations (see Figure 9). These results very clearly and completely invalidate the hypothesis that mitochondrial fusion is needed for maximal respiratory activity and thus for regulation of energy fluxes in muscle cells. In fact, our results show the contrary: in two types of cells of cardiac phenotype the fused reticular mitochondria are seen in HL -1 cells

with significantly decreased respiratory activities, while both in normal adult cardiomyocytes with separate regularly arranged mitochondria and isolated mitochondria the respiratory activities are maximal [14].

The heart is vitally important organ with high energy demand for blood ejection into circulation, totally depending upon permanent mitochondrial respiration and energy supply to contractile system via oxidative phosphorylation and phosphotransfer networks. Both cardiac work performance and oxygen consumption are dependent upon ventricular filling, which in turn depends on pre- or afterload [30-32]. This is the Frank- Starling law of the heart [1]. Stretch-induced increase in the length of sarcomeres of striated cardiac muscle results in changes in the overlapping between thin and thick filaments, alteration in myofilament lattice spacing, increased thin filament cooperativity and, consequently, in the number of force-generating cross-bridges [30]. Length-dependent activation of sarcomeres includes also changes of calcium sensitivity by cardiac myofilaments, which is of major importance particularly for low sarcomere length values [33]. A diminished functional response of the heart to changes in ventricle filling is observed in heart failure [31, 32]. Depending upon the workload, the rate of oxygen consumption by heart can increase rapidly by factor of 20 [].Therefore, the Frank-Starling law describes how the contractile function of myocardium determines the rate of oxygen consumption, substrate uptake, and fuel selection [34-36]. The major substrates used by the heart are carbohydrates and fatty acids [34, 36]. Respiration and energy fluxes in the cardiac cells are regulated on beat-to-beat basis by workload dependent mechanisms of local metabolic feedback signaling between sarcomeres and mitochondria within ICEUs [14].In turn, sarcomere contraction is initiated by excitation-contraction coupling and calcium release by calcium release units, CRU [37-39], the force of sarcomere contraction depending upon its length. Calcium is needed also for

activation of mitochondrial Krebs cycle dehydrogenases [40, 41]. All these mechanisms require very precise structural organization of the cell and very regular arrangement of mitochondria, sarcoplasmic reticulum and sarcomeres and evidently exclude any participation of fusion-fission cycles. In the cells of cardiac phenotype, mitochondrial fusion results in strong decrease of the respiration rate, as it is seen in the non-beating HL-1 cells.

In this paper we again show the role of only one among many other cytoskeletal proteins, the tubulin, that apart for having other physiological roles, they are also a sort of physical barrier between this highly arranged interfibrillar mitochondria preventing them from regular fusion events. Electronic and confocal microscopy imaging have given us a better understanding of cytoskeletal proteins role in cardiac functioning. In addition, tubulin binding to the mitochondrial outer membrane results in formation of a supercomplex, the Mitochondrial Interactosome (MI) [14]. The role of the MI is to ensure continuous recycling of adenine nucleotides in mitochondria, ADP transphosphorylation and metabolic channeling of ATP via ANT to MtCK, and ADP back into matrix, resulting in the export of free energy from mitochondria into cytoplasm as flux of phosphocreatine. The quantitative Metabolic Control Analysis analysis of MI in permeabilized cardiomyocytes revealed a high flux control by ANT, MtCK and the ATP synthasome, involved in ADP/ATP cycling [42-44]. Therefore, the MI is rate-controlling of respiration, conveying local metabolic signal in the ICEUs [42-44]. This is the physiological role of VDAC interaction with βII-tubulin, which restricts the permeability of the mitochondrial outer membrane to adenine nucleotides but not for creatine or PCr and directs the energy transfer via PCr-CK pathway [45-48]. Quantitative in vivo measurements of energy fluxes in the heart with the use of ^{18}O tracer method by Dzeja and Terzic groups showed directly that about 80% of energy is carried out

from mitochondria by PCr fluxes, the remaing flux being carried by other phosphotrasfer pathways [49].

In conclusion, functional and structural studies have revealed the major importance of structure-function relationship in the regulation of cardiac cell metabolism [14, 19, 28, 50, 51]. The regulation of respiration and energy fluxes in cardiac cells occurs on beat-to-beat basis and is thus very rapid (contraction cycle occurs within 200 ms), requiring localized mechanisms of regulation within ICEUs and CRU. The microtubular network (tubulin isotypes), intermediate filaments (plectin, desmin) and microfilaments (actin), form specific structures that represent a vital organization for contraction cycle, and for regulation of energy supply [52-54].

Mitochondrial fusion will evidently need remodeling also the cytoskeletal structures. This explains why it is seen in non-beating HL-1 cells lacking sarcomere structures and beta II tubulin, as well as MtCK [19].

The transfection of non-fixed cardiomyocytes with GFP-α-actinin in the present work let us corroborate previous observations by Beraud *et al*. [6] that under normal conditions mitochondria of adult cardiomyocytes remain in rather fixed positions undergoing rapid-low amplitude fluctuations of their fluorescence centers within the sarcomere. Our observations by high speed scanning showed fast movements of mitochondrial fluorescent centers. This goes in agreement with Beraud's studies [6], where it was suggested that these fluctuation changes may reflect frequent and continuous transitions in the configuration of the mitochondrial inner membrane cristae. Despite the contraction of cardiac cells, the presence of Z-lines was constant through the study in all cardiomyocytes analyzed. These observations are in accordance with previous studies by Yaniv *et al*. [10] where it was showed how

contraction causes mitochondria deformation in three dimensions during cardiomyocytes contraction-relaxation cycle. Therefore, mitochondria expand asymmetrically along the width- and thick-axes during cell contraction. Nevertheless, they did not find apparent fusion nor fission events in the population studied. Absence of fusion-fission phenomena in adult cardiac cells has also been reported by Beraud *et al*. studies where that cytoskeletal structures have an important role in mitochondrial dynamics, especially in fusion and fission events. In healthy adult cardiac cells, mitochondrial fusion seems to be a seldom event. Therefore, the structural organization of cardiac mitochondria has not only a structural role but also a functional role as it has been previously reported by several groups [14].

However, it has been reported the presence of perinuclear clusters in many mammalian cells [24], and that at key stages in cellular differentiation some alterations in mitochondrial shape and distribution are developmentally programmed. On the other side, alterations in mitochondrial distribution and morphology are associated with a variety of pathological conditions, including cardiomyophaties and cancer [17, 24]. Previous reports have shown that in cardiac diseases, mitochondria were found to be disorganized and abnormally small [24]. Also, it has been reported that under various treatments or diseases, heat cells accumulated either abnormally large or abnormally small mitochondria populations [55]. Therefore, we proposed that in healthy adult cardiac cells fusion events of interfibrillar mitochondria hardly ever occur.

ACKNOWLEDGEMENTS

This work was supported by project SYBECAR from Agence de la Recherche Nationale and by INSERM, France, and by National Council of Science and Technology of Mexico (CONACYT).

Technical assistance by Noelia Caro in preparation of cardiac fibers is acknowledged.

REFERENCES

1. Opie, L.H., *The heart: physiology, metabolism, pharmacology, and therapy*. Vol. XII. 1984, London: Orlando: Grune & Stratton. 392.
2. Segretain, D., A. Rambourg, and Y. Clermont, *Three dimensional arrangement of mitochondria and endoplasmic reticulum in the heart muscle fiber of the rat.* Anat Rec, 1981. **200**(2): p. 139-51.
3. Dorn, G.W., 2nd, *Mitochondrial dynamics in heart disease.* Biochim Biophys Acta.
4. Vendelin, M., et al., *Mitochondrial regular arrangement in muscle cells: a "crystal-like" pattern.* Am J Physiol Cell Physiol, 2005. **288**(3): p. C757-67.
5. Aon, M.A., S. Cortassa, and B. O'Rourke, *Mitochondrial oscillations in physiology and pathophysiology.* Adv Exp Med Biol, 2008. **641**: p. 98-117.
6. Beraud, N., et al., *Mitochondrial dynamics in heart cells: very low amplitude high frequency fluctuations in adult cardiomyocytes and flow motion in non beating Hl-1 cells.* J Bioenerg Biomembr, 2009. **41**(2): p. 195-214.
7. Aon, M.A., S. Cortassa, and B. O'Rourke, *Percolation and criticality in a mitochondrial network.* Proc Natl Acad Sci U S A, 2004. **101**(13): p. 4447-52.
8. Vendelin, M., et al., *Intracellular diffusion of adenosine phosphates is locally restricted in cardiac muscle.* Mol Cell Biochem, 2004. **256-257**(1-2): p. 229-41.
9. Gonzalez-Granillo, M., et al., *Studies of the role of tubulin beta II isotype in regulation of mitochondrial respiration in intracellular energetic units in cardiac cells.* J Mol Cell Cardiol. **52**(2): p. 437-47.
10. Yaniv, Y., et al., *Analysis of mitochondrial 3D-deformation in cardiomyocytes during active contraction reveals passive structural anisotropy of orthogonal short axes.* PLoS One. **6**(7): p. e21985.
11. Griffiths, E.J., D. Balaska, and W.H. Cheng, *The ups and downs of mitochondrial calcium signalling in the heart.* Biochim Biophys Acta. **1797**(6-7): p. 856-64.
12. Sauvanet, C., et al., *Energetic requirements and bioenergetic modulation of mitochondrial morphology and dynamics.* Semin Cell Dev Biol. **21**(6): p. 558-65.
13. Guzun, R., et al., *Regulation of respiration in muscle cells in vivo by VDAC through interaction with the cytoskeleton and MtCK within Mitochondrial Interactosome.* Biochim Biophys Acta.
14. Saks, V., et al., *Intracellular Energetic Units regulate metabolism in cardiac cells.* J Mol Cell Cardiol. **52**(2): p. 419-36.
15. Saetersdal, T., G. Greve, and H. Dalen, *Associations between beta-tubulin and mitochondria in adult isolated heart myocytes as shown by immunofluorescence and immunoelectron microscopy.* Histochemistry, 1990. **95**(1): p. 1-10.
16. Stromer, M.H. and M. Bendayan, *Immunocytochemical identification of cytoskeletal linkages to smooth muscle cell nuclei and mitochondria.* Cell Motil Cytoskeleton, 1990. **17**(1): p. 11-8.
17. Yaffe, M.P., *The machinery of mitochondrial inheritance and behavior.* Science, 1999. **283**(5407): p. 1493-7.
18. Chan, D.C., *Mitochondria: dynamic organelles in disease, aging, and development.* Cell, 2006. **125**(7): p. 1241-52.
19. Guzun, R., et al., *Mitochondria-cytoskeleton interaction: Distribution of beta-tubulins in cardiomyocytes and HL-1 cells.* Biochim Biophys Acta. **1807**(4): p. 458-69.
20. Bereiter-Hahn, J. and M. Voth, *Dynamics of mitochondria in living cells: shape changes, dislocations, fusion, and fission of mitochondria.* Microsc Res Tech, 1994. **27**(3): p. 198-219.
21. Westermann, B., *Bioenergetic role of mitochondrial fusion and fission.* Biochim Biophys Acta.
22. Ord, M.J., *The effects of chemicals and radiations within the cell: an ultrastructural and micrurgical study using Amoeba proteus as a single-cell model.* Int Rev Cytol, 1979. **61**: p. 229-81.
23. Brunner, A., Jr., J.A. Bilotta, and D.D. Morena, *Mitochondria, hemosomes and hemoglobin biosynthesis.* Cell Tissue Res, 1983. **233**(1): p. 215-25.

24. Hom, J. and S.S. Sheu, *Morphological dynamics of mitochondria--a special emphasis on cardiac muscle cells.* J Mol Cell Cardiol, 2009. **46**(6): p. 811-20.
25. Chen, H., A. Chomyn, and D.C. Chan, *Disruption of fusion results in mitochondrial heterogeneity and dysfunction.* J Biol Chem, 2005. **280**(28): p. 26185-92.
26. Saks, V.A., Y.O. Belikova, and A.V. Kuznetsov, *In vivo regulation of mitochondrial respiration in cardiomyocytes: specific restrictions for intracellular diffusion of ADP.* Biochim Biophys Acta, 1991. **1074**(2): p. 302-11.
27. Kuznetsov, A.V., et al., *Analysis of mitochondrial function in situ in permeabilized muscle fibers, tissues and cells.* Nat Protoc, 2008. **3**(6): p. 965-76.
28. Saks, V., et al., *Structure-function relationships in feedback regulation of energy fluxes in vivo in health and disease: mitochondrial interactosome.* Biochim Biophys Acta. **1797**(6-7): p. 678-97.
29. Aon, M.A., et al., *Synchronized whole cell oscillations in mitochondrial metabolism triggered by a local release of reactive oxygen species in cardiac myocytes.* J Biol Chem, 2003. **278**(45): p. 44735-44.
30. Patterson, S.W., H. Piper, and E.H. Starling, *The regulation of the heart beat.* J Physiol, 1914. **48**(6): p. 465-513.
31. Katz, A.M., *Ernest Henry Starling, his predecessors, and the "Law of the Heart".* Circulation, 2002. **106**(23): p. 2986-92.
32. Opie, L., *The Heart. Physiology, from cell to circulation*. 1998, Lippincott-Raven Publishers: Philadelphia. p. 43-63.
33. Fukuda, N. and H.L. Granzier, *Titin/connectin-based modulation of the Frank-Starling mechanism of the heart.* J Muscle Res Cell Motil, 2005. **26**(6-8): p. 319-23.
34. Lopaschuk, G.D., et al., *Myocardial fatty acid metabolism in health and disease.* Physiol Rev. **90**(1): p. 207-58.
35. Jaswal, J.S., et al., *Targeting fatty acid and carbohydrate oxidation--a novel therapeutic intervention in the ischemic and failing heart.* Biochim Biophys Acta. **1813**(7): p. 1333-50.
36. Neely, J.R. and H.E. Morgan, *Relationship between carbohydrate and lipid metabolism and the energy balance of heart muscle.* Annu Rev Physiol, 1974. **36**: p. 413-59.
37. Wang, S.Q., et al., *Imaging microdomain Ca2+ in muscle cells.* Circ Res, 2004. **94**(8): p. 1011-22.
38. Maltsev, A.V., et al., *Synchronization of stochastic Ca(2)(+) release units creates a rhythmic Ca(2)(+) clock in cardiac pacemaker cells.* Biophys J. **100**(2): p. 271-83.
39. Rovetti, R., et al., *Spark-induced sparks as a mechanism of intracellular calcium alternans in cardiac myocytes.* Circ Res. **106**(10): p. 1582-91.
40. Hansford, R.G. and D. Zorov, *Role of mitochondrial calcium transport in the control of substrate oxidation.* Mol Cell Biochem, 1998. **184**(1-2): p. 359-69.
41. McCormack, J.G., A.P. Halestrap, and R.M. Denton, *Role of calcium ions in regulation of mammalian intramitochondrial metabolism.* Physiol Rev, 1990. **70**(2): p. 391-425.
42. Tepp, K., et al., *Metabolic control analysis of integrated energy metabolism in permeabilized cardiomyocytes - experimental study.* Acta Biochim Pol. **57**(4): p. 421-30.
43. Kholodenko, B.N., et al., *Subtleties in control by metabolic channelling and enzyme organization.* Mol Cell Biochem, 1998. **184**(1-2): p. 311-20.
44. Kholodenko, B.N. and H.V. Westerhoff, *Metabolic channelling and control of the flux.* FEBS Lett, 1993. **320**(1): p. 71-4.
45. Aliev, M.K. and V.A. Saks, *Compartmentalized energy transfer in cardiomyocytes: use of mathematical modeling for analysis of in vivo regulation of respiration.* Biophys J, 1997. **73**(1): p. 428-45.
46. Saks, V.A., R. Ventura-Clapier, and M.K. Aliev, *Metabolic control and metabolic capacity: two aspects of creatine kinase functioning in the cells.* Biochim Biophys Acta, 1996. **1274**(3): p. 81-8.

47. Vendelin, M., O. Kongas, and V. Saks, *Regulation of mitochondrial respiration in heart cells analyzed by reaction-diffusion model of energy transfer.* Am J Physiol Cell Physiol, 2000. **278**(4): p. C747-64.
48. Saks, V.A., et al., *Role of the creatine/phosphocreatine system in the regulation of mitochondrial respiration.* Acta Physiol Scand, 2000. **168**(4): p. 635-41.
49. Dzeja, P.P., et al., *Adenylate kinase-catalyzed phosphotransfer in the myocardium : increased contribution in heart failure.* Circ Res, 1999. **84**(10): p. 1137-43.
50. Saks, V., N. Beraud, and T. Wallimann, *Metabolic compartmentation - a system level property of muscle cells: real problems of diffusion in living cells.* Int J Mol Sci, 2008. **9**(5): p. 751-67.
51. Saks, V., et al., *Cardiac system bioenergetics: metabolic basis of the Frank-Starling law.* J Physiol, 2006. **571**(Pt 2): p. 253-73.
52. Guerrero, K., et al., *Study of possible interactions of tubulin, microtubular network, and STOP protein with mitochondria in muscle cells.* Mol Cell Biochem. **337**(1-2): p. 239-49.
53. Vertessy, B.G., et al., *Alternative binding of two sequential glycolytic enzymes to microtubules. Molecular studies in the phosphofructokinase/aldolase/microtubule system.* J Biol Chem, 1997. **272**(41): p. 25542-6.
54. Schaper, J., et al., *Structural remodelling in heart failure.* Exp Clin Cardiol, 2002. **7**(2-3): p. 64-8.
55. Kane, L.A. and R.J. Youle, *Mitochondrial fission and fusion and their roles in the heart.* J Mol Med (Berl). **88**(10): p. 971-9.

LEGENDS OF FIGURES

2-D imaging of fixed cardiac cells

Figure 2. Examples of 6 different fixed cardiomyocytes: panels A, B, C, D, E, and F display a section of the confocal merged images of α-actinin (red) with Cy5 immunolabeling and autofluorescence of flavoproteins mitochondria (green) in adult rat cardiomyocytes. All panels show the intracellular distribution of Z-lines (α-actinin) and mitochondria. The white box show on each panel represents the area studied in detail. White bar 5µm.

Figure 3. Analysis of intensity profiles in fixed adult rat cardiac cells: Plots, Fourier and Covariance analyzes of intensity profiles: from panels A, B, C, D, E, and F refer to the respective case shown in Fig. 60.

1. Intensity profiles of immunolabeled α-actinin (dashed-line) with Cy5 and flavoproteins autofluorescence of mitochondria (solid-line), of the selected area.
2. Fourier transforms of the intensity profiles, mitochondria (solid-line) and α-actinin (dashed-line).
3. Covariance analysis of the intensity profiles (mitochondria and α-actinin).

Three dimensional analysis of mitochondrial arrangement in fixed cardiac fibers

Figure 4. Image of three dimensional structure of a cardiac fiber: It shows the intracellular distribution of Z-lines (α-actinin) and mitochondria. Mitochondria (red) were stained with MitoTracker® deep red FM and Z-lines were visualized by immunolabeling of anti-α-actinin

(green). White lines display the areas analyzed. The 3-D movie of adult rat cardiac fiber was built from the confocal sections (12 optical slices) with a total thickness of 2.2 µm. (3-D movie included in supplementary data).

Figure 5. Plots of Intensity profiles, Fourier transforms of intensity profiles and Covariance analyzes of intensity profiles in fixed adult rat cardiac fibers: from lines drew in figure 62 a, b, c, and d different analysis of the intracellular distribution of mitochondria and Z-lines were done. To visualized mitochondria MitoTracker® deep red FM was used and for Z-lines α-actinin immunolabeling was used. Analyzes were done in 1µm (5 optical sections) thick, this corresponds to the thickness of one layer of mitochondria.

1. Intensity profiles of immunolabeled α-actinin (dashed-line) with Cy5 and flavoproteins autofluorescence of mitochondria (solid-line), of the selected area.

2. Fourier transforms of the intensity profiles, mitochondria (solid-line) and α-actinin (dashed-line).

3. Covariance analysis of the intensity profiles (mitochondria and α-actinin).

Mitochondrial dynamics in cultured transfected cells.

Figure 6. Example of a transfected cardiomyocytes with pEGFP-N1 α-actinin and MitoTracker® red FM: Image of a cultured-transfected adult cardiac cell with pEGFP-N1 α-actinin (green) and stain mitochondria (red). Positive-transfected cells were visualized 20-22h after its transfection. A selected area of the transfected cells was recorded by high speed scanning to observe mitochondrial fluctuations of position in their fluorescent centers. White bar 5µm.

Figure 7. Example the clustering technique applied in isolated cardiomyocytes transfected with pEGFP-N1 α-actinin and labeled with MitoTracker® red FM: It displays Z-lines (green), mitochondria (red), and mitochondrial fluorescent centers (blue). (Mitochondrial fluctuations movie is included in supplementary data). White bar 2 μm.

Figure 8. Plots of Intensity profiles, Fourier transforms of intensity profiles and Covariance analyzes of intensity profiles in cultured transfected adult rat cardiac cells: Analyzes were done from the selected area taken by confocal microscopy high speed scanning.

1. Intensity profiles of α-actinin (dashed-line) and mitotracker (solid-line) of the selected area.

2. Fourier transforms of the intensity profiles, mitotracker (solid-line) and α-actinin (dashed-line).

3. Covariance analysis of the intensity profiles (mitochondria and α-actinin).

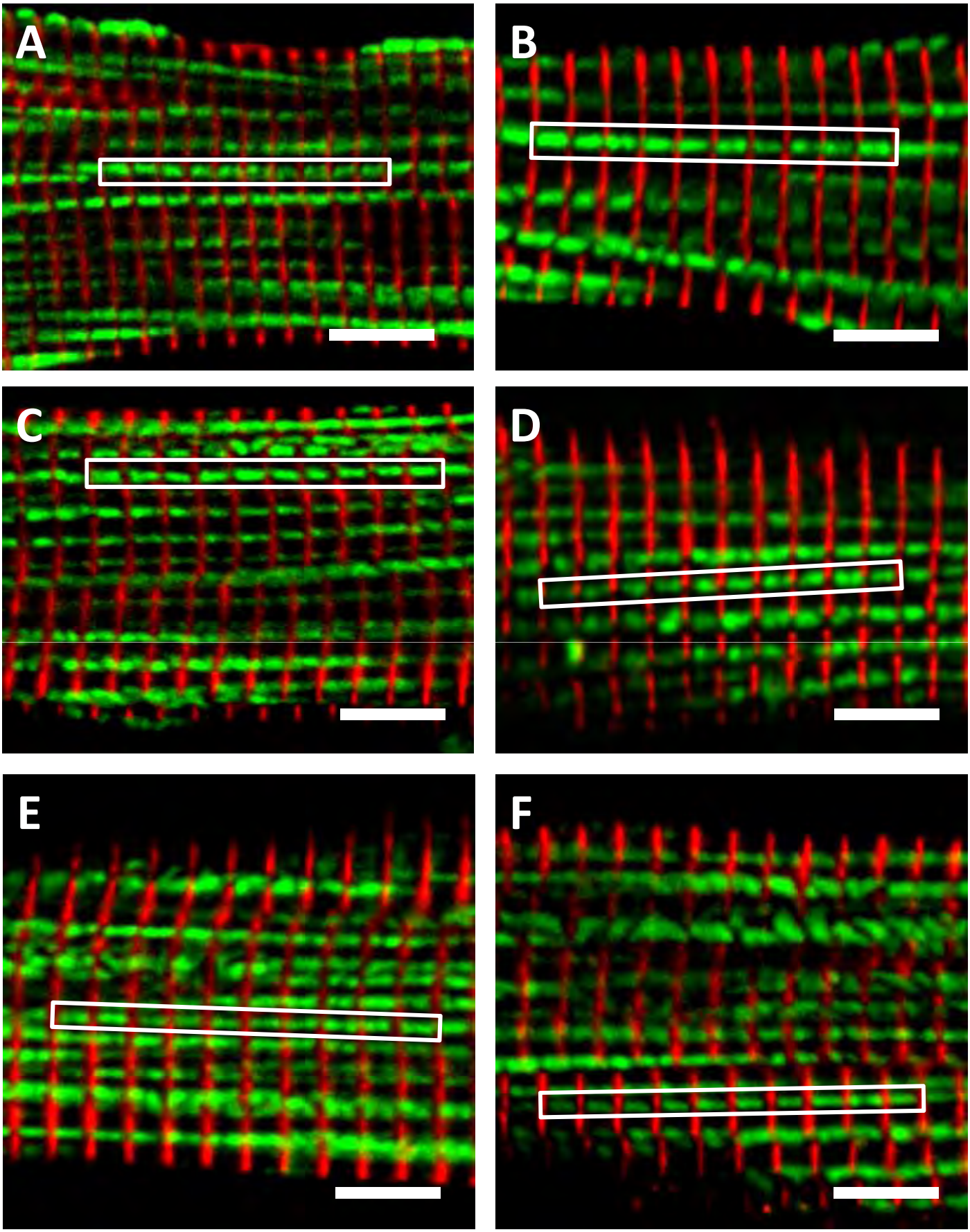

Figure 2

A.1.

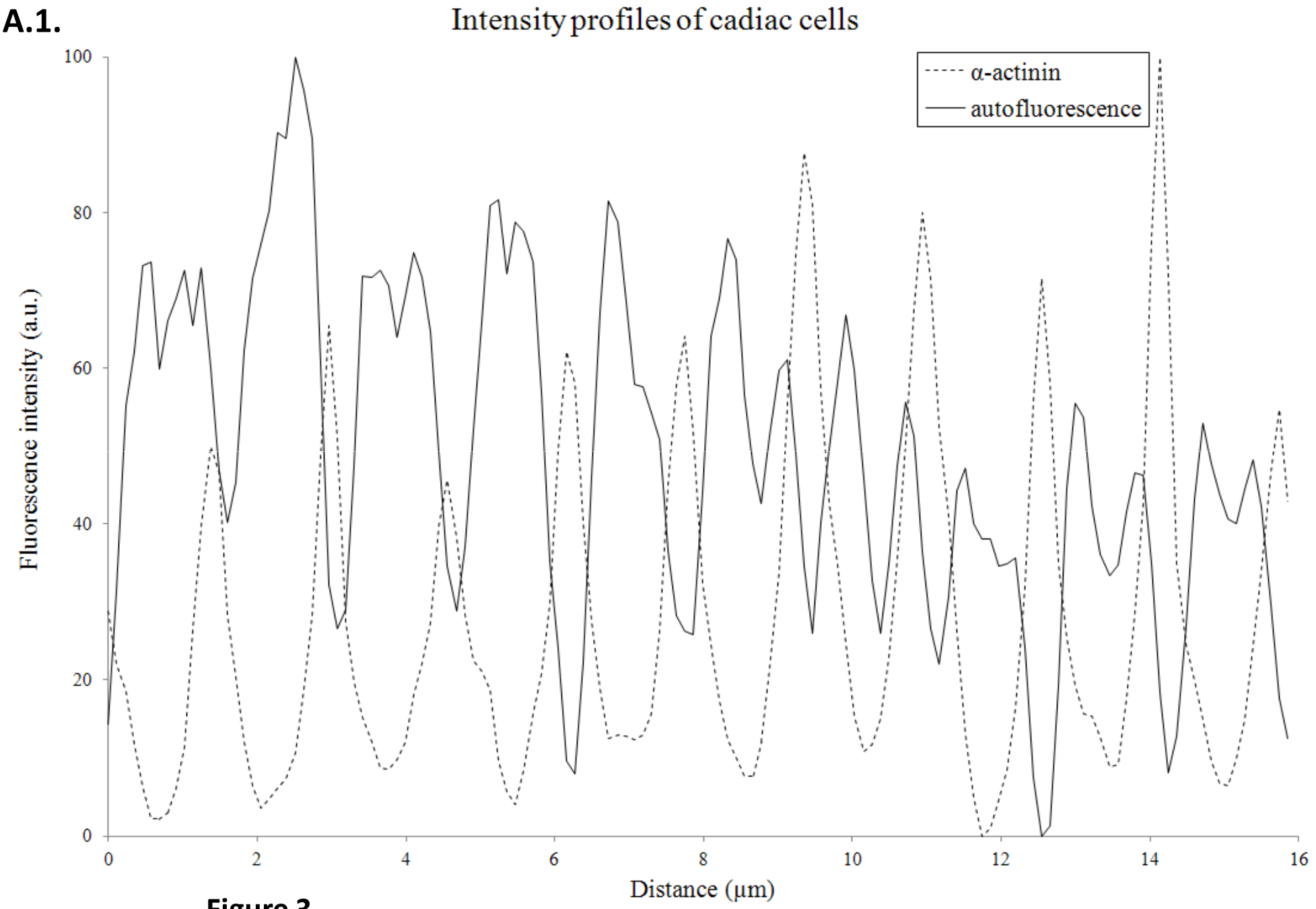
Intensity profiles of cadiac cells
α-actinin
autofluorescence
Fluorescence intensity (a.u.)
Distance (μm)
0
20
40
60
80
100
0
2
4
6
8
10
12
14
16

Figure 3

A.2.

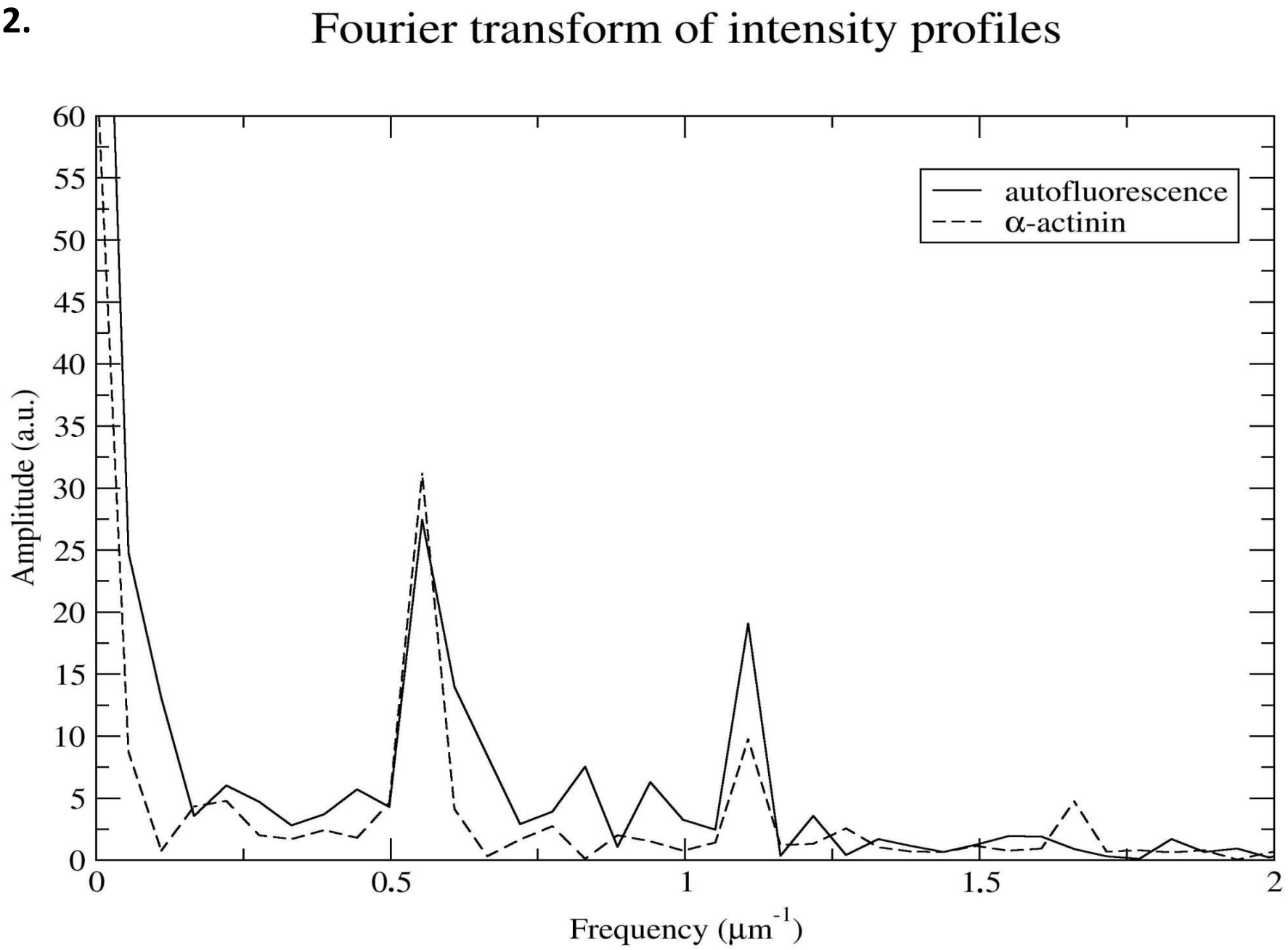
Fourier transform of intensity profiles
autofluorescence
α-actinin
Amplitude (a.u.)
Frequency (μm-1)
0
5
10
15
20
25
30
35
40
45
50
55
60
0
0.5
1
1.5
2

Figure 3

A.3.

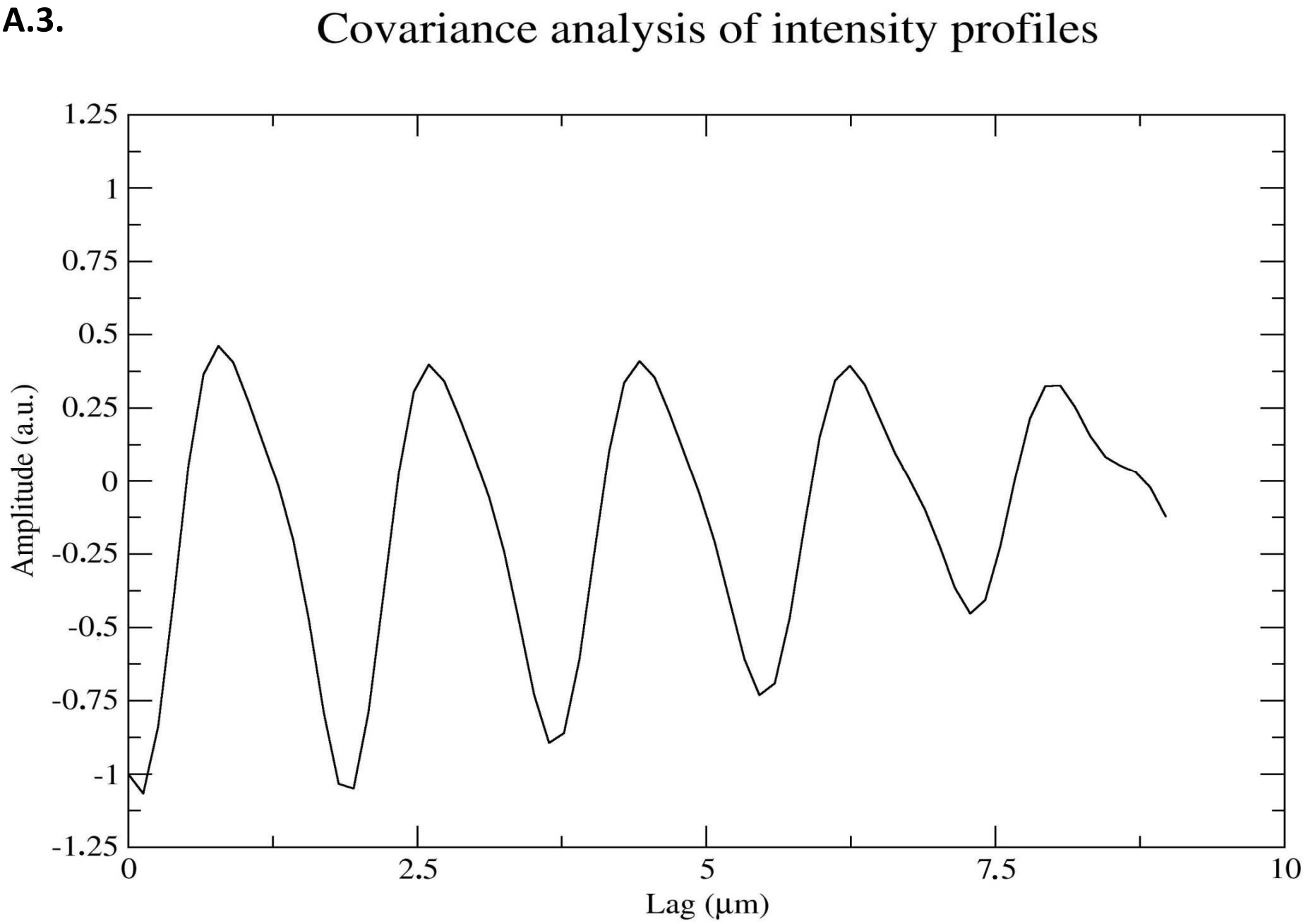
Covariance analysis of intensity profiles
Amplitude (a.u.)
1.25
1
0.75
0.5
0.25
0
-0.25
-0.5
-0.75
-1
-1.25
0
2.5
5
7.5
10
Lag (μm)

Figure 3

B.1.

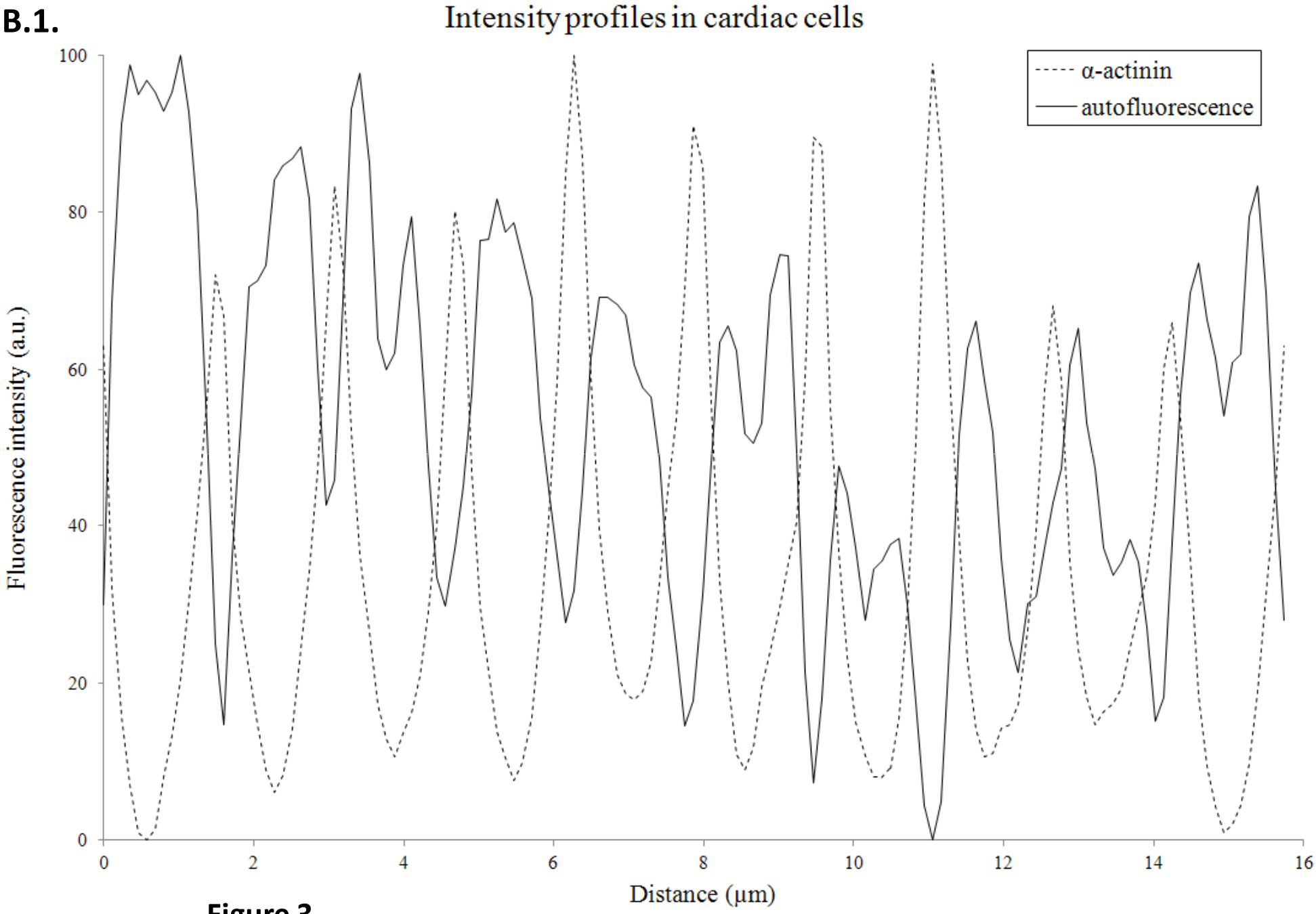
Intensity profiles in cardiac cells
α-actinin
autofluorescence
Fluorescence intensity (a.u.)
Distance (µm)
0
20
40
60
80
100
0
2
4
6
8
10
12
14
16

Figure 3

B.2.

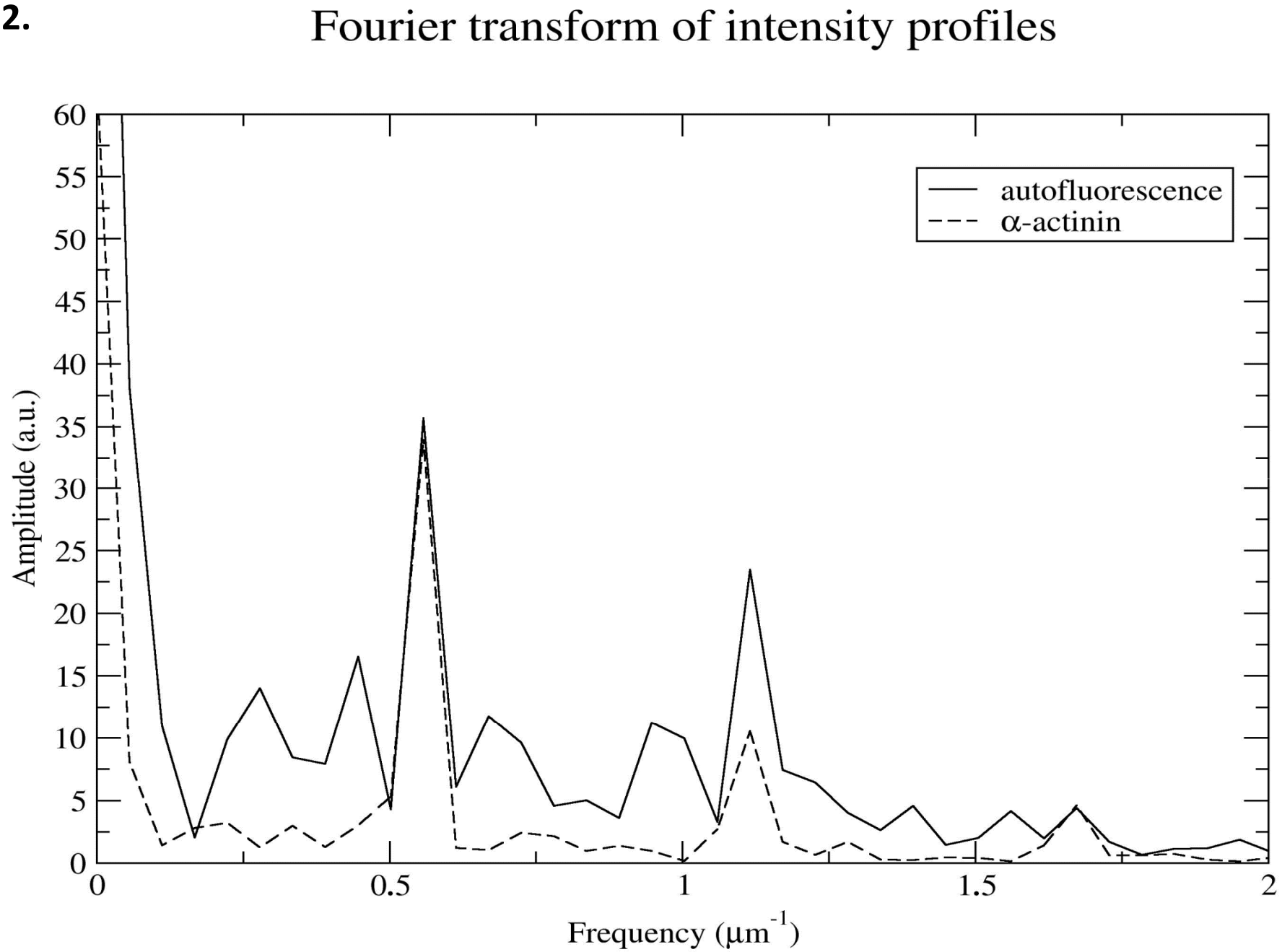
Fourier transform of intensity profiles
autofluorescence
α-actinin
Amplitude (a.u.)
Frequency (μm-1)
0
5
10
15
20
25
30
35
40
45
50
55
60
0
0.5
1
1.5
2

Figure 3

B.3.

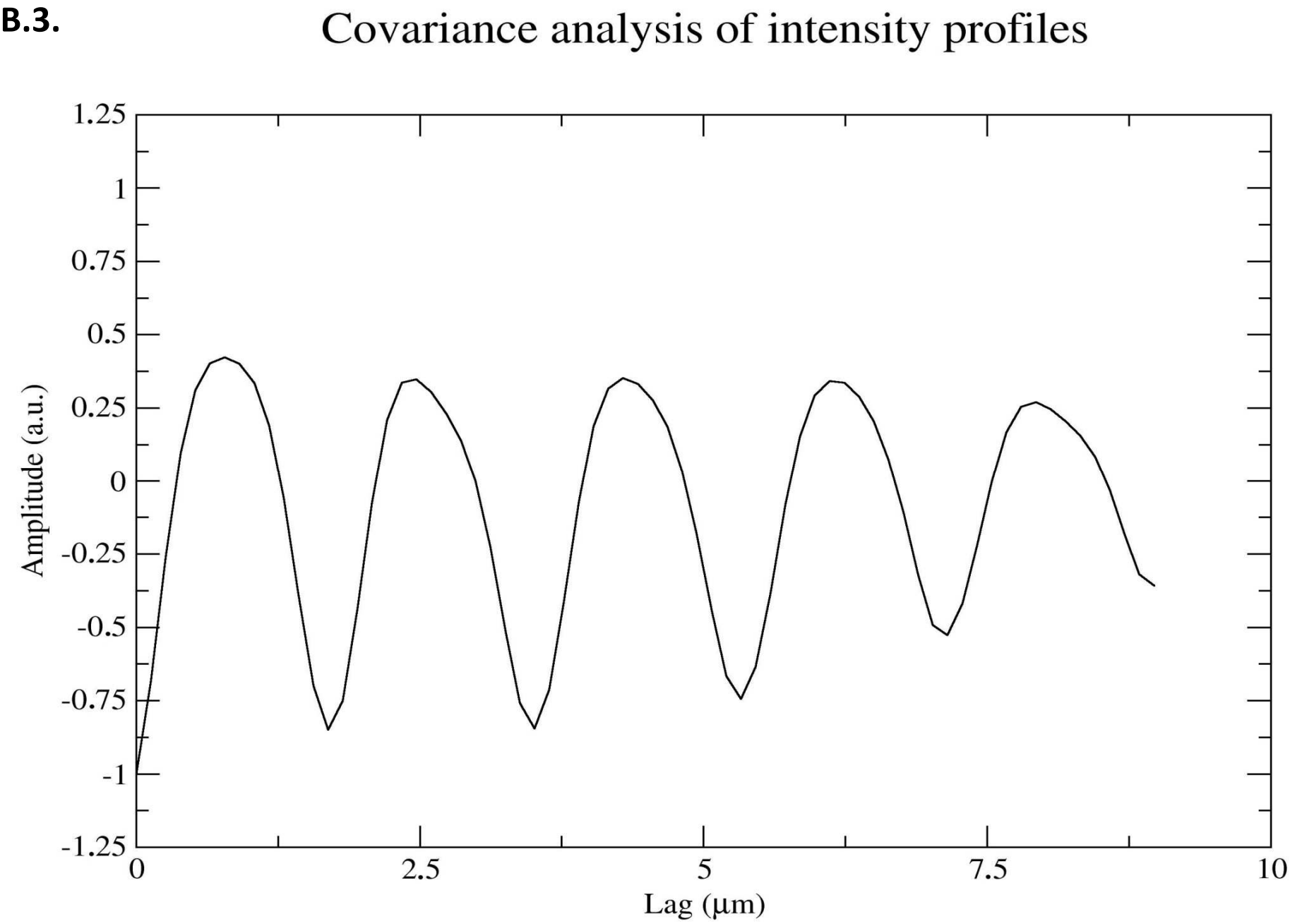
Covariance analysis of intensity profiles
Amplitude (a.u.)
1.25
1
0.75
0.5
0.25
0
-0.25
-0.5
-0.75
-1
-1.25
0
2.5
5
7.5
10
Lag (μm)

Figure 3

C.1.

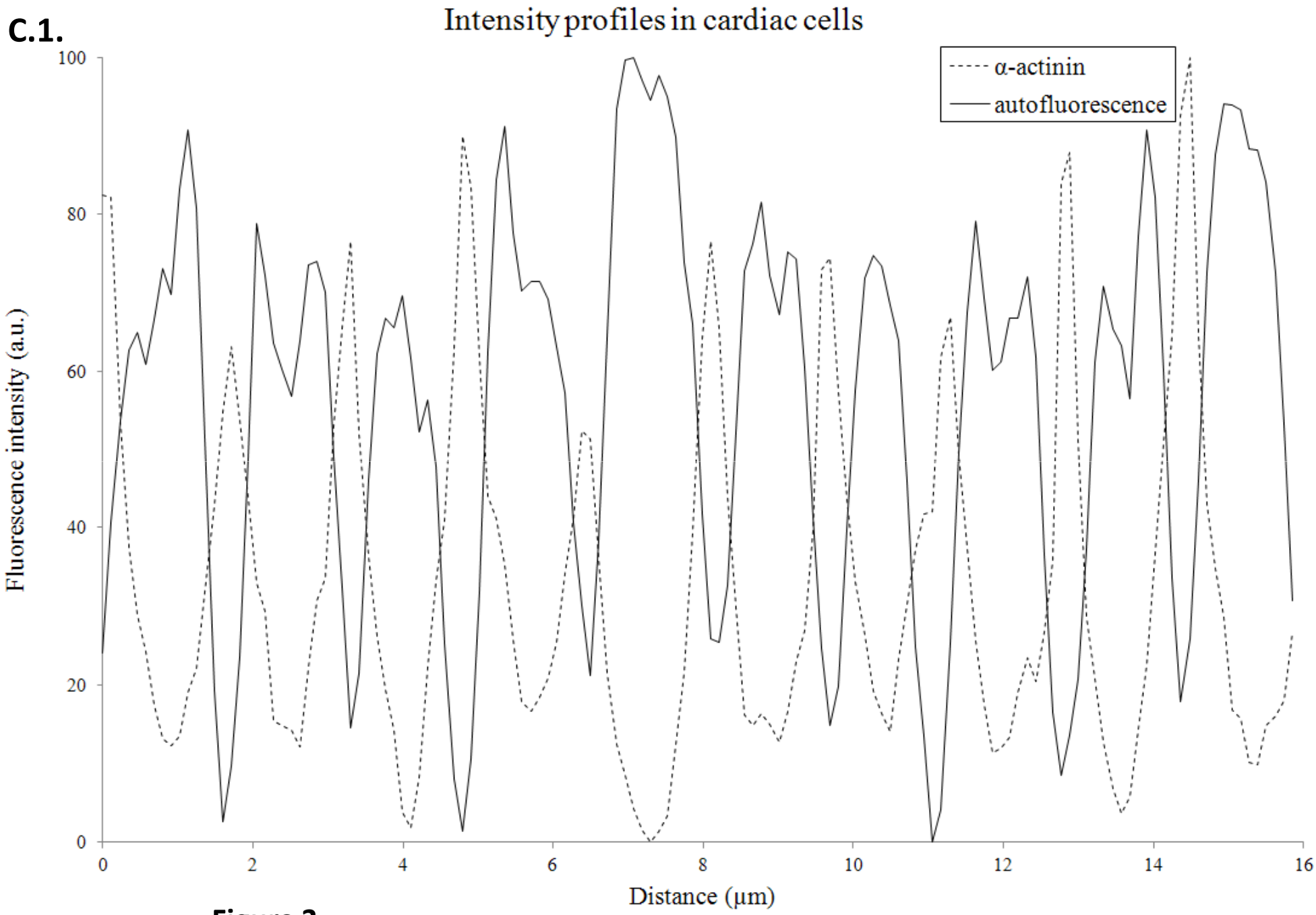
Intensity profiles in cardiac cells
α-actinin
autofluorescence
Fluorescence intensity (a.u.)
Distance (µm)
0
20
40
60
80
100
0
2
4
6
8
10
12
14
16

Figure 3

C.2.

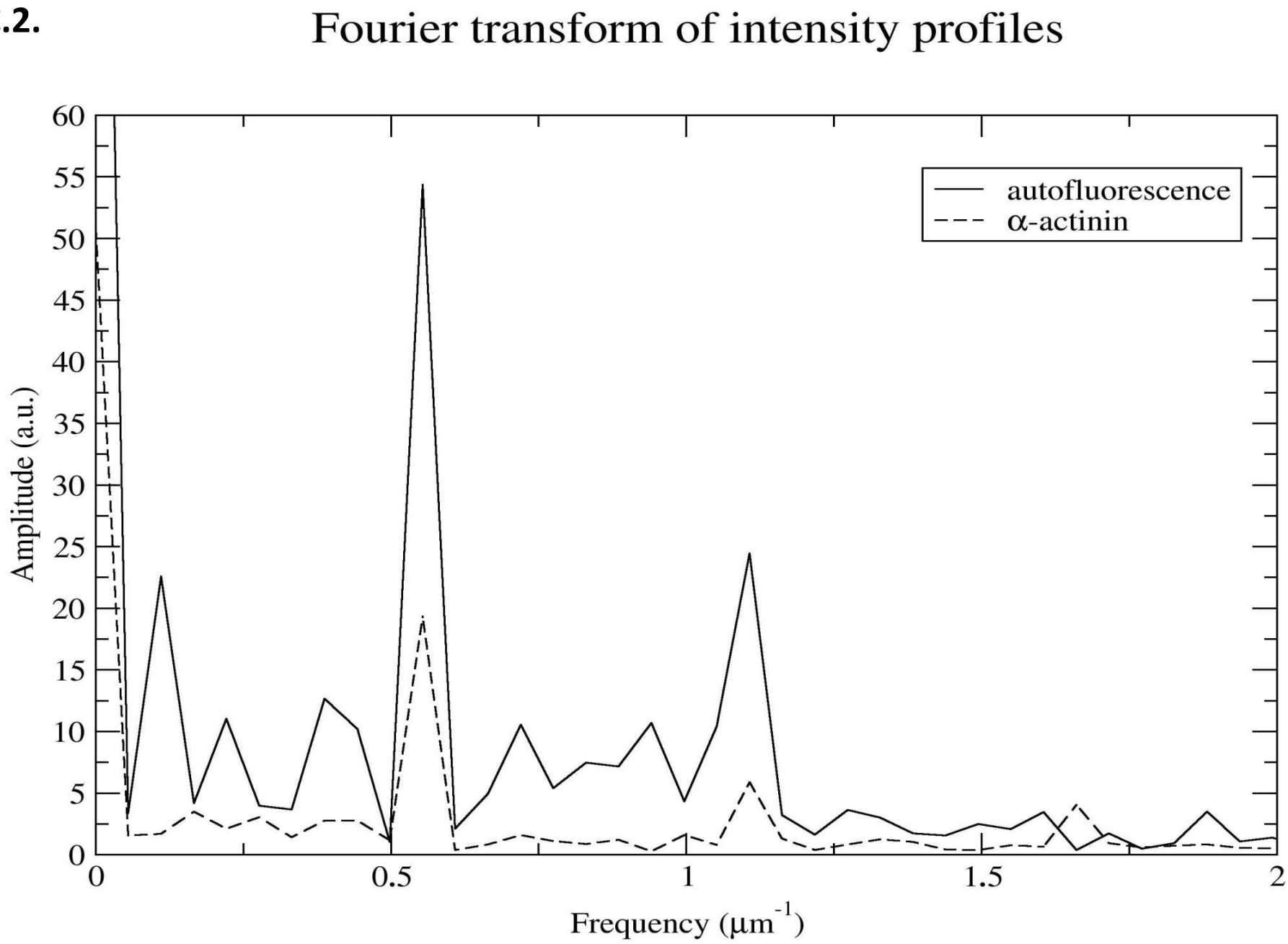
Fourier transform of intensity profiles
autofluorescence
α-actinin
Amplitude (a.u.)
Frequency (μm-1)
0
5
10
15
20
25
30
35
40
45
50
55
60
0
0.5
1
1.5
2

Figure 3

C.3.

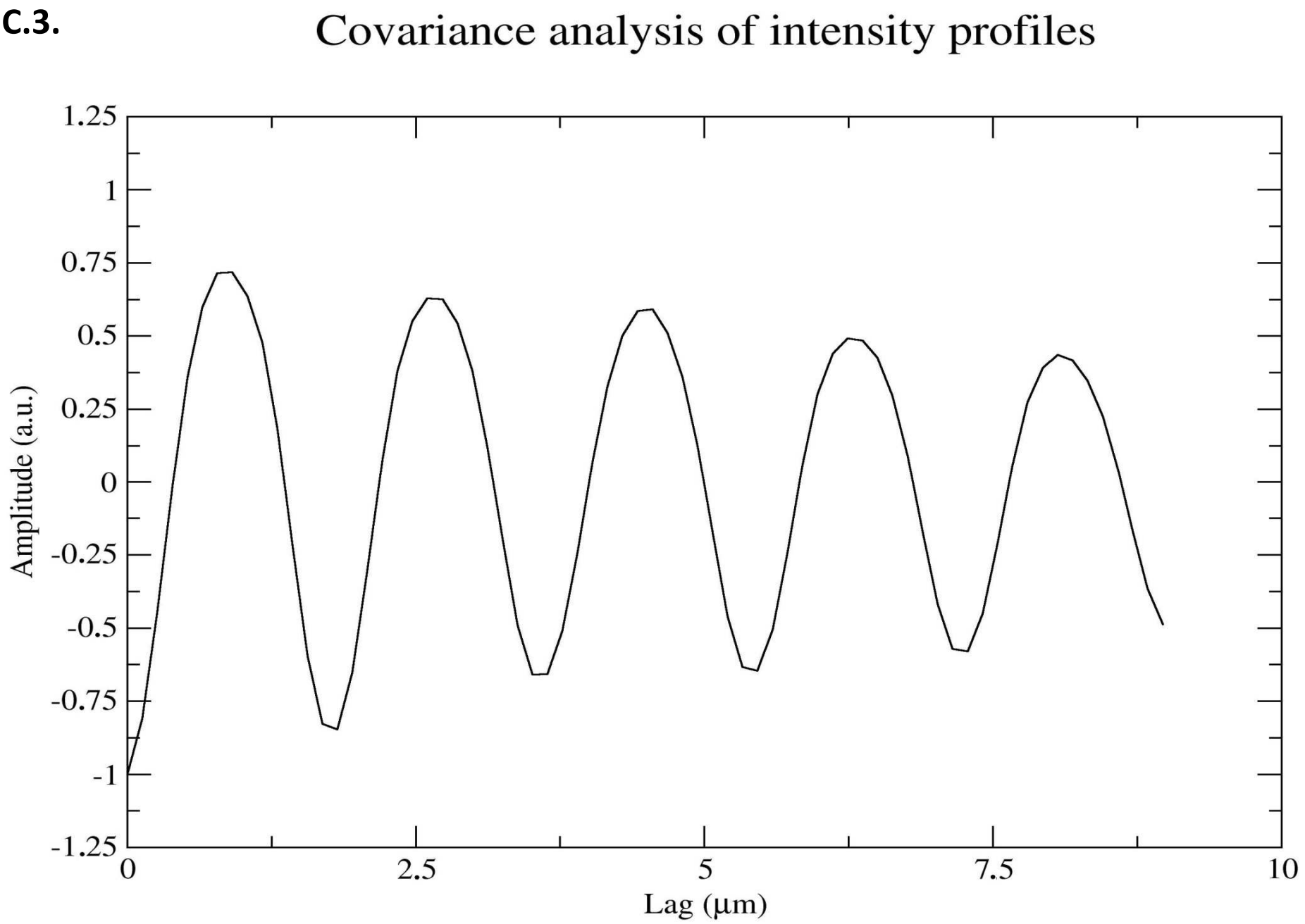
Covariance analysis of intensity profiles
Amplitude (a.u.)
1.25
1
0.75
0.5
0.25
0
-0.25
-0.5
-0.75
-1
-1.25
0
2.5
5
7.5
10
Lag (μm)

Figure 3

D.1.

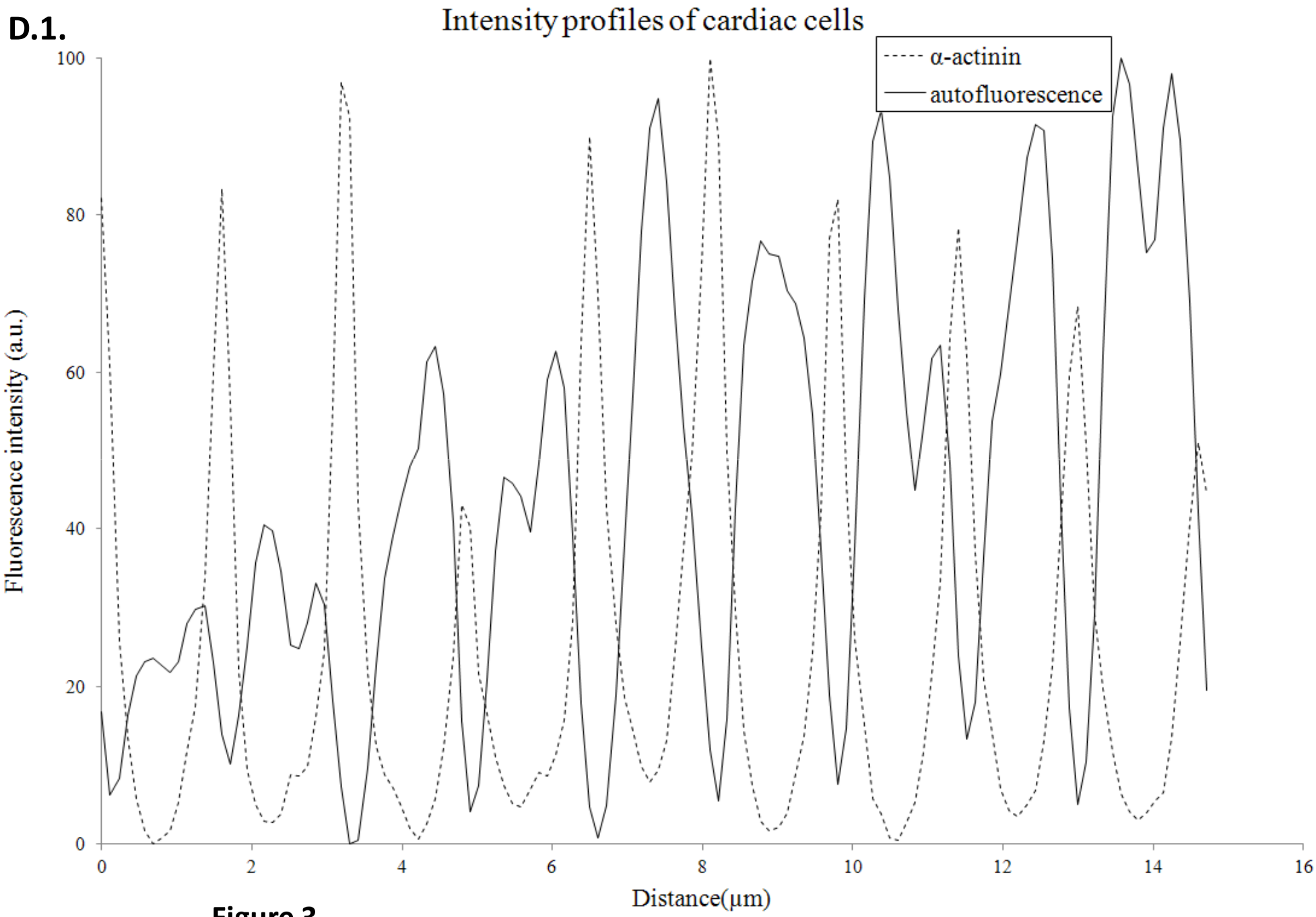
Intensity profiles of cardiac cells
α-actinin
autofluorescence
Fluorescence intensity (a.u.)
Distance(μm)
0
20
40
60
80
100
0
2
4
6
8
10
12
14
16

Figure 3

D.2.

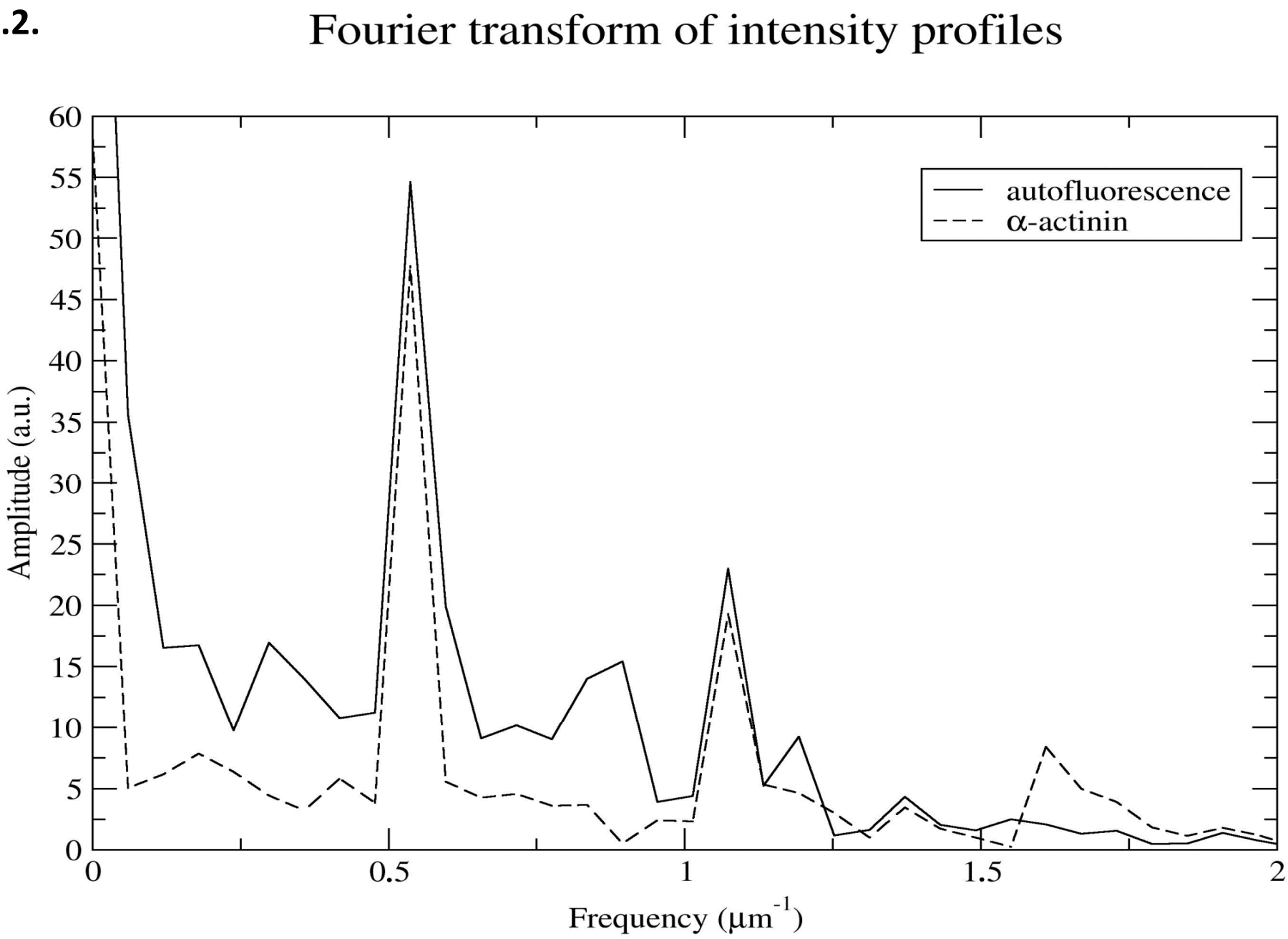
Fourier transform of intensity profiles
autofluorescence
α-actinin
Amplitude (a.u.)
Frequency (μm^-1)
0
5
10
15
20
25
30
35
40
45
50
55
60
0
0.5
1
1.5
2

Figure 3

D.3.

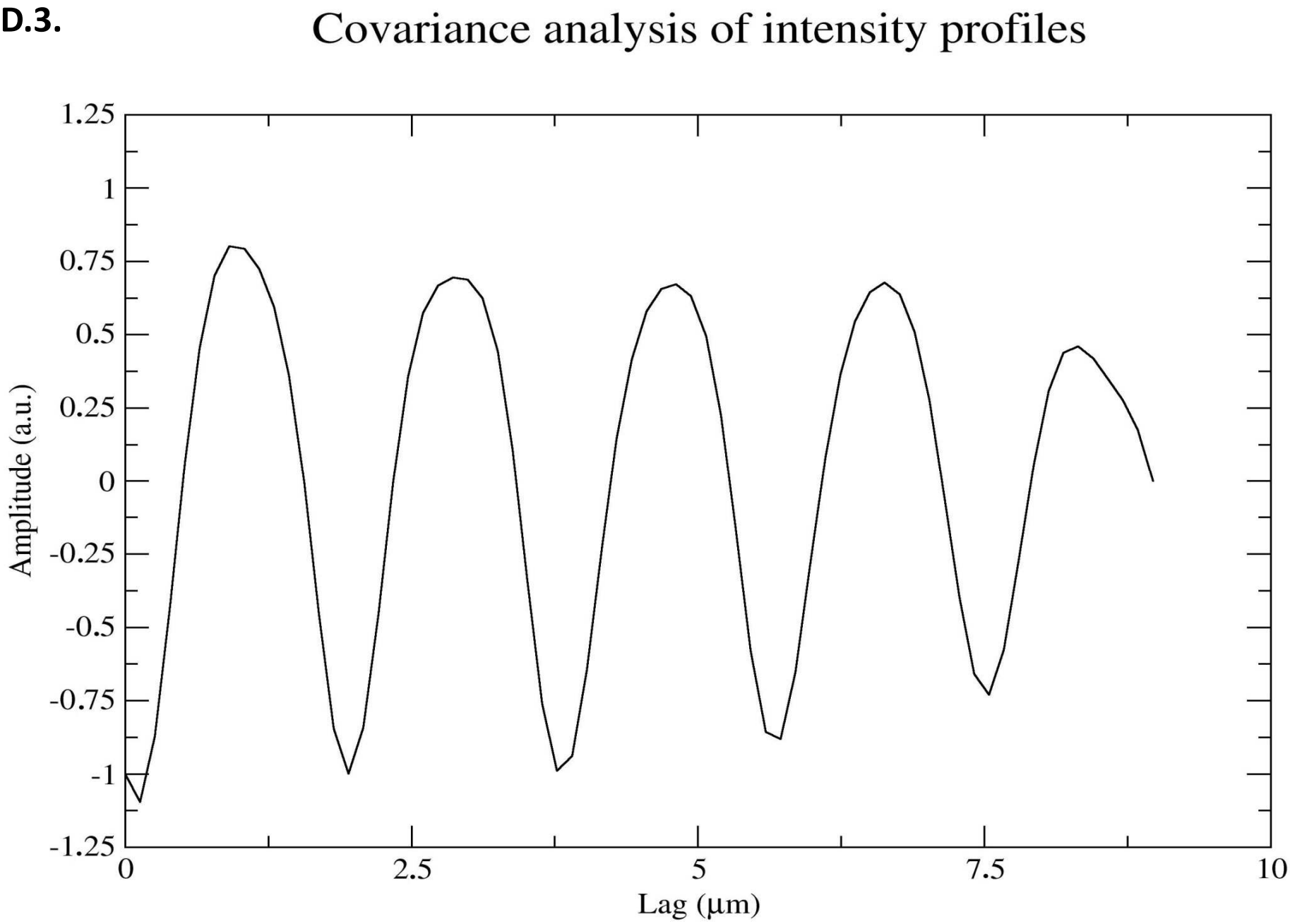
Covariance analysis of intensity profiles
Amplitude (a.u.)
1.25
1
0.75
0.5
0.25
0
-0.25
-0.5
-0.75
-1
-1.25
0
2.5
5
7.5
10
Lag (μm)

Figure 3

E.1.

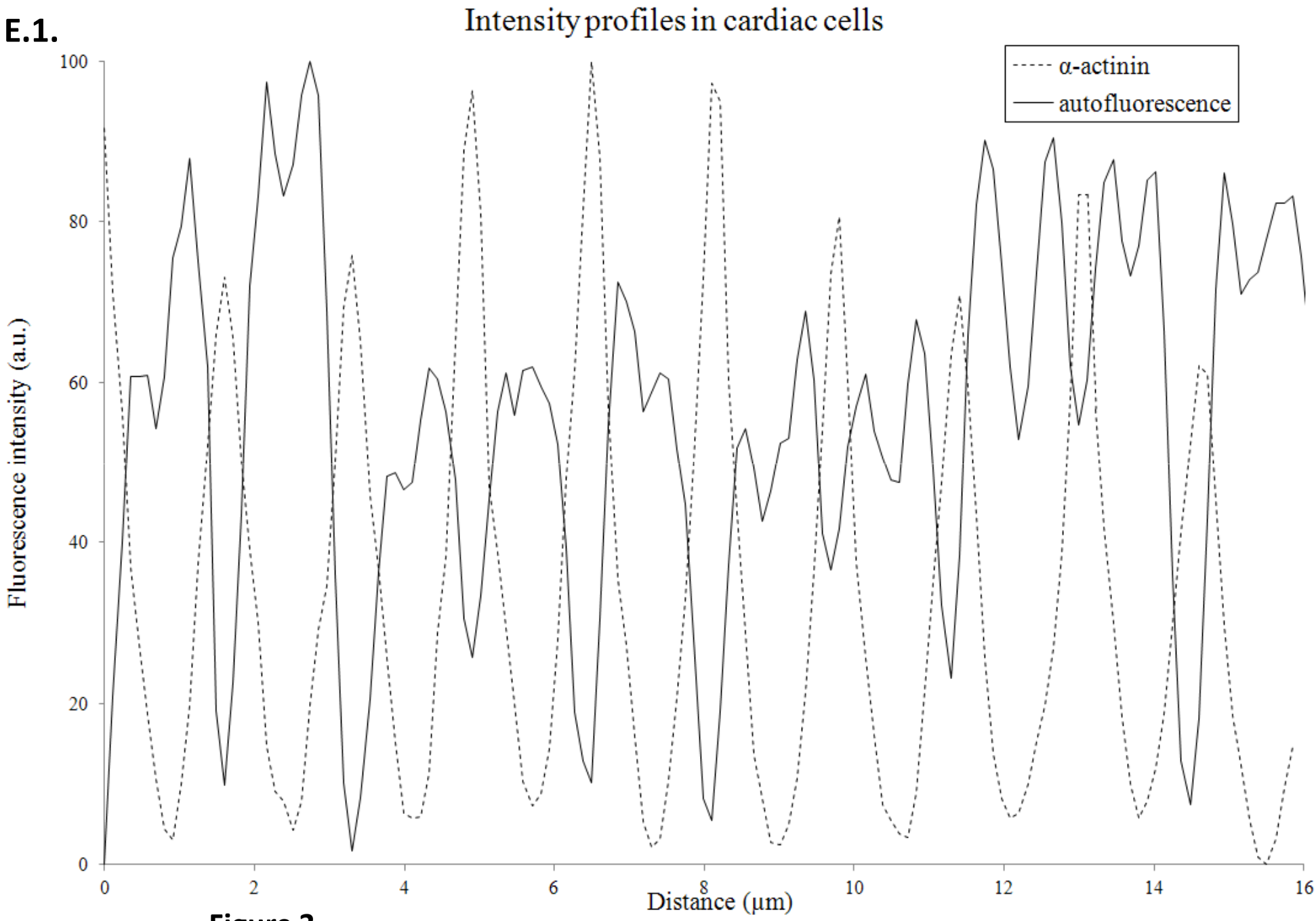
Intensity profiles in cardiac cells
α-actinin
autofluorescence
Fluorescence intensity (a.u.)
Distance (µm)
0
20
40
60
80
100
0
2
4
6
8
10
12
14
16

Figure 3

E.2.

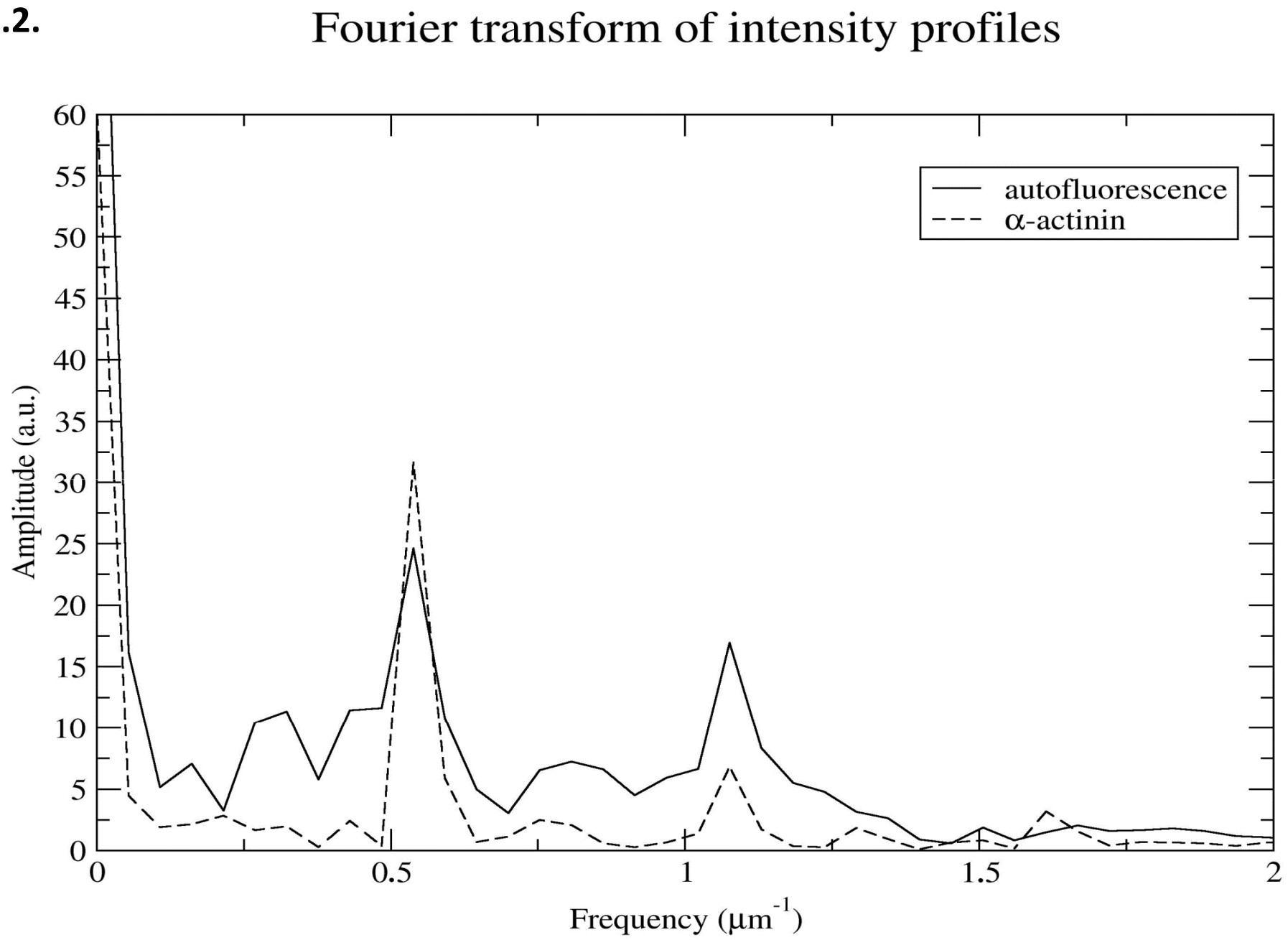
Fourier transform of intensity profiles
autofluorescence
α-actinin
Amplitude (a.u.)
Frequency (μm-1)
0
5
10
15
20
25
30
35
40
45
50
55
60
0
0.5
1
1.5
2

Figure 3

E.3.

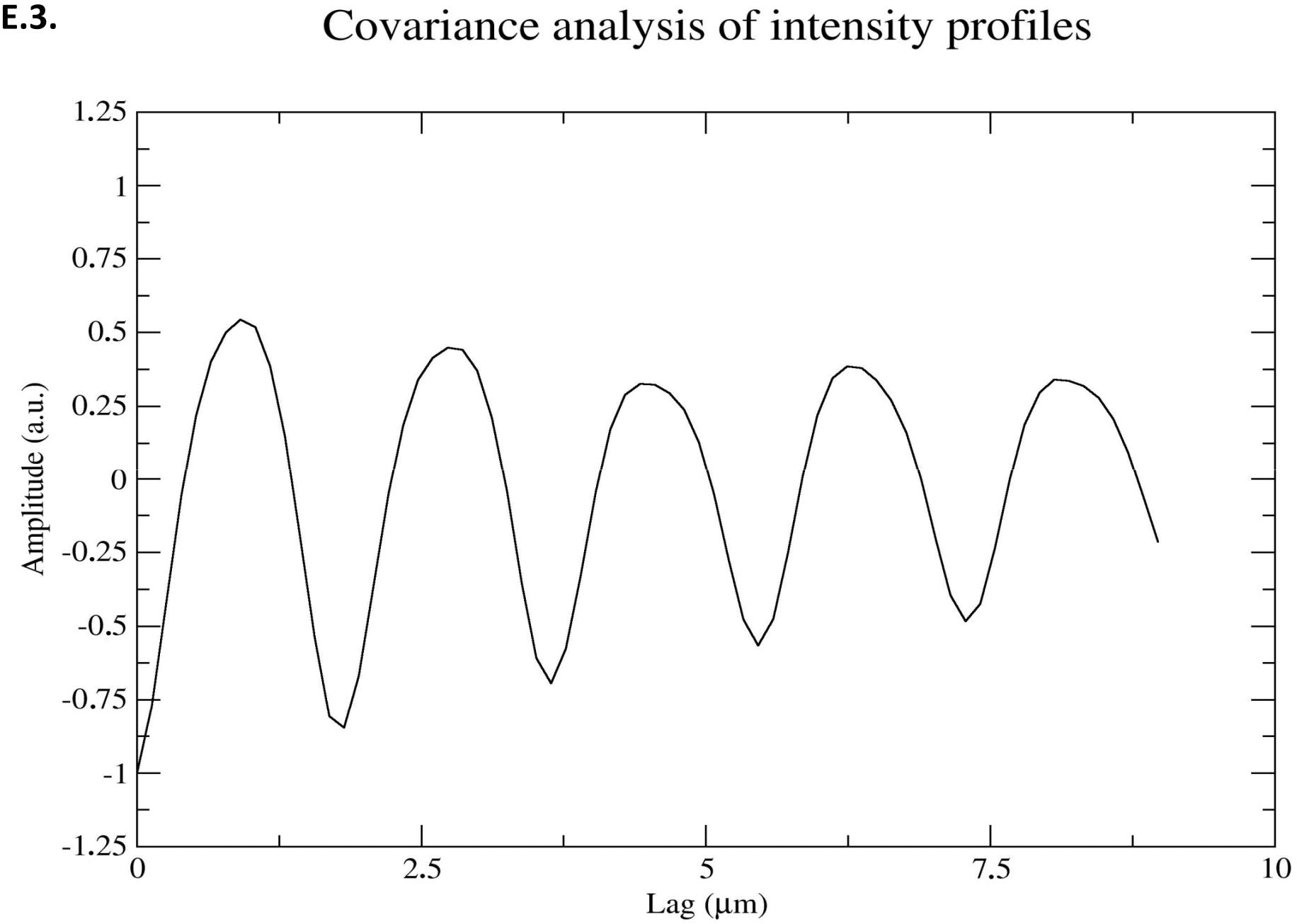
Covariance analysis of intensity profiles
Amplitude (a.u.)
1.25
1
0.75
0.5
0.25
0
-0.25
-0.5
-0.75
-1
-1.25
0
2.5
5
7.5
10
Lag (μm)

Figure 3

F.1.

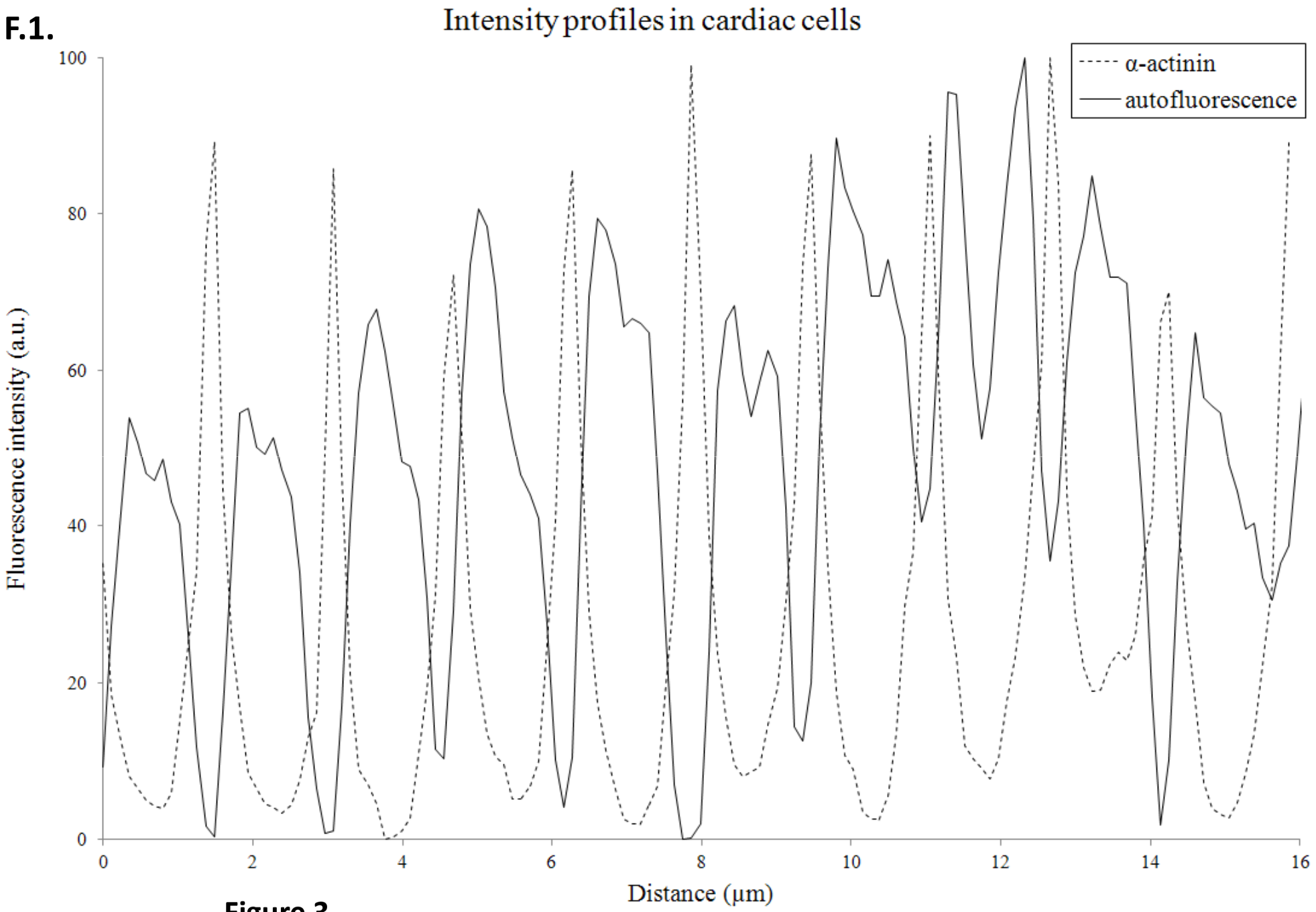
Intensity profiles in cardiac cells
α-actinin
autofluorescence
Fluorescence intensity (a.u.)
Distance (µm)
0
20
40
60
80
100
0
2
4
6
8
10
12
14
16

Figure 3

F.2.

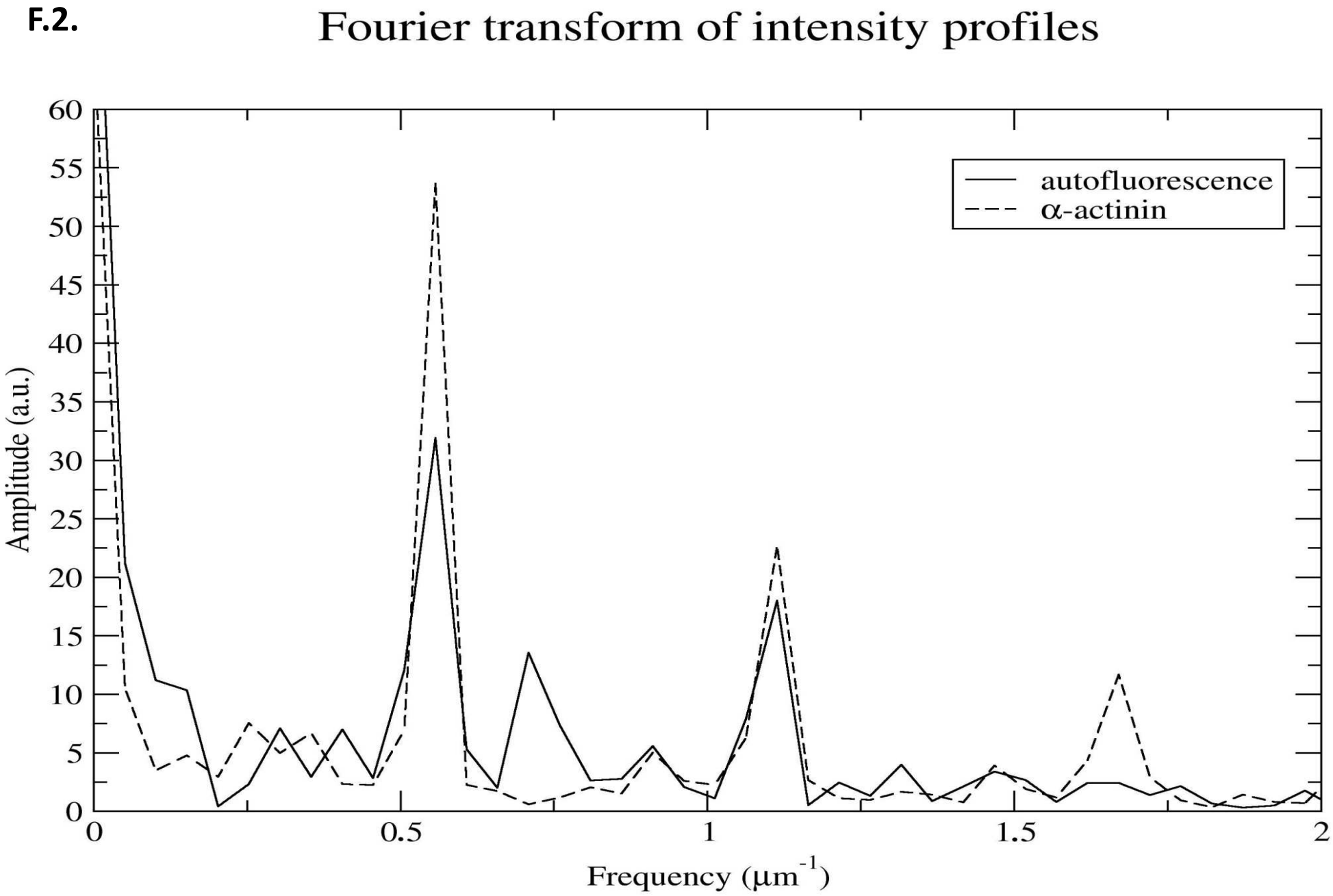
Fourier transform of intensity profiles
autofluorescence
α-actinin
Amplitude (a.u.)
Frequency (μm-1)
0
5
10
15
20
25
30
35
40
45
50
55
60
0
0.5
1
1.5
2

Figure 3

F.3.

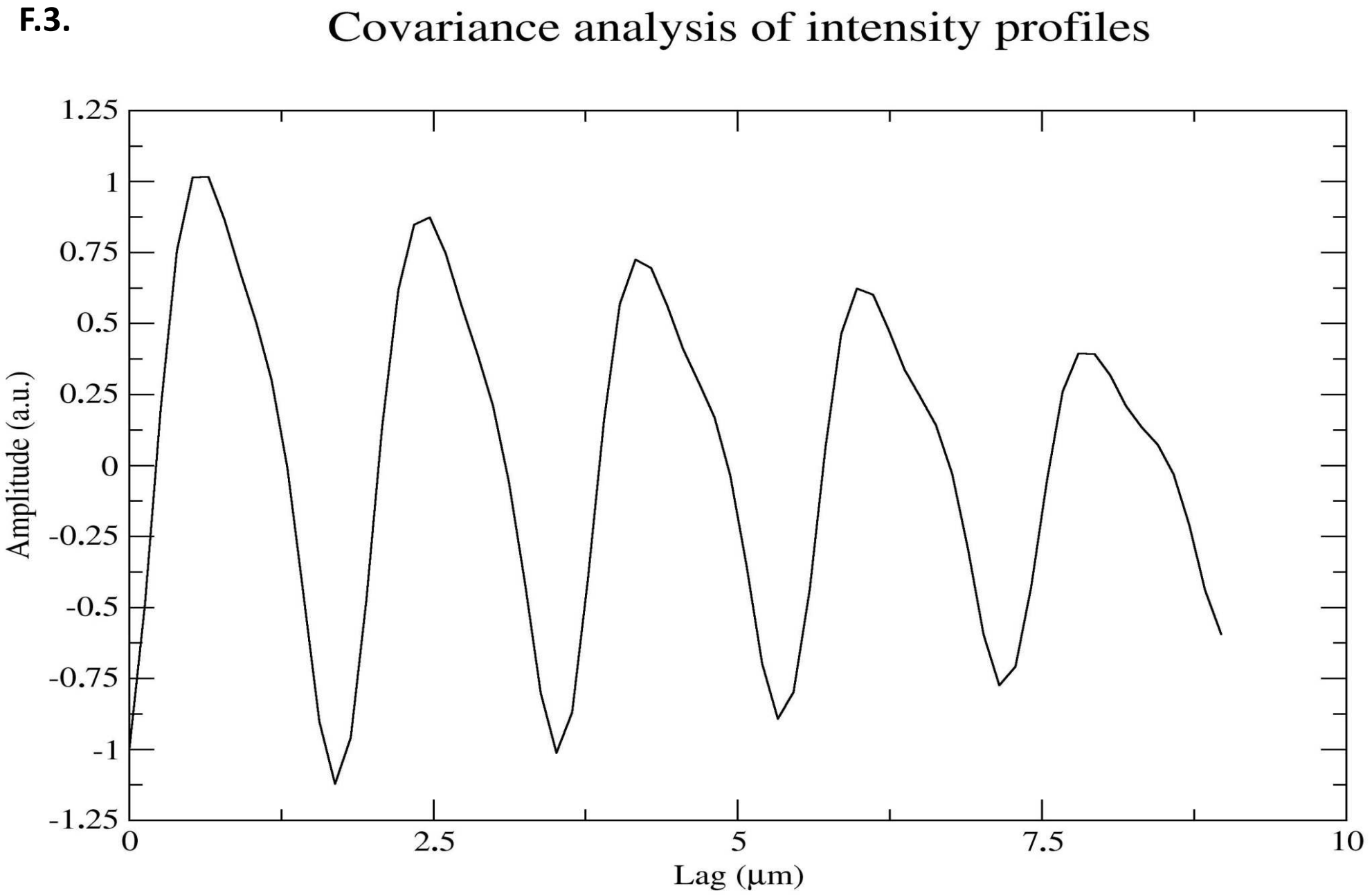
Covariance analysis of intensity profiles
Amplitude (a.u.)
1.25
1
0.75
0.5
0.25
0
-0.25
-0.5
-0.75
-1
-1.25
0
2.5
5
7.5
10
Lag (μm)

Figure 3

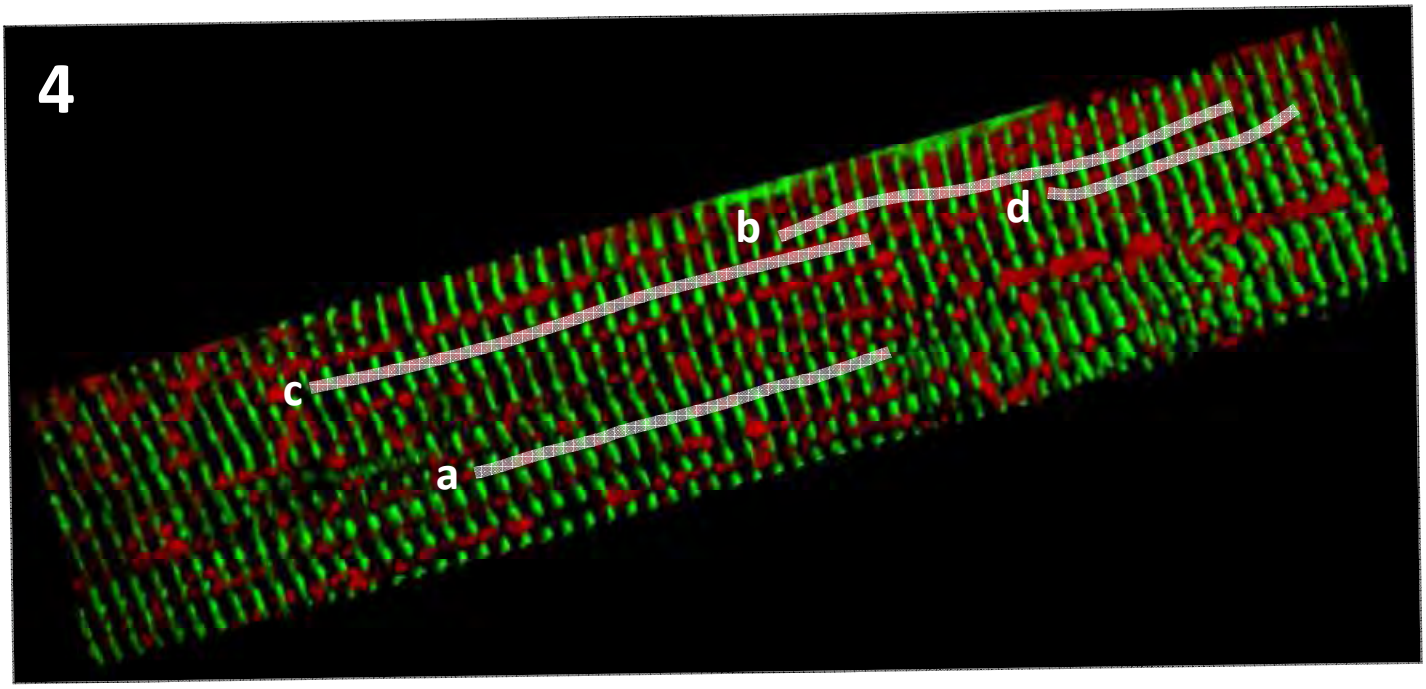

Figure 4

a.1.

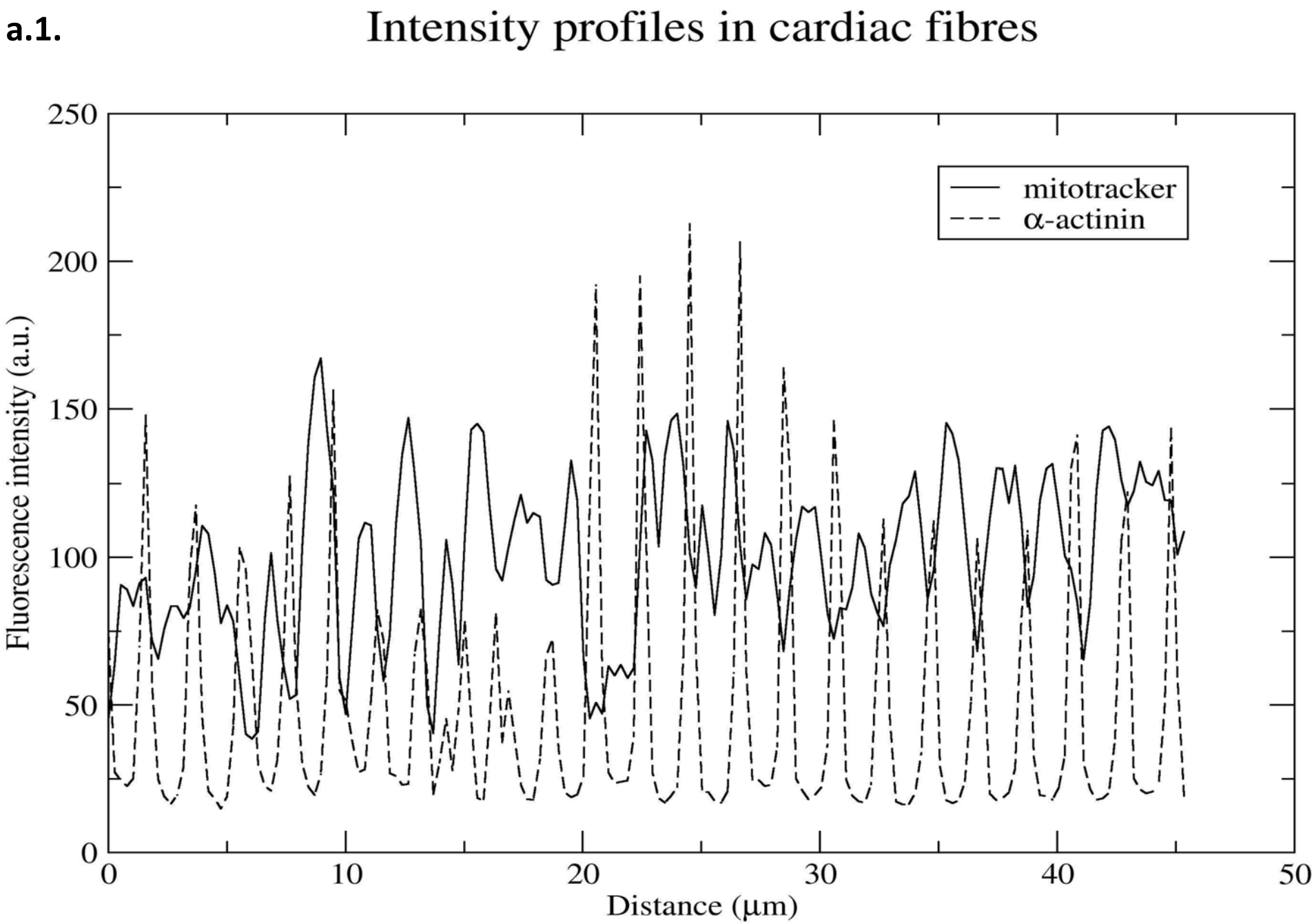
Intensity profiles in cardiac fibres
mitotracker
α-actinin
Fluorescence intensity (a.u.)
Distance (μm)
0
50
100
150
200
250
0
10
20
30
40
50

Figure 5

a.2.

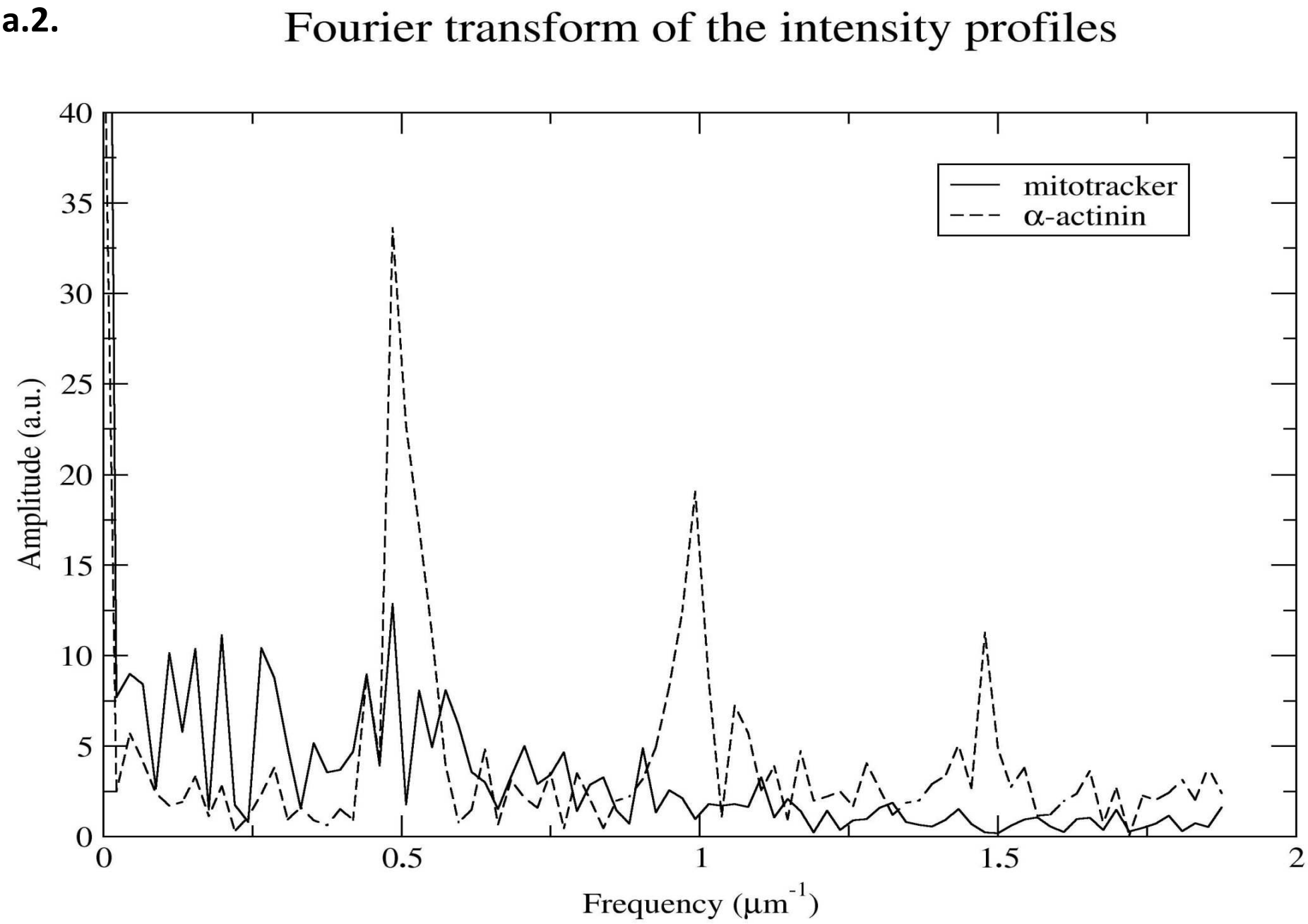
Fourier transform of the intensity profiles
mitotracker
α-actinin
Amplitude (a.u.)
Frequency (μm^-1)
0
5
10
15
20
25
30
35
40
0
0.5
1
1.5
2

Figure 5

a.3.

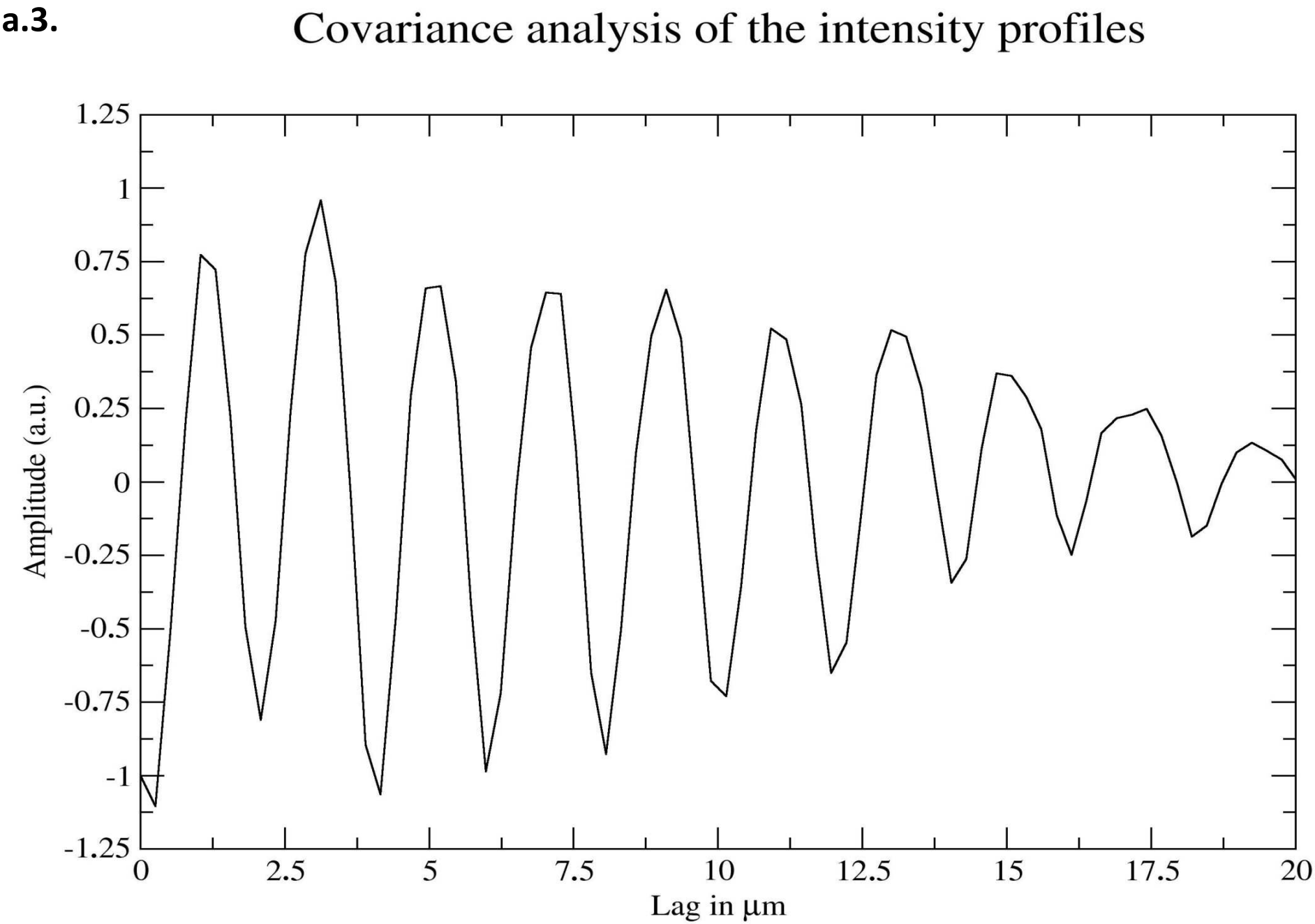
Covariance analysis of the intensity profiles
Amplitude (a.u.)
1.25
1
0.75
0.5
0.25
0
-0.25
-0.5
-0.75
-1
-1.25
0
2.5
5
7.5
10
12.5
15
17.5
20
Lag in μm

Figure 5

b.1.

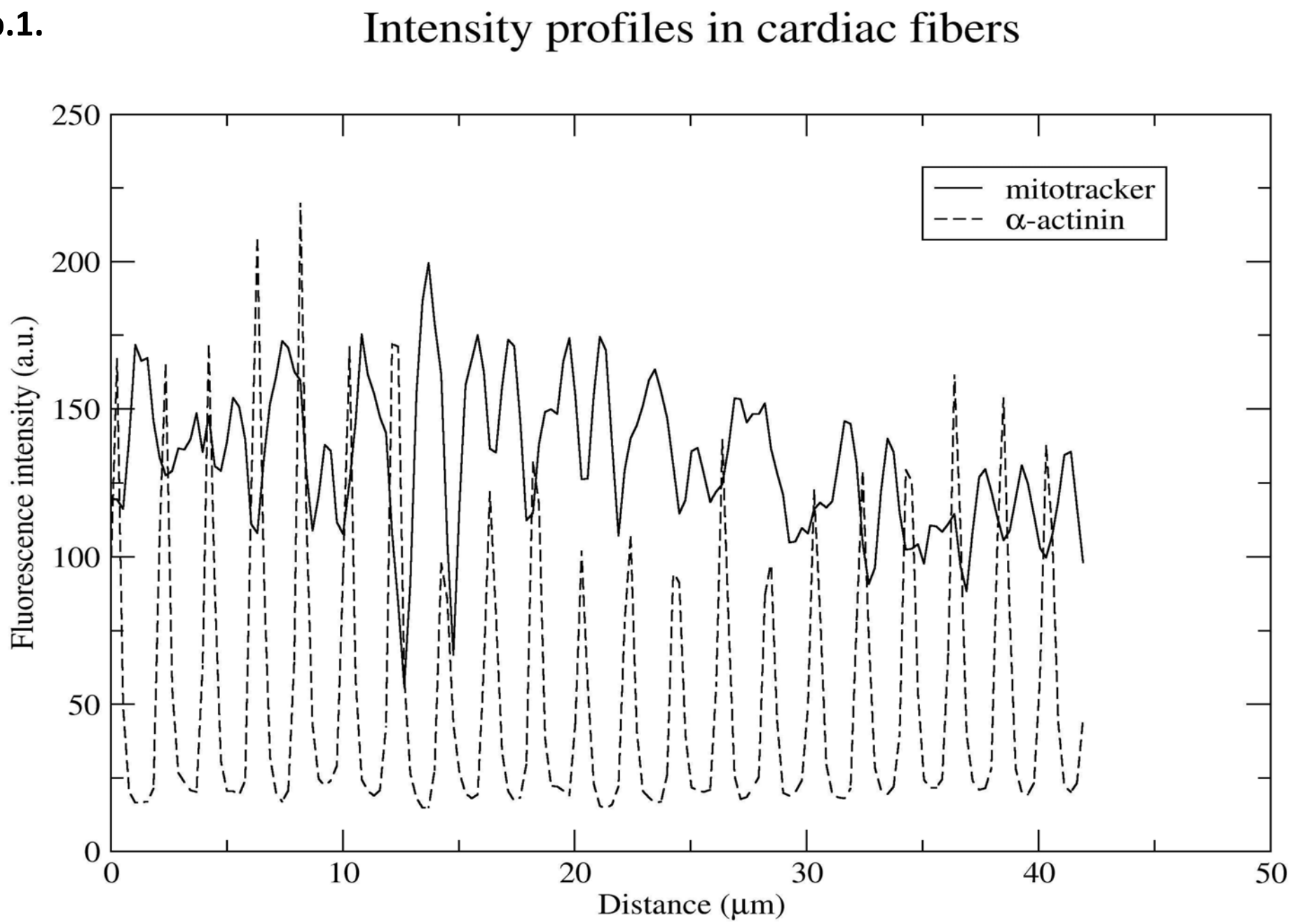
Intensity profiles in cardiac fibers
mitotracker
α-actinin
Fluorescence intensity (a.u.)
Distance (μm)
0
50
100
150
200
250
0
10
20
30
40
50

Figure 5

b.2.

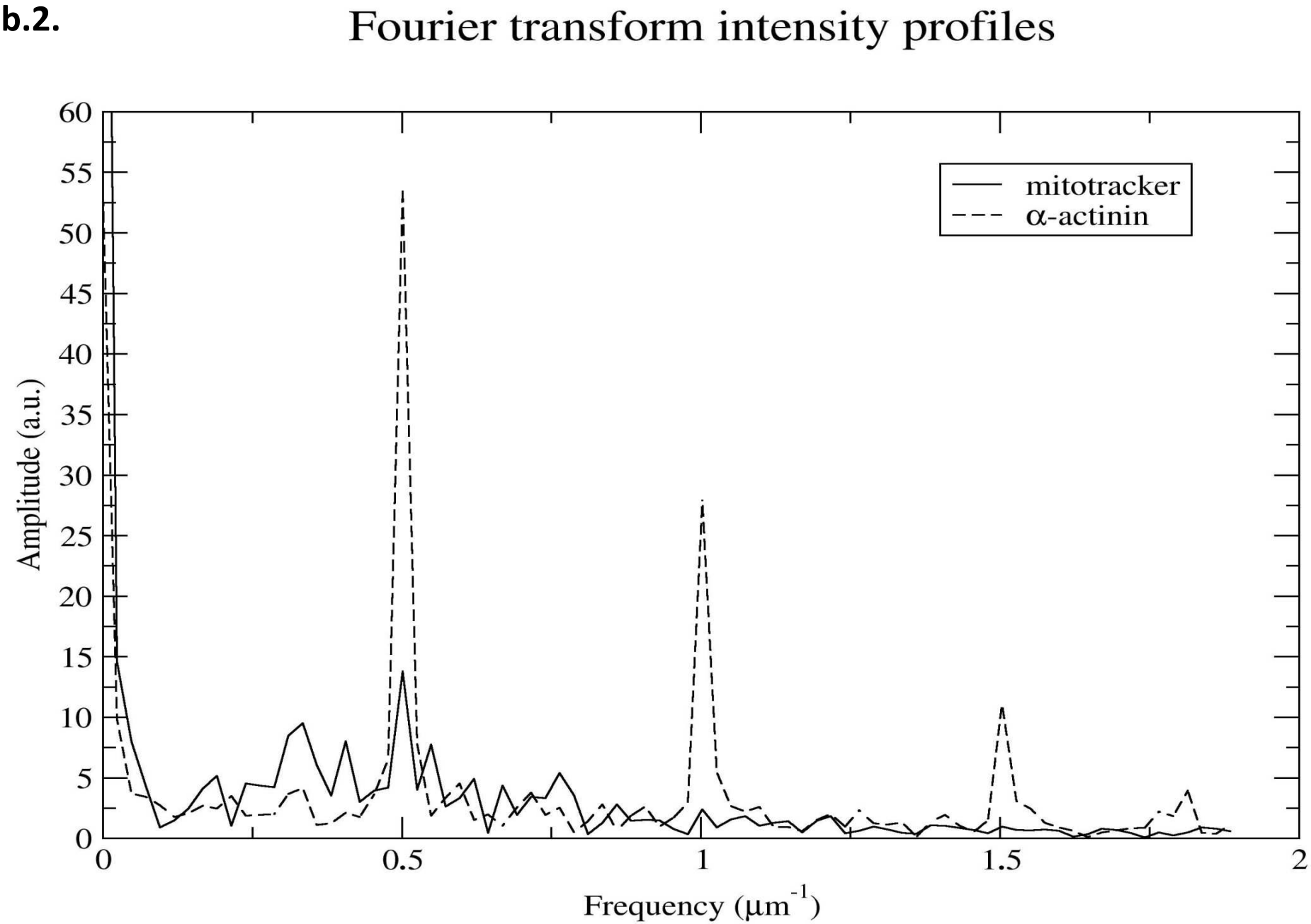
Fourier transform intensity profiles
mitotracker
α-actinin
Amplitude (a.u.)
Frequency (μm-1)
0
5
10
15
20
25
30
35
40
45
50
55
60
0
0.5
1
1.5
2

Figure 5

b.3.

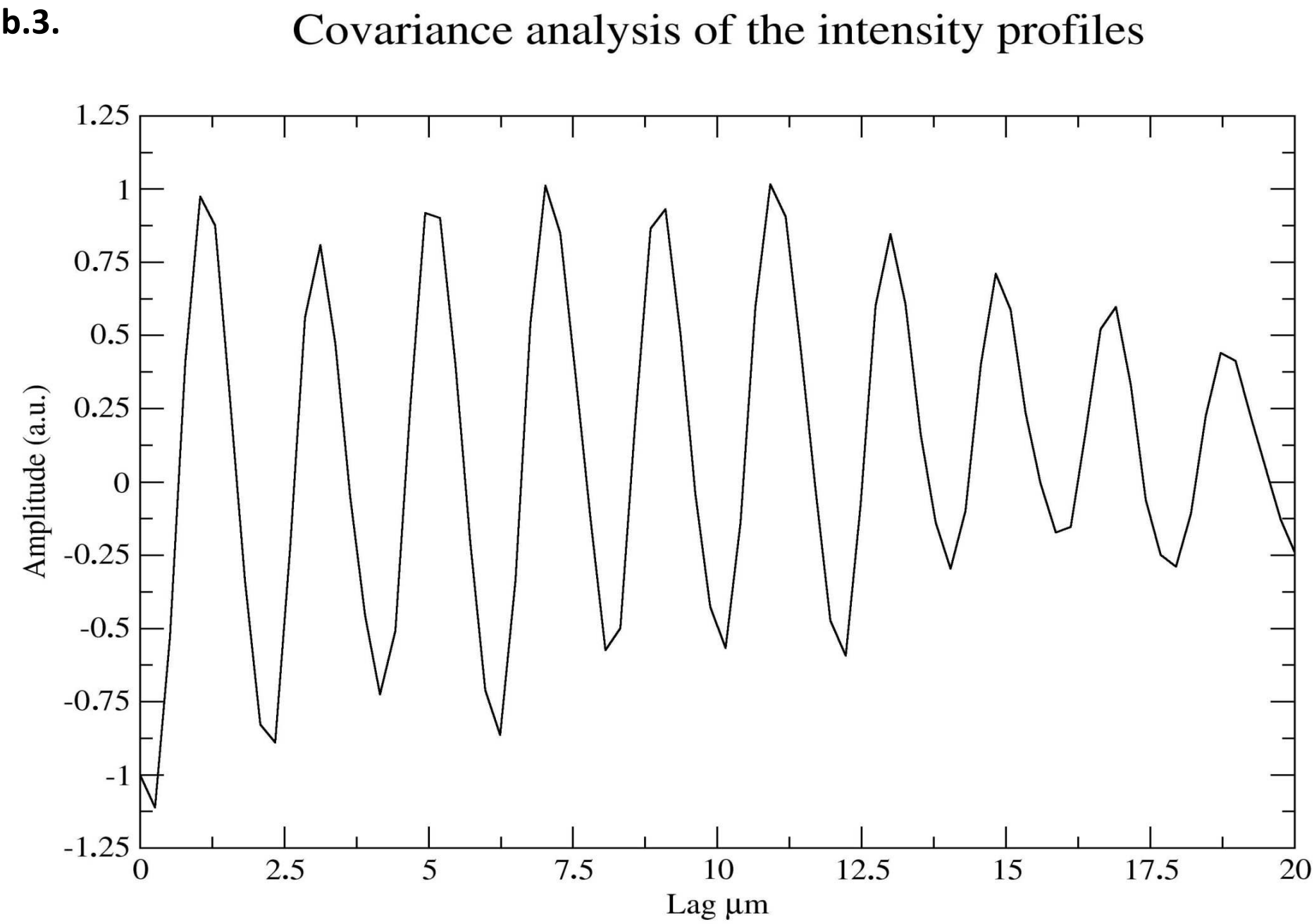
Covariance analysis of the intensity profiles
Amplitude (a.u.)
1.25
1
0.75
0.5
0.25
0
-0.25
-0.5
-0.75
-1
-1.25
0
2.5
5
7.5
10
12.5
15
17.5
20
Lag µm

Figure 5

c.1.

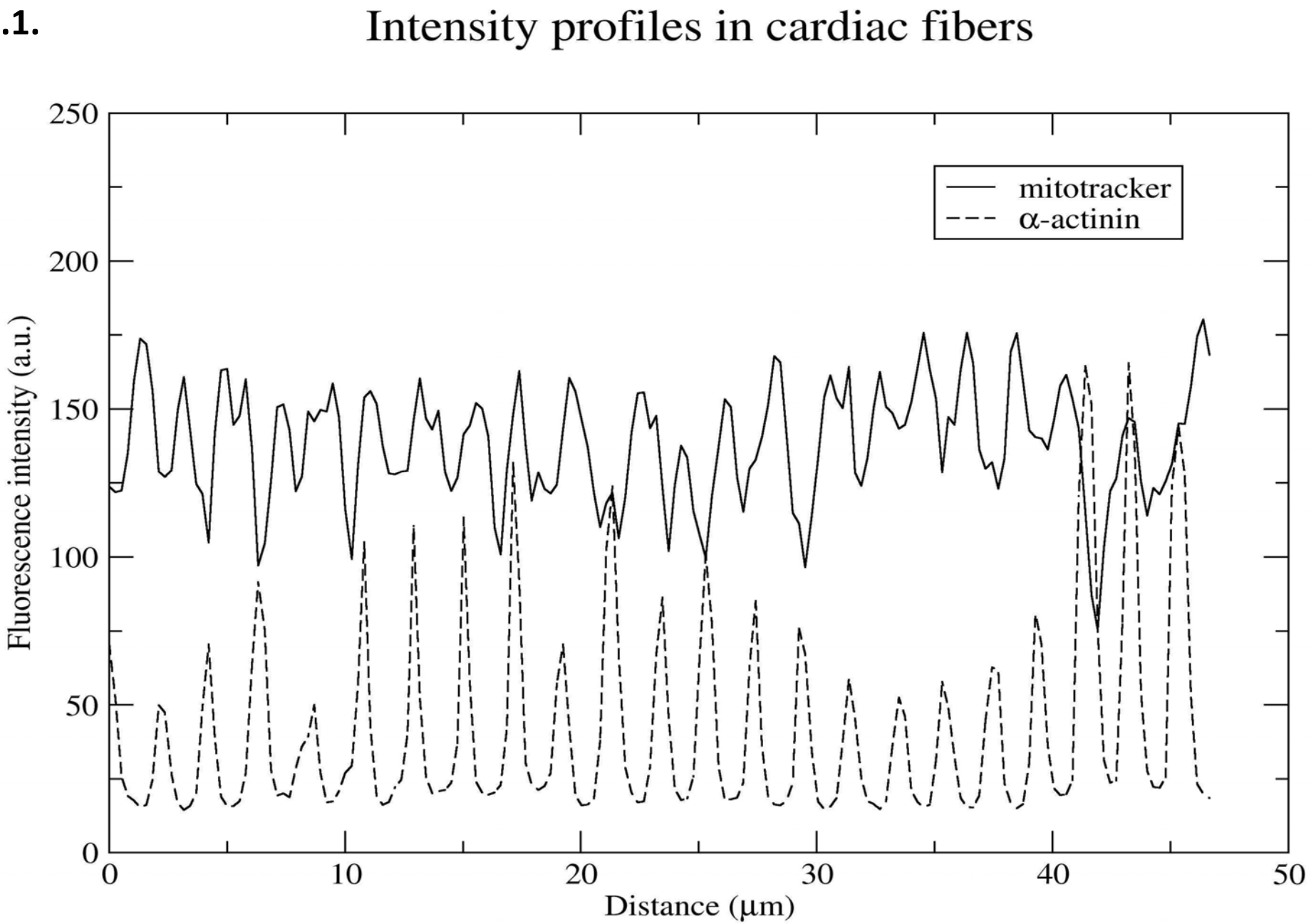
Intensity profiles in cardiac fibers
mitotracker
α-actinin
Fluorescence intensity (a.u.)
Distance (μm)
0
50
100
150
200
250
0
10
20
30
40
50

Figure 5

c.2.

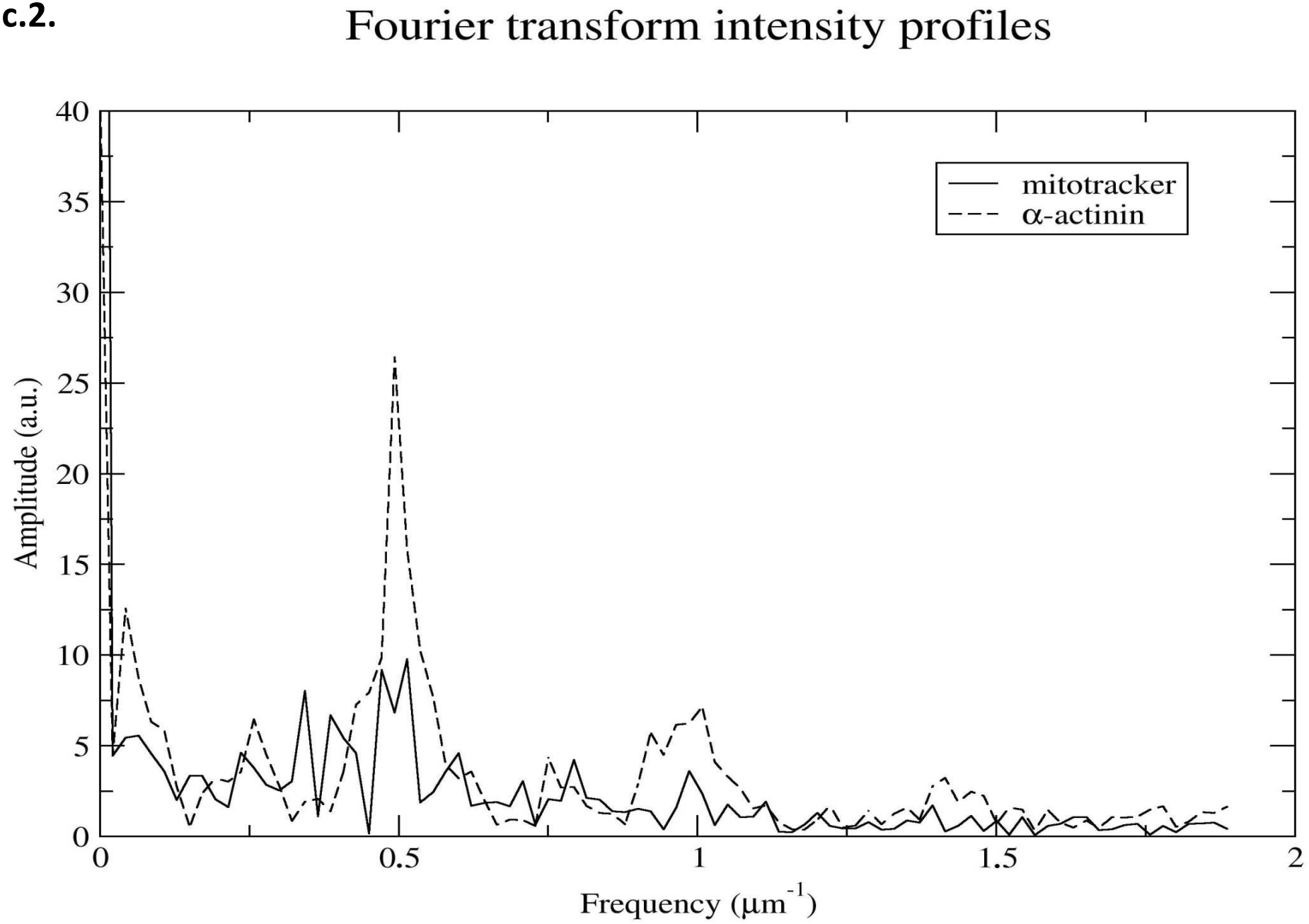
Fourier transform intensity profiles
mitotracker
α-actinin
Amplitude (a.u.)
Frequency (μm-1)
0
5
10
15
20
25
30
35
40
0
0.5
1
1.5
2

Figure 5

c.3.

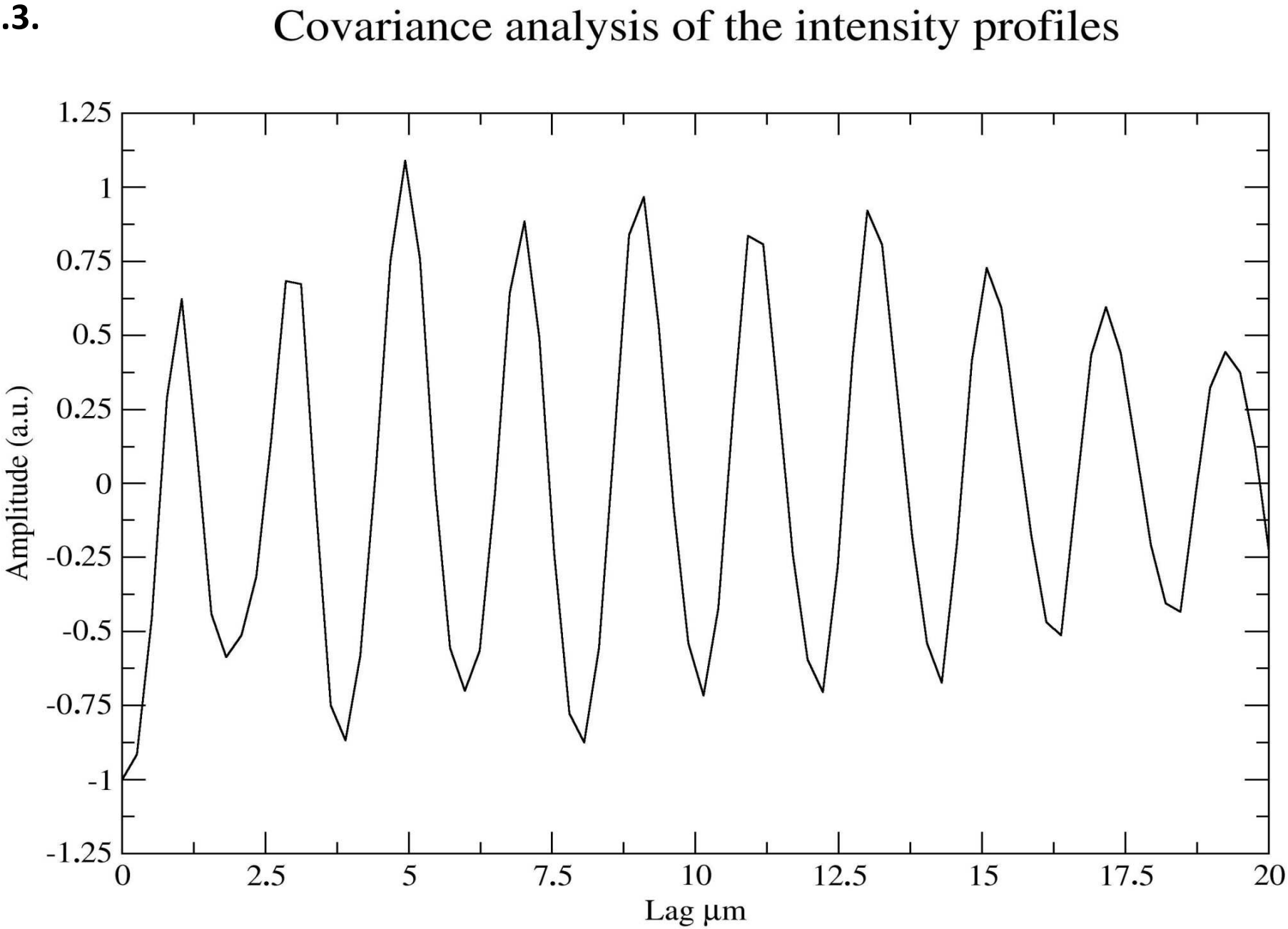
Covariance analysis of the intensity profiles
Amplitude (a.u.)
1.25
1
0.75
0.5
0.25
0
-0.25
-0.5
-0.75
-1
-1.25
0
2.5
5
7.5
10
12.5
15
17.5
20
Lag μm

Figure 5

d.1.

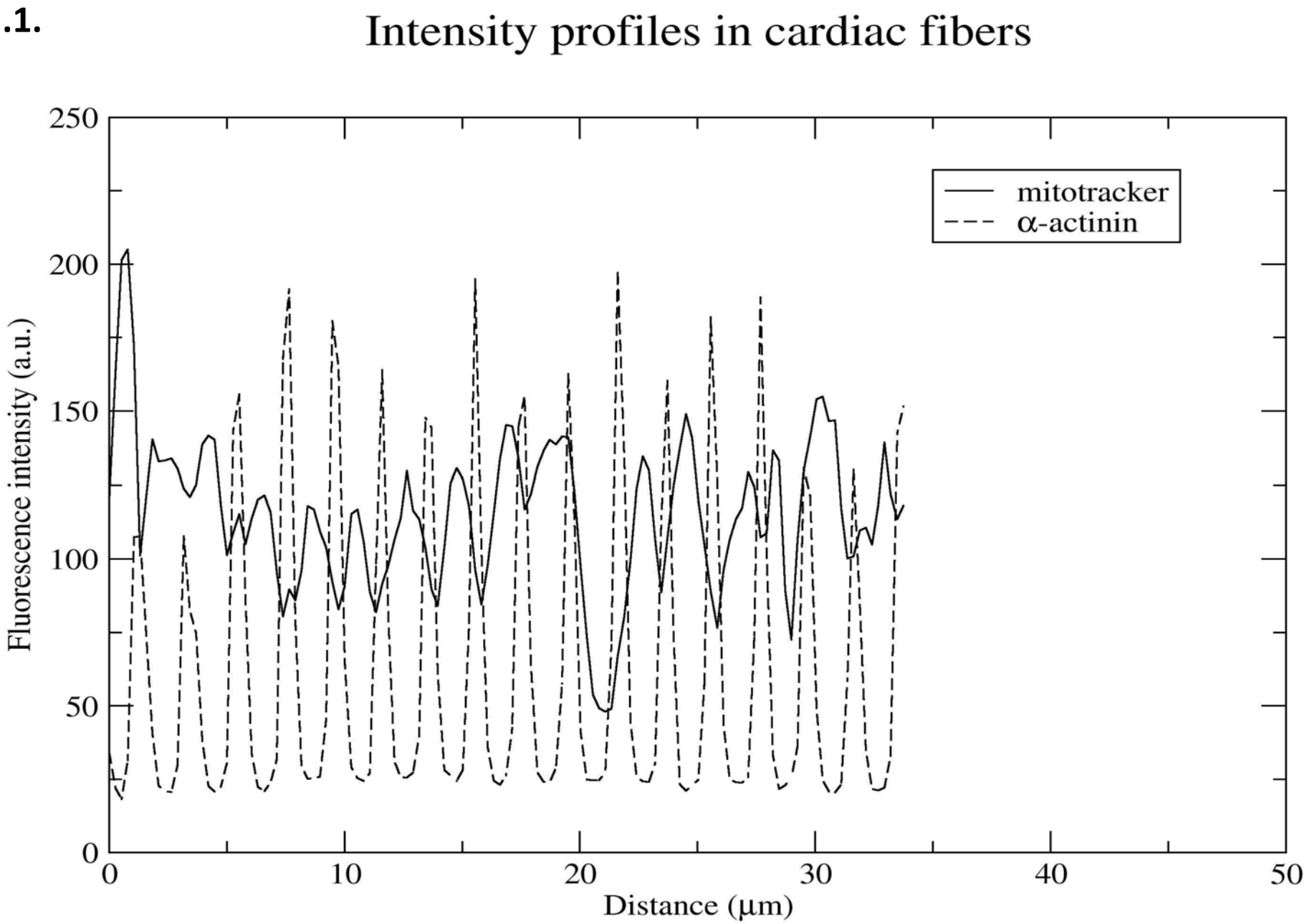
Intensity profiles in cardiac fibers
mitotracker
α-actinin
Fluorescence intensity (a.u.)
Distance (μm)
0
50
100
150
200
250
0
10
20
30
40
50

Figure 5

d.2.

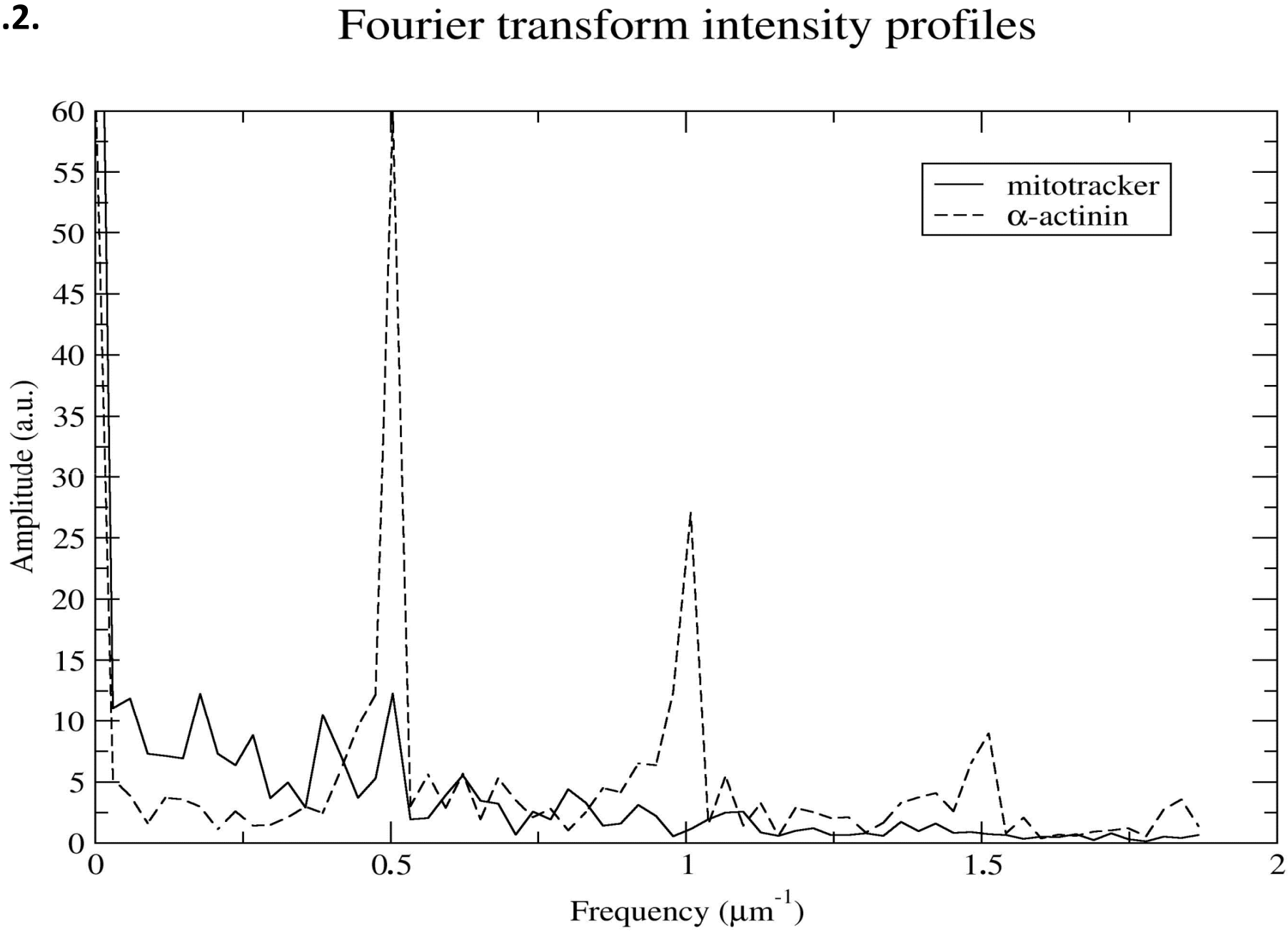
Fourier transform intensity profiles
mitotracker
α-actinin
Amplitude (a.u.)
Frequency (μm-1)
0
5
10
15
20
25
30
35
40
45
50
55
60
0
0.5
1
1.5
2

Figure 5

d.3.

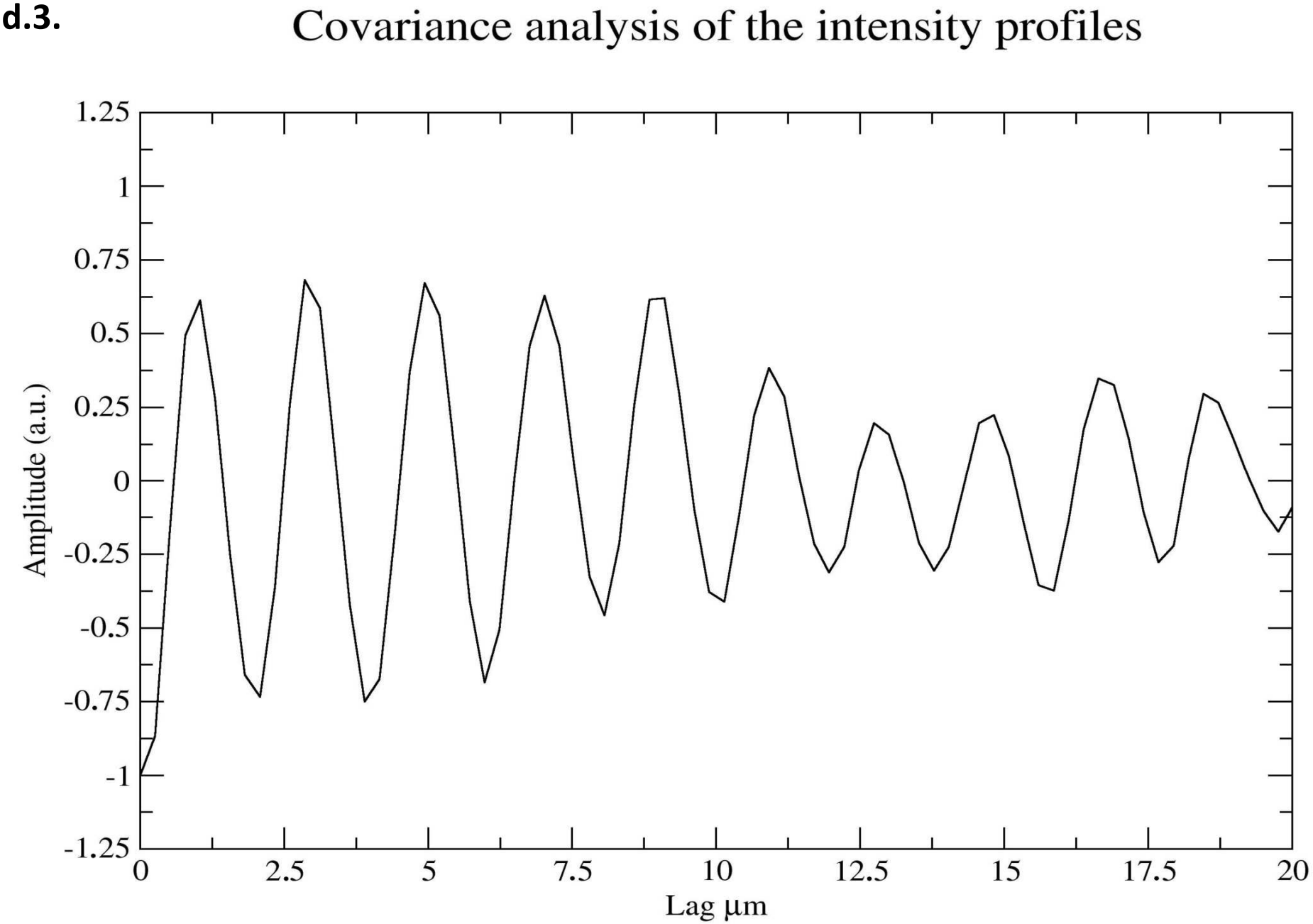
Covariance analysis of the intensity profiles
Amplitude (a.u.)
1.25
1
0.75
0.5
0.25
0
-0.25
-0.5
-0.75
-1
-1.25
0
2.5
5
7.5
10
12.5
15
17.5
20
Lag µm

Figure 5

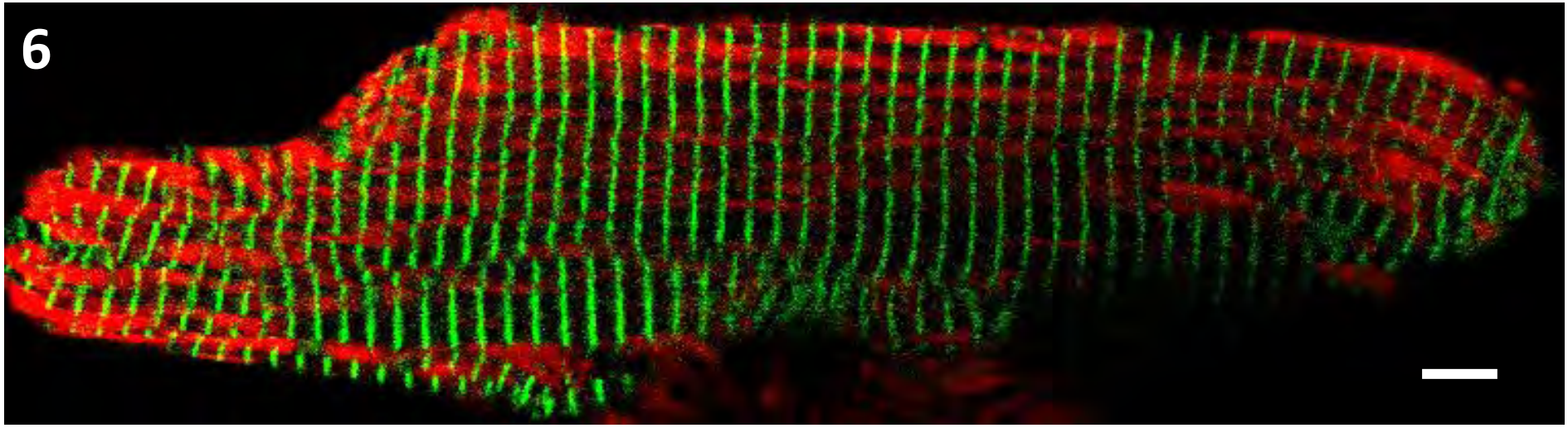

Figure 6

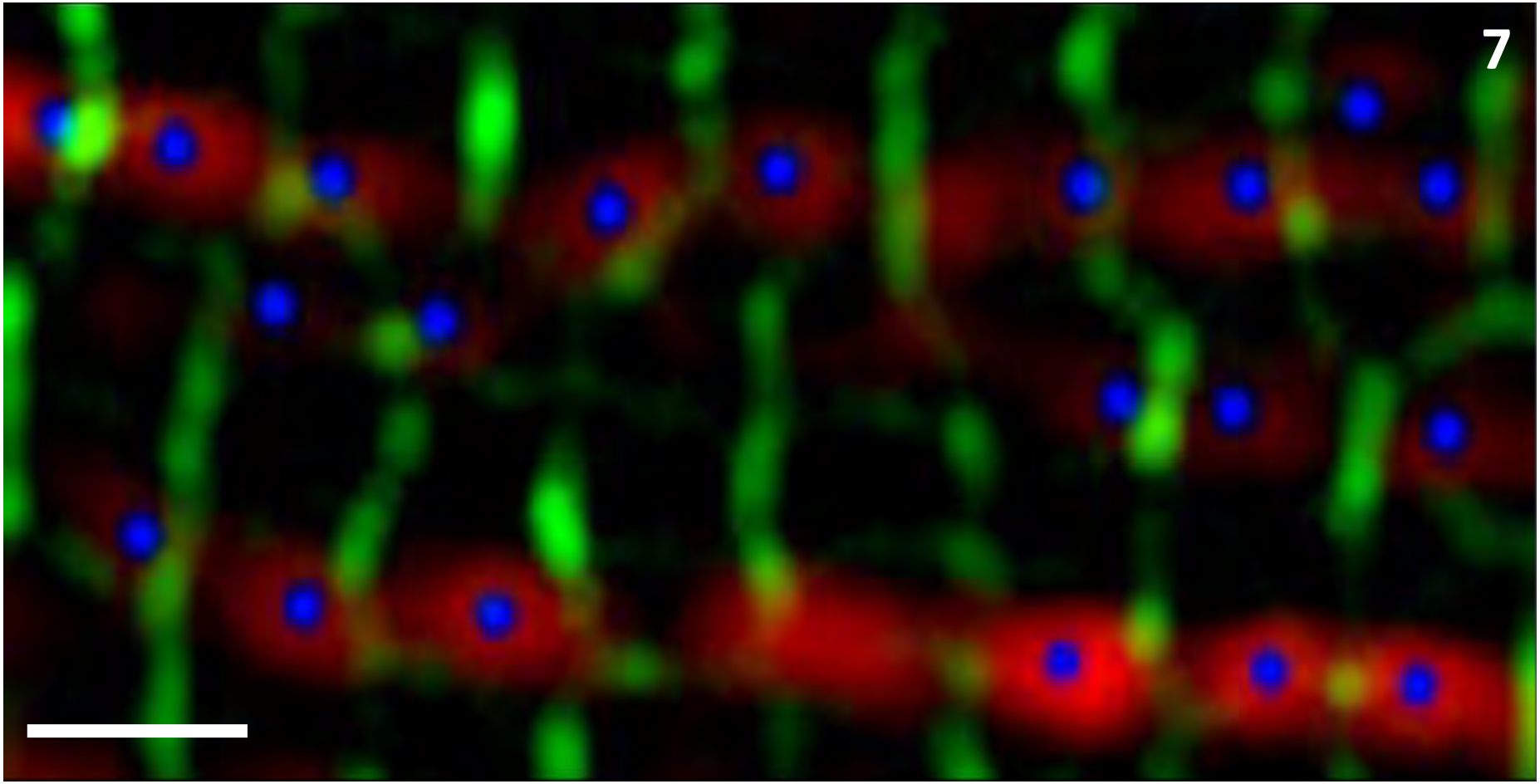

Figure 7

8.1.

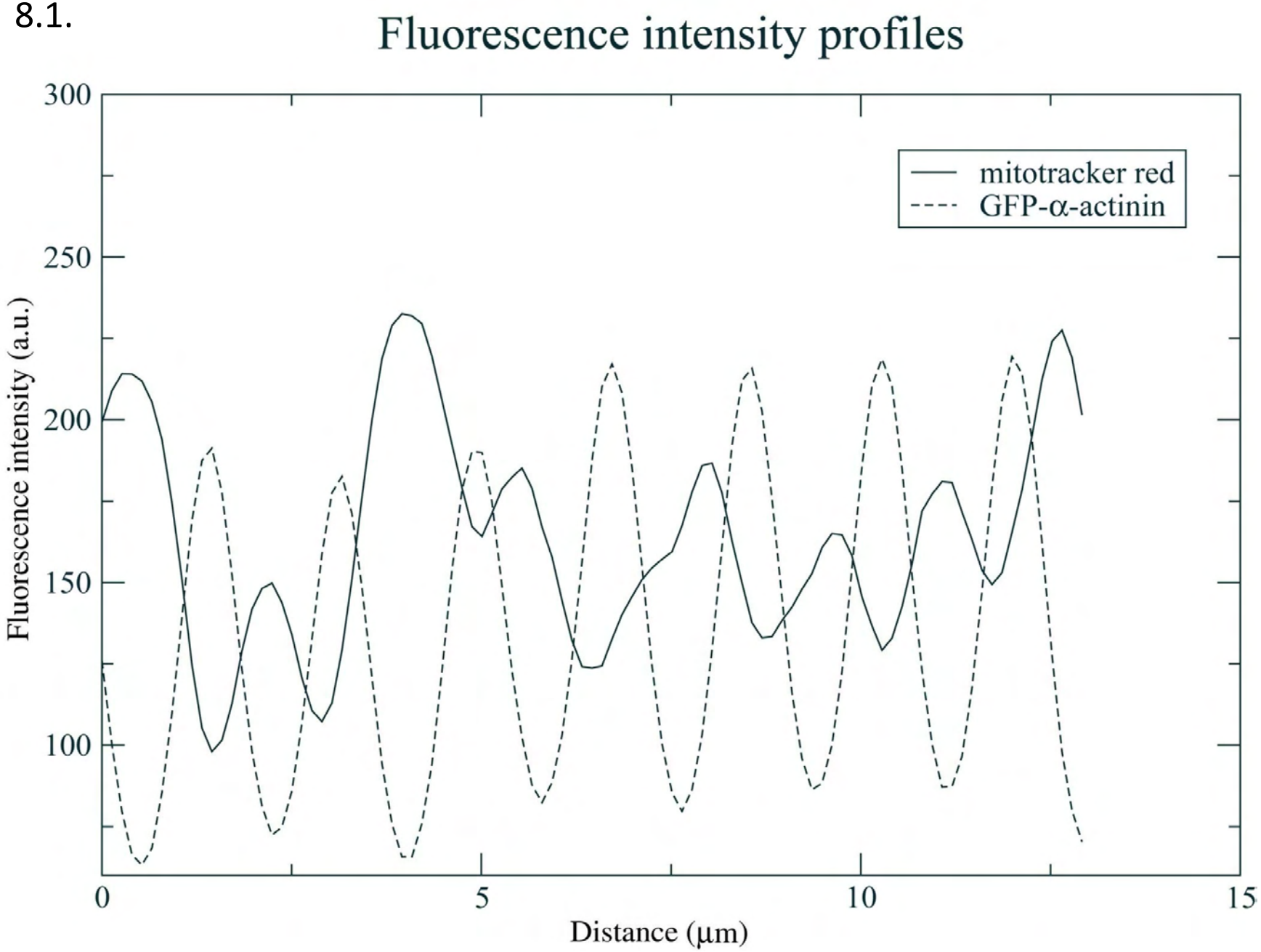
Fluorescence intensity profiles
mitotracker red
GFP-α-actinin
Fluorescence intensity (a.u.)
300
250
200
150
100
0
5
10
15
Distance (μm)

Figure 8

8.2.

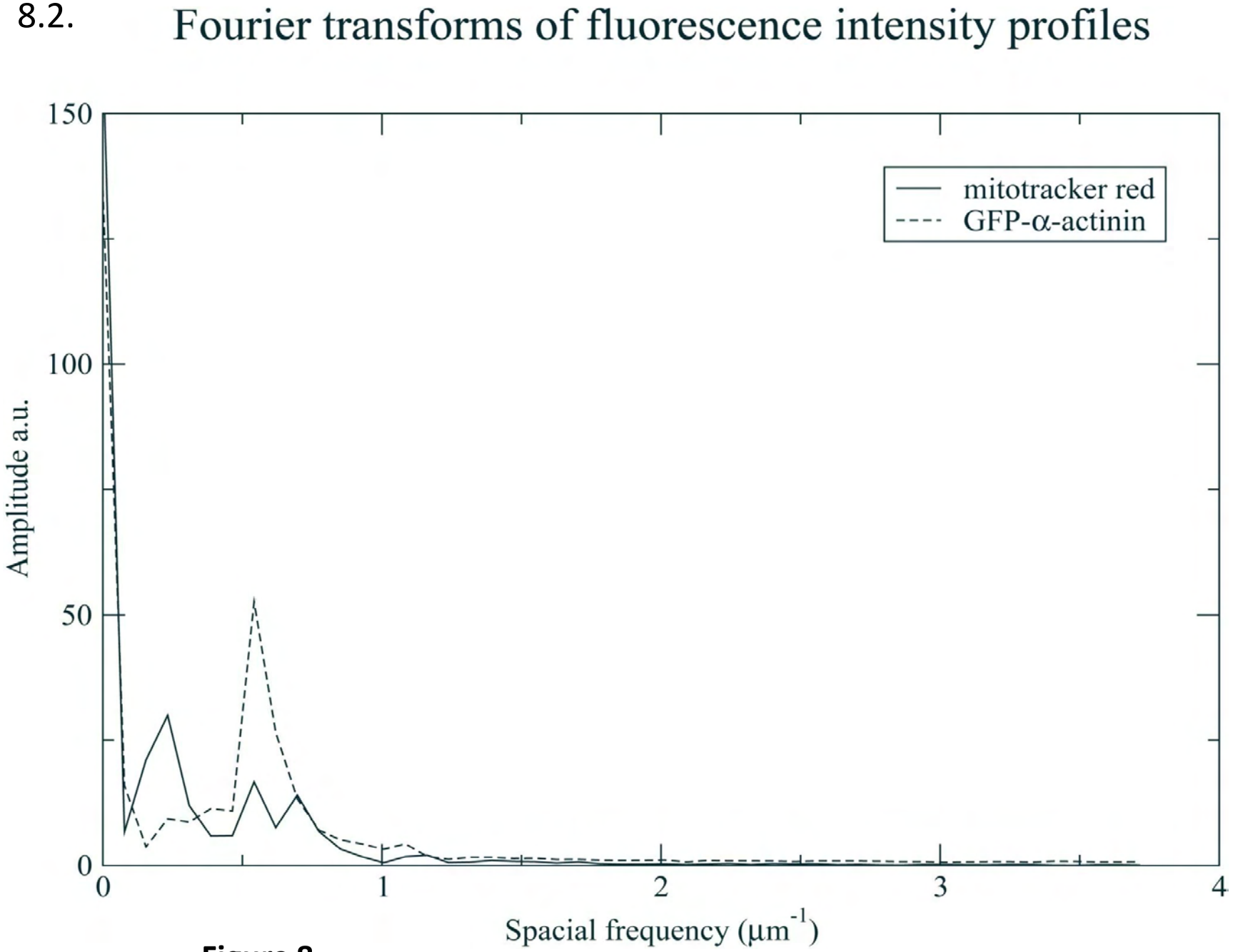
Fourier transforms of fluorescence intensity profiles
150
100
50
0
Amplitude a.u.
0
1
2
3
4
Spacial frequency (μm-1)
mitotracker red
GFP-α-actinin

Figure 8

8.3.

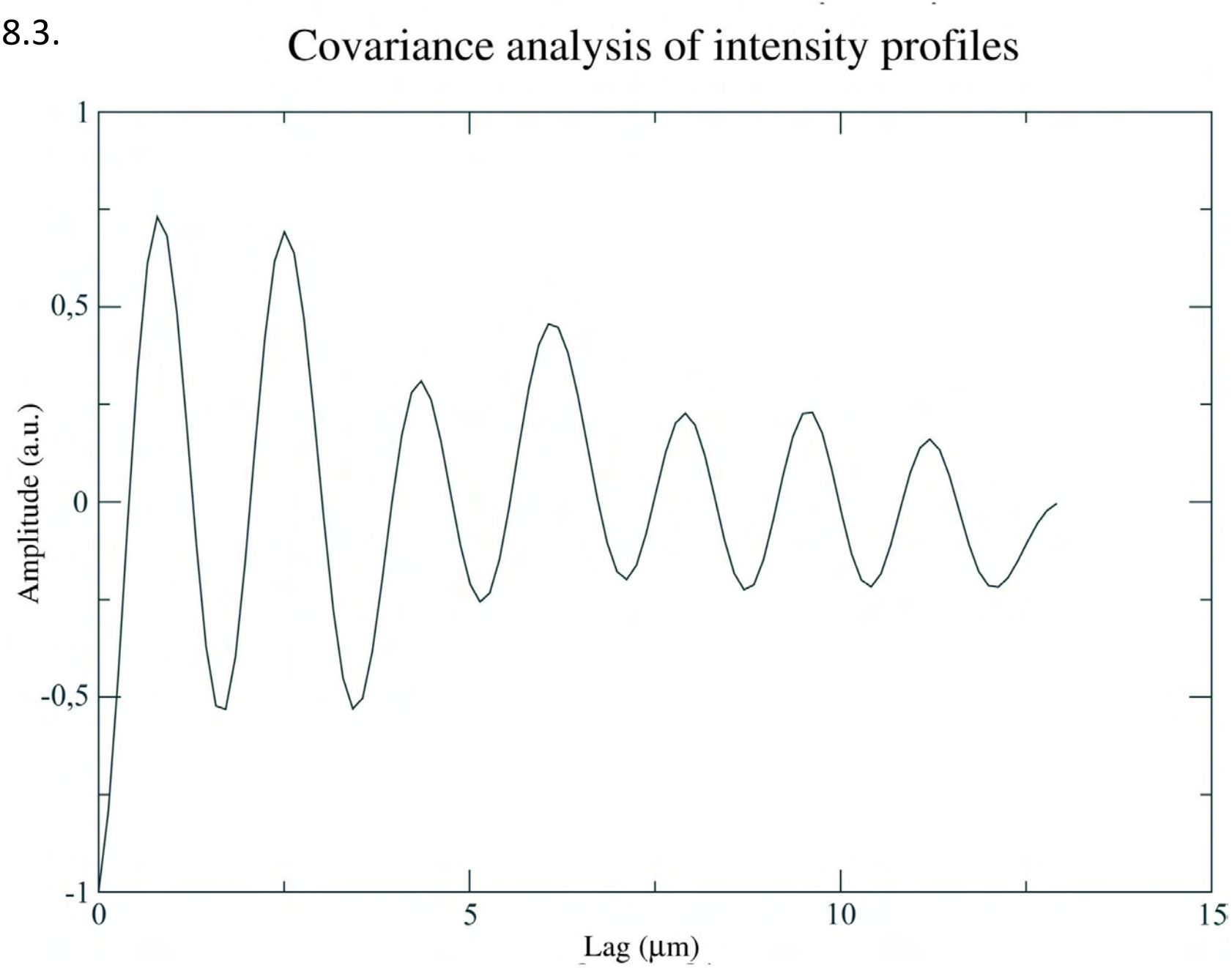
Covariance analysis of intensity profiles
Amplitude (a.u.)
1
0,5
0
-0,5
-1
0
5
10
15
Lag (μm)

Figure 8

Elsevier Editorial System(tm) for BBA - Bioenergetics
Manuscript Draft

Manuscript Number:

Title: Matters of the heart in bioenergetics: mitochondrial fusion into continuous reticulum is not needed for maximal respiratory activity

Article Type: Regular Paper

Keywords: cardiac cells, respiration, mitochondria, fusion-fission, calcium metabolism, energy metabolism.

Corresponding Author: Prof. Valdur A. Saks,

Corresponding Author's Institution: Joseph Fourier University

First Author: Minna Karu-Varikmaa

Order of Authors: Minna Karu-Varikmaa; Marcela Gonzalez-Granillo; Alexey Grichine; Yves Usson; François Boucher; Tuuli Kaambre; Rita Guzun; Valdur A. Saks

Abstract: Mitochondria are dynamic structures which fusion and fission are well characterized for rapidly dividing cells in culture. Recently, these data have been used to formulate new principles of cellular bioenergetics, according to which high respiratory activity is the result of fusion and formation of mitochondrial reticulum, while fission results in fragmented mitochondria with low respiratory activity. In this work we test the validity of this new hypothesis by analysing our own experimental data obtained in the studies of respiration regulation of isolated heart mitochondria, permeabilized cells of cardiac phenotype with different mitochondrial arrangement and dynamics. Additionally, we reviewed published data including electron tomographic investigation of mitochondrial membrane-associated structures in heart cells. Oxygraphic studies show that maximal ADP-dependent respiration rates are equally high both in isolated heart mitochondria and in permeabilized cardiomyocytes. On the contrary, these rates are three times lower in NB HL-1 cells with fused mitochondrial reticulum. Confocal and electron tomographic studies show that there is no mitochondrial reticulum in cardiac cells, where individual mitochondria are regularly arranged at the level of sarcomeres and are at Z-lines separated from each other by membrane structures, including T-tubular system in close connection to sarcoplasmic reticulum. Elaborated T-tubular system supplies calcium, oxygen and substrates from extracellular medium into local domains of the cardiac cells for calcium cycling within Calcium Release Units, associated with respiration and its regulation in Intracellular Energetic Units. Thus, maximal respiratory activity of mitochondria does not depend upon their fusion, which on contrary is characteristic for cardiac cell pathology.

Suggested Reviewers: Be Wieringa
b.wieringa@ncmls.ru.nl
High level expert in the field

Andrey Kuznetsov
Andrey.Kuznetsov@uki.at
Good expert in the field

Michel Rigoulet

Michel.Rigoulet@ibgc.cnrs.fr
High level expert in bioenergetics

Miguel Aon
maon1@jhmi.edu
Very good expert in mitochondrial bioenergetics

Dear Drs. Uli Brandt and Fabrice Rappaport

Executive Editors,
BBA-Bioenergetics

Dear Drs. Uli Brandt and Fabrice Rappaport,

We are submitting herewith our manuscript entitled "Matters of the heart in bioenergetics: mitochondrial fusion into continuous reticulum is not needed for maximal respiratory activity" by Minna Karu-Varikmaa, Marcela Gonzalez-Granillo, Alexei Grichine, Yves Usson, François Boucher, Tuuli Kaambre, Rita Guzun and myself. This manuscript contains our own results and review of literature on the structure of cardiac cell. It was written in response to recent publication by B. Westermann of the review " Bioenergetic role of mitochondrial fusion and fission" in Biochim Biophys Acta (2012) http://dx.doi.org/10.1016/j.bbabio.2012.02.033 and discusses the validity of the new hypothesis of the link between mitochondrial fusion and respiratory activity proposed in that publication. Because of the many contradictions still existing in the literature and because of the importance of the problem, we think that our paper will be interesting for very many investigators working in the area of bioenergetics.

Therefore, we would like to ask you to consider the possibility of its publication in Biochimica Biophysica Acta, section Bioenergetics.

We have requested all permissions needed for reproduction of the data of other authors.

With best regards

Valdur Saks

***Highlights (for review)**

- We compare respiration rates of mitochondrial preparations
- Mitochondrial fusion is not important for respiration
- No mitochondrial reticulum is seen in cardiomyocytes
- T-tubular system is important for mitochondrial arrangement

MATTERS OF THE HEART IN BIOENERGETICS:

MITOCHONDRIAL FUSION INTO CONTINUOUS RETICULUM IS NOT NEEDED FOR MAXIMAL RESPIRATORY ACTIVITY

Minna Karu-Varikmaa[1], Marcela Gonzalez-Granillo[2], Alexei Grichine[3], Yves Usson[3], François Boucher[4], Tuuli Kaambre[1], Rita Guzun[2] and Valdur Saks [1,2]

[1] Laboratory of Bioenergetics,
National Institute of Chemical Physics and Biophysics, Tallinn, Estonia

[2] INSERM U1055
Laboratory of Fundamental and Applied Bioenergetics,
Joseph Fourier University, Grenoble, France

[3] Life science imaging – *in vitro* platform, IAB CRI U823 Inserm /
Joseph Fourier University, France

[4] Experimental, Theoretical and Applied Cardio-Respiratory Physiology,
Laboratory TIMC-IMAG, Joseph Fourier University, Grenoble, France

Address for Correspondence: Pr. Valdur Saks

Laboratory of Bioenergetics
Joseph Fourier University,

2280, Rue de la Piscine

BP53X – 38041

Grenoble Cedex 9, France

e-mail : Valdur.Saks@gujf-grenoble.fr

ABSTRACT

Mitochondria are dynamic structures which fusion and fission are well characterized for rapidly dividing cells in culture. Recently, these data have been used to formulate new principles of cellular bioenergetics, according to which high respiratory activity is the result of fusion and formation of mitochondrial reticulum, while fission results in fragmented mitochondria with low respiratory activity. In this work we test the validity of this new hypothesis by analysing our own experimental data obtained in the studies of respiration regulation of isolated heart mitochondria, permeabilized cells of cardiac phenotype with different mitochondrial arrangement and dynamics. Additionally, we reviewed published data including electron tomographic investigation of mitochondrial membrane-associated structures in heart cells. Oxygraphic studies show that maximal ADP-dependent respiration rates are equally high both in isolated heart mitochondria and in permeabilized cardiomyocytes. On the contrary, these rates are three times lower in NB HL-1 cells with fused mitochondrial reticulum. Confocal and electron tomographic studies show that there is no mitochondrial reticulum in cardiac cells, where individual mitochondria are regularly arranged at the level of sarcomeres and are at Z-lines separated from each other by membrane structures, including T-tubular system in close connection to sarcoplasmic reticulum. Elaborated T-tubular system supplies calcium, oxygen and substrates from extracellular medium into local domains of the cardiac cells for calcium cycling within Calcium Release Units, associated with respiration and its regulation in Intracellular Energetic Units. Thus, maximal respiratory activity of mitochondria does not depend upon their fusion, which on contrary is characteristic for cardiac cell pathology.

Key words: cardiac cells, respiration, mitochondria, fusion-fission, calcium metabolism, energy metabolism.

INTRODUCTION

Pioneering studies of Bereiter-Hahn about twenty years ago have shown that mitochondria are dynamic structures capable to change rapidly their morphological pattern [1,2]. With their work authors opened the way to intensive studies of mitochondrial dynamics in living cells [3-10]. The dynamic morphological changes entail remodeling processes of mitochondria through the fusion and fission phenomena. These opposite events are essential for development, apoptosis, and ageing [5,7]. Fission events associated with major changes in mitochondrial electro-chemical membrane potential ($\Delta\psi_m$) generate functionally divergent daughters required for the removal of damaged and inactive organelles. While fusion mixes the content of parent mitochondria through the rapid diffusion of matrix proteins, due to the slower migration of inner and outer membrane components. Therefore, mitochondrial dynamics has an impact on mitochondrial turnover. Mitochondrial fusion allows efficient mixing of mitochondrial content, and it generates extended mitochondrial networks. Mitochondrial fusion needs essential GTPases proteins, e.g. mitofusin 1 and 2 (Mfn1, Mfn2) and optic atrophy protein 1 (OPA1). In mammals, Mfn1 and Mfn2 are found in mitochondrial outer membrane (MOM), while OPA1 in the intermembrane space closely associated with mitochondrial inner membrane (MIM). It has been suggested that OPA1 play a role in cristae maintenance and its activity is dependent on the bioenergetic state of mitochondria, *i.e*. mitochondrial membrane potential-dependent [5,6,9,10]. Mfns and OPA1 work together to promote mitochondrial fusion. In mitochondrial fusion, MOM and MIM should fuse simultaneously in order to maintain the organelle integrity. It was shown that some cell stressors can trigger increased mitochondrial fusion, called stress-induced mitochondrial hyperfusion, in an Mfn1- and Opa1-dependent manner [9,11].

These intensive studies of mitochondrial fusion and fission, carried out mostly in rapidly dividing cells in culture, have led many authors to conclude that fusion and fission

have important bioenergetic consequences [6,12]. Jezek and Plecita-Hlavata have proposed that only a single mitochondrion consisting of a continuous mitochondrial reticulum exists in a healthy intact cells in the absence of stress signaling [12], and several authors have concluded that mitochondrial fusion is necessary for normal mitochondrial functioning. Thus, Westermann has proposed that mitochondrial morphology adapts depending on the respiratory activity [6]. This model proposes that interconnected mitochondrial networks are frequently present in metabolically and respiratory active cells, whereas small and fragmented mitochondria are more prevalent in quiescent and respiratory inactive cells: when respiratory activity is low, fragmented mitochondria are the preferred morphological state, whereas under respiratory conditions mitochondria undergo fusion to allow spreading of metabolites and macromolecules throughout the entire compartment. Thus, it was suggested that mitochondrial fusion generates extended mitochondrial networks and allows efficient mixing of mitochondrial content that increase the respiratory activity [6]. In other words, it has been proposed by these authors that mitochondrial respiratory activity and thus energy fluxes in the cells *in vivo* are mostly regulated by fusion-fission events. In particular, this has been thought to be important in muscle cells, including heart [6, 13,14]

The aim of our work is to check the validity of this new fundamental hypothesis of cellular bioenergetics. We have taken the advantage of our long-time experience of quantitative studies of the mechanisms of respiration regulation of isolated heart mitochondria and permeabilized cells of cardiac phenotype with very different structures: adult cardiomyocytes with regularly arranged separate mitochondria and cancerous HL-1 cells with mitochondrial reticulum. Also, we have carefully analyzed published structural data on 3-dimensional organization of membrane systems in the heart cells, including T-tubular systems and those responsible for calcium recycling, and mitochondrial intracellular arrangement. All

these experimental data show directly and unequivocally that mitochondrial fusion is not needed for maximal respiratory activity, which is seen in heart in absence of any fused mitochondrial reticulum.

MATERIALS AND METHODS

Cells preparation

For this study we used freshly isolated adult rat cardiomyocytes, isolated rat heart mitochondria and non-beating HL-1 cancerous cell line of cardiac phenotype developed in Dr. W.C. Claycomb laboratory (Louisiana State University Health Science Center, New Orleans, LA, USA).

Isolation of adult cardiac myocytes

Adult cardiomyocytes were isolated after perfusion of the rat heart with collagenase using modified technique described previously [15]. Wistar male rats (300-350g) were anaesthetized with pentobarbital and blood was protected against coagulation by injection of 500 U of heparin. The heart was quickly excised preserving a part of aorta and placed into isolation medium (IM) of the following composition: 117 mM NaCl, 5.7 mM KCl, 4.4 mM $NaHCO_3$, 1.5 mM KH_2PO_4, 1.7 mM $MgCl_2$, 11.7 mM glucose, 10 mM creatine, 20 mM taurine, 10 mM PCr, 2 mM pyruvate and 21 mM HEPES, pH 7.1. The excised rat heart was cannulated by aorta and suspended in Langendorf system for perfusion and washed for 5 min with a flow rate of 15-20 mL/min. The collagenase treatment was performed by switching the perfusion to circulating isolation medium supplemented with 0.5-1 mg/ml Collagenase (Roche) and BSA 2 mg/ml at the flow rate of 5 ml/min for 20-30 min. After the digestion, the heart was washed with IM for 2–3 min and transferred into IM containing 20 μM $CaCl_2$, 10 μM leupeptin, 2 μM soybean trypsin inhibitor and 2 mg/ml fatty acid free BSA. Heart tissue was then gently dissociated using forceps and pipette suction. Cell suspension was filtered through a crude net to remove tissue remnants and let to settle for 3–4 min at room temperature. After 3-4 min the initial supernatant was discarded, pellet of cardiomyocytes resuspended in 10 ml of IM containing 20 μM $CaCl_2$ and the protease inhibitors. This resuspension-sedimentation cycle with calcium-tolerant cells was performed twice, after that

cardiomyocytes were gradually transferred from 20 μM Ca^{2+} IM into free calcium Mitomed (supplemented with protease inhibitors and BSA) and washed 5 times. Each time, slightly turbid supernatant was removed after 4-5 min of the cells' sedimentation. Isolated cells were re-suspended in 1 – 2 ml of Mitomed solution containing 0.5 mM EGTA, 3 mM $MgCl_2$, 60 mM K-lactobionate, 3 mM KH_2PO_4, 20 mM taurine, 20 mM HEPES, 110 mM sucrose, 0.5 mM dithiothreitol (DTT), pH 7.1, 2 mg/mL fatty acid free BSA.

Isolation of mitochondria from cardiac muscle

Heart mitochondria were isolated from adult white Wistar rats 300 g body weight, as described by Saks et al. in 1975 [16]. The final pellet containing mitochondria was re-suspended in 1 ml of isolation medium containing 300 mM sucrose, 10 mM HEPES, pH 7.2, and 0.2 mM EDTA and kept in ice for no longer than 3 h.

Cells culture

Cardiac muscle cell line, designated as HL-1 cells were derived in the Claycomb laboratory from the AT-1 mouse atrial cardiomyocyte tumor lineage (Claycomb 1998). Non-beating HL-1 cells (NB HL-1) were obtained from the HL-1 line developed by W.Claycomb by growing them up in different serum (Gibco fetal bovine serum) [17,18]. These cells maintain cardiac properties characterized by immunolabelling actin, tubulin, desmin, connexin 43, myosin (developmental isoform), dihydropyridine receptors, by the presence of a sodium–calcium exchanger. These cells are devoid of sarcomere structures and possess randomly organized filamentous dynamic mitochondria. NB HL-1 possess electrophysiological characteristics and ionic currents of cardiac cells (cardiac potassium current), but do not display electrical pacemaker activity and do not show spontaneous depolarization [17].

Measurements of oxygen consumption

The rates of oxygen uptake were determined with high-resolution respirometer Oxygraph-2K (OROBOROS Instruments, Austria) in Mitomed solution complemented with 5 mM glutamate and 2 mM malate as respiratory substrates. Respiration was activated by addition of creatine to final concentration of 10 mM in the presence of ATP (2 mM). Maximal respiration rate was measured in the presence of ADP, 2 mM. Measurements were carried out at 25^{o}C; solubility of oxygen was taken as 240 nmol ml^{-1}.

Proteins concentration ware measured using Pierce BCA assay kit.

Measurements of cytochrome aa3 content

Cytochrome aa3 content is representative of respiratory chain in the isolated mitochondria, cardiomyocytes and NB HL-1 cells were measured spectrophotometrically according to [19]. The cells or mitochondria were solubilized with 1% of sodium deoxycholate in phosphate buffer (100 mM KH2PO4, pH 8). The differential spectrum (reduced by dithionite versus oxidized cytochromes) was obtained by scanning from 400 to 650 nm using a Cary 50 Bio spectrophotometer (Varian, Palo Alto, USA). An oxidized-reduced spectrum was obtained by reducing sample with sodium dithionite (final concentration 2 mg/ml). The value of peak at 605 nm was used for quantification of respiratory chaincytochrome aa3 contents (cytochrome c oxidase) using the extinction coefficient e value equal to 24 mM^{-1} cm^{-1}.

Autofluorescence and immunolabeling of α-actinin

Freshly isolated cardiomyocytes were incubated for 10 min in a Petri dish containing oxygen-saturated Mitomed and 5μM of rotenone to produce the oxidation of flavoproteins. Thereafter, cells were fixed using paraformaldehyde (PFA) 4% and Glutaraldehyde 0.1% solutions for 1h at 4°C. Then cells were washed 3 times with PBS (phosphate buffered saline) containing 2% of BSA. Thereafter, cardiac cells were permeabilized with 1% Triton X-100 during 30 min at room temperature (25° C), followed by 3 washes with 2% BSA solution.

Fixed cardiomyocytes with oxidized mitochondria were incubated with anti-alpha actinin antibody [SA-20] (Abcam, ab82247) in PBS containing 2% BSA, overnight. The next day these cardiac cells were washed once with PBS containing 2% BSA and incubated with Cy™ 5-conjugated Afini-Pure goat anti mouse IgG (Jackson Immunoresearch 115-175-146) for 2 hours at room temperature.

Immunolabeling of VDAC and tubulin βII in cardiomyocytes

Freshly isolated cardiomyocytes were fixed in 4% PFA at 37ºC for 15min. After rinsing with PBS, cells were incubated in Antigen Retrieval Buffer (10mM Tris, 5% urea, pH 9.5) at 95ºC for 5 min, washed with PBS, permeabilized in 1% Triton X-100 PBS solution at room temperature for 30 min, washed again with PBS, and blocked in PBS solution containing 2% BSA for 30 min at 25ºC. Fixed and permeabilized cells were incubated overnight with rabbit anti-VDAC antibody (kindly provided by Dr. Catherine Brenner from University Paris-Sud, France). and with mouse anti-tubulin βII (Abcam, ab28036). The next day samples were labelled for 2 h at room temperature with two secondary antibodies DyLight 488 goat anti-rabbit IgG and DyLight549 goat anti-mouse IgG (Abcam, ab96899 and ab96880 correspondingly). Between staining steps samples were repeatedly rinsed with PBS.

Confocal imaging

Fluorescent images were acquired using LSM710NLO confocal microscope (Carl Zeiss) equipped with a 100×/1.4 oil immersion plan-apochromat objective. Laser excitation was 488nm for Dy light 488, and 633nm for Cy5 and MitoTracker® Deep Red FM.

RESULTS AND DISCUSSION

1. *Oxygraphic measurements of respiration rates.*

Figure 1 shows the images of three samples for which we measured maximal rates of respiration stimulated by 2 mM ADP (Vmax). First shown is electron microscopy image (Figure 1A) of isolated mitochondria from rat heart which consist of double membrane - bound spherical or bean-shaped organelles about 1 μm in diameter without any fusion [20,21]. Other two preparations showed by confocal microscopy image are permeabilized adult rat cardiomyocytes (Figure 1B) and cancerous NB HL-1 cells of cardiac phenotype (Figure 1C). The arrangement of intermyofibrillar mitochondria in cardiomyocytes, is remarkably regular following the crystal-like pattern [22-24]. Cancerous NB HL-1 cells of cardiac phenotype display a dense reticulum of fused elongated mitochondrial threads surrounding nuclei (Figure 1C).

Figure 2 shows recordings of oxygen consumption rates of isolated heart mitochondria (Figure 2A), permeabilized cardiomyocytes (Figure 2B) and NB HL-1 cells (Figure 2C). Initially respiration was recorded in the presence of glutamate-malate (basal rate, V_0, State 2 of respiration according to Chance, [25]). Previously, in 1997 Mootha et al., have experimentally found that glutamate-malate is the optimal substrates yielding respiratory rates of heart mitochondria as high as any other substrates [26]. Maximal rate of respiration (Vmax, State 3 of respiration) was activated by the addition of 2 mM ADP. Stable rate of respiration after the addition of 8 μM cytochrome c and the decrease of respiration rate until V0 after the addition of 30 μM atractyloside (State 4 of respiration) indicate the integrity of outer and inner mitochondrial membranes.

Figure 3 shows analysis of respiratory activity of all three preparations studied. Figure 3A shows respiration rates (V0 and Vmax) expressed in nmoles of O_2 consumed per min per

nmoles of cytochrome aa_3. The Respiratory Control Index (RCI) calculated as the ratio between maximal ADP-stimulated respiration and respiration measured in the absence of ADP (States 3 to 4 ratio according to Chance) is about 10 for isolated mitochondria and permeabilized cardiac myocytes, and about 2 for NB HL-1cells. Figure 3B shows the apparent affinity of oxidative phosphorylation for free ADP for these three preparations. The values of apparent Km for ADP are very low for isolated heart mitochondria and NB HL-1 cells (7.9 ± 1.6 µM and 8.6 ± 1.5 µM correspondingly) and very high for permeabilized cardiomyocytes (370.8 ± 30.6 µM) [18,27,28].

Thus, our experiments as many other previous observations show that individual regularly arranged mitochondria of permeabilized cardiomyocytes and isolated heart mitochondria have similar very high maximal ADP-stimulated respiration rates [28-32]. Starting with the works of Britton Chance [25], respiratory activity is measured as the maximum ADP-Pi-driven respiratory rate with saturating levels of oxygen and substrates. Mootha et al. have found that the maximum ADP-Pi driven respiratory rates of the dog heart measured at 37°C in the absence of oxygen or blood flow limitations were 676±31 $nmolO_2 \cdot min^{-1} \cdot nmol\ Cyt\ a^{-1}$. The RCI (ratio of state 3 to state 4 of respiration) ranged in Mootha's experiments between 8 and 15 at 37°C (Mootha 1997). Recalculation of our experimental results, accounting for differences in the temperature, gives the values of respiration rates similar to those found in Mootha's experiments [26].

Kinetic analysis of respiration regulation by ADP revealed significant difference between isolated mitochondria and mitochondria *in situ* surrounded by intracellular structures. The apparent Km for ADP is much higher for permeabilized cardiomyocytes than for isolated mitochondria indicating the low availability of extramitochondrial ADP for adenine nucleotides translocator (ANT) (Figure 3B). It was shown that this effect is due to the limited selective permeability of MOM voltage-dependent anion channel (VDAC) for adenine

nucleotides [27,28,33] which can be increased by the trypsin proteolysis of mitochondrial interactions with cytoskeletal proteins [34]. The NB HL-1 cells display very high affinity for ADP and very low maximal ADP-stimulated respiration rate (Figure 3). Low values of apparent Km for ADP (about 8μM) situated in the range of intracellular ADP concentration (about 50 μM) reflect glycolytic rather than oxidative metabolic pattern characteristic of rapidly proliferating immortalized cell lines, cancerous and embryonic cells. Mitochondria of these cells usually form reticular dynamic network. These experiments confirm that mitochondrial organization and function are cell type- and tissue-specific, and have to be studied separately for every type of cell. Chen et al. studied relationship between mitochondrial organization and respiration activity using only one cell type, mouse embryonic fibroblasts (MEFs) displaying different mitochondrial distribution due to the down- or up-regulation of fusion/fission proteins [35]. Interestingly, cells overexpressing OPA1 with uniform small mitochondrial spheres spread throughout the cytoplasm had similar respiration rates with wild-type MEF cells [35]. Cells underexpressing OPA1 or lacking both Mfn1 and Mfn2 showed highly heterogeneity in mitochondrial size, some were very large mitochondrial spheres (several microns in diameter) accompanied by a scattering of very small mitochondrial fragments. These cells displayed pathological behavior with very slow growth, widespread heterogeneity of mitochondrial membrane potential, and decreased cellular respiration [35].

The conclusion from the first part of this study is that mitochondrial fusion is not needed for maximal mitochondrial respiratory activity in the cells of cardiac phenotype; on the contrary, mitochondrial fusion is seen in the pathological state and results in a decrease of respiratory capacity. Next important question is whether the mitochondrial reticular network exists in intact cardiomyocytes or not, and whether this structure is even possible. This question is analyzed in details below.

2. Confocal microscopic studies

Figure 4A shows the confocal image of autofluorescent mitochondrial flavoproteins (green color) in fixed adult cardiomyocytes and immunnofluorescent labeling of α-actinin (red color) used to visualize Z-lines. Figure 4B shows analysis of fluorescence intensities along the line drawn through the length of sarcomeres. The localization of intensity peaks indicates the regular distribution of separated mitochondria between Z-lines of each sarcomere without any fusion phenomenon. Earlier, studies of mitochondrial dynamics using high speed scanning (1 frame per 400 ms) confocal microscopy and gradient clustering algorithm revealed rapid and limited fluctuations of mitochondria fluorescence centers which could correspond to the conformational changes of MIM [36]. No fusion-fission events of intermyofibrillar mitochondria were observed in adult cardiomyocytes. Using the same technique, Beraud et al., in 2009 quantitatively described dynamic behavior of mitochondrial network also in NB HL-1 cells [36]. Authors showed that mitochondria are continuously moving with the apparent flow velocity V of 6 × 10-4 μm/s when organelles are fragmented and about 2 × 10-4 μm/s when organelles are merged [36]. High degree of freedom of mitochondria in NB HL-1 cells were explained by the lack of sarcomeres and the fusion-fission cycles [36].

One of important factors of the very regular arrangement of individual mitochondria in cardiomyocytes is their interaction with cytoskeleton, in particular with tubulin [28,31,32]. Figure 5A shows the immunofluorescent labelling of VDAC of fixed cardiomyocytes mitochondria, and Figure 5B shows the labelling of tubulin βII by its fluorescent antibodies in these cells. Remarkably, tubulin βII is found to be localized in close association with VDAC (Figure 5C). Biophysical measurements of VDAC permeability *in vitro* and kinetic analysis of regulation of mitochondrial respiration before and after addition of αβ-tubulin revealed that

attachment of this protein to VDAC selectively decreases permeability of the latter for ATP and ADP [33,37]. Additionally, we have shown that phosphocreatine (PCr) and creatine freely diffuse through MOM of isolated mitochondria (avoided of tubulin by trypsin treatment) as well as permeabilized cardiomyocytes which inherently display the co-localization of tubulin βII and mitochondria [27,28,31,38]. NB HL-1 cells, which are characterized by high affinity of oxidative phosphorylation for ADP (Km about 8 μM), do not express tubulin βII. Other studied β-tubulin isotypes (I, III, IV) have structural role with some particularities for cardiomyocytes and NB HL-1 cells. Thus, tubulin βIV is seen in polymerized form creating longitudinally and obliquely oriented microtubules in cardiac cells and filaments, radially distributed from nucleus to cell periphery, creating also inter-connections in NB HL-1 cells. Tubulin βIII is co-colocalized with sarcomeric Z-lines in cardiac cells and have diffuse distribution penetrating into the nucleus in NB HL-1 cells. Tubulin βI have similar diffuse distribution in both cell types [32]. It is important to mention that other cytoskeletal and cytoskeleton-associated proteins (plectin, kinesin, dynein, etc.) can also be involved in regulation of mitochondrial respiration and control MOM permeability for adenine metabolites.

Analysis of structural data published in literature.

Our conclusion from the results shown above is that there is still no direct evidence of the existence of mitochondrial reticulum in heart cells. This conclusion is consistent with the results of very many earlier electron microscopic studies [39-41] and recent observations by confocal microscopy [8,22,31]. Most interestingly, however, the question of mitochondrial morphology and arrangement in cardiac cells was unequivocally and with absolute clarity solved in recent excellent electron tomographic study by Hayashi et al. of membrane structures involved in calcium cycling in heart cells [42]. This advanced technology allowed achieving 5-8 nm resolution 3D microscopic analyses across multiple sarcomeres in

mammalian cardiac muscle [42]. This excellent study and others [43,44] invalidated one of main arguments used by Westermann for development of his hypothesis that in muscle cells mitochondrial filaments connect a dense layer of mitochondria in the oxygen-rich cell periphery with mitochondria in the oxygen-poor core of the muscle fibre, thereby forming a continuous network to dissipate the membrane potential generated in the cell periphery over a large area and to use it to produce ATP in remote parts of the cell [6]. This is not needed and even not possible because of the fine spatial structure of extensions of sarcolemma into the cell interior, called T-tubular system, which is an elaborate network of transversal-axial tubules located at the level of Z-lines or between these lines of each sarcomere in close contact with sarcoplasmic reticulum and mitochondria, making possible the direct supply of calcium, substrates and oxygen from extracellular medium into the cell to each mitochondria in these local areas, and also preventing from mitochondrial fusion. This technique and information was not available when the original hypothesis was proposed [45-47].

a) Calcium release units.

Calcium cycling is the mechanism of the excitation – contraction coupling which regulates the contraction of striated muscle cells [48-50]. In heart, small amount of calcium enters into the cell from extracellular medium during depolarization phase of action potential through sarcolemmal calcium channels called also dyhydropyridine receptors (DHPR) and releases larger amount of calcium from sarcoplasmic reticulum (calcium induced calcium release, CICR) through the channels called ryanodine receptors (RyR). Calcium cycle is terminated by re-accumulation of calcium within sarcoplasmic reticulum (SR) through Ca-dependent ATPase (SERCA) and part of calcium is exported into extracellular medium via Na-Ca exchanger in the sarcolemmal membrane [50]. The elementary event in calcium cycle is a Ca spark, a localized Ca released events due to random and collective opening of RyR channels clustered in the local areas called calcium release units, CRU. Each CRU contains

about 10 sarcolemmal Ca channels and several hundred RyR [51-54]. Different CRU form diffusively coupled networks in cardiomyocytes [53]. Total number of CRUs in one cardiomyocyte has been found to be of the order of 10^4 [53,54].

The calcium released in all diffusively connected CRU activates sarcomere contraction by binding to troponin complex on thin actin filaments and making possible the myosin-actin interaction and thus contraction cycle [49,55]. The force of contraction and cardiac work are regulated also by changes in sarcomere length [55]. This is the length-dependent mechanism of muscle contraction regulation, explaining Frank-Starling law of the heart - the dependence of cardiac performance on left venticular filling [28,56].

b) Mitochondrial arrangement into Intracellular Energetic Units, ICEUs, and respiration regulation.

Mitochondria take part in the calcium cycle, importing calcium by a calcium uniport transporter and exporting it through Na-Ca exchanger [49,57]. In mitochondria, calcium is needed to maintain Krebs cycle dehydrogenases in active state [57]. Mitochondrial respiration and ATP production are dependent both upon calcium entry into mitochondria from CRUs and metabolic signaling from myofibrillar ATPases in sarcomeres, which contraction is regulated by Ca and sarcomere length-dependent mechanism [56,57].

About 50 % of DHPR are located in the T-tubular system, which in the cells is localized transversely and axially [44] close to Z-lines in vicinity of junctional cisterns of SR (jSR) and mitochondria. Hayashi et al. studied the morphology and distribution of T-tubular system, jSR and mitochondria in cardiomyocytes with the use of high resolution electron tomography [42]. Most interesting results of this excellent work are reproduced in Figure 6. Figure 6A shows individual mitochondria localized at the level of A-band of sarcomeres. Figure 6B shows that at the Z-line mitochondria are in close contacts with jSR and T-tubular system forming CRUs, which also separate mitochondria from each other, thus making their

fusion impossible. Figure 6C shows the 3D image of separate mitochondria in another volume that crosscuts of most of myofilaments. Again, one sees individual mitochondria separated from each other by cellular structures. These results are in concord with earlier 3D electron microscopic studies of cardiac cell structures by Segretain reproduced in Figure 7 [39]. Figure 7A shows the crossection of cardiomyocyte at H-band level where separate mitochondria are regularly surrounded by myofibrils. In cross-section taken at Z-line level no mitochondria are seen but T-tubular system and SR (Figure 7B). Figure 7C shows again that at Z-line level mitochondria are separated by T-tubular system and SR, those taking part in CRU.

Finally, Figure 7D shows the 3D reconstruction of T-tubular system in cardiac cell [44]. This is the very elaborated and effective system of supply of Ca, substrates and oxygen from extracellular medium into cardiomyocytes. It plays important role in cellular structural organization, metabolism and mitochondrial arrangement [42,44,58]. Discovery of this elaborated cellular architecture about 12 year ago profoundly changed our knowledge of heart cell structure and mechanisms of regulation of its metabolism [44]. Beraud et al. by using rapid scanning confocal microscopy showed that high frequency oscillations of the mitochondrial fluorescent centers occur only in the limited space between Z-lines [36]. This is in concord with all structural data described above. It has also been shown in many laboratories that there is no electrical conductivity between individual mitochondria in cardiomyocytes [8,36, 54,59-61]. Yaniv et al. [62] measured simultaneously the sarcomere and mitochondrial dimensions *in situ* along the long-axis in isolated cardiomyocytes by registering variations in transmitted light intensity and directly observed mitochondria as micron-sized spheres localized between sarcomeres and distributed throughout the cell in a crystal-like lattice without any fusion. In this organized lattice, transient depolarizations of single mitochondria, known as flickers, due to ROS-induced opening of anion channels in the mitochondrial inner membranes may propagate in cells as depolarization waves [54,61].

Cardiomyocytes were found to contain about 5000 – 10 000 single mitochondria regularly arranged in the cell [54].

All these data lead to the conclusion that the respiration of mitochondria is dependent on the events in the limited area of their localization in the vicinity of sarcomeres, SR and T-tubules. These structurally organized functional domains are called Intracellular Energetic Units, ICEUs [27,28,63] (Figure 8). Due to elaborated structure of T-tubular system, mitochondria in ICEUs are in contact both with myofibrils and sarcolemma, and therefore we cannot distinct between subsarcolemmal or intermyofibrillar populations of mitochondria.

In the heart almost all ATP is synthesized by oxidative phosphorylation, and the linear relationship between heart workload (ATP hydrolysis) and oxygen consumption indicates very effective feedback regulation of mitochondrial respiratory activity in ICEUs [27,28,56]. Furthermore, the large range of changes of ATP turnover rate that may increase 20 times from resting state to maximal physiological workloads [64], is seen in the presence of stable intracellular levels of such energy metabolites as the ADP, Pi, ATP and PCr (metabolic stability or homeostasis) [64-66]. Several mechanisms of regulation of mitochondrial ATP synthesis matching intracellular ATP needs were proposed to explain heart bioenergetics under conditions of metabolic stability. Among them are above discussed Ca-dependent activation of Krebs cycle dehydrogenases [57,65] and the control of oxidative phosphorylation on beat to beat basis by the complex signal consisting of creatine/PCr ratio as well as the ADP, Pi and AMP small-scale local fluctuations within contraction cycle (my). It was demonstrated by Dzeja and Terzic groups with using ^{18}O tracer method that about 80% of mitochondrial ATP is used for phosphocreatine (PCr) production in the mitochondrial creatine kinase (MtCK) reaction, the PCr flux carrying energy to all cites of ATP regeneration for ATPases within ICEUs (Figure 8) [67,68]. Metabolic control analysis of mitochondrial

respiration regulation in cardiomyocytes has shown that by the mechanism of effective recycling of ADP-ATP in mitochondria, the MtCK reaction of PCr production coupled to oxidative phosphorylation is an effective amplifier of metabolic signals within ICEUs [28,69]. Glancy and Balaban have recently also concluded that "a possibility for the observed metabolic homeostasis in intact tissues is the compartmentation of metabolic intermediates in the cytosol much like that demonstrated for Ca^{2+} . The basic concept is that regional changes in ADP, Pi, and creatine in the regions around the mitochondria are major factors in driving mitochondrial ATP production" [57].

Thus, matching of ATP synthesis to ATP hydrolysis for cellular work is the result of compartmentation of integrated metabolic processes, created by the interaction between cellular membranes, cytoskeletal proteins and organelles in the limited space of ICEUs [28]. To overcome the restricted diffusion of metabolites in the structurally organized intracellular medium, the most effective mechanism of functioning of organized metabolic pathways is the metabolic channeling of reaction intermediates within supercomplexes - metabolons [36,70-73]. An example of such a processes is the intracellular glycolytic metabolon, mitochondrial TCA metabolon, β-fatty acids oxidation complex in mitochondrial matrix, PDH complex and even the formation of electron transport chain supercomplexes [74].These reactions occur in ICEUs in closely associated CRUs [28] (Figure 8). A mitochondrial substrate such as pyruvate (final product of anaerobic glycolysis) is directly transferred through the integrated within MIM PDH enzymes complex giving acetyl CoA. The transfer of fatty acids towards the matrix is also dependent on the membrane enzymes: acetyl coenzyme-A synthetase and carnitine palmitoyl transferase (CPT1) in the outer, and CPT2 in the inner membrane. Released into the matrix acyl coenzyme-A enters directly the β-fatty acids oxidation (β-FAO) pathway giving acetyl CoA. Once acetyl CoA is formed, the Krebs cycle begins. Krebs cycle is a big metabolon attached to MIM and forming eight steps of enzymatic transformation of

acetyl into $NADH,H^+$, $FADH_2$ and CO_2. All attempts to disrupt this metabolon will slow down formation of the reducing equivalents for the respiratory chain [75]. The electron transfer complexes ANT, Phosphate Carrier (PC) are incorporated into large assemblies, called supercomplexes, [76,77].

Mixing the contents of all mitochondria into one reticulum may be expected only to destroy all these effective metabolic complexes, increasing diffusion time for intermediates and thus decreasing the energy fluxes (as seen in HL-1 cells), but not elevating the respiration rates, as proposed by Westermann [5,6].

This, if fusion-fission cycle occurs in heart cells, it is a very infrequent phenomenon and does not include the formation of continuous mitochondrial reticulum. It is not excluded that some fusion may occur in the perinuclear mitochondrial clusters. Two main indirect evidences are used for mitochondrial fusion-fission dynamics in cardiac muscle cells [7]. One of them is the presence of fusion-fission proteins in heart muscle and another one consists in pathological remodeling of cardiac cells induced by abrogation of these proteins by genetic manipulations [7]. However, fusion is not an exclusively mitochondrial feature. It is typical for such membranous intracellular structures as the sarcoplasmic reticulum, Golgi apparatus and intracellular vesiculs. Koshiba's et al., have shown that mitochondrial fusions, like other intracellular membrane fusion events, proceeds through a tethering step mediated by heptad repeat region (HR2) [78]. In normal adult cardiac cells fusion proteins may be tethering regularly arranged individual mitochondria to the surrounding membranous structures such as T-tubules and sarcoplasmic reticulum as shown in Scorrano's laboratory [79], rather than to induce fusion. In recent work, Chen Y et al have also shown that Mfn2 is essential for tethering mitochondria to sarcoplasmic reticulum [80].

Moreover, the fusion-fission mitochondrial dynamics becomes evident for cardiac cells under pathological conditions such as the ischemia-reperfusion [7]. It is interesting that

in all these situations mitochondrial fusion-fission is associated with the remodeling of sarcomeres and T-tubules. Cardiac failure *in vivo* due to the loss of fusongenic proteins associated with fragmentation of cardiac mitochondria into small heterogeneous conglomerates [11] can be due to the disorganization of cell structure and metabolic compartmentation (remodeling of mitochondria-associated membrane interactions), impairment of intramitochondrial energy conversion, intracellular distribution of energy fluxes and controlling signals.

In conclusion, one cannot extend knowledge experimentally obtained for one cell-type to all others. For every cell type integrative structural and functional studies should be performed separately for revealing the mechanisms of regulation of their metabolism and energy fluxes.

Acknowledgements

This work was supported by INSERM and Agence Nationale de la Recherche programme SYBECAR, France, by grant No. 7823 from the Estonian Science Foundation and by grant SF0180114Bs08 from Estonia Ministry of Education and Science. The skillful technical assistance by Igor Shevchuk, Vladimir Chekulaev and Maire Peitel is gratefully acknowledged.

BIBLIOGRAPHY

[1] J. Bereiter-Hahn, Behavior of mitochondria in the living cell, Int Rev Cytol 122 (1990) 1-63.

[2] J. Bereiter-Hahn, M. Voth, Dynamics of mitochondria in living cells: shape changes, dislocations, fusion, and fission of mitochondria, Microsc Res Tech 27 (1994) 198-219.

[3] G. Twig, A. Elorza, A.J. Molina, H. Mohamed, J.D. Wikstrom, G. Walzer, L. Stiles, S.E. Haigh, S. Katz, G. Las, J. Alroy, M. Wu, B.F. Py, J. Yuan, J.T. Deeney, B.E. Corkey, O.S. Shirihai, Fission and selective fusion govern mitochondrial segregation and elimination by autophagy, Embo J 27 (2008) 433-46.

[4] M.P. Yaffe, The machinery of mitochondrial inheritance and behavior, Science 283 (1999) 1493-7.

[5] B. Westermann, Mitochondrial fusion and fission in cell life and death, Nat Rev Mol Cell Biol 11 (2010) 872-84.

[6] B. Westermann, Bioenergetic role of mitochondrial fusion and fission, Biochim Biophys Acta (2012) http://dx.doi.org/10.1016/j.bbabio.2012.02.033.

[7] G.W. Dorn, 2nd, Mitochondrial dynamics in heart disease, Biochim Biophys Acta (2012) http://dx.doi.org/10.1016/j.bbamcr.2012.03.008.

[8] A.V. Kuznetsov, M. Hermann, V. Saks, P. Hengster, R. Margreiter, The cell-type specificity of mitochondrial dynamics, Int J Biochem Cell Biol 41 (2009) 1928-39.

[9] H. Chen, D.C. Chan, Emerging functions of mammalian mitochondrial fusion and fission, Hum Mol Genet 14 Spec No. 2 (2005) R283-9.

[10] H. Chen, M. Vermulst, Y.E. Wang, A. Chomyn, T.A. Prolla, J.M. McCaffery, D.C. Chan, Mitochondrial fusion is required for mtDNA stability in skeletal muscle and tolerance of mtDNA mutations, Cell 141 (2010) 280-9.

[11] Y. Chen, Y. Liu, G.W. Dorn, 2nd, Mitochondrial fusion is essential for organelle function and cardiac homeostasis, Circ Res 109 (2012) 1327-31.

[12] P. Jezek, L. Plecita-Hlavata, Mitochondrial reticulum network dynamics in relation to oxidative stress, redox regulation, and hypoxia, Int J Biochem Cell Biol 41 (2009) 1790-804.

[13] J. Hom, S.S. Sheu, Morphological dynamics of mitochondria - A special emphasis on cardiac muscle cells, J Mol Cell Cardiol, 46 (2009) 811-820.

[14] V. Parra, H. Verdejo, A. del Campo, C. Pennanen, J. Kuzmicic, M. Iglewski, J.A. Hill, B.A. Rothermel, S. Lavandero, The complex interplay between mitochondrial dynamics and cardiac metabolism, J Bioenerg Biomembr 43 (2011) 47-51.

[15] V.A. Saks, Y.O. Belikova, A.V. Kuznetsov, In vivo regulation of mitochondrial respiration in cardiomyocytes: specific restrictions for intracellular diffusion of ADP, Biochim Biophys Acta 1074 (1991) 302-11.

[16] V.A. Saks, G.B. Chernousova, D.E. Gukovsky, V.N. Smirnov, E.I. Chazov, Studies of energy transport in heart cells. Mitochondrial isoenzyme of creatine phosphokinase: kinetic properties and regulatory action of Mg2+ ions, Eur J Biochem 57 (1975) 273-90.

[17] S. Pelloux, J. Robillard, R. Ferrera, A. Bilbaut, C. Ojeda, V. Saks, M. Ovize, Y. Tourneur, Non-beating HL-1 cells for confocal microscopy: application to mitochondrial functions during cardiac preconditioning, Prog Biophys Mol Biol 90 (2006) 270-98.

[18] T. Anmann, R. Guzun, N. Beraud, S. Pelloux, A.V. Kuznetsov, L. Kogerman, T. Kaambre, P. Sikk, K. Paju, N. Peet, E. Seppet, C. Ojeda, Y. Tourneur, V. Saks,

Different kinetics of the regulation of respiration in permeabilized cardiomyocytes and in HL-1 cardiac cells. Importance of cell structure/organization for respiration regulation, Biochim Biophys Acta 1757 (2006) 1597-606.

[19] C. Monge, N. Beraud, K. Tepp, S. Pelloux, S. Chahboun, T. Kaambre, L. Kadaja, M. Roosimaa, A. Piirsoo, Y. Tourneur, A.V. Kuznetsov, V. Saks, E. Seppet, Comparative analysis of the bioenergetics of adult cardiomyocytes and nonbeating HL-1 cells: respiratory chain activities, glycolytic enzyme profiles, and metabolic fluxes, Can J Physiol Pharmacol 87 (2009) 318-26.

[20] C.R. Hackenbrock, Ultrastructural bases for metabolically linked mechanical activity in mitochondria. I. Reversible ultrastructural changes with change in metabolic steady state in isolated liver mitochondria, J Cell Biol 30 (1966) 269-97.

[21] F. Appaix, A.V. Kuznetsov, Y. Usson, L. Kay, T. Andrienko, J. Olivares, T. Kaambre, P. Sikk, R. Margreiter, V. Saks, Possible role of cytoskeleton in intracellular arrangement and regulation of mitochondria, Exp Physiol 88 (2003) 175-90.

[22] M. Vendelin, N. Beraud, K. Guerrero, T. Andrienko, A.V. Kuznetsov, J. Olivares, L. Kay, V.A. Saks, Mitochondrial regular arrangement in muscle cells: a "crystal-like" pattern, Am J Physiol Cell Physiol 288 (2005) C757-67.

[23] T.J. Collins, M.J. Berridge, P. Lipp, M.D. Bootman, Mitochondria are morphologically and functionally heterogeneous within cells, Embo J 21 (2002) 1616-27.

[24] M.A. Aon, S. Cortassa, E. Marbán, B. O'Rourke, Synchronized whole cell oscillations in mitochondrial metabolism triggered by a local release of reactive oxygen species in cardiac myocytes, J Biol Chem 278 (2003) 44735-44.

[25] B. Chance, G.R. Williams, The respiratory chain and oxidative phosphorylation, Adv Enzymol. 17(1956) 65-164.

[26] V.K. Mootha , A.E. Arai, R.S. Balaban, Maximum oxidative phosphorylation capacity of the mammalian heart, Am J Physiol 272(1997) H769-75

[27] V. Saks, R. Guzun, N. Timohhina, K. Tepp, M. Varikmaa, C. Monge, N. Beraud, T. Kaambre, A. Kuznetsov, L. Kadaja, M. Eimre, E. Seppet, Structure-function relationships in feedback regulation of energy fluxes in vivo in health and disease: Mitochondrial Interactosome, Biochim Biophys Acta 1797 (2010) 678-97.

[28] V. Saks, A.V. Kuznetsov, M. Gonzalez-Granillo, K. Tepp, N. Timohhina, M. Karu-Varikmaa, T. Kaambre, P. Dos Santos, F. Boucher, R. Guzun, Intracellular Energetic Units regulate metabolism in cardiac cells, J Mol Cell Cardiol 52 (2012) 419-36.

[29] VA Saks, E Vasil'eva, Yu O Belikova, AV Kuznetsov, S Lyapina, L Petrova,. Retarded diffusion of ADP in cardiomyocytes: possible role of mitochondrial outer membrane and creatine kinase in cellular regulation of oxidative phosphorylation. Biochimica et biophysica acta. 1144(1993) 134-48.

[30] Saks V, editor. Molecular System Bioenergetics. Energy for Life. Gmbh, Germany: Wiley-VCH: Weinheim 2007.

[31] R. Guzun, M. Karu-Varikmaa, M. Gonzalez-Granillo, A.V. Kuznetsov, L. Michel, C. Cottet-Rousselle, M. Saaremae, T. Kaambre, M. Metsis, M. Grimm, C. Auffray, V. Saks, Mitochondria-cytoskeleton interaction: Distribution of beta-tubulins in cardiomyocytes and HL-1 cells, Biochim Biophys Acta 1807 (2011) 458-69.

[32] R. Guzun, N. Timohhina, K. Tepp, C. Monge, T. Kaambre, P. Sikk, A.V. Kuznetsov, C. Pison, V. Saks, Regulation of respiration controlled by mitochondrial creatine kinase in permeabilized cardiac cells in situ. Importance of system level properties, Biochim Biophys Acta 1787 (2009) 1089-105.

[33] T.K. Rostovtseva, K.L. Sheldon, E. Hassanzadeh, C. Monge, V. Saks, S.M. Bezrukov, D.L. Sackett, Tubulin binding blocks mitochondrial voltage-dependent anion channel and regulates respiration, Proc Natl Acad Sci U S A 105 (2008) 18746-51.
[34] M. Gonzalez-Granillo, A. Grichine, R. Guzun, Y. Usson, K. Tepp, V. Chekulayev, I. Shevchuk, M. Karu-Varikmaa, A.V. Kuznetsov, M. Grimm, V. Saks, T. Kaambre, Studies of the role of tubulin beta II isotype in regulation of mitochondrial respiration in intracellular energetic units in cardiac cells, J Mol Cell Cardiol 52 (2012) 437-47.
[35] H. Chen, A. Chomyn, D.C. Chan, Disruption of fusion results in mitochondrial heterogeneity and dysfunction, J Biol Chem 280 (2005) 26185-92.
[36] N. Beraud, S. Pelloux, Y. Usson, A.V. Kuznetsov, X. Ronot, Y. Tourneur, V. Saks, Mitochondrial dynamics in heart cells: very low amplitude high frequency fluctuations in adult cardiomyocytes and flow motion in non beating Hl-1 cells, J Bioenerg Biomembr 41 (2009) 195-214.
[37] C. Monge, N. Beraud, A.V. Kuznetsov, T. Rostovtseva, D. Sackett, U. Schlattner, M. Vendelin, V.A. Saks, Regulation of respiration in brain mitochondria and synaptosomes: restrictions of ADP diffusion in situ, roles of tubulin, and mitochondrial creatine kinase, Mol Cell Biochem 318 (2008) 147-65.
[38] N. Timohhina, R. Guzun, K. Tepp, C. Monge, M. Varikmaa, H. Vija, P. Sikk, T. Kaambre, D. Sackett, V. Saks, Direct measurement of energy fluxes from mitochondria into cytoplasm in permeabilized cardiac cells in situ: some evidence for Mitochondrial Interactosome, J Bioenerg Biomembr 41 (2009) 259-75.
[39] D. Segretain, A. Rambourg, Y. Clermont, Three dimensional arrangement of mitochondria and endoplasmic reticulum in the heart muscle fiber of the rat, Anat Rec 200 (1981) 139-51.
[40] D.W. Fawcett, N.S. McNutt, The ultrastructure of the cat myocardium. I. Ventricular papillary muscle, J Cell Biol 42 (1969) 1-45.
[41] C.L. Hoppel, B. Tandler, H. Fujioka, A. Riva, Dynamic organization of mitochondria in human heart and in myocardial disease, Int J Biochem Cell Biol 41 (2009) 1949-56.
[42] T. Hayashi, M.E. Martone, Z. Yu, A. Thor, M. Doi, M.J. Holst, M.H. Ellisman, M. Hoshijima, Three-dimensional electron microscopy reveals new details of membrane systems for Ca2+ signaling in the heart, J Cell Sci 122 (2009) 1005-13.
[43] M. Nivala, E. de Lange, R. Rovetti, Z. Qu, Computational modeling and numerical methods for spatiotemporal calcium cycling in ventricular myocytes, Front Physiol 3 (2012) 114.
[44] C. Soeller, M.B. Cannell, Examination of the transverse tubular system in living cardiac rat myocytes by 2-photon microscopy and digital image-processing techniques, Circ Res 84 (1999) 266-75.
[45] L.E. Bakeeva, S. Chentsov Yu, V.P. Skulachev, Mitochondrial framework (reticulum mitochondriale) in rat diaphragm muscle, Biochim Biophys Acta 501 (1978) 349-69.
[46] A.A. Amchenkova, L.E. Bakeeva, Y.S. Chentsov, V.P. Skulachev, D.B. Zorov, Coupling membranes as energy-transmitting cables. I. Filamentous mitochondria in fibroblasts and mitochondrial clusters in cardiomyocytes, J Cell Biol 107 (1988) 481-95.
[47] V.P. Skulachev, Mitochondrial filaments and clusters as intracellular power-transmitting cables, Trends Biochem Sci 26 (2001) 23-9.
[48] D.M. Bers, Cardiac excitation-contraction coupling, Nature 415 (2002) 198-205.
[49] D. Bers, Excitation-contraction coupling and cardiac contractile force, second ed., Kluwer Academic Publishers, Dordrecht, Netherlands, 2001.

[50] D.M. Bers, K.S. Ginsburg, Na:Ca stoichiometry and cytosolic Ca-dependent activation of NCX in intact cardiomyocytes, Ann N Y Acad Sci 1099 (2007) 326-38.
[51] S.Q. Wang, C. Wei, G. Zhao, D.X. Brochet, J. Shen, L.S. Song, W. Wang, D. Yang, H. Cheng, Imaging microdomain Ca2+ in muscle cells, Circ Res 94 (2004) 1011-22.
[52] C. Soeller, I.D. Jayasinghe, P. Li, A.V. Holden, M.B. Cannell, Three-dimensional high-resolution imaging of cardiac proteins to construct models of intracellular Ca2+ signalling in rat ventricular myocytes, Exp Physiol 94 (2009) 496-508.
[53] M. Nivala, C.Y. Ko, M. Nivala, J.N. Weiss, Z. Qu, Criticality in intracellular calcium signaling in cardiac myocytes, Biophys J 102 (2012) 2433-42.
[54] M. Nivala, P.Korge, M. Nivala, J.N. Weiss, Z. Qu, Linking flickering to waves and whole-cell oscillations in a mitochondrial network model, Biophys J 101(2011) 2102-11.
[55] N.S. Schneider, T. Shimayoshi, A. Amano, T. Matsuda, Mechanism of the Frank-Starling law--a simulation study with a novel cardiac muscle contraction model that includes titin and troponin I, J Mol Cell Cardiol 41 (2006) 522-36.
[56] V. Saks, P. Dzeja, U. Schlattner, M. Vendelin, A. Terzic, T. Wallimann, Cardiac system bioenergetics: metabolic basis of the Frank-Starling law, J Physiol 571 (2006) 253-73.
[57] B. Glancy, R.S. Balaban, Role of mitochondrial Ca2+ in the regulation of cellular energetics, Biochemistry 51 (2012) 2959-73.
[58] M. Nivala, E. de Lange, R. Rovetti, Z. Qu, Computational modeling and numerical methods for spatiotemporal calcium cycling in ventricular myocytes, Front Physiol 3(2012) 114.
[59] D.B. Zorov, C.R. Filburn, L.O. Klotz, J.L. Zweier, S.J. Sollott, Reactive oxygen species (ROS)-induced ROS release: a new phenomenon accompanying induction of the mitochondrial permeability transition in cardiac myocytes, J Exp Med 192 (2000) 1001-14.
[60] T.J. Collins, M.D. Bootman, Mitochondria are morphologically heterogeneous within cells, J Exp Biol 206 (2003) 1993-2000.
[61] L. Zhou, M.A. Aon, T. Liu, B. O'Rourke, Dynamic modulation of Ca2+ sparks by mitochondrial oscillations in isolated guinea pig cardiomyocytes under oxidative stress, J Mol Cell Cardiol 51 (2012) 632-9.
[62] Y. Yaniv, M. Juhaszova, S. Wang, K.W. Fishbein, D.B. Zorov, S.J. Sollott, Analysis of mitochondrial 3D-deformation in cardiomyocytes during active contraction reveals passive structural anisotropy of orthogonal short axes, PLoS One 6 (2011) e21985.
[63] V.A. Saks, T. Kaambre, P. Sikk, M. Eimre, E. Orlova, K. Paju, A. Piirsoo, F. Appaix, L. Kay, V. Regitz-Zagrosek, E. Fleck, E. Seppet, Intracellular energetic units in red muscle cells, Biochem J 356 (2001) 643-57.
[64] J.R. Williamson, C. Ford, J. Illingworth, B. Safer, Coordination of citric acid cycle activity with electron transport flux, Circ Res 38 (1976) I39-51.
[65] R.S. Balaban, Cardiac energy metabolism homeostasis: role of cytosolic calcium, J Mol Cell Cardiol 34 (2002) 1259-71.
[66] J.R. Neely, R.M. Denton, P.J. England, P.J. Randle, The effects of increased heart work on the tricarboxylate cycle and its interactions with glycolysis in the perfused rat heart, Biochem J 128 (1972) 147-59.
[67] P.P. Dzeja, A. Terzic, Phosphotransfer networks and cellular energetics, J Exp Biol 206 (2003) 2039-47.

[68] P.P. Dzeja, K. Hoyer, R. Tian, S. Zhang, E. Nemutlu, M. Spindler, J.S. Ingwall Rearrangement of energetic and substrate utilization networks compensate for chronic myocardial creatine kinase deficiency, J Physiol 589(2011)5 193-211.
[69] K. Tepp, I. Shevchuk, V. Chekulayev, N. Timohhina, A.V. Kuznetsov, R. Guzun, V. Saks, T. Kaambre, High efficiency of energy flux controls within mitochondrial interactosome in cardiac intracellular energetic units, Biochim Biophys Acta 1807 (2011) 1549-61.
[70] J. Ovadi, P.A. Srere, Macromolecular compartmentation and channeling, Int Rev Cytol 192 (2000) 255-80.
[71] V Saks, N Beraud, T Wallimann. Metabolic compartmentation - a system level property of muscle cells: real problems of diffusion in living cells. International journal of molecular sciences. 9 (2008) 751-67.
[72] V. Saks, C. Monge, R. Guzun, Philosophical basis and some historical aspects of systems biology: from hegel to noble - applications for bioenergetic research, Int J Mol Sci 10 (2009) 1161-92.
[73] T. Wallimann, M. Wyss, D. Brdiczka, K. Nicolay, H.M. Eppenberger, Intracellular compartmentation, structure and function of creatine kinase isoenzymes in tissues with high and fluctuating energy demands: the 'phosphocreatine circuit' for cellular energy homeostasis, Biochem J 281 (Pt 1) (1992) 21-40.
[74] G. Lenaz, M.L. Genova, Supramolecular organisation of the mitochondrial respiratory chain: a new challenge for the mechanism and control of oxidative phosphorylation, Adv Exp Med Biol 748 (2012) 107-44.
[75] V. Saks, R. Favier, R. Guzun, U. Schlattner, T. Wallimann, Molecular system bioenergetics: regulation of substrate supply in response to heart energy demands, J Physiol 577 (2006) 769-77.
[76] R. Acin-Perez, P. Fernandez-Silva, M.L. Peleato, A. Perez-Martos, J.A. Enriquez, Respiratory active mitochondrial supercomplexes, Mol Cell 32 (2008) 529-39.
[77] Y.H. Ko, M. Delannoy, J. Hullihen, W. Chiu, P.L. Pedersen, Mitochondrial ATP synthasome. Cristae-enriched membranes and a multiwell detergent screening assay yield dispersed single complexes containing the ATP synthase and carriers for Pi and ADP/ATP, J Biol Chem 278 (2003) 12305-9.
[78] T. Koshiba, S.A. Detmer, J.T. Kaiser, H. Chen, J.M. McCaffery, D.C. Chan, Structural basis of mitochondrial tethering by mitofusin complexes, Science 305(2004) 858-62.
[79] O.M. de Brito, L. Scorrano, Mitofusin 2 tethers endoplasmic reticulum to mitochondria., Nature 456(2008) 605-10.
[80] Y. Chen, G. Csordas, C. Jowdy, T.G. Schneider, N. Csordas, W. Wang, Y. Liu, M. Kohlhaas, M. Meiser, S. Bergem, J.M. Nerbonne, G.W. Dorn, C. Maack, Mitofusin 2-Containing Mitochondrial-Reticular Microdomains Direct Rapid Cardiomyocyte Bioenergetic Responses via Inter-Organelle Ca2+ Crosstalk, Circ Res (2012).

LEGENDS

Figure 1. Different mitochondrial shape and arrangement in experimentally studied samples. A) Electron microscopic image of isolated heart heart mitochondria (without fusion). B) Confocal image of cardiomyocyte labeled with 20 nM MitoTracker Red (regularly arranged mitochondria). C) Confocal image of NB HL-1 cells labeled with 20 nM MitoTracker Red (reticular fused mitochondria are seen).

Figure 2. Respiratory parameters of different mitochondrial preparations

Respiratory control and maximal activity of isolated mitochondria (A), permeabilized cardiomyocytes (B) and NB HL-1 cells (C) was measured using oxygraphy (Oroboros, Austria) in Mitomed medium at 25 °C. Blue line and left axis show oxygen concentrations. Red line and right axis show oxygen flux which is recalculated per nmol cytochrome aa_3. Initial respiration rates (V_0) recorded in the presence of 5 mM glutamate and 2 mM malate correspond to State 2 of respiration according to Chance. Maximal rate of respiration was measured by addition of 2 mM ADP. The addition of cytochrome c (Cyt c, 8 μM) did not change the respiration, indicating that the outer membrane is intact. Atractyloside (Atr, 30 μM) results in a decrease in respiration back to V_0 due to the inhibition of adenine-dinucleotide translocase.

Figure 3. Maximal respiratory activities and kinetic analysis of ADP-stimulated respiration. A) similar Vmax rates of isolated mitochondria and mitochondria *in situ* in permeabilized cardiac muscle cells. The Vmax of NB HL-1 cells is 4 folds lower. B) The apparent affinity of oxidative phosphorylation for ADP of permeabilized adult cardiomyocytes is much lower (app. Km for ADP is 370.8 ± 30.57 μM) than that of isolated mitochondria and NB HL-1 cells for ADP (7.9 ± 1.6 μM and 8.6 ± 1.5 μM correspondingly).

Figure 4. Mitochondrial and alpha-actinin distribution in adult rat cardiomyocyte. **A)** Regular organization of individual mitochondria localized between Z-lines visualized by the

autofluorescence of flavoproteines (green color). Z-lines are marcked using immunofluorescent labeling of α-actinin (red color). B) analysis of fluorescence intensity along selected line in Figure 4A. Peaks of fluorescence intensity corresponding to mitochondria are seen in the regions of "zero" intensity of α-actinin indicating the absence of mitochondrial fusion and "kiss and run" events.

Figure 5 Simultaneous fluorescent immunolabeling of VDAC and βII tubulin in adult rat cardiomyocytes.

A) Fluorescent immunolabeling of VDAC (green color). B) Fluorescent immunolabeling of βII tubulin (red color) using mouse anti-tubulin βII (β2) and Cy5 fluorescent secondary antibody.C) Overlay of images A and B showing close localization of βII tubulin and VDAC. Scale bar: 10 μm

Figure 6. Electron tomographic imaging of mouse cardiac muscle. A) Three-dimensional image of T-tubules (green), junctional sarcoplasmic reticulum (jSR in yellow), mitochondria (magenta). Scale bar: 1 μm. B) Mitochondrial membrane-associated structures and T-tubules at larger magnification. Scale bar 200 nm. C) The 3D mesh models of T-tubules, jSR and mitochondria in volume that crosscuts most of myofilaments. Scale bar 500 nm. Figures are reprinted with permission from Hayashi et al., 2009 [42].

Figure 7. Electron microscopic imaging of cardiac muscle. The cross-section through muscle fiber shows A) at the H-band level (x 55.000) and B) at the Z-line level (x 70.000) mitochondrial membrane-associated structures constituted with endoplasmic reticulum (ER) and T-tubules. C) The longitudinal section through muscle fiber shows tubular cisternae (arrows) running transversely on each side of the T-tubule (T) at the level of Z-lines between two adjacent mitochondria. (G. : glycogen) x 33.000. Figure is reprinted with permission from Segretain et al., 1981 [39]. D) Three-dimensional skeleton of the T-tubular network in a rat ventricular myocyte reconstructed from a stack of fluorescence images. T-tubules create

network mesh with some imposed regularity. Scale bar 55 μm. Figure is reprinted with permission from Soeller et al., 1999 [44].

Figure 8. Functional scheme of the Intracellular Energetic Units of adult cardiac muscle cell. Mitochondria are structurally integrated with T-tubular network, sarcomere, and sarcoplasmic reticulum. Together with cytoskeletal proteins these structures create conditions for compartmentation of metabolic processes and calcium circulation. Substrates,Ca2+ and oxygen are delivered to mitochondria via the system of T-tubuls. Free fatty acids (FFA) taken up by a family of plasma membrane proteins (FATP1), are sterified to acyl-CoA which entering further the β-fatty acids oxidation (β-FAO) pathway which results in acetyl-CoA production. CPT I and CPT II — carnitine palmitoyltransferases I and II, respectively. Electron-transferring flavoprotein (ETF)-ubiquinone oxidoreductase delivers electrons from β-FAO directly to complex III of the respiratory chain (RC). NADH produced by β-FAO is oxidized in the complex I of the RC passing along two electrons and two protons which contribute to the polarization of mitochondrial inner membrane (MIM). Glucose (GLU) is taken up by glucose transporter-4 (GLUT-4) located both in sarcolemma and T-tubules, and oxidized via Embden–Meyerhof pathway. Pyruvate produced from glucose oxidation is transformed by the pyruvate dehydrogenise complex (PDH) into acetyl-CoA. The NADH redox potential resulted from glycolysis enters mitochondrial matrix via malate–aspartate shuttle. Malate generated in the cytosol enters the matrix in exchange for α-ketoglutarate (αKG) and can be used to produce matrix NADH. Matrix oxaloacetate (OAA) is returned to the cytosol by conversion to aspartate (ASP) and exchange with glutamate (Glut). Acetyl-CoA is oxidized to CO2 in the tricarboxylic acids (TCA) cycle generating NADH and FADH2 which are further oxidized in the RC (complexes I, II) with final ATP synthesis. G6P inhibits HK decreasing the rate of glucolysis. The key system in energy transfer from mitochondria to cytoplasm is Mitochondrial Interactosome (MI). MI is a supercomplex,

formed by ATP synthase, adenine nucleotides translocase (ANT), phosphate carriers (PIC), mitochondrial creatine kinase (MtCK), voltage-dependent anion channel (VDAC) with bound cytoskeleton proteins (specifically βII-tubulin). MI is responsible for the narrow coupling of ATP/ADP intramitochondria turnover with phosphorylation of creatine (Cr) into phosphocreatine (PCr). PCr is then used to regenerate ATP locally by CK with ATPases (actomyosin ATPase, sarcoplasmic reticulum SERCA and ion pumps ATPases). The rephosphorylation of ADP in MMCK reaction increases the Cr/PCr ratio which is transferred towards MtCK via CK/PCr shuttle. A small part of ADP issued from ATP hydrolysis creates gradient of concentration transmitted towards the matrix. The shaded area in the upper right corner shows the Calcium Release Unit. Calcium liberated from local intracellular stores during excitation–contraction coupling through calcium-induced calcium release mechanism, (1) activates contraction cycle by binding to troponin C in the troponin–tropomyosin complex of thin filaments and (2) enters the mitochondria mainly via the mitochondrial Ca2+ uniporter (UPC) to activate 3 Krebs cycle dehydrogenases: PDH, αKG, isocitrate dehydrogenase. Figure is reprinted with permission from Saks et al., 2012 [28].

Figure

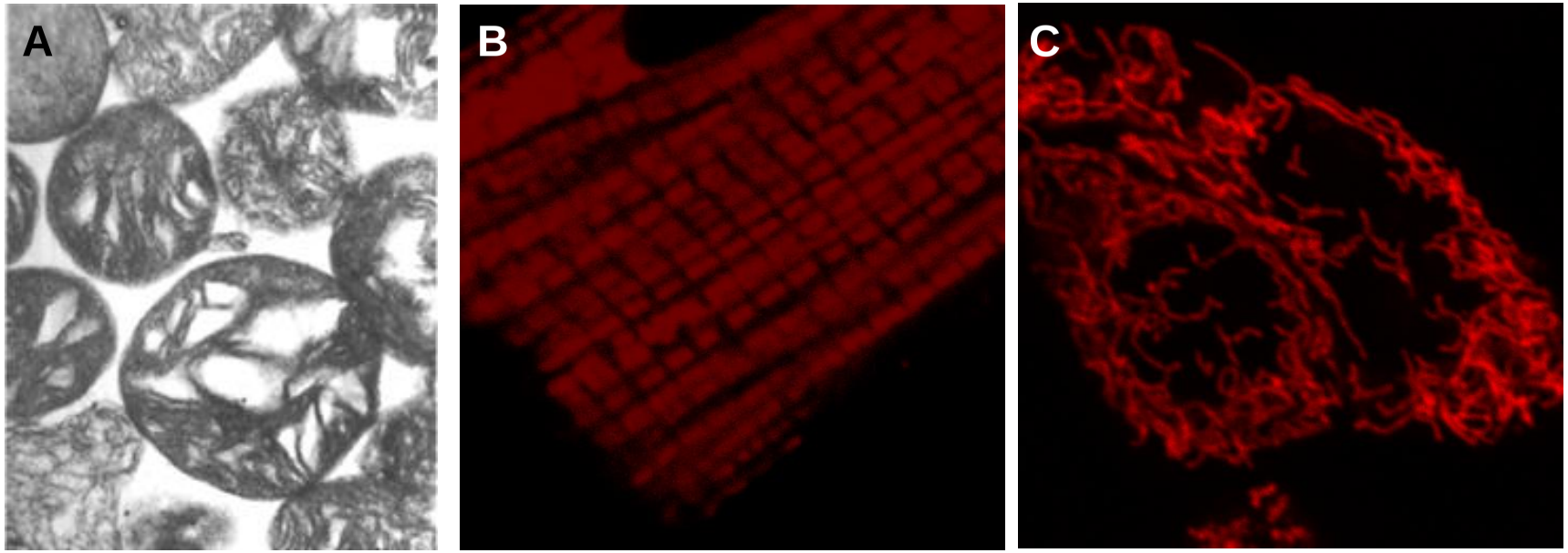

Figure 1

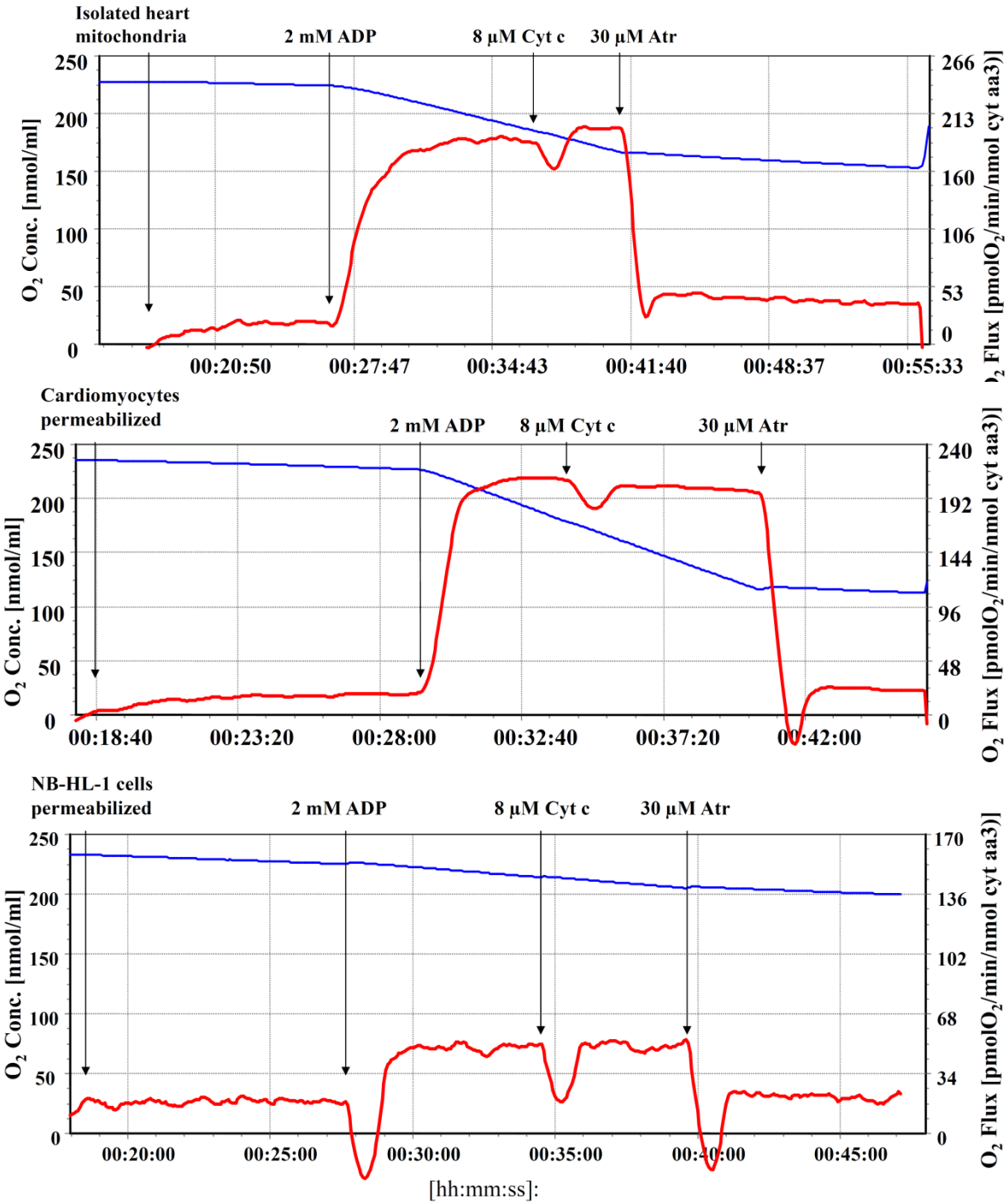
Isolated heart mitochondria
2 mM ADP
8 µM Cyt c
30 µM Atr
O2 Conc. [nmol/ml]
O2 Flux [pmolO2/min/nmol cyt aa3)]
250
200
150
100
50
0
266
213
160
106
53
0
00:20:50
00:27:47
00:34:43
00:41:40
00:48:37
00:55:33
Cardiomyocytes permeabilized
2 mM ADP
8 µM Cyt c
30 µM Atr
O2 Conc. [nmol/ml]
O2 Flux [pmolO2/min/nmol cyt aa3)]
250
200
150
100
50
0
240
192
144
96
48
0
00:18:40
00:23:20
00:28:00
00:32:40
00:37:20
00:42:00
NB-HL-1 cells permeabilized
2 mM ADP
8 µM Cyt c
30 µM Atr
O2 Conc. [nmol/ml]
O2 Flux [pmolO2/min/nmol cyt aa3)]
250
200
150
100
50
0
170
136
102
68
34
0
00:20:00
00:25:00
00:30:00
00:35:00
00:40:00
00:45:00
[hh:mm:ss]:

Figure 2

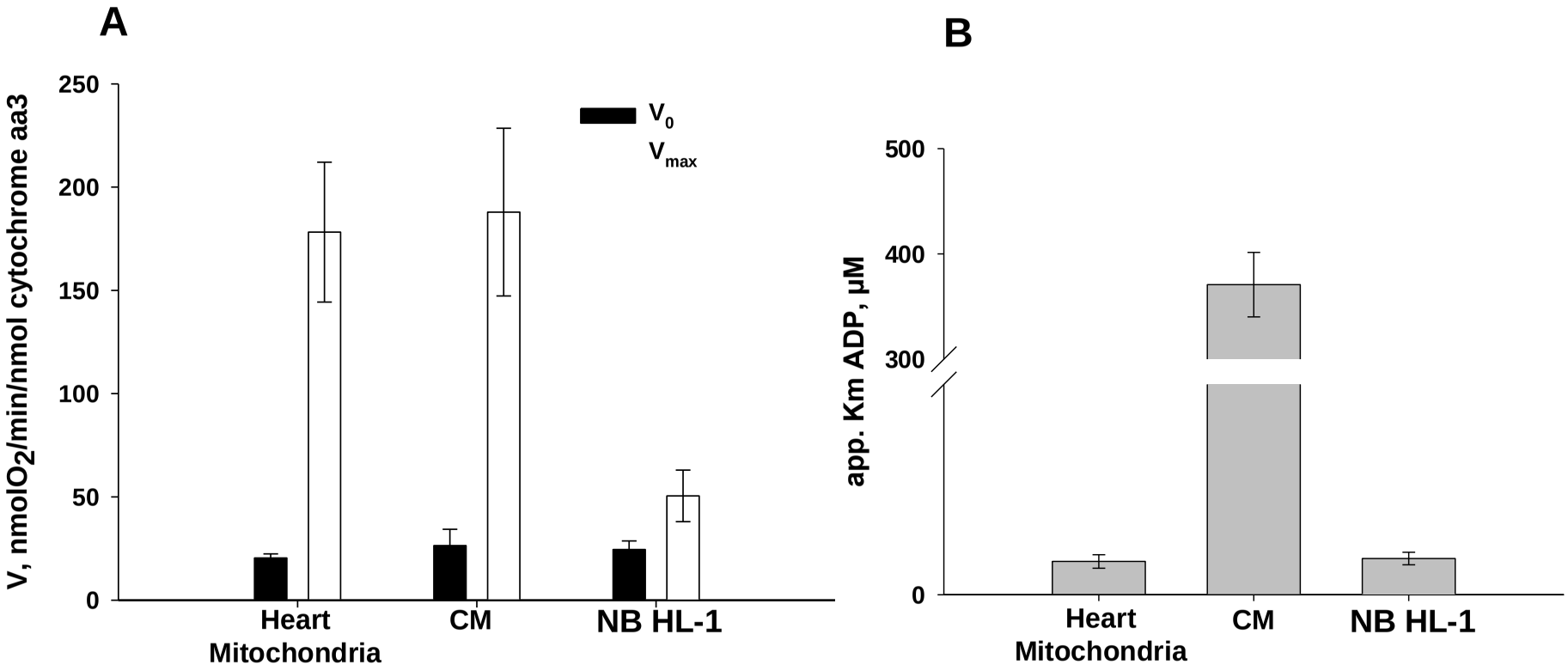
A
B
V, nmolO2/min/nmol cytochrome aa3
250
200
150
100
50
0
V0
Vmax
Heart Mitochondria
CM
NB HL-1
app. Km ADP, µM
500
400
300
0
Heart Mitochondria
CM
NB HL-1

Figure 3

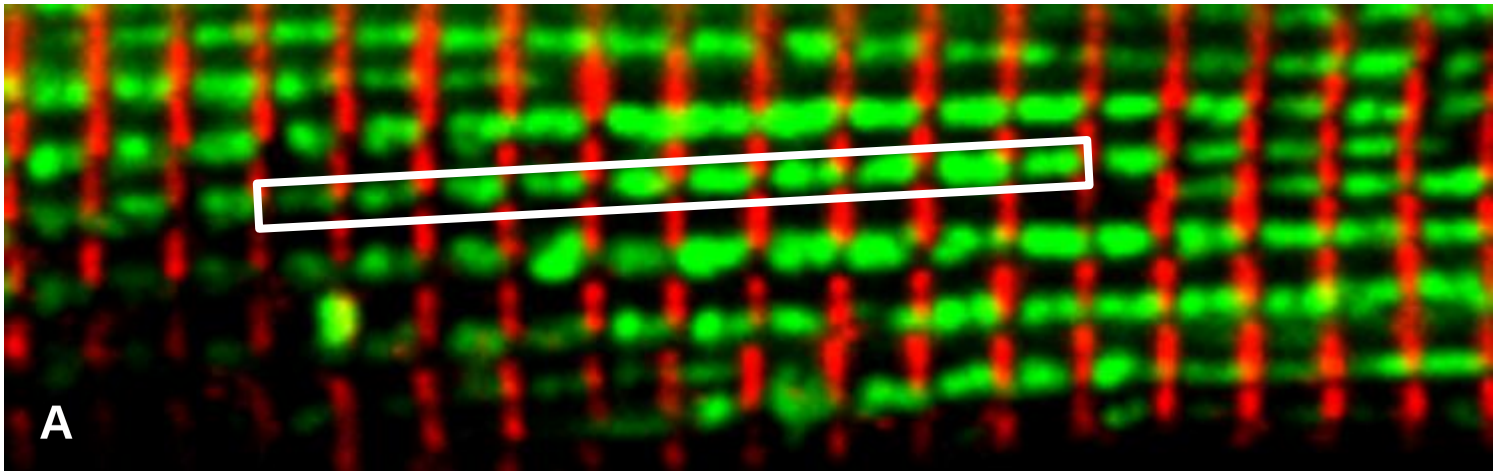

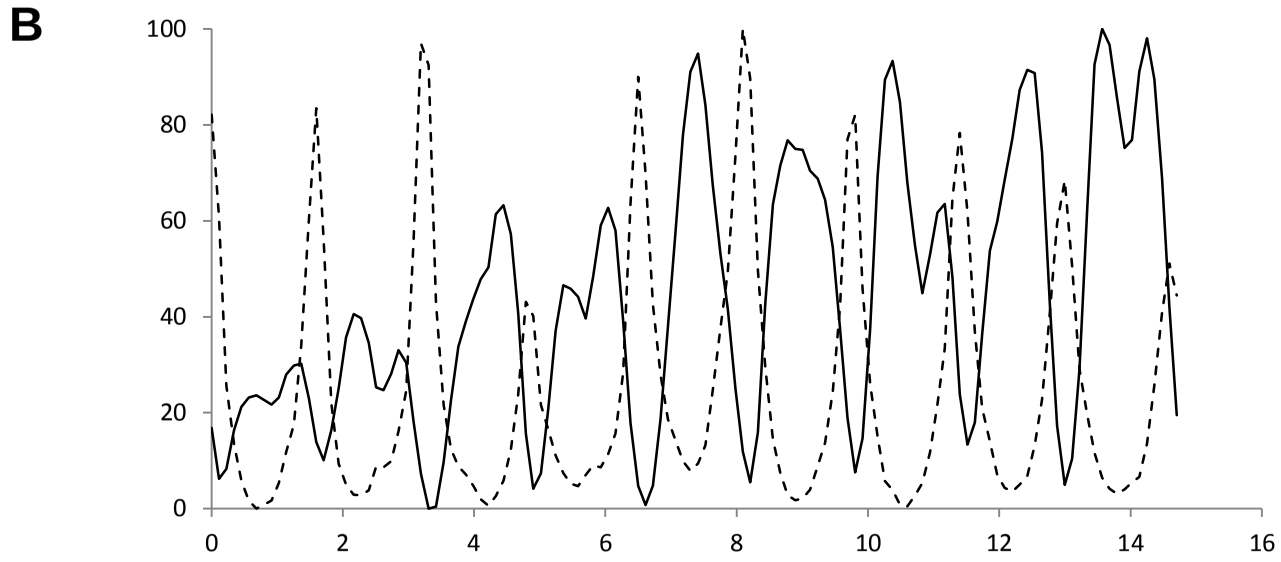

Figure 4

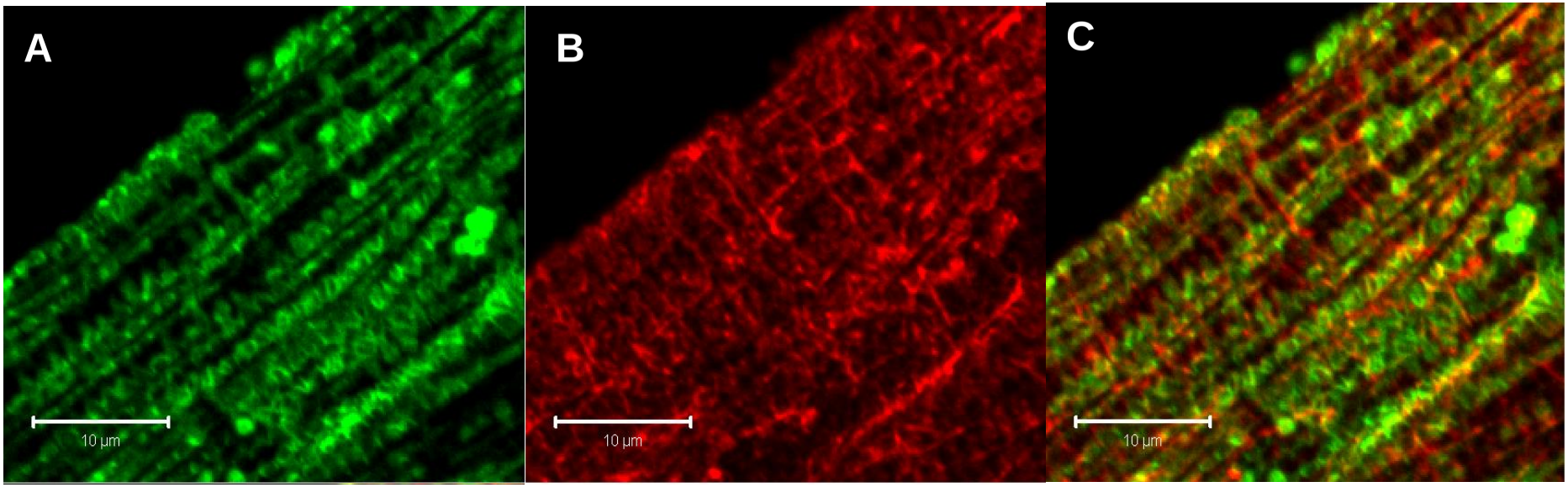

Figure 5

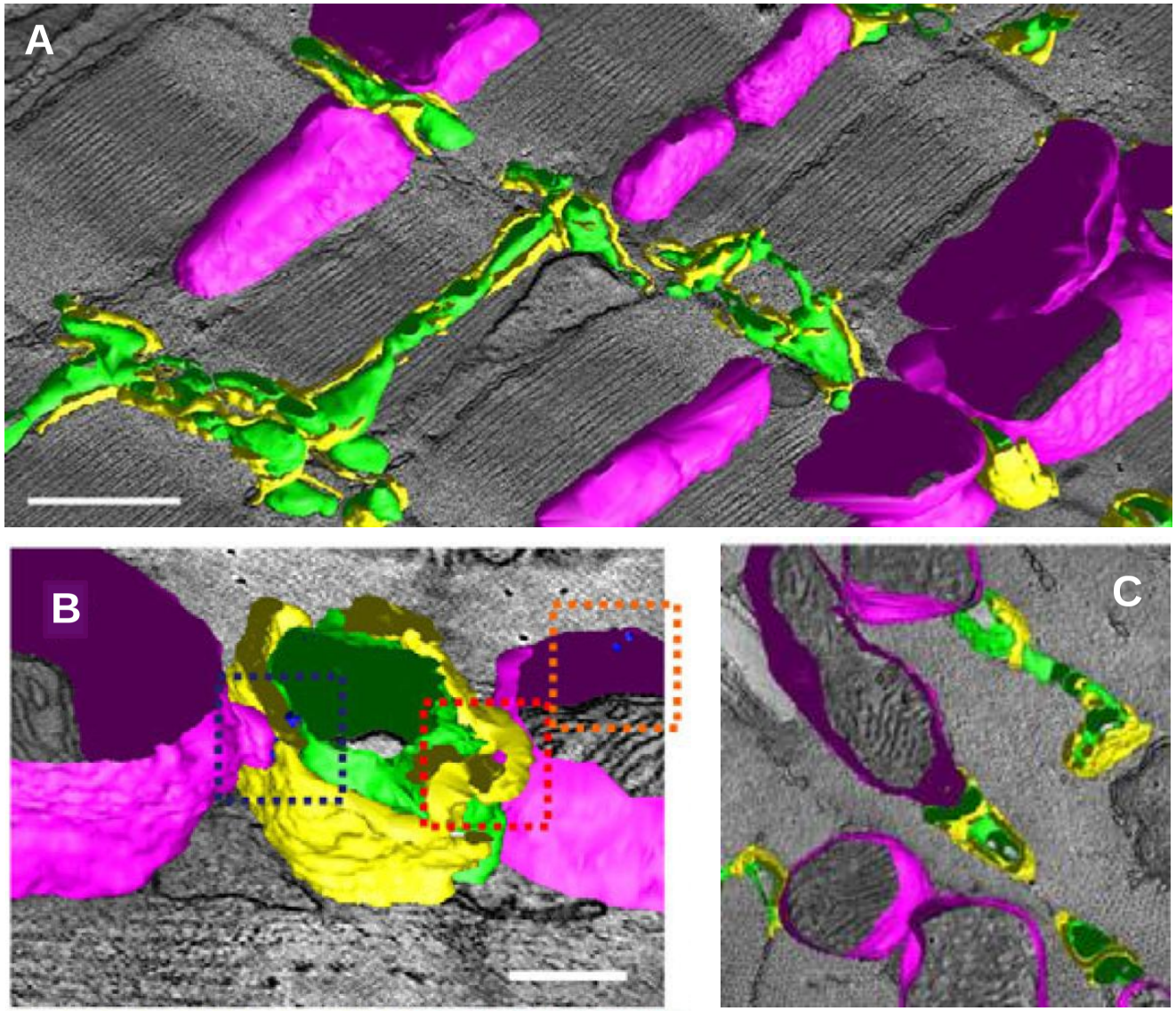

Figure 6

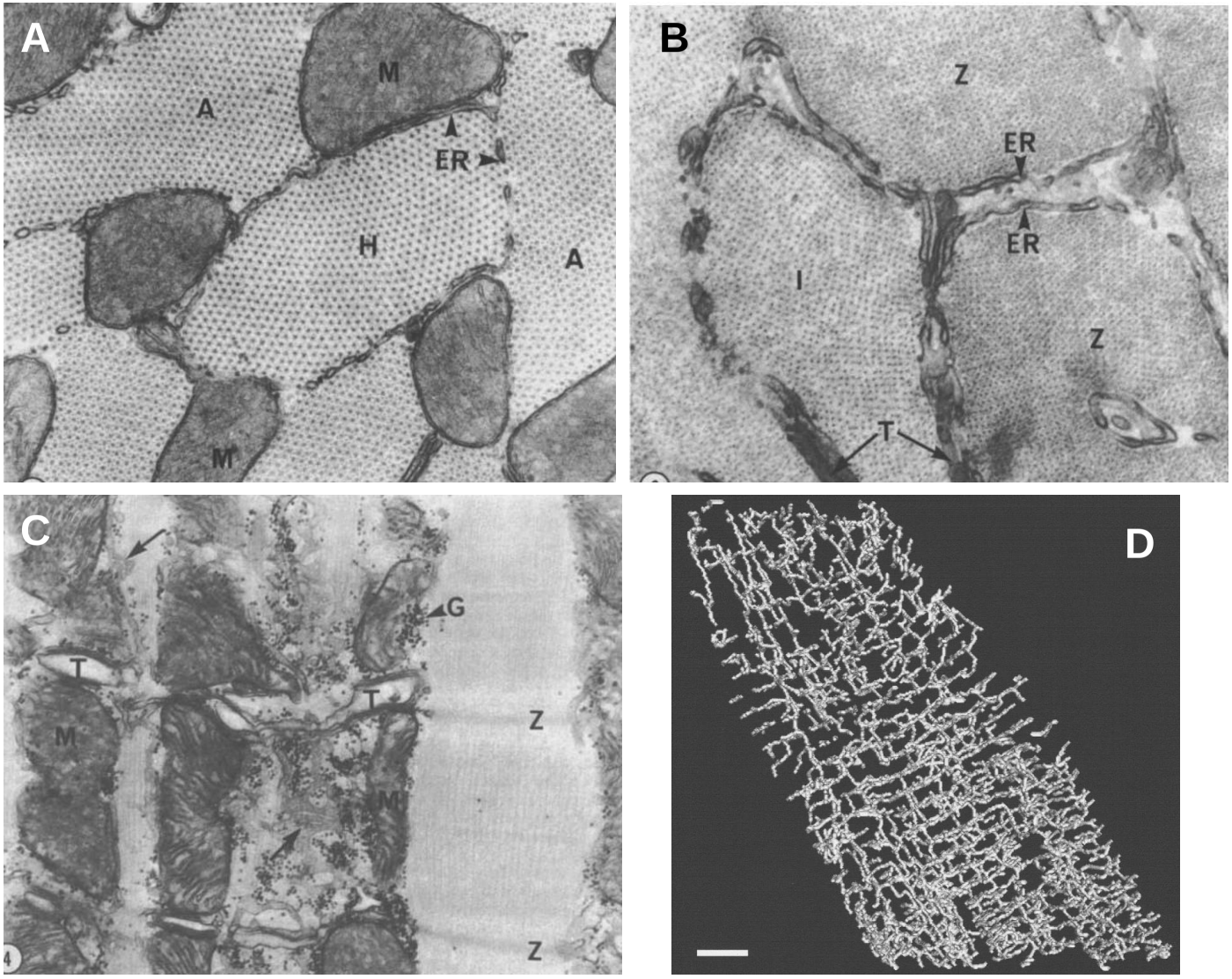

Figure 7

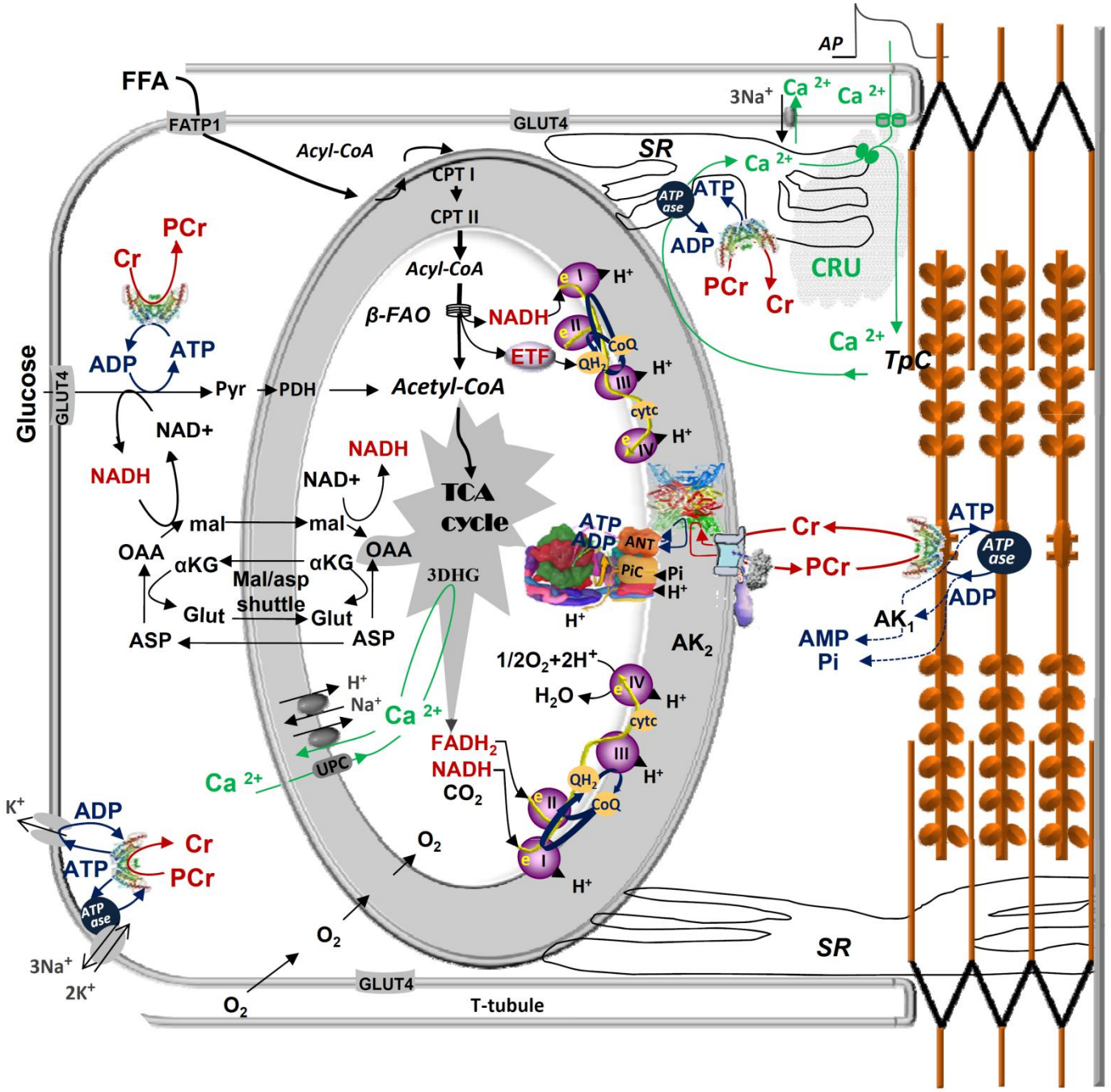
AP
FFA
FATP1
GLUT4
Acyl-CoA
CPT I
CPT II
Acyl-CoA
β-FAO
NADH
ETF
SR
3Na+
Ca 2+
ATP ase
ATP
ADP
PCr
Cr
CRU
TpC
Glucose
GLUT4
Pyr
PDH
Acetyl-CoA
NAD+
NADH
TCA cycle
mal
OAA
αKG
Mal/asp shuttle
Glut
ASP
3DHG
ANT
PiC
Pi
H+
AK2
AK1
AMP
1/2O2+2H+
H2O
cytc
FADH2
CO2
CoQ
QH2
UPC
K+
O2
T-tubule

Figure 8